Technische Universität München
TUM School of Engineering and Design

Development of a Digital System for the Uncertainty Quantification and Minimization of Chemical Kinetic Models

Hongxin Wang

Vollständiger Abdruck der von der TUM School of Engineering and Design der Technischen Universität München zur Erlangung des akademischen Grades eines

Doktors der Ingenieurwissenschaften (Dr.-Ing.)

genehmigten Dissertation.

Vorsitz:

Prof. Dr. Dongsheng Wen

Prüfer*innen der Dissertation:

1. Prof. Dr.-Ing. Oskar J. Haidn
2. Prof. Alexander Konnov, Ph.D.
3. Assistant Prof. Yuval Dagan, Ph.D.

Die Dissertation wurde am 16.08.2022 bei der Technischen Universität München eingereicht und durch die TUM School of Engineering and Design am 29.01.2023 angenommen.

“All models are wrong, but some are useful.”

George E. P. Box

Abstract

This thesis work was performed to develop a digital system for the uncertainty quantification and minimization of chemical kinetic models. In the part of uncertainty quantification, the uncertainties of the reaction rate constants, modeling results, and experimental data were estimated. The reaction rate constants recommended by the literature were analyzed and the Arrhenius equation parameters with uncertainty factors were determined for the reactions of H_2 and hydrocarbon molecules with carbon atoms less than 3. Monte Carlo simulations were conducted with reaction rate constants sampled within the modeling uncertainties and the 2σ bounds of the results were defined as the modeling uncertainties of the parameter set. The uncertainty sources of the collected measured ignition delay times, laminar flame speeds, and concentration profiles were analyzed and the experimental uncertainties were evaluated. In the part of uncertainty minimization, the discrepancy measure was defined and reduced by three methods. The first one is the traditional method relying on the human experience and intuition applied to the update of the ethylene oxidation model, but it may increase the risk of human error. In the second work of the optimization of a hydrogen oxidation model, the methodology of response surface was applied and the uncertainties were reduced based on the probability density function based on the Monte Carlo simulation. The third method was developed based on the particle swarm optimization algorithm and applied to the optimization of a joint hydrogen and syngas oxidation model. With the work presented in this dissertation, the human intervention in the optimization of chemical kinetic models has been reduced and a system with reliable preparation of digital data and automated optimization with quantified uncertainties has been developed.

Zusammenfassung

Diese Arbeit wurde mit dem Ziel durchgeführt, ein digitales System für die Quantifizierung und Minimierung der Unsicherheit chemischer kinetischer Modelle zu entwickeln. Im Teil der Quantifizierung der Unsicherheit wurden die Unsicherheiten der Reaktions-geschwindigkeitskonstanten, der Modellierungsergebnisse und der experimentellen Daten geschätzt. Die in der Literatur empfohlenen Reaktionsgeschwindigkeitskonstanten wurden analysiert und die Parameter der Arrhenius-Gleichung mit Unsicherheitsfaktoren wurden für die Reaktionen von H_2 und Kohlenwasserstoffmolekülen mit weniger als 3 Kohlenstoffatomen bestimmt. Monte-Carlo-Simulationen wurden mit Reaktions-geschwindigkeitskonstanten durchgeführt, die innerhalb der Modellierungsunsicherheiten lagen, und die 2σ-Grenzen der Ergebnisse wurden als Modellierungsunsicherheiten des Parametersatzes definiert. Die Unsicherheitsquellen der erfassten gemessenen Zünd-verzögerungszeiten, laminaren Flammengeschwindigkeiten und Konzentrationsprofile wurden analysiert und die experimentellen Unsicherheiten wurden bewertet. Im Teil der Unsicherheits-minimierung wurde das Diskrepanzmaß definiert und durch drei Methoden reduziert. Die erste ist die traditionelle Methode, die sich auf die menschliche Erfahrung und Intuition bei der Aktualisierung des Ethylenoxidationsmodells stützt, aber sie kann das Risiko menschlicher Fehler erhöhen. In der zweiten Arbeit zur Optimierung eines Wasserstoffoxidationsmodells wurde die Methodik der Reaktionsoberfläche angewandt und die Unsicherheiten wurden anhand der Wahrscheinlichkeitsdichtefunktion auf der Grundlage der Monte-Carlo-Simulation reduziert. Die dritte Methode wurde auf der Grundlage des Algorithmus der Partikel-schwarmoptimierung entwickelt und auf die Optimierung eines gemeinsamen Wasserstoff- und Synthesegas-Oxidationsmodells angewandt. Mit den in dieser Dissertation vorgestellten Arbeiten konnte der menschliche Eingriff in die Optimierung chemischer kinetischer Modelle reduziert und ein System mit zuverlässiger Aufbereitung digitaler Daten und automatisierter Optimierung mit quantifizierten Unsicherheiten entwickelt werden.

Acknowledgment

I would like to express my sincerest gratitude to my supervisor Prof. Oskar Haidn and Dr. Nadezda Slavinskaya for their guidance and support on this project. They opened the door to science for me. They lighted my way to the truth like the sun and lunar in my most difficult time. Thank you for the time spending with me looking for fun in science.

My sincerest gratefulness goes to my parents, Shuangxing Wang and Lanning Shi, and my family. Bringing me into this world is the greatest work for me. Thank you for offering me the chance to experience this life and for taking care of me over the past decades. Thanks to my love Chuting Wu. Without your support, I would never make the achievements today.

I would like to thank Prof. Dongsheng Wen for chairing the thesis evaluation and Prof. Alexander Konnov and Prof. Yuval Dagan for being the examiner and for their valuable feedback. I am also grateful to the TUM Graduate Center for their support during my research and to Frau Helga Bassett for her help with my examination.

I would like to thank my students, Yiting Gao, Siyuan Hu, Chenxi Shi, Chenyi Sun, Guanyu Wang, Yuqian Zhang, Weixuan Yuan, and my coworker, Aziza Kanz, for their creative work. My gratitude extends to my colleagues, Yongchuan Yu, Jianing Liu, Hao Ma, Meng Luo, Ye Hong, Zhendong Yu, Andrej Sternin, Daniel Martinez, and Ibraheem Nasser for their help. I would also like to express my appreciation to Prof. Xu Xu, Prof. Bing Chen, Prof. Liang Tian, Prof. Qingchun Yang, Prof. Xianggeng Wei, Dr. Shaohua Zhu, and Prof. Silong Zhang for their insightful discussions and cooperation.

My doctoral project would not be possible without the support of China Scholarship Council. I sincerely thank Mr. Congbing Wang of Consulate General of the People's Republic of China in Munich, Ms. Zhihong Tang of Chinese-German Center for Technology and Innovation, and Ms. Qian Zhao of Yangtze Delta Region Institute of Tsinghua University.

It is my luck and honor to spend a wonderful time in Munich with my friends. My gratefulness goes to my Alumni from Beihang University Dalong Shi, Siyuan Liu, Xin Guo, and Yang Zhang, my neighboring friends You Xie, Xingcheng Chen, Yuting He, and Youdan Zhang, and my friends from the Verein der Chinese Scholarship Council Academic in München e.V. Shangming Du, Qilin Tang, Mengwen He, Yina Zhang, Difei Han, Yalan Ma, Bailing Li, Haochen Yu, Yiying Hu, Ke Du, Jian Shao, and Jing Ma. Many thanks to cats Sky, Yaya, and Ronnie for warming me in the coldest winter. There are so many words of thanks and so many of them that I cannot list them all here.

List of papers

The thesis is based on the work presented in the following papers:

Paper-I. Hongxin Wang, Nadezda Slavinskaya, Aziza Kanz, Moldir Auyelkhankyzy, Yiting Gao, Oskar Haidn, A comprehensive kinetic modeling study of ethylene combustion with data uncertainty analysis, Fuel 299 (2021) 120833. DOI: 10.1016/j.fuel.2021.120833.

Paper-II. Hongxin Wang, Nadezda Slavinskaya, Oskar Haidn, A comprehensive kinetic modeling study of hydrogen combustion with uncertainty quantification, Fuel 319 (2022) 123705. DOI: 10.1016/j.fuel.2022.123705.

Paper-III. Hongxin Wang, Chenyi Sun, Oskar Haidn, Askarova Aliya, Chiara Manfletti, Nadezda Slavinskaya, A joint hydrogen and syngas chemical kinetic model optimized with particle swarm optimization, Fuel 332 (2023) 125945. DOI: 10.1016/j.fuel.2022.125945.

Related work

Gajana Walter, **Hongxin Wang**, Aziza Kanz, Alexander Kolbasseff, Xu Xu, Oskar Haidn, Nadezda Slavinskaya, Experimental error assessment of laminar flame speed measurements for digital chemical kinetics databases, Fuel 266 (2020) 117012. DOI: 10.1016/j.fuel.2020.117012.

Content

List of Figures

List of Tables

List of Abbreviation

Abbreviation	Definition	Unit
T	Temperature	K
p	Pressure	atm, bar
φ	Equivalence ratio	dimensionless
k	Reaction rate constant	order 1: s^{-1} order 2: $cm^3 \cdot mole^{-1} \cdot s^{-1}$ order 3: $cm^6 \cdot mole^{-2} \cdot s^{-1}$
η_M	Relative collision efficiency for M	dimensionless
E_a	Activation energy	K
f	Uncertainty factor of the RRC	dimensionless
σ	Standard deviation	*
y^{exp}	Experimental data	*
y^{mod}	Modeling data	*
y^{pre}	Response surface prediction data	*
x, $\boldsymbol{X}$	Normalized RRC parameter	dimensionless
α_i, β_{ij}	1st-/2nd- order polynomial coefficient	dimensionless
u	Uncertainty of the experimental data	*
Ψ	Model discrepancy measure	dimensionless
C	Uncertainty contribution	*
C_r	Relative uncertainty contribution	dimensionless
r	Pearson correlation coefficients	Dimensionless
IDT	Ignition delay time	s
LFS	Laminar flame speed	cm/s
RRC	Reaction rate constant	
ST	Shock tube	
RCM	Rapid compression machine	
PFR	Plug flow reactor	
PSR	Perfectly stirred reactor	
PDF	Probability density function	
PSO	Particle swarm optimization	

*Depend on the type of the measurement

1. Introduction

The history of humanity making use of combustion is more than one million years. Thanks to the development of the steam engine in the First Industrial Revolution and the widespread use of electricity and oil in the Second Industrial Revolution, in which combustion played a crucial role, mankind's productivity increased to an unprecedented level [1, 2]. Combustion has become a fundamental technology for heating, transportation, electricity generation, manufacturing, etc. Since the Third Industrial Revolution, also known as the digital revolution, computer simulations have rapidly grown to become a significant component in science and engineering, and the simulation of chemical reactions has become an essential aspect of combustion research [3].

The first chemical kinetic systems to be modeled were developed for the decomposition of hydrazine, nitric oxide, and ozone [4]. Over the past seven decades, as the computational power has increased, more detailed chemical kinetic models with large number of elementary reactions have been proposed. With the increasing number of species and steps required to describe a particular oxidation process, the design of a reaction mechanism relying heavily on intuition and rules of thumb should be replaced by the computer-aided design approach [5]. In the upcoming Fourth Industrial Revolution, or Industry 4.0 [6], the integration of artificial intelligence into traditional industry will lead to increased automation and self-monitoring, and the use of digital systems that can analyze and diagnose issues without human intervention [7, 8].

Chemical kinetic models are used to describe the transformation of reactants into products at the molecular level. A complete chemical kinetic model consists of elementary reactions that show changes in the concentration of a reactant or a product over time, thermal properties of each species, such as enthalpy, entropy, and heat capacities, and the transport process characterizing the molecular transport of species, momentum, and energy.

One of the most important concepts of kinetics is the reaction rate of chemical reaction, which shows the change of concentration of a reactant or a product over time. With advancements in technologies such as mass spectrometry [9], laser absorption technology [10], and transition-state theory [11, 12], various experimental [13-17] and theoretical methods [18-20] have been developed to determine reaction rate constants (RRCs). However, the RRCs

obtained conditionally "directly" or calculated via quantum chemistry calculations often exhibit high uncertainties [21, 22], thereby posing a major challenge in developing reliable chemical kinetic models.

One practical approach to estimate RRCs is the reverse chemical kinetic problem, where the reaction rates are determined from simulations of macro experimental kinetic data, such as ignition delay times, laminar flame speeds, and concentration profiles. The Bound-to-Bound Data Collaboration (B2BDC) [23] is a useful method that employs robust control to identify the actual bounds of parameter uncertainties and ensure consistency between model parameters and experimental data. By deploying semidefinite programming algorithms [24], the initial bounds on unknowns are combined with the initial bounds of experimental data, which shows the model predictions out of the experimental errors. The initially calculated deterministic uncertainty bounds, called feasible parameter sets, are further used for prediction in new settings. The output variables produced in different numerical experiments for discrete points (random samplings) in feasible parameter space are fitted with a second-order polynomial function into a response surface (solution mapping methodology [25]), which is further used in subsequent uncertainty analyses to optimize the model and produce a final feasible set of model parameters [26] and to determine the validity range of the model. The model optimization is carried out after data consistency analyses: the potential outliers from a training set are identified with a quantitative measure of an agreement between the model and raw experimental data.

In this thesis, a digital system combining the methodologies of response surface [28] and artificial intelligence algorithm for the uncertainty quantification and minimization of chemical kinetic models has been developed. The chemical kinetic model and simulation model of macro experimental kinetic data measured in shock tubes, rapid compression machines, premixed laminar flames, perfectly stirred reactors, and plug flow reactors will be briefly introduced in Chapter 2. In Chapter 3, the uncertainty quantifications of the experimental data, reaction rate constants, and the chemical kinetic model will be presented, which with the initial uncertainty bounds can be determined. In Chapter 4, the discrepancy measure, which shows the prediction ability of the chemical kinetic model, will be defined. The response surface methodology is developed on the Monte Carlo simulation for revealing the input-output characteristics of the chemical kinetic modeling. The uncertainty reduction based on the probability density function and particle swarm optimization will be described. Lastly, Chapter 5 gives an outline of the uncertainty quantification and minimization and summarizes the thesis.

Through the work described in this thesis, 3 major aims will be achieved:

(1) To develop the database and method for the uncertainty quantification and data consistency analysis of the reaction rate constants (RRCs), experimental data, and modeling results of hydrogen and small hydrocarbon oxidation.

(2) To develop a digital system combining the methodologies of response surface [27] and artificial intelligence algorithm for the uncertainty quantification and minimization of chemical kinetic models.

(3) Test the established method by figuring out the feasible parameter sets of a detailed chemical kinetic model with good prediction ability for the currently available experimental data of H_2 and syngas oxidation.

Through these aims, a digital system for the automatic optimization of chemical kinetic models will be developed. In Paper-I, a revision and upgrade of the ethylene (C_2H_4) oxidation kinetic sub-model were carried out as the next step in the optimization of the $C_{<3}$ chemistry. Uncertainty quantification was conducted for the RRCs of small hydrocarbon reactions and a database was developed based on the literature. Data consistency and uncertainties were figured out for the experimental data of C_2H_4 oxidation. In Paper-II, a 19-reactions H_2 oxidation chemical kinetic sub-model has been optimized with uncertainty quantification. The system input-output response behavior was studied with the help of Monte Carlo simulation and the method of response surface. The probability density functions of RRCs were calculated for 4 key channels to reduce their large uncertainty intervals. In Paper-III, a syngas oxidation model has been optimized with re-optimization of the H_2 model by particle swarm optimization (PSO) algorithm. The feasible parameter set was determined based on a statistical analysis of the optimums obtained by PSO.

2. Chemical kinetic model and simulation

Numerical simulation of reactive kinetic systems requires accurate knowledge about model parameter values to be predictive. Besides experimental measurements of reaction rates and quantum chemical/statistical calculations, the reverse chemical kinetic problem when the reaction rates are determined from simulations of experimental macro kinetic data, ignition delay times (IDTs), laminar flame speeds (LFSs), and concentration profiles, are applied to determine RRCs. Different experimental methods have been designed to create near-ideal reaction environments to avoid the influence of redundant factors on the system's input-output behavior. However, the non-ideal phenomena make it difficult to achieve ideal conditions such as local constant pressure or local constant temperature in reactive systems. Idealized models with non-ideal factors taken into account are the basis for the accurate prediction of the measured parameters and the study of the reactive system input-output characteristics. In this chapter, the reaction rate constants of the studied kinetic models will be defined. Short descriptions of the idealized models for the simulation of shock tubes (STs), rapid compression machines (RCMs), premixed laminar flames, perfectly stirred reactors (PSRs), and plug flow reactors (PFRs) will be presented.

2.1 Reaction rate constant

The chemical kinetic is composed of the elementary reaction which can be described by the equation:

$$a\mathrm{A} + b\mathrm{B} + c\mathrm{C} \ldots = d\mathrm{D} + e\mathrm{E} + f\mathrm{F} \ldots \quad (1)$$

where A, B, C … are the reactants and D, E, F … are the products. The reaction rate can be expressed by the concentration change of reactant A:

$$\frac{\mathrm{d[A]}}{\mathrm{dt}} = -k \cdot [\mathrm{A}]^a[\mathrm{B}]^b[\mathrm{C}]^c \ldots \quad (2)$$

where *a*, *b*, *c* … are the reaction orders concerning the species A, B, C … and *k* is the RRC for the elementary reaction in Eq. (1). In this thesis, the unit of RRC is dependent on the overall reaction order, which is the sum of exponents *a*, *b*, *c*… in Eq. (2). The units of the RRC for first-, second-, and third- order reactions are s^{-1}, $cm^3mole^{-1}s^{-1}$, and $cm^6mole^{-2}s^{-1}$ respectively.

Most RRCs depend strongly in a nonlinear way on the temperature, which can be described by the Arrhenius equation:

$$k(T) = AT^n \exp\left(-\frac{E_a}{T}\right), (\text{cm}^3, \text{s, mole, K}) \quad (3)$$

where T is the absolute temperature in Kelvin, A is the pre-exponential factor, n is a constant representing the temperature dependence, and E_a is the activation energy for the reaction in the unit of Kelvin.

The pressure dependence of RRCs is described by the F-center treatment of Troe [28]. The third body M is added to the Arrhenius expression for the RRC in the fall-off range, then k_∞ and k_0 are determined for the high- and low- pressure limitation:

$$a\text{A} + b\text{B} = d\text{D} + e\text{E} \quad (4)$$

$$a\text{A} + b\text{B} + \text{M} = d\text{D} + e\text{E} + \text{M} \quad (5)$$

Here M can be any molecule, and the relative collision efficiency, η_M, is defined for different bath gases M:

$$\eta_M = \frac{k_{0,M}}{k_{0,Ar}} \quad (6)$$

which describes that the bath gas M promotes the reaction as a ratio of low-pressure limit RRC $k_{0,Ar}$, in which Ar is the reference bath gas. In the developed models, η_M is given for the commonly used diluent gases such as Ar, N_2, and He and the main reactants and products such as H_2, CO, H_2O, and CO_2.

Four parameters a, T^{***}, T^*, and T^{**} are used to determine the F_{cent} value:

$$F_{cent} = a \cdot \exp\left(\frac{T}{T^*}\right) + \exp\left(\frac{T}{T^{**}}\right) + (1+a) \cdot \exp\left(\frac{T}{T^{***}}\right) \quad (7)$$

which is used to calculate the value F:

$$\log F = \log F_{cent} \left[1 + \left(\frac{\log P_r + c}{n - d\cdot(\log P_r + c)}\right)^2\right]^{-1} \quad (8)$$

where

$$c = -0.4 - 0.67 \log F_{cent} \quad (9)$$

$$n = 0.75 - 1.27 \log F_{cent} \quad (10)$$

$$P_r = \frac{k_0[\text{M}]}{k_\infty} \quad (11)$$

With F and P_r, the RRC for reactions (4) and (5) at a certain pressure and temperature can be described as:

$$k = k_\infty \left(\frac{P_r}{1+P_r}\right) F \quad (12)$$

In this thesis, all the simulations were conducted with Ansys Chemkin Pro [29]. Three

chemical kinetic models with thermal data and transport data in the format for Ansys Chemkin Pro have been presented in the supplementary:
Paper-I: a model with 63 species 534 reactions for C_2H_4 with polycyclic aromatic hydrocarbon and soot formation;
Paper-II: a model with 11 species and 19 reactions for H_2 oxidation;
Paper-III: a model with 16 species and 41 reactions for H_2 and syngas oxidation.

2.2 Shock tube

A shock tube is a tube with closed ends split by the diaphragm into two sections: the high-pressure driver section filled with super-compressed carrier inert gas and the low-pressure driven section filled with the test gas mixture. During the experiment, the gas in the driver section is pressurized until the diaphragm bursts so that the incident shock wave quickly forms and propagates through the driven section. After reaching the end of the driven section, the incident shock wave is reflected from the wall and propagates back towards the driver section, stagnating and further compressing and heating the test gas to the pre-ignition temperature (T_5) and pressure (p_5).

The ideal model assumes that in a reflected shock wave experiment, the incident shock is planar and moves at a constant speed. The likewise planar reflected shock compresses the driven gas instantaneously. A homogeneous uniform zone of test gas can be produced behind the shock wave, which can be treated as a 0-dimensional (perfectly homogeneous) adiabatic, isochoric, or isobaric uniform reactor with constant internal energy or enthalpy, without any hydrodynamic processes, so that the IDT would be controlled only by chemistry.

In this thesis, the closed homogeneous model with constrained volume is applied to calculate IDTs measured in shock tubes. The energy equation is solved with initial temperature, T_5, and pressure, p_5. The IDT could be recorded as occurring either at the time of maximum rate of change or of the peak value of some species such as OH* and CH* [30, 31], or maximum gradient of temperature or pressure [32, 33], or could be based on an extrapolation of the maximum slope to the zero-signal level [30, 34]. In the work of Petersen et al. [30], the IDTs defined by the measured peak of OH* mole fraction ($\tau_{[OH]peak}$) and the maximum rate of the OH* curve to the zero line (τ_{zero}) were recorded. Fig. 1a shows the different definitions of the IDTs of the $H_2/O_2/Ar$ mixture at T_5 = 1181 K, in which the OH* mole fraction is replaced by the OH mole fraction. As shown by the comparison of the modeling results and experimental data [30] with 20% uncertainty in Fig. 1b, the optimized H_2 oxidation model predicts both

definitions of IDTs very well.

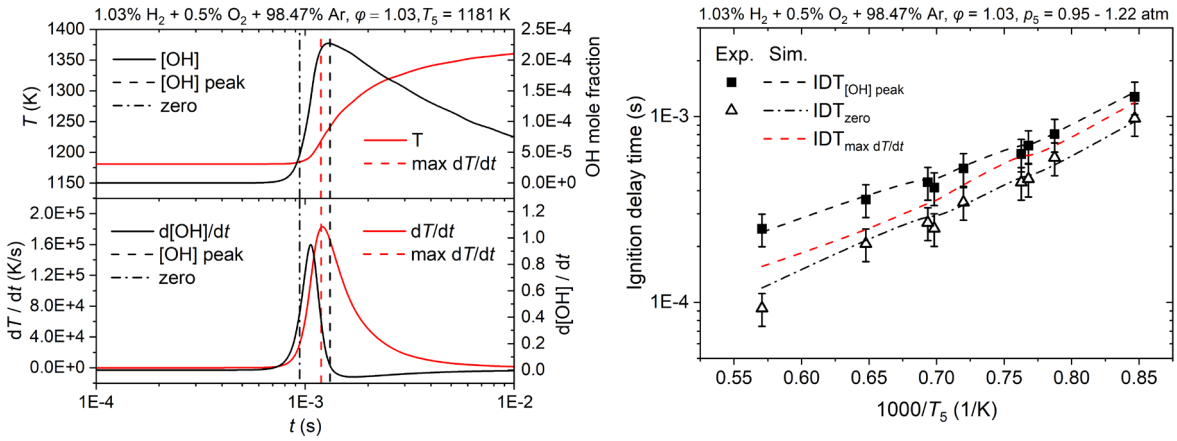

(a) **(b)**

Fig. 1. (a) Temperature, OH mole fraction (up), and their gradients (low) of the IDT simulation at T_5 = 1181 K; (b) Comparison of the IDTs determined by different definitions (Exp. by Petersen et al. [30] with 20% uncertainties, Sim. by H_2 oxidation model in Paper-II).

2.3 Rapid compression machine

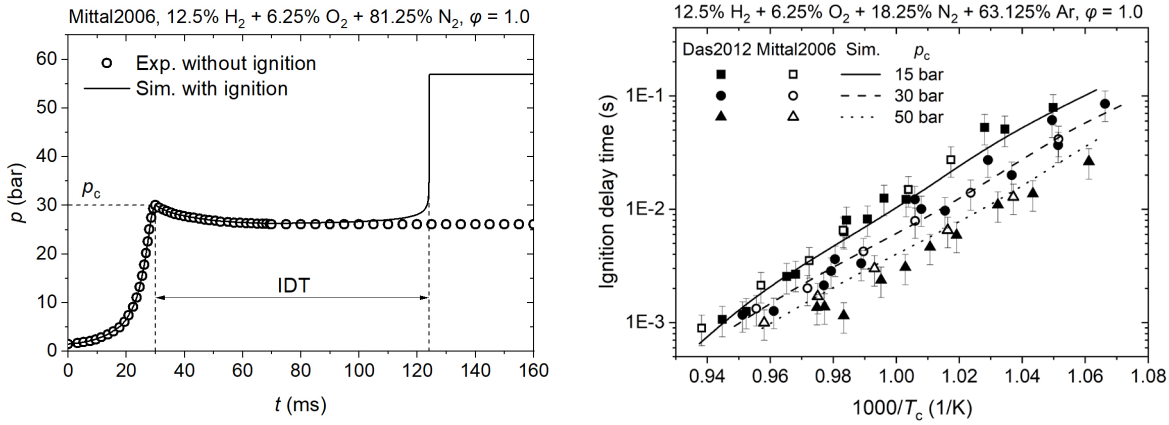

(a) **(b)**

Fig. 2. (a) Pressure profiles measured in the RCM experiment [35] and simulated with the volume profile; (b) Comparison of the measured [35, 36] and simulated IDTs in the RCMs.

The rapid compression machine (RCM) is used to simulate a single compression stroke of an internal combustion engine [37]. It can be used as an alternative to the shock tube for measuring the low to intermediate-temperature IDTs. In the experiment of RCM, the fuel-oxidizer mixture in the chamber is rapidly compressed by a piston assembly in a process close to adiabatic compression. The rapid compression results in elevated temperature (T_c) and high-pressure (p_c) conditions in the reaction chamber, as shown in Fig. 2a, which can be used to

investigate the autoignition characteristics.

The closed homogeneous model with constrained volume is applied to calculate IDTs measured in RCMs. The volume profile is used for each mixture to reproduce the real compression process. A comparison of the measured and simulated pressure is presented in Fig. 2a. The possible pre-ignition reaction and pressure decrease after the rapid compression caused by heat transfer are well predicted, and the modeling IDTs show good agreement with the measured data, as shown in Fig. 2b.

2.4 Premixed laminar flame

Premixed combustion consists of the chemical reactions within a flow of a premixture of reacting species. The laminar flame speed (LFS) and concentration profile measured in the premixed laminar flame are the most important characteristics for combustion investigation. The flame speed is defined as the velocity of the unburned gases through the combustion wave in the direction normal to the wave surface. The method of Bunsen flame, spherical flame [38, 39], counterflow flame [40], and flat flame [41] have been developed for the measurement of LFSs in the past decades.

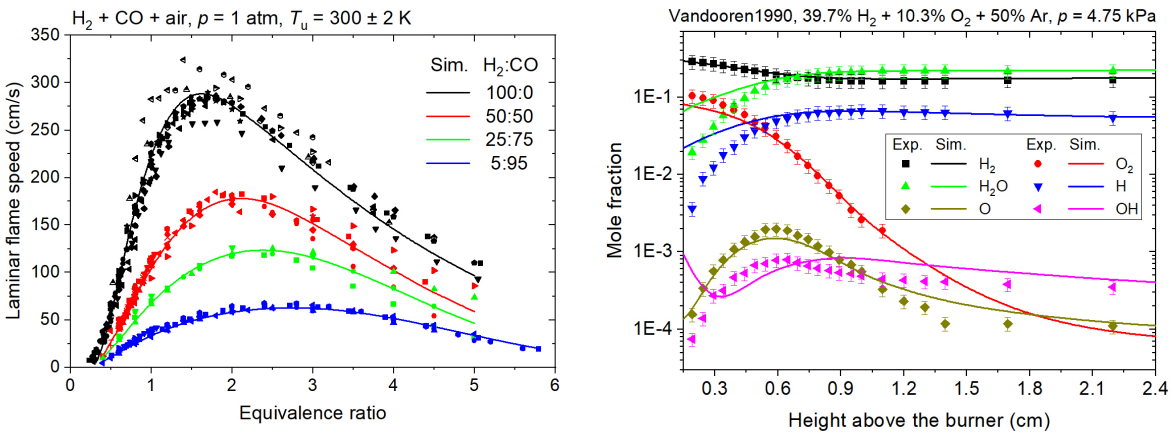

(a) **(b)**

Fig. 3. Comparison of the experimental data (symbols) and modeling results (lines) of premixed laminar flame: (a) laminar flame speeds of H_2 and syngas mixtures at 1 atm; (b) concentration profiles in H_2/O_2/Ar premixed laminar flame (Vandooren et al. [42]).

The ideal model of the premixed laminar flame is assumed to be a one-dimensional flow with uniform inlet conditions. The model solves the set of governing differential equations that describe the flame dynamics using implicit finite difference methods, as well as, a combination of time-dependent and steady-state methods [29]. Some results for laminar flame speeds and

concentration profiles of premixed laminar flames are presented in Fig. 3.

2.5 Perfectly stirred reactor

The jet stirred reactor [43] is a classical apparatus for studying the chemical kinetics of combustion reactions. The perfectly stirred reactor (PSR) is a jet stirred reactor in which perfect mixing (homogeneity) is achieved inside the control volume and the process in this volume is controlled by chemical reaction rates but not mixing processes. In the PSR, reactants are jetted into the mixing chamber through several nozzles and maintained at elevated temperatures for reaction. The constant temperature zone in the chamber is established by the heating system [44, 45]. The temperature in the PSR is monitored by thermocouples and the heater is controlled to achieve a constant temperature condition in the reaction zone. At the end of residence time, samples of the reacting mixtures are taken and analyzed by instruments [46, 47].

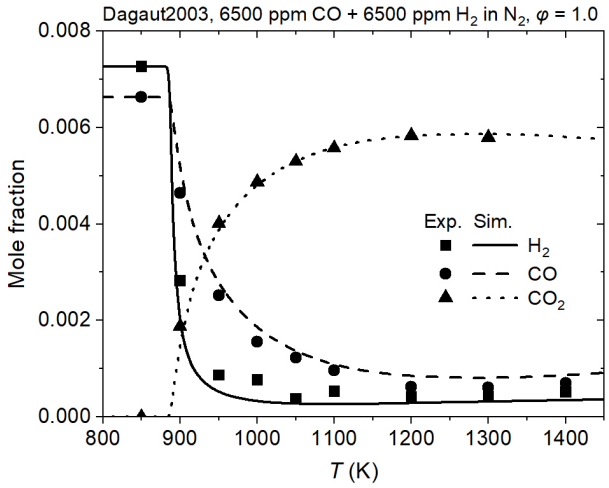

Fig. 4. Concentration profiles measured in the PFR (Dagaut et al. [48]) and simulated with the developed syngas oxidation model.

The 0-dimensional ideal stirred reactor model assumes that the reactor is sufficiently mixed to be described well by spatially averaged or bulk properties. An assumption that the mixing time scale is much smaller than either the residence time scale or the chemical time scale is made for a PSR model. The closed homogeneous model with constrained pressure and temperature is applied to the simulation of PSR. The concentration profiles of the mixtures at the end of reaction time (residence time) are compared with the measured data. A comparison of the measured and simulated concentration profiles in the PSR [48] is presented in Fig. 4.

2.6 Plug flow reactor

The PFR has mostly tube flow configuration to study continuous processes at a steady state. The reactions take place in a tubular reactor with electric resistance heating tapes [49].

The reactor temperature is monitored by thermocouples and the heating tape is controlled to achieve a nearly constant temperature condition in the reaction zone with a steep temperature increase at the inlet and a steep temperature drop at the reactor outlet. The product gas sample is extracted at the end of the reaction zone and analyzed for composition.

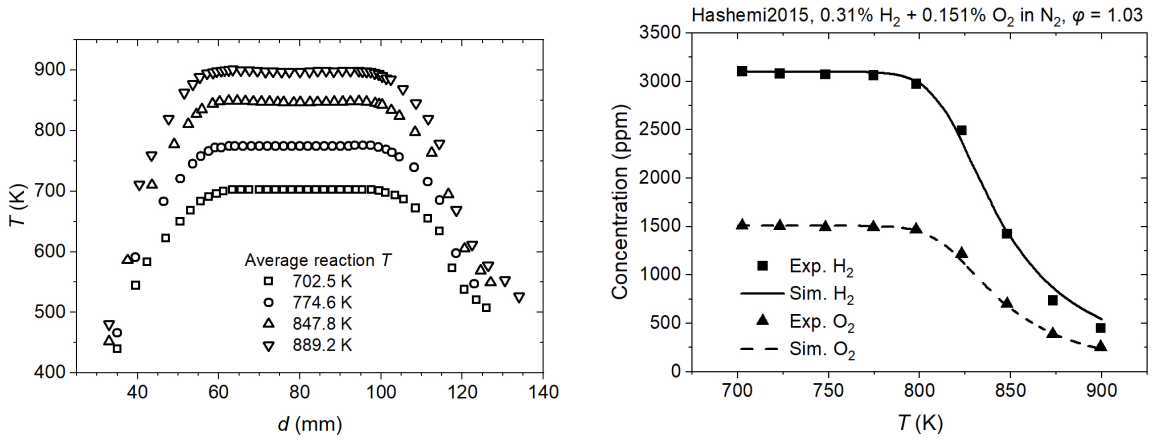

(a) **(b)**

Fig. 5. Comparison of the concentration profiles measured in the PFR [50] and the modeling results obtained with the optimized H_2 oxidation model in Paper-II.

The 1-dimensional model included transport phenomena is applied to the simulation of the PFR experiments with temperature profiles [50-52]. As shown in Fig. 5b, the concentration profiles simulated with the temperature profiles, in Fig. 5a, show good agreement with the measured data [50]. For the PFR experiments with residence time, the idealized 0-D model assumes that there is no mixing in the flow direction but perfect mixing in the transverse direction(s).

3. Uncertainty quantification

To study the input-output characteristics of reactive kinetic systems, uncertainty quantification should be conducted for both input (RRCs and experimental setup) and output (measured and simulated IDTs, LFSs, and concentration profiles) parameters. In this chapter, statistical analysis is applied to the RRCs recommended by the literature of direct experimental measurements, theoretical calculation, and review works. RRCs with uncertainty factors have been obtained for reactions of H_2 and $C_{<3}$ molecules. The modeling uncertainties and uncertainty contributions of the simulated output data are defined as corresponding to the uncertainties of the input RRCs. The experimental methods are analyzed and the uncertainty sources of the measured data are identified. The uncertainties of the collected experimental data for model optimization are carefully evaluated, which has been described in the previous work [26, 53].

3.1 Uncertainty quantification of the reaction rate constant

Arrhenius equation parameters for RRCs and their specific temperature ranges recommended by literature of experimental measurements, theoretical calculations, and the review works of Baulch et al. [21, 54-56] were collected for the uncertainty evaluation described below.

The standard deviations of the Arrhenius expression parameters, A, n, and E_a in Eq. (3), are calculated in the determining the margin, $\Delta(T)$, of the rate-coefficient error. The uncertainty factor, $f(T)$, is used to determine the uncertainty level for $k(T)$:

$$f(T) = \log_{10}\left(\frac{k_0(T)}{k_{\mathrm{low}}(T)}\right) = \log_{10}\left(\frac{k_{\mathrm{up}}(T)}{k_0(T)}\right) \tag{13}$$

where $k_0(T)$ is the nominal RRC, and $k_{\mathrm{low}}(T)$ and $k_{\mathrm{up}}(T)$ are the lower and upper bounds respectively.

The statistical treatment of the rate coefficients is complicated due to the limited amount of available data, but if several datasets are present the simple analysis of uncertainty k based on the least-squares regression can be done. Parameter errors, $s(x_\alpha)$, describe the confidence level of the rate coefficient parameters and can be further used for the calculation of:

$$k_{\mathrm{low}}(T) = 10^{\log_{10}(A)-s(\log_{10}(A))}T^{(\mathrm{n}-s(\mathrm{n}))}\exp\left(-\frac{E_\mathrm{a}+s(E_\mathrm{a})}{T}\right) \quad (14)$$

$$k_{\mathrm{up}}(T) = 10^{\log_{10}(A)+s(\log_{10}(A))}T^{(\mathrm{n}+s(\mathrm{n}))}\exp\left(-\frac{E_\mathrm{a}-s(E_\mathrm{a})}{T}\right) \quad (15)$$

where $s(\log_{10}(A))$, $s(\mathrm{n})$, and $s(E_\mathrm{a})$ can be found from the covariance matrix of the applied statistical method of nonlinear regression [57, 58].

Implementation of the nonlinear least-squares method was realized numerically using FUMILI [59], which linearizes a model $f(\vec{y},\vec{x})$ and approximates the data of *m* observations with a model of *n* unknown parameters (*m* > *n*). This algorithm [59, 60] has been successfully used for the estimation of intermolecular potential parameters and their uncertainties from experimental data of different types [58, 61].

The evaluation of parameters can be obtained through minimization of the objective function $\phi(\vec{y},\vec{x})$ (following the model linearization by a first-order Taylor series expansion of the parameters)

$$\phi(\vec{y},\vec{x}) = \sum_{j=1}^{m}\omega_j\left[Y_j^{\exp} - \left(f_0(\vec{y},\vec{x}^*) + \sum_{k=1}^{n}\frac{\partial f_j(\vec{y},\vec{x})}{\partial x_k}\Delta x_k\right)\right]^2 \quad (16)$$

where $\vec{y}$ is the vector of "coordinates", i.e., temperature, pressure, etc.; $\vec{x}$ is the vector of Arrhenius parameters *A, n,* and E_a; ω_j is the weight of an observation; $Y_j^{\exp}$ is the experimental data. The different sets of rate coefficients following experiments, quantum-chemical calculations or reaction models can be assumed as statistical samplings, i.e., $Y_j^{\exp}$.

The vector of the parameter corrections Δx_k is obtained from *n* differential equations (related to each parameter) following from minimization of the objective function:

$$\begin{cases}\sum_{j=1}^{m}\omega_j\left(Y_j^{\exp} - f_0(\vec{y},\vec{x}^*)\right)\frac{\partial f_j(\vec{y},\vec{x})}{\partial x_1} = \sum_{j=1}^{m}\omega_j\sum_{k=1}^{n}\frac{\partial f_j}{\partial x_k}\frac{\partial f_j}{\partial x_1}\Delta x_k \\ \cdots \\ \sum_{j=1}^{m}\omega_j\left(Y_j^{\exp} - f_0(\vec{y},\vec{x}^*)\right)\frac{\partial f_j(\vec{y},\vec{x})}{\partial x_n} = \sum_{j=1}^{m}\omega_j\sum_{k=1}^{n}\frac{\partial f_j}{\partial x_k}\frac{\partial f_j}{\partial x_n}\Delta x_k\end{cases} \quad (17)$$

Let us denote:

$$\gamma_{\alpha\beta} = \sum_{j=1}^{m}\omega_j\frac{\partial f_j}{\partial x_\alpha}\frac{\partial f_j}{\partial x_\beta},\ \alpha,\beta = 1,\ldots,n \quad (18)$$

$$\eta_\alpha = \sum_{j=1}^{m}\omega_j\left(Y_j^{\exp} - f_0(\vec{y},\vec{x}^*)\right)\frac{f_j(\vec{y},\vec{x})}{\partial x_\alpha} \quad (19)$$

then the vector Δx_k can be written as:

$$\Delta x_k = \sum_{i=1}^{n}(\gamma^{-1})_{ki}\eta_i \quad (20)$$

The error matrix (or the covariance matrix), $\Lambda = \gamma^{-1}$, provides information about parameter errors, $s(x_\alpha)$, and deviations of calculated functions (mean values of coefficients k_0), $\Delta f(\vec{y},\vec{x})$:

$$s(x_\alpha) = \sqrt{\frac{\phi}{m-n} D(x_\alpha)} \tag{21}$$

$$\Delta f = t_s \sqrt{\frac{\phi}{m-n} \sum_{\alpha=1}^{n} \sum_{\beta=1}^{n} \frac{\partial f}{\partial x_\alpha} \frac{\partial f}{\partial x_\beta} cov(x_\alpha, x_\beta)} \tag{22}$$

Here, ϕ is the final sum of the reduced squares of the deviations, $cov(x_\alpha, x_\beta)$ are the covariance elements of matrix Λ, $D(x_\alpha) = \Lambda(x_{\alpha\alpha})$, $\sqrt{\frac{\phi}{m-n}}$ provides an estimate for the reduced standard deviation of the observations and t_s is the coefficient of proportionality for $\Delta f / s(f)$ with a certain confidence probability.

The overall correlation coefficients provide further useful information, characterizing the connection (dependence) of one parameter with all others, and can be calculated from the matrix Λ as

$$Q_\alpha = \sqrt{1 - 1/R_\alpha} \tag{23}$$

where $R_\alpha = \Lambda(x_{aa}) \cdot \Lambda(x_{aa})^{-1}$.

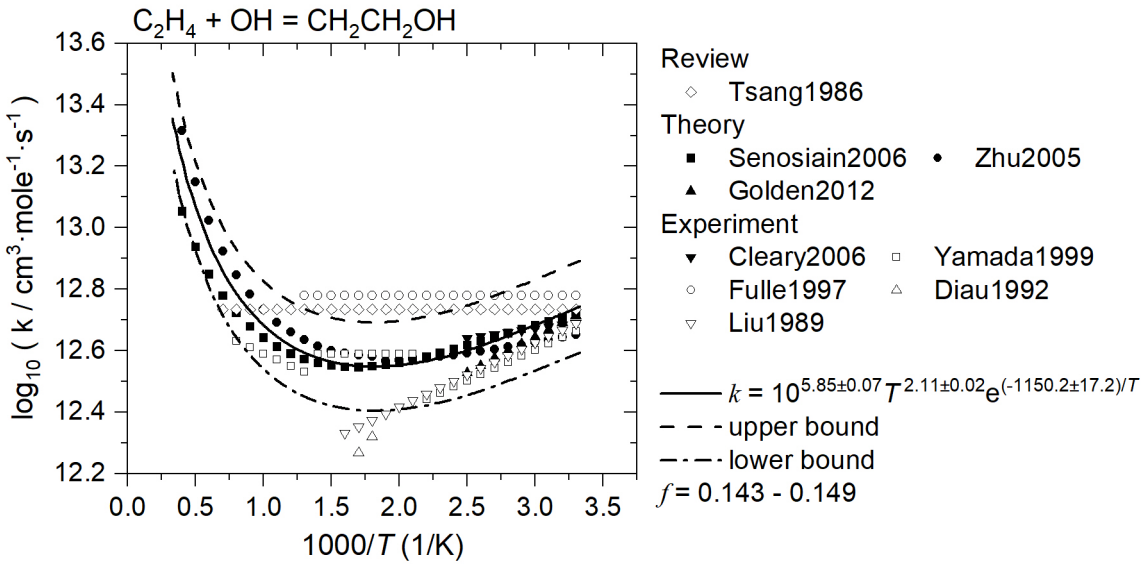

Fig. 6. Recommended RRCs for reaction C_2H_4 + OH = CH_2CH_2OH with evaluated uncertainty intervals (detailed Arrhenius equation parameters and reference information are presented in Supplementary-2 of Paper-I)

The uncertainty analysis of RRCs described above has been applied to the study of H_2, C_1, and C_2 reactions. An example of the collected RRCs recommended in the literature and the calculated uncertainty intervals are presented in Fig. 6. The detailed results are presented in Supplementary-2 of Paper-I, Supplementary-1 of Paper-II, and Supplementary-1 of Paper-III.

3.2 Uncertainty quantification of the chemical kinetic model

To evaluate the uncertainty of chemical kinetic models, the Arrhenius expression parameters are sampled within the determined uncertainty intervals (Eq. (14) and (15)) using the Latin Hypercube sampling method [62]. Monte Carlo simulation is carried out with the model based on the randomly sampled RRCs and a large number of modeling results can be obtained. The two-standard deviation (2σ) of the results, which covers > 90% of the distribution probability, is defined as the modeling uncertainty [63, 64]. Fig. 7a shows an example of uncertainty bounds (shadow) for the modeling IDTs from [31] and [65], which are determined by the Monte Carlo simulations, as shown in Fig. 7b.

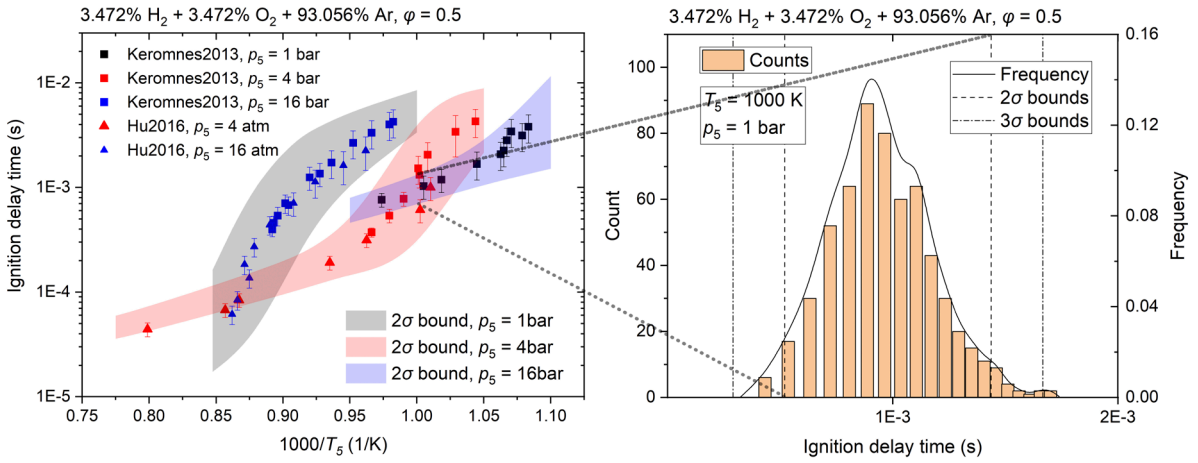

(a) **(b)**

Fig. 7. (a) IDTs of H_2/O_2/Ar mixture measured by Kéromnès et al. [31] and Hu et al. [65] and the modeling uncertainties determined by 2σ (shadows); (b) Histogram and probability density distribution of IDT (T_5 = 1000K) simulated with Monte Carlo method.

To figure out the source of the modeling uncertainty, the uncertainty contributed by the parameter x_i is defined as

$$C(x_i) = \left[y_{\max}^{\mathrm{mod}}(x_i) - y_{\min}^{\mathrm{mod}}(x_i)\right]\Big|_{x_j=\bar{x}_j, j\neq i} \tag{24}$$

where $y^{\mathrm{mod}}(x_i)$ is the modeling target and $\bar{x}_j$ is the average value of x_j, The relative uncertainty contribution of parameter x_i among the total N number of model parameters is defined as:

$$C_r(x_i) = \frac{C(x_i)}{\sum_{i=1}^{N} C(x_i)} \tag{25}$$

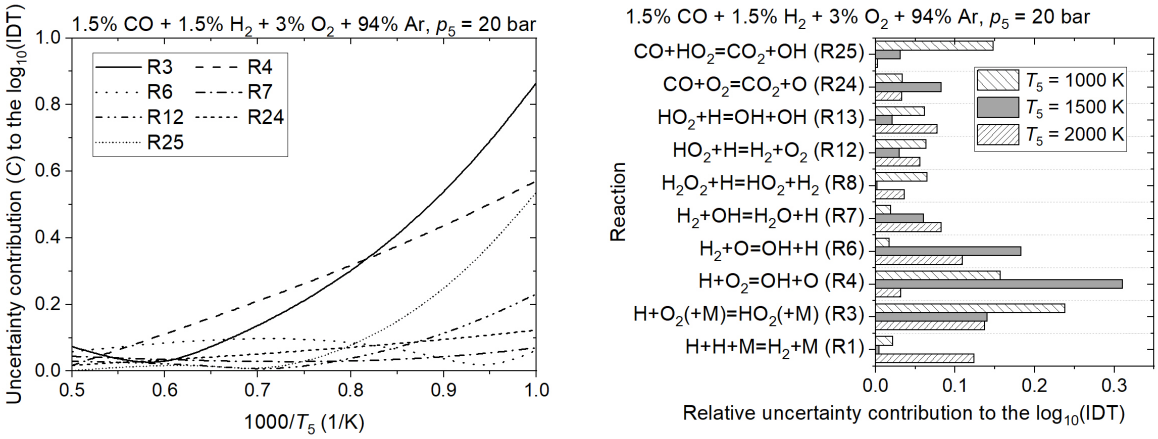

(a) **(b)**

Fig. 8. (a) Uncertainty contributions (*C*) and (b) relative uncertainty contributions (C_r) of different channels to the modeling IDTs of CO/H_2/O_2/Ar mixture at p_5 = 20 bar.

The uncertainty contribution, C, and the relative uncertainty contributions, C_r, to the simulated IDTs of CO/H_2/O_2/Ar mixture from Paper-III are presented in Fig. 8. The uncertainties contributed by reactions

$$H + O_2 + M = HO_2 + M \quad \text{(R3)}$$

$$H + O_2 = OH + O \quad \text{(R4)}$$

$$CO + HO_2 = CO_2 + OH \quad \text{(R25)}$$

show an obvious negative correlation with T_5, as shown in Fig. 8a. The channels related to O_2 and HO_2 gain dominance of the IDT uncertainties at low-temperature. The relative uncertainty contributions of the channels to the IDTs are presented in Fig. 8b, in which reactions (R3) and (R4) show the highest importance, followed by reactions (R1), (R6), (R8), (R24), and (R25). In Paper-II and Paper-III, the uncertainty contributions to the simulated results have been analyzed and the reactions with $C_r > 0.1$ are identified as the key reactions for optimization.

3.3 Uncertainty quantification of the experimental data

High-quality experimental data is critical for the optimization of chemical kinetic models. However, most researchers who work on experiments do not offer detailed uncertainty analysis for their experimental data. The uncertainty of the data set used for model validation should be carefully evaluated. In this thesis, the uncertainty sources of measured IDTs, concentration profiles, and laminar flame speeds were analyzed following the estimation given in [26, 53]. The uncertainties sourced from the experimental setup, operating conditions, measurement facilities, equipment, and nonideality during the test are analyzed and quantified.

3.3.1 Ignition delay times measured in shock tubes

In practical shock tubes, the unavoidable non-idealities exist in the shocked gases and the reaction rate coefficients obtained as a solution to the reverse kinetic problem during IDT simulations cannot be considered as a result of chemical processes only. An integrated impact of facility-dependent nonidealities, which influence the character of kinetic times, should be evaluated and accounted for in the experimental uncertainty. The evaluation of uncertainty sources and intervals for IDTs measured by shock tube experiments are listed in Table 1, which is described in detail in the work of [26]. With the developed evaluation method, an average uncertainty of 20% was obtained for the measured IDTs used in this thesis.

Table 1. Evaluation of uncertainty intervals for IDTs measured by shock tube experiments.

Source	Parameter	Uncertainty
Driven-section length (m)	> 8	+ 0%
	< 8	+ 5%
Driven-section internal diameter (cm)	> 10	+ 0%
	< 10	+ 5%
Temperature interval	T_5 < 1000 K	+ 5%
	T_5 > 1600 K	+ 5%
Pressure	p_5 > 15 atm	+ 5%
	p_5 > 30 atm	+ 5%
Dilution	< 90%	+ 5%
IDT (μs)	0 - 50	+ 5%
	50 - 500	+ 0%
	500 - 1000	+ 5%
	1000 - 1500	+ 10%

3.3.2 Laminar flame speeds

The source of the inaccuracy of laminar flame speed (LFS) data can be from the equipment, experimental procedures, and data processing. It is necessary to figure out different sources of uncertainty and establish a universal method to evaluate objectively uncertainties of measured data. In the related work [53], the four most commonly used methods including heat–flux method, Bunsen flame method, spherical flame method, and counterflow method were analyzed. The uncertainty sources shared by the different experimental methods are presented in Table 2, and the detailed analyses of the four studied methods can be found in [53].

Table 2. Evaluation of uncertainties for measured laminar flame speeds (Λ*: measuring error self-calibrated or specified by the manufacturer).

Source	Uncertainty
Specific material properties of the burner	+ 0.2%
Length of the heating tube	L > 2 m: + 0.2%
Mass flow controller	Λ*
Pressure sensor	Λ*
Thermocouple	Λ*
Composition of the air	+ 0.2%
Specific properties of the fuel	liquid: + 0.5%, gaseous: + 0.2%
Stoichiometry	φ < 0.8: + 0.5%, φ > 1.4: + 0.5%
Pressure	up to 1.5%, p > 4atm + 0.5%
Temperature	up to 2%
Radiation	+ 0.1%
Data interpretation	linear: + 0.5%

3.3.3 Concentration profiles measured in PFRs and PSRs

Table 3. Uncertainty sources for experiments of PSR and PFR (Λ*: measuring error self-calibrated or specified by the manufacturer).

Source	Uncertainty
Gas purity, mixture concentration	Up to ± 5.5% *
Specific properties of the reactants	liquid +0.5%; gaseous + 0.2%
Mass flow controller	Up to 10% *
Composition of the air	+ 0.2%
Stoichiometry	φ < 0.8 + 0.5%; φ > 1.4 + 0.5%
Reactor material	Λ*
Thermocouple	± 2 K to ± 5 K *
Radiation	+ 2%
Heat release	+ 2%
Temperature control	+ 2%
Residence time	average residence time: + 2%
Pressure sensor	Λ*
Sampling	+ 2%
Concentration measurements, analyzer	up to 20% *
Reproducibility	Λ*

PFRs and PSRs are used in chemical kinetics research by analyzing the products of oxidation and pyrolysis. As the chemically reacting flow involve transport phenomena in addition to kinetics and thermodynamics, rigorous reactor models are by necessity multidimensional, therefore the non-idealities in temperature, pressure, special concentration,

and heat release are existing in experiments of PFRs and PSRs. The uncertainties caused by the facilities and the non-ideal phenomena in the measurements performed in PSRs and PFRs are analyzed based on the studies of PFR [49, 51, 66-76] and PSR [43-45, 77-87]. The uncertainties resulting from reactant gases, temperature and pressure control systems, and measurement facilities are listed in Table 3.

4. Uncertainty minimization

In this project, three ways have been explored for the uncertainty minimization of chemical kinetic models. In Paper-I, the discrepancy measure between the experimental data and the modeling data was defined as the optimization target, and the traditional method based on human experience and intuition was applied to reduce the discrepancy measure. To reduce the human intervention in the optimization of chemical kinetic models, the probability density functions (PDFs) based on the Monte Carlo (MC) simulation were applied to reduce the discrepancy measure in Paper-II, however, only 4 reactions with the highest sensitivities are recognized for uncertainty reduction. In Paper-III, an uncertainty reduction method based on the particle swarm optimization (PSO) algorithm was developed. In this chapter, the discrepancy measure will be defined, and the methodologies of response surface, uncertainty reduction based on PDFs, and PSO algorithm will be described. A brief overview of the results of uncertainty minimization will be presented.

4.1 Discrepancy measure

To evaluate the predictive ability of the model, the model discrepancy measure, Ψ, is defined as:

$$\Psi = \frac{1}{M}\sum_{i=1}^{M}\frac{1}{N_i}\sum_{j=1}^{N_i}\Psi_{ij}^{\mathrm{mod}} \tag{26}$$

in which M is the number of the experimental data sets and N_i is the point number of the i_{th} data set. The Ψ_{ij}^{mod} for the j_{th} target in the i_{th} data set is defined as follows:

$$\Psi_{ij}^{\mathrm{mod}} = \left(\frac{y_{ij}^{\mathrm{mod}} - y_{ij}^{\mathrm{exp}}}{u\left(y_{ij}^{\mathrm{exp}}\right)}\right)^2 \tag{27}$$

where y_{ij}^{exp} is the experimentally measured data and y_{ij}^{mod} is the modeling result. The experimental uncertainty, $u\left(y_{ij}^{exp}\right)$, is adopted from references or evaluated based on the uncertainty analysis of experiments, which is described in Chapter 3.1.

4.2 Response surface methodology

The response surface methodology allows evaluation of the effects of multiple factors and their interactions on one or more response variables [88, 89]. It is widely used to learn system input-output response behavior. To determine the mapping of the multidimensional system of the model input-output responses, Monte Carlo simulations were conducted for the development of the response surface [27, 90]. The second-order polynomial regression was applied to express the predicted properties as a function of the model parameters. However, the magnitudes of the Arrhenius expression parameters show a huge difference, which may reduce the accuracy of the predictions, so that the Arrhenius expression parameters are normalized to space [0,1] as follow:

$$x_i = \frac{f_{\mathrm{l},i}+\log_{10}(A_i)-\log_{10}(A_{0,i})}{f_{\mathrm{l},i}+f_{\mathrm{u},i}},\ \log_{10}(A_i) \in \left[\log_{10}(A_{0,i}) - f_{\mathrm{l},i}\ ,\ \log_{10}(A_{0,i}) + f_{\mathrm{u},i}\right] \quad (28)$$

in which $\varepsilon_{0,i}$ is the fitted average value and $s(\varepsilon_i)$ is the standard deviation for the i_{th} parameter, which can be calculated following Chapter 3.1. In this way, the Arrhenius expression parameters, $\varepsilon(\varepsilon_1, \varepsilon_2, \ldots \varepsilon_n)$, sampled within the determined uncertainty intervals can be mapped to the normalized RRC parameters $\boldsymbol{X}$ ($x_1, x_2 \ldots x_n$). In contrast, the Arrhenius expression parameters can be determined by x_i as follow:

$$\log_{10}(A_i) = \log_{10}(A_{0,i}) - f_{\mathrm{l},i} + x_i(f_{\mathrm{l},i} + f_{\mathrm{u},i}),\ x_i \in [0,1] \quad (29)$$

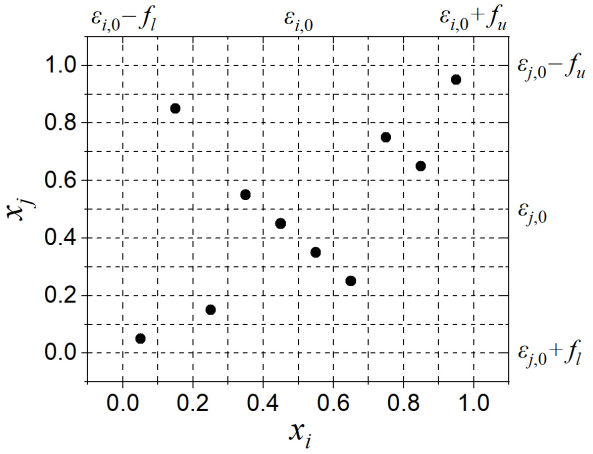

Fig. 9. Random numbers sampled with the Latin hypercube method and the determined Arrhenius expression parameters.

To cover as many parameter combinations as possible and reduce the amount of computation required for the polynomial regression, the normalized RRC parameters $\boldsymbol{X}$ were sampled within space [0,1] using the Latin Hypercube sampling method [48], and for each sample, a model with randomly determined Arrhenius expression parameters can be developed,

as shown in Fig. 9. With these developed chemical kinetic models, Monte Carlo simulation is conducted in Chemkin Pro [29] to obtain the direct simulation results, $y^{\mathrm{mod}}(\boldsymbol{X})$, based on which the second-order polynomial regression was carried out to express the response function, $y^{\mathrm{pre}}(\boldsymbol{X})$, throughout the total of N number of model parameters:

$$y^{\mathrm{mod}}(\boldsymbol{X}) \approx y^{\mathrm{pre}}(\boldsymbol{X}) = y_0 + \sum_{i=1}^{N} \alpha_i x_i + \sum_{i=1}^{N} \sum_{j=1}^{N} \beta_{ij} x_i x_j \tag{30}$$

in which the first- and second-order polynomial coefficients ($\boldsymbol{\alpha}$ and $\boldsymbol{\beta}$) were determined using the least square method realized in an in-house python numerical code [91]. By replacing y^{mod} in Eq. (27) with y^{pre}, the Ψ_{ij}^{mod} for the j_{th} target in the i_{th} data set can be estimated by

$$\Psi_{ij}^{\mathrm{mod}} = \left(\frac{y_{ij}^{\mathrm{mod}} - y_{ij}^{\mathrm{exp}}}{u\left(y_{ij}^{\mathrm{exp}}\right)} \right)^2 \approx \left(\frac{y_{ij}^{\mathrm{pre}} - y_{ij}^{\mathrm{exp}}}{u\left(y_{ij}^{\mathrm{exp}}\right)} \right)^2 \tag{31}$$

Substituting Eq. (29) and Eq. (30) into Eq. (31), the predictive ability of a model depended on $\boldsymbol{X}$ can be evaluated by $\Psi(\boldsymbol{X})$.

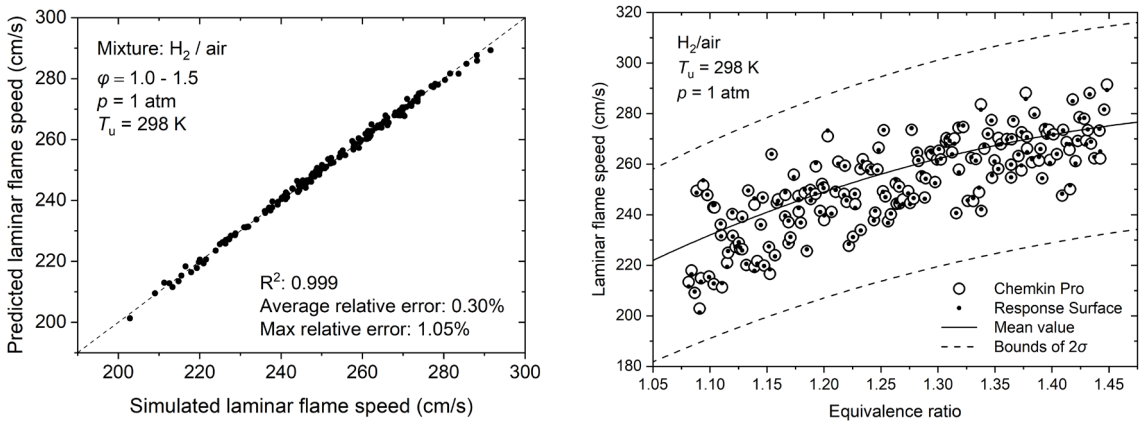

(a) **(b)**

Fig. 10. Results predicted by the response surface versus directly simulated with Chemkin Pro [29] for the laminar flame speeds of H_2/air mixtures.

To evaluate the predictive ability of the response surface, the coefficient of determination [92], R^2, was used. If $\overline{y^{\mathrm{pre}}}$ is the mean value of n number of predicted targets:

$$\overline{y^{\mathrm{pre}}} = \frac{1}{n} \sum_{i=1}^{n} y_i^{\mathrm{pre}} \tag{32}$$

The residual sum of squares is

$$SS_{\mathrm{res}} = \sum_{i}^{n} (y_i^{\mathrm{pre}} - y_i^{\mathrm{mod}})^2 = \sum_{i}^{n} e_i^2 \tag{33}$$

in which e_i is the residual. The total sum of squares is

$$SS_{\text{tot}} = \sum_i^n (y_i^{\text{pre}} - \overline{y^{\text{pre}}})^2 \tag{34}$$

Then the coefficient of determination is defined as

$$R^2 = 1 - \frac{SS_{\text{res}}}{SS_{\text{tot}}} \tag{35}$$

which is the proportion of the variation in the predicted values that is predictable from the modeling results.

Fig. 10 demonstrates the comparison of results predicted by the constructed response surface (y-axis) and the results directly simulated with Chemkin Pro [29] (x-axis). The relative error defined as:

$$\left| \frac{y_i^{\text{pre}} - y_i^{\text{exp}}}{y_i^{\text{exp}}} \right| \times 100\% \tag{36}$$

is also presented. In Paper-II and Paper-III, R^2 higher than 0.98 was obtained for the polynomial regression of IDTs measured by shock tubes and 0.99 for the other experimental data. The developed response surface can well predict the input-output properties of the chemical simulation.

4.3 RRC uncertainty reduction based on the PDF

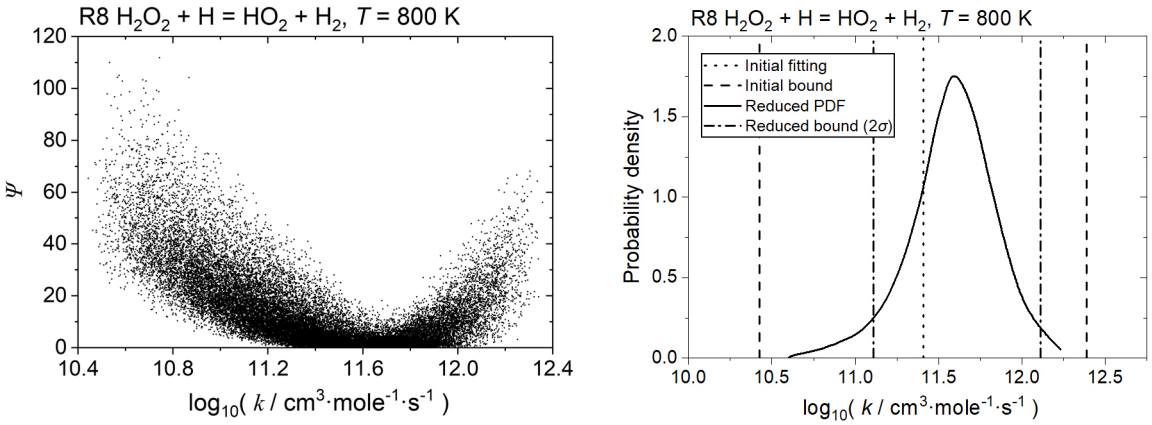

(a) **(b)**

Fig. 11. (a) The distribution of Ψ obtained from Monte Carlo simulation; (b) PDF of the RRC calculated based on Ψ.

Monte Carlo simulation is conducted to determine the probability density functions (PDFs) of the studied RRCs. In Paper-II, the Arrhenius expression parameters of the studied reactions were sampled within the uncertainty intervals. With the developed response function, the distribution of Ψ can be obtained, as shown in Fig. 11a. For the RRC of reaction (R8) H_2O_2 + H = HO_2 + H_2, the lowest discrepancies are concentrated around $\log_{10}(k_{R8}) = 11.7$. The initially

defined uniform uncertainty distributions of the studied RRCs are replaced by the PDFs calculated as follows:

$$P(a \le k \le b) = \frac{\sum_{j=1}^{m} W_j}{\sum_{i=1}^{n} W_i} \quad (a \le k_j \le b) \tag{37}$$

where $P(a \le k \le b)$ is the probability that the RRC, k, is located between a and b; n is the total number of the samples and m is the number of parameters sets in which $a \le k_j \le b$. The weight, W, is defined as the reciprocal of the discrepancy measure:

$$W = \frac{1}{\Psi} \tag{38}$$

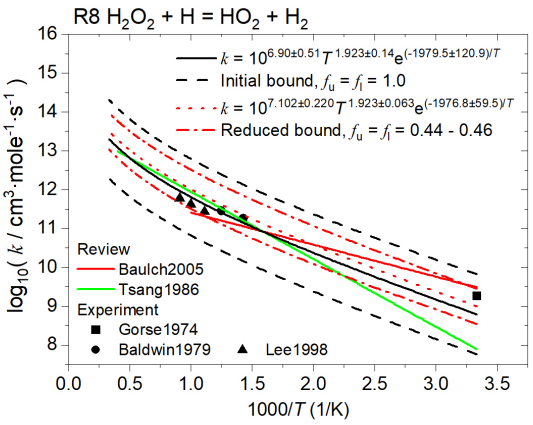

Fig. 12. Comparison of the initial and reduced uncertainty bounds for the RRC of reaction (R8) $H_2O_2 + H = HO_2 + H_2$.

As shown by the calculated PDF presented in Fig. 11b, the highest probability of the RRC locates around the value where Ψ is lower. The 2 times standard deviation (2σ) bounds, which cover >95% of the probability, are determined as the reduced uncertainty bounds. The initially determined and reduced uncertainty intervals for the RRC of reaction (R8) are presented in Fig. 12. The uncertainty factor was reduced from 1.0 to 0.44-0.46. In Paper-II, 4 most important reactions were recognized and the uncertainty intervals of these RRCs were reduced using the method described above.

4.4 RRC uncertainty reduction based on PSO

Particle swarm optimization (PSO) is an evolutionary computation technique developed by Kennedy and Eberhart [93]. The PSO algorithm was developed through simplified social model simulation such as bird flocking and fishing schooling [94]. The PSO algorithm has been proved to be a good tool for multidimensional and nonlinear search [95-97].

In Paper-III, In the PSO algorithm, particles with position $\boldsymbol{X}$ present the surrogates of the chemical kinetic model, $\boldsymbol{M(X)}$ based on $\boldsymbol{X}$, Eq. (28); the discrepancy measure $\Psi(\boldsymbol{X})$, Eq. (26) is defined as the fitness function. The set of particles is initialized as $p = \{p_i, i \in [1{:}N_p]\}$, where N_p is the size of the population (all possible surrogates). The particles can move in a 20-

dimensional (number of RRC parameters under consideration) search space. The current position of the particle p_i in the different iterations (t = 0, 1, 2 … t_{max}) is defined with a vector of its coordinates $\boldsymbol{X_{pi,t}}\left(x_{pi,1}^{t}, x_{pi,2}^{t}, \cdots, x_{pi,D}^{t}\right)$ and a vector of its velocity $\boldsymbol{V_{pi,t}}\left(v_{pi,1}^{t}, v_{pi,2}^{t}, \cdots, v_{pi,D}^{t}\right)$. The position of each particle will be tracked, which is associated with the lowest $\Psi(\boldsymbol{X})$ achieved up till for the particle with the personal best, $\boldsymbol{X^{per}}$. The global best, $\boldsymbol{X^{glo}}$, keeps track of the lowest $\Psi(\boldsymbol{X})$ obtained so far by all particles within the population. In canonical PSO on the t^{th} iteration, the particle p_i updates its velocity and position of the j^{th}-dimension in the $(t+1)^{th}$ iteration by tracking the personal best position ($\boldsymbol{X^{per}}$) and global best position ($\boldsymbol{X^{glo}}$) as follows [93]:

$$v_{pi,j}^{t+1} = wv_{pi,j}^{t} + c_1 r_{pi,1}\left(x_{pi,j}^{\text{per}} - x_{pi,j}^{t}\right) + c_2 r_{pi,2}\left(x_{j}^{\text{glo}} - x_{pi,j}^{t}\right) \tag{39}$$

$$x_{pi,j}^{t+1} = x_{pi,j}^{t} + v_{pi,j}^{t+1} \tag{40}$$

where $x_{pi,j}^{\text{per}}$ and x_{j}^{glo} are the j^{th} components of the personal best location and the global best location respectively; w is the inertia weight determining the "inertial" properties of particles. It reflects the impact of the particle's current velocity on the next iteration. $r_{pi,1}$ and $r_{pi,2}$ are the random numbers that are uniformly distributed between [0, 1] on each iteration. c_1 and c_2 are the acceleration coefficients: c_1 controls the tendency of the particle towards its personal best location, and c_2 adjusts the trend of the particle approaching the global best location. With Eq. (39) and Eq. (40), the particles can update their velocities in each iteration and converge towards the optimal position, as shown in Fig. 13a. To describe the neighbor relationship and interaction between particles, a global topology, Fig. 13b, is used [98, 99].

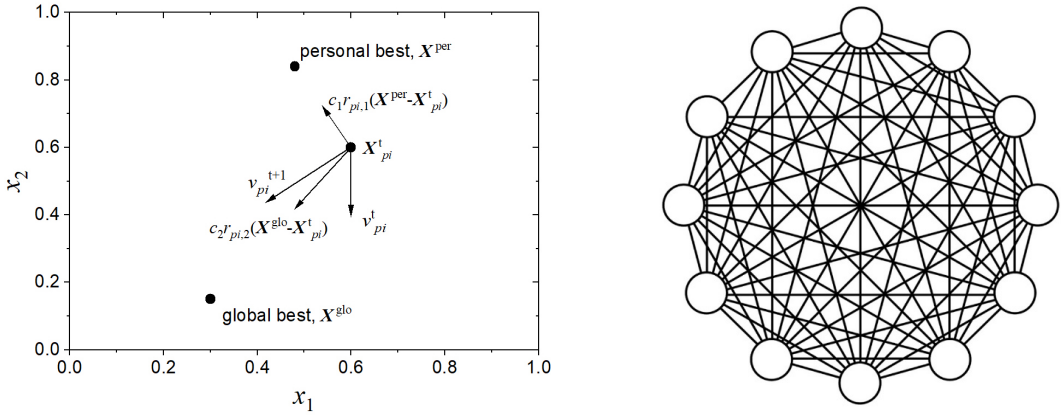

(a) **(b)**

Fig. 13. (a) Update of the particle velocity in the $(t+1)^{th}$ iteration; (b) global topology of the PSO, circles are particles, in our case surrogates $M(X)$.

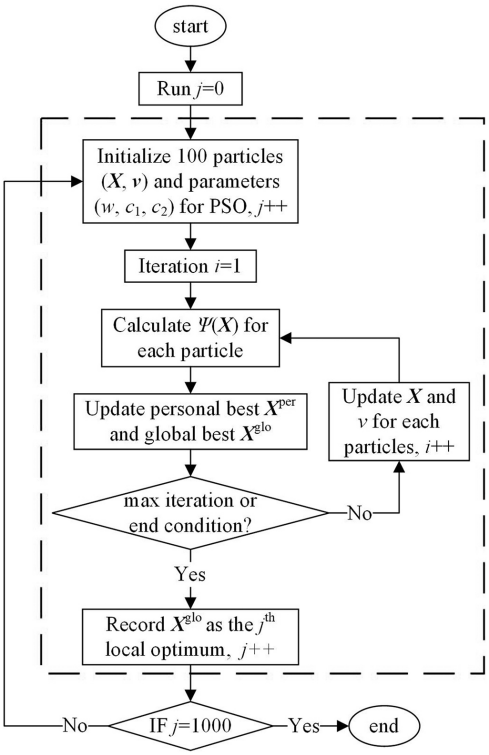

Fig. 14. Flow chart of the particle swarm optimization algorithm.

As shown by the flow chart of the PSO in Fig. 14 (in the dashed rectangle), in each iteration step, the position and velocity of each particle will be changed by moving towards the personal best and global best. As the computation progresses, particles aggregate or converge around the global best by exploring and exploiting known personal bests in the search space. With the finally obtained global best, $\boldsymbol{X}^{glo}$, the Arrhenius expression parameters of the optimized model can be determined by Eq. (29).

The PSO algorithm was applied to search an Arrhenius parameter set with the best predictive ability for the experimental targets in Paper-III. As shown by the 100 particles in the ternary graph of Fig. 15a, the positions of the parameters were initialized randomly within the search space and concentrated towards the location of the optimal solution as the iteration processes. The algorithm stops searching as the Ψ stabilizes after the 15th iteration, as shown by the history of the predicted Ψ in Fig. 15b. The RRCs of the optimized model are determined by substituting the position ($\boldsymbol{X}^{glo}$) of the particle with the lowest Ψ into Eq. (29).

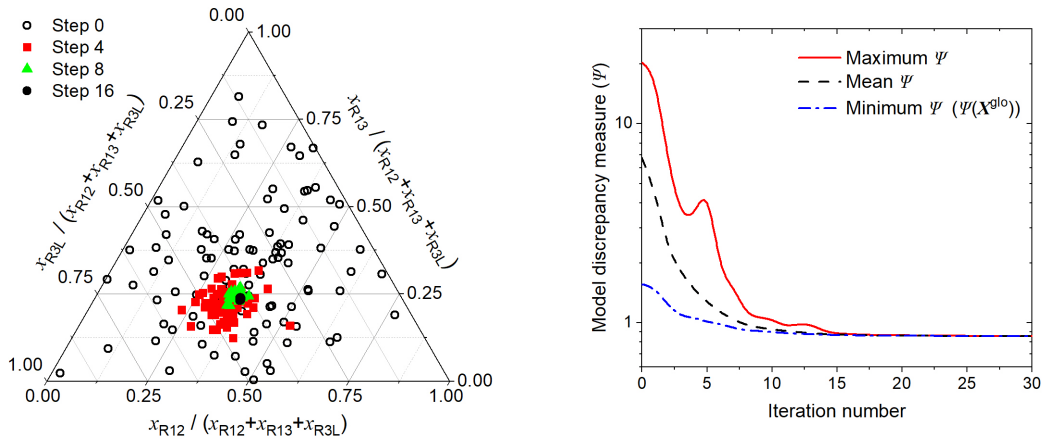

(a) **(b)**

Fig. 15. (a) The distributions of the particle swarm at different iteration steps; (b) The history of model discrepancy measure (Ψ).

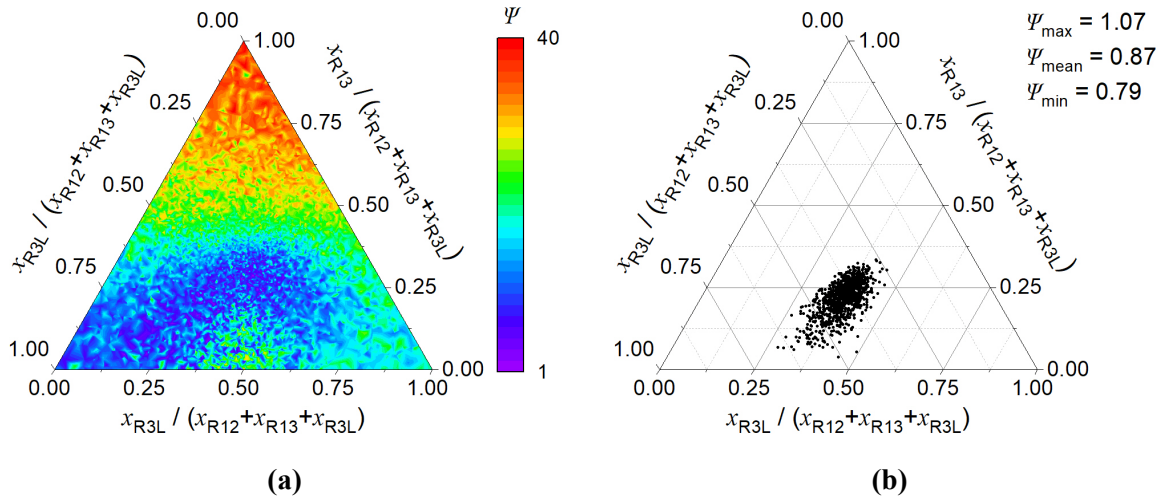

(a) **(b)**

Fig. 16. (a) Distribution of the discrepancy measure (Ψ) in the space of RRCs of reaction (R3L), (R12), and (R13); (b) distribution of the recorded 1000 local optimums.

The inherent randomness of PSO is realized with the initialization of input parameters for PSO which are randomly defined on each new run: random searching parameters $r_{pi,1}$ and $r_{pi,2}$, the acceleration coefficients c_1 and c_2, and randomly defined Arrhenius preexponents. Fig. 16a demonstrates the space of solutions, Ψ, for randomly modified rate coefficients of three reactions. The preferable parameters of the RRCs are located within the dark zone where the discrepancy measure has minimal values. Due to the randomness in the initialization of the particles in each repetition of the PSO run, and the particle velocity update in each PSO iteration (the j^{th} iteration in Fig. 14), the statistic representative array of the local optimums can be calculated, which are further used for the definition of the confidence region for the model parameters. It is performed through the main step of the framework shown in Fig. 14:

(1) Initialized the parameters and particles for the j^{th} run of PSO;

(2) Calculate $\boldsymbol{\Psi}(\boldsymbol{X})$ for each particle and update the personal best $\boldsymbol{X}^{per}$ and global best $\boldsymbol{X}^{glo}$ for the i^{th} iteration of PSO;

(3) Update the position ($\boldsymbol{X}$) and velocity ($\boldsymbol{v}$) for each particle and return to step (2) until i reaches the max iteration number or the $\Psi(\boldsymbol{X}^{glo})$ stabilizes after 10 iterations;

(4) Record the $\boldsymbol{X}^{glo}$ as the j^{th} local optimum and go to step (1) until j = 1000.

The PSO algorithm is repeated to select 1000 local optimums, which are scattered in an area where a lower Ψ has a high probability to be obtained, Fig. 16b. The standard deviations are calculated for each parameter based on the 1000 local optimums and the 2σ bounds are determined as the reduced uncertainty bounds for the studied parameters.

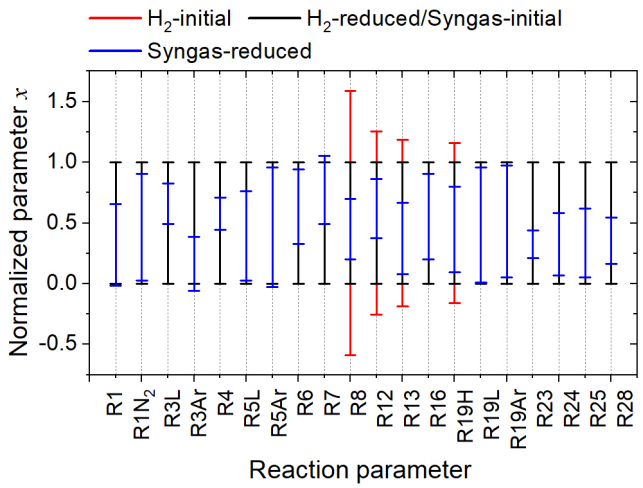

Fig. 17. The reduced uncertainties of the normalized RRC parameters *X*.

The reduced uncertainties of H_2 reactions obtained in Paper-II were used as the initial uncertainty bounds in Paper-III, as shown by the red uncertainty bars in Fig. 17, which were normalized to $X \in [0, 1]$. With the help of PSO algorithm, the possible reductions of the studied uncertainties were recognized automatically. All the modified RRCs were re-evaluated, as shown by the blue uncertainty bars in Fig. 17. Compared to the uncertainty reduction based on the PDF, the application of PSO algorithm reduced the reliance on human experience and intuition and increased the automation and self-monitoring of the chemical kinetic model optimization works.

4.5 Reduction of the modeling uncertainty

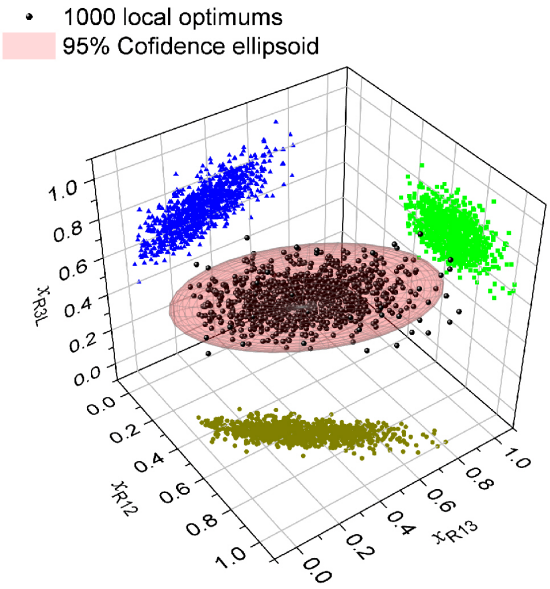

Fig. 18. The 95% confidence ellipsoid of the 1000 local optimums for x_{R3L}, x_{R12}, and x_{R13}.

The high-level correlation between RRCs and experimental parameters is organically accounted for in the PSO through the calculation of the particles' positions and velocities in the searching space, which is especially effective for optimization of the multichannel reactions. Let us take again reactions (R3L), (R12), and (R13):

$$H + O_2 + M = HO_2 + M \quad \text{(R3L)}$$

$$HO_2 + H = H_2 + O_2 \quad \text{(R12)}$$

$$HO_2 + H = OH + OH \quad \text{(R13)}$$

Fig. 18 presents the 95% confidence ellipsoid obtained for the calculated 1000 local optimums in coordinates of the three reactions. The projections of the particles on the

RRC axes are pointed with colored symbols. The projected symbols of the pair reactions (R12)-(R13) show an obvious correlation compared with that of pairs (R3L)-(R12) and (R3L)-(R13). The Pearson correlation coefficients (r) [100] are calculated for the RRCs based on the 1000 local optimums. x_{R12} and x_{R13} demonstrate a significant positive correlation, r = 0.91 (Fig. 19a), and define the branching ratio for these two branches of HO_2 + H reaction. The reaction (R3L) is weakly correlated with (R12), r = 0.25, points fill the full confidence region so that the RRC uncertainty bounds are approximately not affected with correlation, Fig. 19b.

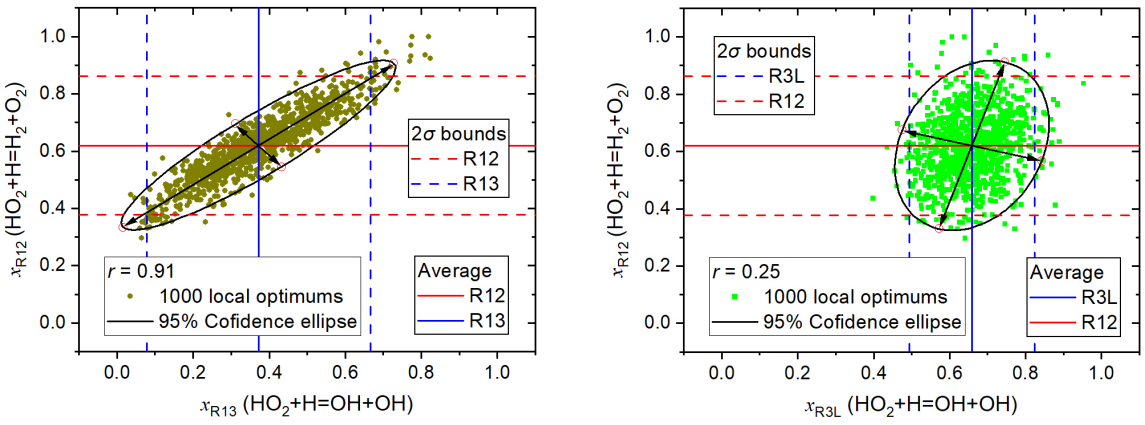

(a) **(b)**

Fig. 19. Distribution of the 1000 local optimums: **(a) reactions (R13)-(R12), r = 0.91; (b) reactions (R3L)-(R12), r = 0.25.**

In Paper-III, the high correlation coefficient reaction pairs ($|r| > 0.5$) are recognized. For these high-$|r|$ pairs, the confidence ellipses for the 1000 local optimums are calculated:

$$\begin{bmatrix} x_i - \bar{x}_i \\ x_j - \bar{x}_j \end{bmatrix}^{\mathrm{T}} \boldsymbol{cov}(x_i, x_j)^{-1} \begin{bmatrix} x_i - \bar{x}_i \\ x_j - \bar{x}_j \end{bmatrix} < S \tag{41}$$

where S defines the scale of the ellipse (95% confidence corresponds to S = 5.991) and $\boldsymbol{cov}(x_i, x_j)^{-1}$ is the inverse of the covariance matrix of x_i and x_j based on the 1000 local optimums:

$$\boldsymbol{cov}(x_i, x_j)^{-1} = \begin{bmatrix} cov(x_i, x_i) & cov(x_i, x_j) \\ cov(x_j, x_i) & cov(x_j, x_j) \end{bmatrix}^{-1} \tag{42}$$

The intersection of the 2σ bounds and the 95% confidence ellipse determines the final feasible parameter set. The sampling of x_i and x_j follows the rule of:

$$\begin{cases} \bar{x}_i - 2\sigma_i < x_i < \bar{x}_i + 2\sigma_i \\ \bar{x}_j - 2\sigma_j < x_j < \bar{x}_j + 2\sigma_j \\ \begin{bmatrix} x_i - \bar{x}_i \\ x_j - \bar{x}_j \end{bmatrix}^{\mathrm{T}} \boldsymbol{cov}(x_i, x_j)^{-1} \begin{bmatrix} x_i - \bar{x}_i \\ x_j - \bar{x}_j \end{bmatrix} < 5.991 \end{cases} \tag{43}$$

where σ_i and σ_j are the standard deviations based on the respective statistical analysis on parameter x_i and x_i, and the third line defines the 95% confidence ellipse shown in Fig. 19a.

By reducing the uncertainty intervals of RRCs, feasible parameter ranges are obtained. With the model parameters located within the feasible ranges, there are high probabilities to develop a model with good prediction ability. The modeling uncertainty defined in Section 3.3 is used to evaluate the prediction ability of the as-compiled model with the reduced uncertainty intervals.

In the work of Paper-II for the H_2 oxidation model, the RRCs of 10 reactions were modified and the RRC uncertainty intervals of 4 reactions were reduced due to their high initial uncertainties and key roles in the simulation of the available experimental data. The modeling uncertainties with the RRCs located within the reduced RRC uncertainty intervals are calculated and compared with the initial estimated values. As presented in Fig. 20a, compared with the initial modeling uncertainties of the concentration profiles in the PFR [50], the uncertainties based on the feasible parameter ranges are reduced by about 50%. As shown by the simulated IDTs in the RCMs [35, 36], the results of Monte Carlo simulation with RRCs sampled within the reduced uncertainty intervals show a clear tendency to converge to the experimental data.

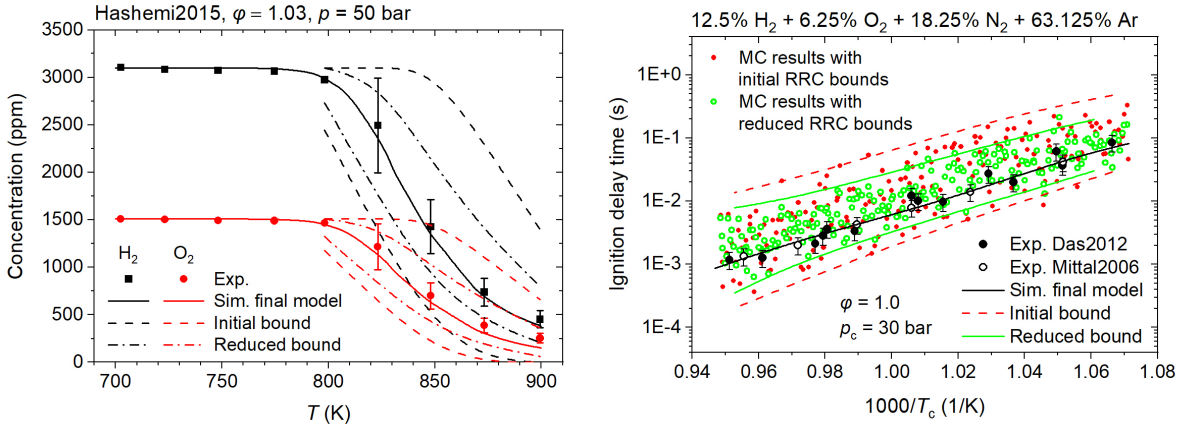

(a) **(b)**

Fig. 20. Initial and reduced modeling uncertainties of (a) concentration profiles measured in the PFR [50]; (b) ignition delay times measured in the RCMs [35, 36].

In the work of Paper-III for the H_2 and syngas oxidation model, the reduced RRC uncertainties of the H_2 reactions were inherited from Paper-II as the initial uncertainties, which guaranteed the model a good prediction ability for the H_2 oxidation data. With the more comprehensive study for syngas oxidation and the re-optimization of the H_2 sub-mechanism, the modeling uncertainties were further reduced. The RRCs were sampled within the initial and reduced uncertainty intervals respectively for the Monte Carlo simulation, and the comparison

of the modeling results is presented in Fig. 21. The uncertainty reduction improves the model accuracy and reduces its uncertainties for predicting the IDTs.

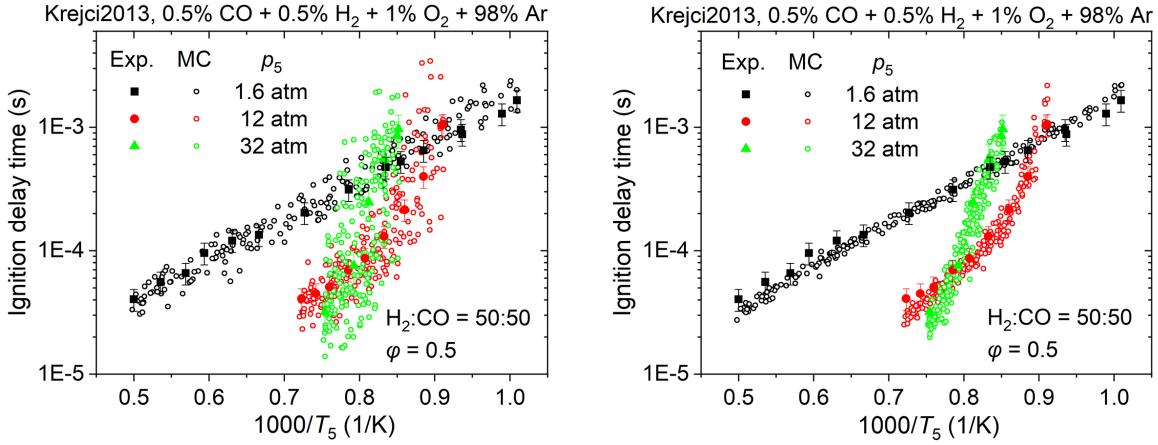

(a) **(b)**

Fig. 21. IDTs measured by Krejci et al. [101] and simulated with the Monte Carlo method: (a) with the initial uncertainty bounds; (b) with the reduced uncertainty bounds (small symbols).

5. Concluding remarks

5.1 Summary

The aims and achievements of this thesis were:

(1) To develop the database and method for the uncertainty quantification and data consistency analysis of the reaction rate constants (RRCs), experimental data for validation, and modeling results of hydrogen and small hydrocarbon oxidation. Thousands of references have been reviewed to collect the recommended RRCs and their validated temperature and pressure ranges. Uncertainty analysis has been conducted for the H_2, C_1 and C_2 reactions and uncertainty intervals have been determined for the Arrhenius expression parameters. Detailed results for the RRC uncertainties are presented in Supplementary-2 in Paper-I, Supplementary-1 in Paper-II, and Supplementary-1 in Paper-III. Uncertainty quantification methods have been developed and applied to the measured ignition delay times, laminar flame speeds, and concentration profiles. Hundreds of data sets from the experiments of shock tubes, rapid compression machines, premixed laminar flames, and flow reactors have been collected and validated.

(2) To combine the methodologies of response surface [27], Bound-to-Bound Data Collaboration [23, 102], and artificial intelligence algorithm for the uncertainty quantification and minimization of chemical kinetic models. A digital system that enables uncertainty analysis of RRCs, uncertainty quantification of combustion experimental data, Monte Carlo simulation, development of response surface, probability analysis, and particle swarm optimization has been successfully developed for the optimization of chemical kinetic models.

(3) To figure out the feasible parameter sets for RRCs of hydrogen and small hydrocarbons oxidation, and develop detailed chemical kinetic models for hydrogen and small hydrocarbons with good prediction ability for the currently available experimental data. The uncertainty intervals of RRCs were reduced for the H_2 and syngas oxidation model in Paper-II and paper-III. Feasible parameter sets were determined and the modeling uncertainties were reduced for the available experimental data. Three chemical kinetic models have been developed and optimized for the oxidation of H_2, syngas, and C_2H_4. The

obtained models show good prediction abilities for the ignition delay times, laminar flame speed, and concentration profiles. The detailed comparisons of the experimental data and the simulated data are presented in Supplementary-3 and 4 in Paper-I, Supplementary-3 in Paper-II, and Supplementary-2 in Paper-III.

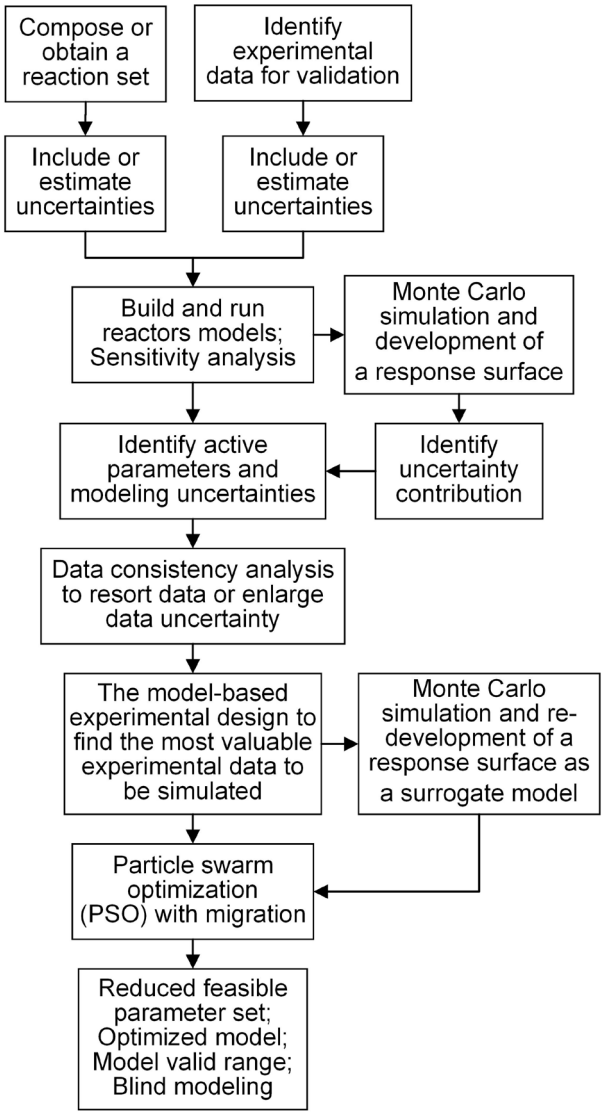

Fig. 22. Framework of the uncertainty quantification and minimization in this thesis.

The process diagram of this thesis is presented in Fig. 22. The work starts with a literature review for the collection of the existing theoretical and experimental data. The validated temperature and pressure ranges and the uncertainties are carefully included or estimated. Based on the initial data sets, reaction models are established and the Monte Carlo simulation is conducted for the development of the response surface. With the help of the response surface, uncertainty contributions are calculated for the studied reactions of the as-compiled model. The active parameters are identified for uncertainty reduction and model optimization. Data consistency analysis is carried out to ensure the reliability of the optimization targets, and the unreliable data are excluded from the optimization or given higher uncertainties. The response surface is developed to reveal the input-output property between the active model parameters and the modeling results for the optimization targets. The particle swarm optimization algorithm is applied to search the minimum discrepancy measure and the feasible parameter sets are determined. The modeling uncertainties of the model based on the parameters sampled within the feasible sets show a significant reduction, and the model with the lowest discrepancy measure is selected as the final optimized model.

5.2 Outlook

By applying the methodology in this thesis, a digital system has been developed for the uncertainty quantification and minimization of chemical kinetic models. Based on the optimized sub-models and feasible parameter sets for H_2 and syngas oxidation, the studies on the oxidation of C_1, C_2, and C_3 hydrocarbons will be conducted, after which the model of polycyclic aromatic hydrocarbon and soot formation will be optimized.

The application of uncertainty analysis and particle swarm optimization helped to diminish the weight of human experience and intuition in the research of chemical kinetic models. More artificial intelligence tools such as genetic algorithms and neural networks are expected to improve optimization efficiency and prediction accuracy.

References

[1] Crafts NF. The first industrial revolution: A guided tour for growth economists. The American Economic Review 1996:197-201.

[2] Mokyr J, Strotz RH. The second industrial revolution, 1870-1914. Storia dell'economia Mondiale 1998;21945(1).

[3] Westbrook CK, Mizobuchi Y, Poinsot TJ, Smith PJ, Warnatz J. Computational combustion. Proceedings of the Combustion Institute 2005;30(1):125-57.

[4] Hirschfelder J, Curtiss C, Campbell DE. The theory of flame propagation. IV. The Journal of Physical Chemistry 1953;57(4):403-14.

[5] Simmie JM. Detailed chemical kinetic models for the combustion of hydrocarbon fuels. Progress in energy and combustion science 2003;29(6):599-634.

[6] Lasi H, Fettke P, Kemper H-G, Feld T, Hoffmann M. Industry 4.0. Business & information systems engineering 2014;6(4):239-42.

[7] Philbeck T, Davis N. The fourth industrial revolution. Journal of International Affairs 2018;72(1):17-22.

[8] Lee M, Yun JJ, Pyka A, Won D, Kodama F, Schiuma G, et al. How to respond to the fourth industrial revolution, or the second information technology revolution? Dynamic new combinations between technology, market, and society through open innovation. Journal of Open Innovation: Technology, Market, and Complexity 2018;4(3):21.

[9] Domon B, Aebersold R. Mass spectrometry and protein analysis. Science 2006;312(5771):212-7.

[10] Hanson RK, Davidson DF. Recent advances in laser absorption and shock tube methods for studies of combustion chemistry. Progress in Energy and Combustion Science 2014;44:103-14.

[11] Truhlar DG, Garrett BC, Klippenstein SJ. Current status of transition-state theory. The Journal of physical chemistry 1996;100(31):12771-800.

[12] Pollak E, Talkner P. Reaction rate theory: What it was, where is it today, and where is it going? Chaos: An Interdisciplinary Journal of Nonlinear Science 2005;15(2):026116.

[13] Morin J, Bedjanian Y, Romanias MN. Rate Constants of the Reactions of O (3P) Atoms with Ethene and Propene over the Temperature Range 230–900 K. International Journal of Chemical Kinetics 2017;49(1):53-60.

[14] Goulay F, Osborn DL, Taatjes CA, Zou P, Meloni G, Leone SR. Direct detection of polyynes formation from the reaction of ethynyl radical (C2H) with propyne (CH3-C[triple bond]CH) and allene (CH2=C=CH2). Physical Chemistry Chemical Physics 2007;9(31):4291-300.

[15] Peukert SL, Labbe NJ, Sivaramakrishnan R, Michael JV. Direct measurements of rate constants for the reactions of CH3 radicals with C2H6, C2H4, and C2H2 at high temperatures. The Journal of Physical Chemistry A 2013;117(40):10228-38.

[16] Vasu SS, Hong Z, Davidson DF, Hanson RK, Golden DM. Shock tube/laser absorption measurements of the reaction rates of OH with ethylene and propene. The Journal of Physical Chemistry A 2010;114(43):11529-37.

[17] Meana-Pañeda R, Truhlar DG, Fernández-Ramos A. High-level direct-dynamics variational transition state theory calculations including multidimensional tunneling of the thermal rate constants, branching ratios, and

kinetic isotope effects of the hydrogen abstraction reactions from methanol by atomic hydrogen. The Journal of Chemical Physics 2011;134(9):094302.

[18] Shan X, Clary DC. Application of one-dimensional semiclassical transition state theory to the CH3OH + H ⇌ CH2OH/CH3O + H2 reactions. Philosophical Transactions of the Royal Society A: Mathematical, Physical and Engineering Sciences 2018;376(2115):20170147.

[19] Klippenstein SJ, Georgievskii Y, Harding LB. Predictive theory for the combination kinetics of two alkyl radicals. Physical Chemistry Chemical Physics 2006;8(10):1133-47.

[20] Xu K, Xu Z, Lin M-C. Ab initio kinetic prediction of branching rate constants for reactions of H atoms with CH3O and CH2OH. Molecular Physics 2007;105(19-22):2763-76.

[21] Baulch DL, Bowman CT, Cobos CJ, Cox RA, Just T, Kerr JA, et al. Evaluated Kinetic Data for Combustion Modeling: Supplement II. Journal of Physical and Chemical Reference Data 2005;34(3):757-1397.

[22] Wang H, Sheen DA. Combustion kinetic model uncertainty quantification, propagation and minimization. Progress in Energy and Combustion Science 2015;47:1-31.

[23] Iavarone S, Oreluk J, Smith ST, Hegde A, Li W, Packard A, et al. Application of Bound-to-Bound Data Collaboration approach for development and uncertainty quantification of a reduced char combustion model. Fuel 2018;232:769-79.

[24] Frenklach M, Packard A, Garcia-Donato G, Paulo R, Sacks J. Comparison of statistical and deterministic frameworks of uncertainty quantification. SIAM/ASA Journal on Uncertainty Quantification 2016;4(1):875-901.

[25] Frenklach M, Wang H, Rabinowitz MJ. Optimization and analysis of large chemical kinetic mechanisms using the solution mapping method—combustion of methane. Progress in Energy and Combustion Science 1992;18(1):47-73.

[26] Slavinskaya N, Abbasi M, Starcke JH, Whitside R, Mirzayeva A, Riedel U, et al. Development of an uncertainty quantification predictive chemical reaction model for syngas combustion. Energy & Fuels 2017;31(3):2274-97.

[27] Khuri AI, Mukhopadhyay S. Response surface methodology. Wiley Interdisciplinary Reviews: Computational Statistics 2010;2(2):128-49.

[28] Gilbert R, Luther K, Troe J. Theory of thermal unimolecular reactions in the fall-off range. II. Weak collision rate constants. Berichte der Bunsengesellschaft für physikalische Chemie 1983;87(2):169-77.

[29] DESIGNS ME. Chemkin-pro. 2011.

[30] Petersen EL, Kalitan DM, Rickard MJ. Reflected Shock Ignition of SiH4/H2/O2/Ar andSiH4/CH4/O2/Ar Mixtures. Journal of Propulsion and Power 2004;20(4):665-74.

[31] Kéromnès A, Metcalfe WK, Heufer KA, Donohoe N, Das AK, Sung C-J, et al. An experimental and detailed chemical kinetic modeling study of hydrogen and syngas mixture oxidation at elevated pressures. Combustion and Flame 2013;160(6):995-1011.

[32] Pang G, Davidson D, Hanson R. Experimental study and modeling of shock tube ignition delay times for hydrogen–oxygen–argon mixtures at low temperatures. Proceedings of the Combustion Institute 2009;32(1):181-8.

[33] Aul CJ, Metcalfe WK, Burke SM, Curran HJ, Petersen EL. Ignition and kinetic modeling of methane and ethane fuel blends with oxygen: A design of experiments approach. Combustion and Flame 2013;160(7):1153-67.

[34] Pan L, Hu E, Zhang J, Zhang Z, Huang Z. Experimental and kinetic study on ignition delay times of DME/H2/O2/Ar mixtures. Combustion and Flame 2014;161(3):735-47.

[35] Mittal G, Sung CJ, Yetter RA. Autoignition of H2/CO at elevated pressures in a rapid compression machine.

International Journal of Chemical Kinetics 2006;38(8):516-29.

[36] Das AK, Sung C-J, Zhang Y, Mittal G. Ignition delay study of moist hydrogen/oxidizer mixtures using a rapid compression machine. International Journal of Hydrogen Energy 2012;37(8):6901-11.

[37] Sung C-J, Curran HJ. Using rapid compression machines for chemical kinetics studies. Progress in Energy and Combustion Science 2014;44:1-18.

[38] Dowdy DR, Smith DB, Taylor SC, Williams A. The use of expanding spherical flames to determine burning velocities and stretch effects in hydrogen/air mixtures. *Symposium (International) on Combustion.* 23. Elsevier; 1991:325-32.

[39] Babkin V, Kononenko YG. Equations for determining normal flame velocity in a constant-volume spherical bomb. Combustion, Explosion, and Shock Waves 1967;3(2):168-71.

[40] Chao B, Egolfopoulos F, Law CK. Structure and propagation of premixed flame in nozzle-generated counterflow. Combustion and flame 1997;109(4):620-38.

[41] Konnov AA, Riemeijer R, Kornilov V, de Goey L. 2D effects in laminar premixed flames stabilized on a flat flame burner. Experimental Thermal and Fluid Science 2013;47:213-23.

[42] Vandooren J, Bian J. Validation of H2/O2 reaction mechanisms by comparison with the experimental structure of a rich hydrogen-oxygen flame. *Symposium (International) on Combustion.* 23. Elsevier; 1990:341-6.

[43] Dagaut P, Cathonnet M, Rouan J, Foulatier R, Quilgars A, Boettner J, et al. A jet-stirred reactor for kinetic studies of homogeneous gas-phase reactions at pressures up to ten atmospheres ($\approx$ 1 MPa). Journal of Physics E: Scientific Instruments 1986;19(3):207.

[44] Dagaut P, Cathonnet M, Boettner J-c. Kinetics of ethane oxidation. International Journal of Chemical Kinetics 1991;23(5):437-55.

[45] Dagaut P, Dayma G, Nicolle A. Experimental and detailed chemical kinetic modeling study of the oxidation of hydrogen-enriched natural gas blends. *European Combustion Meeting (ECM 2005), Louvain-la-Neuve, Belgium, April.* 2005:3-6.

[46] Le Cong T, Dagaut P. Experimental and detailed modeling study of the effect of water vapor on the kinetics of combustion of hydrogen and natural gas, impact on NO x. Energy & Fuels 2009;23(2):725-34.

[47] Dagaut P, Boettner J, Cathonnet M. Kinetic modeling of ethanol pyrolysis and combustion. Journal de chimie physique 1992;89:867-84.

[48] Dagaut P, Lecomte F, Mieritz J, Glarborg P. Experimental and kinetic modeling study of the effect of NO and SO2 on the oxidation of CO-H2 mixtures. International journal of chemical kinetics 2003;35(11):564-75.

[49] Sen F, Shu B, Kasper T, Herzler J, Welz O, Fikri M, et al. Shock-tube and plug-flow reactor study of the oxidation of fuel-rich CH4/O2 mixtures enhanced with additives. Combustion and Flame 2016;169:307-20.

[50] Hashemi H, Christensen JM, Gersen S, Glarborg P. Hydrogen oxidation at high pressure and intermediate temperatures: Experiments and kinetic modeling. Proceedings of the Combustion Institute 2015;35(1):553-60.

[51] Hashemi H, Jacobsen JG, Rasmussen CT, Christensen JM, Glarborg P, Gersen S, et al. High-pressure oxidation of ethane. Combustion and Flame 2017;182:150-66.

[52] Hashemi H, Christensen JM, Glarborg P. High-pressure pyrolysis and oxidation of ethanol. Fuel 2018;218:247-57.

[53] Walter G, Wang H, Kanz A, Kolbasseff A, Xu X, Haidn O, et al. Experimental error assessment of laminar flame speed measurements for digital chemical kinetics databases. Fuel 2020;266.

[54] Baulch D, Cobos C, Cox R, Esser C, Frank P, Just T, et al. Evaluated kinetic data for combustion modelling. Journal of Physical and Chemical Reference Data 1992;21(3):411-734.

[55] Atkinson R, Baulch D, Cox R, Hampson Jr R, Kerr J, Rossi M, et al. Evaluated kinetic, photochemical and heterogeneous data for atmospheric chemistry: Supplement V. IUPAC Subcommittee on Gas Kinetic Data Evaluation for Atmospheric Chemistry. Journal of Physical and Chemical Reference Data 1997;26(3):521-1011.

[56] Tsang W, Hampson R. Chemical kinetic data base for combustion chemistry. Part I. Methane and related compounds. Journal of physical and chemical reference data 1986;15(3):1087-279.

[57] Wang H, Slavinskaya N, Kanz A, Auyelkhankyzy M, Gao Y, Haidn O. A comprehensive kinetic modeling study of ethylene combustion with data uncertainty analysis. Fuel 2021;299:120833.

[58] Slavinskaya N, Mirzayeva A, Whitside R, Starke J, Abbasi M, Auyelkhankyzy M, et al. A modelling study of acetylene oxidation and pyrolysis. Combustion and Flame 2019;210:25-42.

[59] Kurbatov V, Silin I. New method for minimizing regular functions with constraints on parameter region. Nuclear Instruments and Methods in Physics Research Section A 1994;345(2):346-50.

[60] Sokolov S, Silin I. Preprint JINR D-810. Dubna 1961.

[61] Fokin LR, Slavinskaya N. Thermophysical parameter correlation for low-density gas mixtures: Ar-Xe. Institute for High Temperatures, USSR Academy of Sciences 1987;25(1):40-5.

[62] Stein M. Large sample properties of simulations using Latin hypercube sampling. Technometrics 1987;29(2):143-51.

[63] Sheen DA, You X, Wang H, Løvås T. Spectral uncertainty quantification, propagation and optimization of a detailed kinetic model for ethylene combustion. Proceedings of the Combustion Institute 2009;32(1):535-42.

[64] Prager J, Najm HN, Sargsyan K, Safta C, Pitz WJ. Uncertainty quantification of reaction mechanisms accounting for correlations introduced by rate rules and fitted Arrhenius parameters. Combustion and Flame 2013;160(9):1583-93.

[65] Hu E, Pan L, Gao Z, Lu X, Meng X, Huang Z. Shock tube study on ignition delay of hydrogen and evaluation of various kinetic models. International Journal of Hydrogen Energy 2016;41(30):13261-80.

[66] Manzello SL, Lenhert DB, Stroud CB, Tsang W. The effects of aromatic species on soot particle size distribution and species concentration in a well stirred reactor/plug flow reactor. Fuel 2007;2(2):N2.

[67] Rasmussen CL, Jakobsen JG, Glarborg P. Experimental measurements and kinetic modeling of CH4/O2and CH4/C2H6/O2 conversion at high pressure. International Journal of Chemical Kinetics 2008;40(12):778-807.

[68] Rasmussen CL, Hansen J, Marshall P, Glarborg P. Experimental measurements and kinetic modeling of CO/H2/O2/NOx conversion at high pressure. International Journal of Chemical Kinetics 2008;40(8):454-80.

[69] Lopez JG, Rasmussen CL, Alzueta MU, Gao Y, Marshall P, Glarborg P. Experimental and kinetic modeling study of C2H4 oxidation at high pressure. Proceedings of the Combustion Institute 2009;32(1):367-75.

[70] Gimenez-Lopez J, Rasmussen CT, Hashemi H, Alzueta MU, Gao Y, Marshall P, et al. Experimental and Kinetic Modeling Study of C2H2Oxidation at High Pressure. International Journal of Chemical Kinetics 2016;48(11):724-38.

[71] Djokic M, Carstensen H-H, Van Geem KM, Marin GB. The thermal decomposition of 2, 5-dimethylfuran. Proceedings of the Combustion Institute 2013;34(1):251-8.

[72] Harper MR, Van Geem KM, Pyl SP, Marin GB, Green WH. Comprehensive reaction mechanism for n-butanol pyrolysis and combustion. Combustion and Flame 2011;158(1):16-41.

[73] Stachler RD, Heyne JS, Stouffer S, Miller JD, Roquemore M. Investigation of combustion emissions from conventional and alternative aviation fuels in a well-stirred reactor. *55th AIAA Aerospace Sciences Meeting.* 2017:0382.

[74] Sen F, Kasper T, Bergmann U, Hegner R, Atakan B. Partial oxidation of methane at elevated pressures and

effects of propene and ethane as additive: experiment and simulation. Zeitschrift für Physikalische Chemie 2015;229(6):955-76.

[75] Arutyunov V, Rudakov V, Savchenko V, Sheverdenkin E, Sheverdenkina O, Zheltyakov AY. Partial alkane oxidation kinetics at high pressures: methane oxidation in stainless steel and quartz reactors. Theoretical Foundations of Chemical Engineering 2002;36(5):472-6.

[76] Gil I, Mocek P. CFD analysis of mixing intensity in jet stirred reactors. Chemical and Process Engineering 2012;33(3):397-410.

[77] Maurice L, Blust J, Leung K, Lindstedt R. Emissions from combustion of hydrocarbons in a well-stirred reactor. *37th Aerospace Sciences Meeting and Exhibit.* 1999:1038.

[78] Zabarnick S, Zelina J. Chemical kinetics of NOx production in a well stirred reactor. *Intersociety Energy Conversion Engineering Conference.* 1994:3828.

[79] Blust J, Getz M, Zabarnick S, Blust J, Getz M, Zabarnick S. Probe design optimization for the well stirred reactor. *35th Aerospace Sciences Meeting and Exhibit.* 1997:907.

[80] Blust J, Ballal D, Sturgess G. Fuel effects on lean blowout and emissions from a well-stirred reactor. Journal of Propulsion and Power 1999;15(2):216-23.

[81] Ayass WW, Nasir EF, Farooq A, Sarathy SM. Mixing-structure relationship in jet-stirred reactors. Chemical Engineering Research and Design 2016;111:461-4.

[82] Bensabath T, Monnier H, Glaude P-A. Detailed kinetic modeling of the formation of toxic polycyclic aromatic hydrocarbons (PAHs) coming from pyrolysis in low-pressure gas carburizing conditions. Journal of Analytical and Applied Pyrolysis 2016;122:342-54.

[83] Reich R, Frayne C, Zelina J, Mayfield H, Stouffer S, Katta V. Particulate matter and polycyclic aromatic hydrocarbon determination using a well-stirred reactor. *41st Aerospace Sciences Meeting and Exhibit.* 2003:664.

[84] Norinaga K, Deutschmann O, Hüttinger KJ. Analysis of gas phase compounds in chemical vapor deposition of carbon from light hydrocarbons. Carbon 2006;44(9):1790-800.

[85] Wagnon SW, Thion S, Nilsson EJ, Mehl M, Serinyel Z, Zhang K, et al. Experimental and modeling studies of a biofuel surrogate compound: laminar burning velocities and jet-stirred reactor measurements of anisole. Combustion and Flame 2018;189:325-36.

[86] Vermeire FH, Carstensen H-H, Herbinet O, Battin-Leclerc F, Marin GB, Van Geem KM. The thermal decomposition of furfural: molecular chemistry unraveled. Proceedings of the Combustion Institute 2019;37(1):445-52.

[87] Marinov NM, Malte PC. Ethylene oxidation in a well-stirred reactor. International Journal of Chemical Kinetics 1995;27(10):957-86.

[88] Li G, Rosenthal C, Rabitz H. High dimensional model representations. The Journal of Physical Chemistry A 2001;105(33):7765-77.

[89] Tomlin AS. The use of global uncertainty methods for the evaluation of combustion mechanisms. Reliability Engineering & System Safety 2006;91(10-11):1219-31.

[90] Wang H. Uncertainty quantification and minimization. Computer Aided Chemical Engineering. Elsevier; 2019, p. 723-62.

[91] Shi C. Development of a Program for the Optimization of Chemical Kinetic Mechanism. *Department of Mechanical Engineering.* Master Semester Thesis. Munich: Technical University of Munich; 2021.

[92] Nagelkerke NJ. A note on a general definition of the coefficient of determination. Biometrika 1991;78(3):691-2.

[93] Kennedy J, Eberhart R. Particle swarm optimization. *Proceedings of ICNN'95-international conference on neural networks.* 4. IEEE; 1995:1942-8.

[94] Shi Y. Particle swarm optimization. IEEE connections 2004;2(1):8-13.

[95] Schwaab M, Biscaia Jr EC, Monteiro JL, Pinto JC. Nonlinear parameter estimation through particle swarm optimization. Chemical Engineering Science 2008;63(6):1542-52.

[96] Hu X, Eberhart R. Solving constrained nonlinear optimization problems with particle swarm optimization. *Proceedings of the sixth world multiconference on systemics, cybernetics and informatics.* 5. Citeseer; 2002:203-6.

[97] Wang X, Xiao J. PSO-based model predictive control for nonlinear processes. *International Conference on Natural Computation.* Springer; 2005:196-203.

[98] Blackwell T, Kennedy J. Impact of communication topology in particle swarm optimization. IEEE Transactions on Evolutionary Computation 2018;23(4):689-702.

[99] Figueiredo EM, Ludermir TB. Investigating the use of alternative topologies on performance of the PSO-ELM. Neurocomputing 2014;127:4-12.

[100] Lee Rodgers J, Nicewander WA. Thirteen ways to look at the correlation coefficient. The American Statistician 1988;42(1):59-66.

[101] Krejci MC, Mathieu O, Vissotski AJ, Ravi S, Sikes TG, Petersen EL, et al. Laminar flame speed and ignition delay time data for the kinetic modeling of hydrogen and syngas fuel blends. Journal of Engineering for Gas Turbines and Power 2013;135(2).

[102] Seiler P, Frenklach M, Packard A, Feeley R. Numerical approaches for collaborative data processing. Optimization and Engineering 2006;7(4):459-78.

Summary of paper

Paper-I: A comprehensive kinetic modeling study of ethylene combustion with data uncertainty analysis

A revision and upgrade of the ethylene (C_2H_4) oxidation kinetic sub-mechanism were carried out as the next step in the optimization of the $C_{<3}$ chemistry, which is a base for the upcoming PAH sub-model improvement. The main emphasis of the work was focused on the assessment of uncertainties of the thermo-kinetical and experimental data used to achieve reasonable model parameter corrections. The principal targets of mechanism extension and update are: inspection of the reaction rate coefficients with accounting for recently published pressure-dependent reactions and analysis of reaction paths related to the C_2H_4 low-temperature oxidation and the formation of aromatic precursors. The experimental data (auto-ignition, premixed laminar flame speeds, and concentration profiles) with evaluated uncertainty and consistency were used for model optimization. The uncertainty bounds of the key reaction rate coefficients were evaluated from the statistical treatment of the published data, which provided constraints on the reaction rate parameters. The rate parameters of 57 reactions of C_2H_4 and key intermediates were optimized. The revised reaction mechanism demonstrates a good agreement with the majority of the existing experimental data. Results of the sensitivity and rate of production analyses were performed for several kinetic mechanisms from the literature and compared to visualize the variations and ambiguity in the importance of reaction paths and highlight the problems in mechanism optimization and integration.

Paper-II: A comprehensive kinetic modeling study of hydrogen combustion with uncertainty quantification

A 19-reactions H_2 oxidation chemical kinetic model has been optimized with uncertainty quantification. The uncertainties of the reaction rate constant (RRC) parameters have been first estimated based on the recommended direct measurements and review works. This deterministic approach was further combined with the probabilistic treatment of RRC to decrease the uncertainty intervals and to extend the temperature validity range for RRCs with the highest uncertainty level, for which two quantities, discrepancy measures and uncertainty contributions, were introduced in the developed framework. Monte Carlo simulations with randomly sampled RRCs and polynomial regression were performed to develop the response

surface with high coefficients of determination to be utilized in the model optimization procedure. 10 key channels were selected for further optimization, and the probability density functions were calculated based on discrepancy measures for 4 channels to reduce their large uncertainty intervals. The training set was collected from carefully validated measured data following experiments of shock tubes, rapid compression machines, jet stirred reactors, plug flow reactors, and premixed laminar flames. Inconsistent experimental targets were fixed and excluded from considerations. The optimized chemical kinetic model demonstrates good predicting ability for the H2 combustion experimental data from both the training set and the conditions outside the tested range (blind modeling).

Paper-III: A joint hydrogen and syngas chemical kinetic model optimized with particle swarm optimization.

A joint H_2 and syngas oxidation chemical kinetic model has been successfully developed and optimized by applying the heuristic algorithm, namely canonic particle swarm optimization (PSO). In comparison with deterministic and probabilistic optimization algorithms, the method of PSO is more effective and robust in coping with uncertainties and incomplete information. The review work and uncertainty analysis have been conducted for the reaction rate constants and 15 key reactions were recognized for optimization. Kinetic experimental data selected for model fitness were measured in shock tubes, jet stirred reactors, plug flow reactors, flow reactors, and premixed laminar flames, and cover wide ranges of temperature, pressure, equivalence ratio, and H_2/CO ratios. The final dataset has been produced with data uncertainty quantification and data consistency analysis. The set of optimums was obtained with the developed PSO framework by repeating optimization steps. The optimum with the lowest discrepancy measure was selected as the global and the corresponding surrogate model was recognized as the final optimized model. The initially evaluated uncertainties of the studied reaction rate constants were significantly constrained. The reaction rate constants for the H_2 oxidation sub-model were re-optimized and their uncertainties were further reduced.

Paper I

Fuel 299 (2021) 120833

Contents lists available at ScienceDirect

Fuel

journal homepage: www.elsevier.com/locate/fuel

Full Length Article

A comprehensive kinetic modeling study of ethylene combustion with data uncertainty analysis

Hongxin Wang [a], Nadezda Slavinskaya [b,c,*], Aziza Kanz [d], Moldir Auyelkhankyzy [c,e], Yiting Gao [a], Oskar Haidn [a]

[a] Department of Aerospace and Geodesy, Technical University of Munich, 85748 Garching, Germany
[b] GRS Association for Plant and Reactor Safety, 85748 Garching, Germany
[c] Al-Farabi Kazakh National University, 050040 Almaty, Kazakhstan
[d] DLR German Aerospace Center, Institute of Combustion Technology, 70569 Stuttgart, Germany
[e] Institute of Combustion Problems, 050012 Almaty, Kazakhstan

ARTICLE INFO

Keywords:
Ethylene
Chemical kinetic mechanism
Uncertainty
Auto-ignition
Laminar flame

ABSTRACT

A revision and upgrade of the ethylene (C_2H_4) oxidation kinetic sub-mechanism were carried as a next step in the optimization of the $C_{<3}$ chemistry, which is a base for the upcoming PAH sub-model improvement. The main emphasis of the work was focused on the assessment of uncertainties of the thermo-kinetical and experimental data to involve that principally in the methodology of reaction model uncertainty. The principal targets of mechanism extension and update are: inspection of the reaction rate coefficients with accounting recently published pressure-dependent reactions and analysis of reaction paths related to the C_2H_4 low-temperature oxidation and the formation of aromatic precursors. The experimental data (auto-ignition, premixed laminar flame speeds, and concentration profiles) with evaluated uncertainty and consistency were used for model optimization. The uncertainty bounds of the key reaction rate coefficients were evaluated from the statistical treatment of the published data, which provided constraints in the reaction rate parameters. The rate parameters of 57 reactions of C_2H_4 and key intermediates were optimized. The revised reaction mechanism demonstrates a good agreement with the majority of the existing experimental data. Results of the sensitivity and rate of production analyses performed for several kinetic mechanisms from the literature were compared to visualize the variations and ambiguity in the importance of reaction paths and highlight the uncertainty problems in mechanism optimization and integration.

1. Introduction

Ethylene (C_2H_4) is an important fuel and a key intermediate in the combustion of hydrocarbons. Its oxidation and pyrolysis reactions are also important for the formation of polycyclic aromatic hydrocarbons (PAH) and soot precursors. The C_2H_4 chemistry has been explored in sufficient breadth and depth over the past decades [1–10] to assume that the completeness of current chemistry is achieved and most important qualitative improvements of models could be done by further optimizations of poorly understood reaction rate coefficients (RRC).

Despite great efforts and constantly emerging new data, most elementary reaction rate parameters are not known with sufficient accuracy [11–14]. Uncertainties of the available data remain unknown in most cases. The reaction mechanism updating becomes a permanent process, which initiates the question: what is the final version and how it can be defined? The easiest answer is making sure that all the conceivable reactions are included and all RRCs in the model are obtained from the "first principals" with acceptable accuracy. However, it is not yet possible now. We do not have a hallmark to be sure a model includes all conceivable reactions. The RRCs from "first principals" are restricted, in the case of experiments, by ranges of measurement conditions and parameter fitting, and in the case of quanta-chemical calculations, by applied theoretical evaluations and numerical methods.

Most of the RRCs, especially for $C_{\geq 2}$ fuels, are derived from semi-empirical methods and model calibrating against combustion data performed by different workgroups. Some of these RRCs are successfully used in different reaction mechanisms, which will be regarded as statistical samplings, so these RRCs can be classified as "quasi first

* Corresponding author.
E-mail address: Nadezda.Slavinskaya@grs.de (N. Slavinskaya).

https://doi.org/10.1016/j.fuel.2021.120833
Received 18 January 2021; Received in revised form 3 April 2021; Accepted 7 April 2021
Available online 5 May 2021

principal" empirical data of high quality. Unfortunately, significantly more data obtained in this way were evaluated for conditions of the individual study interest or from fitting the model parameters to better match some experimental data within their respective range of applications. Today the expanding growth of publications with experimental, quanta-chemical data and reaction mechanisms do this process more efficient, but simultaneously more complicate: it involves much more data; it needs an analyses both of data physical sense, and also the data quality. Despite that, the technology development needs simulation tools with evaluated validity range. As the hydrocarbon models have hierarchical structure, the rick of error propagation is high. In our work we present our technology to develop reaction model with well understood model valid range. The development of numerical tools for reaction model fitting can further sharpen this problem: direct matching the experimental data of the different quality levels can lead to unwarranted modifications of the RRCs, which can be further traced in different models published in the literature [15].

In the following analysis of model parameters, we tried to recognize these problems.

The work presented in this study inherits the gradual upgrade of the German Aerospace Center (DLR) reaction database [16]. The updated C_2H_4 mechanism can be applied to the computational fluid dynamics simulation of combustion in engines fueled on C_2H_4 or small hydrocarbons [17–20], and also belongs to the upgrade of the kerosene combustion model with PAH formation [9,10,16,21–23]. Now the C_1-C_3 oxidation chemistry is under optimization without changes in the PAH formation sub-mechanism, which will be updated after the final inspection of the C_1-C_3 oxidation chemistry. The reaction paths for the PAH formation are strongly coupled with both $C_{\leq 3}$ chemistry and the products of the larger hydrocarbons, part of which are the PAH precursors. The including PAH reactions in the C_1-C_3 oxidation chemistry allow avoiding the model tailoring and the artificial breaking of the atom flows, and serve as a bridge between small and large molecules oxidation. The well-parameterized detailed chemistry of PAH precursors is expected to reduce the re-optimization efforts in upcoming updates of the $C_{\geq 4}$ combustion chemistry models. Another reason for following this strategy is the extremely high data scattering for kinetics of poly-aromatic molecules. Despite high-level theoretical calculations, the progress here can be achieved through the model calibration against measured concentration profiles, which follow mostly from the small-molecule combustion study. The well-optimized small chemistry can increase the chance to obtain stable and physically reasonable parameters of RRCs for PAH reactions in the future.

The paper is organized as follows: The second section discusses the model update strategy, the statistical method, and the uncertainty intervals for the initial steps of C_2H_4 oxidation. The third section presents the improvements in model optimization. The fourth section reports the validation results, i.e. simulations of experimental data for ignition delay times, laminar flame speeds and concentration profiles, and discussion. The work is supported by the supplement materials 1, 2, 3, 4, and the updated chemical kinetic model.

Additionally, the obtained model was compared with the models for small hydrocarbons published within the last two decades, including mechanisms of Aramco 3.0 [12], USC 2.0 [11], UCSD [13], Lopez et al. [6], Konnov [14], Dias et al. [7], NTUA [2], and GRI 3.0 [24]. The performed comparison of different mechanisms highlights the uncertainty problem in chemical kinetics. An overview of these modeling studies is presented in Supplementary-1.

2. Method

2.1. Mechanism update strategy

Detailed reaction mechanisms of hydrocarbon combustion chemistry have the hierarchical structure and logical passes from H_2 to larger chemical species with offshoots for pollution formation (NO_x, sulfuric acid, PAH, soot, etc.). It remains unclear [25] whether RRCs derived by optimization of small hydrocarbon mechanisms need to be re-optimized by modeling the oxidation of larger fuel molecules. In the current work, it is assumed that the re-optimization of some empirical RRCs by the optimization and extension in the next hierarchy sub-model is inevitable. Such re-optimization was performed through calibration of all "smaller" sub-models and was adopted only if the facility of sub-models were not disturbed. Parameters of RRCs obtained from the first principal were re-optimized exclusively if the new data of higher quality were published or found. This strategy is kept to reduce re-optimization efforts and to narrow the uncertainty intervals of the "anchoring reactions" which support the structure of the reaction database under development.

In this study, the C_2H_4 sub-mechanism optimization continues the development of the basic small chemistry reaction model [15,22,26,27]. The optimization is based on the first principals considering the most recent investigations and discoveries in the field of kinetic chemistry with estimated uncertainties and the comprehensive model validation against representative high-fidelity experiments for a wide application domain. Considering that the studied model is a part of the reaction mechanism for kerosene combustion with PAH formation, the model is constructed to keep reasonable size, and therefore unimportant channels and channels with high level of uncertainties were ignored.

The model inspection and optimization were based on the following axes: (1) final issue of the reaction mechanism for acetylene combustion [16]; (2) the literature review and analysis of the components and reactions involved in the ethylene oxidation; (3) the uncertainty analysis of RRCs; (4) analysis of uncertainties and consistency of the experimental data used for model validation and optimization; (5) the model calibration and optimization on experimental data for ignition delay times, laminar flame speeds and species concentration profiles.

All the calculations were performed with the Ansys Chemkin Pro [28] software. The models of closed homogeneous reactor, premixed laminar flame speed calculation, and premixed stabilized flame were applied to the modeling of ignition delay times, laminar flame speeds, and concentration profiles in premixed laminar flames respectively. The detailed parameters for shock tubes and premixed laminar flame burner can be found in the Section 4 and in Supplementary-3, Supplementary-4.

2.2. Uncertainty analysis of the reaction rate parameters

To fix the size of the feasible parameter region and to understand the uncertainty intervals for RRCs, we performed the statistical analysis [15,29–31] of the literature data for important reactions. The detailed theory has been presented in our former work [16], therefore only a brief review of the analysis parameters is shown here.

The standard deviations of the Arrhenius expression parameters A, n, and E_a:

$$k(T) = AT^n \exp\left(-\frac{E_a}{T}\right), (\mathrm{cm}^3,\ \mathrm{s},\ \mathrm{mole},\ \mathrm{K}) \tag{1}$$

calculated in the applied method of nonlinear regression [15,29–31], determine the margin, $\Delta k(T)$, of the rate-coefficient error. The uncertainty factor $f(T)$ [32,33] is used to determine the uncertainty level for $k(T)$:

$$f(T) = \log_{10}\left(\frac{k_{\mathrm{up}}(T)}{k_0(T)}\right) = \log_{10}\left(\frac{k_0(T)}{k_{\mathrm{low}}(T)}\right) \tag{2}$$

where k_0 is the nominal RRC and k_{low} and k_{up} are the lower and upper bounds respectively. Errors of the Arrhenius expression parameters [16], $s(x_a)$, describing the confidence level of RRC parameters, were used for calculation of:

$$k_{\mathrm{low}}(T) = (A - s(A))T^{(n-s(n))}\exp\left(-\frac{E_a + s(E_a)}{T}\right) \tag{3}$$

$$k_{up}(T) = (A + s(A))T^{(n+s(n))}\exp(-\frac{E_a - s(E_a)}{T}) \quad (4)$$

and finally, for the evaluation of the uncertainty factors, Eq. (2).

For the investigated uncertainty intervals, experimental measurements and theoretical calculations of RRCs were collected from the NIST Chemical Kinetics Database [34] and recently published references. Baulch et al. [32,35–39] conducted a series of reviews on RRCs, but the recommendations in their early works [35–39] show relatively high uncertainties due to the limitation of available data so that only the newest work [32] was applied in the uncertainty analysis.

The uncertainty ranges evaluated by the review work of Baulch et al. [32] are implemented in the applied statistical tool. As an example of performed statistical analysis, the obtained uncertainty factor for the reaction of $C_2H_4 + OH = C_2H_3 + H_2O$ is shown in Table 1 and Fig. 1. As mentioned above, the RRCs recommended in the early review works of Tsang et al. [39] and Warnatz [38] show high uncertainties so that RRCs from these works are depicted only for comparisons and were not applied in the statistical analysis. Other uncertainty factors and uncertainty bounds for the analyzed channels are presented in Table S2-1 and Fig. S2-1 in Supplementary-2.

3. Model improvements

3.1. Inspection and update of reaction rate constants

The original mechanism [16] based on our previous work [9,10,22,46,47] is referred as model-1, and the obtained newly optimized model for C_2H_4 is referred as model-2. Our initial mechanism for the PAH formation [47] was developed on the base of methane oxidation model of Hughes et al. [46] which was constructed at that time with a tough requirement of first principal application. Over time this base principal turned into a disadvantage. For example, a number of RRCs adopted in [9,10,16,22,47] from [46] were originated from experiments relevant to the limited temperature intervals; third body reactions have a large uncertainty for low-pressure limit and collider definitions, etc. The out coming chemistry traced from the model [42] in the model releases [9,10,16,22,47] initiated the mechanism revision and improvement.

Critical analysis of matches between simulations with model-1 and experiments on ignition delay times and laminar flame speeds has been performed and highlighted the problems to be solved: model-1 over-predicted ignition delay times and laminar flame speeds of C_2H_4. By scanning results of sensitivity analysis (Fig. S2-2 in Supplementary-2) accounted for the representative set of experimental data, reactions with the highest potential to provide the model improvement were determined [16] and all known sources of the RRCs were analyzed. The reactions to be inspected were related mostly to the low-temperature reactions of C_2H_4 oxidation and reactions of the key intermediates such as ethylenyl (C_2H_3), ethyl radical (C_2H_5), ketene (CH_2CO), and acetaldehyde (CH_2CHO). Special attention was paid to the pressure-dependent RRCs and the reactions important for the formation of PAH precursors.

The reactions could be modified on data for ignition delay times, laminar flame speeds and concentration profiles are shown in Table 2.

Table 1
Uncertainty factors calculated from the literature sources for the reaction $C_2H_4 + OH = C_2H_3 + H_2O$, $k(T) = AT^n exp(-E_a/T)$.

Reaction	Reference	T range, K	k, cm^3, s, mole, K		
			A	n	E_a
$C_2H_4 + OH = C_2H_3 + H_2O$ $f = 0.301 - 0.318$	Ali2011 [40]	200–400	6.20E + 11	4.20	−433.0
	Senosiain2006 [41]	650–1500	1.31E - 01	0.00	2990.0
	Baulch2005 [32]	200–5000	2.05E + 13	2.01	585.0
	Liu2002 [42]	1003–1253	2.10E + 06	0.00	2990.0
	Westbrook1989 [43]	650–901	2.00E + 13	0.00	2990.0
	Tully1988 [44]	748–1170	2.02E + 13	0.00	2100.0
	Liu1987 [45]	300–2500	1.45E + 13	2.75	2100.0
	Tsang1986 [39]	500–2000	1.57E + 04	0.00	1500.0
	Warnatz1984 [38]		3.00E + 13		

3.2. Modification of reaction rate constants

The further rate constant adjustments of the C_2H_4 chemistry rate parameters were carried out on the base of simulations of experimental data with model-2 applying sensitivity and rate of production analyses. Fig. 2 illustrates the scattering in normalized sensitivity coefficients calculated for the reactions of model-2 by simulations of ignition delay times and laminar flame speeds. Top 15 reactions related to C_2 species are shown. According to the sensitivity coefficients, channels related to O_2 and HO_2, such as reactions of $C_2H_3 + O_2$, $C_2H_4 + HO_2$, and $C_2H_5 + O_2$, are the most important channels for the low-temperature ($T_5 \leq 1000$ K) oxidation of C_2H_4. For the higher temperature ($T_5 = 1800$ K), reactions related to O and H and the decomposition of C_2H_4 become more important, as shown in Fig. 2.

The optimization approach and protocol were essentially identical to the one used in [16,27]. The k values to be modified were tested iteratively until the best optimization was obtained. The known kinetic data was applied in the model improvement: experimental C_2H_4 ignition delay times from publications

[1,3,5,48–52] measured for $T_5 = 1000$–2238 K, $p_5 = 1$–60 atm and equivalence ratios of 0.5 to 3.0; laminar flame speeds of C_2H_4/air mixtures measured by heat flux method, counter flow flames and spherical flames [53–59]; concentration profiles obtained in premixed flat flames [2,7,60–62], as shown in Table 3. The modifications of the RRCs are controlled within the calculated uncertainty bounds. The data published within the last twenty years or recommendations from recently developed or updated mechanisms are preferred, but for some reactions, only a small amount of data or references could be found. The detailed description of revised reactions and modification work is reported in Supplementary-2. The collections of RRCs and the final list of updated values are shown in Tables S2-1 and S2-2 in Supplementary-2.

4. Results and discussion

4.1. Ignition delay times

The detailed experimental data and modeling results of ignition delay times are presented in Supplementary-3. Large scattering of experimental data generates difficulties for the proper optimization of the mechanism. Brown et al. [48], Kalitan et al. [50], and Saxena et al. [5] conducted shock tube experiments with the same mixture (1% C_2H_4 + 3% O_2 + 96% Ar) at similar pressure ($p_5 = 1$–3 atm). A comparison of these experimental data [5,48,50] with the modeling results simulated with model-2 is presented in Fig. 3a. It can be seen that model-2 can predict the ignition delay times from Kalitan et al. [3] and Saxena et al. [4] quite well but cannot reproduce the data measured by Brown et al. [48]. Similar results obtained by the simulation with Aramco 3.0 [12], USC 2.0 [11], and UCSD [13] mechanisms are presented in Supplementary-3, and the compared mechanisms tend to be consistent with the results measured by Kalitan et al. [3] and Saxena et al. [4].

The same problem occurs in the ignition delay times of the C_2H_4/air mixtures measured by Penyazkov et al. [7] and Kopp et al. [6], as shown in Fig. 3b. Penyazkov et al. [7] and Kopp et al. [6] measured ignition delay times for the same mixture at different pressures with shock tubes,

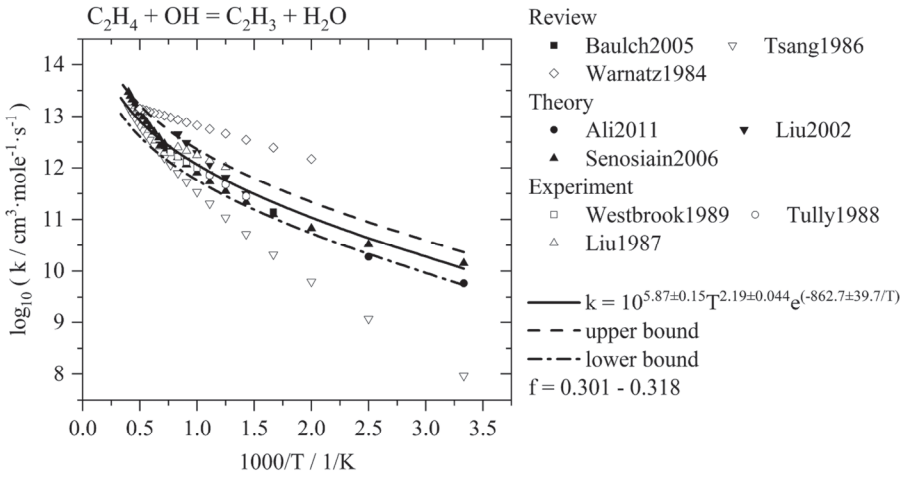

Fig. 1. Determination of k_{low} (lower bound) and k_{up} (upper bound) and the uncertainty factor for the reaction $C_2H_4 + OH = C_2H_3 + H_2O$ from the statistical analysis of the literature data (solid symbols for the data published after the year 2000, and open symbols for the data published before the year 2000).

Table 2
Reactions optimized on the measured data for ignition delay time, laminar flame speed and concentration profile.

No.	Reaction	Ignition delay time		Laminar flame speed	Concentration profile
		low-T	high-T		
R2a	$C_2H_4 + O = CH_3 + HCO$		√		√
R2b	$C_2H_4 + O = CH_2CHO + H$		√	√	√
R2c	$C_2H_4 + O = CH_2O + CH_2$			√	√
R2d	$C_2H_4 + O = CH_2CO + H_2$		√		√
R3a	$C_2H_4 + OH = C_2H_3 + H_2O$	√	√	√	√
R3d	$C_2H_4 + OH = C_2H_3OH + H$				√
R4a	$C_2H_4 + H = C_2H_3 + H_2$		√		√
R4b	$C_2H_4 + H = C_2H_5$				√
R5a	$C_2H_4 = C_2H_3 + H$		√	√	√
R5b	$C_2H_4 = H_2CC + H_2$	√	√		
R6	$C_2H_4 + HO_2 = CH_2OCH_2 + OH$	√			
R7a	$C_2H_5 + O_2 = C_2H_4 + HO_2$	√			√
R8a	$CH_3 + CH_3 = C_2H_5 + H$			√	
R8b	$C_2H_5 + H = C_2H_4 + H_2$			√	
R10, R11	CH_2CO			√	√
R12	CH_3CO				√
R13, R14	CH_2CHO				√
R15-20	H_2CC		√	√	√
R21-26	CH_2OCH_2	√			

but the data measured by Penyazkov et al. [7] shows a trend of over-prediction at temperatures lower than 1250 K (1000/T > 0.8). Fig. 3 illustrates a problem arising at the model calibrating in a case of inconsistent experimental data. As the data are measured under the same conditions, the dominants reactions are the same for both measured sets. Conclusions following from these data simulations are contradictory and rate constant optimization in such cases can lead to the parameters lying beyond physical and theoretical reasonable ranges. To meet a decision about data quality, in similar controversial cases we simulated data with various models to analyze the scattering in simulations.

To follow the optimization progress, the global average error of modeling ignition delay times against the measured data is defined as follows [64]:

$$E = \frac{1}{N}\sum_{i=1}^{N}\frac{1}{N_i}\sum_{j=1}^{N_i} e_{ij} \tag{6}$$

where N is the number of data sets, N_i is the number of data points in the ith data set. The error of modeling results based on the uncertainty e_{ij} which is defined as:

$$e_{ij} = \ln\left(\frac{t_{ij}^{sim} - t_{ij}^{exp}}{u_{ij}}\right)^2 \tag{7}$$

where t_{ij}^{exp} is the experimental value of the ignition delay time, t_{ij}^{sim} is the simulated result and u_{ij} is the experimental uncertainty.

Most authors who measured ignition delay times evaluated the uncertainties for specific experiment settings or an average uncertainty for the measured ignition delay times [1,5,50]. In this study, the uncertainties, u_{ij}, were evaluated based on the similar strategy shown in our previous work [27,65]. The distribution of evaluated uncertainties of the collected 461 ignition delay time targets [1,3,5,49,50,52] versus T_5, p_5, and equivalence ratio are illustrated in Fig. 4a. The points are colored in green for $10\% \le u_{ij} \le 15\%$, blue for $20\% \le u_{ij} \le 25\%$, and red for $u_{ij} \ge 30\%$. The biggest uncertainties are evaluated for the data obtained mostly for fuel-rich mixtures at lower temperatures ($T_5 < 1200$ K) and high temperatures ($T_5 > 1600$ K), where more experimental targets are needed for uncertainty analysis and data quality analysis. Fig. 4b shows the distribution of modeling errors (e_{ij}, Eq. (7)) for the ignition delay time targets. The points are colored in green for $e_{ij} < 0.001$, blue for $0.001 \le e_{ij} \le 0.005$, and red for $e_{ij} > 0.005$. The biggest discrepancies have been achieved for data measured at $T_5 < 1100$ K and $\varphi > 2.5$ for all studied pressures.

Fig. 5 demonstrates progress in the e_{ij} (Eq. (7)) calculated for modeling ignition delay times with model-1 and model-2. Considering the contradiction of the experimental data, the ignition delay times measured by Brown et al. [48] are excluded from the data set used for mechanism optimization. The comparison of the errors of the two models shows a significant improvement in predicting the ignition delay

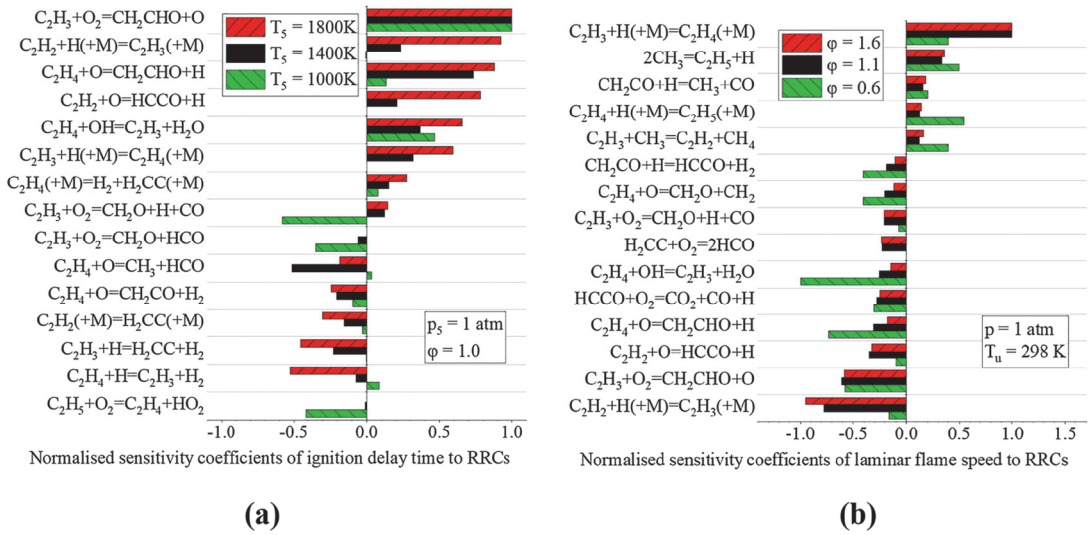

Fig. 2. Comparison of normalized sensitivity coefficients calculated with model-2 for: (a) ignition delay times of C_2H_4/O_2/Ar mixtures with $\varphi = 1.0$, $p_5 = 1$ atm and $T_5 = 1000$, 1400, 1800 K; (b) laminar flame speeds of C_2H_4/air mixtures with $T_u = 298$ K, p = 1 atm and $\varphi = 0.6$, 1.1, 1.6.

Table 3
Overview of the ignition delay times (ST for shock tube), laminar flame speeds (HF for heat flux method, CF for counterflow flame, SF for spherical flame) and concentration profiles (PFF for premixed flat flame) used for validation.

Ignition delay time	**T_5 / K**	**p_5 / atm**	**Mixture and method**
Brown et al. 1999 [48]	1074–2238	1–5	C_2H_4/O_2/Ar, $\varphi = 1.0$, ST $C_2H_4/O_2/N_2$, $\varphi = 1.0$, ST
Colket et al. 2001 [49]	1125–1380	5–8	C_2H_4/O_2/Ar, $\varphi = 0.5$–1.0, ST
Kalitan et al. 2005 [50]	1115–1754	1–3	C_2H_4/O_2/Ar, $\varphi = 0.5$, 1.0, ST
Penyazkov et al. 2009 [51]	1120–1520	6–15	C_2H_4/air, $\varphi = 0.5$–2.0, ST
Saxena et al. 2011 [5]	1000–1634	2–18	C_2H_4/O_2/Ar, $\varphi = 1.0$, 3.0, ST
Kopp et al. 2014 [3]	1106–1310	1–25	C_2H_4/air, $\varphi = 0.3$–1.0, ST
Deng et al. 2017 [52]	1090–1600	1.2–10	C_2H_4/O_2/Ar, $\varphi = 1.0$, ST
Shao et al. 2018 [1]	1095–1317	15, 60	C_2H_4/O_2/Ar, $\varphi = 1.0$, 2.0, ST
Laminar flame speed	**T_u / K**	**p / atm**	**Mixture and method**
Egolfopolous et al. 1991 [63]	298	1	C_2H_4/air, CF
Hassan et al. 1998 [53]	298	0.5–4	C_2H_4/air, SF
Hirasawa et al. 2002 [54]	298	1	C_2H_4/air, CF
Jomaas et al. 2005 [55]	298	1	C_2H_4/air, CF
Kumar et al. 2008 [56]	298	1	C_2H_4/air, CF
Park et al. 2013 [57]	298	1	C_2H_4/air, CF
Ravi et al. 2015 [58]	298	1	C_2H_4/air, SF
Treek et al. 2020 [59]	298	1	C_2H_4/air, HF
Concentration profile	**T_u / K**	**p**	**Mixture and method**
Xu et al. 1997 [60]	298	98.7 kPa	C_2H_4/air, PFF
Delfau et al. 2007 [61]	298	1 atm	$C_2H_4/O_2/N_2$, PFF
Dias et al. 2011 [7]	298	0.05 bar	33%C_2H_4 + 40%O_2 + 27%Ar, PFF
Korobeinichev et al. 2011 [62]	298	0.04 bar	28%C_2H_4 + 42%O_2 + 30%Ar, PFF
Malliotakis et al. 2018 [2]	298	0.05 bar	30%C_2H_4 + 40%O_2 + 30%Ar, PFF

times. The e_{ij} errors for other compared mechanisms [2,6,7,11–14,24] are shown in Fig. S3-1 in Supplementary-3.

Although lots of ignition delay time data are measured today, it is not enough to cover all the operating conditions of practical interests. Kinetic models are generally validated over a particular set of experimental data but are frequently used for the reaction conditions which are far from validation parameters, and this can lead to high uncertainties in the model predictions. The deficit of the experimental data or their high uncertainties do not allow justifying a feasible range of RRCs, model tailoring or final valid parameter range of a kinetic model. In our previous study [16] we introduced the criterion for applicability of an experimental target, E_{ap} (a relation between experimental error and parameter constrain), and showed, that far not all experimental data we have are useful for the RRCs' improvement, also if they have low errors, because these data are not sensitive to the studied RRCs. The measurement planning needs methods for evaluating the problem-oriented operating conditions of experiments. The combination of rigorous methods for uncertainty and consistency analyses of the big amount of data and methods for model optimization is the way to handle kinetic data today. That can be realized only with advanced computing systems like PrIMe [27,66], which is now in standby modus.

4.2. Laminar flame speeds

The experimental data versus modeling results performed with the studied model and the compared models are presented in Fig. 6. The spread of points measured by different groups in Fig. 6a shows that uncertainties for laminar flame speeds can be>10% at the peak ($\varphi = 1.1$) [65]. As shown in Fig. 6, model-1 predicted higher laminar flame speeds than the experimental targets, which was revised by the upgrade work in model-2. The mechanism improvement was achieved by revision RRCs of reactions (R2), (R3), (R4b), and (R5a) (see Table 2 and Supplementary-2). The simulation of laminar flame speeds at various pressures also shows a good agreement with the data measured by Hassan et al. [53]. The compared models, Aramco 3.0 [12], UCSD [13], and USC 2.0 [11], also show acceptable results for the collected data.

4.3. Concentration profiles

Reactions related to C_2H_5, CH_2CO, CH_3CO, and CH_2CHO (reaction R7-14) were triggers of progress in concentration simulations (see Table 2 and Supplementary-2), as they are the key intermediates of C_2H_4 oxidation. Generally, the developed model demonstrates satisfactory agreement with the simulated data. Detailed results are shown in Supplementary-4.

Fig. 7 reports simulations of concentration profiles measured in laminar premixed ethylene flames by Xu et al. [60] and Delfau et al. [61]. The last experimental data were recorded in very short flame, above 0.4 cm from the burner. Data of Xu et al. [60] are in excellent accordance with simulations, while data of Delfau et al. [61] are

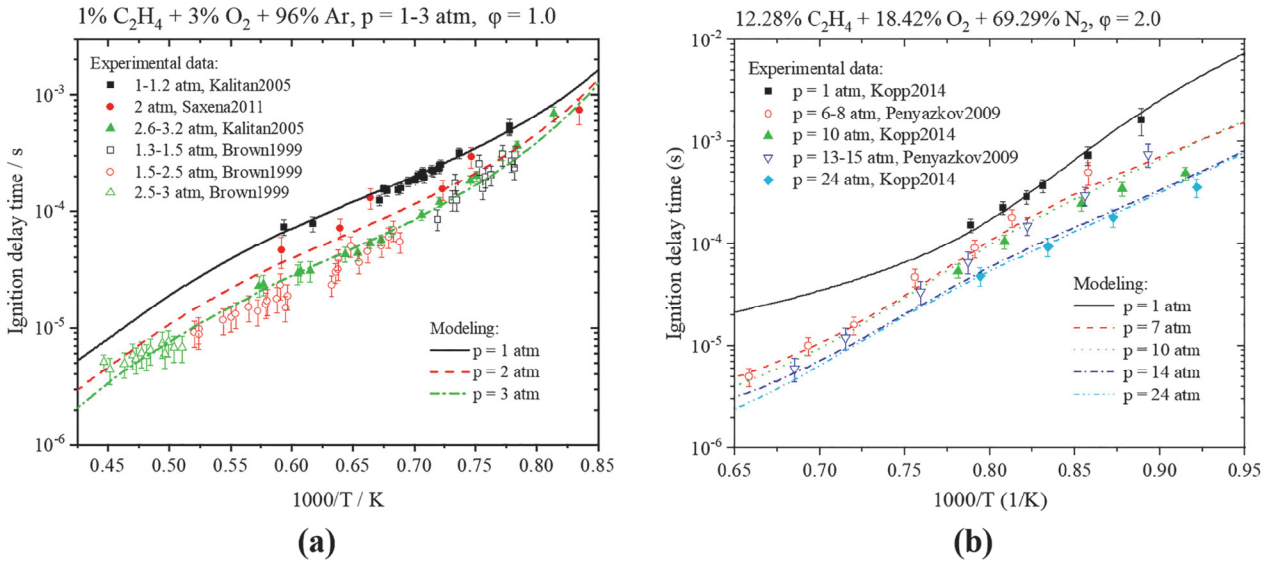

Fig. 3. The experimental ignition delay times measured by the different groups (Brown1999 [48], Kalitan2005 [50], Saxena2011 [5], Penyazkov2009 [51], Kopp2014 [3]) versus simulations performed with model-2.

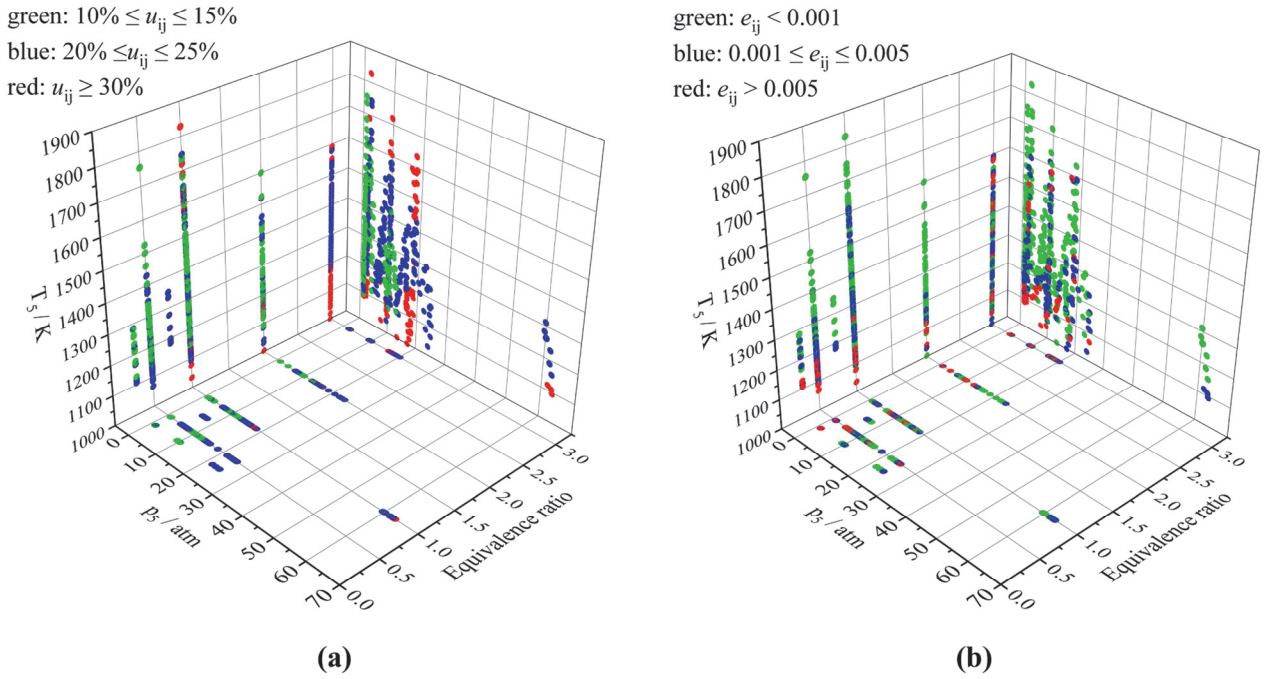

Fig. 4. (a) Uncertainties of the used experimental ignition delay times vs T_5, p_5 and equivalence ratio: green points for $10\% \leq u_{ij} \leq 15\%$, blue points for $20\% \leq u_{ij} \leq 25\%$ and red points for $u_{ij} \geq 30\%$; (b) Errors for modeling ignition delay times with model-2: green points for $e_{ij} < 0.001$, blue points for $0.001 \leq e_{ij} \leq 0.005$ and red points for $e_{ij} > 0.005$. (For interpretation of the references to color in this figure legend, the reader is referred to the web version of this article.)

described with some discrepancies, but in accordance with trends and values of simulation results with other models, as shown in Fig. 7b.

Compared to the ignition delay time and laminar flame speed data, the concentration profiles demonstrate a higher uncertainty/inconsistency level. Some of the measurements conducted under the similar conditions by different workgroups demonstrate huge discrepancies between reported concentration profiles.

Fig. 8 presents the concentration profiles of H_2 in the fuel rich premixed flat flames measured by Dias et al. [7], Korobeinichev et al. [62] and Malliotakis et al. [2] and the modeling results simulated with the model-2. The three experiments were carried out to investigate the PAH and soot formation in the rich C_2H_4 premixed flames at similar pressure with similar mixing ratio,

Table 3. Although the specific settings of the experimental devices are different, all the facilities are designed to obtain ideal one-dimensional premixed flames in flat flame burner. The experimentally determined temperature profiles have been imposed to calculations so that the heat losses to the burner are explicitly taken into account [2]. Nonetheless, as it can be seen in Fig. 8, the difference in results reaches factor of 3. By comparing the data measured by Dias et al. [7] and

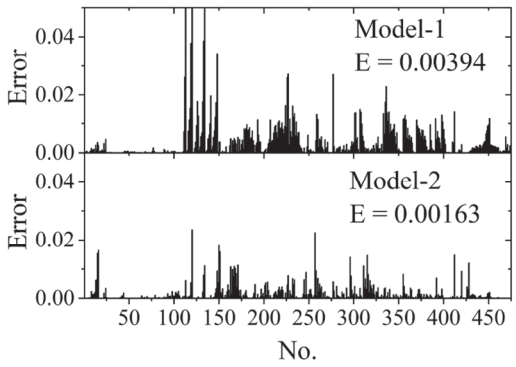

Fig. 5. Modeling errors (e_{ij}, Eq. (7)) for ignition delay times obtained with model-1 and model-2.

Malliotakis et al. [2], it can be concluded that difference of 3% in the initial C_2H_4 concentration can lead to a 20% increase in the H_2 mole fraction. To point out which data could be used for the model optimization we performed simulations with the models Aramco 3.0 [12], UCSD [13], Dias et al. [7] and Malliotakis et al. [2] (NTUA 2015) as well. Results of model comparison are shown in Supplementary-4 and will be described in the next section.

Based on these simulations, the RRCs were not fixed for concentration profiles intentionally. The experimentally measured mole fractions are only used for preventing major deviations during the modification work.

4.4. Discussion

Fig. 9 summarizes the studied channels for the oxidation of C_2H_4 [2,6,7,11–14,24] adopted for the model-2 structure. The channels marked with red color were not included in the model due to their weak impact on the validation data. If these reactions were added in the

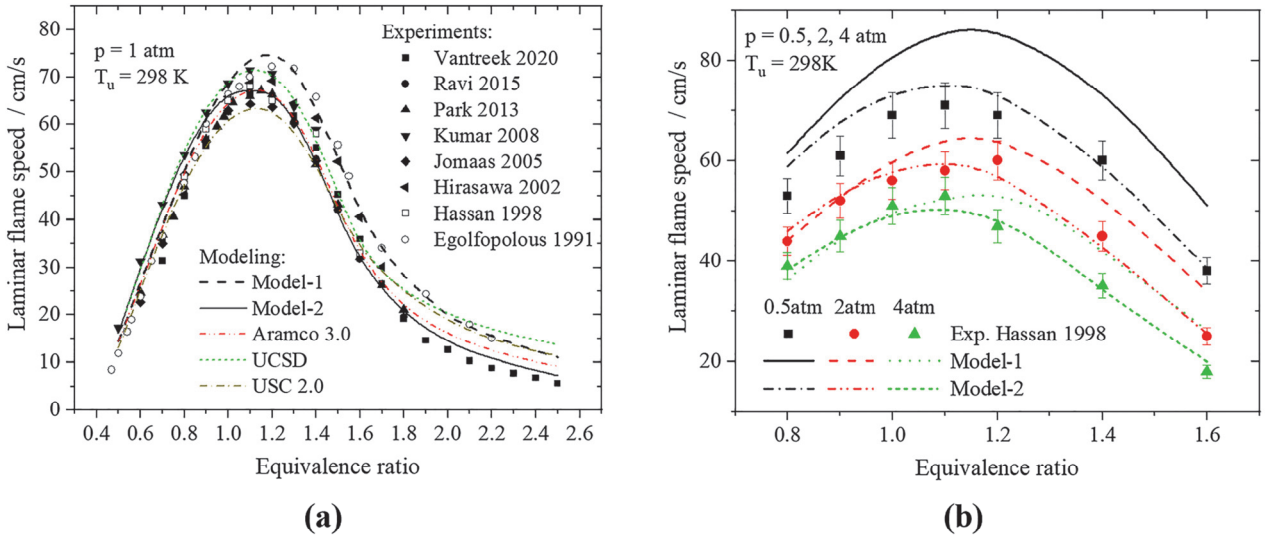

Fig. 6. Experimental laminar flame speed data (Hassan et al. [53], Hirasawa et al. [54], Jomaas et al. [55], Ibarreta et al. [8], Kumar et al. [56], Park et al. [57], Ravi et al. [58]) versus modeling results performed with model-1, model-2, Aramco 3.0 [12], UCSD [13], USC 2.0 [11] mechanisms.

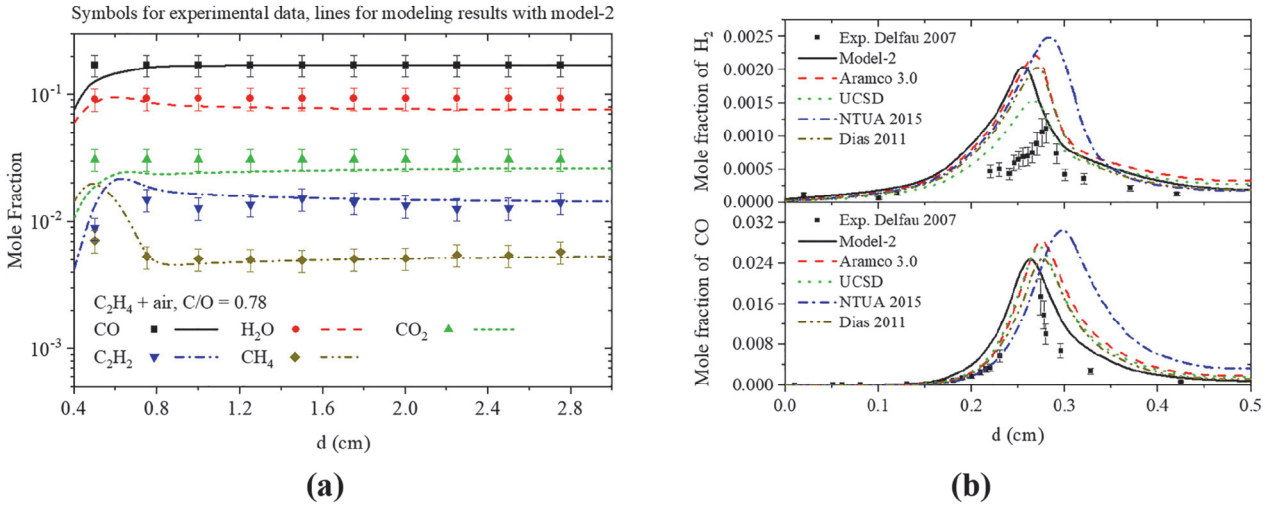

Fig. 7. The concentration profiles measured in premixed laminar flame of C_2H_4/air versus modeling results: (a) Xu et al. [60] vs model-2 (b) Delfau et al. [61] vs model-2, Aramco 3.0 mechanism [12], UCSD mechanism [13], USC 2.0 mechanism [11].

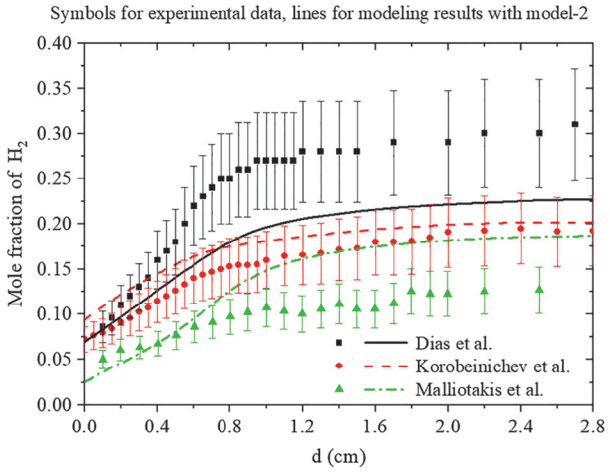

Fig. 8. Comparison of H_2 concentration profiles measured by Dias et al. [7], Korobeinichev et al. [62] and Malliotakis et al. [2] (presented with 20% uncertainties) at similar conditions and modeling results simulated with model-2.

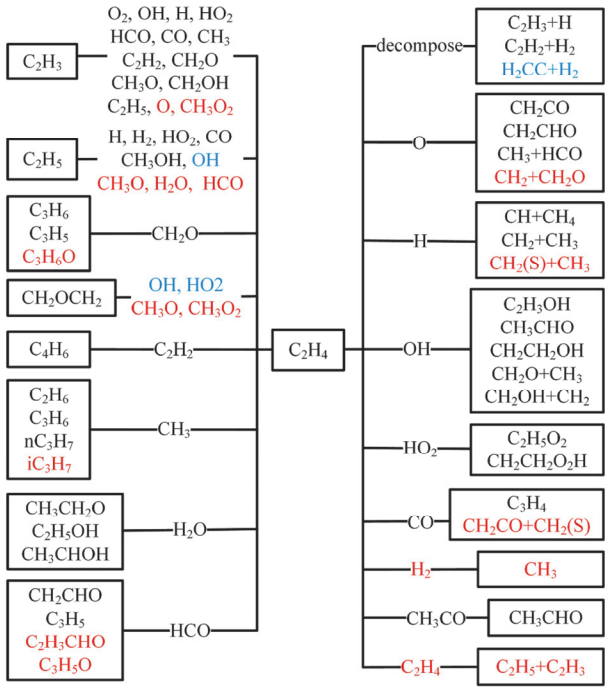

Fig. 9. Channels for the initial steps of C_2H_4 oxidation and pyrolysis (coloured in black are the channels which model-1 contains, coloured in red are the channels which model-1 and model-2 lack, coloured in blue are the reactions which have been added to model-2). (For interpretation of the references to color in this figure legend, the reader is referred to the web version of this article.)

model, the new RRCs could not be validated by the existing experimental data, so that it is unnecessary to introduce these channels with uncontrollable uncertainties. New channels for C_2H_5, H_2CC and CH_2OCH_2 (blue) were added according to the sensitivity analysis and their important roles in the formation of PAH.

Performed improvements of the model-1 resulted in the redistribution of atomic flows simulated with model-2. The percentages for different channels are calculated based on the top 20 rates of productions. Statistical results of rates of production for C_2H_4 oxidation at 1000 K (numbers out of the brackets) and 1800 K (numbers inside the brackets) are shown in Fig. 10. New channels added in model-2 are highlighted with color blue. The main changes are related to the reactions of CH_2OCH_2, H_2CC, C_2H_4 and C_2H_5. Channels of CH_2OCH_2, which are important for the low-temperature reactions, are added as new paths. Reactions of $C_2H_4 + O$ and $C_2H_5 + O$ are revised and found to play an important role in the high-temperature condition. The RRCs of $C_2H_4 + O$ channels are replaced by the newest recommendations of Morin et al. [67,68]. The channels from C_2H_4 to PAH precursors (C_2H_2, H_2CC, C_2H_3) are rebuilt following the work of Laskin et al. [69] and Wang et al. [70]. The detailed update work and discussion on the RRCs are shown in Supplementary-2.

The final list of new reactions and sources of their RRCs is given in Table S2-2 in Supplementary-2. The final obtained capabilities in comparison to model-1 are integrated in Table 4. Significant improvement is made to the C_2H_4 oxidation model by the upgrade work and the prediction ability for C_2H_2 oxidation [16,71–74] is retained as well.

The reaction flow diagram from C_2H_4 to benzene (A_1) of model-2, presented in Fig. 11, fixes the actual logic of aromatic molecule formation and main directions of the following work: reactions of C_2H_6, C_2H_5 and C_2H_5OH will be further investigated followed by sub-mechanisms of C_3H_4, C_3H_6, and C_3H_8.

4.5. Comparison of mechanisms

In the following paragraph, we would like to briefly present a comparison of reaction models once again to focus on the problem of the structure of a chemical reaction model and its valid parameter range. As the different criteria for defining the valid model parameter range are based on the sensitivity coefficients [75], we highlight the problem using the results of sensitivity analysis of ignition delay times to RRCs performed for four models: model-2 (115 species, 971 reactions), Aramco 3.0 [12] (581 species, 3037 reactions), USC 2.0 [11] (111 species, 784 reactions) and UCSD [13] (58 species 207 reactions) at $T_5 = 1000$ K and 1800 K, Fig. 12. Detailed comparison of measured ignition delay times and modeling results with model-1, model-2, Aramco 3.0 [12] and UCSD [13] are shown in Supplementary-3.

For the condition of $T_5 = 1000$ K, the most obvious discrepancies among these models occur in the channels of $C_2H_3 + O_2 = CH_2O + H + CO$, $C_2H_3 + O_2 = CH_2O + HCO$, and $C_2H_3 + O_2 = C_2H_2 + HO_2$. The model-2 and Aramco 3.0, which have the RRCs for reactions of $C_2H_3 + O_2$ adopted from Goldsmith et al. [76], show the similar sensitivities to these channels compared to the other two models, which have RRCs from [77,78]. For all the models, channel $C_2H_3 + O_2 = CH_2CHO + O$ demonstrates the highest importance at lower temperature, Fig. 12a.

For higher temperatures, the distribution between sensitivity coefficients obtained for analyzed models is much higher and for the reaction $C_2H_4 + H = C_2H_3 + H_2$ they are even opposite: in the model UCSD [13], this reaction has a negative effect on the ignition delay times, Fig. 12b. The UCSD model lacks the component H_2CC, which is the important product of C_2H_4 decomposition at high temperature, as shown in Fig. 12b. The highest sensitivity of the ignition delay time to reaction $C_2H_3 + H = C_2H_2 + H_2$ demonstrated by the model of Aramco 3.0 [12] can be explained with the modification performed in this mechanism: the RRC of this channel has been increased to a much higher value than the recommendations [36,38]. Reaction $C_2H_4 + O = C_2H_3 + OH$ of the USC 2.0 model shows the importance for both low- and high-temperature conditions, but this channel tends to be an overall reaction and was not studied in the newest works [68,79–81].

Apparent disagreements in the sensitivity coefficients follow from various distributions of atom fluxes in the models, which in turn are defined with individual combinations between the reaction channels and correlations between the rate parameters. Differences in the model structures can be unnoticeable at the simulation of macro processes: analyzed reaction mechanisms are different in choices of elementary reactions and their rate parameters, but the ignition delay times are

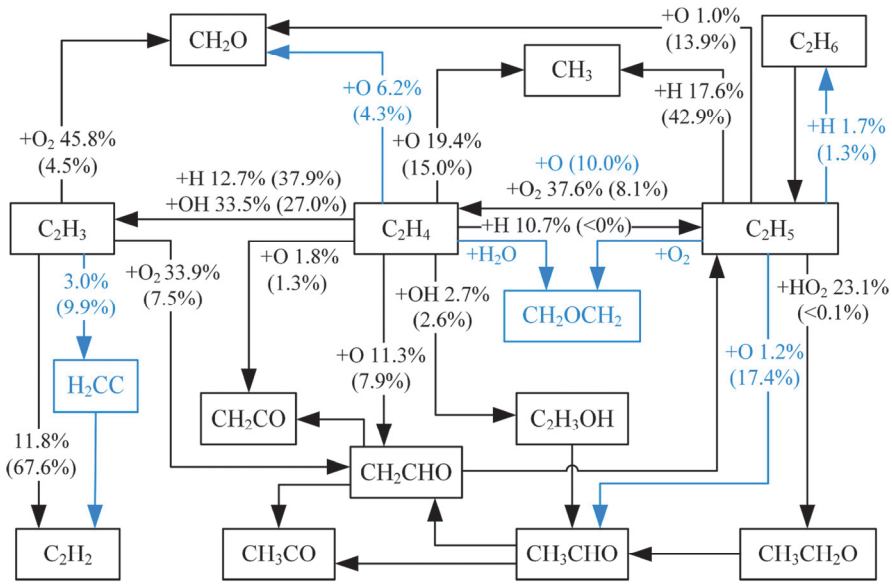

Fig. 10. Reaction flow diagrams of C_2H_4 oxidation at $\varphi = 1$, $p = 1$ atm, $T = 1000$ K (*percentages out of the brackets*) and $T = 1800$ K (*percentages inside of the* brackets) with model-2 (blue colour for the new reactions added in model-2). (For interpretation of the references to color in this figure legend, the reader is referred to the web version of this article.)

Table 4
Validation information and average errors for ignition delay times and laminar flame speeds for C_2H_4 and C_2H_2 with model-1 and model-2.

Mechanism	Average error E for C_2H_4 ignition delay times	Average error E for C_2H_2 ignition delay times	Average error E for C_2H_4 laminar flame speeds
Model-2	0.00163	0.00092	4.35
Model-1	0.00394	0.00098	7.32

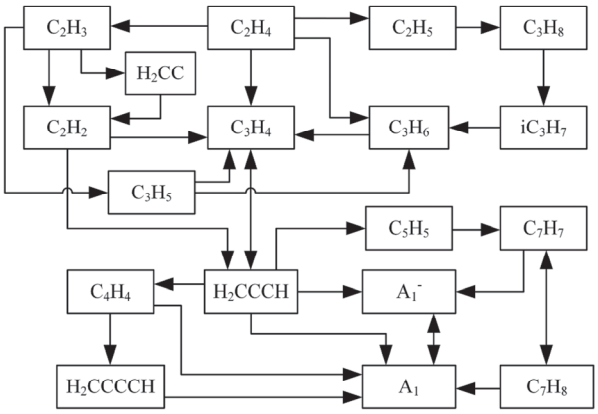

Fig. 11. Reaction flow diagram of C_2H_4 to benzene (A_1) *in the simulation of* premixed laminar flame of Korobeinichev et al. [62] with model-2.

reproduced well with all analyzed models in most cases (detailed comparisons of measured ignition delay times and modeling results are shown in Supplementary-3).

Average errors (Eq. (6)) for C_2H_4 ignition delay times simulated with model-1, model-2, and mechanisms [6,11–14,16,24,78] are listed in Table 5. As expected, the updated new mechanism with its specific adaptation for C_2H_4 yields generally better results in comparison with the analyzed models. The highest errors among the compared mechanisms were obtained for models of Dias et al. [7] and NTUA [2] following from the process of model construction. These two reaction mechanisms were developed based on measurements performed by authors of [2,7] in premixed laminar flame. The application scope of these models [2,7] might be restricted without comprehensive research. The high error value shown by GRI 3.0 [24] logically follows from the limitation of available experimental data during the creation of the model.

It can be concluded from Fig. 12, the figured dominance channels for modeled processes are mostly related to the individual model structure and not to the nature of the process. In any case we do not have criteria to recognize that, and simple enumerating the chemical species and elementary reactions with used RRCs are not enough for that. The special objective methods should be developed for evaluating the model structure quality and tools for model comparison. It is worth mentioning that simple adaptations of RRCs from different mechanisms may jeopardize the prediction capabilities of mechanism.

Modeling concentration profiles especially clearly demonstrates the effect of model structure on the results. Unfortunately, the lack of such data and some inconsistency of the available data do not allow us to draw final conclusions and use these data for final model optimization.

The calculations of the concentration profiles of H_2 and H_2O with five models (model-2 and Aramco 3.0 [12], UCSD [13], Dias 2011 [7] and NTUA [2]) are compared with the measured data obtained in [7], [62] and [2], as shown in Fig. 13. As it was previously described, these data obtained under similar conditions,

Table 3, are not consistent, Fig. 8. Data of Korobeinichev et al. [62] are predicted within their experimental errors by all models, excepting *models of Dias et al. [7] and NTUA [2] developed for the restricted* calibration conditions and having the highest error for most of the concentration profiles. No one model describes hydrogen profile measured by Malliotakis et al. [2]; all models have a trend to underpredict results of Dias et al. [7] and to over-predict results of Malliotakis et al. [2] for H_2. The opposite results are obtained for H_2O simulations: all studied models over-predict the experimental data from Dias et al. [7] und under-predict the data of Malliotakis et al. [2]. The Aramco 3.0 [12] mechanism shows the lowest values for hydrogen concentration and the highest values for water concentration measured in [7], [62] and [2] data, as shown in Fig. 13.

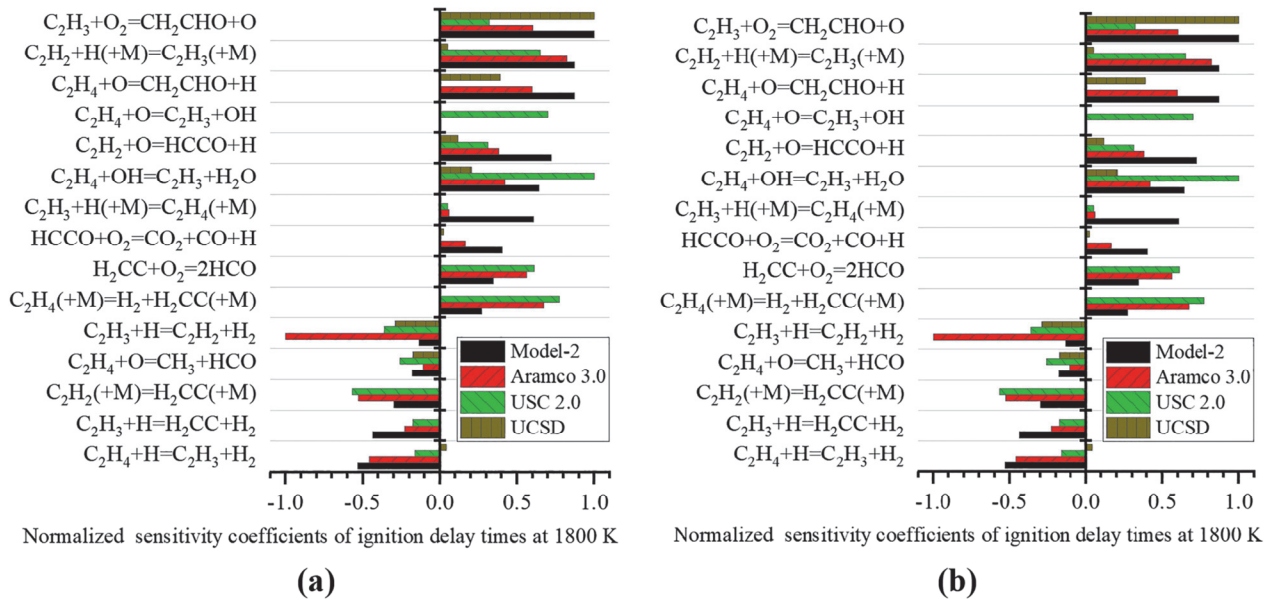

Fig. 12. Comparison of normalized sensitivity coefficients of ignition delay times simulated with model-2 (this study), Aramco 3.0 [12], USC 2.0 [11] and UCSD [13] to the RRCs for $C_2H_4/O_2/Ar$ mixture with $\varphi = 1.0$, $p_5 = 1$ atm and (a) $T_5 = 1000$ K; (b) $T_5 = 1800$ K.

Table 5
Validation information and average errors for C_2H_4 ignition delay times simulated by different mechanisms.

Mechanism	Year	Recent validation for C_2H_4	Average error for C_2H_4	Average error for C_2H_2
Model-2 (this study)	2021	this study	0.00163	0.00092
Aramco 3.0 [12]	2018	Kopp et al. 2014 [82]	0.00183	0.00085
UCSD [13]	2016	UCSD 2015 [13]	0.00380	0.00089
Lopez et al. [6]	2009	Lopez et al. 2009 [6]	0.00386	0.00397
Model-1 [16]	2019	None	0.00394	0.00098
USC 2.0 [11]	2009	None	0.00497	0.00236
Konnov [14]	2009	None	0.00508	0.00305
GRI 3.0 [24]	1999	None	0.01856	0.01019
Dias et al. [7]	2011	Dias et al. 2011 [7]	0.01890	0.00550
NTUA 2015 [2]	2015	Malliotakis et al [2]	0.03635	0.00453

5. Conclusion

The upgrade and extension of the detailed C_2H_4 combustion mechanism have been successfully performed based on the simulations of the experimental data for auto-ignition [1,3,5,48–52], premixed laminar flame speeds [53–59,63], and concentration profiles measured in premixed flat flame [2,7,60–62]. Hundreds of heterogenic experimental targets measured over a wide spectrum of experimental conditions by different research groups have been analyzed for model optimization.

It is shown, there is an on-going and growing need to provide validation of chemical kinetics models.

Sensitivity and rate of production analyses have been conducted to identify the key reactions and intermediates. The selected modifications of RRCs were performed within the uncertainty intervals estimated with statistical methods. The following features have been studied:

(1) Initial reaction paths of the C_2H_4 oxidation and pyrolysis, including channels related to the newly added H_2CC, CH_2OCH_2, and CH_2OCH (reaction R15-26);
(2) Pressure-dependent reaction rate coefficients for reactions of $C_2H_4 + OH$, $C_2H_5 + O_2$, CH_2CO, CH_3CO, and CH_2CHO (reaction R3, R7, and R11-14);
(3) Reactions of $C_2H_4 + HO_2$, CH_2OCH_2, and CH_2OCH (reaction R6, R7a, and R21-26) for the low-temperature chemistry;
(4) Reactions related to the key intermediates for the aromatic precursor formation (C_2H_2, H_2CC, C_2H_3, and C_2H_5).

Comparison with the other chemical kinetic models [2,6,7,11–14,24] shows that the updated model demonstrates a good ability to predict auto-ignition delay times and laminar flame speeds, and satisfactory results for reproduction of concentration profiles. The model is well prepared for the next step of optimization: upgrade of C_2H_6 and C_2H_5OH sub-mechanisms and further improvement of the PAH formations reaction paths [2,7,62].

Problems of the inconsistency of the experimental data have been shown and discussed. The reported conflicting results of the used experimental data, measured by the different groups make it difficult to draw the final univocal conclusions about the studied kinetic model optimization.

More effort should be put into the development of the methods and numerical tools for the model quality analysis, data uncertainty, uncertainty propagation analyses and evaluation of the model valid parameter range. The simple comparison of simulations with measured data cannot be considered as a final assessment of model quality and model ability to reproduce the real natural micro-processes. Without such objective assessments, the different reaction mechanisms can be regarded as statistical samplings for gathering information about process and to make some assumptions about the entire system's behaviour.

CRediT authorship contribution statement

Hongxin Wang: Investigation, Writing - original draft. **Nadezda Slavinskaya:** Investigation, Methodology, Supervision. **Aziza Kanz:** Validation, Writing - review & editing. **Moldir Auyelkhankyzy:** Validation, Funding acquisition, Writing - review & editing. **Yiting Gao:** Investigation. **Oskar Haidn:** Methodology, Supervision.

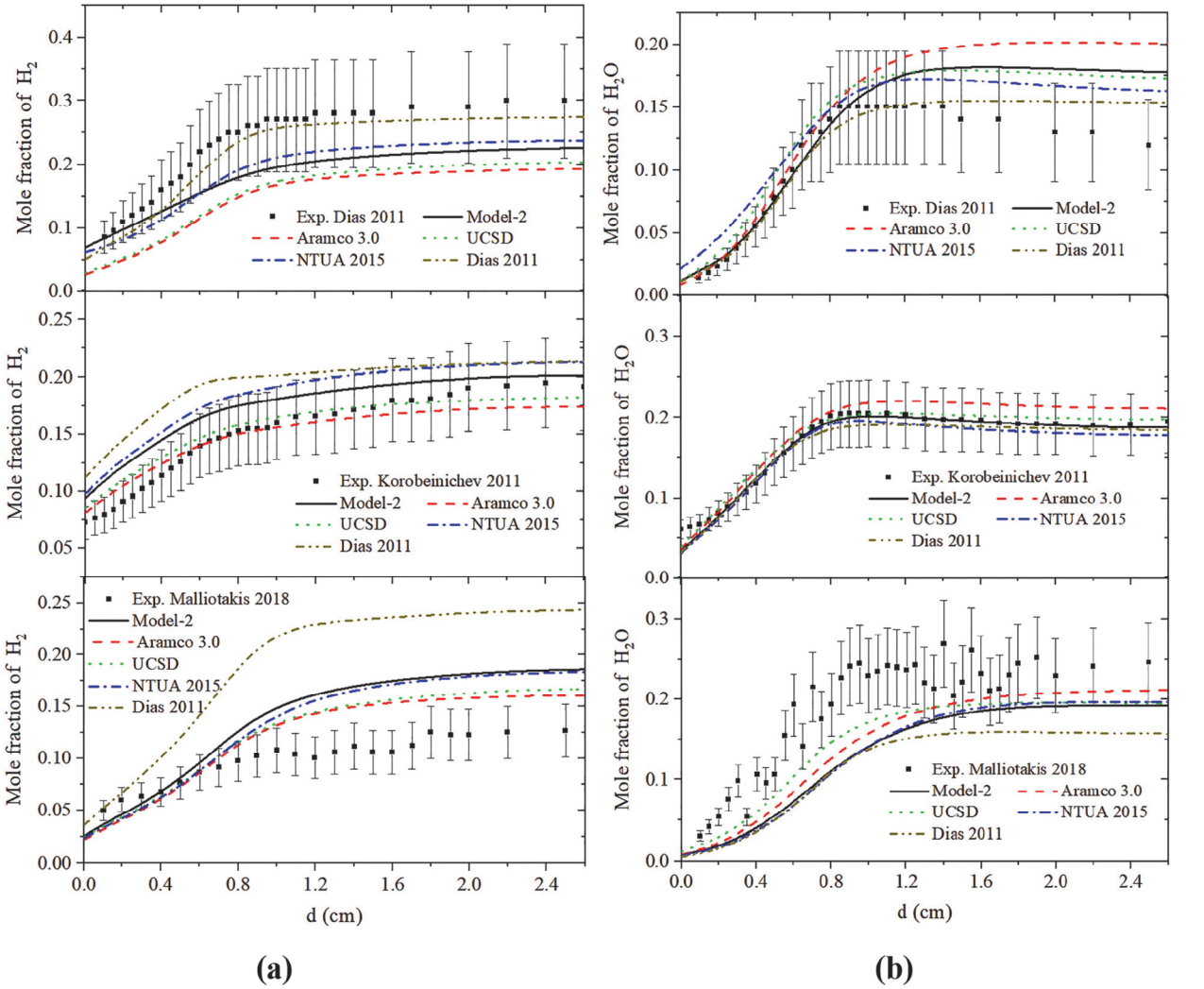

Fig. 13. Comparison of the concentration profiles measured by Dias et al. [7], Korobeinichev et al. [62] and Malliotakis et al. [2] and simulation results obtained with model-2, Aramco 3.0 [12], UCSD [13], Dias 2011 [7] and NTUA 2015 (Malliotakis et al.) [2]: (a) mole fractions of H_2; (b) mole fractions of H_2O.

Declaration of Competing Interest

The authors declare that they have no known competing financial interests or personal relationships that could have appeared to influence the work reported in this paper.

Acknowledgments

The authors would like to thank China Scholarship Council, and acknowledge the Ministry of Education and Science of Republic of Kazakhstan for funding this work through the project IRN AP05133755. The authors would also like to acknowledge the full financial support of one of the co-authors, Mrs. Kanz, by the DAAD German Academic Exchange Service within the framework of DLR-DAAD Research Fellowship.

Appendix A. Supplementary data

Supplementary data to this article can be found online at https://doi.org/10.1016/j.fuel.2021.120833.

References

[1] Shao J, Davidson DF, Hanson RK. A shock tube study of ignition delay times in diluted methane, ethylene, propene and their blends at elevated pressures. Fuel 2018;225:370–80.
[2] Malliotakis Z, Leplat N, Vourliotakis G, Keramiotis C, Skevis G, Founti MA, et al. An Experimental and Detailed Chemical Kinetic Investigation of the Addition of C2 Oxygenated Species in Rich Ethylene Premixed Flames. Combust Sci Technol 2018: 1–24.
[3] Kopp MM, Donato NS, Petersen EL, Metcalfe WK, Burke SM, Curran HJ. Oxidation of Ethylene-Air Mixtures at Elevated Pressures, Part 1: Experimental Results. J Propul Power 2014;30(3):790–8.
[4] Xu C, Konnov AA. Validation and analysis of detailed kinetic models for ethylene combustion. Energy 2012;43(1):19–29.
[5] Saxena S, Kahandawala MSP, Sidhu SS. A shock tube study of ignition delay in the combustion of ethylene. Combust Flame 2011;158(6):1019–31.
[6] Lopez JG, Rasmussen CL, Alzueta MU, Gao Y, Marshall P, Glarborg P. Experimental and kinetic modeling study of C2H4 oxidation at high pressure. Proc Combust Inst 2009;32(1):367–75.
[7] Dias V, Vandooren J. Experimental and modeling studies of C2H4/O2/Ar, C2H4/methylal/O2/Ar and C2H4/ethylal/O2/Ar rich flames and the effect of oxygenated additives. Combust Flame 2011;158(5):848–59.
[8] Ibarreta AF, Sung C-J, Wang H. Experimental characterization of premixed spherical ethylene/air flames under sooting conditions. Proc Combust Inst 2007;31 (1):1047–54.
[9] Chernov V, Thomson MJ, Dworkin SB, Slavinskaya NA, Riedel U. Soot formation with C1 and C2 fuels using an improved chemical mechanism for PAH growth. Combust Flame 2014;161(2):592–601.

[10] Dworkin SB, Zhang Q, Thomson MJ, Slavinskaya NA, Riedel U. Application of an enhanced PAH growth model to soot formation in a laminar coflow ethylene/air diffusion flame. Combust Flame 2011;158(9):1682–95.

[11] Wang H, You X, Joshi AV, Davis SG, Laskin A, Egolfopoulos F, et al. USC Mech Version II. High-Temperature Combustion Reaction Model of H2/CO/C1-C4 Compounds. http://ignisuscedu/USC_Mech_IIhtm May 2007.

[12] Zhou C-W, Li Y, Burke U, Banyon C, Somers KP, Ding S, et al. An experimental and chemical kinetic modeling study of 1,3-butadiene combustion: Ignition delay time and laminar flame speed measurements. Combust Flame 2018;197:423–38.

[13] Chemical-Kinetic Mechanisms for Combustion Applications Mechanical and Aerospace Engineering (Combustion Research), University of California at San Diego, San Diego Mechanism web page, http://combustion.ucsd.edu.

[14] Konnov AA. Implementation of the NCN pathway of prompt-NO formation in the detailed reaction mechanism. Combust Flame 2009;156(11):2093–105.

[15] Methling T, Braun-Unkhof M, Riedel U. An optimised chemical kinetic model for the combustion of fuel mixtures of syngas and natural gas. Fuel 2020;262:116611. https://doi.org/10.1016/j.fuel.2019.116611.

[16] Slavinskaya N, Mirzayeva A, Whitside R, Starke J, Abbasi M, Auyelkhankyzy M, et al. A modelling study of acetylene oxidation and pyrolysis. Combust Flame 2019;210:25–42.

[17] Wei B, Xu X, Yan M, Shi X, Yang Y. Study on aeroramp injector/gas-pilot flame in a supersonic combustor. J Propul Power 2012;28(3):486–95.

[18] Wei B, Zhang Y, Tian L, Song G, Xu X. Experimental study on combustion mode transition in an aero-ramp based scramjet. 48th AIAA/ASME/SAE/ASEE Joint Propulsion Conference & Exhibit. 2012;3923.

[19] Werling L, Perakis N, Hochheimer B, Ciezki HK, Schlechtriem S. Experimental investigations based on a demonstrator unit to analyze the combustion process of a nitrous oxide/ethene premixed green bipropellant. 5th CEAS Air & Space Conference. 7. 2015.

[20] Perakis N, Werling L, Ciezki H, Schlechtriem S. Numerical Calculation of Heat Flux Profiles in a N2O/C2H4 Premixed Green Propellant Combustor using an Inverse Heat Conduction Method. Space Propulsion Conference. 1. 2016.

[21] Eckel G, Grohmann J, Cantu L, Slavinskaya N, Kathrotia T, Rachner M, et al. LES of a swirl-stabilized kerosene spray flame with a multi-component vaporization model and detailed chemistry. Combust Flame 2019;207:134–52.

[22] Slavinskaya NA, Riedel U, Dworkin SB, Thomson MJ. Detailed numerical modeling of PAH formation and growth in non-premixed ethylene and ethane flames. Combust Flame 2012;159(3):979–95.

[23] Valencia-López AM, Bustamante F, Loukou A, Stelzner B, Trimis D, Frenklach M, et al. Effect of benzene doping on soot precursors formation in non-premixed flames of producer gas (PG). Combust Flame 2019;207:265–80.

[24] Smith GP, Golden DM, Frenklach M, Moriarty NW, Eiteneer B, Goldenberg M, et al. GRI 3.0 Mechanism. Gas Research Institute (http://combustion.berkeley.edu/gri-mech/) 1999.

[25] Qin Z, Lissianski VV, Yang H, Gardiner WC, Davis SG, Wang H. Combustion chemistry of propane: a case study of detailed reaction mechanism optimization. Proc Combust Inst 2000;28(2):1663–9.

[26] Slavinskaya N, Abbasi M, Starcke J-H, Mirzayeva A, Haidn OJ. Skeletal mechanism of the methane oxidation for space propulsion applications. 52nd AIAA/SAE/ASEE Joint Propulsion Conference. 2016;4781.

[27] Slavinskaya N, Abbasi M, Starcke JH, Whitside R, Mirzayeva A, Riedel U, et al. Development of an uncertainty quantification predictive chemical reaction model for syngas combustion. Energy Fuels 2017;31(3):2274–97.

[28] DESIGNS ME. Chemkin-pro. 2011.

[29] Fokin LR, Slavinskaya N. Thermophysical parameter correlation for low-density gas mixtures: Ar-Xe. Institute for High Temperatures, USSR Academy of Sciences 1987;25(1):40–5.

[30] Sokolov S, Silin I. "Preprint JINR D-810," Dubna 1961.

[31] Kurbatov V, Silin I. New method for minimizing regular functions with constraints on parameter region. Nucl Instrum Methods Phys Res, Sect A 1994;345(2):346–50.

[32] Baulch DL, Bowman CT, Cobos CJ, Cox RA, Just T, Kerr JA, et al. Evaluated Kinetic Data for Combustion Modeling: Supplement II. J Phys Chem Ref Data 2005;34(3):757–1397.

[33] Nagy T, Valkó É, Sedyó I, Zsély IG, Pilling MJ, Turányi T. Uncertainty of the rate parameters of several important elementary reactions of the H2 and syngas combustion systems. Combust Flame 2015;162(5):2059–76.

[34] Manion J, Huie R, Levin R, Burgess Jr D, Orkin V, Tsang W, et al. NIST chemical kinetics database. NIST standard reference database 2008;17:20899–8320.

[35] Baulch D, Bowers M, Malcolm D, Tuckerman R. Evaluated Kinetic Data for High-Temperature Reactions. Volume 5. Part 1. Homogeneous Gas Phase Reactions of the Hydroxyl Radical with Alkanes. J Phys Chem Ref Data 1986;15(2):465–592.

[36] Baulch D, Cobos C, Cox R, Esser C, Frank PT, Just JAK, et al. J Phys Chem Ref Data 1992;21(3):411–569.

[37] Baulch DL, Cobos CJ, Cox RA, Frank P, Hayman G, Just T, et al. Evaluated Kinetic Data for Combustion Modeling. Supplement I. J Phys Chem Ref Data 1994;23(6):847–8.

[38] Warnatz J. Rate coefficients in the C/H/O system. Combustion chemistry. Springer 1984:197–360.

[39] Tsang W, Hampson RF. Chemical Kinetic Data Base for Combustion Chemistry. Part I. Methane and Related Compounds. J Phys Chem Ref Data 1986;15(3):1087–279.

[40] Ali MA, Upendra B, Rajakumar B. Kinetic parameters of abstraction reactions of OH radical with ethylene, fluoroethylene, cis-and trans-1, 2-difluoroethylene and 1, 1-difluoroethylene, in the temperature range of 200–400 K: Gaussian-3/B3LYP theory. Chem Phys Lett 2011;511(4–6):440–6.

[41] Senosiain JP, Klippenstein SJ, Miller JA. Reaction of ethylene with hydroxyl radicals: a theoretical study. The Journal of Physical Chemistry A 2006;110(21):6960–70.

[42] Liu G, Ding Y, Li Z, Fu Q, Huang X, Sun C, et al. Theoretical study on mechanisms of the high-temperature reactions C2H3 + H2O and C2H4 + OH. PCCP 2002;4(6):1021–7.

[43] Westbrook CK, Thornton MM, Pitz WJ, Malte PC. A kinetic study of ethylene oxidation in a well-stirred reactor. Symp (Int) Combust 1989;22(1):863–71.

[44] Tully FP. Hydrogen-atom abstraction from alkenes by OH, ethene and 1-butene. Chem Phys Lett 1988;143(5):510–4.

[45] Liu A-D, Mulac WA, Jonah CD. Pulse radiolysis study of the reaction of OH radicals with C2H4 over the temperature range 343–1173 K. Int J Chem Kinet 1987;19(1):25–34.

[46] Hughes K, Turányi T, Clague A, Pilling M. Development and testing of a comprehensive chemical mechanism for the oxidation of methane. Int J Chem Kinet 2001;33(9):513–38.

[47] Slavinskaya N, Frank P. A modelling study of aromatic soot precursors formation in laminar methane and ethene flames. Combust Flame 2009;156(9):1705–22.

[48] Brown CJ, Thomas GO. Experimental studies of shock-induced ignition and transition to detonation in ethylene and propane mixtures. Combust Flame 1999;117(4):861–70.

[49] Colket MB, Spadaccini LJ. Scramjet Fuels Autoignition Study. J Propul Power 2001;17(2):315–23.

[50] Kalitan DM, Hall JM, Petersen EL. Ignition and Oxidation of Ethylene-Oxygen-Diluent Mixtures with and Without Silane. J Propul Power 2005;21(6):1045–56.

[51] Penyazkov OG, Sevrouk KL, Tangirala V, Joshi N. High-pressure ethylene oxidation behind reflected shock waves. Proc Combust Inst 2009;32(2):2421–8.

[52] Deng F, Pan Y, Sun W, Yang F, Zhang Y, Huang Z. Comparative Study of the Effects of Nitrous Oxide and Oxygen on Ethylene Ignition. Energy Fuels 2017;31(12):14116–28.

[53] Hassan MI, Aung KT, Kwon OC, Faeth GM. Properties of Laminar Premixed Hydrocarbon/Air Flames at Various Pressures. J Propul Power 1998;14(4):479–88.

[54] Hirasawa T, Sung CJ, Joshi A, Yang Z, Wang H, Law CK. Determination of laminar flame speeds using digital particle image velocimetry: Binary Fuel blends of ethylene, n-Butane, and toluene. Proc Combust Inst 2002;29(2):1427–34.

[55] Jomaas G, Zheng XL, Zhu DL, Law CK. Experimental determination of counterflow ignition temperatures and laminar flame speeds of C2–C3 hydrocarbons at atmospheric and elevated pressures. Proc Combust Inst 2005;30(1):193–200.

[56] Kumar K, Mittal G, Sung C, Law C. An experimental investigation of ethylene/O2/diluent mixtures: Laminar flame speeds with preheat and ignition delays at high pressures. Combust Flame 2008;153(3):343–54.

[57] Park O, Veloo PS, Egolfopoulos FN. Flame studies of C2 hydrocarbons. Proc Combust Inst 2013;34(1):711–8.

[58] Ravi S, Sikes TG, Morones A, Keesee CL, Petersen EL. Comparative study on the laminar flame speed enhancement of methane with ethane and ethylene addition. Proc Combust Inst 2015;35(1):679–86.

[59] Van Treek L, Roth N, Seidel L, Mauß F. Measurements of the laminar burning velocities of rich ethylene/air mixtures. Fuel 2020;275:117938.

[60] Xu F, Sunderland P, Faeth G. Soot formation in laminar premixed ethylene/air flames at atmospheric pressure. Combust Flame 1997;108(4):471–93.

[61] Delfau J-L, Biet J, Idir M, Pillier L, Vovelle C. Experimental and numerical study of premixed, lean ethylene flames. Proc Combust Inst 2007;31(1):357–65.

[62] Korobeinichev OP, Yakimov SA, Knyazkov DA, Bolshova TA, Shmakov AG, Yang J, et al. A study of low-pressure premixed ethylene flame with and without ethanol using photoionization mass spectrometry and modeling. Proc Combust Inst 2011;33(1):569–76.

[63] Egolfopoulos FN, Zhu DL, Law CK. Experimental and numerical determination of laminar flame speeds: Mixtures of C2-hydrocarbons with oxygen and nitrogen. Symp (Int) Combust 1991;23(1):471–8.

[64] Olm C, Varga T, Valkó É, Hartl S, Hasse C, Turányi T. Development of an Ethanol Combustion Mechanism Based on a Hierarchical Optimization Approach. Int J Chem Kinet 2016;48(8):423–41.

[65] Walter G, Wang H, Kanz A, Kolbasseff A, Xu X, Haidn O, et al. Experimental error assessment of laminar flame speed measurements for digital chemical kinetics databases. Fuel 2020;266.

[66] You X, Packard A, Frenklach M. Process informatics tools for predictive modeling: Hydrogen combustion. Int J Chem Kinet 2012;44(2):101–16.

[67] Morin J, Bedjanian Y. Reaction of O (3P) with C2H4: Yield of the Reaction Products as a Function of Temperature. The Journal of Physical Chemistry A 2016;120(45):9063–70.

[68] Morin J, Bedjanian Y, Romanias MN. Rate Constants of the Reactions of O (3P) Atoms with Ethene and Propene over the Temperature Range 230–900 K. Int J Chem Kinet 2017;49(1):53–60.

[69] Laskin A, Wang H, Law CK. Detailed kinetic modeling of 1,3-butadiene oxidation at high temperatures. Int J Chem Kinet 2000;32(10):589–614.

[70] Wang H. A new mechanism for initiation of free-radical chain reactions during high-temperature, homogeneous oxidation of unsaturated hydrocarbons: Ethylene, propyne, and allene. Int J Chem Kinet 2001;33(11):698–706.

[71] Rickard M, Hall J, Petersen E. Effect of silane addition on acetylene ignition behind reflected shock waves. Proc Combust Inst 2005;30(2):1915–23.

[72] Eiteneer B, Frenklach M. Experimental and modeling study of shock-tube oxidation of acetylene. Int J Chem Kinet 2003;35(9):391–414.

[73] Hidaka Y, Hattori K, Okuno T, Inami K, Abe T, Koike T. Shock-tube and modeling study of acetylene pyrolysis and oxidation. Combust Flame 1996;107(4):401–17.

[74] Fournet R, Bauge J, Battin-Leclerc F. Experimental and modeling of oxidation of acetylene, propyne, allene and 1, 3-butadiene. Int J Chem Kinet 1999;31(5): 361 79.
[75] Wang H, Sheen DA. Combustion kinetic model uncertainty quantification, propagation and minimization. Prog Energy Combust Sci 2015;47:1–31.
[76] Goldsmith CF, Harding LB, Georgievskii Y, Miller JA, Klippenstein SJ. Temperature and pressure-dependent rate coefficients for the reaction of vinyl radical with molecular oxygen. The Journal of Physical Chemistry A 2015;119(28):7766–79.
[77] Mebel A, Diau E, Lin M, Morokuma K. Ab initio and RRKM calculations for multichannel rate constants of the C2H3+ O2 reaction. J Am Chem Soc 1996;118 (40):9759–71.
[78] Marinov NM, Pitz WJ, Westbrook CK, Vincitore AM, Castaldi MJ, Senkan SM, et al. Aromatic and Polycyclic Aromatic Hydrocarbon Formation in a Laminar Premixed n-Butane Flame. Combust Flame 1998;114(1–2):192–213.
[79] Nguyen TL, Vereecken L, Hou XJ, Nguyen MT, Peeters J. Potential energy surfaces, product distributions and thermal rate coefficients of the reaction of O(3P) with C2H4(X1Ag): a comprehensive theoretical study. The Journal of Physical Chemistry A 2005;109(33):7489–99.
[80] Balucani N, Leonori F, Casavecchia P, Fu B, Bowman JM. Crossed molecular beams and quasiclassical trajectory surface hopping studies of the multichannel nonadiabatic O (3P)+ ethylene reaction at high collision energy. The Journal of Physical Chemistry A 2015;119(50):12498–511.
[81] Li X, Jasper AW, Zádor J, Miller JA, Klippenstein SJ. In: Proceedings of the Combustion Institute; 2017. p. 219–27.
[82] Kopp MM, Petersen EL, Metcalfe WK, Burke SM, Curran HJ. Oxidation of Ethylene—Air Mixtures at Elevated Pressures, Part 2: Chemical Kinetics. J Propul Power 2014;30(3):799–811.

Supplementary Material - 1

A Comprehensive Kinetic Modelling Study of Ethylene Combustion with Data Uncertainty Analysis

Hongxin Wang[a], Nadezda Slavinskaya[b, c], Aziza Kanz[d], Moldir Auyelkhankyzy[c, e], Yiting Gao[a], Oskar Haidn[a]

a. Department of Aerospace and Geodesy, Technical University of Munich, 85748 Garching, Germany

b. GRS Association for Plant and Reactor Safety, 85748 Garching, Germany

c. Al-Farabi Kazakh National University, 050040 Almaty, Kazakhstan

d. DLR German Aerospace Center, Institute of Combustion Technology, 70569 Stuttgart, Germany

e. Institute of Combustion Problems, 050012 Almaty, Kazakhstan

An overview of ethylene oxidation models published in the last two decades and their experimental validations.

Table S1-1. Overview of recent studies on major C_2 kinetic mechanisms and their experimental validations on the oxidation of C_2H_4.

Model	Ignition delay time	Concentration profile	Laminar flame speed
J. Lopez et al. [1]		plug flow reactor [1] p = 60 bar T = 600–900 K $C_2H_4/O_2/N_2$ φ = 0.2, 0.98, 19.8	
USC 2.0 [2] UCSD [3]	shock tube [4, 5] p_5 = 1.1–60 atm, T_5 = 950–1800 K C_2H_4/O_2/Ar, φ = 0.3 - 2.0 rapid compression machine [6] p = 15, 30, 50 bar T = 850–1050 K $C_2H_4/O_2/N_2$/Ar, φ = 1.0		[6-13] p = 0.5–5 atm T_0 = 298, 360, 400, 470 K mixture: C_2H_4/Air
Aramco [14]	shock tube [4, 5, 15-17] p_5 = 1.1–60 atm, T_5 = 950–1800 K C_2H_4/O_2/Ar, φ = 0.3–2.0 C_2H_4/air, φ = 0.5–2.0	plug flow reactor [1] p = 60 bar T = 600–900 K $C_2H_4/O_2/N_2$, φ = 0.981	[6-13, 18] p = 1, 2, 5 atm T_0 = 298 K C_2H_4/Air
A. Konnov [19] N. Marinov et al. [20]	shock tube [16, 21] p_5 = 1, 2, 3 bar, T_5 = 1100–1740 K C_2H_4/O_2/Ar, φ = 1.0, 2.0		[6, 8-13] p = 0.5, 1, 2, 5 atm, T_0 = 298, 360, 400, 470 K C_2H_4/Air
Dias [22, 23]		premixed flat flame [22, 23] p = 0.05 bar φ = 2.5, 33%C_2H_4+40%O_2+27%Ar	
Korobeinichev [24]		premixed flat flame [24] p = 0.04 bar φ = 2.0 28%C_2H_4+42%O_2+30%Ar	
This study	shock tube [4, 5, 15-17, 25, 26] p_5 = 1-60 atm, T_5 = 1000–2238 K C_2H_4/O_2/Ar, φ = 0.5-3.0 $C_2H_4/O_2/N_2$, φ = 1.0 C_2H_4/air, φ = 0.3-2.0	premixed flat flame [23, 24, 27-29] C_2H_4/O_2/Ar, $C_2H_4/O_2/N_2$	[6, 7, 9, 11, 12, 18, 30] p = 0.5, 1, 2, 5 atm, T_0 = 298, 360, 400, 470 K C_2H_4/Air

Modeling studies focusing on C_2H_4 oxidation in the past ten years are collected and accomplished with experimental data used for models' validation, as shown in Table S1-1.

Lopez et al. [1] updated a mechanism for ethylene oxidation using data measured in a high-pressure plug flow reactor based on the earlier studied combustion models of CO/H_2, CH_4, and CH_4/C_2H_6 proposed by Rasmussen and Glarborg et al. [31, 32]. In this work [1], the importance of the hydroxyethyl and 2-hydroperoxyethyl radicals, formed from the addition of OH and HO_2 to C_2H_4, and vinyl peroxide, formed from $C_2H_3+O_2$, was studied in details.

Wang et al. [2] developed a mechanism of 111 species and 784 reactions for H2/CO/C_1-C_4 kinetic modeling based on their former studies on H_2/CO [33], C_3 fuel [34], 1,3-butadiene [35], ethylene and acetylene [36] combustion. This USC 2.0 mechanism has been validated for a wide variety of C_2H_4 combustion scenarios [10-12, 17, 37-40], but some of these experimental data were published a long time ago so that they will not be considered as validation data in this study. The combustion research group of University California, San Diego (UCSD) proposed a reaction model [3] with sub-mechanisms for the chemistry of JP10, heptane, and dimethyl ether, and updates were made to several sensitive reactions involving formaldehyde, methane, ethane, ethylene, acetylene, and methanol in 2005 [3]. Kumar et al. [6] applied these two models [2, 3] to simulate their laminar flame speeds measured in a counterflow configuration burner and ignition delay times measured in a rapid compression machine. Analysis of reaction flow and sensitivity for ignition delay times at low-temperature and high-pressure conditions and laminar flame speeds at high-temperature conditions were conducted to compare the two mechanisms. The analysis reveals that the main difference between the two mechanisms is the channels related to CH_2O and CH_2CHO which are important intermediates for the oxidation of C_2H_4, and the UCSD mechanism showed better agreements with both laminar flame speeds and ignition delay times than the USC 2.0.

Kopp et al. [14] updated the C_2H_4 sub-mechanism of AramcoMech, which was developed by Metcalfe et al. [41] for C_1-C_4 chemistry. In this work [14], the chemical kinetic model was improved to better agree with the ignition delay time data measured in shock tube experiments for undiluted C_2H_4-air mixtures [5], although the model still tends to over-predict ignition delay times at low pressures for the fuel-lean cases. Kopp et al. [14] also compared the optimized model with mechanisms of USC 2.0 and UCSD, and the comparison shows that their study can be used to make further improvements in the mechanisms from other groups.

Marinov et al. [20] in Lawrence Livermore National Laboratory (LLNL) conducted an experimental work of atmospheric pressure premixed n-Butane flat flame and developed a detailed chemical kinetic model for C_1-C_4 with PAH formation. Konnov [19] developed a detailed reaction mechanism for small hydrocarbons combustion including reactions of

nitrogen focusing on reactions of NO, CN, NCN and HNCN. In the study of Xu and Konnov [13], mechanisms of Konnov [19], USC 2.0 [2], UCSD [3] and LLNL [20] were validated for C_2H_4 oxidation with experimental data of ignition delays [13, 16, 21, 28, 29] and laminar flame speeds [6, 8-13]. Differences in reaction rate constants and routes of C_2H_4 and vinyl chemistry were analyzed and discussed. The results show that H-O and C_1 chemistry reactions significantly influence the laminar flame speeds in lean C_2H_4/air flames, while C_2 chemistry reactions become of increasing importance in fuel-rich flames.

Dias et al. [22, 23] used a Spalding–Botha type burner to investigate the effect of the addition of methylal ($C_3H_8O_2$) and ehtylal ($C_5H_{12}O_2$), and a kinetic model was elaborated to simulate the investigated flames. Malliotakis et al. [29] studied the addition of C2 oxygenated species in rich C_2H_4 premixed flames with the flat flame burner at the University of Louvain (UCL), and detailed kinetic mechanisms of NTUA [42, 43] and UCL [44-46] were utilized for analysis.

Korobeinichev et al. [24] conducted an experimental study to understand the influence of ethanol on the process of polycyclic aromatic hydrocarbons (PAH) and soot formation in C_2H_4 flames. A detailed mechanism composed of the mechanisms of Marinov et al. [47] and Appel et al. [48] was applied to analyze the benzene formation in C_2H_4 flames.

References:

[1] Lopez JG, Rasmussen CL, Alzueta MU, Gao Y, Marshall P, Glarborg P. Experimental and kinetic modeling study of C2H4 oxidation at high pressure. Proceedings of the Combustion Institute 2009;32(1):367-75.

[2] Wang H, You X, Joshi AV, Davis SG, Laskin A, Egolfopoulos F, et al. USC Mech Version II. High-Temperature Combustion Reaction Model of H2/CO/C1-C4 Compounds. http://ignisuscedu/USC_Mech_IIhtm May 2007.

[3] Chemical-Kinetic Mechanisms for Combustion Applications. Mechanical and Aerospace Engineering (Combustion Research), University of California at San Diego, San Diego Mechanism web page, http://combustionucsdedu.

[4] Shao J, Davidson DF, Hanson RK. A shock tube study of ignition delay times in diluted methane, ethylene, propene and their blends at elevated pressures. Fuel 2018;225:370-80.

[5] Kopp MM, Donato NS, Petersen EL, Metcalfe WK, Burke SM, Curran HJ. Oxidation of Ethylene–Air Mixtures at Elevated Pressures, Part 1: Experimental Results. Journal of Propulsion and Power 2014;30(3):790-8.

[6] Kumar K, Mittal G, Sung C, Law C. An experimental investigation of ethylene/O2/diluent mixtures: Laminar flame speeds with preheat and ignition delays at high pressures. Combustion and Flame 2008;153(3):343-54.

[7] Park O, Veloo PS, Egolfopoulos FN. Flame studies of C2 hydrocarbons. Proceedings of the Combustion Institute 2013;34(1):711-8.

[8] Coppens F, Deruyck J, Konnov A. The effects of composition on burning velocity and nitric oxide formation in laminar premixed flames of CH4 + H2 + O2 + N2. Combustion and Flame 2007;149(4):409-17.

[9] Hirasawa T, Sung CJ, Joshi A, Yang Z, Wang H, Law CK. Determination of laminar flame speeds using digital particle image velocimetry: Binary Fuel blends of ethylene, n-Butane, and toluene. Proceedings of the

Combustion Institute 2002;29(2):1427-34.
[10] Egolfopoulos FN, Zhu DL, Law CK. Experimental and numerical determination of laminar flame speeds: Mixtures of C2-hydrocarbons with oxygen and nitrogen. Symposium (International) on Combustion 1991;23(1):471-8.
[11] Jomaas G, Zheng XL, Zhu DL, Law CK. Experimental determination of counterflow ignition temperatures and laminar flame speeds of C2–C3 hydrocarbons at atmospheric and elevated pressures. Proceedings of the Combustion Institute 2005;30(1):193-200.
[12] Hassan MI, Aung KT, Kwon OC, Faeth GM. Properties of Laminar Premixed Hydrocarbon/Air Flames at Various Pressures. Journal of Propulsion and Power 1998;14(4):479-88.
[13] Xu C, Konnov AA. Validation and analysis of detailed kinetic models for ethylene combustion. Energy 2012;43(1):19-29.
[14] Kopp MM, Petersen EL, Metcalfe WK, Burke SM, Curran HJ. Oxidation of Ethylene—Air Mixtures at Elevated Pressures, Part 2: Chemical Kinetics. Journal of Propulsion and Power 2014;30(3):799-811.
[15] Saxena S, Kahandawala MSP, Sidhu SS. A shock tube study of ignition delay in the combustion of ethylene. Combustion and Flame 2011;158(6):1019-31.
[16] Kalitan DM, Hall JM, Petersen EL. Ignition and Oxidation of Ethylene-Oxygen-Diluent Mixtures with and Without Silane. Journal of Propulsion and Power 2005;21(6):1045-56.
[17] Brown CJ, Thomas GO. Experimental studies of shock-induced ignition and transition to detonation in ethylene and propane mixtures. Combustion and Flame 1999;117(4):861-70.
[18] Ravi S, Sikes TG, Morones A, Keesee CL, Petersen EL. Comparative study on the laminar flame speed enhancement of methane with ethane and ethylene addition. Proceedings of the Combustion Institute 2015;35(1):679-86.
[19] Konnov AA. Implementation of the NCN pathway of prompt-NO formation in the detailed reaction mechanism. Combustion and Flame 2009;156(11):2093-105.
[20] Marinov NM, Pitz WJ, Westbrook CK, Vincitore AM, Castaldi MJ, Senkan SM, et al. Aromatic and Polycyclic Aromatic Hydrocarbon Formation in a Laminar Premixed n-Butane Flame. Combustion and Flame 1998;114(1-2):192-213.
[21] Baker JA, Skinner GB. Shock-tube studies on the ignition of ethylene-oxygen-argon mixtures. Combustion and Flame 1972;19(3):347-50.
[22] Dias V, Renard C, Vandooren J. Modeling of Rich Premixed C2H4/O2/Ar and C2H4/Dimethoxymethane/O2/Ar Flames. Zeitschrift für Physikalische Chemie 2009;223(4-5):565-77.
[23] Dias V, Vandooren J. Experimental and modeling studies of C2H4/O2/Ar, C2H4/methylal/O2/Ar and C2H4/ethylal/O2/Ar rich flames and the effect of oxygenated additives. Combustion and Flame 2011;158(5):848-59.
[24] Korobeinichev OP, Yakimov SA, Knyazkov DA, Bolshova TA, Shmakov AG, Yang J, et al. A study of low-pressure premixed ethylene flame with and without ethanol using photoionization mass spectrometry and modeling. Proceedings of the Combustion Institute 2011;33(1):569-76.
[25] Colket MB, Spadaccini LJ. Scramjet Fuels Autoignition Study. Journal of Propulsion and Power 2001;17(2):315-23.
[26] Penyazkov OG, Sevrouk KL, Tangirala V, Joshi N. High-pressure ethylene oxidation behind reflected shock waves. Proceedings of the Combustion Institute 2009;32(2):2421-8.
[27] Xu F, Sunderland P, Faeth G. Soot formation in laminar premixed ethylene/air flames at atmospheric pressure. Combustion and Flame 1997;108(4):471-93.
[28] Delfau J-L, Biet J, Idir M, Pillier L, Vovelle C. Experimental and numerical study of premixed, lean ethylene

flames. Proceedings of the Combustion Institute 2007;31(1):357-65.
[29] Malliotakis Z, Leplat N, Vourliotakis G, Keramiotis C, Skevis G, Founti MA, et al. An Experimental and Detailed Chemical Kinetic Investigation of the Addition of C2 Oxygenated Species in Rich Ethylene Premixed Flames. Combustion Science and Technology 2018:1-24.
[30] Van Treek L, Roth N, Seidel L, Mauß F. Measurements of the laminar burning velocities of rich ethylene/air mixtures. Fuel 2020;275:117938.
[31] Rasmussen CL, Jakobsen JG, Glarborg P. Experimental measurements and kinetic modeling of CH4/O2and CH4/C2H6/O2conversion at high pressure. International Journal of Chemical Kinetics 2008;40(12):778-807.
[32] Rasmussen CL, Hansen J, Marshall P, Glarborg P. Experimental measurements and kinetic modeling of CO/H2/O2/NOxconversion at high pressure. International Journal of Chemical Kinetics 2008;40(8):454-80.
[33] Davis SG, Joshi AV, Wang H, Egolfopoulos F. An optimized kinetic model of H2/CO combustion. Proceedings of the Combustion Institute 2005;30(1):1283-92.
[34] Davis SG, Law CK, Wang H. Propene pyrolysis and oxidation kinetics in a flow reactor and laminar flames. Combustion and Flame 1999;119(4):375-99.
[35] Laskin A, Wang H, Law CK. Detailed kinetic modeling of 1,3-butadiene oxidation at high temperatures. International Journal of Chemical Kinetics 2000;32(10):589-614.
[36] Wang H, Laskin A. A comprehensive kinetic model of ethylene and acetylene oxidation at high temperatures. Progress Report for an AFOSR New World Vista Program 1998.
[37] Hidaka Y, Nishimori T, Sato K, Henmi Y, Okuda R, Inami K, et al. Shock-tube and modeling study of ethylene pyrolysis and oxidation. Combustion and Flame 1999;117(4):755-76.
[38] Homer JB, Kistiakowsky G. Oxidation and pyrolysis of ethylene in shock waves. The Journal of Chemical Physics 1967;47(12):5290-5.
[39] Bhargava A, Westmoreland PR. Measured Flame Structure and Kinetics in a Fuel-Rich Ethylene Flame. Combustion and Flame 1998;113(3):333-47.
[40] Sun C, Sung C, Wang H, Law CK. On the structure of nonsooting counterflow ethylene and acetylene diffusion flames. Combustion and flame 1996;107(4):321-35.
[41] Metcalfe WK, Burke SM, Ahmed SS, Curran HJ. A Hierarchical and Comparative Kinetic Modeling Study of C1− C2Hydrocarbon and Oxygenated Fuels. International Journal of Chemical Kinetics 2013;45(10):638-75.
[42] Vourliotakis G, Skevis G, Founti MA. A Detailed Kinetic Modeling Study of Benzene Oxidation and Combustion in Premixed Flames and Ideal Reactors. Energy & Fuels 2011;25(5):1950-63.
[43] Vourliotakis G, Skevis G, Founti MA. Some aspects of combustion chemistry of C1–C2 oxygenated fuels in low pressure premixed flames. Proceedings of the Combustion Institute 2015;35(1):437-45.
[44] Leplat N, Seydi A, Vandooren J. An Experimental Study of the Structure of a Stoichiometric Ethanol/Oxygen/Argon Flame. Combustion Science and Technology 2008;180(3):519-32.
[45] Leplat N, Vandooren J. Experimental Investigation and Numerical Simulation of the Structure of CH3CHO/O2/Ar Flames at Different Equivalence Ratios. Combustion Science and Technology 2010;182(4-6):436-48.
[46] Leplat N, Vandooren J. Numerical and experimental study of the combustion of acetic acid in laminar premixed flames. Combustion and Flame 2012;159(2):493-9.
[47] Marinov NM. A detailed chemical kinetic model for high temperature ethanol oxidation. International Journal of Chemical Kinetics 1999;31(3):183-220.
[48] Appel J, Bockhorn H, Frenklach M. Kinetic modeling of soot formation with detailed chemistry and physics: laminar premixed flames of C2 hydrocarbons. Combustion and flame 2000;121(1-2):122-36.

Supplementary Material - 2

A Comprehensive Kinetic Modelling Study of Ethylene Combustion with Data Uncertainty Analysis

Hongxin Wang[a], Nadezda Slavinskaya[b, c], Aziza Kanz[d], Moldir Auyelkhankyzy[c, e], Yiting Gao[a], Oskar Haidn[a]

a. Department of Aerospace and Geodesy, Technical University of Munich, 85748 Garching, Germany

b. GRS Association for Plant and Reactor Safety, 85748 Garching, Germany

c. Al-Farabi Kazakh National University, 050040 Almaty, Kazakhstan

d. DLR German Aerospace Center, Institute of Combustion Technology, 70569 Stuttgart, Germany

e. Institute of Combustion Problems, 050012 Almaty, Kazakhstan

Model analysis and reaction review

A discussion on the update of RRCs

Table S2-1. Parameters for Arrhenius equation and uncertainty factors, $k(T) = AT^n exp(-E_a/T)$, $k(T) = A_1 T^{n_1} exp\left(-\frac{E_{a1}}{T}\right) + A_2 T^{n_2} exp\left(-\frac{E_{a2}}{T}\right)$ for duplications (dup).

Reaction		Reference	ΔT, K	k, cm^3, s, mole, K		
				A	n	E_a, K
R1a	$C_2H_4+O_2=C_2H_3+H_2O$	Hua2005 [1]	300-2500	4.17E+03	2.99	28070.0
		Tsang1986 [2]	300-2500	4.20E+13	0.00	29000.0
R2	C_2H_4+O=products	Li2017 [3]	300-2500	7.58E+07	1.65	277.0
	f = 0.135 - 0.142	Morin2017 [4, 5]	230-902	5.20E+07	1.70	206.0
		Nguyen2005 [6]	200-2000	1.02E+08	1.66	331.0
		Baulch2005 [7]	220-2000	1.35E+07	1.88	92.0
		Baulch1992 [8]	300-2000	2.46E+06	2.08	0.0
		Klemm1990 [9]	1000-2300	5.80E+13	0.00	2770.0
		Mahmud1987 [10]	300-850	1.60E+08	1.44	267.0
		Klemm1987 dup1 [11]	244-1052	6.14E+12	0.00	753.0
		Klemm1987 dup2 [11]	244-1052	1.66E+14	0.00	4220.0
		Umemoto1985 [12]	240-450	8.39E+12	0.00	712.0
		Perry1984 [13]	258-861	1.28E+11	0.63	689.0
		Fonderie1984 [14]	300-850	1.10E+13	0.00	1010.0
		Browarzik1984 [15]	197-372	5.06E+12	0.00	758.0
		Nicovich1982 [16]	298-500	7.350E+12	0.00	870.0
		Singleton1976 [17]	298-400	6.980E+12	0.00	845.0
		Davis1972 [18]	232- 500	3.270E+12	0.00	569.0
		Fenimore1963 [19]	1400-1860	3.160E+13	0.00	0.0
		Elias1963 [20]	223- 613	8.430E+12	0.00	805.0
R3a	$C_2H_4+OH=C_2H_3+H_2O$	Ali2011 [21]	200-400	6.20E+11	0.00	1400.0
	f = 0.301 - 0.318	Senosiain2006 [22]	250-2500	1.31E-01	4.20	-433.0
		Liu2002 [23]	200-5000	2.10E+06	2.01	585.0
		Baulch1992 [8]	650-1500	2.05E+13	0.00	2990.0
		Westbrook1989 [24]	1003-1253	2.00E+13	0.00	2990.0
		Tully1988 [25]	650-901	2.02E+13	0.00	2990.0
		Liu1987 [26]	748-1170	1.45E+13	0.00	2100.0
		Tsang1986 [2]	300-2500	1.57E+04	2.75	2100.0
		Warnatz1984 [27]	500- 2000	3.00E+13	0.00	1500.0
R3b	$C_2H_4+OH=CH_2CH_2OH$	Golden2012 [28]	200-400	7.35E+12	-0.31	-431.0
	f = 0.143 - 0.149	Cleary2006 [29]	200-400	3.02E+12	0.00	-148.0
		Senosiain2006 dup1 [22]	250-2500	6.02E+37	-8.88	2602.0
		Senosiain2006 dup2 [22]	250-2500	4.46E+07	1.55	-787.0
		Zhu2005 [30]	200-500	1.81E+10	0.72	-425.0
		Zhu2005 [30]	600-3000	2.26E+05	2.28	-1241.0
		Yamada1999 [31]	290-450	1.00E+12	0.00	-463.0
		Yamada1999 [31]	450-700	3.89E+12	0.00	0.0
		Yamada1999 [31]	700-1200	6.19E+12	0.00	463.0
		Fulle1997 [32]	300- 800	6.03E+12	0.00	0.0
		Diau1992 [33]	544-590	2.41E+11	0.00	-1200.0

Reaction		Reference	ΔT, K	k, cm^3, s, mole, K		
				A	A	A
R3c	$C_2H_4+OH=CH_2O+CH_3$	Senosiain2006 [22]	250-2500	1.78E+05	1.68	1036.9
R3d	$C_2H_4+OH=C_2H_3OH+H$	Senosiain2006 [22]	250-2500	3.20E+05	2.19	2644.9
R3e	$C_2H_4+OH=CH_3CHO+H$	Senosiain2006 [22]	250-2500	2.38E-02	3.91	867.0
R4a	$C_2H_4+H=C_2H_3+H_2$	Huynh2007 [34]	300-3000	1.26E+05	2.75	5862.0
	f = 0.847 - 0.898	Baulch2005 [7]	400-2000	2.35E+02	3.62	5670.0
		Knyazev1996 [35]	200-3000	5.06E+07	1.93	6520.0
		Baulch1992 [8]	700-2000	5.42E+14	0.00	7500.0
		Manion1988 [36]	872-1080	1.00E14	0.00	7550.0
		Tsang1986 [2]	300-2500	1.32E+06	2.53	6160.3
		Warnatz1984 [27]	700-2000	1.50E+14	0.00	5140.4
		Just1977 [37]	1070-2000	5.00E+15	0.00	11500.4
R4b	$C_2H_4+H(+M)=C_2H_5(+M)$	Ding2011 [38]	200-3000	4.80E+08	1.50	1317.0
	(high-pressure limit)	Curran2006 [39]	298-2000	1.70E+10	1.07	729.7
	f = 0.22	Michael2005 [40]	200-2000	2.53E+08	1.75	604.9
		Miller2004 [41]	300-2000	1.40E+09	1.46	681.9
		Baulch1994 [42]	300-800	3.97E+09	1.28	650.0
		Feng1993 [43]	200-1100	1.08E+12	0.45	917.0
		Lightfoot1987 [44]	193-604	2.64E+13	0.00	1087.0
		Tsang1986 [2]	300-2500	8.42E+08	1.49	499.0
		Warnatz1984 [27]	700-2000	1.00E+13	0.00	757.7
		Sugawara1981 [45]	206-461	2.83E+13	0.00	1096.0
	$C_2H_4+H(+M)=C_2H_5(+M)$	Baulch2005 [7]	300-800	4.71E+18	0.00	380.0
	(low-pressure limit)	Miller2004 [41]	300-2000	2.00E+39	-6.64	2903.1
		Baulch1994 [42]	300-800	2.79E+18	0.00	380.0
		Lightfoot1987 [44]	193-607	5.04E+18	0.00	569.0
R5a$^-$	$C_2H_3+H=C_2H_4$	Harding2008[46]	200-2000	3.88E+13	0.20	0.0
		Duran1988 [47]	700-1300	5.36E+14	0.00	494.0
R6	$C_2H_4+HO_2=CH_2OCH_2+OH$	Baulch1992 [8]	600-900	2.23E+12	0.00	8650.0
		Baldwin1986[48]	673-773	2.82E+12	0.00	8610.0
		Baldwin1984[49]	673-773	3.80E+12	0.00	8980.0
R7a	$C_2H_5+O_2=C_2H_4+HO_2$	Klippenstein2017 [50]	300-2500	2.47E+09	0.51	582.2
	f = 0.231 - 0.241	Carstensen2005 [51]	300-850	2.43E+17	-1.90	2229.3
		DeSain2003 [52]	300-700	1.84E+07	1.13	-362.6
		Miller2001 [53]	300-2000	1.40E+07	1.09	-993.9
		Baulch1992 [8]	600-1200	1.02E+11	0.00	-1100.0
		Bozzelli1990 [54]	250-1200	2.56E+19	-2.77	995.0
		Tsang1986 [2]	300-2500	8.43E+11	0.00	1950.0
		Warnatz1984 [27]	700-2000	2.00E+12	0.00	2510.0
		Baldwin1980 [55]	673-813	5.51E+11	0.00	1950.0
		Baker1971 [56]	713-896	2.17E+11	0.00	694.0
		Cooke1971 [57]	1400-1800	3.16E+12	0.00	2520.0

Reaction		Reference	ΔT, K	k, cm^3, s, mole, K		
				A		
R7a	$C_2H_5+O_2=C_2H_4+HO_2$	Klippenstein2017 [50]	300-2500	2.47E+09	0.51	582.2
	f = 0.231 - 0.241	Carstensen2005 [51]	300-850	2.43E+17	-1.90	2229.3
		DeSain2003 [52]	300-700	1.84E+07	1.13	-362.6
		Miller2001 [53]	300-2000	1.40E+07	1.09	-993.9
		Baulch1992 [8]	600-1200	1.02E+11	0.00	-1100.0
		Bozzelli1990 [54]	250-1200	2.56E+19	-2.77	995.0
		Tsang1986 [2]	300-2500	8.43E+11	0.00	1950.0
		Warnatz1984 [27]	700-2000	2.00E+12	0.00	2510.0
		Baldwin1980 [55]	673-813	5.51E+11	0.00	1950.0
		Baker1971 [56]	713-896	2.17E+11	0.00	694.0
		Cooke1971 [57]	1400-1800	3.16E+12	0.00	2520.0
R7b	$C_2H_5+O_2=C_2H_5O_2$	Klippenstein2017 [50]	300-2500	3.98E+42	-9.86	4088.4
	f = 0.491 - 0.511	Fernandes2015 [58]	300-500	8.61E+14	-1.00	0.0
		Carstensen2005 [51]	300-850	9.42E+36	-8.01	3068.6
		DeSain2003 [52]	300-700	9.36E+59	-15.3	7120.0
		Sheng2002 [59]	300-1000	2.94E+13	-0.44	0.0
		Miller2001 [53]	298-2000	2.02E+10	0.98	-32.0
		Bozzelli1990 [60]	250-1200	2.00E+42	-10.3	3060.0
		Wagner1990 [61]	300-2000	2.21E+10	0.77	-287.0

Table S2-2. Update of RRCs for major initial reactions of C_2H_4 oxidation and key intermediates.

No.	Reaction	Reference	
		Model-1	Model-2
R1a	$C_2H_4+O_2=C_2H_3+H_2O$	Tsang1986 [2]	Hua2005 [1]
R1b	$C_2H_4+O_2=CH_2CHO+OH$	Glarborg1998 [62]	-
R2a	$C_2H_4+O=CH_3+HCO$	Baulch2005 [7]	Morin2017 [4, 5]
R2b	$C_2H_4+O=CH_2CHO+H$	Baulch2005 [7]	
R2c	$C_2H_4+O=CH_2O+CH_2$	-	
R2d	$C_2H_4+O=CH_2CO+H_2$	Baulch2005 [7]	
R3a	$C_2H_4+OH=C_2H_3+H_2O$	Vasu2010 [63]	Senosian2006 [22]
R3b	$C_2H_4+OH=CH_2O+CH_3$	Baulch2005 [7]	
R3c	$C_2H_4+OH=C_2H_3OH+H$		
R3d	$C_2H_4+OH=CH_3CHO+H$		
R3e	$C_2H_4+OH=CH_2CH_2OH$	Senosian2006 [22]	
R4a	$C_2H_4+H=C_2H_3+H_2$	Hughes2001 [64]	Huynh2007 [34]
R4b	$C_2H_4+H=C_2H_5$	Baulch1994 [7]	Miller2004 [41]
R5a	$C_2H_4=C_2H_3+H$	Hughes2001 [64]	Baulch2005 [7]
R5b	$C_2H_4= H_2CC+H_2$	Hughes2001 [64]	Laskin2000 [65]
R6	$C_2H_4+HO_2=CH_2OCH_2+OH$	-	Baulch2005 [7]

No.	Reaction	Reference	
		Original model	New model
R7a	$C_2H_5+O_2=C_2H_4+HO_2$	Marinov1996 [66]	Klippenstein2017 [50]
R7b	$C_2H_5+O_2=C_2H_5O_2$	Miller2001 [53]	
R7c	$C_2H_5+O_2=CH_2OCH_2+OH$	-	
R8a	$CH_3+CH_3=C_2H_5+H$	Hughes2001 [64]	Baulch2005 [7]
R8b	$C_2H_5+H=C_2H_4+H_2$	-	
R8c	$C_2H_5+H=C_2H_6$	-	Wang2003 [67]
R9a	$C_2H_5+O=CH_2O+CH_3$	-	Slagle1988 [68]
R9b	$C_2H_5+O=CH_3CHO+H$	-	
R9c	$C_2H_5+O=C_2H_4+OH$	-	
R10	$CH_2CO+O=HCCO+OH$	-	Xiong2014 [69]
R11a	$CH_2CO+H=HCCO+H_2$	-	Zhou2008 [70]
R11b	$CH_2CO+H=CH_3+CO$	Frank1986 [71]	Senosiain2006 [72]
R11c	$CH_2CO+H=CH_2CHO$	Senosiain2006 [72]	
R11d	$CH_2CO+H=CH_3CO$	Senosiain2006 [72]	
R12	$CH_3CO=CH_3+CO$	Konnov2009 [73]	
R13a	$CH_2CHO=CH_3+CO$	Rasmussen2004 [74]	
R13b	$CH_2CHO=CH_3CO$	Lindstedt2000 [75]	Lee2003 [76]
R14a	$CH_2CHO+H=CH_3+HCO$	Glarborg1998 [62]	Labbe2015 [77]
R14b	$CH_2CHO+H=CH_3CO+H$		
R15	$H_2CC+OH=CH_2CO+H$	-	Laskin2000 [65] Wang2001 [78]
R16	$H_2CC+O_2=HCO+HCO$		
R17	$H_2CC+H=C_2H_2+H$		
R18	$H_2CC+C_2H_2=C_4H_4$		
R19	$C_2H_2=H_2CC$		
R20	$C_2H_3+H=H_2CC+H_2$		
R21a	$CH_2OCH_2=CH_3CHO$	-	Joshi2005 [79]
R21b	$CH_2OCH_2=CH_3+HCO$	-	
R21c	$CH_2OCH_2=CH_4+CO$	-	
R21d	$CH_2OCH_2=CH_3CO+H$	-	
R21e	$CH_2OCH_2=CH_2CHO+H$	-	
R21f	$CH_2OCH_2=CH_2CO+H2$	-	
R21g	$CH_2OCH_2=C_2H_2+H2O$	-	
R22	$CH_2OCH=CH_3+CO$	-	
R22	$CH_2OCH=CH_2CO+H$	-	
R22	$CH_2OCH=CH_2CHO$	-	
R23a	$CH_2OCH_2+H=CH_3CHO+H$	-	
R23b	$CH_2OCH_2+H=CH_2OCH+H_2$	-	Lifshitz1983 [80]
R23c	$CH_2OCH_2+H=C_2H_4+OH$	-	
R24	$CH_2OCH_2+O=CH_2OCH+OH$	-	Bogan1978 [81]
R25	$CH_2OCH_2+OH=CH_2OCH+H_2O$	-	Baldwin1984 [49]
R26	$CH_2OCH_2+CH_3=CH_2OCH+CH_4$	-	

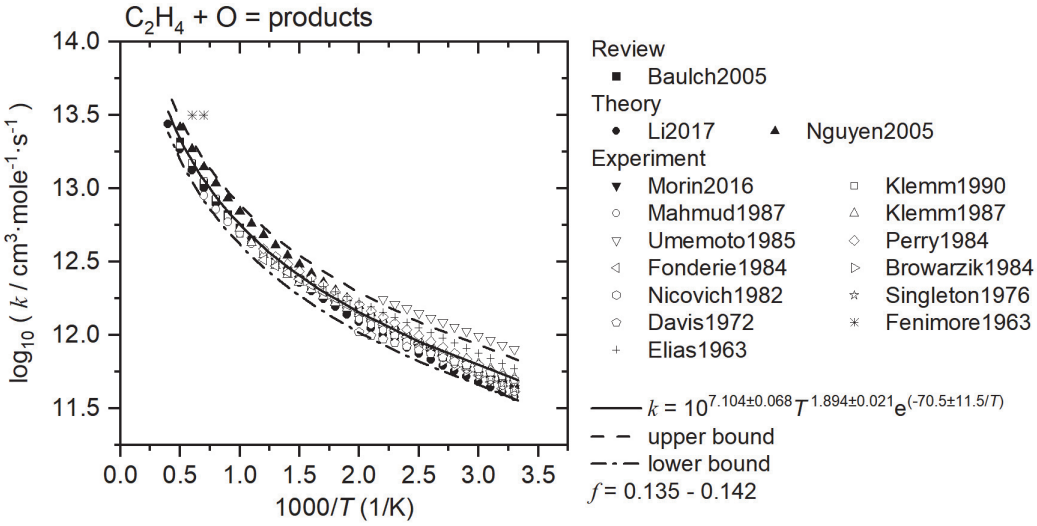

R2 $C_2H_4 + O$ = products

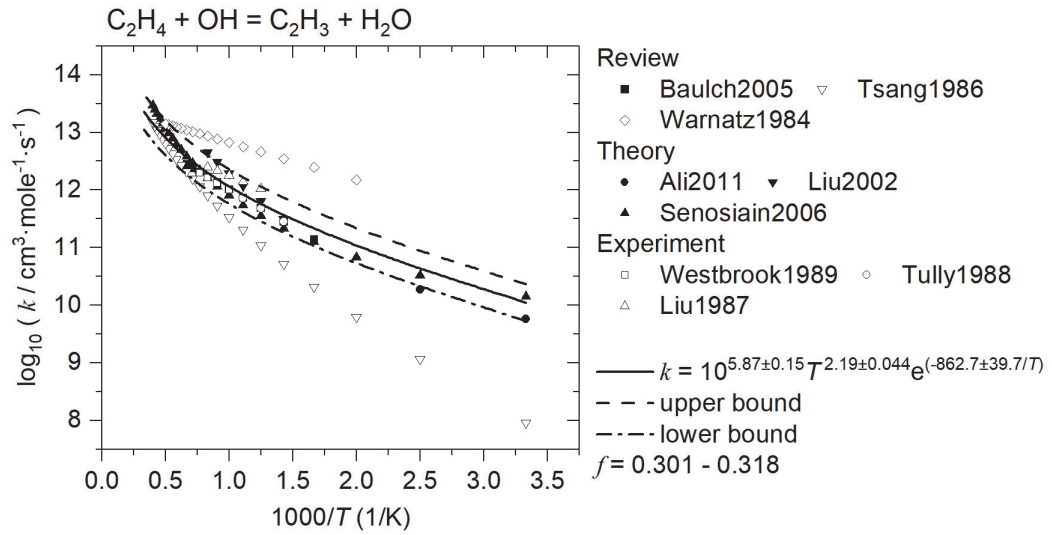

R3a $C_2H_4 + OH = C_2H_3 + H_2O$

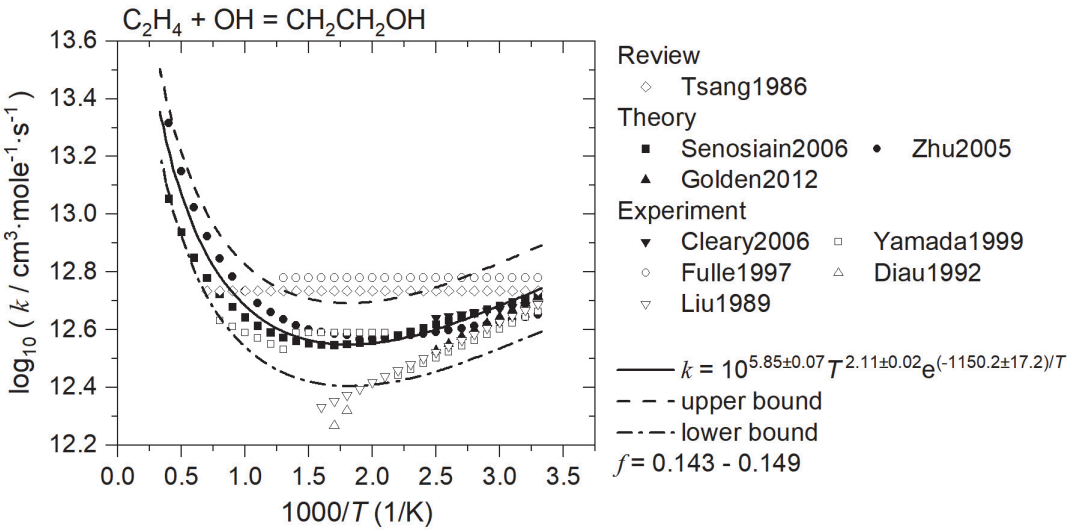

R3b $C_2H_4 + OH = CH_2CH_2OH$ (high-pressure limit)

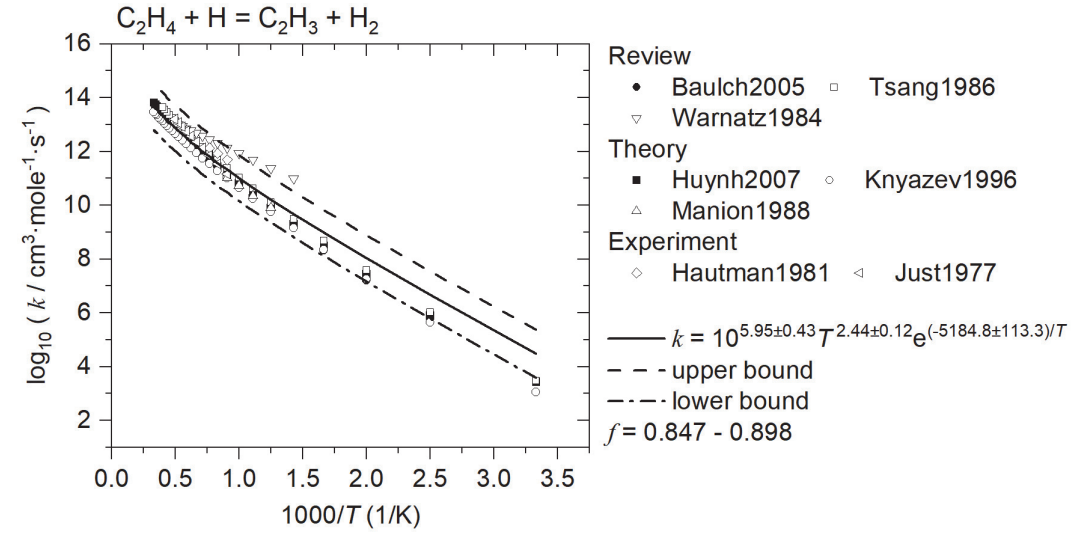

R4a $C_2H_4 + H = C_2H_3 + H_2$

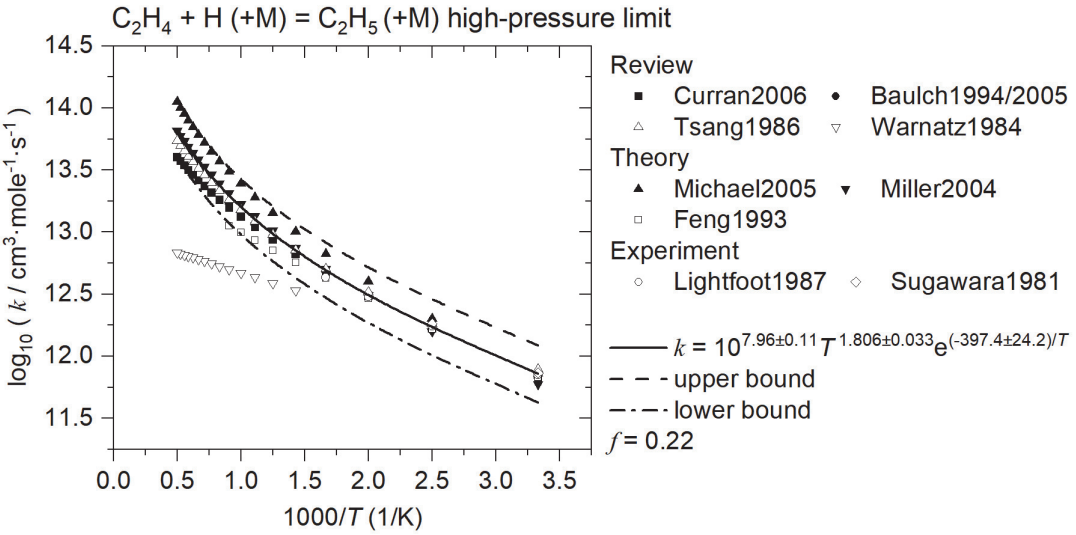

R4b $C_2H_4 + H (+M) = C_2H_5 (+M)$ (high-pressure limit)

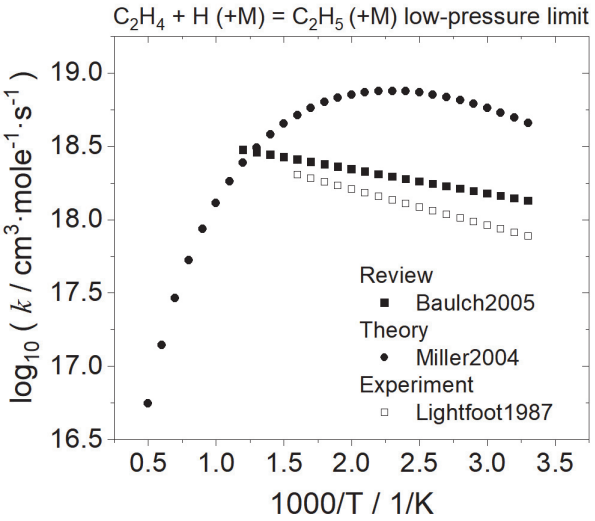

R4b $C_2H_4 + H (+M) = C_2H_5 (+M)$ (low-pressure limit)

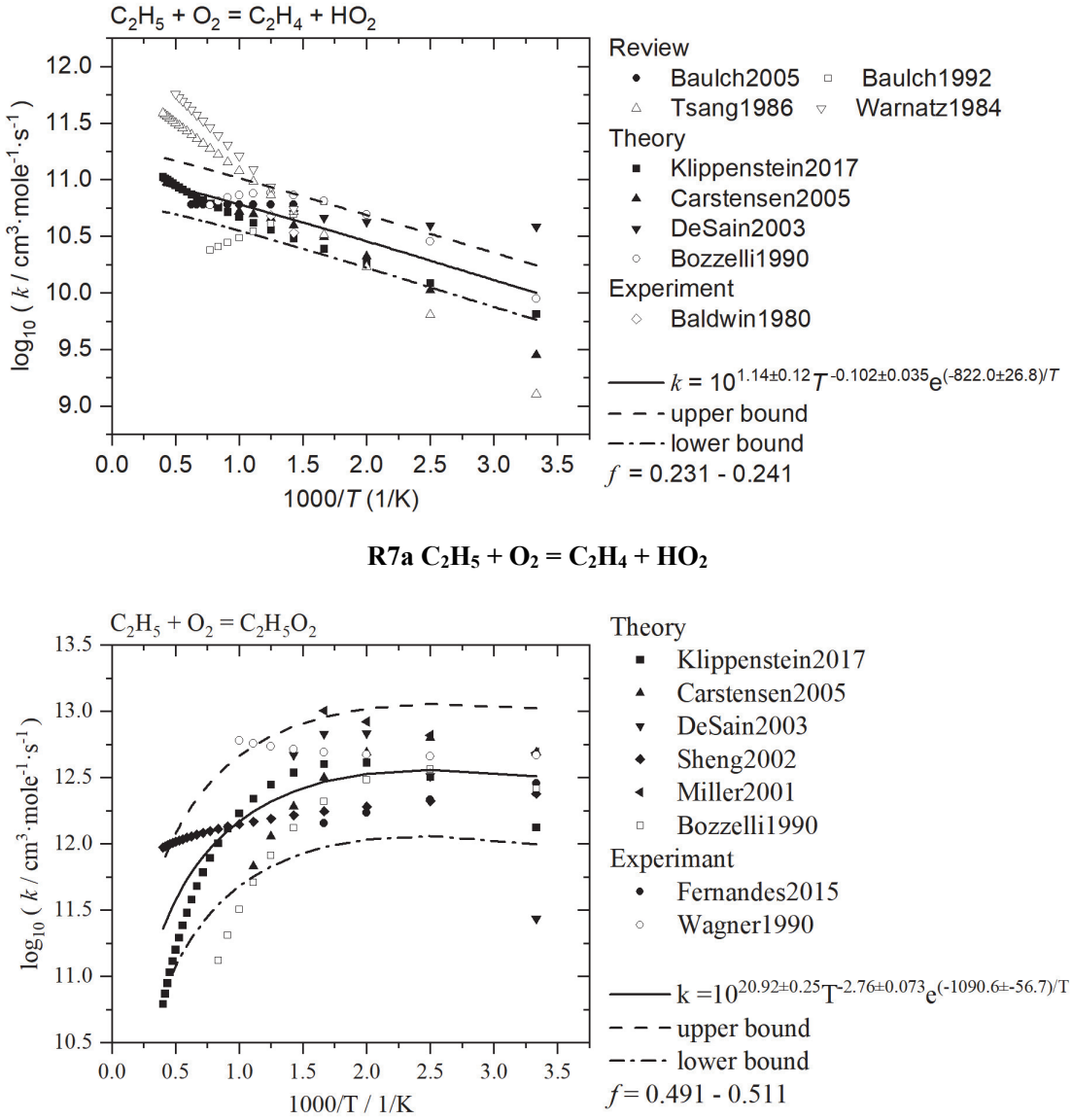

Figure S2-1. Determination of uncertainty bounds and factors for rate coefficients from statistical analysis of literature data.

A discussion on the update of RRCs is presented as follows:

$C_2H_4 + O_2 = C_2H_3 + H_2O$ (R1a)

For this RRC, Tsang et al. [2] gave a recommendation with a high level of uncertainty. The ab initio calculation conducted by Hua et al. [1] showed similar results, which was further adopted in model-2.

$C_2H_4 + O_2 = CH_2CHO + OH$ (R1b)

The RRC of reaction (R1b) was adopted from the kinetic model developed by Glarborg et al. [62] and the work of Benson et al. [82], in which reaction (R1b) was studied as an overall reaction containing reactions of C_2H_3, CH_2CH_2OO and CH_2CHOH. Considering the existing

detailed channels for these species, reaction (R1b) has been deleted in model-2.

$C_2H_4 + O$ = products (R2)

$C_2H_4 + O = CH_3 + HCO$ (R2a)

$C_2H_4 + O = CH_2CHO + H$ (R2b)

$C_2H_4 + O = CH_2O + CH_2$ (R2c)

$C_2H_4 + O = CH_2CO + H_2$ (R2d)

Reaction (R2) has been experimentally studied over a wide range of temperature [4, 6, 9-11, 83]. Reactions (R2a-d) are the most important channels for the reaction of C_2H_4+O and the branching ratios are studied both experimentally and theoretically. Baulch et al. [7] recommended the RRC well fitted on previous works on reaction (R2). The theoretical results obtained by Nguyen et al. [6] agreed well with the experimental results at temperatures in the range of 287-607K. The calculation of Li et al. [3] showed similar results as Nguyen et al. [6] at low temperatures, but also a sharp decrease of the branching fractions of the channels (R2a) and (R2d) at temperatures above 750K, where no experimental branching information is available. However, later experiments conducted by Morin et al. [4, 5] showed that the branching ratios are nearly non-temperature dependent at temperatures up to 900K. In model-2, the RRCs and branching ratios measured by Morin et al. [4, 5] have been adopted.

$C_2H_4 + OH = C_2H_3 + H_2O$ (R3a)

$C_2H_4 + OH = CH_2CH_2OH$ (R3b)

$C_2H_4 + OH = CH_2O + CH_3$ (R3c)

$C_2H_4 + OH = C_2H_3OH + H$ (R3d)

$C_2H_4 + OH = CH_3CHO + H$ (R3e)

Limited to the available data, Tsang et al. [2] obtained a calculated RRC with high uncertainty for the reaction (R3a). Baulch et al. [8] gave a fitted RRC for the reaction R3a in their early work, but the same RRC was recommended for the sum of reactions (R3c-e) in their later work [7]. Hidaka et al. [83], Zhu et al. [30], Cleary et al. [29] and Senosiain et al. [22] conducted quantum chemistry calculations for the reaction system of C_2H_4+OH. The theoretical results showed a good agreement with previous experimental data [26, 32, 33, 84] and self-consistency. The channel (R3b) becomes dominant at low temperatures and shows a strong pressure dependence. In model-2, the calculations over the temperature range of 250-2500K in the work of Senosiain et al. [22] have been adopted for the reactions (R3a-e).

$C_2H_4 + H = C_2H_3 + H_2$ (R4a)

Reaction (R4a) is one of the key reactions for C_2H_4 oxidation at high temperatures and most of the experimental works [7, 27] focused on the temperature range of 900-2000K. Huynh et al. [34] studied the hydrogen abstraction reaction class of the H+alkene using the reaction class transition state theory and the results showed good agreement with the previous experimental

data and review works. In model-2, the RRC recommended by Huynh et al. [34] has been adopted for the reaction (R4a).

$C_2H_4 + H = C_2H_5$ (R4b)

Except the RRC recommended by the early work of Warnatz [27], which showed an underestimation of results at high temperatures due to the lack of available data, the rest of the collections were applied to the statistical analysis of the RRC for the reaction (R4b) at the high-pressure limit. The reference sources for the reaction (R4b) at the low-pressure range are limited. Miller et al. [41] investigated the kinetics of the $H+C_2H_2$ and $H+C_2H_4$ reactions and applied the variational transition-state theory to compute rate coefficients. The results of Miller et al. [41] showed that the RRC recommended by Baulch et al. [7, 42] for the temperature range of 300-800K could be overestimated at high temperatures. In model-2, the RRCs and fall-off data calculated by Miller et al. [41] have been adopted.

$C_2H_4 = C_2H_3 + H$ (R5a)

The previous studies [37, 85-87] on the decomposition of C_2H_4 mainly focused on the very high-temperature range (T>1500K). To avoid possible large uncertainties at low temperatures, the RRC for reaction (R5a) has been replaced by the RRC recommended by Baulch et al. [7].

$C_2H_4 = H_2CC + H_2$ (R5b)

Laskin et al. [65] and Wang [78] studied the reactions related to H_2CC in detail, and their recommendations for reaction (R5b) and channels related to H_2CC are adopted in model-2.

$C_2H_4 + HO_2 = CH_2OCH_2 + OH$ (R6)

CH_2OCH_2 is a key intermediate of C_2H_4 oxidation at low temperatures, but this channel was missing in model-1. The RRC for the reaction R6 fitted by Baulch et al. [7] and the theoretical results obtained by Joshi et al. [79] for reactions related to CH_2OCH_2 have been adopted in model-2.

Reactions of C_2H_5 (R7-9)

The RRCs for reactions of $C_2H_5+O_2$, which are important for the low-temperature C_2H_4 oxidation, have been updated with the recent theoretical studies conducted by Klippenstein et al. [50, 88]. RRCs for the channels of C_2H_5+H recommended by Baulch et al. [7] and Harding et al. [46] are adopted in model-2. Harding et al. [89] also conducted a theoretical investigation on the reactions of C_2H_5+O, but the results appear to underestimate the previous experimental data [90, 91] so that the RRCs recommended by Slagle et al. have been adopted in model-2. C_2H_5 is also the main product of the initial steps of C_2H_6 oxidation, and these channels related to C_2H_5 will be studied in detail in our later work on C_2H_6.

Reactions related to CH_2CO, CH_3CO and CH_2CHO (R10-14)

Compared to the reactions of C_2H_4 and C_2H_5, the available data for the reactions related to CH_2CO, CH_3CO, and CH_2CHO are limited. The theoretical results calculated by Senosian et al.

[72] and the RRCs recommended by the recent works of Xiong et al. [69], Labbe et al. [77], and Wang [92] have been adopted in model-2.

Reactions of H_2CC and CH_2OCH_2 (R15-26)

New species of vinylidene (H_2CC) and ethylene oxide (CH_2OCH_2) and their related reactions were added to the model due to their important roles in the formation of PAH and low-temperature C_2H_4 oxidation, following the work of Laskin et al. [65] and Joshi et al. [79].

References

[1] H. Hua, B. Ruscic, B. Wang, Theoretical calculations on the reaction of ethylene with oxygen, Chemical Physics 311(3) (2005) 335-341.

[2] W. Tsang, R.F. Hampson, Chemical Kinetic Data Base for Combustion Chemistry. Part I. Methane and Related Compounds, Journal of Physical and Chemical Reference Data 15(3) (1986) 1087-1279.

[3] X. Li, A.W. Jasper, J. Zádor, J.A. Miller, S.J. Klippenstein, Theoretical kinetics of O + C2H4, Proceedings of the Combustion Institute 36(1) (2017) 219-227.

[4] J. Morin, Y. Bedjanian, M.N. Romanias, Rate Constants of the Reactions of O (3P) Atoms with Ethene and Propene over the Temperature Range 230–900 K, International Journal of Chemical Kinetics 49(1) (2017) 53-60.

[5] J. Morin, Y. Bedjanian, Reaction of O (3P) with C2H4: Yield of the Reaction Products as a Function of Temperature, The Journal of Physical Chemistry A 120(45) (2016) 9063-9070.

[6] T.L. Nguyen, L. Vereecken, X.J. Hou, M.T. Nguyen, J. Peeters, Potential energy surfaces, product distributions and thermal rate coefficients of the reaction of O(3P) with C2H4(X1Ag): a comprehensive theoretical study, The Journal of Physical Chemistry A 109(33) (2005) 7489-99.

[7] D.L. Baulch, C.T. Bowman, C.J. Cobos, R.A. Cox, T. Just, J.A. Kerr, M.J. Pilling, D. Stocker, J. Troe, W. Tsang, R.W. Walker, J. Warnatz, Evaluated Kinetic Data for Combustion Modeling: Supplement II, Journal of Physical and Chemical Reference Data 34(3) (2005) 757-1397.

[8] D. Baulch, C. Cobos, R. Cox, C. Esser, P. Frank, Th. Just, JA Kerr, MJ Pilling, J. Troe, RW Walker, and J. Warnatz, Journal of Physical and Chemical Reference Data 21(3) (1992) 411-569.

[9] R.B. Klemm, J.W. Sutherland, M.A. Wickramaaratchi, G. Yarwood, Flash photolysis-shock tube kinetic study of the reaction of atomic oxygen(3P) with ethylene: 1052K.ltoreq.T.ltoreq.2284K, The Journal of Physical Chemistry 94(8) (1990) 3354-3357.

[10] K. Mahmud, P. Marshall, A. Fontijn, A high-temperature photochemistry kinetics study of the reaction of oxygen(3P) atoms with ethylene from 290 to 1510 K, The Journal of Physical Chemistry 91(6) (1987) 1568-1573.

[11] R.B. Klemm, F.L. Nesbitt, E.G. Skolnik, J.H. Lee, J.F. Smalley, Direct rate constant measurements for the reaction of ground-state atomic oxygen with ethylene, 244-1052K, Journal of Physical Chemistry 91(6) (1987) 1574-1580.

[12] H. Umemoto, K. Sugiyama, S. Tsunashima, S. Sato, The Arrhenius parameters for the reactions of O atoms with ethene and five fluoroethenes, Bulletin of the Chemical Society of Japan 58(4) (1985) 1228-1233.

[13] R.A. Perry, Absolute rate constants for the reaction of O (3 P) atoms with ethylene, propylene, and propylene‐d 6 over the temperature range 258–861 K, The Journal of chemical physics 80(1) (1984) 153-158.

[14] V. Fonderie, D. Maes, J. Peeters, The Kinetic Coefficient of the C 2 H 4+ O Reaction Over Extended Pressure and Temperature Ranges, Physico-Chemical Behaviour of Atmospheric Pollutants, Springer1984, pp. 274-282.

[15] R. Browarzik, F. Stuhl, Temperature dependence of the rate constants for the reactions of oxygen atoms with ethene, propene, and 1-butene, The Journal of Physical Chemistry 88(24) (1984) 6004-6009.

[16] J. Nicovich, A. Ravishankara, A study of the reaction of O (3P) with ethylene, Symposium (International) on Combustion, Elsevier, 1982, pp. 23-30.

[17] D. Singleton, R. Cvetanovic, Temperature dependence of the reaction of oxygen atoms with olefins, Journal of the American Chemical Society 98(22) (1976) 6812-6819.
[18] D.D. Davis, R.E. Huie, J.T. Herron, M.J. Kurylo, W. Braun, Absolute rate constants for the reaction of atomic oxygen with ethylene over the temperature range 232–500° K, The Journal of Chemical Physics 56(10) (1972) 4868-4876.
[19] C. Fenimore, G. Jones, The decomposition of ethylene and ethane in premixed hydrocarbon-oxygen-hydrogen flames, Symposium (International) on Combustion, Elsevier, 1963, pp. 597-606.
[20] L. Elias, Reinvestigation of some absolute rate measurements of O ‐ atom reactions with olefins, The Journal of Chemical Physics 38(4) (1963) 989-995.
[21] M.A. Ali, B. Upendra, B. Rajakumar, Kinetic parameters of abstraction reactions of OH radical with ethylene, fluoroethylene, cis-and trans-1, 2-difluoroethylene and 1, 1-difluoroethylene, in the temperature range of 200–400 K: Gaussian-3/B3LYP theory, Chemical Physics Letters 511(4-6) (2011) 440-446.
[22] J.P. Senosiain, S.J. Klippenstein, J.A. Miller, Reaction of ethylene with hydroxyl radicals: a theoretical study, The Journal of Physical Chemistry A 110(21) (2006) 6960-70.
[23] G. Liu, Y. Ding, Z. Li, Q. Fu, X. Huang, C. Sun, A. Tang, Theoretical study on mechanisms of the high-temperature reactions C2H3 + H2O and C2H4 + OH, Physical Chemistry Chemical Physics 4(6) (2002) 1021-1027.
[24] C.K. Westbrook, M.M. Thornton, W.J. Pitz, P.C. Malte, A kinetic study of ethylene oxidation in a well-stirred reactor, Symposium (International) on Combustion 22(1) (1989) 863-871.
[25] F.P. Tully, Hydrogen-atom abstraction from alkenes by OH, ethene and 1-butene, Chemical Physics Letters 143(5) (1988) 510-514.
[26] A.-D. Liu, W.A. Mulac, C.D. Jonah, Pulse radiolysis study of the reaction of OH radicals with C2H4 over the temperature range 343-1173 K, International Journal of Chemical Kinetics 19(1) (1987) 25-34.
[27] J. Warnatz, Rate coefficients in the C/H/O system, Combustion chemistry, Springer1984, pp. 197-360.
[28] D.M. Golden, The reaction OH+ C2H4: an example of rotational channel switching, The Journal of Physical Chemistry A 116(17) (2012) 4259-4266.
[29] P.A. Cleary, M.T.B. Romero, M.A. Blitz, D.E. Heard, M.J. Pilling, P.W. Seakins, L. Wang, Determination of the temperature and pressure dependence of the reaction OH+ C 2 H 4 from 200–400 K using experimental and master equation analyses, Physical Chemistry Chemical Physics 8(48) (2006) 5633-5642.
[30] R.S. Zhu, J. Park, M.C. Lin, Ab initio kinetic study on the low-energy paths of the HO+C2H4 reaction, Chemical Physics Letters 408(1-3) (2005) 25-30.
[31] T. Yamada, J.W. Bozzelli, T. Lay, Kinetic and Thermodynamic Analysis on OH Addition to Ethylene: Adduct Formation, Isomerization, and Isomer Dissociations, The Journal of Physical Chemistry A 103(38) (1999) 7646-7655.
[32] D. Fulle, H. Hamann, H. Hippler, C. Jänsch, The High Pressure Range of the Addition of OH to C2H2 and C2H4, Berichte der Bunsengesellschaft für physikalische Chemie 101(10) (1997) 1433-1442.
[33] E.W.G. Diau, Y.P. Lee, Detailed rate coefficients and the enthalpy change of the equilibrium reaction OH+C2H4=MHOC2H4 over the temperature range 544–673 K, The Journal of Chemical Physics 96(1) (1992) 377-386.
[34] L.K. Huynh, S. Panasewicz, A. Ratkiewicz, T.N. Truong, Ab initio study on the kinetics of hydrogen abstraction for the H+alkene-->H2+alkenyl reaction class, The Journal of Physical Chemistry A 111(11) (2007) 2156-65.
[35] V.D. Knyazev, Á. Bencsura, S.I. Stoliarov, I.R. Slagle, Kinetics of the C2H3+ H2⇄ H+ C2H4 and CH3+ H2 ⇄ H+ CH4 Reactions, The Journal of Physical Chemistry 100(27) (1996) 11346-11354.
[36] J.A. Manion, R. Louw, Gas-phase hydrogenolysis of chloroethene: rates, products, and computer modelling,

Journal of the Chemical Society, Perkin Transactions 2 (8) (1988) 1547-1555.
[37] T. Just, P. Roth, R. Damm, Production of hydrogen atoms during the thermal dissociation of ethylene between 1700 and 2200 K, Symposium (International) on Combustion, Elsevier, 1977, pp. 961-969.
[38] J. Ding, L. Zhang, K. Han, Thermal rate constants of the pyrolysis of n-heptane, Combustion and flame 158(12) (2011) 2314-2324.
[39] H.J. Curran, Rate constant estimation for C1 to C4 alkyl and alkoxyl radical decomposition, International journal of chemical kinetics 38(4) (2006) 250-275.
[40] J. Michael, M.-C. Su, J. Sutherland, L. Harding, A. Wagner, Rate constants for D+ C2H4→ C2H3D+ H at high temperature: Implications to the high pressure rate constant for H+ C2H4→ C2H5, Proceedings of the Combustion Institute 30(1) (2005) 965-973.
[41] J.A. Miller, S.J. Klippenstein, The H + C2H2(+M) ⇄ C2H3(+M) and H + C2H2(+M) ⇄ C2H5(+M) reactions: Electronic structure, variational transition-state theory, and solutions to a two-dimensional master equation, Physical Chemistry Chemical Physics 6(6) (2004) 1192-1202.
[42] D.L. Baulch, C.J. Cobos, R.A. Cox, P. Frank, G. Hayman, T. Just, J.A. Kerr, T. Murrells, M.J. Pilling, J. Troe, R.W. Walker, J. Warnatz, Evaluated Kinetic Data for Combustion Modeling. Supplement I, Journal of Physical and Chemical Reference Data 23(6) (1994) 847-848.
[43] Y. Feng, J. Niiranen, A. Bencsura, V. Knyazev, D. Gutman, W. Tsang, Weak collision effects in the reaction ethyl radical. dblarw. ethene+ hydrogen, The Journal of Physical Chemistry 97(4) (1993) 871-880.
[44] P.D. Lightfoot, M.J. Pilling, Temperature and pressure dependence of the rate constant for the addition of hydrogen atoms to ethylene, Journal of Physical Chemistry 91(12) (1987) 3373-3379.
[45] K.-i. Sugawara, K. Okazaki, S. Sato, Temperature dependence of the rate constants of H and D-atom additions to C2H4, C2H3D, C2D4, C2H2, and C2D2, Bulletin of the Chemical Society of Japan 54(10) (1981) 2872-2877.
[46] L.B. Harding, Y. Georgievskii, S.J. Klippenstein, Predictive theory for hydrogen atom− hydrocarbon radical association kinetics, The Journal of Physical Chemistry A 109(21) (2005) 4646-4656.
[47] R. Duran, V. Amorebieta, A. Colussi, Is the homogeneous thermal dimerization of acetylene a free-radical chain reaction? Kinetic and thermochemical analysis, The Journal of Physical Chemistry 92(3) (1988) 636-640.
[48] R.R. Baldwin, C.E. Dean, R.W. Walker, Relative rate study of the addition of HO 2 radicals to C 2 H 4 and C 3 H 6, Journal of the Chemical Society, Faraday Transactions 2: Molecular and Chemical Physics 82(9) (1986) 1445-1455.
[49] R.R. Baldwin, A. Keen, R.W. Walker, Studies of the decomposition of oxirane and of its addition to slowly reacting mixtures of hydrogen and oxygen at 480° C, Journal of the Chemical Society, Faraday Transactions 1: Physical Chemistry in Condensed Phases 80(2) (1984) 435-456.
[50] S.J. Klippenstein, From theoretical reaction dynamics to chemical modeling of combustion, Proceedings of the Combustion Institute 36(1) (2017) 77-111.
[51] H.-H. Carstensen, C.V. Naik, A.M. Dean, Detailed modeling of the reaction of C2H5+ O2, The Journal of Physical Chemistry A 109(10) (2005) 2264-2281.
[52] J.D. DeSain, S.J. Klippenstein, J.A. Miller, C.A. Taatjes, Measurements, Theory, and Modeling of OH Formation in Ethyl + O2and Propyl + O2Reactions, The Journal of Physical Chemistry A 107(22) (2003) 4415-4427.
[53] J.A. Miller, S.J. Klippenstein, The reaction between ethyl and molecular oxygen II: Further analysis, International Journal of Chemical Kinetics 33(11) (2001) 654-668.
[54] A. Dean, J. Bozzelli, Chemical activation analysis of the reaction of C2H5 with 02, J; Phys. Chem 94(8) (1990) 3313-3317.
[55] R.R. Baldwin, I.A. Pickering, R.W. Walker, Reactions of ethyl radicals with oxygen over the temperature range 400–540° C, Journal of the Chemical Society, Faraday Transactions 1: Physical Chemistry in Condensed

Phases 76 (1980) 2374-2382.
[56] R. Baker, R. Baldwin, R. Walker, The use of the H2+ O2 reaction in determining the velocity constants of elementary reaction in hydrocarbon oxidation, Symposium (International) on Combustion, Elsevier, 1971, pp. 291-299.
[57] D. Cooke, A. Williams, Shock-tube studies of the ignition and combustion of ethane and slightly rich methane mixtures with oxygen, Symposium (International) on Combustion, Elsevier, 1971, pp. 757-766.
[58] R.X. Fernandes, K. Luther, G. Marowsky, M.P. Rissanen, R. Timonen, J.r. Troe, Experimental and Modeling Study of the Temperature and Pressure Dependence of the Reaction C2H5+ O2 (+ M)→ C2H5O2 (+ M), The Journal of Physical Chemistry A 119(28) (2015) 7263-7269.
[59] C.Y. Sheng, J.W. Bozzelli, A.M. Dean, A.Y. Chang, Detailed kinetics and thermochemistry of C2H5+ O2: Reaction kinetics of the chemically-activated and stabilized CH3CH2OO• adduct, The Journal of Physical Chemistry A 106(32) (2002) 7276-7293.
[60] J.W. Bozzelli, A.M. Dean, Chemical activation analysis of the reaction of ethyl radical with oxygen, Journal of Physical Chemistry 94(8) (1990) 3313-3317.
[61] D. Walter, H.-H. Grotheer, J.W. Davies, M.J. Pilling, A.F. Wagner, Experimental and theoretical study of the recombination reaction CH3+ CH3→ C2H6, Symposium (International) on Combustion, Elsevier, 1990, pp. 107-114.
[62] P. Glarborg, M.U. Alzueta, K. Dam-Johansen, J.A. Miller, Kinetic Modeling of Hydrocarbon/Nitric Oxide Interactions in a Flow Reactor, Combustion and Flame 115(1-2) (1998) 1-27.
[63] S.S. Vasu, Z. Hong, D.F. Davidson, R.K. Hanson, D.M. Golden, Shock tube/laser absorption measurements of the reaction rates of OH with ethylene and propene, The Journal of Physical Chemistry A 114(43) (2010) 11529-37.
[64] K. Hughes, T. Turányi, A. Clague, M. Pilling, Development and testing of a comprehensive chemical mechanism for the oxidation of methane, International Journal of Chemical Kinetics 33(9) (2001) 513-538.
[65] A. Laskin, H. Wang, C.K. Law, Detailed kinetic modeling of 1,3-butadiene oxidation at high temperatures, International Journal of Chemical Kinetics 32(10) (2000) 589-614.
[66] N.M. Marinov, W.J. Pitz, C.K. Westbrook, M.J. Castaldi, S.M. Senkan, Modeling of Aromatic and Polycyclic Aromatic Hydrocarbon Formation in Premixed Methane and Ethane Flames, Combustion Science and Technology 116-117(1-6) (1996) 211-287.
[67] B. Wang, H. Hou, L.M. Yoder, J.T. Muckerman, C. Fockenberg, Experimental and theoretical investigations on the methyl− methyl recombination reaction, The Journal of Physical Chemistry A 107(51) (2003) 11414-11426.
[68] I.R. Slagle, D. Sarzyński, D. Gutman, J.A. Miller, C.F. Melius, Kinetics of the reaction between oxygen atoms and ethyl radicals, Journal of the Chemical Society, Faraday Transactions 2: Molecular and Chemical Physics 84(5) (1988) 491-503.
[69] S.-Z. Xiong, Q. Yao, Z.-R. Li, X.-Y. Li, Reaction of ketenyl radical with hydroxyl radical over C2H2O2 potential energy surface: A theoretical study, Combustion and flame 161(4) (2014) 885-897.
[70] C.-W. Zhou, Y. Li, U. Burke, C. Banyon, K.P. Somers, S. Ding, S. Khan, J.W. Hargis, T. Sikes, O. Mathieu, E.L. Petersen, M. AlAbbad, A. Farooq, Y. Pan, Y. Zhang, Z. Huang, J. Lopez, Z. Loparo, S.S. Vasu, H.J. Curran, An experimental and chemical kinetic modeling study of 1,3-butadiene combustion: Ignition delay time and laminar flame speed measurements, Combustion and Flame 197 (2018) 423-438.
[71] P. Frank, A high temperature shock tube study on fast reactions of methylene and methyl radicals, Proceeding of International Symposium Rarefied Gas Dynamics, 1986, pp. 422-426.
[72] J.P. Senosiain, S.J. Klippenstein, J.A. Miller, Pathways and rate coefficients for the decomposition of vinoxy and acetyl radicals, The Journal of Physical Chemistry A 110(17) (2006) 5772-81.
[73] A.A. Konnov, Implementation of the NCN pathway of prompt-NO formation in the detailed reaction

mechanism, Combustion and Flame 156(11) (2009) 2093-2105.
[74] M.S. Skjøth-Rasmussen, P. Glarborg, M. Østberg, J. Johannessen, H. Livbjerg, A. Jensen, T. Christensen, Formation of polycyclic aromatic hydrocarbons and soot in fuel-rich oxidation of methane in a laminar flow reactor, Combustion and Flame 136(1-2) (2004) 91-128.
[75] R. Lindstedt, G. Skevis, Molecular growth and oxygenated species formation in laminar ethylene flames, Proceedings of the Combustion Institute 28(2) (2000) 1801-1807.
[76] J. Lee, J.W. Bozzelli, Reaction of H+ ketene to formyl methyl and acetyl radicals and reverse dissociations, International journal of chemical kinetics 35(1) (2003) 20-44.
[77] N.J. Labbe, R. Sivaramakrishnan, S.J. Klippenstein, The role of radical + fuel-radical well-skipping reactions in ethanol and methylformate low-pressure flames, Proceedings of the Combustion Institute 35(1) (2015) 447-455.
[78] H. Wang, A new mechanism for initiation of free‐radical chain reactions during high‐temperature, homogeneous oxidation of unsaturated hydrocarbons: Ethylene, propyne, and allene, International Journal of Chemical Kinetics 33(11) (2001) 698-706.
[79] A. Joshi, X. You, T.A. Barckholtz, H. Wang, Thermal decomposition of ethylene oxide: potential energy surface, master equation analysis, and detailed kinetic modeling, The Journal of Physical Chemistry A 109(35) (2005) 8016-8027.
[80] A. Lifshitz, H. Ben-Hamou, Thermal reactions of cyclic ethers at high temperatures. 1. Pyrolysis of ethylene oxide behind reflected shocks, The Journal of Physical Chemistry 87(10) (1983) 1782-1787.
[81] D.J. Bogan, C.W. Hand, Absolute rate constant, kinetic isotope effect and mechanism of the reaction of ethylene oxide with oxygen (3P) atoms, The Journal of Physical Chemistry 82(19) (1978) 2067-2073.
[82] S.W. Benson, Oxygen initiated combustion: Thermochemistry and kinetics of unsaturated hydrocarbons, International Journal of Chemical Kinetics 28(9) (1996) 665-672.
[83] Y. Hidaka, T. Nishimori, K. Sato, Y. Henmi, R. Okuda, K. Inami, T. Higashihara, Shock-tube and modeling study of ethylene pyrolysis and oxidation, Combustion and Flame 117(4) (1999) 755-776.
[84] F.P. Tully, Elementary Combustion Reactions: Laser Photolysis-Laser-Induced Fluorescence Kinetic Studies, ACS Publications1984.
[85] J. Kiefer, S. Kapsalis, M. Al-Alami, K. Budach, The very high temperature pyrolysis of ethylene and the subsequent reactions of product acetylene, Combustion and Flame 51 (1983) 79-93.
[86] T. Tanzawa, W. Gardiner Jr, Thermal decomposition of ethylene, Combustion and Flame 39(3) (1980) 241-253.
[87] P. Roth, T. Just, Messungen zum homogenen thermischen Zerfall von Äthylen, Berichte der Bunsengesellschaft für physikalische Chemie 77(12) (1973) 1114-1118.
[88] H. Hashemi, J.G. Jacobsen, C.T. Rasmussen, J.M. Christensen, P. Glarborg, S. Gersen, M. van Essen, H.B. Levinsky, S.J. Klippenstein, High-pressure oxidation of ethane, Combustion and Flame 182 (2017) 150-166.
[89] L.B. Harding, S.J. Klippenstein, Y. Georgievskii, Reactions of oxygen atoms with hydrocarbon radicals: a priori kinetic predictions for the CH3+ O, C2H5+ O, and C2H3+ O reactions, Proceedings of the Combustion Institute 30(1) (2005) 985-993.
[90] I.R. Slagle, Q. Feng, D. Gutman, Kinetics of the reaction of ethyl radicals with molecular oxygen from 294 to 1002 K, The Journal of Physical Chemistry 88(16) (1984) 3648-3653.
[91] W. Hack, K. Hoyermann, M. Olzmann, T. Zeuch, Mechanisms and rates of the reactions C2H5+ O and 1-C3H7+ O, Proceedings of the Combustion Institute 29(1) (2002) 1247-1255.
[92] Z. Wang, Measurement of laminar burning speed and flame instablity study of syngas/oxygen/helium premixed flame, Northeastern University2016.

Supplementary Material - 3

A Comprehensive Kinetic Modelling Study of Ethylene Combustion with Data Uncertainty Analysis

Hongxin Wang[a], Nadezda Slavinskaya[b, c], Aziza Kanz[d], Moldir Auyelkhankyzy[c, e], Yiting Gao[a], Oskar Haidn[a]

a. Department of Aerospace and Geodesy, Technical University of Munich, 85748 Garching, Germany

b. GRS Association for Plant and Reactor Safety, 85748 Garching, Germany

c. Al-Farabi Kazakh National University, 050040 Almaty, Kazakhstan

d. DLR German Aerospace Center, Institute of Combustion Technology, 70569 Stuttgart, Germany

e. Institute of Combustion Problems, 050012 Almaty, Kazakhstan

Experimental data and modeling results for ignition delay times

Table S3-1. References of the validated ignition delay times of ethylene oxidation.

No.	Author	Journal/Congress	Title
[1]	M.B. Colket L. J. Spadaccini	*Journal of Propulsion and Power* 17 (2001) 315-323.	Scramjet fuels autoignition study
[2]	D. M. Kalitan. J. M. Hall E. L. Petersen	*Journal of Propulsion and Power* 21 (2005) 1045-1056.	Ignition and Oxidation of Ethylene-Oxygen-Diluent Mixtures with and Without Silane
[3]	O.G. Penyazkov K.L. Sevrouk V. Tangirala N. Joshi	*Proceedings of the Combustion Institute* 32 (2009) 2421-2428.	High-pressure ethylene oxidation behind reflected shock waves
[4]	S. Saxena, M.S.P. Kahandawala, S. S. Sidhu	*Combustion and Flame* 158 (2011) 1019-1031.	A shock tube study of ignition delay in the combustion of ethylene
[5]	M. M. Kopp E. L. Petersen W. K. Metcalfe S. M. Burke H. J. Curran	*Journal of Propulsion and Power* 30 (2014) 790-798.	Oxidation of ethylene-air mixtures at elevated pressures, part 2 chemical kinetics
[6]	F. Deng Y. Pan W. Sun F. Yang Y. Zhang Z. Huang	*Energy & Fuels* 31 (2017) 14116-14128	Comparative study of the effects of nitrous oxide and oxygen on ethylene ignition
[7]	J. Shao, D. F. Davidson, R. K. Hanson	*Fuel* 225 (2018) 370-380.	A shock tube study of ignition delay times in diluted methane, ethylene, propene and their blends at elevated pressures
[8]	C. J. Brown G. O. Thomas	*Combustion and Flame* 117 (1999) 861-870.	Experimental studies of shock-induced ignition and transition to detonation in ethylene and propane mixtures

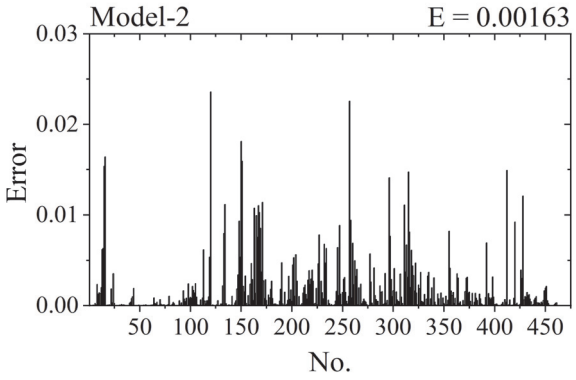
Model-2
E = 0.00163
Error
No.

(a)

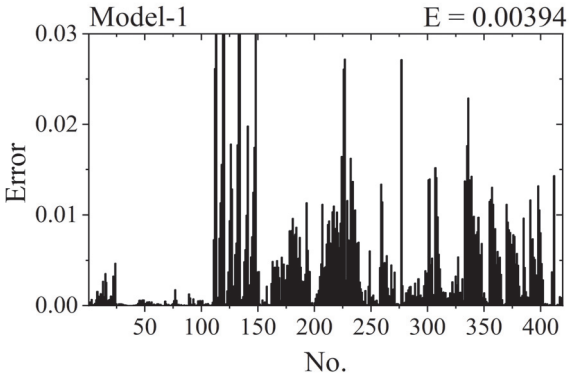
Model-1
E = 0.00394
Error
No.

(b)

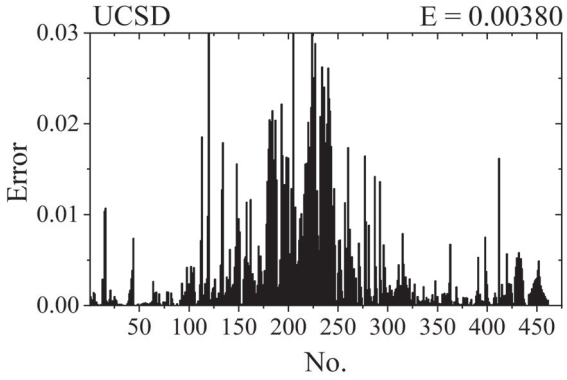
UCSD
E = 0.00380
Error
No.

(c)

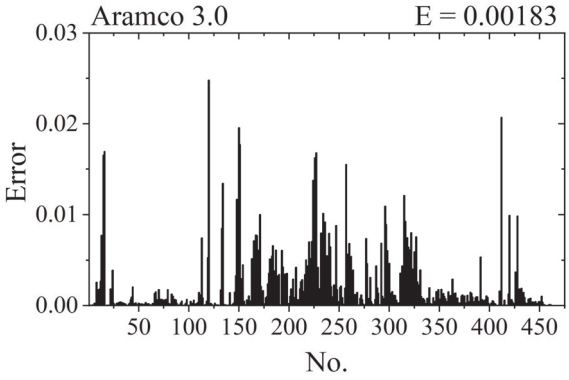
Aramco 3.0
E = 0.00183
Error
No.

(d)

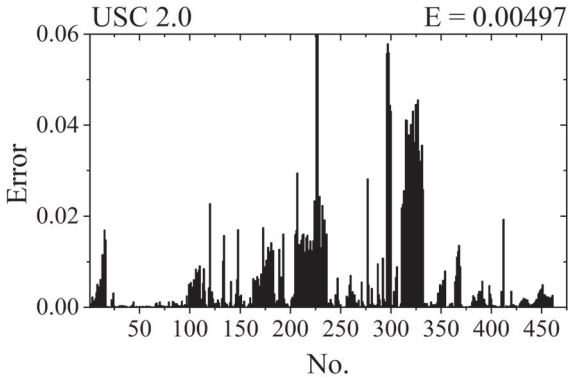
USC 2.0
E = 0.00497
Error
No.

(e)

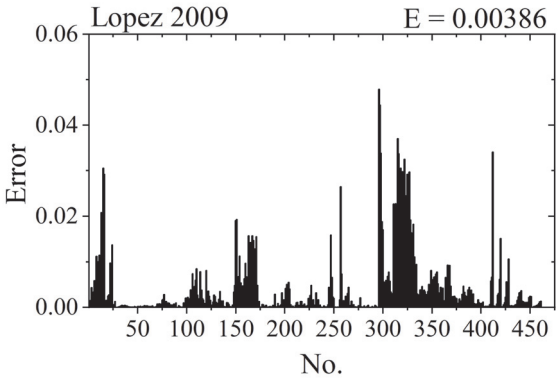
Lopez 2009
E = 0.00386
Error
No.

(f)

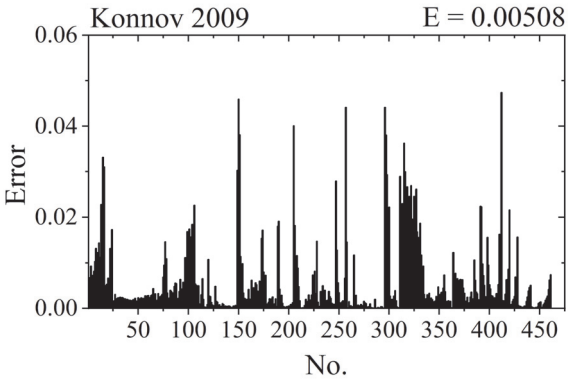
Konnov 2009
E = 0.00508
Error
No.

(g)

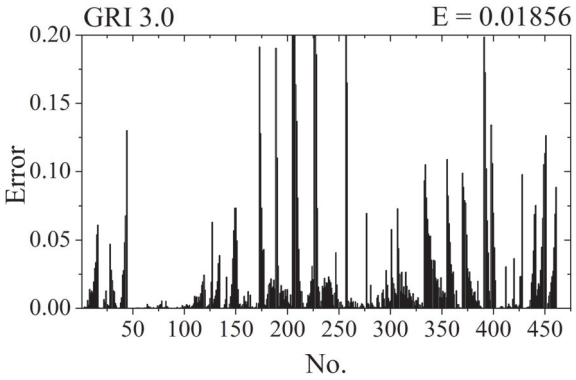
GRI 3.0
E = 0.01856
Error
No.

(h)

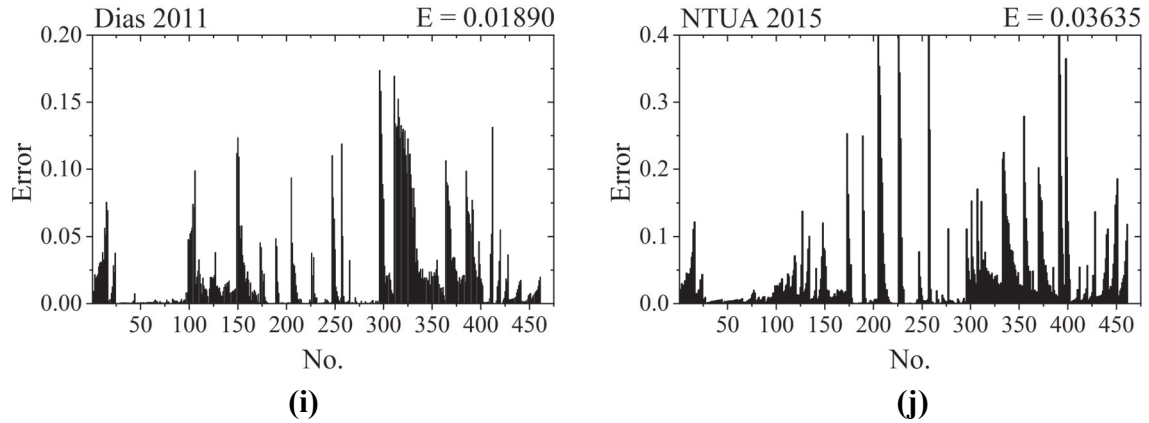

(i) **(j)**

Figure S3-1. Errors (e_{ij}, equation 7) for modelling ignition delay times with mechanism of model-1, model-2 (this study), Aramco 3.0 [9], UCSD [10], Lopez [11], USC 2.0 [12], Konnov [13], GRI 3.0 [14], Dias [15], NTUA 2015 [16].

Journal: *Journal of Propulsion and Power* 17 (2001) 315-323
Article: Scramjet fuels autoignition study
Author: M.B. Colket. L. J. Spadaccini

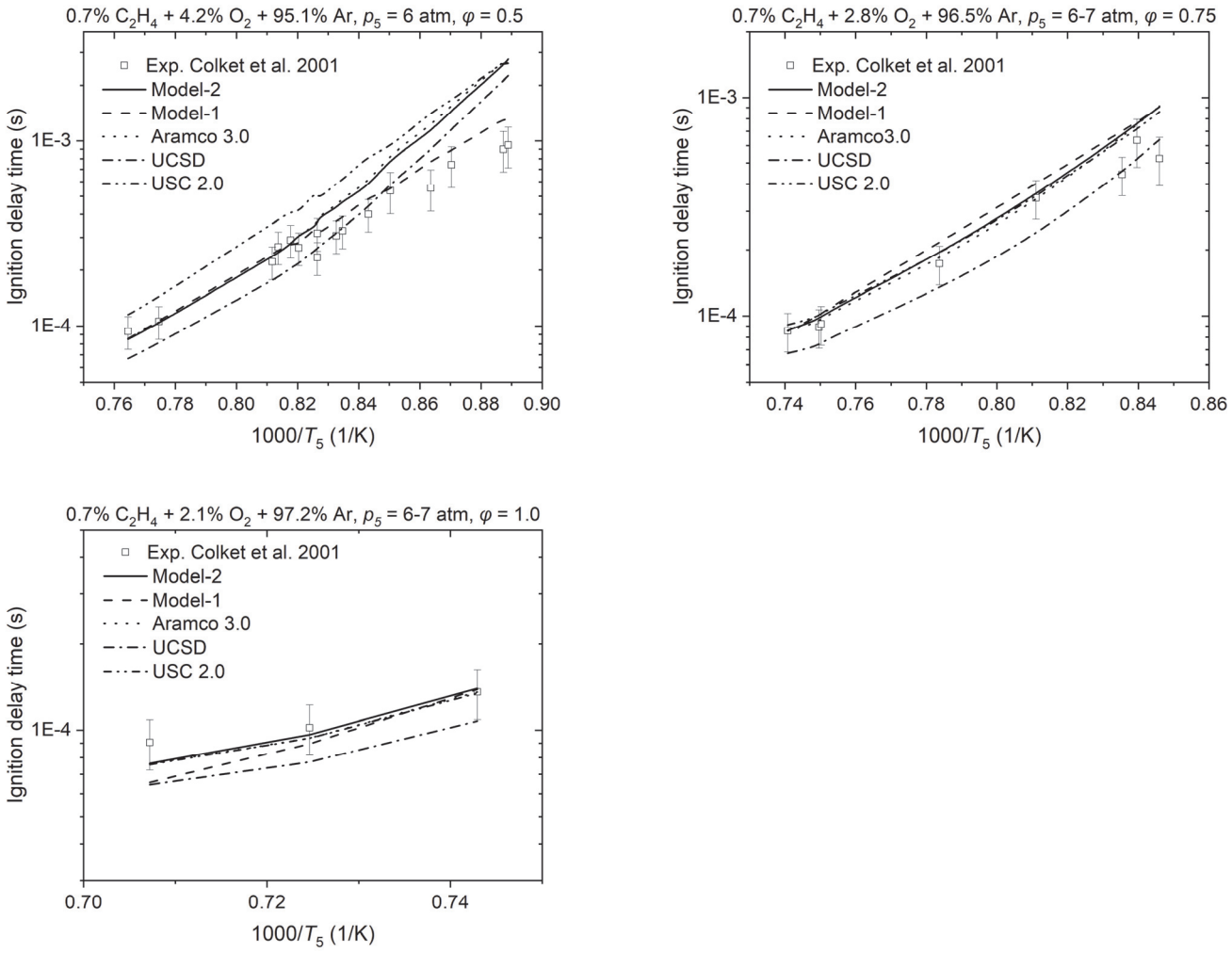

Journal: *Journal of Propulsion and Power* 21 (2005) 1045-1056.
Article: Ignition and oxidation of ethylene-oxygen-diluent mixtures with and without silane
Author: D. M. Kalitan. J.M. Hall. E.L. Petersen

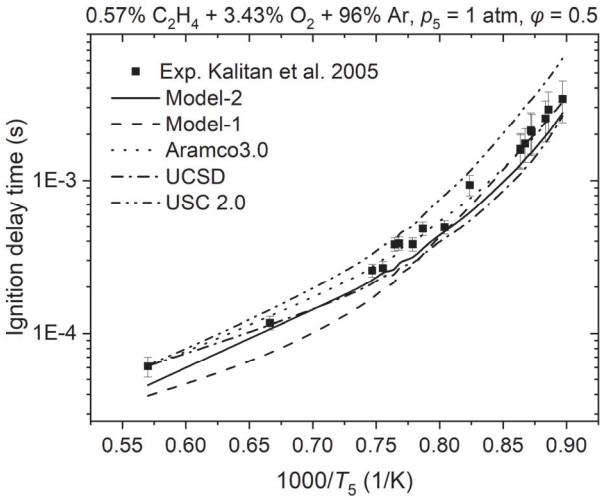

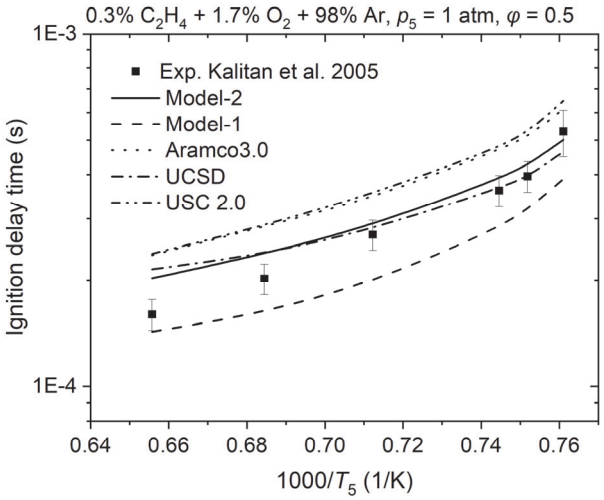

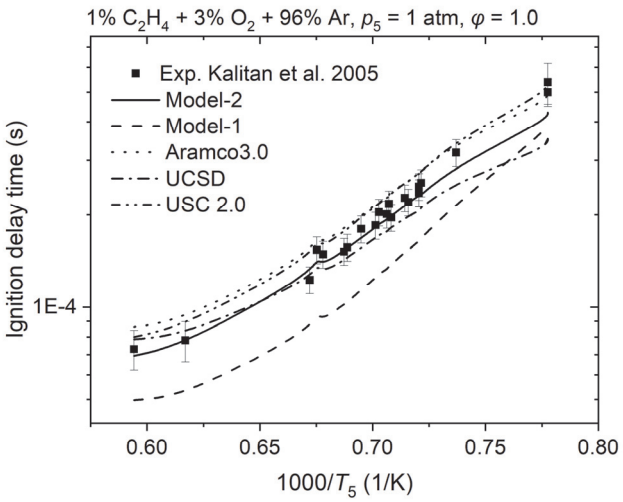

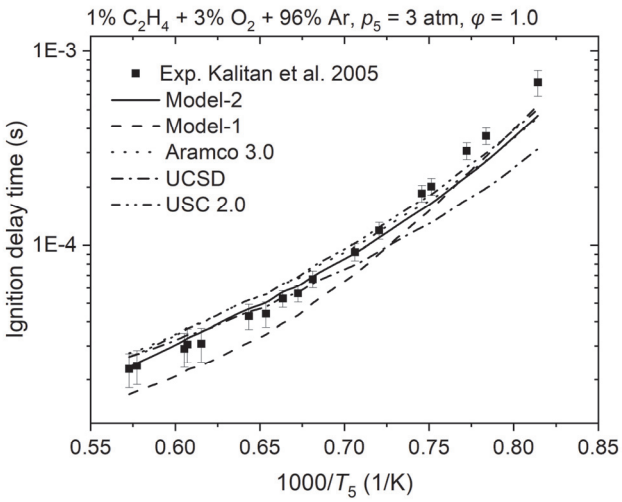

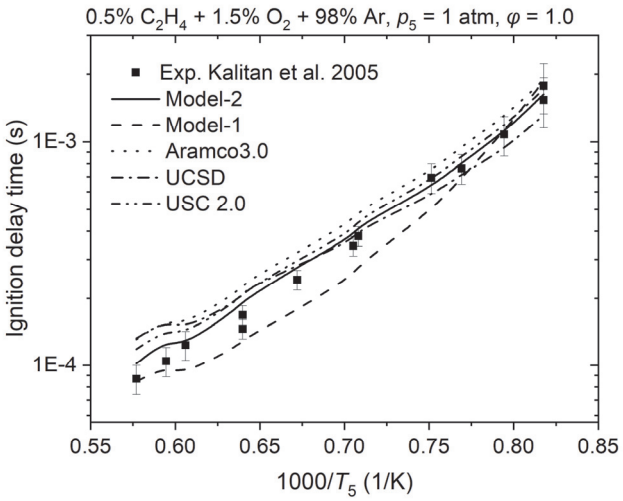

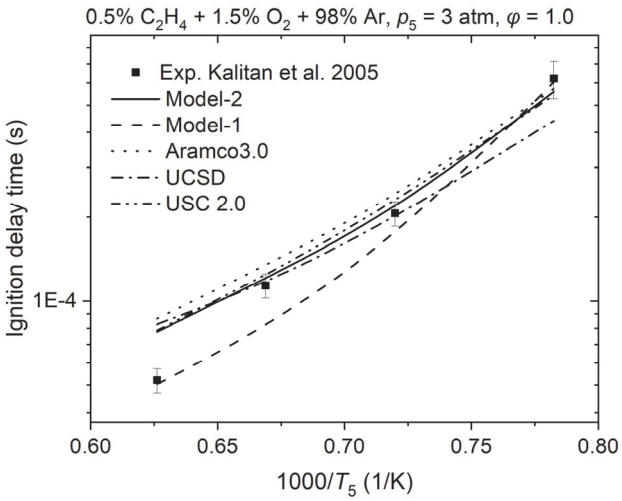

Journal: Proceedings of the Combustion Institute 32 (2009) 2421–2428
Article: High-pressure ethylene oxidation behind reflected shock waves
Author: O.G. Penyazkov, K.L. Sevrouk, V. Tangirala, N. Joshi

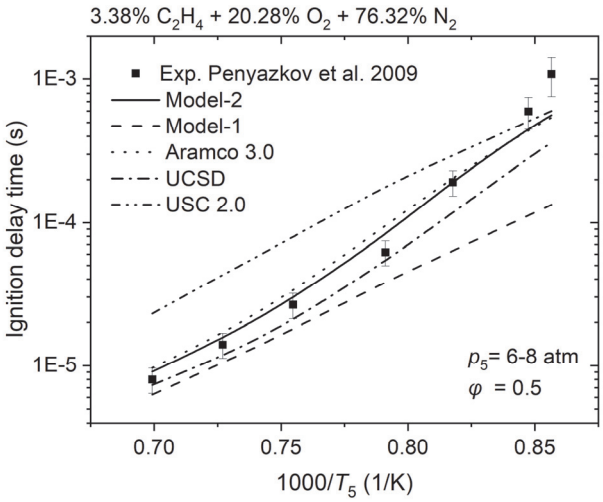

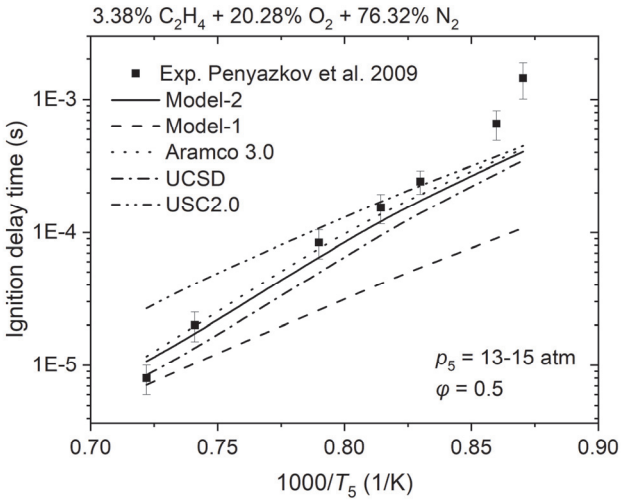

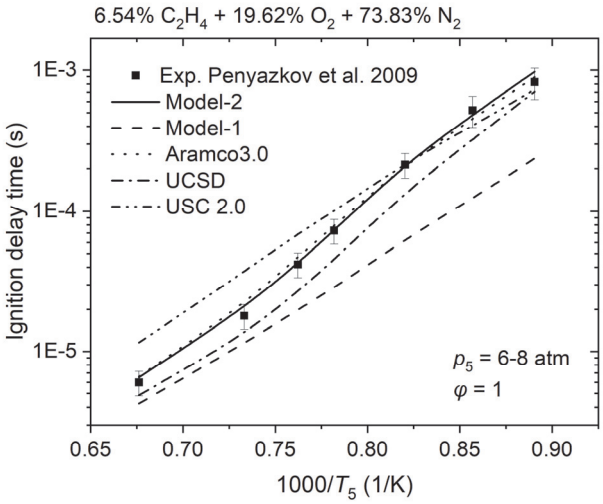

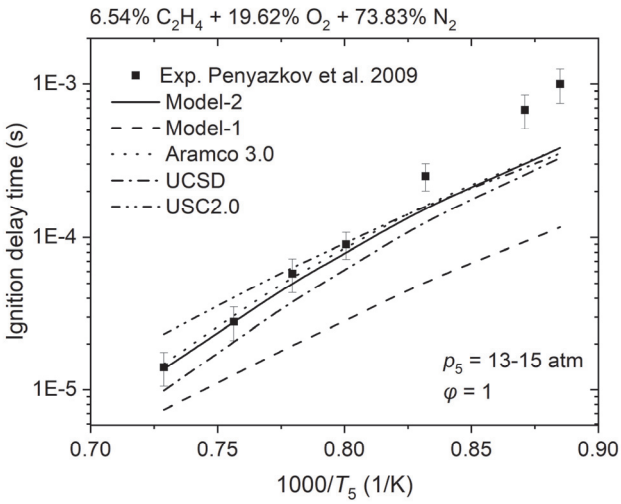

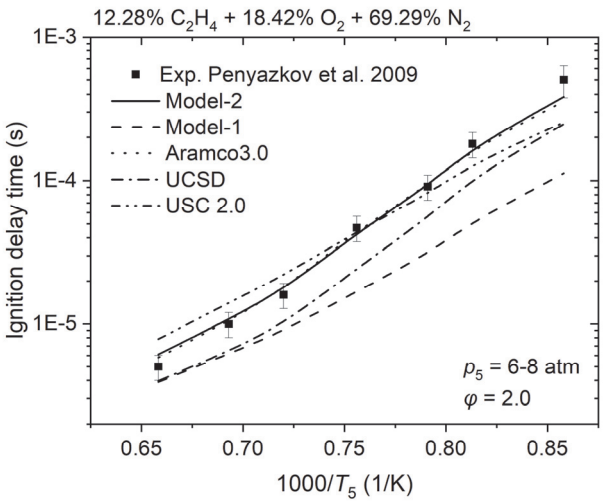

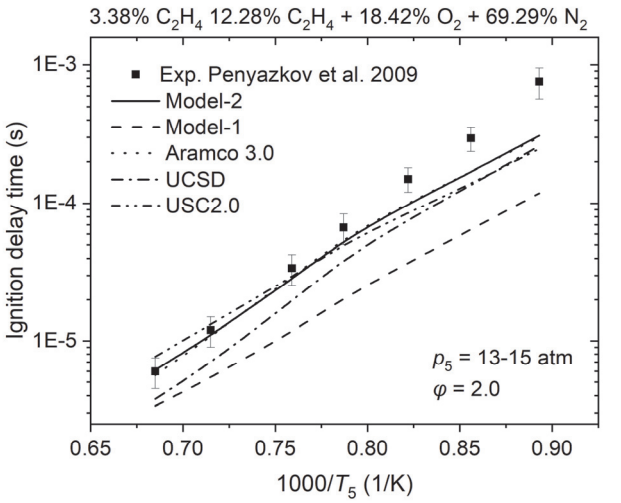

Journal: *Combustion and Flame* 158 (2011) 1019–1031
Article: A shock tube study of ignition delay in the combustion of ethylene
Author: S. Saxena, M.S.P. Kahandawala, S. S. Sidhu

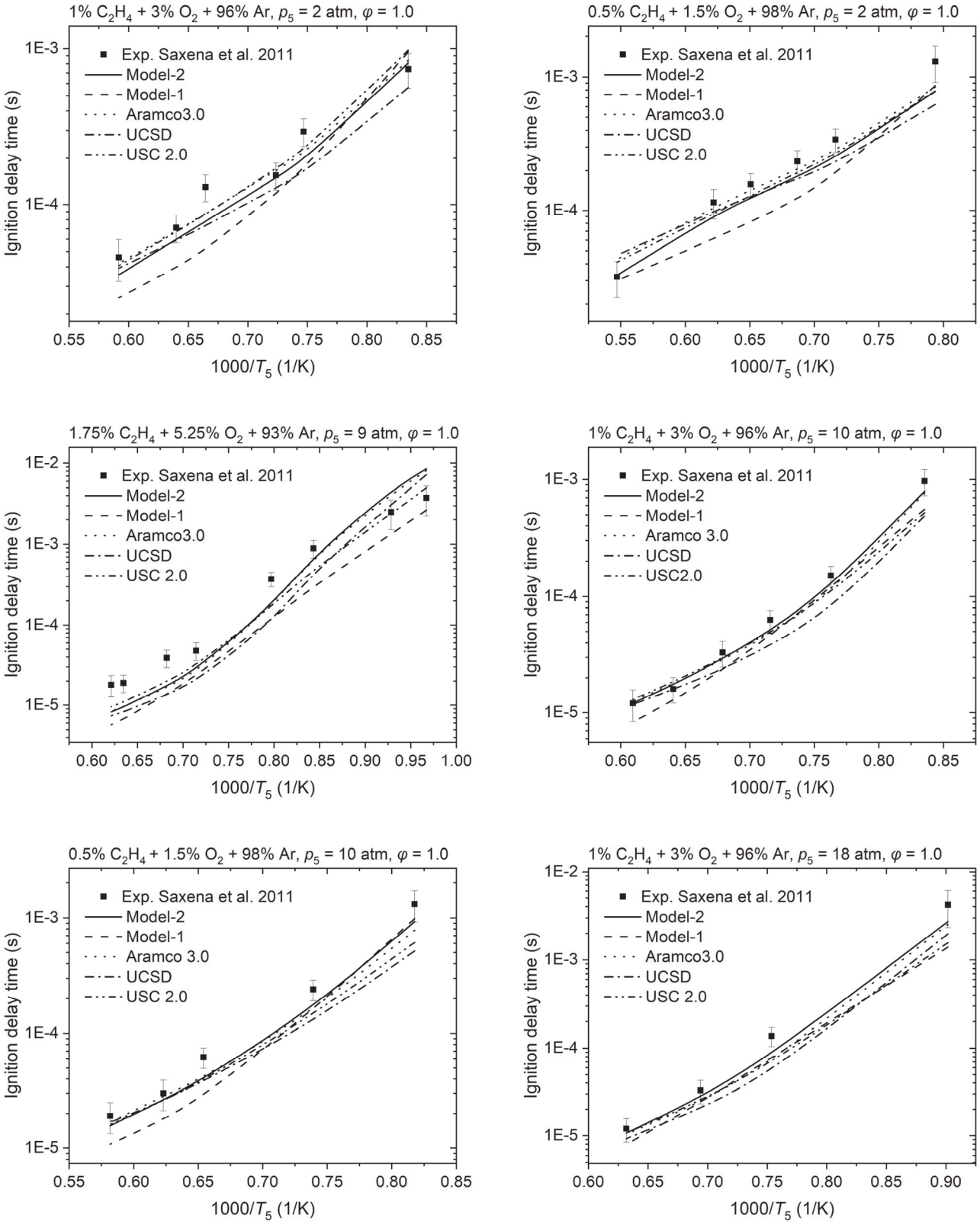

Journal: *Combustion and Flame* 158 (2011) 1019–1031
Article: A shock tube study of ignition delay in the combustion of ethylene
Author: S. Saxena, M.S.P. Kahandawala, S. S. Sidhu

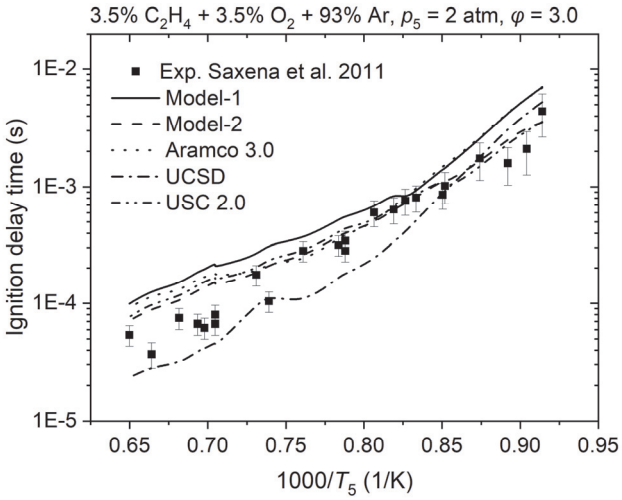

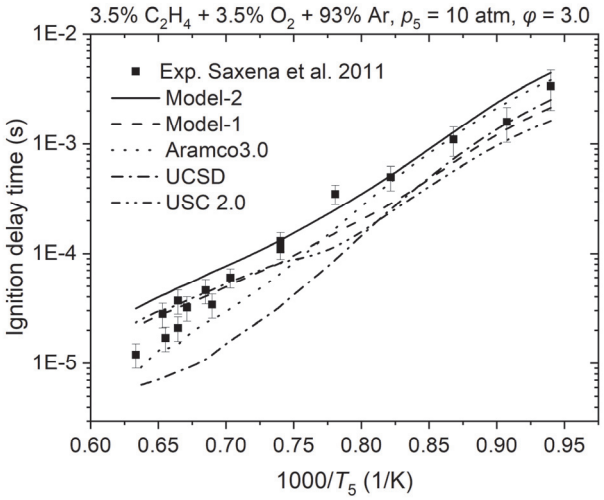

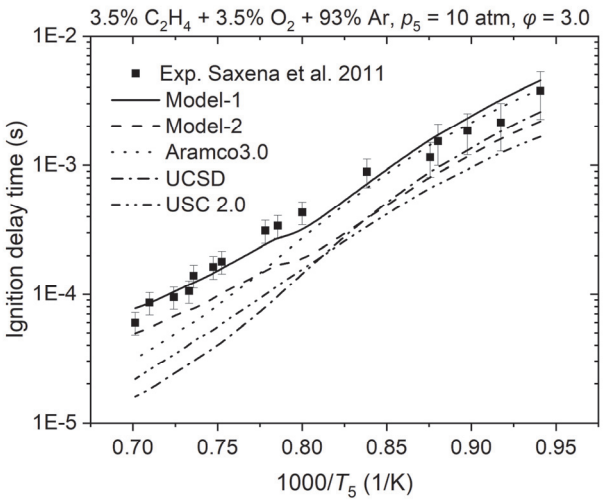

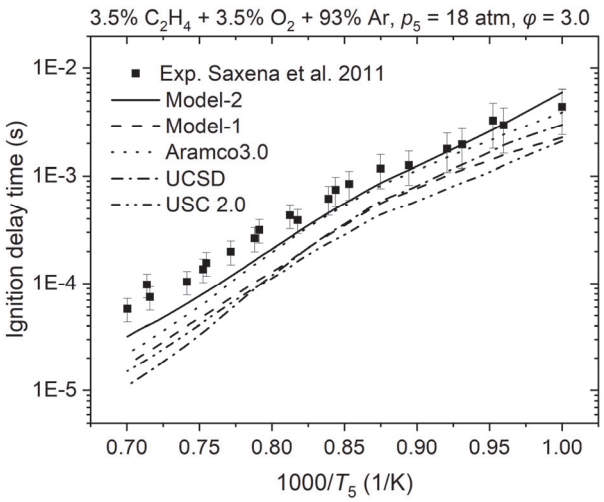

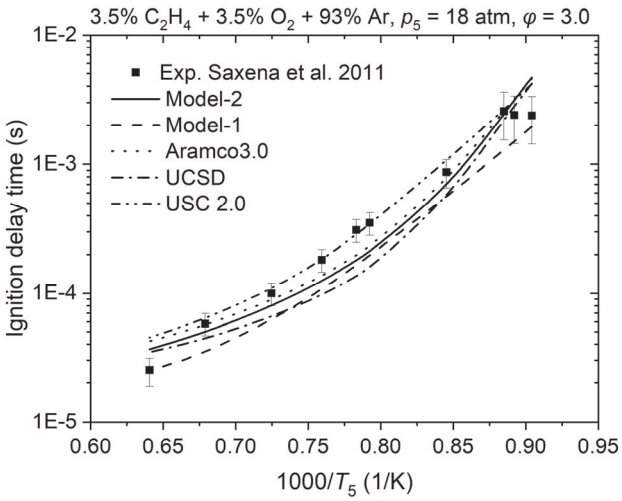

Journal: *Journal of Propulsion and Power* 30 (2014) 790-798.
Article: Oxidation of Ethylene—Air Mixtures at Elevated Pressures
Author: M. M. Kopp, E. L. Petersen, W. K. Metcalfe, S. M. Burke, H. J. Curran

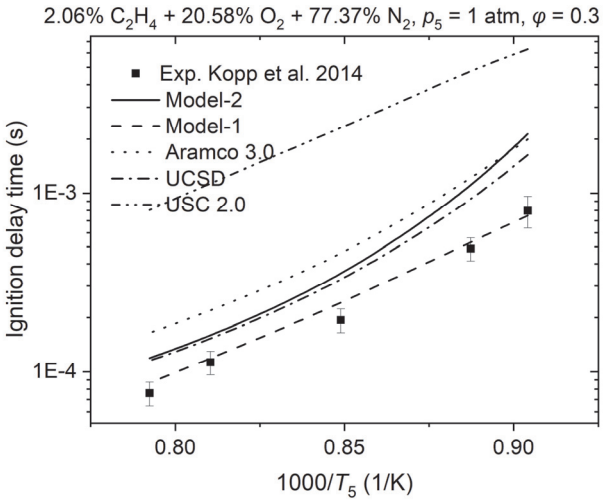

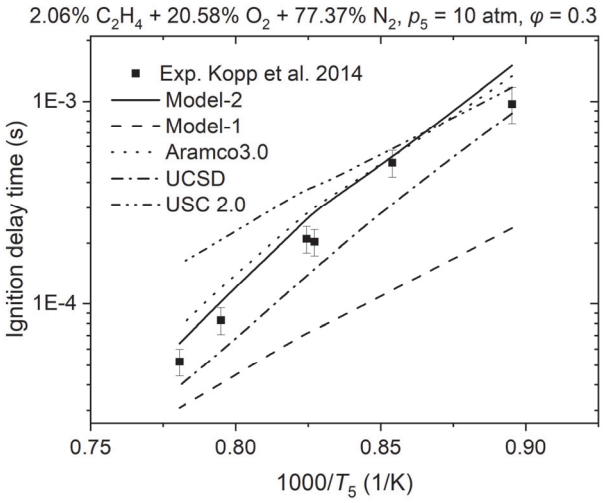

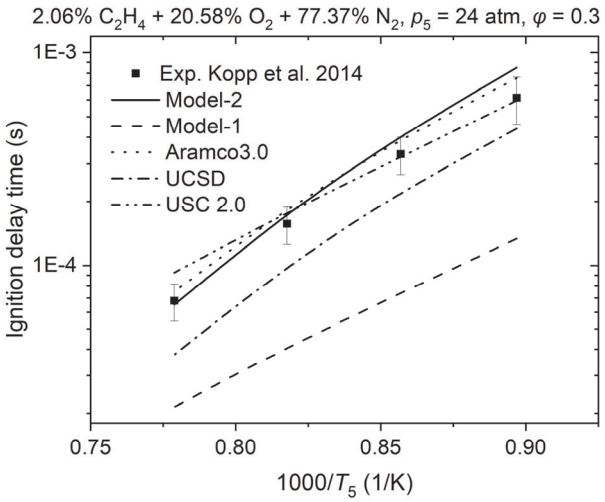

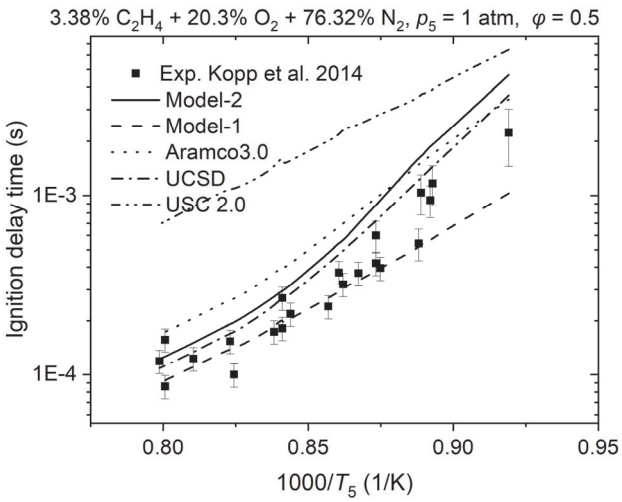

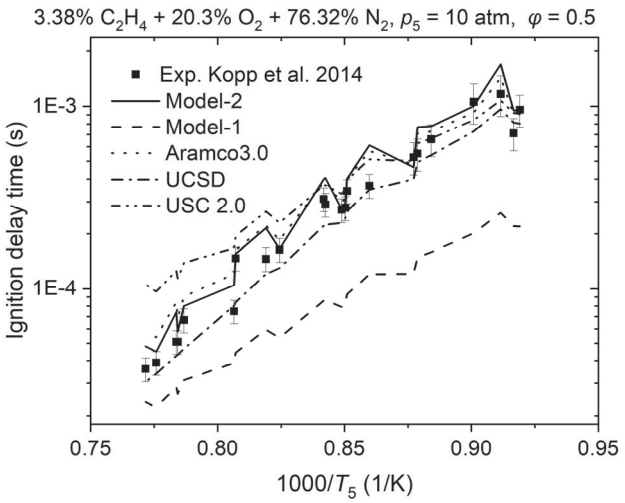

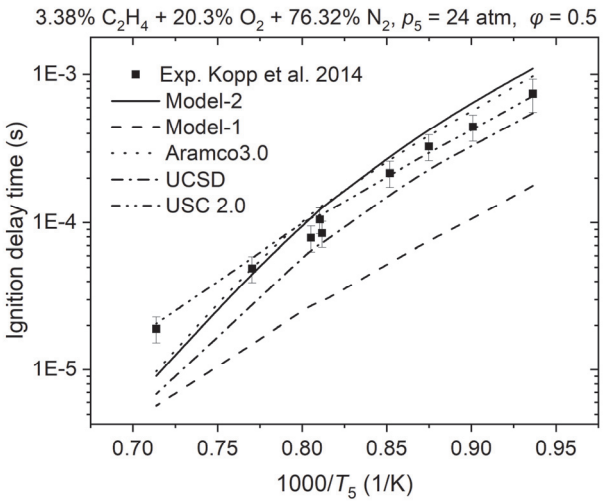

Journal: *Journal of Propulsion and Power* 30 (2014) 790-798.
Article: Oxidation of Ethylene—Air Mixtures at Elevated Pressures
Author: M. M. Kopp, E. L. Petersen, W. K. Metcalfe, S. M. Burke, H. J. Curran

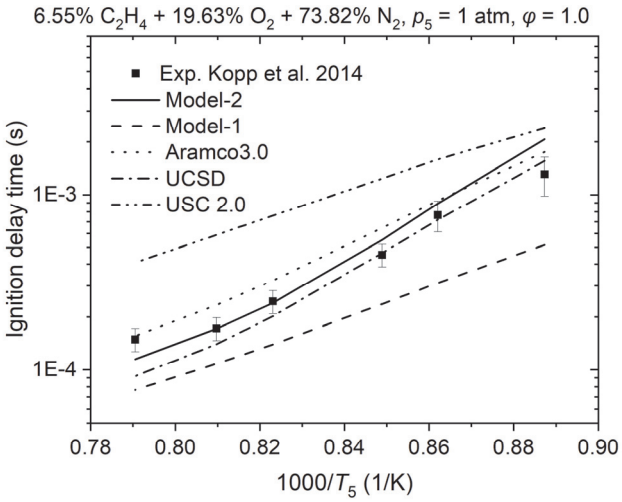

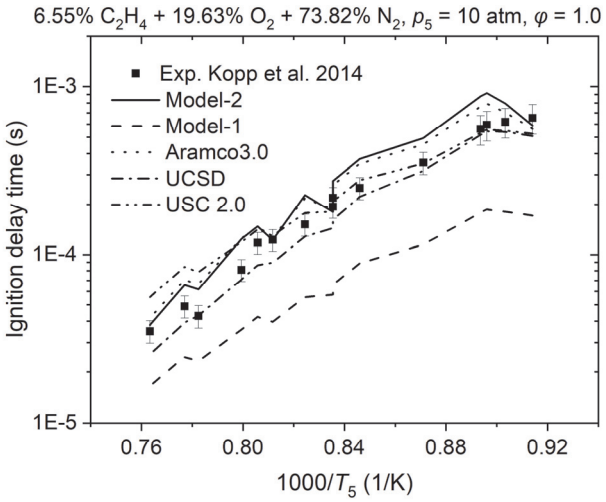

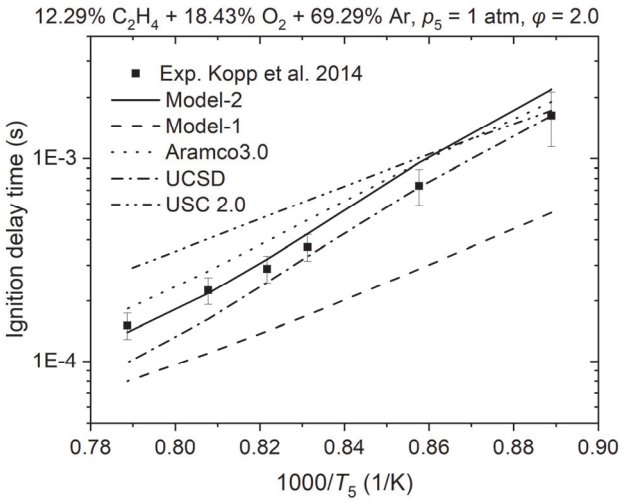

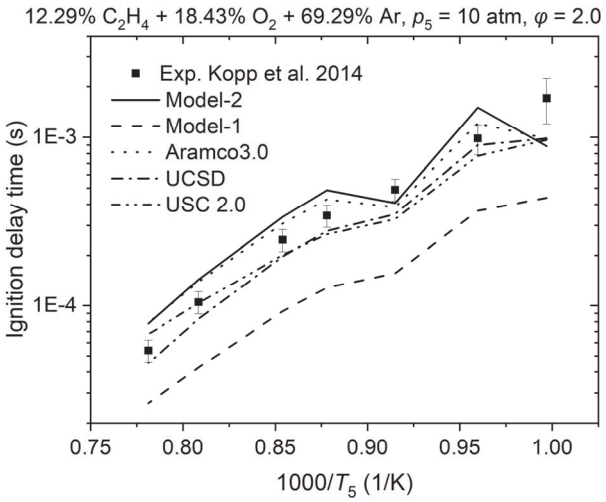

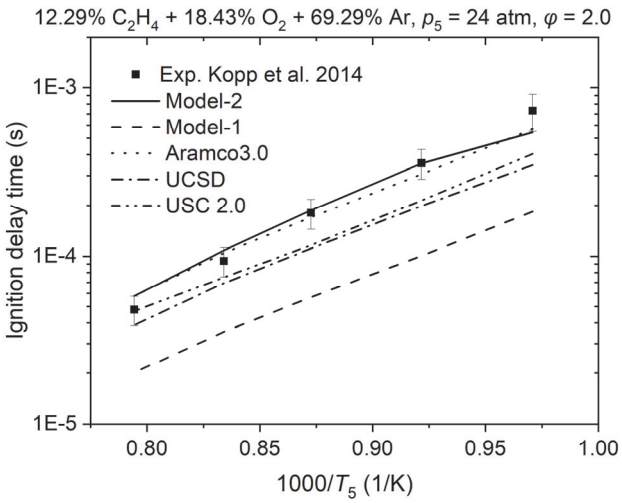

Journal: *Energy & Fuels* 31 (2017) 14116-14128.
Article: Comparative study of the effects of nitrous oxide and oxygen on ethylene ignition
Author: F. Deng, Y. Pan, W. Sun, F. Yang, Y. Zhang, Z. Huang

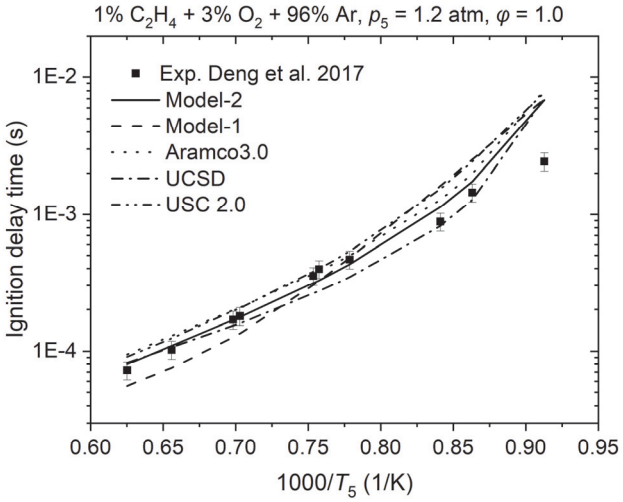

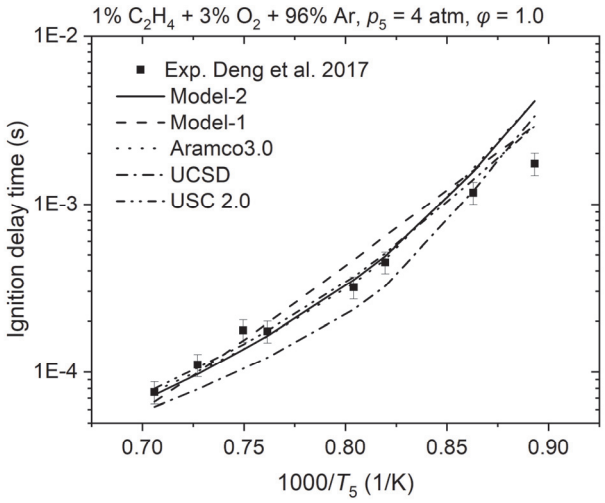

Journal: *Fuel* 225 (2018) 370-380.
Article: A shock tube study of ignition delay times in diluted methane, ethylene, propene and their blends at elevated pressures
Author: J. Shao, D. F. Davidson, R. K. Hanson

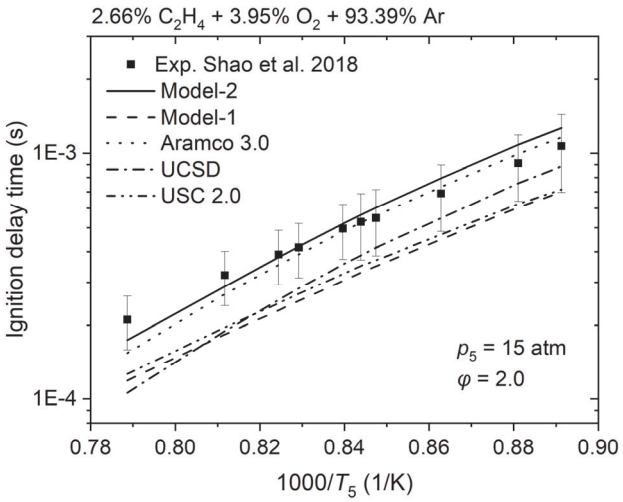

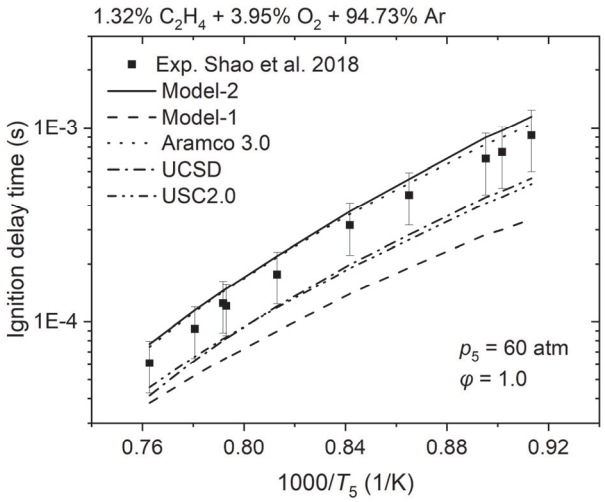

Journal: *Combustion and Flame* 117 (1999) 861-870.
Article: Experimental studies of shock-induced ignition and transition to detonation in ethylene and propane mixtures
Author: C. J. Brown and G. O. Thomas

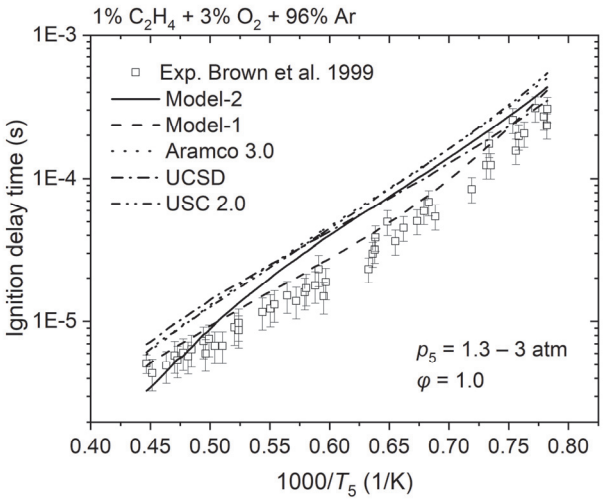

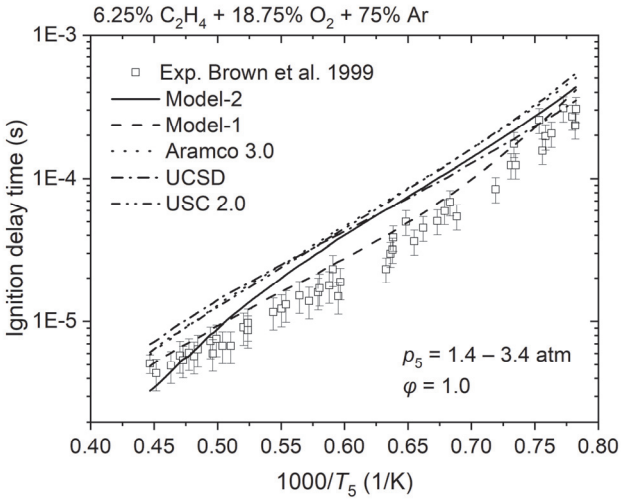

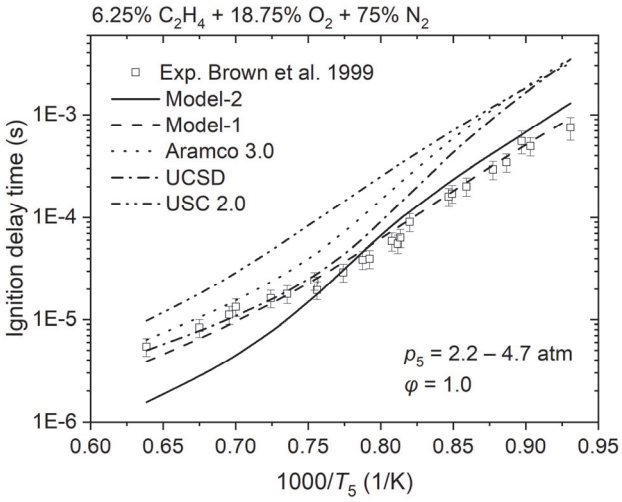

Reference:

[1] M.B. Colket, L.J. Spadaccini, Scramjet Fuels Autoignition Study, Journal of Propulsion and Power 17(2) (2001) 315-323.
[2] D.M. Kalitan, J.M. Hall, E.L. Petersen, Ignition and Oxidation of Ethylene-Oxygen-Diluent Mixtures with and Without Silane, Journal of Propulsion and Power 21(6) (2005) 1045-1056.
[3] O.G. Penyazkov, K.L. Sevrouk, V. Tangirala, N. Joshi, High-pressure ethylene oxidation behind reflected shock waves, Proceedings of the Combustion Institute 32(2) (2009) 2421-2428.
[4] S. Saxena, M.S.P. Kahandawala, S.S. Sidhu, A shock tube study of ignition delay in the combustion of ethylene, Combustion and Flame 158(6) (2011) 1019-1031.
[5] M.M. Kopp, N.S. Donato, E.L. Petersen, W.K. Metcalfe, S.M. Burke, H.J. Curran, Oxidation of Ethylene–Air Mixtures at Elevated Pressures, Part 1: Experimental Results, Journal of Propulsion and Power 30(3) (2014) 790-798.
[6] F. Deng, Y. Pan, W. Sun, F. Yang, Y. Zhang, Z. Huang, Comparative Study of the Effects of Nitrous Oxide and Oxygen on Ethylene Ignition, Energy & Fuels 31(12) (2017) 14116-14128.
[7] J. Shao, D.F. Davidson, R.K. Hanson, A shock tube study of ignition delay times in diluted methane, ethylene, propene and their blends at elevated pressures, Fuel 225 (2018) 370-380.
[8] C.J. Brown, G.O. Thomas, Experimental studies of shock-induced ignition and transition to detonation in ethylene and propane mixtures, Combustion and Flame 117(4) (1999) 861-870.
[9] C.-W. Zhou, Y. Li, U. Burke, C. Banyon, K.P. Somers, S. Ding, S. Khan, J.W. Hargis, T. Sikes, O. Mathieu, E.L. Petersen, M. AlAbbad, A. Farooq, Y. Pan, Y. Zhang, Z. Huang, J. Lopez, Z. Loparo, S.S. Vasu, H.J. Curran, An experimental and chemical kinetic modeling study of 1,3-butadiene combustion: Ignition delay time and laminar flame speed measurements, Combustion and Flame 197 (2018) 423-438.
[10] Chemical-Kinetic Mechanisms for Combustion Applications, Mechanical and Aerospace Engineering (Combustion Research), University of California at San Diego, San Diego Mechanism web page, http://combustion.ucsd.edu.
[11] J.G. Lopez, C.L. Rasmussen, M.U. Alzueta, Y. Gao, P. Marshall, P. Glarborg, Experimental and kinetic modeling study of C2H4 oxidation at high pressure, Proceedings of the Combustion Institute 32(1) (2009) 367-375.
[12] H. Wang, X. You, A.V. Joshi, S.G. Davis, A. Laskin, F. Egolfopoulos, C.K. Law, USC Mech Version II. High-Temperature Combustion Reaction Model of H2/CO/C1-C4 Compounds., http://ignis.usc.edu/USC_Mech_II.htm (May 2007).
[13] A.A. Konnov, Implementation of the NCN pathway of prompt-NO formation in the detailed reaction mechanism, Combustion and Flame 156(11) (2009) 2093-2105.
[14] G.P. Smith, D.M. Golden, M. Frenklach, N.W. Moriarty, B. Eiteneer, M. Goldenberg, C.T. Bowman, R.K. Hanson, S. Song, W.C. Gardiner Jr, GRI 3.0 Mechanism, Gas Research Institute (http://www.me.berkeley.edu/gri_mech) (1999).
[15] V. Dias, J. Vandooren, Experimental and modeling studies of C2H4/O2/Ar, C2H4/methylal/O2/Ar and C2H4/ethylal/O2/Ar rich flames and the effect of oxygenated additives, Combustion and Flame 158(5) (2011) 848-859.
[16] Z. Malliotakis, N. Leplat, G. Vourliotakis, C. Keramiotis, G. Skevis, M.A. Founti, J. Vandooren, An Experimental and Detailed Chemical Kinetic Investigation of the Addition of C2 Oxygenated Species in Rich Ethylene Premixed Flames, Combustion Science and Technology (2018) 1-24.

Supplementary Material - 4

A Comprehensive Kinetic Modelling Study of Ethylene Combustion with Data Uncertainty Analysis

Hongxin Wang[a], Nadezda Slavinskaya[b, c], Aziza Kanz[d], Moldir Auyelkhankyzy[c, e], Yiting Gao[a], Oskar Haidn[a]

a. Department of Aerospace and Geodesy, Technical University of Munich, 85748 Garching, Germany

b. GRS Association for Plant and Reactor Safety, 85748 Garching, Germany

c. Al-Farabi Kazakh National University, 050040 Almaty, Kazakhstan

d. DLR German Aerospace Center, Institute of Combustion Technology, 70569 Stuttgart, Germany

e. Institute of Combustion Problems, 050012 Almaty, Kazakhstan

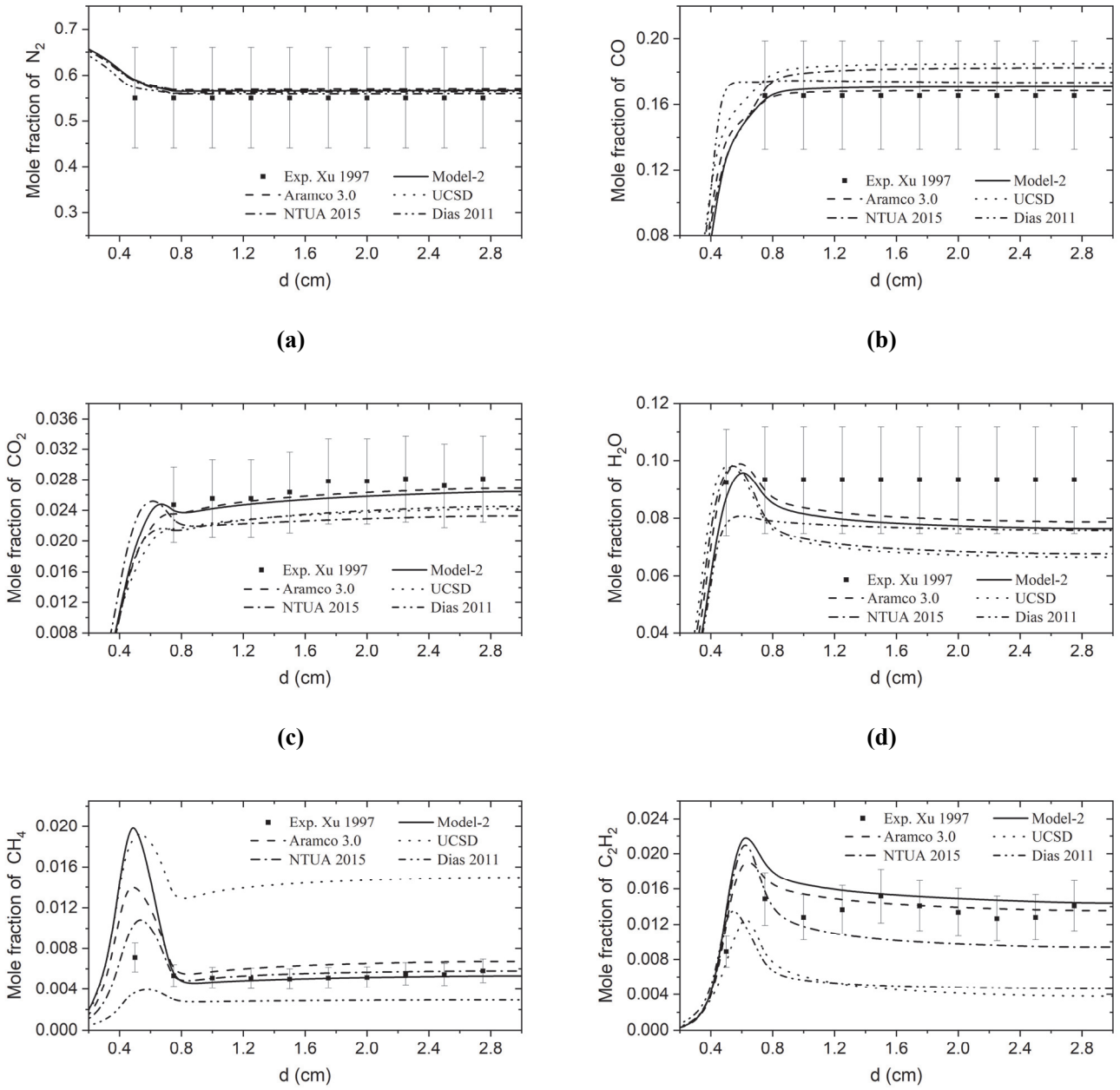

Figure S4-1. Comparison of concentration profiles in a premixed laminar flame of C_2H_4/air measured by Xu et al. [1] (scatters), 14%C_2H_4 + 18%O_2 + 68%N_2, p = 98.7 kPa, with simulations using model-2 (this study), Aramco 3.0 [2], UCSD [3], NTUA2015 [4], Dias2011 [5].

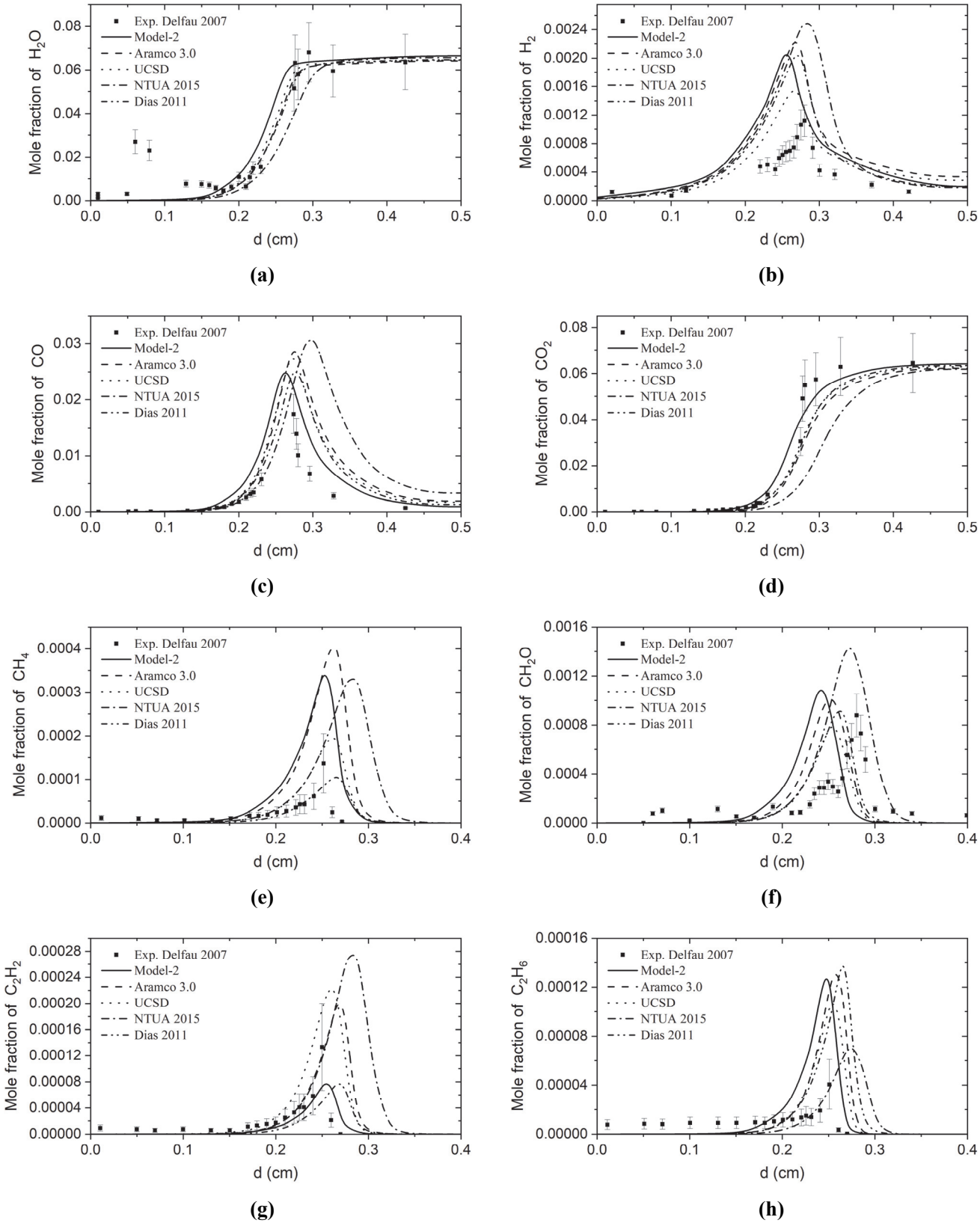

Figure S4-2. Comparison of concentration profiles in a premixed laminar flame measured by Delfau et al. [6] (scatters), 3.28%C_2H_4 + 19.79%O_2 + 76.93%Ar, φ = 0.5, p = 1 atm, with simulations using model-2 (this study), Aramco 3.0 [2], UCSD [3], NTUA2015 [4], Dias2011 [5].

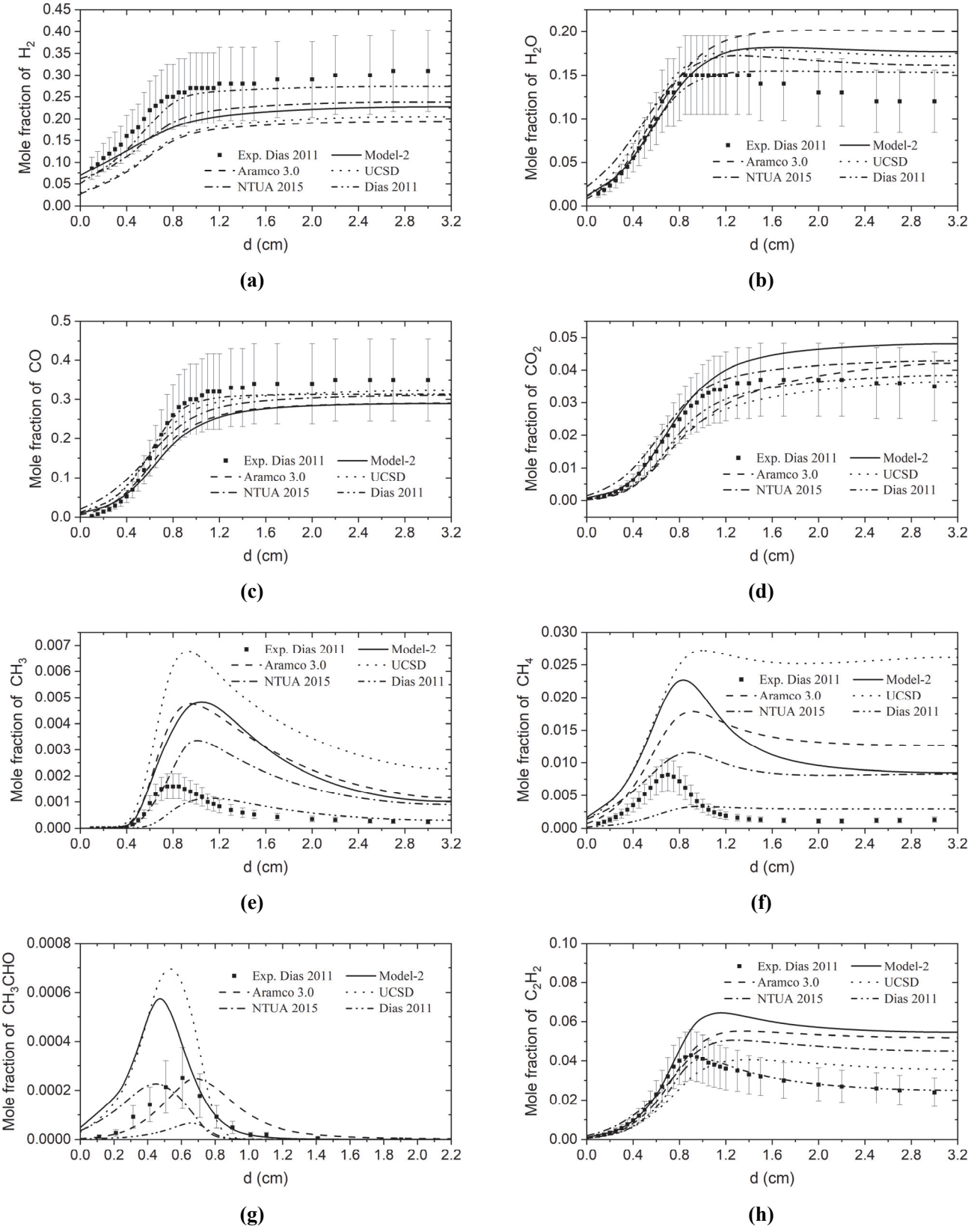

Figure S4-3. Comparison of concentration profiles in a premixed laminar flame measured by Dias et al. [5] (scatters), 33%C_2H_4 + 40%O_2 + 27%Ar, φ = 2.5, p = 0.05 bar, with simulations using model-2 (this study), Aramco 3.0 [2], UCSD [3], NTUA2015 [4], Dias2011 [5].

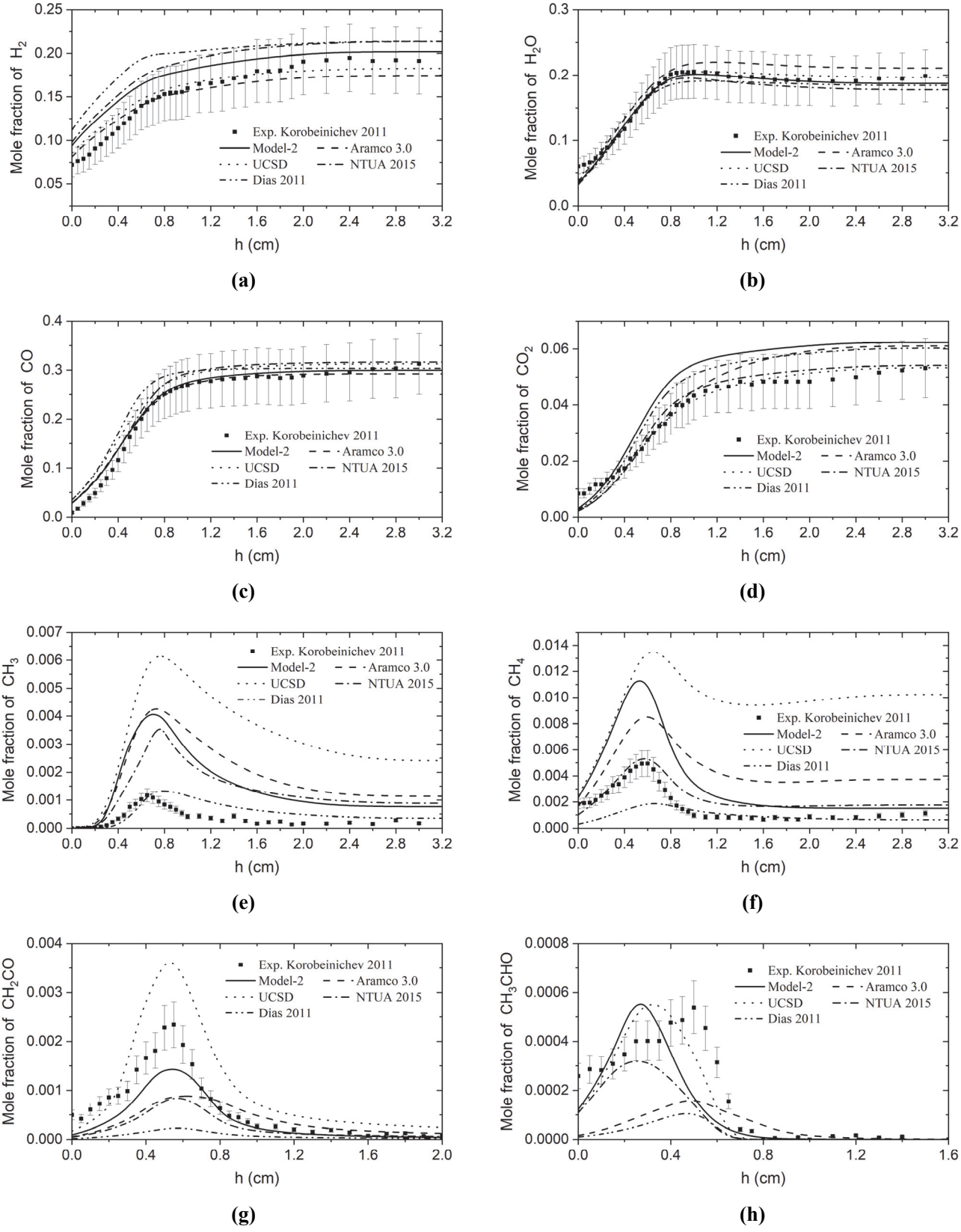

Figure S4-4. Comparison of concentration profiles measured in a premixed laminar flame of $C_2H_4/O_2/Ar$ by Korobeinichev et al. [7] (scatters), 28%C_2H_4 + 42%O_2 + 30%Ar, φ = 2.0, p = 0.04 bar, with simulations using model-2 (this study), Aramco 3.0 [2], UCSD [3], NTUA2015 [4], Dias2011 [5].

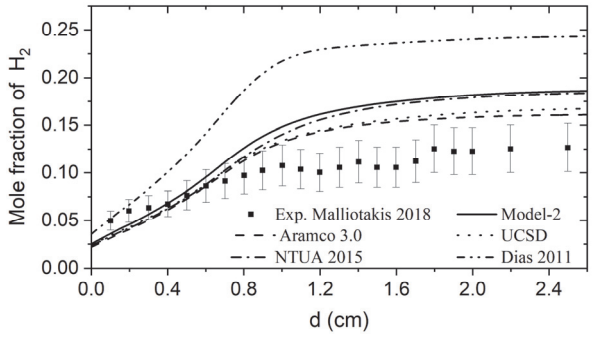

(a)

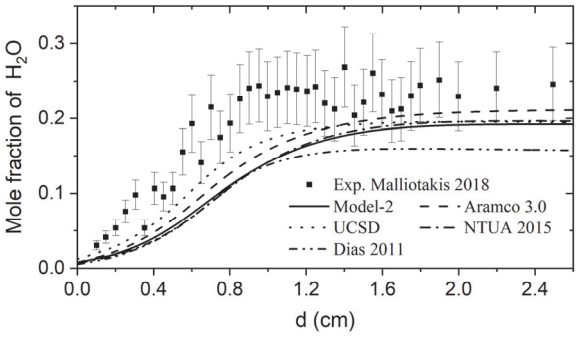

(b)

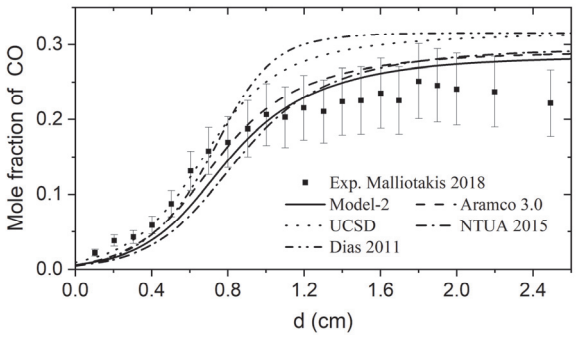

(c)

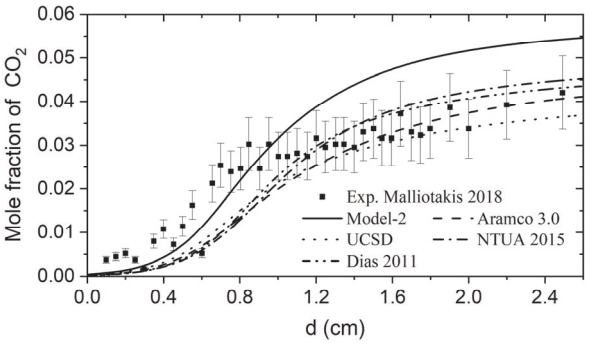

(d)

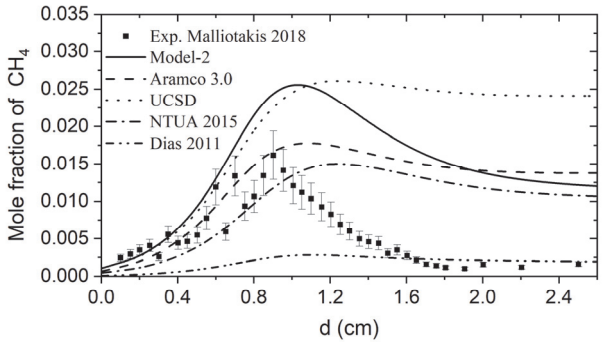

(e)

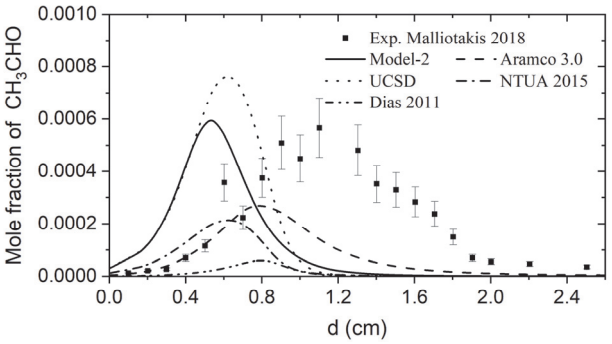

(f)

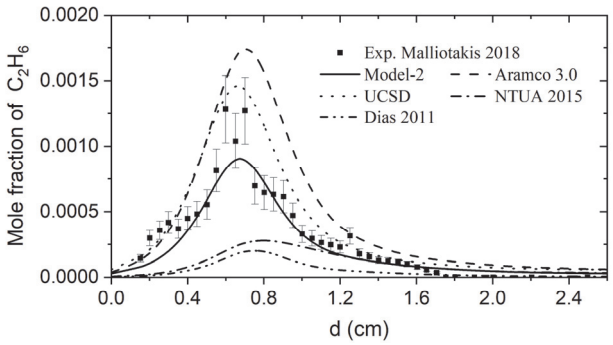

(g)

Figure S4-5. Comparison of concentration profiles measured in a premixed laminar flame of C_2H_4/O_2/Ar by Malliotakis et al. [4] (scatters), 30%C_2H_4 + 40%O_2 + 30%Ar, φ = 2.25, p = 0.04 bar, with simulations using model-2 (this study), Aramco 3.0 [2], UCSD [3], NTUA2015 [4], Dias2011 [5].

Reference:

[1] F. Xu, P. Sunderland, G. Faeth, Soot formation in laminar premixed ethylene/air flames at atmospheric pressure, Combustion and Flame 108(4) (1997) 471-493.

[2] C.-W. Zhou, Y. Li, U. Burke, C. Banyon, K.P. Somers, S. Ding, S. Khan, J.W. Hargis, T. Sikes, O. Mathieu, E.L. Petersen, M. AlAbbad, A. Farooq, Y. Pan, Y. Zhang, Z. Huang, J. Lopez, Z. Loparo, S.S. Vasu, H.J. Curran, An experimental and chemical kinetic modeling study of 1,3-butadiene combustion: Ignition delay time and laminar flame speed measurements, Combustion and Flame 197 (2018) 423-438.

[3] Chemical-Kinetic Mechanisms for Combustion Applications, Mechanical and Aerospace Engineering (Combustion Research), University of California at San Diego, San Diego Mechanism web page, http://combustion.ucsd.edu.

[4] Z. Malliotakis, N. Leplat, G. Vourliotakis, C. Keramiotis, G. Skevis, M.A. Founti, J. Vandooren, An Experimental and Detailed Chemical Kinetic Investigation of the Addition of C2 Oxygenated Species in Rich Ethylene Premixed Flames, Combustion Science and Technology (2018) 1-24.

[5] V. Dias, J. Vandooren, Experimental and modeling studies of C2H4/O2/Ar, C2H4/methylal/O2/Ar and C2H4/ethylal/O2/Ar rich flames and the effect of oxygenated additives, Combustion and Flame 158(5) (2011) 848-859.

[6] J.-L. Delfau, J. Biet, M. Idir, L. Pillier, C. Vovelle, Experimental and numerical study of premixed, lean ethylene flames, Proceedings of the Combustion Institute 31(1) (2007) 357-365.

[7] O.P. Korobeinichev, S.A. Yakimov, D.A. Knyazkov, T.A. Bolshova, A.G. Shmakov, J. Yang, F. Qi, A study of low-pressure premixed ethylene flame with and without ethanol using photoionization mass spectrometry and modeling, Proceedings of the Combustion Institute 33(1) (2011) 569-576.

Paper II

Fuel 319 (2022) 123705

Contents lists available at ScienceDirect

Fuel

journal homepage: www.elsevier.com/locate/fuel

Full Length Article

A comprehensive kinetic modeling study of hydrogen combustion with uncertainty quantification

Hongxin Wang [a], Nadezda Slavinskaya [b,c,*], Oskar Haidn [a]

[a] Department of Aerospace and Geodesy, Technical University of Munich, 85748 Garching, Germany
[b] GRS Association for Plant and Reactor Safety, 85748 Garching, Germany
[c] Al-Farabi Kazakh National University, 050040 Almaty, Kazakhstan

ARTICLE INFO

Keywords:
Hydrogen
Chemical kinetic model
Combustion
Uncertainty quantification

ABSTRACT

A 19-reactions H_2 oxidation chemical kinetic model has been optimized with uncertainty quantification. The uncertainties of the reaction rate constant (RRC) parameters have been first estimated based on the recommended direct measurements and review works. This deterministic approach was further combined with the probabilistic treatment of RRC to decrease the uncertainty intervals and to extend the temperature validity range for RRCs with the highest uncertainty level, for which two quantities, discrepancy measures and uncertainty contributions, were introduced in the developed framework. Monte Carlo simulations with randomly sampled RRCs and polynomial regression were performed to develop the response surface with high coefficients of determination to be utilized in the model optimization procedure.10 key channels were selected for further optimization, and the probability density functions were calculated on the basis of discrepancy measures for 4 channels to reduce their large uncertainty intervals. The training set was collected from carefully validated measured data following experiments of shock tubes, rapid compression machines, jet stirred reactors, plug flow reactors, and premixed laminar flames. Inconsistent experimental targets were fixed and excluded from considerations. The optimized chemical kinetic model demonstrates good predicting ability for the H_2 combustion experimental data from both the training set and the conditions outside the tested range (blind modeling).

List of Abbreviation

Abbreviation	Definition	Unit
T	Temperature	K
p	Pressure	atm, bar
φ	Equivalence ratio	Dimensionless
RRC	Reaction rate constant	
k	Reaction rate constant	order 1: s^{-1} order 2: $cm^3 \cdot mole^{-1} \cdot s^{-1}$ order 3: $cm^6 \cdot mole^{-2} \cdot s^{-1}$
E_a	Activation energy	K
f	Uncertainty factor of the RRC	Dimensionless
Y^{exp}	Experimental data	*
u	Uncertainty of the experimental data	*
ε^L, ε^U	The lower and upper bounds for experimental data	*
Y^{mod}	Modeling data	*
σ	Standard deviation of modeling data	*

(*continued on next column*)

List of Abbreviation (*continued*)

Abbreviation	Definition	Unit
ξ^L, ξ^U	The lower and upper bounds for simulation outputs	*
Ψ	Model discrepancy measure	Dimensionless
Y^{pre}	Response surface prediction data	*
X	Normalized RRC parameter	Dimensionless
α_i, β_{ij}	1st-/2nd- order polynomial coefficient	Dimensionless
c	Uncertainty contribution	*
c_r	Relative uncertainty contribution	Dimensionless
P	Probability	Dimensionless
W	Reverse discrepancy measure	Dimensionless
IDT	Ignition delay time	s
LFS	Laminar flame speed	cm/s
MC	Monte Carlo	
ST	Shock tube	
RCM	Rapid compression machine	
PLF	Premixed laminar flame	
PFR	Plug flow reactor	
JSR	Jet stirred reactor	

(*continued on next page*)

* Corresponding author.
E-mail address: Nadezda.Slavinskaya@grs.de (N. Slavinskaya).

https://doi.org/10.1016/j.fuel.2022.123705
Received 15 December 2021; Received in revised form 22 February 2022; Accepted 25 February 2022
Available online 17 March 2022

List of Abbreviation (*continued*)

Abbreviation	Definition	Unit
B2BDC	Bound-to-bound data Collaboration	
PDF	Probability density function	

*Depend on the type of the measurement.

1. Introduction

Due to the increasing demand for electric and renewable energy, the German Federal government presented a long-term political timetable for climate protection and the transformation of the energy supply, which calls for emissions of greenhouse gases in Germany to be reduced by 80% to 95% from the 1990 level by the year 2050 [1]. The national energy strategies of different countries give hydrogen the central role in the successful conversion of the energy systems to renewable, environmentally friendly, low-carbon energy technologies. Hydrogen is a perfect and ecological [2] energy carrier that is efficient and practically inexhaustible in nature. It is used as a feedstock in refineries and the chemical industry and as a possible substitute for coke in steel production. In the view of energy density, it shows the promising application in fuel cell vehicles [3] and is the most powerful propellant for rocket and air-breathing engines [4,5]. "Hydrogen World", i.e., production, storage, transport, and use of gray, blue, and green H_2 in various technical processes and industrial technologies strongly confronts with "problems" of hydrogen: extremely high diffusivity and flammability (hydrogen requires less than 7% of the energy to ignite natural gas), tendency to explode, very low temperatures for storage and transport. These characteristics make safe H_2 handling a challenge.

To control the safety of hydrogen technologies, numerical tools are needed which can reproduce/predict the possible accident scenario based on the simulation of different processes such as hydrogen leakage, ignition, flame propagation, explosion. As the high flammability of H_2 is caused by its oxidation chemistry, such tools should use the detailed chemical kinetic model for hydrogen combustion. Due to the high uncertainty of the related thermochemical data [6] and high requirements for assessing the likelihood of accidents, the reaction model should be developed with the actual estimated valid range. The main uncertainty source in chemical kinetic models, even for the key channels of hydrogen oxidation [7], is the reaction rate constants (RRCs), which can be measured only conditionally "directly" (actually, never directly), calculated with quanta-chemical methods, or evaluated by fitting the experimental data obtained for the macro chemical processes such as ignition delay times, laminar flame speeds, and concentration profiles.

During the past few decades, different approaches [8-10], have been developed to quantify the uncertainty of the kinetic model (*forward problem*) [8] and to define/reduce the uncertainty of the kinetic-model parameters (*inverse problem*) [11,12]. The underlying frameworks can be categorized as probabilistic and deterministic, depending on how the uncertainty of model parameters is treated. The probabilistic approaches address the uncertainty of parameters and models with probability density functions [13]. In contrast, the deterministic approach prescribes fixed uncertainty bounds for the involved parameters.

The most developed methodology, based on the deterministic approach, is the Bound-to-Bound Data Collaboration (B2BDC) [14]. It is employed using robust control of the actual limits for parameter uncertainties and consistency of the model parameters and related experiments. By deploying semidefinite programming algorithms [13], the initial bounds on unknowns are combined with the initial bounds of experimental data to outsource the parameter values, which give model predictions out of experimental errors. So initially calculated deterministic uncertainty bounds, called feasible parameter sets, are further used for prediction in new settings. The output variables produced in different numerical experiments for discrete points (random samplings) in feasible parameter space are fitted with a second-order polynomial function into a response surface (solution mapping methodology [11]), which is further used in subsequent uncertainty analysis to optimize the model and produce a final feasible set of model parameters [15] and to determine the model valid range. The model optimization is carried out after data consistency analysis: the potential outliers from a training set are identified with a quantitative measure of an agreement between the model and raw experimental data.

The probabilistic uncertainty quantification is aimed to evaluate the probability density function (PDF) of model parameters from the statistics of model outputs, i.e., quality of simulations of experimental data. Najm and co-workers [16-20] have implemented an approach, based on a spectral description of uncertain parameters and field quantities using polynomial chaos expansions for a stochastic representation of uncertainty. In the developed approach, an uncertain model parameter is described not as a deterministic quantity but as a random variable with a distribution described by a PDF. Sheen et al. [21-23] combined the deterministic and stochastic spectral expansion of parameters, solution mapping approach, and polynomial chaos expansions to develop the single unified theoretical and computational toolkit, termed the Method of Uncertainty Minimization using Polynomial Chaos Expansions, to quantify the model uncertainty and constrain the parameter uncertainties. The method was successfully applied to the detailed H_2/CO/C_1–C_4 kinetic model and ethylene combustion data by Sheen et al. [22] and at minimization of the uncertainty of an *n*-pentane combustion model by Cai and Pitsch [24]. Nagy and Turanyi estimated priori uncertainties of RRCs based on "direct" measurements and theoretical calculations of the Arrhenius parameters [25]. A method similar to Sheen et al. [22] was applied to the optimization procedure [26], but the systematic deviation between the simulated and experimental values was taken into account. The initial Gaussian distribution probability density function (PDF) within the determined uncertainties are narrowed in an iterative manner [26], and much lower uncertainties were obtained for the RRCs within the validated temperature range.

Despite the big effort in the uncertainty quantification methods, there are open questions related to the sampling design, solution surface approximation, data consistency, re-optimization problem on the new data, data correlations. The high correlations of the RRCs can lead to the restriction of the applicability of the results obtained with probabilistic methods: the evaluated constraints of model parameters are strongly linked with the studied model and used a training set of experimental data.

Due to the limited experimental conditions, the earlier hydrogen oxidation models [27,28] and the models optimized for specific experiments [29,30] have a limited range of their applications. Most of the studies for detailed chemical kinetic models were carried out with hands and intuition without uncertainty analysis [31]. Konnov [32] gave a review of recommended RRCs and their uncertainties in the modeling study of H_2 oxidation. The developed detailed H_2 oxidation model [32] was further updated in the work of Alekseev et al. [33] and the study devoted to the excited species in hydrogen combustion [34]. Conaire et al. [35] developed an H_2 oxidation model fitted for a variety of experimental data, and the model was updated in the modeling study of the H_2 and syngas oxidation by Keromnes [36]. The RRCs were optimized at fitting the ignition delay time targets measured in shock tubes and the rapid compression machines [36,37]. Based on the H_2 combustion model of Keromnes [36], Varga et al. [38] minimized the modeling uncertainty for ignition delay times and laminar flame speeds using the method [26] mentioned above. Varga et al. [38] used the response surfaces [11] approach for the 'first stage' optimization, but ignition delay times were directly calculated in the 'second stage' optimization. Li et al. [39] modified the H_2 oxidation model of Mueller et al. [28] with newly recommended RRCs, and Burke et al. [40] updated the model of Li et al. [39] with special attention to high-pressure flames. Zhang et al. [41] also conducted a modeling study of H_2 oxidation for high-pressure conditions, in which the uncertainties of RRCs were analyzed, but only a few ignition delay times measured in a rapid

compression machine [42] were utilized for the model validation at high-pressures.

In this paper, the statistical treatments of the reaction models described in [43,44] were further developed and applied to the optimization of the H_2 oxidation (19 reactions, 11 components) sub-model from our previous studies [15,45,46] to produce an actual H_2 combustion reaction model with evaluated uncertainty range and reduced feasible set of parameters (RRCs). The combined deterministic and probabilistic approach using the next methods, principles, and tools were applied: statistical procedure from our previous work [45] to evaluate uncertainty boundaries of RRCs used in the model as-complied; experimental uncertainties of experimental data follow from data sources or our evaluations [15,47]; the Latin Hypercube method [48] for the random parameter samplings; Monte Carlo (MC) [44] calculations and evaluation of the model uncertainty; polynomial regression [43] for construction of the multitarget high-dimensional input–output response function; the global sensitivity analysis [49,50], the relative uncertainty contribution of parameters for the determination of key reaction channels, construction of PDFs and model optimization. Experimental data for the model calibration and optimization are collected from the recently published measurements carried out in the shock tube (ST), rapid compression machine (RCM), premixed laminar flame (PLF), plug flow reactor (PFR), and jet stirred reactor (JSR).

2. Methodology

2.1. Uncertainty analysis of reaction rate constants

The statistical analysis has been performed for the recommended in literature RRCs to evaluate the uncertainty boundaries of the RRCs used in the model as-complied. In this study, Arrhenius equation parameters for RRCs recommended by experimental measurements, theoretical calculations, and the review works of Baulch et al. [7,51-53] were collected with specific temperature ranges. Recommendations from models, which were fitted on the macro experimental combustion data, were not used in the uncertainty analysis. Collection of detailed information for the used RRC parameters and references for the analyzed reactions and graphics for obtained uncertainty intervals are presented in Supplementary-1.

The statistical method of nonlinear regression established in the authors' previous works [45,46] was applied to calculate the standard deviations $s(A), s(n), s(E_a)$ of the Arrhenius expression parameters A, n, and E_a.

$$k(T) = AT^n \exp\left(-\frac{E_a}{T}\right), (\mathrm{cm}^3,\ \mathrm{s},\ \mathrm{mole},\ \mathrm{K}) \tag{1}$$

$s(A), s(n), s(E_a)$ can be found from the covariation matrix of applied statistical approach [45,46,54-56]. After that the lower, k_{low}, and upper, k_{up}, boundaries of RRC can be calculated:

$$k_{low}(T) = 10^{\log_{10}(A)-s(A)} T^{(n-s(n))} \exp\left(-\frac{E_a + s(E_a)}{T}\right) \tag{2}$$

$$k_{up}(T) = 10^{\log_{10}(A)+s(A)} T^{(n+s(n))} \exp\left(-\frac{E_a - s(E_a)}{T}\right) \tag{3}$$

Then the integrated uncertainty factor for the RRC, $f(T)$, is defined as follows:

$$f(T) = \log_{10}\left(\frac{k_{up}(T)}{k_0(T)}\right) = \log_{10}\left(\frac{k_0(T)}{k_{low}(T)}\right) \tag{4}$$

where k_0 is the nominal RRC.

The main problem at the RRCs uncertainty evaluation arises from the deficit and incompleteness of the data. An illustration of the problem can be done with data analysis performed for recommendations available only for limited temperature range: the uncertainty bounds evaluated only on low-temperature or high-temperature data can result in an underestimation of the RRC uncertainty for the given temperature range, Fig. 1, or can lead to erroneous trends in uncertainty bounds for the temperature range where the data are missing.

Due to the different levels of attention and technical limitations, the number of available RRCs data for each reaction is various and some reactions are only studied around standard state temperature (298 K). Deficit of data can result in higher uncertainty intervals, Table 1, even for such key reactions for the low temperature H_2 oxidation as (R8) and (R13). For well-investigated reactions more sources are available and relatively lower uncertainties can be obtained, reactions (R6) and (R7), Table 1. One of the aims of the proposed optimization framework is to reduce the uncertainty intervals for reactions with data deficit. The uncertainties of the third factors and relevant center broadening factors for the pressure-dependent reactions are not considered in the current work due to the available experimental studies on dilution gas and pressure.

2.2. Combustion experimental targets

To optimize the H_2 model, the fundamental combustion heterogenic experimental targets were carefully selected over a wide spectrum of experimental conditions, Table 2. The published experimental results of ignition delay times (IDTs) [36,42,57-64], laminar flame speeds (LFSs) [65-83], and flow reactor species profiles [29,30,84,85] were used as the training set for the model. Each target is assigned with uncertainty, $u\left(Y_{ij}^{\exp}\right)$, following from data source or carefully evaluated based on the earlier published studies [15,47], and finally presented with error bars in the figures. The uncertainty in measuring experiment targets is further used to constrain the uncertainty of the model predictions and the feasible parameter set reducing. The experimental data with poor quality were recognized by the consistency analysis, which will be shown in the following chapter, and were removed from the training set. All the simulations in this work were conducted with Ansys Chemkin Pro [50]. "Mixture-averaged transport option" was used for LFS 196 simulations.

2.3. Uncertainty of the as-compiled reaction model and discrimination of inconsistent training targets

The uncertainty of the as-compiled chemical kinetic model is assessed by direct MC simulations of targets from the training set. The Arrhenius expression parameters ($\log_{10}(A)$, n, and E_a in Eq. (1)) of the 19 reactions were sampled using the Latin Hypercube sampling method

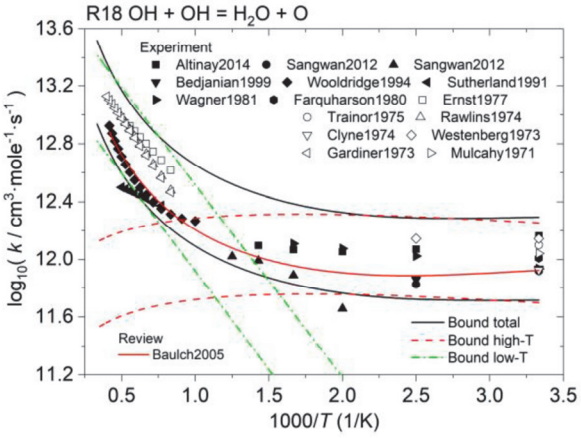

Fig. 1. Recommended RRCs for reaction $OH + OH = H_2O + O$ with evaluated bounds based on both, high-temperature and low-temperature recommendations (the detailed reference information is presented in Supplementary-1).

Table 1
The calculated uncertainty intervals for the 19 reactions in the as-compiled reaction model for the H_2 oxidation (H for high-pressure limit, L for low-pressure limit).

No.	Reaction	Number of used RRC sources	Initial uncertainty intervals f_u/f_l
R1	$2H + M = H_2 + M$	12	0.36–0.38
R2	$H + O + M = OH + M$	1	0.50
R3H	$H + O_2(+M) = HO_2(+M)$ high-p	5	0.09
R3L	$H + O_2(+M) = HO_2(+M)$ low-p	9	0.16–0.17
R4	$H + O_2 = OH + O$	21	0.19–0.20
R5H	$H + OH(+M) = H_2O(+M)$ high-p	1	0.50
R5L	$H + OH(+M) = H_2O(+M)$ low-p	6	0.50
R6	$H_2 + O = OH + H$	17	0.27–0.29
R7	$H_2 + OH = H_2O + H$	23	0.20–0.21
R8	$H_2O_2 + H = HO_2 + H_2$	3	1.00
R9	$H_2O_2 + H = H_2O + OH$	3	1.00
R10	$H_2O_2 + O = HO_2 + OH$	3	0.30
R11	$H_2O_2 + OH = H_2O + HO_2$	11	0.13
R12	$H + HO_2 = H_2 + O_2$	5	0.56–0.59
R13	$H + HO_2 = 2OH$	3	0.42–0.44
R14	$2HO_2 = H_2O_2 + O_2$	21	0.29–0.30
R15	$HO_2 + O = O_2 + OH$	7	0.15
R16	$HO_2 + OH = H_2O + O_2$	19	0.26–0.27
R17	$2O + M = O_2 + M$	6	0.18–0.23
R18	$2OH = H_2O + O$	15	0.28–0.29
R19H	$H_2O_2(+M) = 2OH(+M)$ high-p	4	1.0
R19L	$H_2O_2(+M) = 2OH(+M)$ low-p	5	0.20–0.22

Table 2
Used H_2 oxidation experiments and their test conditions.

IDT measured in the ST	T_5/K	p_5/bar	Mixture
DLR [36,57]	889 – 2110	1.0 – 19.7	$H_2/O_2/N_2/Ar$, $\varphi = 0.1 – 4.0$
TAMU [36]	965 – 1736	1.67 – 34.24	$H_2/O_2/Ar$, $\varphi = 0.3 – 1.0$
XJTU [58-60]	905 – 1463	1.22 – 20.0	$H_2/O_2/Ar$, $\varphi = 0.5 – 2.0$
UCF [61,62]	1009 – 1752	0.96 – 1.38	$H_2/O_2/Ar$, $\varphi = 0.4 – 1.47$
Stanford [63]	858 – 1131	3.04 – 4.42	$H_2/O_2/Ar$, $\varphi = 0.4 – 1.0$
IDT measured in the RCM	**T_c/K**	**p_c/bar**	**Mixture**
CWRU [42,64]	907 – 1065	10 – 70	$H_2/O_2/H_2O/N_2/Ar$, $\varphi = 1.0$
NUIG [36]	926 – 1013	8, 16, 32	$H_2/O_2/N_2/Ar$, $\varphi = 0.5$
Laminar flame speed	**T_u/K**	**p/atm**	**Mixture**
Bunsen flame [65-68]	298	1	H_2/air, $\varphi = 0.5 – 3.0$
Counterflow flame [69-73]	298	1	H_2/air, $\varphi = 0.26 – 1.5$
Spherical flame [74-83]	298 – 443	0.3 – 20.0	H_2/air, $\varphi = 0.23 – 5.08$ $H_2/O_2/N_2/He/Ar$, $\varphi = 0.45 – 4.5$
Concentration profile	**T/K**	**p**	**Mixture**
PLF [84]	–	1 atm	$H_2/O_2/N_2$, $\varphi = 2.05$
PLF [85]	–	4.75 kPa	$H_2/O_2/Ar$, $\varphi = 1.93$
JSR [29]	800 – 1150	1, 10 atm	$H_2/O_2/N_2$, $\varphi = 0.2 – 2.33$
PFR [30]	700 – 900	50 bar	$H_2/O_2/N_2$, $\varphi =$ 0.0009–12.07

[48]. Uniform distributions were defined for the rate parameters within the evaluated uncertainty intervals, Table 1. Fig. 2a shows an example of a histogram of the predicted IDT for $H_2/O_2/Ar$ mixture at $T_5 = 1000$ K and $p_5 = 1$ bar obtained with 600 MC simulations with randomly sampled RRC parameters. The two-standard deviation (2σ), which covers > 90% of the distribution probability, is defined as the modeling uncertainty [21,86]. So calculated uncertainty bounds for the simulations of the IDT from [36] and [59] with the as-compiled model are shown in Fig. 2b.

To minimize the uncertainty propagation problem, data points which were not reconciled with both other targets and studied reaction model within the reported/calculated measurement errors and evaluated model uncertainties were recognized as inconsistent. For that, the lower and upper bounds for simulation outputs, $\xi_{ij}^{L} and \xi_{ij}^{U}$, and experimental targets, $\varepsilon_{ij}^{L} and \varepsilon_{ij}^{U}$, of the j_{th} target in the i_{th} data set are defined as.

$$\varepsilon_{ij}^{L} = \overline{Y}_{ij}^{mod} - 2\sigma_{ij} \text{and} \varepsilon_{ij}^{U} = \overline{Y}_{ij}^{mod} + 2\sigma_{ij} \tag{5}$$

$$\xi_{ij}^{L} = Y_{ij}^{exp} - u\left(Y_{ij}^{exp}\right) \text{and} \xi_{ij}^{U} = Y_{ij}^{exp} + u\left(Y_{ij}^{exp}\right) \tag{6}$$

where $\overline{Y}_{ij}^{mod}$ is the average value of MC simulation results, σ_{ij} is the standard deviation of MC simulation results, Y_{ij}^{exp} is the experimentally measured data, and $u\left(Y_{ij}^{exp}\right)$ is the uncertainty of the experimental target. Then the condition for target discrimination is described as:

$$\xi_{ij}^{U} < \varepsilon_{ij}^{L} \text{or} \xi_{ij}^{L} > \varepsilon_{ij}^{U} \tag{7}$$

In this way, the measured data with potential high uncertainties have been fixed and removed from the training set collected in Table 2. One example is shown in Fig. 3: data measured by Qin et al [65], Liu et al. [68], and Gunther et al. [73] are more likely to be over-measured and inconsistent with other points and simulations within their uncertainty boundaries. On this way measured data following from studies [58,62,65,68,73] (Table 2) were finally excluded from the model optimization procedure due to their potential high uncertainties.

It should be noted that measured and simulated uncertainties of the LFS for very lean and 234 very reach mixtures are higher than uncertainty of data around stoichiometric mixtures. For these 235 conditions, when a heat release effect does not further hardly suppressed diffusion and number of 236H radicals is low, the special experimental setups and more accurate models for the 237 multicomponent diffusion are necessary.

2.4. Reaction model optimization

2.4.1. Definition of the model discrepancy measure

To evaluate the predictive ability of the model, the model discrepancy measure, $\overline{\Psi}$, is defined as:

$$\overline{\Psi} = \frac{1}{M}\sum_{i=1}^{M}\frac{1}{N_i}\sum_{j=1}^{N_i}\Psi_{ij}^{mod} \tag{8}$$

in which M is the number of the experimental data sets and N_i is the point number of the i_{th} data set. The Ψ_{ij}^{mod} for the j_{th} target in the i_{th} data set is defined as following:

$$\Psi_{ij}^{mod} = \left(\frac{Y_{ij}^{mod} - Y_{ij}^{exp}}{u\left(Y_{ij}^{exp}\right)}\right)^2 \tag{9}$$

where Y_{ij}^{exp} is the experimentally measured data and Y_{ij}^{mod} is the modeling result. The experimental uncertainty, $u\left(Y_{ij}^{exp}\right)$, is adopted form the reference or evaluated based on the uncertainty analysis of experiments [15,47].

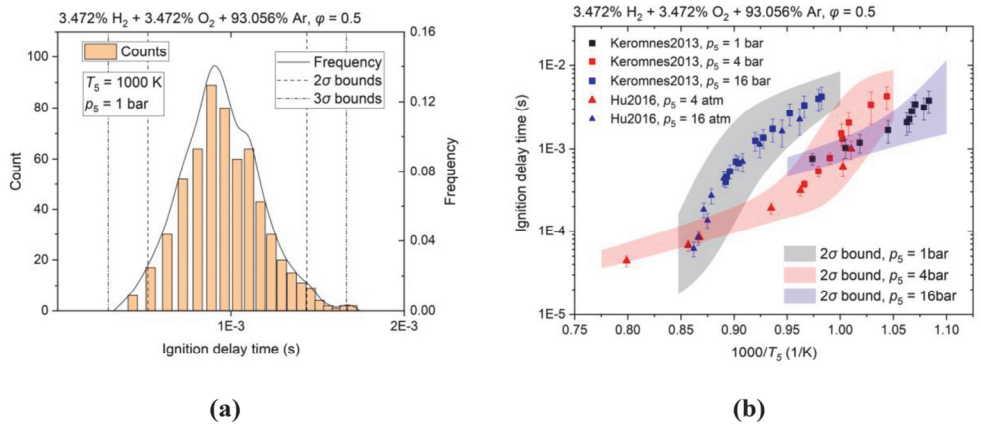

Fig. 2. (a) Histogram and probability density distribution of IDT (T_5 = 1000 K, Keromnes et al. [36]) simulated with MC method. (b) IDTs of H_2/O_2/Ar mixture measured by Keromnes et al. [36] and Hu et al. [59] and the modeling uncertainties determined by 2σ (shadows).

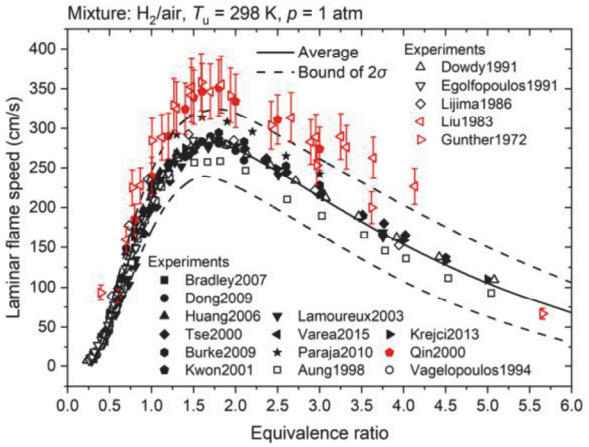

Fig. 3. LFSs of H_2/air mixtures and evaluated modeling uncertainty of the as-compiled reaction model (10% uncertainty for the experimental data).

2.4.2. Response surface

To optimize the reaction kinetic model, the global sensitivity analysis is explored to describe the multivariate contributions of high dimensional input variables, acting not independently and not necessarily linearly, in the model outputs. To learn system input–output response behavior, an interpolation of the heterogenic system outputs throughout the input variable space (mapping) with response surface is widely used [8,87]. The model outputs $y(x)$ are replaced with response surface approach expressed as a finite function expansion in terms of the input variables. In this study, the second-order polynomial regression [43] was used to construct the response surface for simulated outputs of IDTs, LFSs, and concentration profiles.

The Arrhenius expression parameters $\boldsymbol{X}$ ($\log_{10}(A)$, n, and E_a in Eq. (1)) were normalized within the uncertainty intervals (Table 1) to the space of [0,1]. The outputs $\boldsymbol{Y}^{mod}(\boldsymbol{X})$ directly simulated with Chemkin Pro [50] are presented as the second-order polynomial to express the response function $\boldsymbol{Y}^{\mathrm{pre}}(\boldsymbol{X})$ throughout the total of N number of model parameters:

$$\boldsymbol{Y}^{mod}(\boldsymbol{X}) \approx \boldsymbol{Y}^{\mathrm{pre}}(\boldsymbol{X}) = Y_0 + \sum_{i=1}^{N} \alpha_i X_i + \sum_{i=1}^{N}\sum_{j=1}^{N} \beta_{ij} X_i X_j \tag{10}$$

where $\boldsymbol{Y}_0$ is the intercept; $\boldsymbol{\alpha}$ and $\boldsymbol{\beta}$ are the first- and second-order polynomial coefficients of the second-order polynomial. They have been determined using least square method realized in in-home python numerical code [88].

With the help of the response surface, the simulated results, $\boldsymbol{Y}^{mod}$ obtained by solving the Navier-Stokes equations with Chemkin Pro can be replaced by the $\boldsymbol{Y}^{\mathrm{pre}}$ determined by second-order polynomial regression. The quality of the model with a specific Arrhenius expression parameter set can be evaluated quickly without solving the chemical and physical equations, which can produce a large amount of data and makes the application of statistical method possible. By replacing $\boldsymbol{Y}^{mod}$ in Eq. (9) with $\boldsymbol{Y}^{\mathrm{pre}}$ in Eq. (10), the discrepancy between experimental data and simulations can be presented in objective function as.

$$\Psi_{ij}^{\mathrm{mod}} \approx \Psi_{ij}^{\mathrm{pre}} = \left(\frac{Y_{ij}^{\mathrm{pre}} - Y_{ij}^{\mathrm{exp}}}{u\left(Y_{ij}^{\mathrm{exp}}\right)} \right)^2 \tag{11}$$

To evaluate the predictive ability of the response surface, the coefficient of determination [89], R^2, and the relative error, which is defined as:

$$\left| \frac{Y_{ij}^{\mathrm{pre}} - Y_{ij}^{\mathrm{exp}}}{Y_{ij}^{\mathrm{exp}}} \right| \times 100\% \tag{12}$$

are calculated. An average relative error of 1% between the data predicted by response surface and experimental data has been obtained, and R^2 higher than 0.98 was obtained for the polynomial regression of IDTs measured by STs and 0.99 for the other experiments. Fig. 4 demonstrates the comparison of results predicted by the constructed response surface and the results directly simulated with Chemkin Pro [50]. As shown by the examples, the LFSs and IDTs predicted by the response surface agree well with the directly simulated results. More results for the comparison of the simulated and predicted results are shown in Fig. S2-1 in Supplementary-2.

2.4.3. Uncertainty contribution of the RRCs

Uncertainty analysis based on the sensitivity analysis [90-92] quantify the uncertainty in the model output given by the defined uncertainties in the model input. In this study, the relative uncertainty contribution of parameter X_i among the total N number of model parameters is defined as:

$$c_r(X_i) = \frac{c(X_i)}{\sum_{i=1}^{N} c(X_i)} \tag{13}$$

where.

$$c(X_i) = \left[Y_{\max}^{\mathrm{pre}}(X_i) - Y_{\min}^{\mathrm{pre}}(X_i) \right] \Big|_{X_j = \overline{X}_j, j \neq i} \tag{14}$$

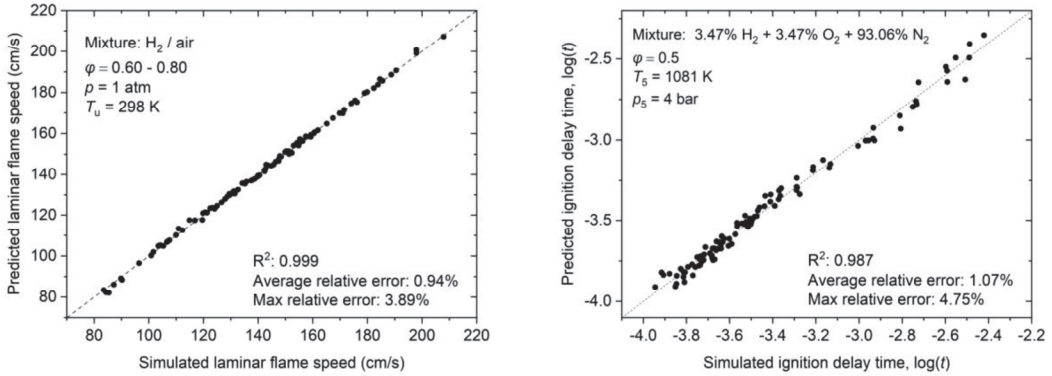

Fig. 4. Results predicted by the response surface versus directly simulated with Chemkin Pro [50] for (a) LFSs of H_2/air mixtures and (b) IDTs of $H_2/O_2/N_2$ mixture.

and $\overline{X}_j$ is the average value ofX_j..

Compared to the sensitivity analysis, the relative uncertainty contributions can reveal the influence of the RRCs uncertainties on simulation results and identifying thereby reactions which have the highest potential to be improved. To identify these reactions all the 19 reactions were analyzed for uncertainty contributions over the studied experimental conditions for IDTs, LFSs, and concentration profiles. Reactions with$c_r > 10\%$ were taken as optimization targets. More details are explained in Fig. S2-2 in Supplementary-2. Here Fig. 5a and Fig. 5b demonstrate an example of the comparison of normalized sensitivity coefficients [50] and the relative uncertainty contributions (Eq. (13)) for IDTs. Only the top 10 channels and 3 different cases for IDTs are shown in Fig. 5. Both spectrums reveal the dominance of reaction (R3) and (R4), and importance of reactions (R8), (R13), and (R19) at high pressures. Although reaction (R4) shows higher sensitivity than reaction (R8) at 16 bar in Fig. 5a, reaction (R8) contributes a higher uncertainty to the modeling of IDT (Fig. 5b) due to its larger uncertainty factor (Table 1). Also, simulations of RCM and PFR are strongly influenced by reaction (R8) and (R19), Fig. 6.

2.4.4. *Reduction of feasible parameter set and modeling uncertainties*

With the criteria described in the previous paragraph, 10 most contributing in uncertainty channels have been defined as objects for the model optimization, Fig. S2-2 in Supplementary-2. The 33 parameters of the selected 10 channels were randomly sampled within the uncertainty intervals and MC simulations were conducted for the PFR [30] and RCM [64]. Reaction (R8) and (R19) were specially analyzed for these two kinds of reactors due to their dominance in the uncertainty contributions, Fig. 6.

The discrepancy measure,$\overline{\Psi}$, obtained from the random sampling of the RRC of reaction $H_2O_2 + H = HO_2 + H_2$ (R8) is shown in Fig. 7a. The lowest discrepancies were concentrated around $\log_{10}(k_{R8}) = 11.7$ (Fig. 7a), and the uncertainty intervals for the RRC of reaction (R8) are expected to be reduced. The combined influence of the two reaction uncertainties, (R8) and (R19H), on the discrepancy between experimental data [30,42,64] and simulations is presented in Fig. 7b. Although reaction (R19H) (y-axis direction) does not have the same dominant position as reaction (R8) (x-axis direction), its correlation with (R8) affects the discrepancy measure distribution indicating that an optimized model should be developed as result of integrated effect of key RRCs under consideration.

From the distribution of discrepancy between experimental data and model predictions the PDFs for the studied RRCs have been calculated to replace the initially defined uniform uncertainty distribution. The probability density function of the RRC is calculated as follow:

$$P(a \le k \le b) = \frac{\sum_{j=1}^{m} W_j}{\sum_{i=1}^{n} W_i}(a \le k_j \le b) \tag{15}$$

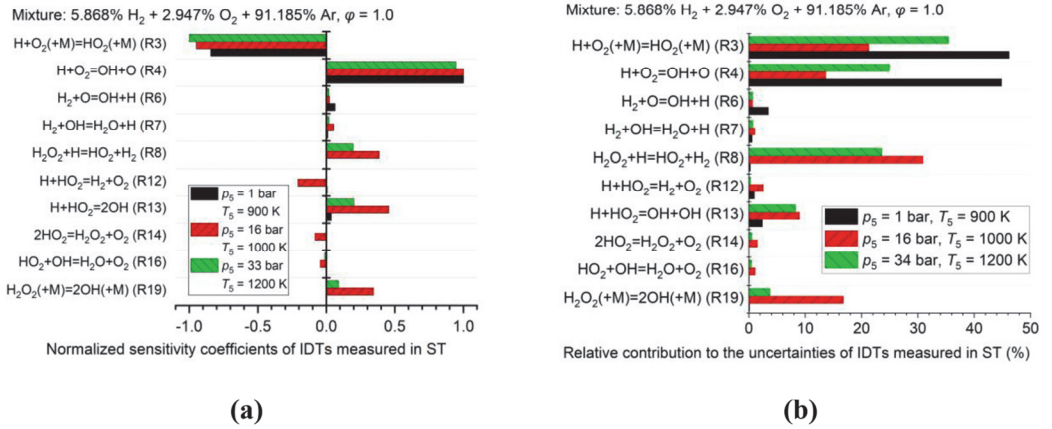

Fig. 5. (a) Normalized sensitivity coefficients of IDTs for H_2/O_2/Ar mixtures; (b) Comparison of the relative uncertainty contributions of different channels to the modeling IDTs in the ST.

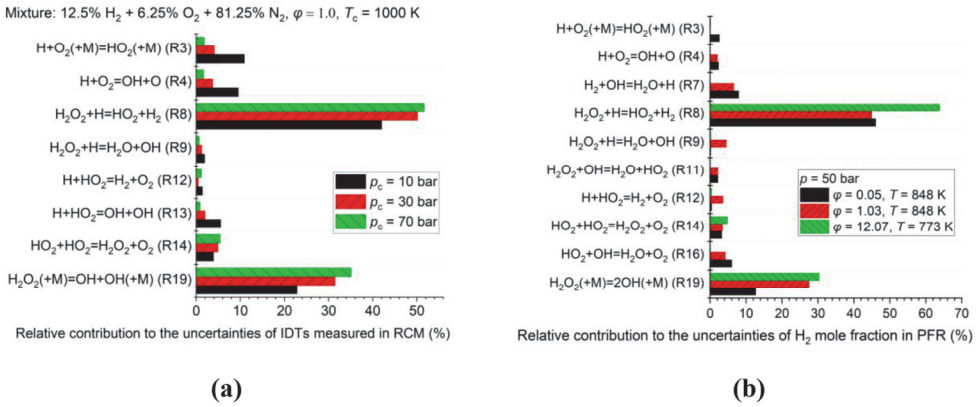

Fig. 6. Comparison of the relative uncertainty contributions of different channels to the (a) IDTs measured in the RCM (b) H_2 mole fractions measured in the PFR [30].

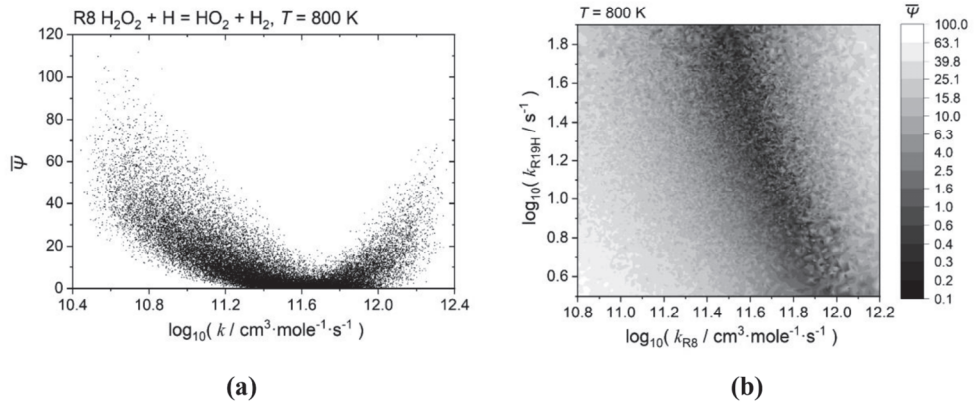

Fig. 7. (a) The distribution of discrepancy measure obtained from random sampling of the RRC of reaction $H_2O_2 + H = HO_2 + H_2$ (R8); (b) the combined influence of uncertainties of reactions $H_2O_2 + H = HO_2 + H_2$ (R8) and $H_2O_2 = OH + OH$ (R19H) on the simulation of IDTs measured in the RCM [42,64] and mole fractions measured in the PFR [30].

where $P(a \le k \le b)$ is the probability that the RRC, k, is located between a and b; n is the total number of the samples and m is the number of parameters sets in which $a \le k_j \le b$. The weight, W, is defined as the reciprocal of the discrepancy measure:

$$W = \frac{1}{\overline{\Psi}} \tag{16}$$

The so calculated smoothed PDF and the reduced 2σ bounds are shown in Fig. 8a for (R8) $H_2O_2 + H = HO_2 + H_2$ as example. The final

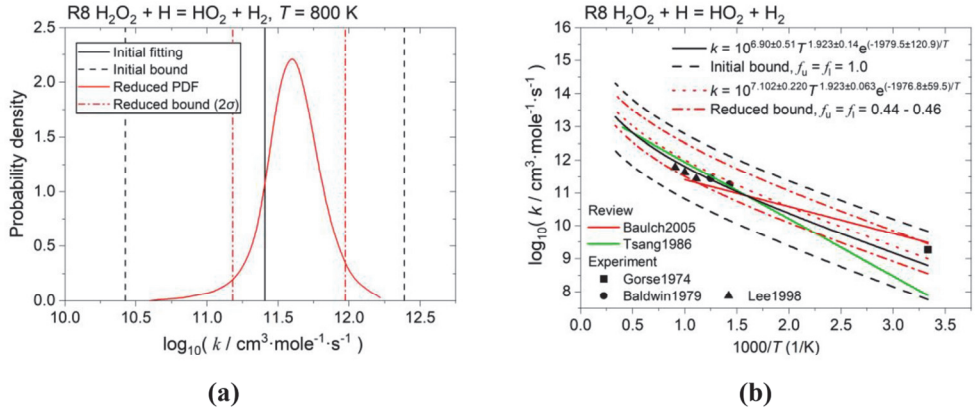

Fig. 8. (a) The probability density function of the RRC calculated based on the discrepancy measure; (b) Comparison of the initial uncertainty bounds and the reduced bounds for the RRC of reaction (R8) $H_2O_2 + H = HO_2 + H_2$ [7,27,53,93,94].

uncertainty interval for reaction (R8) was reduced on this way from 1 to 0.44–0.46, Fig. 8b. Applying this procedure the input temperature intervals of recommended RRCs have been extended to the effective validated temperature range, which follows from the experimental test conditions (800 to 1000 K for the PFR [30] and RCM [42,64]). To keep the validity of expressions for the uncertainty of the RRC, Eq. (2) and (3), the RRC uncertainty bounds outside of the test temperature range, where validation data are lacked, are shifted following the bounds inside the validated temperature range. The reduced uncertainties are expected to be further studied and re-optimized in the future when experimental data covering wider temperature and pressure ranges appear.

The distributions of the discrepancy measures obtained from random samplings of the RRCs of reactions (R8), (R12), (R13), and (R19H) are shown in Fig. S2-3 in Supplementary-2. The probability density functions and the reduced uncertainties for these RRCs are shown in Figs. S2-4 and S2-5 in Supplementary-2.

3. Results and discussion

The process diagram of the current study is presented in Fig. 9. The deterministic and probabilistic approaches are combined for the RRC uncertainty treatment to extend the RRC input temperature validity range. With the method shown in the previous sections, uncertainties of the RRCs were estimated and the high uncertainty intervals of reaction (R8), (R12), (R13), and (R19H) were reduced with the method presented in this study. The modeling uncertainty of RCM, PFR, and JSR have been obviously reduced, which will be shown in Figs. 11, 13, and 15.

Within the reduced bounds, the Arrhenius parameters of the selected 10 key reactions were randomly sampled and one of the models with lowest $\overline{\Psi}$ were selected as the final optimized model. It should be emphasized that this study aims at reducing the uncertainties of the studied RRCs. The final model was specially fitted for the published experimental results, Table 2, filtered with uncertainty analysis. The determined RRCs of the final model will be further optimized with newly published experimental researches and optimization work of combustion models of hydrocarbons.

In this section, the results simulated with the reduced RRC uncertainty bounds and the final model will be presented. The $\overline{\Psi}$ for IDTs measured in STs [36,57,59,60,62,63] and RCMs [36,42,64], LFSs [66,67,69-72,74-83], and concentration profiles measured in a JSR [29] and a PFR [30] were calculated. The results of [58,62,65,68,73,84,85] were not applied to the optimization due to their potential high uncertainties or limited amount of data, but the modeling results will also be shown. Limited by the length of the article, most results are presented in Supplementary-3. The H_2 oxidation chemical kinetic model, thermal data, and transport data for the reproduction of the simulations were uploaded as Supplementary-4.

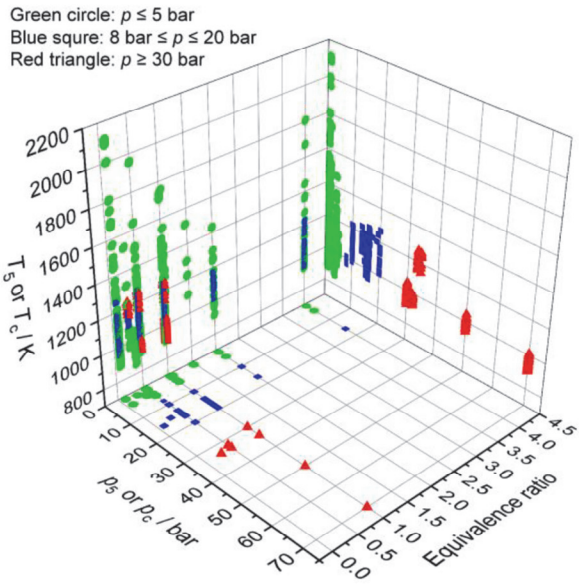

Fig. 10. Available data of IDTs measured in STs and RCMs.

3.1. Ignition delay times

The temperature, pressure, and equivalence ratio distributions of the

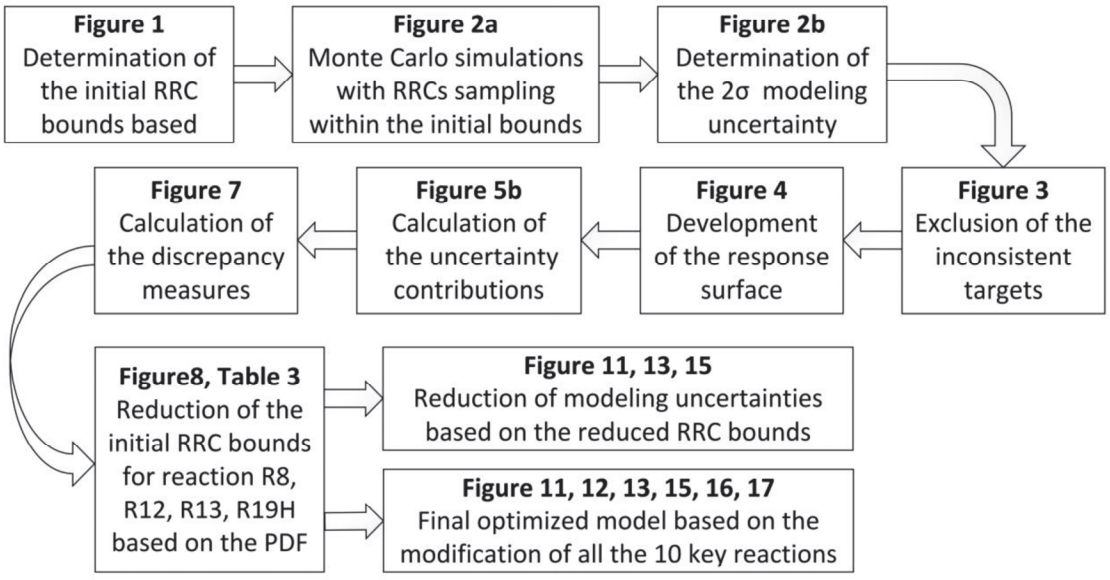

Fig. 9. Framework of the uncertainty reduction and model optimization of the current study.

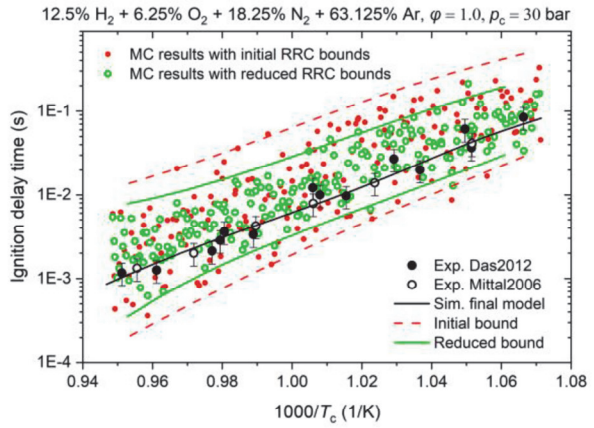

Fig. 11. Comparison of the IDTs measured in RCMs [42,64] and the modeling results obtained with the as-compiled model and with the optimized model.

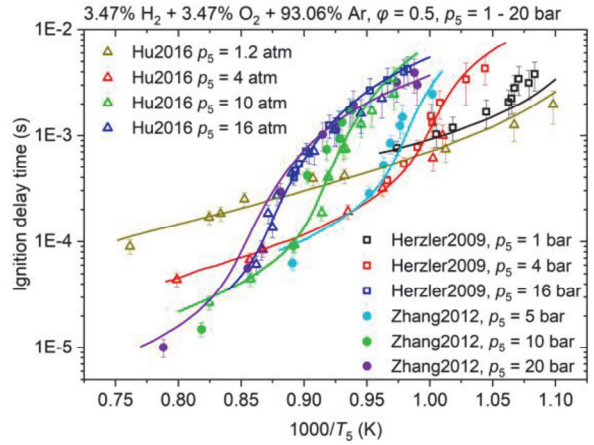

Fig. 12. Comparison of the simulated with the optimized model and measured IDTs in STs (lines: modeling results, symbols: Kéromnès et al. [36,57], Herzler et al. [36,57], Hu et al. [59,60], Zhang et al. [58]).

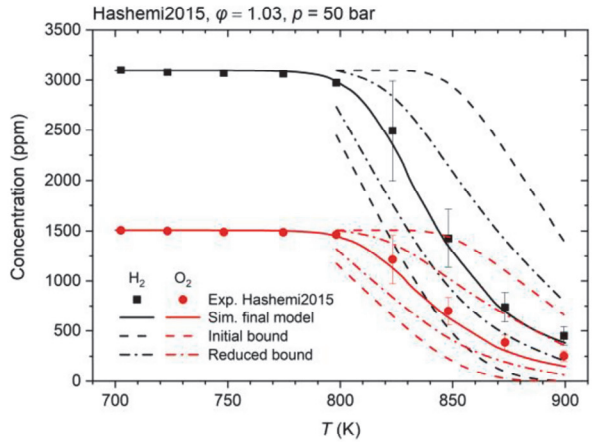

Fig. 13. Comparison of the concentration profiles measured in the PFR [30] and the modeling results obtained with the as-compiled model and with the optimized model.

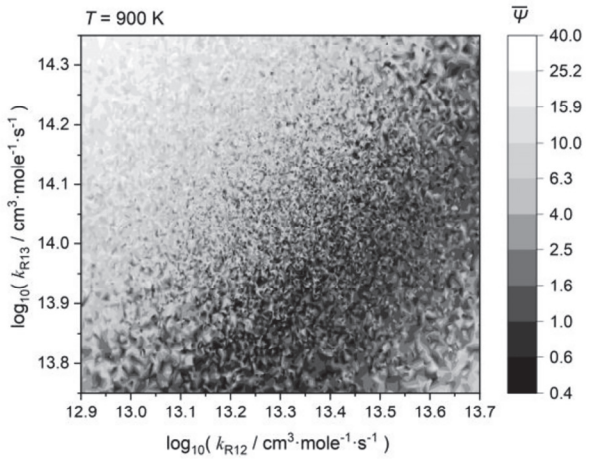

Fig. 14. The distribution of $\overline{\Psi}$[29] due to the combined influence of reactions $HO_2 + H = H_2 + O_2$ (R12) and $HO_2 + H = OH + OH$ (R13).

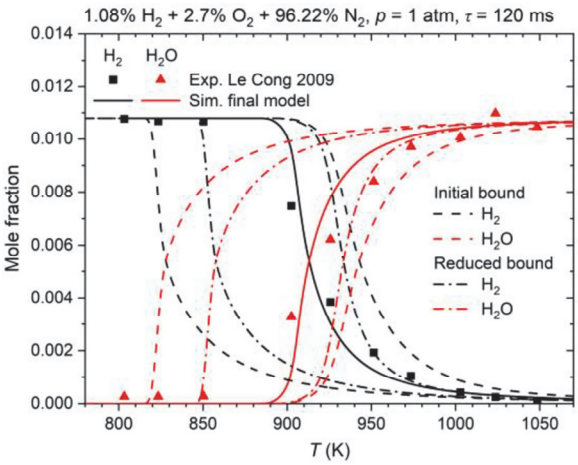

Fig. 15. Comparison of the concentration profiles measured in the JSR [29] and the modeling results obtained with the as-compiled model and with the optimized model.

available measured IDTs (Table 2) are presented in Fig. 10. Most of the experimental studies focus on the relatively low-pressure conditions (green symbols). The higher-pressure data (blue and red symbols) concentrated from 1000 K to 1200 K, and only few tests were conducted at pressure higher than 30 bar (red symbols). The lack of data at high pressure and temperature become an obstacle to the calibration of the model in this range.

Traditionally, sensitivity and uncertainty analysis (Fig. 5) shown that the reactions of H and O_2 (R3, R4) have the highest impact on the ignition of H_2/O_2 mixtures, especially at low pressures. These two reactions have received lots of attentions and narrow uncertainty intervals were obtained initially with the recommended RRCs.

$$H + O_2 (+M) - HO_2 (+M) \quad \text{(R3)}$$

$$H + O_2 = OH + O \quad \text{(R4)}$$

$$H_2O_2 + H = HO_2 + H_2 \quad \text{(R8)}$$

$$H_2O_2 (+M) = OH + OH (+M) \quad \text{(R19)}$$

As the pressure rises, the role of H_2O_2 becomes more important and

reaction (R8) and (R19) show higher uncertainty contributions, as shown in Fig. 5b and Fig. 6a. As described in the previous section, due to the lack of reliable recommended direct data for the RRCs of reaction (R8) and (R19), the initially estimated large uncertainties of these two channels were reduced in this study.

Mittal et al. [64] measured the IDTs of $H_2/O_2/N_2$/Ar mixture and with a RCM, and Das et al. [42] built a similar facility and extend the test conditions. A comparison of the initial and reduced modeling bounds for a test case shared by Mittal et al. [64] and Das et al. [42] is presented in Fig. 11. From the initial MC simulation (red closed symbols) to the reduced one (green open symbols), obvious improvement has been achieved in the predictive ability for the IDTs. More results for the simulation of IDTs measured in RCMs are presented in Fig. S3-1 in Supplementary-3.

The authors of [36,57] and Xi'an Jiaotong University (XJTU) [58-60] measured the IDTs of H_2/O_2/Ar mixtures in STs with similar conditions. Increases of 2%/ms to 6%/ms were set to the pressure of the homogeneous model to reproduce the real reaction processes in STs. The measurements covered a wide temperature and pressure ranges, and one comparison of the modeling results and the experimental data is presented in Fig. 12. It should be noted that the IDTs measured by Zhang et al. [58] were not used for the uncertainty minimization. More results for the simulation of IDTs measured in STs are presented in Figs. S3-2, 3, 4, 5, and 6 in Supplementary-3.

3.2. Plug flow reactor

H_2 oxidation under highly diluted conditions was studied with a PFR and the concentration profiles of H_2 and O_2 were measured with a gas chromatograph by Hashemi et al. [30]. Reaction (R8) and (R19) were specially fitted for the simulation of concentration profiles of H_2 and O_2 in the PFR. A comparison of the simulated and measured concentration profiles of $H_2/O_2/N_2$ mixture with an equivalence ratio of 1.03 is presented in Fig. 13. The 2σ bounds of the predicted concentration profiles in the PFR [30] based on the initial (dash lines) and reduced (dash-dot lines) RRC bounds are compared in Fig. 13, and the newly calculated standard deviation σ is 50% or less of the initial value. More results for the fuel-lean and fuel-rich conditions are presented in Fig. S3-7 in Supplementary-3.

3.3. Jet stirred reactor

$$HO_2 + H = H_2 + O_2 \quad \text{(R12)}$$

$$HO_2 + H = OH + OH \quad \text{(R13)}$$

The oxidation of H_2 over the temperature range of 800–1300 K was studied in a jet-stirred reactor by Le Cong and Dagaut [29]. 10% water was added to the mixture for the investigation of H_2 oxidation model. Uncertainty analysis shows that the reactions of $HO_2 + H$ (R12, R13) play decisive roles in the modeling of JSR (Fig. S2-2e in Supplementary-2). However, only very few directly measured data were found for the RRCs of these two reactions. The distribution of discrepancy measure, $\overline{\Psi}$, following from the combined impact of the RRCs for (R12) and (R13) is presented in Fig. 14. The initially estimated large uncertainties of the RRCs were reduced based on the modeling of the jet-stirred reactor. The probability density functions for the RRCs of these two reactions were determined based on $\overline{\Psi}$, which are shown in Fig. S2-4c and S2-4d in Supplementary-2.

By reducing the RRCs uncertainty bounds for reaction (R12) and (R13), the modeling bounds of the predicted unstable process in JSR were narrowed, as shown in Fig. 15, and the final optimized model can well predict the concentration profiles. More results for the simulation of JSR [29] can be found in Fig. S3-8in in Supplementary-3.

3.4. Laminar flame speed

The Bunsen flame, counterflow flame, and spherical flame are commonly used experimental technologies for the measurement of LFSs. Most of the tests were conducted with H_2/air mixtures with unburn temperatures of 298 K at atmospheric pressure. Bradley et al. [72] and Hu et al. [80] measured the LFSs of H_2/air mixtures at variable temperature and pressure with the spherical flame method. Kwon et al. [77] investigated the effect of different dilution gases on the LFSs. Tse et al. [76] measured the laminar mass burning rate of H_2/O_2/He mixtures in the spherical flame at variable pressures up to 20 atm. In this study, only the LFSs of H_2/air mixtures measured at atmospheric pressure and T_u = 298 K were selected as optimization targets and blind simulation was conducted for the other data.

Most of the studied reactions show importance to the simulated LFSs, as shown in Fig. S2-2c in Supplementary-2. The uncertainty intervals of the RRCs were not specially reduced for the modeling of LFSs. As shown by the comparison of the simulated and measured LFSs of H_2/air mixtures in Fig. 16, the low $\overline{\Psi}$ was obtained with the final optimized model (the inconsistent targets are not shown). The results for the LFS simulations at variable temperature, pressure, and dilution gases are presented in Figs. S3-9, 10, and 11 in Supplementary-3. All the predictions show good agreement with the experimental data.

3.5. Premixed laminar flame structure

Vandooren et al. [85] investigated the flame structure of the rich H_2/O_2/Ar flame at low pressure and measured the mole fractions of H_2, O_2, H_2O, H, O, and OH with the mass spectrometric analysis. In the earlier work of Dixon-lewis et al. [84], the structure of the rich $H_2/O_2/N_2$ flame was studied at atmospheric pressure, but only the concentration profiles of three stable components of the flame, H_2, O_2, and H_2O, were measured. Considering the limited number of tests, the concentration profiles measured in PLF were not specially fitted, and blind simulations were conducted for the two experiments with good predictions of the concentration profiles, Fig. 17.

4. Conclusion

The optimization of a 19-reactions H_2 oxidation chemical kinetic model has been successfully performed with the developed strategy for reduction of the rate constant uncertainties for reactions having the high uncertainty contributions to the modeling results. Experimental data with strongly evaluated errors from shock tubes, rapid compression machines, jet stirred reactors, plug flow reactors, and premixed laminar

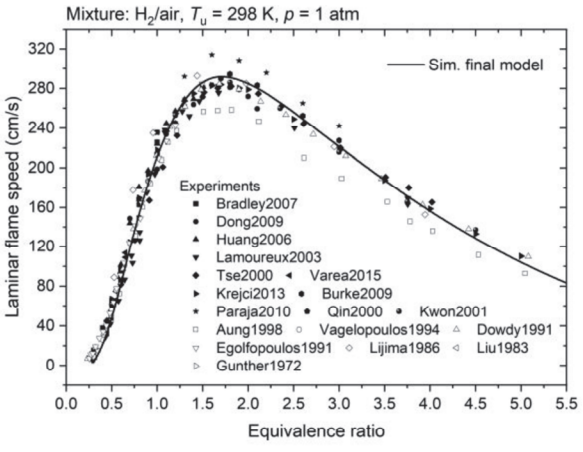

Fig. 16. LFSs of H_2/air mixtures at 298 K and 1 atm.

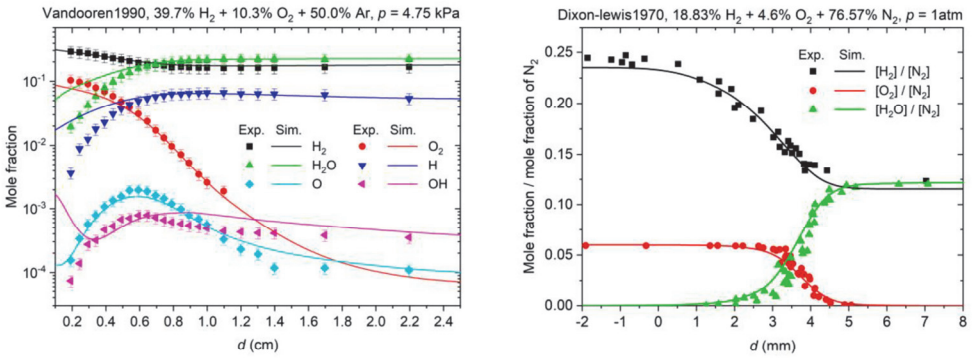

Fig. 17. Simulations of concentration profiles with the optimized model measured by (a) Vandooren et al. [85]; (b) Dixon-lewis et al. [84] in PLF for H_2, O_2, H_2O, H, O, and OH.

flames were used as the training set. The inconsistent targets were fixed and excluded from the optimization.

The discrepancy measure was introduced in the developed framework for quantification of the model prediction quality. The relative uncertainty contributions were calculated to characterize the impact of the reaction rate uncertainties on the model prediction quality and to select the reaction rates with the highest potential to be optimized on the base of the defined training set. 10 key channels (33 rate parameters) were selected from the analysis of uncertainty contributions.

Uncertainty intervals of the studied reaction rate constants were first decided by the statistical analysis of reliable data recommended by direct measurements and theoretical calculations. Monte Carlo simulation with randomly sampled reaction rate constants and polynomial regression were performed to develop the response surface with a very high coefficient of determination to be utilized in the model optimization procedure.

The probability density functions were calculated for the 4 key channels with highest uncertainty contributions, and the initially estimated uncertainties for both RRCs and modeling were reduced. The proposed framework through combination of deterministic and probabilistic approaches for the RRC uncertainty treatment allows to extend the RRC input temperature validity range.

The final model optimization is performed through the discrepancy measure minimization. The predictions of ignition delay times, laminar flame speeds, and concentration profiles obtained with the final optimized model demonstrate the lowest discrepancy measure and the model's good application potential in the computational fluid dynamic simulation of hydrogen combustion.

The applied statistical methods can be effective for the mathematical treatment of complex reaction systems for the development of predictive reaction models with a quantified valid range. The uncertainty parameters of the reaction rate constants and the obtained reaction model will be a good basement for the development of complex kinetic models for the hydrocarbon oxidation with narrowed uncertainty intervals.

CRediT authorship contribution statement

Hongxin Wang: Investigation, Formal analysis, Writing – original draft. **Nadezda Slavinskaya:** Writing – review & editing, Supervision. **Oskar Haidn:** Conceptualization, Writing – review & editing, Supervision.

Declaration of Competing Interest

The authors declare that they have no known competing financial interests or personal relationships that could have appeared to influence the work reported in this paper.

Appendix A. Supplementary data

Supplementary data to this article can be found online at https://doi.org/10.1016/j.fuel.2022.123705.

References

[1] Pregger T, Nitsch J, Naegler T. Long-term scenarios and strategies for the deployment of renewable energies in Germany. Energy Policy 2013;59:350–60.
[2] Schultz MG, Diehl T, Brasseur GP, Zittel W. Air pollution and climate-forcing impacts of a global hydrogen economy. Science 2003;302(5645):624–7.
[3] Ajanovic A, Haas R. Prospects and impediments for hydrogen and fuel cell vehicles in the transport sector. Int J Hydrogen Energy 2021;46(16):10049–58.
[4] Smith JJ, Schneider G, Suslov D, Oschwald M, Haidn O. Steady-state high pressure LOx/H2 rocket engine combustion. Aerosp Sci Technol 2007;11(1):39–47.
[5] Wang H, Yang Q, Xu X. Effect of thermal choking on ejection process in a rocket-based combined cycle engine. Appl Therm Eng 2017;116:197–204.
[6] Sánchez AL, Williams FA. Recent advances in understanding of flammability characteristics of hydrogen. Prog Energy Combust Sci 2014;41:1–55.
[7] Baulch DL, Bowman CT, Cobos CJ, Cox RA, Just T, Kerr JA, et al. Evaluated Kinetic Data for Combustion Modeling: Supplement II. J Phys Chem Ref Data 2005;34(3):757–1397.
[8] Tomlin AS. The use of global uncertainty methods for the evaluation of combustion mechanisms. Reliab Eng Syst Saf 2006;91(10–11):1219–31.
[9] Russi T, Packard A, Frenklach M. Uncertainty quantification: Making predictions of complex reaction systems reliable. Chem Phys Lett 2010;499(1–3):1–8.
[10] Bertolino A, Fürst M, Stagni A, Frassoldati A, Pelucchi M, Cavallotti C, et al. An evolutionary, data-driven approach for mechanism optimization: theory and application to ammonia combustion. Combust Flame 2021;229:111366.
[11] Frenklach M, Wang H, Rabinowitz MJ. Optimization and analysis of large chemical kinetic mechanisms using the solution mapping method—combustion of methane. Prog Energy Combust Sci 1992;18(1):47–73.
[12] Elliott L, Ingham D, Kyne A, Mera N, Pourkashanian M, Wilson C. Incorporation of physical bounds on rate parameters for reaction mechanism optimization using genetic algorithms. Combust Sci Technol 2003;175(4):619–48.
[13] Frenklach M, Packard A, Garcia-Donato G, Paulo R, Sacks J. Comparison of statistical and deterministic frameworks of uncertainty quantification. SIAM/ASA J Uncertainty Quantif 2016;4(1):875–901.
[14] Iavarone S, Oreluk J, Smith ST, Hegde A, Li W, Packard A, et al. Application of Bound-to-Bound Data Collaboration approach for development and uncertainty quantification of a reduced char combustion model. Fuel 2018;232:769–79.
[15] Slavinskaya N, Abbasi M, Starcke JH, Whitside R, Mirzayeva A, Riedel U, et al. Development of an uncertainty quantification predictive chemical reaction model for syngas combustion. Energy Fuels 2017;31(3):2274–97.
[16] Le Maitre OP, Reagan MT, Najm HN, Ghanem RG, Knio OM. A stochastic projection method for fluid flow: II. Random process. J Comput Phys 2002;181(1):9–44.
[17] Knio OM, Najm HN, Ghanem RG. A stochastic projection method for fluid flow: I. basic formulation. J Comput Phys 2001;173(2):481–511.
[18] Reagana MT, Najm HN, Ghanem RG, Knio OM. Uncertainty quantification in reacting-flow simulations through non-intrusive spectral projection. Combust Flame 2003;132(3):545–55.

[19] Reagan M, Najm H, Debusschere B, Le Maître O, Knio O, Ghanem R. Spectral stochastic uncertainty quantification in chemical systems. Combust Theor Model 2004;8(3):607.
[20] Najm HN, Debusschere BJ, Marzouk YM, Widmer S, Le Maître O. Uncertainty quantification in chemical systems. Int J Numer Meth Eng 2009;80(6–7):789–814.
[21] Sheen DA, You X, Wang H, Løvås T. Spectral uncertainty quantification, propagation and optimization of a detailed kinetic model for ethylene combustion. Proc Combust Inst 2009;32(1):535–42.
[22] Sheen DA, Wang H. The method of uncertainty quantification and minimization using polynomial chaos expansions. Combust Flame 2011;158(12):2358–74.
[23] Sheen DA, Wang H. Combustion kinetic modeling using multispecies time histories in shock-tube oxidation of heptane. Combust Flame 2011;158(4):645–56.
[24] Cai L, Pitsch H. Mechanism optimization based on reaction rate rules. Combust Flame 2014;161(2):405–15.
[25] Nagy T, Turanyi T. Uncertainty of Arrhenius parameters. Int J Chem Kinet 2011;43 (7):359–78.
[26] Turányi T, Nagy T, Zsély IG, Cserháti M, Varga T, Szabó B, et al. Determination of rate parameters based on both direct and indirect measurements. Int J Chem Kinet 2012;44(5):284–302.
[27] Lee D, Hochgreb S. Hydrogen autoignition at pressures above the second explosion limit (0.6–4.0 MPa). Int J Chem Kinet 1998;30(6):385–406.
[28] Mueller M, Kim T, Yetter R, Dryer F. Flow reactor studies and kinetic modeling of the H2/O2 reaction. Int J Chem Kinet 1999;31(2):113–25.
[29] Le Cong T, Dagaut P. Experimental and detailed modeling study of the effect of water vapor on the kinetics of combustion of hydrogen and natural gas, impact on NO x. Energy Fuels 2009;23(2):725–34.
[30] Hashemi H, Christensen JM, Gersen S, Glarborg P. Hydrogen oxidation at high pressure and intermediate temperatures: Experiments and kinetic modeling. Proc Combust Inst 2015;35(1):553–60.
[31] Simmie JM. Detailed chemical kinetic models for the combustion of hydrocarbon fuels. Prog Energy Combust Sci 2003;29(6):599–634.
[32] Konnov AA. Remaining uncertainties in the kinetic mechanism of hydrogen combustion. Combust Flame 2008;152(4):507–28.
[33] Alekseev VA, Christensen M, Konnov AA. The effect of temperature on the adiabatic burning velocities of diluted hydrogen flames: A kinetic study using an updated mechanism. Combust Flame 2015;162(5):1884–98.
[34] Konnov AA. On the role of excited species in hydrogen combustion. Combust Flame 2015;162(10):3755–72.
[35] Ó Conaire M, Curran HJ, Simmie JM, Pitz WJ, Westbrook CK. A comprehensive modeling study of hydrogen oxidation. Int J Chem Kinet 2004;36(11):603–22.
[36] Kéromnès A, Metcalfe WK, Heufer KA, Donohoe N, Das AK, Sung C-J, et al. An experimental and detailed chemical kinetic modeling study of hydrogen and syngas mixture oxidation at elevated pressures. Combust Flame 2013;160(6):995–1011.
[37] Keromnes A, Donohoe N, Curran H, Herzler J, Naumann C, Griebel P. Ignition Delay Time Measurements and Validation of Reaction Mechanism for Hydrogen at Gas Turbine Relevant Conditions. *5th International Conference of The Future of Gas Turbine Technology*. 86. Brussels, Belgium; 2010.
[38] Varga T, Nagy T, Olm C, Zsély IG, Pálvölgyi R, Valkó É, et al. Optimization of a hydrogen combustion mechanism using both direct and indirect measurements. Proc Combust Inst 2015;35(1):589–96.
[39] Li J, Zhao Z, Kazakov A, Dryer FL. An updated comprehensive kinetic model of hydrogen combustion. Int J Chem Kinet 2004;36(10):566–75.
[40] Burke MP, Chaos M, Ju Y, Dryer FL, Klippenstein SJ. Comprehensive H2/O2 kinetic model for high-pressure combustion. Int J Chem Kinet 2012;44(7):444–74.
[41] Zhang Y, Fu J, Xie M, Liu J. Improvement of H2/O2 chemical kinetic mechanism for high pressure combustion. Int J Hydrogen Energy 2021;46(7):5799–811.
[42] Das AK, Sung C-J, Zhang Y, Mittal G. Ignition delay study of moist hydrogen/oxidizer mixtures using a rapid compression machine. Int J Hydrogen Energy 2012; 37(8):6901–11.
[43] Wang H. Uncertainty quantification and minimization. In: Comput Aided Chemical Engineering. Elsevier; 2019. p. 723–62.
[44] Rubinstein RY, Kroese DP. Simulation and the Monte Carlo method. John Wiley & Sons; 2016.
[45] Wang H, Slavinskaya N, Kanz A, Auyelkhankyzy M, Gao Y, Haidn O. A comprehensive kinetic modeling study of ethylene combustion with data uncertainty analysis. Fuel 2021;299:120833.
[46] Slavinskaya N, Mirzayeva A, Whitside R, Starke J, Abbasi M, Auyelkhankyzy M, et al. A modelling study of acetylene oxidation and pyrolysis. Combust Flame 2019; 210:25–42.
[47] Walter G, Wang H, Kanz A, Kolbasseff A, Xu X, Haidn O, et al. Experimental error assessment of laminar flame speed measurements for digital chemical kinetics databases. Fuel 2020;266.
[48] Stein M. Large sample properties of simulations using Latin hypercube sampling. Technometrics 1987;29(2):143–51.
[49] Saito H, Scriven L. Study of coating flow by the finite element method. J Comput Phys 1981;42(1):53–76.
[50] DESIGNS ME. Chemkin-pro. 2011.
[51] Baulch D, Cobos C, Cox R, Esser C, Frank P, Just T, et al. Evaluated kinetic data for combustion modelling. J Phys Chem Ref Data 1992;21(3):411–734.
[52] Atkinson R, Baulch D, Cox R, Hampson Jr R, Kerr J, Rossi M, et al. Evaluated kinetic, photochemical and heterogeneous data for atmospheric chemistry: Supplement V. IUPAC Subcommittee on Gas Kinetic Data Evaluation for Atmospheric Chemistry. J Phys Chem Ref Data 1997;26(3):521–1011.
[53] Tsang W, Hampson R. Chemical kinetic data base for combustion chemistry. Part I. Methane and related compounds. J Phys Chem Ref Data 1986;15(3):1087–279.
[54] Fokin LR, Slavinskaya N. Thermophysical parameter correlation for low-density gas mixtures: Ar-Xe. Institute for High Temperatures, USSR Academy of Sciences 1987;25(1):40–5.
[55] Sokolov S, Silin I. Preprint JINR D-810. Dubna 1961.
[56] Kurbatov V, Silin I. New method for minimizing regular functions with constraints on parameter region. Nucl Instrum Methods Phys Res, Sect A 1994;345(2):346–50.
[57] Herzler J, Naumann C. Shock-tube study of the ignition of methane/ethane/hydrogen mixtures with hydrogen contents from 0% to 100% at different pressures. Proc Combust Inst 2009;32(1):213–20.
[58] Zhang Y, Huang Z, Wei L, Zhang J, Law CK. Experimental and modeling study on ignition delays of lean mixtures of methane, hydrogen, oxygen, and argon at elevated pressures. Combust Flame 2012;159(3):918–31.
[59] Hu E, Pan L, Gao Z, Lu X, Meng X, Huang Z. Shock tube study on ignition delay of hydrogen and evaluation of various kinetic models. Int J Hydrogen Energy 2016;41 (30):13261–80.
[60] Pan L, Hu E, Zhang J, Zhang Z, Huang Z. Experimental and kinetic study on ignition delay times of DME/H2/O2/Ar mixtures. Combust Flame 2014;161(3): 735–47.
[61] Petersen EL, Kalitan DM, Rickard MJ. Reflected Shock Ignition of SiH4/H2/O2/Ar andSiH4/CH4/O2/Ar Mixtures. J Propul Power 2004;20(4):665–74.
[62] Ninnemann E, Koroglu B, Pryor O, Barak S, Nash L, Loparo Z, et al. New insights into the shock tube ignition of H2/O2 at low to moderate temperatures using high-speed end-wall imaging. Combust Flame 2018;187:11–21.
[63] Pang G, Davidson D, Hanson R. Experimental study and modeling of shock tube ignition delay times for hydrogen–oxygen–argon mixtures at low temperatures. Proc Combust Inst 2009;32(1):181–8.
[64] Mittal G, Sung CJ, Yetter RA. Autoignition of H2/CO at elevated pressures in a rapid compression machine. Int J Chem Kinet 2006;38(8):516–29.
[65] Qin X, Kobayashi H, Niioka T. Laminar burning velocity of hydrogen–air premixed flames at elevated pressure. Exp Therm Fluid Sci 2000;21(1–3):58–63.
[66] Dong C, Zhou Q, Zhao Q, Zhang Y, Xu T, Hui S. Experimental study on the laminar flame speed of hydrogen/carbon monoxide/air mixtures. Fuel 2009;88(10): 1858–63.
[67] Pareja J, Burbano HJ, Ogami Y. Measurements of the laminar burning velocity of hydrogen–air premixed flames. Int J Hydrogen Energy 2010;35(4):1812–8.
[68] Liu D, MacFarlane R. Laminar burning velocities of hydrogen-air and hydrogen-air steam flames. Combust Flame 1983;49(1–3):59–71.
[69] Egolfopoulos F, Law CK. An experimental and computational study of the burning rates of ultra-lean to moderately-rich H2/O2/N2 laminar flames with pressure variations. *Symposium (international) on combustion*. 23. Elsevier; 1991:333-40.
[70] Vagelopoulos CM, Egolfopoulos FN, Law CK. Further considerations on the determination of laminar flame speeds with the counterflow twin-flame technique. *Symposium (international) on combustion*. Elsevier; 1994:1341–7.
[71] Huang Z, Zhang Y, Zeng K, Liu B, Wang Q, Jiang D. Measurements of laminar burning velocities for natural gas–hydrogen–air mixtures. Combust Flame 2006; 146(1–2):302–11.
[72] Bradley D, Lawes M, Liu K, Verhelst S, Woolley R. Laminar burning velocities of lean hydrogen–air mixtures at pressures up to 1.0 MPa. Combust Flame 2007;149 (1–2):162–72.
[73] Günther R, Janisch G. Measurements of burning velocity in a flat flame front. Combust Flame 1972;19(1):49–53.
[74] Dowdy DR, Smith DB, Taylor SC, Williams A. The use of expanding spherical flames to determine burning velocities and stretch effects in hydrogen/air mixtures. In: *Symposium (International) on Combustion*. 23. Elsevier; 1991. p. 325–32.
[75] Aung K, Hassan M, Faeth G. Effects of pressure and nitrogen dilution on flame/stretch interactions of laminar premixed H2/O2/N2 flames. Combust Flame 1998; 112(1–2):1–15.
[76] Tse SD, Zhu D, Law CK. Morphology and burning rates of expanding spherical flames in H2/O2/inert mixtures up to 60 atmospheres. Proc Combust Inst 2000;28 (2):1793–800.
[77] Kwon O, Faeth G. Flame/stretch interactions of premixed hydrogen-fueled flames: measurements and predictions. Combust Flame 2001;124(4):590–610.
[78] Lamoureux N, Paillard C-E, Vaslier V. Low hydrocarbon mixtures ignition delay times investigation behind reflected shock waves. Shock Waves 2002;11(4): 309–22.
[79] Burke MP, Chen Z, Ju Y, Dryer FL. Effect of cylindrical confinement on the determination of laminar flame speeds using outwardly propagating flames. Combust Flame 2009;156(4):771–9.
[80] Hu E, Huang Z, He J, Miao H. Experimental and numerical study on laminar burning velocities and flame instabilities of hydrogen–air mixtures at elevated pressures and temperatures. Int J Hydrogen Energy 2009;34(20):8741–55.
[81] Krejci MC, Mathieu O, Vissotski AJ, Ravi S, Sikes TG, Petersen EL, et al. Laminar flame speed and ignition delay time data for the kinetic modeling of hydrogen and syngas fuel blends. J Eng Gas Turbines Power 2013;135(2).
[82] Varea E, Beeckmann J, Pitsch H, Chen Z, Renou B. Determination of burning velocities from spherically expanding H2/air flames. Proc Combust Inst 2015;35 (1):711–9.
[83] Zhang Z, Cheng P, Tan J, Liang J, Li Y, Li G. The uncertainty of laminar burning velocity of premixed H2-air flame induced by the non-uniform initial temperature field inside the constant-volume combustion vessel. Int J Hydrogen Energy 2018; 43(45):21049–59.
[84] Dixon-Lewis G, Sutton MM, Williams A. Flame structure and flame reaction kinetics-IV. Experimental investigations of a fuel-rich hydrogen+ oxygen+ nitrogen flame at atmospheric pressure. Proceedings of the Royal Society of London A Mathematical and Physical Sciences 1970;317(1529):227–34.

[85] Vandooren J, Bian J. Validation of H2/O2 reaction mechanisms by comparison with the experimental structure of a rich hydrogen-oxygen flame. In: *Symposium (International) on Combustion.* 23. Elsevier; 1990. p. 341–6.
[86] Prager J, Najm HN, Sargsyan K, Safta C, Pitz WJ. Uncertainty quantification of reaction mechanisms accounting for correlations introduced by rate rules and fitted Arrhenius parameters. Combust Flame 2013;160(9):1583–93.
[87] Li G, Rosenthal C, Rabitz H. High dimensional model representations. J Phys Chem A 2001;105(33):7765–77.
[88] Shi C. Development of a Program for the Optimization of Chemical Kinetic Mechanism. *Department of Mechanical Engineering.* Master Semester Thesis. Munich: Technical University of Munich; 2021.
[89] Nagelkerke NJ. A note on a general definition of the coefficient of determination. Biometrika 1991;78(3):691–2.
[90] Metcalfe WK, Burke SM, Ahmed SS, Curran HJ. A Hierarchical and Comparative Kinetic Modeling Study of C1–C2 Hydrocarbon and Oxygenated Fuels. Int J Chem Kinet 2013;45(10):638–75.
[91] Konnov AA. Implementation of the NCN pathway of prompt-NO formation in the detailed reaction mechanism. Combust Flame 2009;156(11):2093–105.
[92] Hashemi H, Christensen JM, Gersen S, Levinsky H, Klippenstein SJ, Glarborg P. High-pressure oxidation of methane. Combust Flame 2016;172:349–64.
[93] Gorse R, Volman D. Photochemistry of the gaseous hydrogen peroxide—carbon monoxide system. II: Rate constants for hydroxyl radical reactions with hydrocarbons and for hydrogen atom reactions with hydrogen peroxide. J Photochem 1974;3(1):115–22.
[94] Baldwin RR, Walker RW. Rate constants for hydrogen+ oxygen system, and for H atoms and OH radicals+ alkanes. J Chem Soc, Faraday Trans 1 F 1979;75:140–54.

Supplementary-1

A Comprehensive Kinetic Modelling Study of Hydrogen Combustion with Data Uncertainty Analysis

Hongxin Wang[a], Nadezda Slavinskaya[b, c], Oskar Haidn[a]

a. Department of Aerospace and Geodesy, Technical University of Munich, 85748 Garching, Germany

b. GRS Association for Plant and Reactor Safety, 85748 Garching, Germany

c. Al-Farabi Kazakh National University, 050040 Almaty, Kazakhstan

Recommendations of the reaction rate constants and calculated uncertainty parameters.

Table S1-1. Parameters for Arrhenius equation and uncertainty factors, $k(T) = AT^n exp(-E_a/T)$, $k(T) = A_1 T^{n_1} exp\left(-\frac{E_{a1}}{T}\right) + A_2 T^{n_2} exp\left(-\frac{E_{a2}}{T}\right)$ for duplications (dup).

Reaction		+M	Reference	ΔT, K	k, cm^3, s, mole, K		
					A	n	E_a, K
R1	H+H+M=H_2+M	H_2	Baulch2005 [1]	200-5000	1.02E+17	-0.60	0.0
		Ar	Baulch2005 [1]	200-2500	6.53E+17	-1.00	0.0
		He	Mitchell1977 [2]	297	2.10E+15	0.00	0.0
		H_2	Lynch1976 [3]	298	3.08E+15	0.00	0.0
		He	Lynch1976 [3]	298	2.50E+15	0.00	0.0
		Ar	Lynch1976 [3]	298	2.90E+15	0.00	0.0
		N_2	Lynch1976 [3]	298	3.48E+15	0.00	0.0
		H_2	Walkauskas1975 [4]	298	2.94E+15	0.00	0.0
		He	Walkauskas1975 [4]	298	2.54E+15	0.00	0.0
		Ar	Walkauskas1975 [4]	298	3.34E+15	0.00	0.0
		N_2	Walkauskas1975 [4]	295	3.30E+15	0.00	0.0
		CH_4	Walkauskas1975 [4]	295	5.55E+15	0.00	0.0
		CO_2	Walkauskas1975 [4]	295	5.93E+15	0.00	0.0
		H_2	Trainor1973 [5]	298	2.94E+15	0.00	0.0
		He	Trainor1973 [5]	298	2.54E+15	0.00	0.0
		Ar	Trainor1973 [5]	298	3.34E+15	0.00	0.0
		H_2	Bennett1971 [6]	298	3.40E+15	0.00	0.0
		Ar	Bennett1971 [6]	298	5.78E+15	0.00	0.0
		He	Bennett1971 [6]	298	7.51E+15	0.00	0.0
		CO_2	Bennett1971 [6]	298	1.20E+16	0.00	0.0
		N_2	Bennett1971 [6]	298	1.32E+16	0.00	0.0
		CH_4	Bennett1971 [6]	298	2.25E+16	0.00	0.0
		H_2	Ham1970 [7]	298	3.01E+15	0.00	0.0
		Ar	Mallard1974 [8]	1300-1700	1.00E+15	0.00	0.0
		Ar	Halstead1970 [9]	1800-2000	1.80E+15	0.00	0.0
		He	Halstead1970 [9]	1800-2000	1.80E+15	0.00	0.0
		N_2	Halstead1970 [9]	1800-2000	1.90E+15	0.00	0.0
		CO_2	Halstead1970 [9]	1800-2000	5.40E+15	0.00	0.0
		CO	Halstead1970 [9]	1800-2000	5.40E+15	0.00	0.0
		H_2	Hurle1969 [10]	2500-7000	1.44E+15	-0.25	-2649.5
		Ar	Hurle1969 [10]	2500-7000	4.52E+15	-0.35	-3735.1
		Ar	Getzinger1969 [11]	1260-1910	7.50E+14	0.00	0.0
		Ar	Jocobs1967 [12]	2900-4700	1.00E+18	-1.00	0.0
		H_2	Jocobs1967 [12]	2900-4700	2.50E+18	-1.00	0.0
		Ar	Schott1964 [13]	1700-1700	4.00E+14	0.00	0.0
		Ar	Rink1962 [14]	2800-5000	1.50E+18	-1.00	0.0
		H_2	Rink1962 [14]	2800-5000	3.00E+18	-1.00	0.0
		Ar	Patch1962 [15]	2950-5330	7.50E+17	-1.00	0.0
		H_2	Patch1962 [15]	2950-5330	7.50E+18	-1.00	0.0

Reaction		+M	Reference	ΔT, K	k, cm^3, s, mole, K		
					A	n	E_a, K
R2	H+O+M=OH+M	-	Tsang1986 [16]	300- 2500	4.71E+18	-1.00	0.0
		Ar	Naudet2001 [17]	2950-3700	6.75E+18	-1.00	0.0
R3	H+O_2(+M)=HO_2(+M) low-pressure limit	Ar	Baulch2005 [1]	298-2000	6.89E+18	-1.20	0.0
		N_2	Baulch2005 [1]	298-2000	2.65E+19	-1.30	0.0
		H_2O	Baulch2005 [1]	298-2000	3.63E+19	-1.00	0.0
		Ar	Sellevag2008 [18]	300-3000	3.30E+19	-1.40	134.0
		N_2	Sellevag2008 [18]	300-3000	7.25E+20	-1.73	270.0
		Ar	Troe2000 [19]	300-2000	7.49E+18	-1.20	0.0
		N_2	Troe2000 [19]	300-2000	5.75E+19	-1.40	0.0
		Ar	Fernandes2008 [20]	300-900	4.75E+18	-1.12	0.0
		N_2	Fernandes2008 [20]	300-900	1.74E+19	-1.23	0.0
		He	Fernandes2008 [20]	300-900	6.13E+18	-1.20	0.0
		Ar	Hahn2004 [21]	300-700	1.51E+19	-1.30	0.0
		N_2	Michael2002 [22]	482-712	1.75E+19	-1.23	0.0
		Ar	Michael2002 [22]	471-698	4.57E+18	-1.12	0.0
		H_2O	Michael2002 [22]	296	1.81E+17	0.00	0.0
		Ar	Bates2001 [23]	1050-1250	6.81E+18	-1.20	0.0
		N_2	Bates2001 [23]	1050-1250	2.65E+19	-1.30	0.0
		H2O	Bates2001 [23]	1050-1250	3.70E+19	-1.00	0.0
		N_2	Ashman1998 [24]	750-900	2.25E+15	0.00	-680.0
		H_2O	Ashman1998 [24]	750-900	2.39E+16	0.00	-680.0
		CO_2	Ashman1998 [24]	750-900	5.40E+15	0.00	-680.0
		Ar	Ashman1998 [24]	750-900	1.26E+15	0.00	-680.0
		H_2O	Carleton1993 [25]	575-750	1.42E+16	0.00	-600.0
		N_2	Carleton1993 [25]	298-580	1.05E+15	0.00	-825.0
		Ar	Carleton1993 [25]	298	7.62E+15	0.00	0.0
		N_2	Hsu1987 [26]	298-693	2.36E+15	0.00	-680.0
		H_2O	Hsu1987 [26]	298-693	6.89E+15	0.00	-1050.0
		He	Hsu1987 [26]	298-693	1.45E+15	0.00	-560.0
		Ar	Cobos1985 [27]	298	1.02E+16	0.00	0.0
		N_2	Cobos1985 [27]	298	2.36E+16	0.00	0.0
		CH_4	Cobos1985 [27]	298	5.44E+16	0.00	0.0
		Ar	Pratt1983 [28]	231-512	2.85E+14	0.00	-796.0
R3	H+O_2(+M)=HO_2(+M) high-pressure limit		Baulch2005 [1] dup	298-1500	1.93E+12	0.56	0.0
			Baulch2005 [1] dup	298-1500	1.75E+17	-1.70	0.0
			Sellevag2008 [18] dup	300-3000	1.51E+14	-0.37	0.0
			Sellevag2008 [18] dup	300-3000	4.52E+11	0.70	0.0
			Troe2000 [19]	300-2000	4.65E+12	0.44	0.0
			Fernandes2008 [20]	300-900	4.65E+12	0.44	0.0
			Hahn2004 [21]	300-700	4.65E+12	0.44	0.0
			Cobos1985 [27]	298	4.52E+13	0.00	0.0

Reaction		Reference	ΔT, K	k, cm^3, s, mole, K		
				A	n	E_a, K
R4	$H+O_2=OH+O$	Wang2017 [29]	1428-1685	8.04E+13	0.00	7370.0
		Hong2011 [30]	1100-3370	1.04E+14	0.00	7705.0
		Hong2011 [30]	1100-1530	1.12E+14	0.00	7805.0
		Yang1994 [31]	1850-3550	1.00E+14	0.00	7690.0
		Du1992 [32]	2050-2950	9.33E+13	0.00	7270.0
		Yuan1991 [33]	1050-2700	1.59E+17	-0.93	8490.0
		Shin1991 [34]	1100-2060	6.92E+13	0.00	6920.0
		Masten1990 [35]	1450-3370	9.33E+13	0.00	7450.0
		Pirraglia1989 [36]	962-1700	1.68E+14	0.00	8120.0
		Fujii1988 [37]	1900-2650	6.00E+14	0.00	11400.0
		Frank1985 [38]	1700-2500	2.44E+14	0.00	8700.0
		Aleksandrov1984 [39]	773	2.89E+09	0.00	0.0
		Dixon-Lewis1983 [40]	700-1500	1.80E+14	0.00	8450.0
		Schott1973 [41]	1250-2500	1.22E+17	-0.91	8370.0
		Eberius1971 [42]	650-1000	2.30E+14	0.00	8450.0
		Jachimowski1970 [43]	1200-1800	9.91E+13	0.00	7560.0
		Myerson1968 [44]	1700-2700	6.02E+12	0.50	8930.0
		Kurzius1968 [45]	300-1650	1.69E+14	0.00	8400.0
		Gutman1967 [46]	1290-1670	7.76E+13	0.00	7270.0
		Gutman1967[46]	975-2060	9.55E+13	0.00	7400.0
R4-	$OH+H=H+O_2$	Robertson2006 [47]	136-377	6.74E+13	-0.32	-177.0
		Robertson2002 [48]	295	1.91E+13	0.00	0.0
		Smith1994 [49]	158-294	3.06E+10	0.98	-337.0
		Brune1983 [50]	300	1.87E+13	0.00	0.0
		Howard1981 [51]	250-515	4.00E+14	-0.50	0.0
		Lewis1980 [52]	221-499	1.21E+13	0.00	-112.0
		Howard1980 [53]	298	2.29E+13	0.00	0.0
		Campbell1977	425	2.65E+13	0.00	0.0
		Breen1970 [54]	298	2.59E+13	0.00	0.0
		Kurzius1968 [45]	300	1.69E+13	0.00	0.0

Reaction		+M	Reference	ΔT, K	k, cm^3, s, mole, K		
					A	n	E_a, K
R5	H+OH(+M)=H_2O(+M) low-pressure limit	Ar	Baulch2005 [1]	300-3000	8.34E+21	-2.00	0.0
		N_2	Baulch2005 [1]	300-3000	2.21E+22	-2.00	0.0
		H_2O	Baulch2005 [1]	300-3000	1.41E+23	-2.00	0.0
		Ar	Sellevag2008 [18]	300-3000	3.12E+20	-1.53	185.0
		N_2	Sellevag2008 [18]	300-3000	4.53E+21	-1.81	251.0
		Ar	Javoy2003 [55]	2790-3200	3.75E+21	-2.10	0.0
		H_2O	Javoy2003 [55]	2790-3200	6.75E+22	-2.10	0.0
		N_2	Goodings1988 [56]	1600-2200	3.64E+19	-1.00	0.0
		He	Zellner1977 [57]	230-300	1.56E+23	-2.60	0.0
		CO_2	Zellner1977 [57]	300-300	3.27E+17	0.00	0.0
		N_2	Zellner1977 [57]	300-300	1.74E+17	0.00	0.0
		Ar	Zellner1977 [57]	300-300	8.34E+16	0.00	0.0
		OH	Davis1974 [58]	1740-1860	8.34E+15	0.00	0.0
		Ar	Homer1970 [59]	2570-3290	1.50E+25	-2.60	0.0
		H_2O	Homer1970 [59]	2570-3290	7.51E+23	-2.60	0.0
		Ar	Halstead1970 [9]	1800-2000	3.20E+15	0.00	0.0
		He	Halstead1970 [9]	1800-2000	8.00E+15	0.00	0.0
		N_2	Halstead1970 [9]	1800-2000	3.20E+15	0.00	0.0
		H_2O	Halstead1970 [9]	1800-2000	2.70E+16	0.00	0.0
		H_2O	Getzinger1969 [11]	1259-1912	6.61E+16	0.00	0.0
		Ar	Getzinger1969 [11]	1259-1912	3.30E+14	0.00	0.0
		N_2	Getzinger1969 [11]	1259-1912	8.59E+15	0.00	0.0
		Ar	Getzinger1967 [60]	1310-1850	5.40E+15	0.00	0.0
		N_2	Lewis1962 [61]	1070-1070	3.80E+15	0.00	0.0
R5	H+OH+M=H_2O+M high-pressure limit		Sellevag2008 [18]	300-3000	2.51E+13	0.23	-57.5
R5-	H_2O+M= H+OH+M low-pressure limit	Ar	Javoy2003 [55]	2790-3200	3.95E+14	0.00	53690.0
		H_2O	Javoy2003 [55]	2790-3200	7.10E+15	0.00	53690.0
		Ar	Homer1970 [59]	2570-3290	4.00E+23	-2.20	59414.5
		H_2O	Homer1970 [59]	2570-3290	8.00E+24	-2.20	59414.5
		Ar	Cathro1972 [62]	2000-2400	8.99E+14	0.00	52800.0
		H_2O	Cathro1972 [62]	2000-2400	1.80E+16	0.00	52800.0
		Ar	Olschewski1967 [63]	2700-6000	5.01E+14	0.00	52800.0

Reaction		Reference	ΔT, K	k, cm^3, s, mole, K		
				A	n	E_a, K
R6	H_2+O=OH+H	Balakrishnan2004 [64]	300	4.28E+06	0.00	0.0
		Javoy2003 [55]	2021-3356	7.10E+06	2.10	4140.0
		Javoy2000 [65]	2690-3360	9.25E+14	0.00	9740.0
		Ryu1995 [66]	1424-2427	1.88E+14	0.00	6897.0
		Yang1993 [67]	1600-2250	3.70E+14	0.00	7817.7
		Davidson1990 [68]	2120-2750	8.13E+14	0.00	9540.0
		Shin1989 [69]	1790-2250	7.90E+14	0.00	9381.2
		Sutherland1988 [70]	880-2495	1.87E+14	0.00	6853.8
		Sutherland1988 [70]	504-923	4.34E+13	0.00	5248.6
		Natarajan1987 [71]	1713-3532	3.72E+06	2.17	4080.0
		Marshall1987 [72]	430-1420	4.41E+03	2.93	2980.0
		Presser1985 [73]	297-471	3.16E+12	0.00	3980.0
		Pamidimukkala1982 [74]	1919-2781	2.30E+14	0.00	6915.7
		Light1980 [75]	298	5.50E+06	0.00	0.0
		Dubinsky1975 [76]	347-832	5.00E+12	0.00	4329.8
		Schott1974 [77]	1400-1900	2.20E+14	0.00	6915.7
		Brabbs1971 [78]	1200-1600	2.96E+13	0.00	4931.5
		Dean1970 [79]	1700-2600	9.04E+13	0.00	5030.0
		Jachimowski1970 [43]	1200-1800	7.50E+13	0.00	5590.0
R7	H_2+OH=H_2O+H	Baulch2005 [1]	250-2500	2.17E+08	1.52	1740.0
		Lam2013 [80]	902-1518	4.38E+13	0.00	3518.0
		Nguyen2011 [81]	200-2500	2.53E+07	1.78	1453.0
		Orkin2006 [82]	250-479	2.87E+05	2.41	1240.0
		Krasnoperov2004 [83]	832-1359	3.28E+13	0.00	3220.0
		Haworth2002 [84]	1000-2000	8.32E+05	2.34	1761.0
		Talukdar1996 [85]	238-400	4.33E+04	2.69	1150.0
		Bott1989 [86]	1200-1200	2.70E+12	0.00	0.0
		Schmidt1985 [87]	295	3.49E+09	0.00	0.0
		Frank1985 [38]	1700-2500	4.74E+13	0.00	3070.0
		Ravishankara1981 [88]	250-400	2.95E+12	0.00	1990.0
		Ravishankara1981 [88]	250-1050	2.48E+05	2.44	1280.0
		Trainor1975 [89]	300	3.19E+09	0.00	0.0
		Overend1975 [90]	295	3.49E+09	0.00	0.0
		Atkinson1975 [91]	297-434	3.56E+12	0.00	2010.0
		Smith1974 [92]	210-460	1.08E+13	0.00	2330.0
		Gardiner1974 [93]	1350-1600	5.20E+13	0.00	3250.0
		Westenberg1973 [94]	298-745	1.86E+00	4.05	444.0
		Stuhl1972 [95]	298	4.28E+09	0.00	0.0
		Eberius1971 [42]	500-1500	1.00E+13	0.00	2420.0
		Brabbs1971 [78]	1100-1600	2.10E+13	0.00	2570.0

Reaction		Reference	ΔT, K	k, cm^3, s, mole, K		
				A	n	E_a, K
R8	$H_2O_2+H=HO_2+H_2$	Baulch2005 [1]	300-1000	1.69E+12	0.00	1890.0
		Tsang1986 [16]	300-2500	4.82E+13	0.00	4000.0
		Gorse1974 [96]	298-298	1.87E+09	0.00	0.0
		Baldwin1979 [97]	713-773	6.30E+12	0.00	2480.0
		Lee1998 [98]	950-1050	2.30E+13	0.00	4000.0
R9	$H_2O_2+H=H_2O+OH$	Baulch2005 [1]	300-1000	1.02E+13	0.00	1800.0
		Tsang1986 [16]	300-2500	2.41E+13	0.00	2000.0
		Gorse1974 [96]	298	3.44E+09	0.00	0.0
		Baldwin1979 [97]	713-773	8.00E+14	0.00	4580.0
		Forst1958 [99]	700-740	3.21E+13	0.00	3520.0
R10	$H_2O_2+O=HO_2+OH$	Baulch2005 [1]	283-500	8.43E+11	0.00	2000.0
		Tsang1986 [16]	300-2500	9.63E+06	2.00	2000.0
		Wine1983 [100]	298-386	6.81E+11	0.00	2000.0
		Davis1974 [101]	283-368	1.66E+12	0.00	2120.0
		Albers1971 [102]	370-800	2.80E+13	0.00	3220.0
R11	$H_2O_2+OH=H_2O+HO_2$	Baulch2005 [1] dup	240-1700	1.64E+18	0.00	14800.0
		Baulch2005 [1] dup	240-1700	1.93E+12	0.00	215.0
		Hong2010 [103]	1020-1460	4.60E+13	0.00	2630.0
		Jimenez2004 [104]	254-356	1.75E+12	0.00	110.0
		Vakhtin2003 [105]	96-296	4.10E+11	0.00	-285.0
		Vaghjiani1990 [106]	298	1.20E+12	0.00	0.0
		Hippler1995 [107] dup	930-1680	1.70E+18	0.00	14800.0
		Hippler1995 [107] dup	930-1680	2.00E+12	0.00	215.0
		Hippler1990 [108]	1100-1100	3.00E+12	0.00	0.0
		Lamb1983 [109]	241-413	4.20E+04	2.50	-838.0
		Marinelli1982 [110]	298	1.09E+12	0.00	0.0
		Kurylo1982 [111]	250-370	1.75E+12	0.00	161.0
		Wine1981 [112]	273-410	2.23E+12	0.00	260.0
		Troe1969 [113]	950-1450	2.45E+11	0.50	603.0
R12	$HO_2+H=H_2+O_2$	Baulch2005 [1]	250-1000	1.05E+14	0.00	1030.0
		Mousavipour2007 [114]	200-3000	6.70E+07	1.77	-286.0
		Karkach1999 [115]	298-1000	6.18E+11	0.47	230.0
		Baldwin1979 [97]	370-773	2.80E+13	0.00	0.0
		Sridharan1982 [116]	296	4.01E+12	0.00	0.0
		Keyser1986 [117]	245-300	4.19E+12	0.00	0.0
R13	$HO_2+H=OH+OH$	Baulch2005 [1]	250-1000	4.46E+14	0.00	700.0
		Mousavipour2007 [114]	200-3000	2.20E+11	0.88	-32.5
		Sridharan1982 [116]	296	3.88E+13	0.00	0.0
		Keyser1986 [117]	245-300	4.72E+13	0.00	0.0

Reaction	Reference	ΔT, K	k, cm^3, s, mole, K

				A	*n*	E_a, K
R14	$HO_2+HO_2=H_2O_2+O_2$	Baulch2005 [1] dup	550-1250	4.22E+14	0.00	6030.8
		Baulch2005 [1] dup	550-1250	1.32E+11	0.00	820.3
		zhou2012 [118] dup	200-2000	1.18E+09	0.77	918.2
		zhou2012 [118] dup	200-2000	1.25E+12	0.30	3724.7
		Kappel2002 [119] dup	300-1250	1.03E+14	0.00	5556.0
		Kappel2002 [119] dup	300-1250	1.94E+11	0.00	709.0
		Thiébaud2006 [120]	298	1.14E+12	0.00	0.0
		Kanno2006 [121]	250-350	1.14E+11	0.00	670.0
		Stone2005 [122]	236-309	1.08E+10	0.00	1500.0
		Sehested1997 [123]	295-295	2.11E+12	0.00	0.0
		Maricq1994 [124]	210-363	1.69E+11	0.00	594.0
		Dobis1993 [125]	243-368	2.71E+11	0.00	520.0
		Crowley1991 [126]	298	1.45E+12	0.00	0.0
		Crowley1991 [126]	298	1.71E+12	0.00	0.0
		Hippler1990 [108] dup	750-1120	4.20E+14	0.00	6030.0
		Hippler1990 [108] dup	750-1120	1.30E+11	0.00	820.0
		Andersson1988 [127]	278-299	5.55E+09	0.00	1700.0
		McAdam1987 [128]	298	1.75E+12	0.00	0.0
		Takacs1986 [129]	253-390	1.21E+11	0.00	595.0
		Mozurkewich1985 [130]	241-417	3.77E+09	0.00	2250.0
		Sander1984 [131]	298	9.04E+11	0.00	0.0
		Rozenshtein1984 [132]	300	9.93E+11	0.00	0.0
		Thrush1982 [133]	298-358	1.45E+11	0.00	560.0
		Patrick1982 [134]	298-510	2.49E+11	0.00	630.0
		Lii1981 [135]	298-373	5.55E+10	0.00	1060.0
		Hochanadel1980 [136]	296	4.00E+12	0.00	0.0
R15	$HO_2+O=O_2+OH$	Baulch2005 [1]	220-1000	1.63E+13	0.00	-224.0
		Ravishankara1983 [137]	298	3.73E+13	0.00	0.0
		Keyser1982 [138]	229-372	1.87E+13	0.00	-200.0
		Sridharan1982 [116]	296	3.13E+13	0.00	0.0
		Lii1980 [139]	298	4.22E+13	0.00	0.0
		Burrows1979 [140]	298	1.87E+13	0.00	0.0
		Hack1979 [141]	298	2.00E+13	0.00	0.0

Reaction		+M	Reference	ΔT, K	k, cm^3, s, mole, K		
					A	n	E_a, K
R16	$HO_2+OH=H_2O+O_2$		Baulch2005 [1]	250-400	2.89E+13	0.00	-250.0
			Baulch2005 [1]	1300-2000	9.27E+15	0.00	8810.0
			Tsang1986 [16]	300-2500	1.75E+13	0.00	-200.0
			Assaf2016 [142]	298	6.14E+13	0.00	0.0
			Hong2010 [143]	1600-2200	3.30E+13	0.00	0.0
			Srinivasan2006 [144]	1242-1533	4.03E+13	0.00	0.0
			Hippler1990 [108]	1100-1100	3.00E+13	0.00	0.0
			Schwab1989 [145]	298	4.82E+13	0.00	0.0
			Keyser1988 [146]	254-382	2.89E+13	0.00	-250.0
			Goodings1988 [56]	1800-2550	6.03E+13	0.00	0.0
			Dransfeld1987 [147]	298	3.60E+13	0.00	0.0
			Sridharan1984 [148]	252-420	1.02E+13	0.00	-416.0
			Rozenshtein1984 [132]	300	3.13E+13	0.00	0.0
			Temps1982 [149]	296	4.00E+13	0.00	0.0
			DeMore1982 [150]	298	7.23E+13	0.00	0.0
			Braun1982 [151]	298	6.62E+13	0.00	0.0
			Thrush1981 [152]	298	3.49E+13	0.00	0.0
			Kurylo1981 [153]	298	9.04E+13	0.00	0.0
			Cox1981 [154]	308	5.96E+13	0.00	0.0
			Burrows1981 [155]	288	3.73E+13	0.00	0.0
			Lii1980 [139]	308	5.96E+13	0.00	0.0
			Hochanadel1980 [136]	296	7.00E+13	0.00	0.0
R17	$O+O+M=O_2+M$	-	Tsang1986 [16]	200-4000	1.89E+13	0.00	-900.0
		N_2	Campbell1973 [156]	196-298	3.43E+14	0.00	-485.0
		O_2	Tchen1972 [157]	298	3.63E+15	0.00	0.0
		Ar	Campbell1967 [158]	298	2.98E+15	0.00	0.0
		N_2	Campbell1967	298	3.88E+15	0.00	0.0
		He	Campbell1967	298	1.36E+15	0.00	0.0
		O_2	Marshall1962 [159]	300	1.63E+15	0.00	0.0
		Ar	Reeves1960 [160]	298	9.79E+14	0.00	0.0
		N_2	Morgan1960 [161]	298	3.23E+15	0.00	0.0
R17-	$O_2+M=O+O+M$	N_2	Javoy2003 [55]	2740-3460	6.80E+14	0.00	55700.0
		Ar	Jerig1991 [162]	2400-4100	1.60E+18	-1.00	59380.0
		N_2	Jerig1991 [162]	2400-4100	3.40E+18	-1.00	59380.0
		Ar	Watt1969 [163]	2850-5000	1.85E+11	0.50	48158.1

Reaction		+M	Reference	ΔT, K	k, cm^3, s, mole, K		
					A	n	E_a, K
R18	OH+OH=H_2O+O		Baulch2005 [1]	250-2400	3.35E+04	2.42	-970.0
			Altinay2014 [164]	295-701	2.88E+06	1.79	-879.0
			Sangwan2012 [165]	295-414	6.34E+13	-0.76	0.0
			Sangwan2012 [165]	555-773	2.12E+32	-6.07	4924.4
			Bedjanian1999 [166]	233-360	4.28E+11	0.00	-210.0
			Wooldridge1994 [167]	1050-2380	9.40E-05	4.77	-4570.0
			Sutherland1991 [168]	1290-2030	5.36E+12	0.00	1060.0
			Wagner1981 [169]	250-580	1.93E+12	0.00	242.0
			Farquharson1980 [170]	298	1.02E+12	0.00	0.0
			Ernst1977 [171]	1200-1800	3.40E+13	0.00	2530.0
			Trainor1975 [89]	300	1.26E+12	0.00	0.0
			Rawlins1974 [172]	1200-2000	5.50E+13	0.00	3490.0
			Clyne1974 [173]	300	8.43E+11	0.00	0.0
			Westenberg1973 [94]	350	1.40E+12	0.00	0.0
			Gardiner1973 [174]	1200-2500	5.50E+13	0.00	3520.0
			Mulcahy1971 [175]	298	1.10E+12	0.00	0.0
R18-	H_2O+O=OH+OH		Sutherland1991 [168]	1290-2030	5.55E+13	0.00	9610.0
			Lifshitz1991 [176]	1500-2400	6.75E+13	0.00	9120.0
			Albers1971 [102]	753- 1040	4.00E+13	0.00	8710.0
R19	H_2O_2(+M)=2OH	Ar	Baulch2005 [1]	1000-1500	2.29E+16	0.00	21960.0
	(+M)	N_2	Baulch2005 [1]	700-1500	1.20E+17	0.00	22900.0
	low-pressure limit	Ar	Troe2011 [177]	500-1500	2.49E+24	-2.30	24534.0
		N_2	Troe2011 [177]	500-1500	3.66E+24	-2.30	24534.0
		Ar	Selleva2009 [178]	500-3000	8.43E+31	-4.57	26322.0
		Ar	Hong2009 [179]	1000-1200	1.32E+16	0.00	21650.0
		Ar	Hong2009 [179]	1000-1200	8.32E+15	0.00	21060.0
		Ar	Hong2009 [179]	1000-1200	5.62E+15	0.00	20770.0
		Ar	Kijewski1971 [180]	1000-1400	1.58E+16	0.00	21638.4
R19	H_2O_2(+M)=2OH		Baulch2005 [1]	700-1500	3.00E+14	0.00	24400.0
	(+M)		Troe2011 [177]	500-1500	2.00E+12	0.90	24500.0
	high-pressure limit		Brouwer1987 [181]	1000-1500	2.95E+14	0.00	24400.0
			Giguere1957 [182]	673-773	1.00E+13	0.00	24200.0
			McLane1949 [183]	762-815	9.14E+10	0.00	20200.0

Reaction		+M	Reference	ΔT, K	k, cm^3, s, mole, K		
					A	n	E_a, K
R19-	OH+OH(+M)=H_2O_2(+M) low-pressure limit	N_2	Baulch2005 [1]	200-400	2.39E+19	-0.80	0.0
		H_2O	Baulch2005 [1]	200-400	1.45E+18	0.00	0.0
		N_2	Troe2011 [177]	200-700	2.76E+25	-3.20	0.0
		He	Selllevag2009 [178]	200-3000	1.60E+28	-4.30	340.0
		He	Sangwan2012 [165]	296-834	1.56E+26	-3.50	0.0
		N_2	Zellner1988 [184]	298	2.50E+17	0.00	0.0
		H_2O	Zellner1988 [184]	298	1.45E+18	0.00	0.0
		N_2	Trainor1975 [89]	298	9.07E+16	0.00	0.0
		He	Caldwell1965 [185]	298	3.08E+17	0.00	0.0
		Ar	Caldwell1965 [185]	298	3.52E+17	0.00	0.0
		N_2	Caldwell1965 [185]	298	1.20E+18	0.00	0.0
		O_2	Caldwell1965 [185]	298	1.85E+18	0.00	0.0
		CO_2	Caldwell1965 [185]	298	1.52E+18	0.00	0.0
		H_2O	Caldwell1965 [185]	298	6.53E+18	0.00	0.0
		He	Black1962 [186]	298	4.71E+15	0.00	0.0
		Ar	Black1962 [186]	298	5.44E+15	0.00	0.0
		N_2	Black1962 [186]	298	1.85E+16	0.00	0.0
		O_2	Black1962 [186]	298	2.87E+16	0.00	0.0
		CO_2	Black1962 [186]	298	2.32E+16	0.00	0.0
		H_2O	Black1962 [186]	298	1.02E+17	0.00	0.0
R19-	OH+OH(+M)=H_2O_2(+M) high-pressure limit		Baulch2005 [1]	200-400	1.57E+13	0.00	0.0
			Sangwan2012 [165]	200-400	2.50E+14	-0.50	0.0
			Fulle1996 [187]	200-700	1.57E+13	0.00	0.0
			Forster1995 [188]	298	1.32E+13	0.00	0.0
			Zellner1988 [184]	253-353	9.04E+12	0.00	0.0
			Greiner1968 [189]	300	3.90E+13	0.00	0.0
			Troe2011 [177]	200-700	3.96E+15	-0.50	0.0
			Brouwer1987 [181]	200-1500	7.49E+13	-0.37	0.0

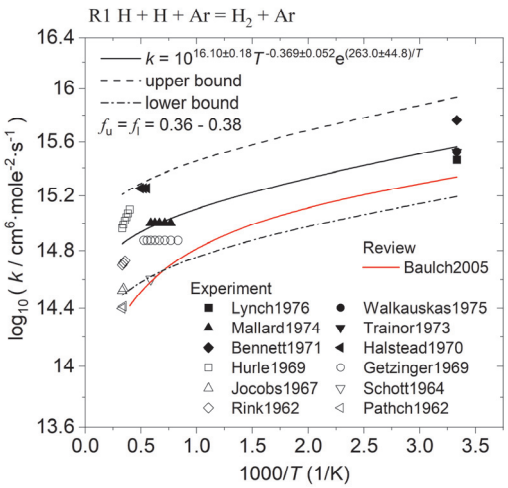

Figure S1-1 (R1) H + H + Ar = H_2 + Ar

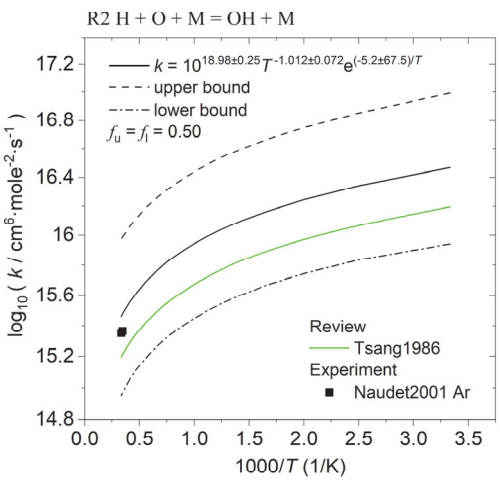

Figure S1-2 (R2) H + O + M = OH + M

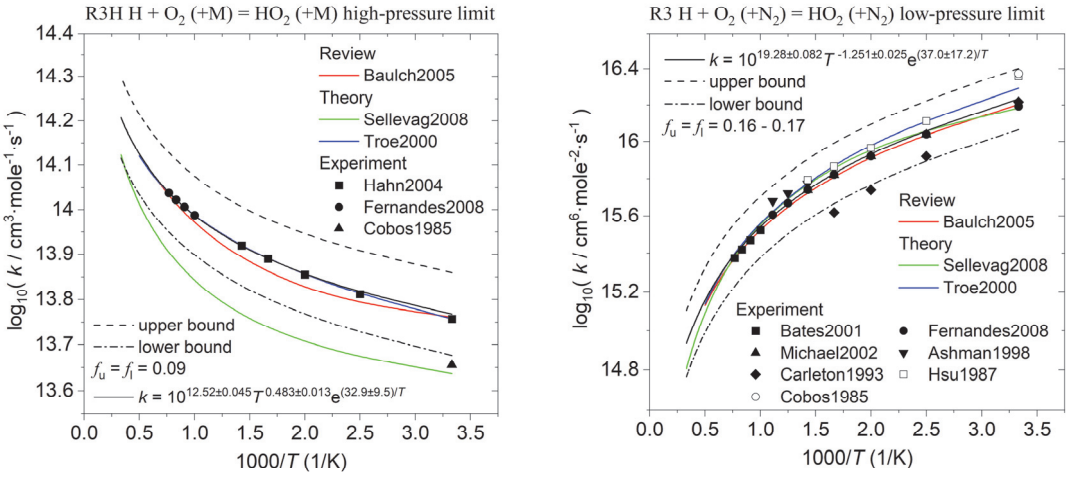

Figure S1-3 (R3) H + O_2 (+M) = HO_2 (+M)

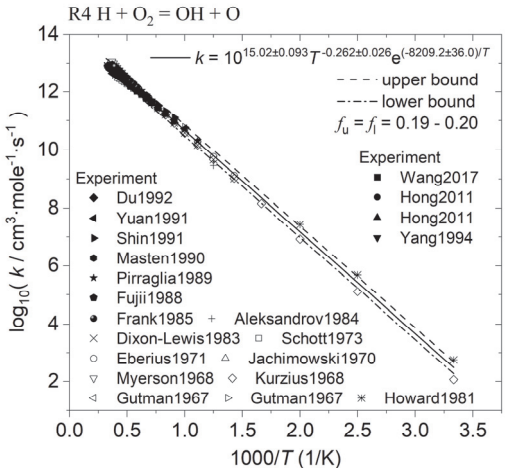

Figure S1-4 (R4) H + O_2 = OH + O

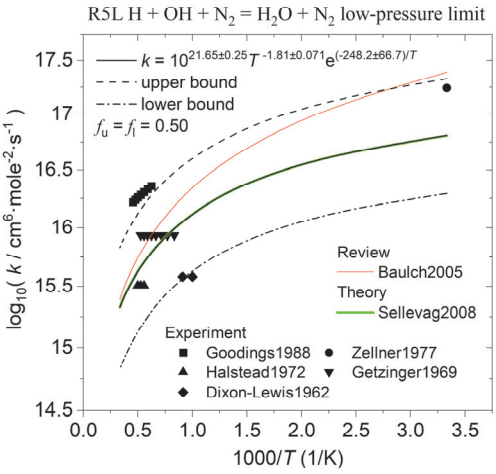

Figure S1-5 (R5) H + OH + N_2 = H_2O + N_2

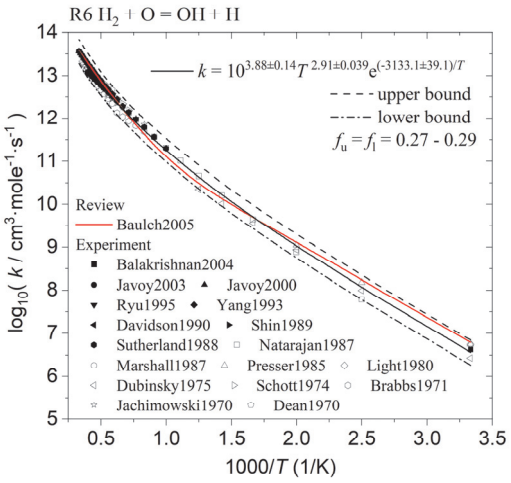

Figure S1-6 (R6) H_2 + O = OH + H

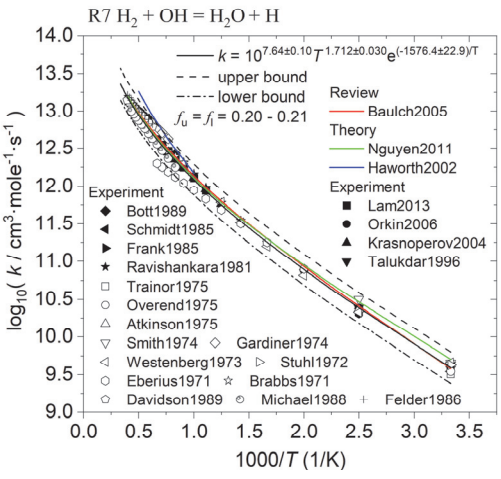

Figure S1-7 (R7) H_2 + OH = H_2O + H

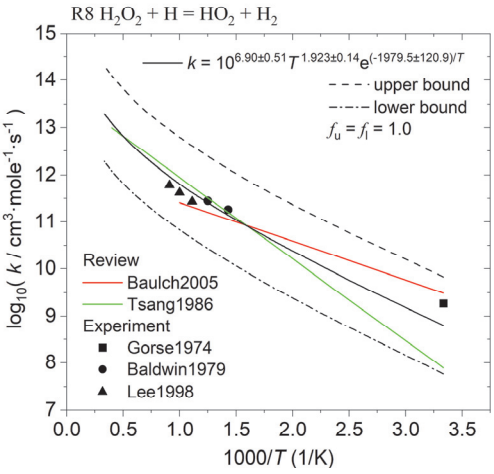

Figure S1-8 (R8) $H_2O_2 + H = HO_2 + H_2$

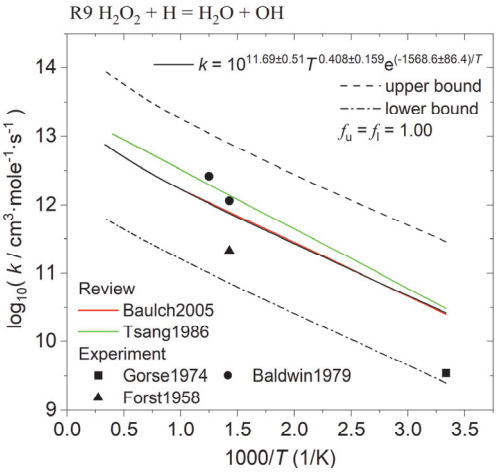

Figure S1-9 (R9) $H_2O_2 + H = H_2O + OH$

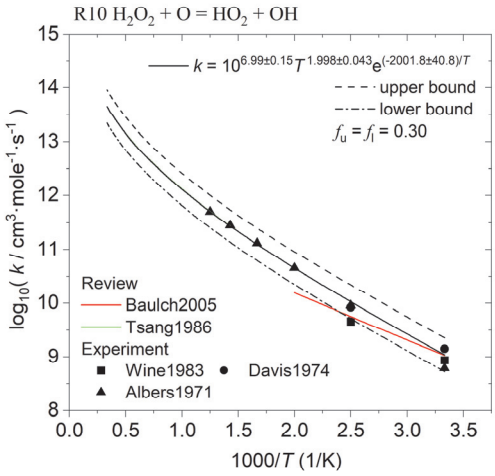

Figure S1-10 (R10) $H_2O_2 + O = HO_2 + OH$

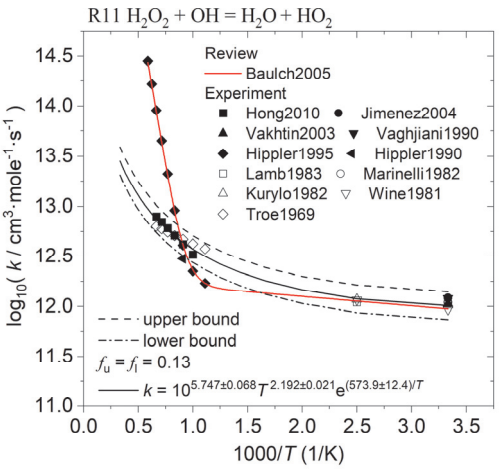

Figure S1-11 (R11) $H_2O_2 + OH = H_2O + HO_2$

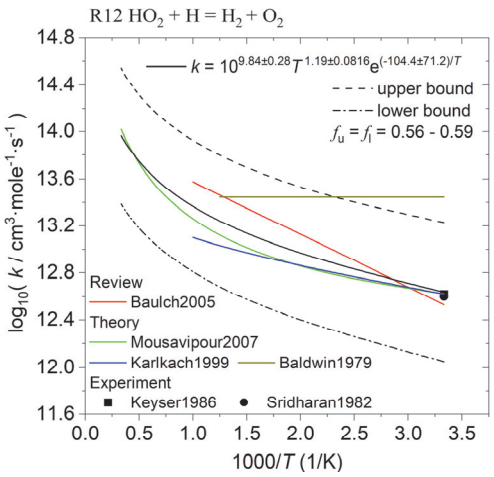

Figure S1-12 (R12) $HO_2 + H = H_2 + O_2$

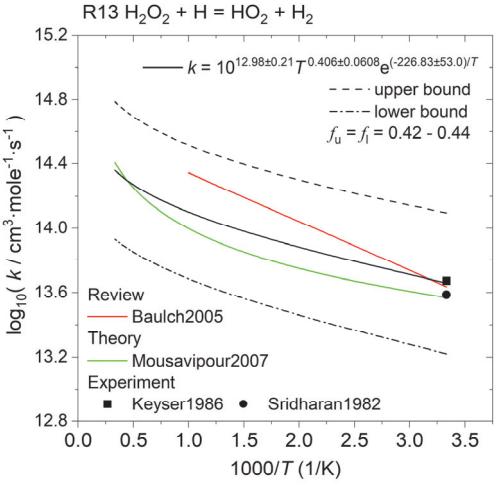

Figure S1-13 (R13) $HO_2 + H = OH + OH$

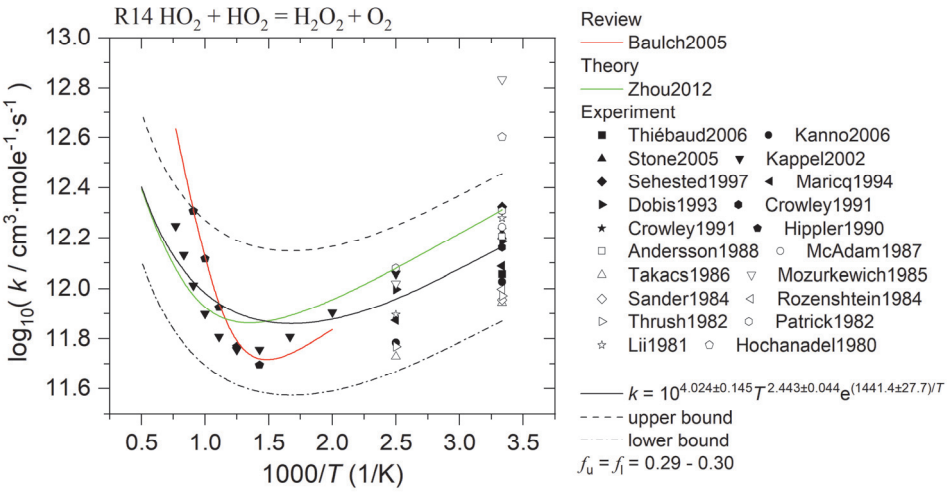

Figure S1-14 (R14) $HO_2 + HO_2 = H_2O_2 + O_2$

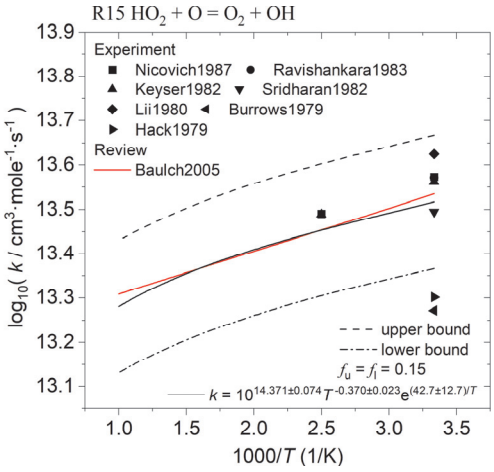

Figure S1-15 (R15) $HO_2 + O = O_2 + OH$

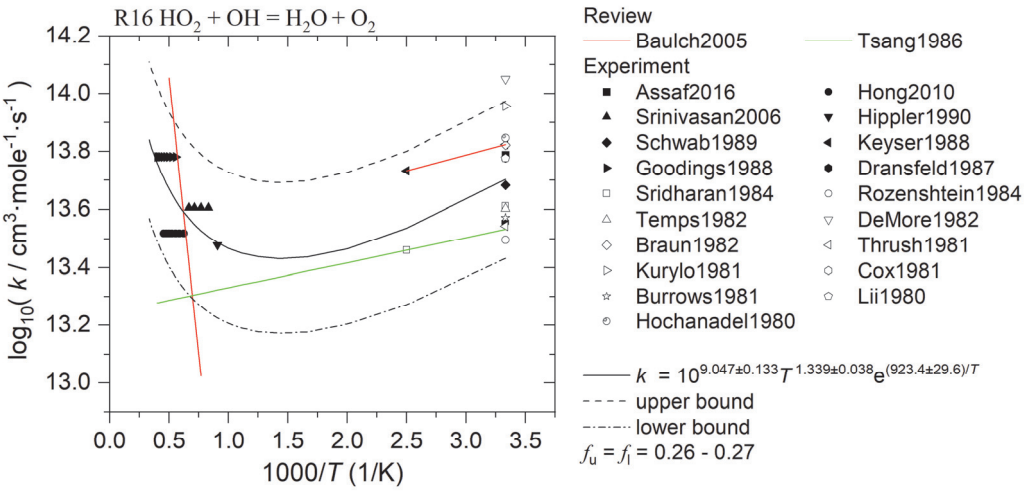

Figure S1-16 (R16) $HO_2 + OH = H_2O + O_2$

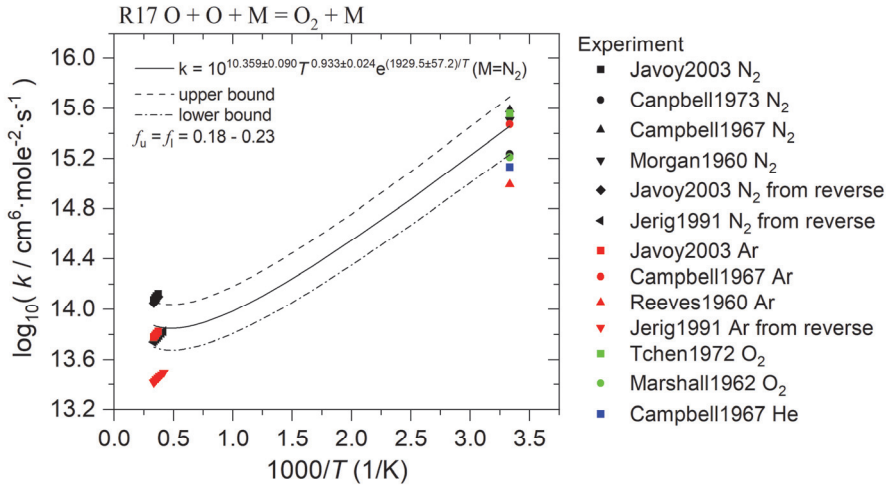

Figure S1-17 (R17) O + O + M = O_2 + M

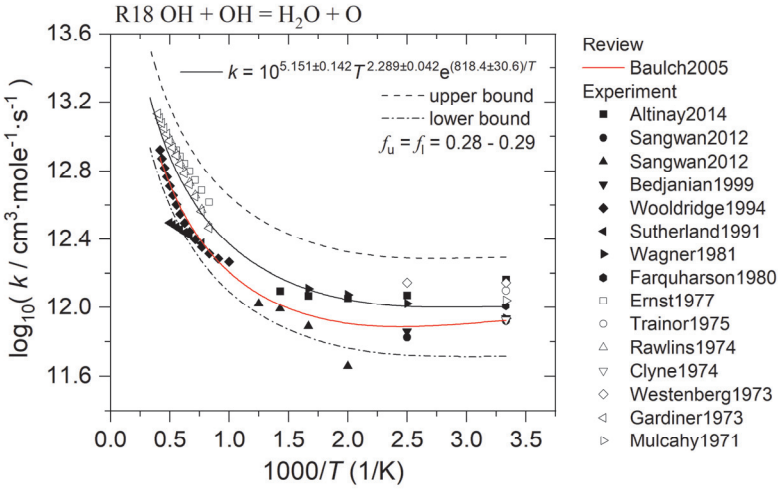

Figure S1-18 (R18) OH + OH = H_2O + O

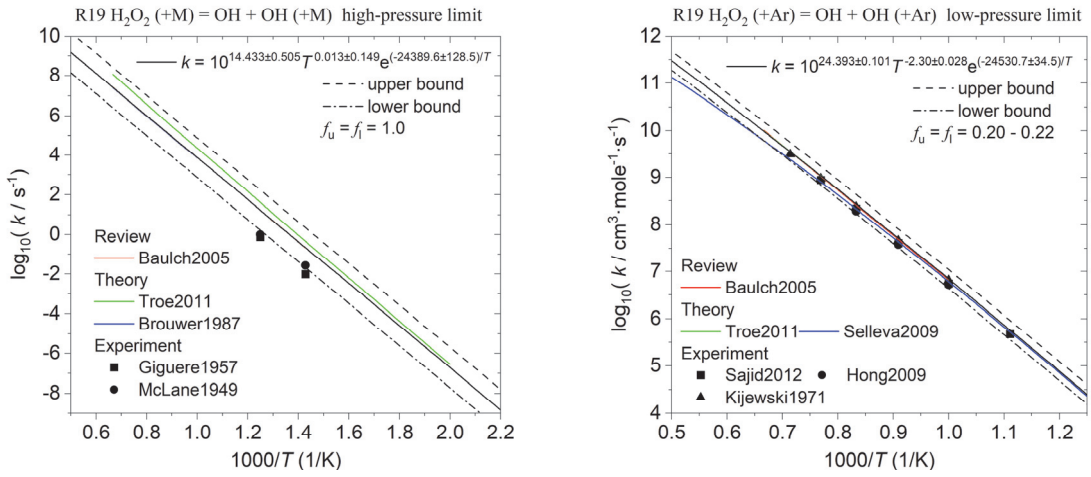

Figure S1-19 (R19) H_2O_2 (+M) = OH + OH (+M)

References

[1] D.L. Baulch, C.T. Bowman, C.J. Cobos, R.A. Cox, T. Just, J.A. Kerr, M.J. Pilling, D. Stocker, J. Troe, W. Tsang, R.W. Walker, J. Warnatz, Evaluated Kinetic Data for Combustion Modeling: Supplement II, Journal of Physical and Chemical Reference Data 34(3) (2005) 757-1397.

[2] D. Mitchell, D. LeRoy, An experimental test of the orbiting resonance theory of hydrogen atom recombination at room temperature, The Journal of Chemical Physics 67(3) (1977) 1042-1050.

[3] K. Lynch, T. Schwab, J. Michael, Lyman - α absorption photometry at high pressure and atom density kinetic results for H recombination, International Journal of Chemical Kinetics 8(5) (1976) 651-671.

[4] L. Walkauskas, F. Kaufman, Gas phase hydrogen atom recombination, Symposium (International) on Combustion, Elsevier, 1975, pp. 691-699.

[5] D.W. Trainor, D.O. Ham, F. Kaufman, Gas phase recombination of hydrogen and deuterium atoms, The Journal of Chemical Physics 58(10) (1973) 4599-4609.

[6] J. Bennett, D. Blackmore, Rates of gas-phase hydrogen-atom recombination at room temperature in the presence of added gases, Symposium (International) on Combustion, Elsevier, 1971, pp. 51-59.

[7] D.O. Ham, D.W. Trainor, F. Kaufman, Gas Phase Kinetics of H+ H+ H2→ 2H2, The Journal of Chemical Physics 53(11) (1970) 4395-4396.

[8] W. Mallard, J. Owen, Rate constant for H+ H+ Ar= H2+ Ar from 1300 to 1700 K, International Journal of Chemical Kinetics 6(5) (1974) 753-761.

[9] C. Halstead, D.R. Jenkins, Rates of H+ H+ M→ H2+ M and H+ OH+ M→ H2O+ M reactions in flames, Combustion and Flame 14(3) (1970) 321-323.

[10] I. Hurle, A. Jones, J. Rosenfeld, Shock-wave observations of rate constants for atomic hydrogen recombination from 2500 to 7000 K: collisional stabilization by exchange of hydrogen atoms, Proceedings of the Royal Society of London. A. Mathematical and Physical Sciences 310(1501) (1969) 253-276.

[11] R. Getzinger, L. Blair, Recombination in the hydrogen-oxygen reaction: A shock tube study with nitrogen and water vapour as third bodies, Combustion and Flame 13(3) (1969) 271-284.

[12] T. Jacobs, R. Giedt, N. Cohen, Kinetics of hydrogen halides in shock waves. ii. a new measurement of the hydrogen dissociation rate, The Journal of Chemical Physics 47(1) (1967) 54-57.

[13] G.L. Schott, P.F. Bird, Kinetic Studies of Hydroxyl Radicals in Shock Waves. IV. Recombination Rates in Rich Hydrogen—Oxygen Mixtures, The Journal of Chemical Physics 41(9) (1964) 2869-2876.

[14] J.P. Rink, Shock tube determination of dissociation rates of hydrogen, The Journal of Chemical Physics 36(1) (1962) 262-265.

[15] R.W. Patch, Shock - Tube Measurement of Dissociation Rates of Hydrogen, The Journal of Chemical Physics 36(7) (1962) 1919-1924.

[16] W. Tsang, R.F. Hampson, Chemical Kinetic Data Base for Combustion Chemistry. Part I. Methane and Related Compounds, Journal of Physical and Chemical Reference Data 15(3) (1986) 1087-1279.

[17] V. Naudet, S. Javoy, C.-E. Paillard, A high temperature chemical kinetics study of the reaction: OH+ Ar= H+ O+ Ar by atomic resonance absorption spectrophotometry, Combustion science and technology 164(1) (2001) 113-128.

[18] S.R. Sellevåg, Y. Georgievskii, J.A. Miller, The temperature and pressure dependence of the reactions H+ O2 (+ M)→ HO2 (+ M) and H+ OH (+ M)→ H2O (+ M), The Journal of Physical Chemistry A 112(23) (2008) 5085-5095.

[19] J. Troe, Detailed modeling of the temperature and pressure dependence of the reaction H+ O2 (+ M)→ HO2 (+ M), Proceedings of the combustion institute 28(2) (2000) 1463-1469.

[20] R. Fernandes, K. Luther, J. Troe, V. Ushakov, Experimental and modelling study of the recombination reaction

H+ O 2 (+ M)→ HO 2 (+ M) between 300 and 900 K, 1.5 and 950 bar, and in the bath gases M= He, Ar, and N 2, Physical Chemistry Chemical Physics 10(29) (2008) 4313-4321.
[21] J. Hahn, L. Krasnoperov, K. Luther, J. Troe, Pressure dependence of the reaction H+ O 2 (+ Ar)→ HO 2 (+ Ar) in the range 1 – 900 bar and 300 – 700 K, Physical Chemistry Chemical Physics 6(9) (2004) 1997-1999.
[22] J. Michael, M.-C. Su, J. Sutherland, J. Carroll, A. Wagner, Rate constants for H+ O2+ M→ HO2+ M in seven bath gases, The Journal of Physical Chemistry A 106(21) (2002) 5297-5313.
[23] R.W. Bates, D.M. Golden, R.K. Hanson, C.T. Bowman, Experimental study and modeling of the reaction H+ O 2+ M→ HO 2+ M (M= Ar, N 2, H2O) at elevated pressures and temperatures between 1050 and 1250 K, Physical Chemistry Chemical Physics 3(12) (2001) 2337-2342.
[24] P.J. Ashman, B.S. Haynes, Rate coefficient of H+ O2+ M→ HO2+ M (M= H2O, N2, Ar, CO2), Symposium (International) on Combustion, Elsevier, 1998, pp. 185-191.
[25] K.L. Carleton, W.J. Kessler, W.J. Marinelli, Hydrogen atom+ oxygen+ M (= N2, H2O, Ar) three-body rate coefficients at 298-750 K, The Journal of Physical Chemistry 97(24) (1993) 6412-6417.
[26] K.-J. Hsu, J. Durant, F. Kaufman, Rate constants for H+ O2+ M at 298 K for M= He, N2, and H2O, Journal of physical chemistry (1952) 91(7) (1987) 1895-1899.
[27] C. Cobos, J. Troe, Theory of thermal unimolecular reactions at high pressures. II. Analysis of experimental results, The Journal of chemical physics 83(3) (1985) 1010-1015.
[28] G.L. Pratt, S.W. Wood, Stoichiometry and rate of reaction of hydrogen atoms with oxygen, Journal of the Chemical Society, Faraday Transactions 1: Physical Chemistry in Condensed Phases 79(11) (1983) 2597-2604.
[29] S. Wang, D.F. Davidson, R.K. Hanson, Shock Tube and Laser Absorption Study of CH2O Oxidation via Simultaneous Measurements of OH and CO, J Phys Chem A 121(45) (2017) 8561-8568.
[30] Z. Hong, D.F. Davidson, E.A. Barbour, R.K. Hanson, A new shock tube study of the H+O2→OH+O reaction rate using tunable diode laser absorption of H2O near 2.5 μm, Proceedings of the Combustion Institute 33(1) (2011) 309-316.
[31] H. Yang, W.C. Gardiner, K.S. Shin, N. Fujii, Shock tube study of the rate coefficient of H + O2 → OH + O, Chemical Physics Letters 231(4-6) (1994) 449-453.
[32] H. Du, J.P. Hessler, Rate coefficient for the reaction H+O2→OH+O: Results at high temperatures, 2000 to 5300 K, The Journal of Chemical Physics 96(2) (1992) 1077-1092.
[33] T. Yuan, C. Wang, C.L. Yu, M. Frenklach, M.J. Rabinowitz, Determination of the rate coefficient for the reaction hydrogen atom + oxygen .fwdarw. hydrogen + oxygen atom by a shock tube/laser absorption/detailed modeling study, The Journal of Physical Chemistry 95(3) (1991) 1258-1265.
[34] K.S. Shin, J.V. Michael, Rate constants for the reactions H+O2→OH+O and D+O2→OD+O over the temperature range 1085 – 2278 K by the laser photolysis – shock tube technique, The Journal of Chemical Physics 95(1) (1991) 262-273.
[35] D.A. Masten, R.K. Hanson, C.T. Bowman, Shock tube study of the reaction hydrogen atom + oxygen .fwdarw. hydroxyl + oxygen atom using hydroxyl laser absorption, The Journal of Physical Chemistry 94(18) (1990) 7119-7128.
[36] A. Pirraglia, J. Michael, J. Sutherland, R. Klemm, A flash photolysis-shock tube kinetic study of the H atom reaction with O2: H+ O2⇄ OH+ O (962 K≤ T≤ 1705 K) and H+ O2+ Ar⇄ HO2+ Ar (746 K≤ T≤ 987 K), Journal of physical chemistry (1952) 93(1) (1989) 282-291.
[37] N. Fujii, K.S. Shin, Rate constant for H+ O2→ O+ OH by laser absorption spectroscopy of OH in shock-heated H2-O2-Ar mixtures, Chemical physics letters 151(4-5) (1988) 461-465.
[38] P. Frank, T. Just, High temperature reaction rate for H+ O2= OH+ O and OH+ H2= H2O+ H, Berichte der Bunsengesellschaft für physikalische Chemie 89(2) (1985) 181-187.

[39] E.N. Aleksandrov, V.S. Arutyunov, I.V. Dubrovina, S.N. Kozlov, Kinetics of hydrogen oxidation near the lower explosion limit, International Journal of Chemical Kinetics 16(7) (1984) 817-834.
[40] G. Dixon-Lewis, Spherically symmetric flame propagation in hydrogen-air mixtures, Combustion science and technology 34(1-6) (1983) 1-29.
[41] G.L. Schott, Further studies of exponential branching rates in reflected-shock heated, nonstoichiometric H2COO2 systems, Combustion and Flame 21(3) (1973) 357-370.
[42] K.H. Eberius, K. Hoyermann, H.G. Wagner, Experimental and mathematical study of a hydrogen-oxygen flame, Symposium (International) on Combustion 13(1) (1971) 713-721.
[43] C.J. Jachimowski, W.M. Houghton, Shock-tube study of the induction-period kinetics of the hydrogen-oxygen reaction, Combustion and Flame 15(2) (1970) 125-132.
[44] A. Myerson, W. Watt, Atom‐Formation Rates behind Shock Waves in Hydrogen and the Effect of Added Oxygen, The Journal of Chemical Physics 49(1) (1968) 425-433.
[45] S.C. Kurzius, M. Boudart, Kinetics of the branching step in the hydrogen-oxygen reaction, Combustion and Flame 12(5) (1968) 477-491.
[46] D. Gutman, G.L. Schott, Shock‐Tube Study of Chain Branching during the Induction Period of the Hydrogen—Oxygen Reaction, The Journal of Chemical Physics 46(12) (1967) 4576-4584.
[47] R. Robertson, G.P. Smith, Temperature Dependence of O+ OH at 136− 377 K Using Ozone Photolysis, The Journal of Physical Chemistry A 110(21) (2006) 6673-6679.
[48] R. Robertson, G.P. Smith, Photolytic measurement of the O+ OH rate constant at 295 K, Chemical physics letters 358(1-2) (2002) 157-162.
[49] I.W. Smith, D.W. Stewart, Low-temperature kinetics of reactions between neutral free radicals. Rate constants for the reactions of OH radicals with N atoms (103⩽ T/K⩽ 294) and with O atoms (158⩽ T/K⩽ 294), Journal of the Chemical Society, Faraday Transactions 90(21) (1994) 3221-3227.
[50] W.H. Brune, J.J. Schwab, J. Anderson, Laser magnetic resonance, resonance fluorescence, resonance absorption studies of the reaction kinetics of atomic oxygen+ hydroxyl. fwdarw. atomic hydrogen+ molecular oxygen, atomic oxygen+ perhydroxyl. fwdarw. hydroxyl+ molecular oxygen, atomic nitrogen+ hydroxyl. fwdarw. atomic hydrogen+ nitric oxide, atomic nitrogen+ perhydroxyl. fwdarw. products at 300 K between 1 and 5 torr, The Journal of Physical Chemistry 87(22) (1983) 4503-4514.
[51] M.J. Howard, I.W. Smith, Direct rate measurements on the reactions N+ OH→ NO+ H and O+ OH→ O 2+ H from 250 to 515 K, Journal of the Chemical Society, Faraday Transactions 2: Molecular and Chemical Physics 77(6) (1981) 997-1008.
[52] R. Lewis, R. Watson, Temperature dependence of the reaction O (3P)+ OH (2II). fwdarw. O2+ H, The Journal of Physical Chemistry 84(26) (1980) 3495-3503.
[53] M.J. Howard, I.W. Smith, Direct rate measurements on the reactions N+ OH→ NO+ H And O+ OH→ O2+ H, Chemical Physics Letters 69(1) (1980) 40-44.
[54] J. Breen, G. Glass, Rate of some hydroxyl radical reactions, The Journal of Chemical Physics 52(3) (1970) 1082-1086.
[55] S. Javoy, V. Naudet, S. Abid, C. Paillard, Elementary reaction kinetics studies of interest in H2 supersonic combustion chemistry, Experimental thermal and fluid science 27(4) (2003) 371-377.
[56] J.M. Goodings, A.N. Hayhurst, Heat release and radical recombination in premixed fuel-lean flames of H 2+ O 2+ N 2. Rate constants for H+ OH+ M→ H 2 O+ M and HO 2+ OH→ H 2 O+ O 2, Journal of the Chemical Society, Faraday Transactions 2: Molecular and Chemical Physics 84(6) (1988) 745-762.
[57] R. Zellner, K. Erler, D. Field, Kinetics of the recombination reaction OH+ H+ M→ H2O+ M at low temperatures, Symposium (International) on Combustion, Elsevier, 1977, pp. 939-948.

[58] M. Davis, W. McGregor, A. Mason, OH chemiluminescent radiation from lean hydrogen‐oxygen flames, The Journal of Chemical Physics 61(4) (1974) 1352-1356.
[59] J. Homer, I. Hurle, The dissociation of water vapour behind shock waves, Proceedings of the Royal Society of London. A. Mathematical and Physical Sciences 314(1519) (1970) 585-598.
[60] R.W. Getzinger, A shock-wave study of recombination in near-stoichiometric hydrogen-oxygen mixtures, Symposium (International) on Combustion, Elsevier, 1967, pp. 117-124.
[61] G. Dixon-Lewis, M. Sutton, A. Williams, The kinetics of hydrogen atom recombination, Discussions of the Faraday Society 33 (1962) 205-212.
[62] W. Cathro, J. Mackie, Lithium hydroxide and the dissociation kinetics of water vapour, Journal of the Chemical Society, Faraday Transactions 1: Physical Chemistry in Condensed Phases 68 (1972) 150-159.
[63] H. Olschewski, J. Troe, H.G. Wagner, Studies of unimolecular reactions of triatomic molecules, Symposium (International) on Combustion, Elsevier, 1967, pp. 155-161.
[64] N. Balakrishnan, Quantum calculations of the O (3 P)+ H 2→ OH+ H reaction, The Journal of chemical physics 121(13) (2004) 6346-6352.
[65] S. Javoy, V. Naudet, S. Abid, C. Paillard, Rate constant for the reaction of O with H2 at high temperature by resonance absorption measurements of O atoms, International Journal of Chemical Kinetics 32(11) (2000) 686-695.
[66] S.-O. Ryu, S.M. Hwang, M.J. Rabinowitz, Rate coefficient of the O+ H2= OH+ H reaction determined via shock tube-laser absorption spectroscopy, Chemical physics letters 242(3) (1995) 279-284.
[67] H.-X. Yang, K.S. Shin, W. Gardiner, Rate coefficients for O+ H2→ OH+ H and O+ D2→ OD+ D by kinetic laser absorption spectroscopy in shock waves, Chemical physics letters 207(1) (1993) 69-74.
[68] D. Davidson, R. Hanson, A direct comparison of shock tube photolysis and pyrolysis methods in the determination of the rate coefficient for O+ H2→ OH+ H, Combustion and flame 82(3-4) (1990) 445-447.
[69] K.S. Shin, N. Fujii, W.C. Gardiner Jr, Rate constant for O+ H2→ OH+ H by laser absorption spectroscopy of OH in shock-heated H2 O2 Ar mixtures, Chemical physics letters 161(3) (1989) 219-222.
[70] J. Sutherland, J. Michael, A. Pirraglia, F. Nesbitt, R. Klemm, Rate constant for the reaction of O (3P) with H2 by the flash photolysis—shock tube and flash photolysis—Resonance fluorescence techniques; 504K≤ T≤ 2495K, Symposium (International) on Combustion, Elsevier, 1988, pp. 929-941.
[71] K. Natarajan, P. Roth, High temperature rate coefficient for the reaction of O (3P) with H2 obtained by the resonance absorption of O and H atoms, Combustion and flame 70(3) (1987) 267-279.
[72] P. Marshall, A. Fontijn, HTP kinetics studies of the reactions of O (2 3 PJ) atoms with H2 and D2 over wide temperature ranges, The Journal of chemical physics 87(12) (1987) 6988-6994.
[73] N. Presser, R.J. Gordon, The kinetic isotope effect in the reaction of O (3 P) with H2, D2, and HD, The Journal of chemical physics 82(3) (1985) 1291-1297.
[74] K.M. Pamidimukkala, G.B. Skinner, Resonance absorption measurements of atom concentrations in reacting gas mixtures. VIII. Rate constants for O+ H2→ OH+ H and O+ D2→ OD+ D from measurements of O atoms in oxidation of H2 and D2 by N2O, The Journal of Chemical Physics 76(1) (1982) 311-315.
[75] G.C. Light, J.H. Matsumoto, Experimental measurement of the rate of the reaction o (3P)+ H2 (v= 0)→ OH (v= 0)+ H at T= 298 K, International Journal of Chemical Kinetics 12(7) (1980) 451-468.
[76] R.N. Dubinsky, D.J. McKenney, Determination of the Rate Constant of the O+ H2→ OH+ H Reaction using Atomic Oxygen Resonance Fluorescence and the Air Afterglow Techniques, Canadian Journal of Chemistry 53(23) (1975) 3531-3541.
[77] G.L. Schott, R.W. Getzinger, W.A. Seitz, Transient oxygen atom yields in H2 O2 ignition and the rate coefficient for O+ H2→ OH+ H, International Journal of Chemical Kinetics 6(6) (1974) 921-943.

[78] T. Brabbs, F. Belles, R. Brokaw, Shock-tube measurements of specific reaction rates in the branched-chain H2-CO-O2 system, Symposium (International) on Combustion, Elsevier, 1971, pp. 129-136.
[79] A. Dean, G. Kistiakowsky, Oxidation of carbon monoxide by oxygen in shock waves, The Journal of Chemical Physics 53(2) (1970) 830-838.
[80] K.Y. Lam, D.F. Davidson, R.K. Hanson, A shock tube study of H2+ OH→ H2O+ H using OH laser absorption, International Journal of Chemical Kinetics 45(6) (2013) 363-373.
[81] T.L. Nguyen, J.F. Stanton, J.R. Barker, Ab initio reaction rate constants computed using semiclassical transition-state theory: HO + H2 --> H2O + H and isotopologues, J Phys Chem A 115(20) (2011) 5118-26.
[82] V.L. Orkin, S.N. Kozlov, G.A. Poskrebyshev, M.J. Kurylo, Rate Constant for the Reaction of OH with H2 between 200 and 480 K, The Journal of Physical Chemistry A 110(21) (2006) 6978-6985.
[83] L.N. Krasnoperov, J.V. Michael, Shock Tube Studies Using a Novel Multipass Absorption Cell: Rate Constant Results For OH + H2and OH + C2H6, The Journal of Physical Chemistry A 108(26) (2004) 5643-5648.
[84] N.L. Haworth, G.B. Bacskay, J.C. Mackie, The Role of Phosphorus Dioxide in the H + OH Recombination Reaction: Ab Initio Quantum Chemical Computation of Thermochemical and Rate Parameters, The Journal of Physical Chemistry A 106(8) (2002) 1533-1541.
[85] R.K. Talukdar, T. Gierczak, L. Goldfarb, Y. Rudich, B.M. Rao, A. Ravishankara, Kinetics of hydroxyl radical reactions with isotopically labeled hydrogen, The Journal of Physical Chemistry 100(8) (1996) 3037-3043.
[86] J. Bott, N. Cohen, A shock tube study of the reaction of the hydroxyl radical with H2, CH4, c‐C5H10, and i‐C4H10, International journal of chemical kinetics 21(7) (1989) 485-498.
[87] V. Schmidt, G.-Y. Zhu, K. Becker, E. Fink, Study of OH reactions at high pressures by excimer laser photolysis—dye laser fluorescence, Berichte der Bunsengesellschaft für physikalische Chemie 89(3) (1985) 321-322.
[88] A. Ravishankara, J. Nicovich, R. Thompson, F. Tully, Kinetic study of the reaction of hydroxyl with hydrogen and deuterium from 250 to 1050 K, The Journal of Physical Chemistry 85(17) (1981) 2498-2503.
[89] D.W. Trainor, C.W. von Rosenberg, Energy partitioning in the products of elementary reactions involving OH-radicals, Symposium (International) on Combustion 15(1) (1975) 755-764.
[90] R.P. Overend, G. Paraskevopoulos, R.J. Cvetanović, Rates of OH Radical Reactions. I. Reactions with H2, CH4, C2H6, and C3H8 at 295 K, Canadian Journal of Chemistry 53(22) (1975) 3374-3382.
[91] R. Atkinson, D.A. Hansen, J.N. Pitts, Rate constants for the reaction of the OH radical with H2 and NO (M=Ar and N2), The Journal of Chemical Physics 62(8) (1975) 3284-3288.
[92] I.W.M. Smith, R. Zellner, Rate measurements of reactions of OH by resonance absorption. Part 3.—Reactions of OH with H2, D2and hydrogen and deuterium halides, J. Chem. Soc., Faraday Trans. 2 70(0) (1974) 1045-1056.
[93] W.C. Gardiner, W.G. Mallard, J.H. Owen, Rate constant of OH + H2 = H2O + H from 1350 to 1600 K, The Journal of Chemical Physics 60(6) (1974) 2290-2295.
[94] A.A. Westenberg, N. deHaas, Rates of CO + OH and H2 + OH over an extended temperature range, The Journal of Chemical Physics 58(10) (1973) 4061-4065.
[95] F. Stuhl, H. Niki, Pulsed Vacuum‐uv Photochemical Study of Reactions of OH with H2, D2, and CO Using a Resonance‐Fluorescent Detection Method, The Journal of Chemical Physics 57(9) (1972) 3671-3677.
[96] R. Gorse, D. Volman, Photochemistry of the gaseous hydrogen peroxide—carbon monoxide system. II: Rate constants for hydroxyl radical reactions with hydrocarbons and for hydrogen atom reactions with hydrogen peroxide, Journal of Photochemistry 3(1) (1974) 115-122.
[97] R.R. Baldwin, R.W. Walker, Rate constants for hydrogen+ oxygen system, and for H atoms and OH radicals+ alkanes, Journal of the Chemical Society, Faraday Transactions 1: Physical Chemistry in Condensed Phases 75 (1979) 140-154.

[98] D. Lee, S. Hochgreb, Hydrogen autoignition at pressures above the second explosion limit (0.6–4.0 MPa), International journal of chemical kinetics 30(6) (1998) 385-406.
[99] W. Forst, P.A. Giguere, Inhibition by Hydrogen Peroxide of the Second Explosion Limit of the Hydrogen-Oxygen Reaction, The Journal of Physical Chemistry 62(3) (1958) 340-343.
[100] P. Wine, J. Nicovich, R. Thompson, A. Ravishankara, Kinetics of atomic oxygen (3PJ) reactions with hydrogen peroxide and ozone, The Journal of Physical Chemistry 87(20) (1983) 3948-3954.
[101] D. Davis, W. Wong, R. Schiff, Dye laser flash photolysis kinetics study of the reaction of ground-state atomic oxygen with hydrogen peroxide, The Journal of Physical Chemistry 78(4) (1974) 463-464.
[102] E. Albers, K. Hoyermann, H.G. Wagner, J. Wolfrum, Absolute measurements of rate coefficients for the reactions of H and O atoms with H2O2 and H2O, Symposium (International) on Combustion, Elsevier, 1971, pp. 81-88.
[103] Z. Hong, R.D. Cook, D.F. Davidson, R.K. Hanson, A shock tube study of OH+ H2O2→ H2O+ HO2 and H2O2+ M→ 2OH+ M using laser absorption of H2O and OH, The Journal of Physical Chemistry A 114(18) (2010) 5718-5727.
[104] E. Jiménez, T. Gierczak, H. Stark, J.B. Burkholder, A. Ravishankara, Reaction of OH with HO2NO2 (peroxynitric acid): rate coefficients between 218 and 335 K and product yields at 298 K, The Journal of Physical Chemistry A 108(7) (2004) 1139-1149.
[105] A.B. Vakhtin, D.C. McCabe, A. Ravishankara, S.R. Leone, Low-temperature kinetics of the reaction of the OH radical with hydrogen peroxide, The Journal of Physical Chemistry A 107(49) (2003) 10642-10647.
[106] G.L. Vaghjiani, A. Ravishankara, Photodissociation of h2o2 and ch3ooh at 248 nm and 298 k: Quantum yields for oh, o (3 p) and h (2 s), The Journal of chemical physics 92(2) (1990) 996-1003.
[107] H. Hippler, H. Neunaber, J. Troe, Shock wave studies of the reactions HO+ H2O2→ H2O+ HO2 and HO+ HO2→ H2O+ O2 between 930 and 1680 K, The Journal of chemical physics 103(9) (1995) 3510-3516.
[108] H. Hippler, J. Troe, J. Willner, Shock wave study of the reaction HO2+ HO2→ H2O2+ O2: Confirmation of a rate constant minimum near 700 K, The Journal of chemical physics 93(3) (1990) 1755-1760.
[109] J.J. Lamb, L.T. Molina, C.A. Smith, M.J. Molina, Rate constant of the hydroxy radical+ hydrogen peroxide. fwdarw. hydroperoxo radical+ water reaction, The Journal of Physical Chemistry 87(22) (1983) 4467-4470.
[110] W.J. Marinelli, H.S. Johnston, Reaction rates of hydroxyl radical with nitric acid and with hydrogen peroxide, The Journal of Chemical Physics 77(3) (1982) 1225-1234.
[111] M.J. Kurylo, J.L. Murphy, G.S. Haller, K.D. Cornett, A flash photolysis resonance fluorescence investigation of the reaction OH+ H2O2→ HO2+ H2O, International Journal of Chemical Kinetics 14(10) (1982) 1149-1161.
[112] P. Wine, D. Semmes, A. Ravishankara, A laser flash photolysis kinetics study of the reaction OH+ H2O2→ HO2+ H2O, The Journal of Chemical Physics 75(9) (1981) 4390-4395.
[113] J. Troe, Ultraviolettspektrum und Reaktionen des HO2 - Radikals im thermischen Zerfall von H2O2, Berichte der Bunsengesellschaft für physikalische Chemie 73(10) (1969) 946-952.
[114] S.H. Mousavipour, V. Saheb, Theoretical study on the kinetic and mechanism of H+ HO2 reaction, Bulletin of the Chemical Society of Japan 80(10) (2007) 1901-1913.
[115] S.P. Karkach, V.I. Osherov, Ab initio analysis of the transition states on the lowest triplet H 2 O 2 potential surface, The Journal of chemical physics 110(24) (1999) 11918-11927.
[116] U. Sridharan, L. Qiu, F. Kaufman, Kinetics and product channels of the reactions of perhydroxyl with oxygen and hydrogen atoms at 296 K, The Journal of Physical Chemistry 86(23) (1982) 4569-4574.
[117] L.F. Keyser, Absolute rate constant and branching fractions for the atomic hydrogen+ hydroperoxyl radical reaction from 245 to 300 K, The Journal of Physical Chemistry 90(13) (1986) 2994-3003.
[118] D.D. Zhou, K. Han, P. Zhang, L.B. Harding, M.J. Davis, R.T. Skodje, Theoretical determination of the rate

coefficient for the HO2+ HO2→ H2O2+ O2 reaction: Adiabatic treatment of anharmonic torsional effects, The Journal of Physical Chemistry A 116(9) (2012) 2089-2100.
[119] C. Kappel, K. Luther, J. Troe, Shock wave study of the unimolecular dissociation of H 2 O 2 in its falloff range and of its secondary reactions, Physical Chemistry Chemical Physics 4(18) (2002) 4392-4398.
[120] J. Thiebaud, C. Fittschen, Near infrared cw-CRDS coupled to laser photolysis: Spectroscopy and kinetics of the HO 2 radical, Applied Physics B 85(2-3) (2006) 383-389.
[121] N. Kanno, K. Tonokura, M. Koshi, Equilibrium constant of the HO2 - H2O complex formation and kinetics of HO2+ HO2 - H2O: Implications for tropospheric chemistry, Journal of Geophysical Research: Atmospheres 111(D20) (2006).
[122] D. Stone, D.M. Rowley, Kinetics of the gas phase HO 2 self-reaction: Effects of temperature, pressure, water and methanol vapours, Physical Chemistry Chemical Physics 7(10) (2005) 2156-2163.
[123] J. Sehested, T. Møgelberg, K. Fagerström, G. Mahmoud, T.J. Wallington, Absolute rate constants for the self reactions of HO2, CF3CFHO2, and CF3O2 radicals and the cross reactions of HO2 with FO2, HO2 with CF3CFHO2, and HO2 with CF3O2 at 295 K, International journal of chemical kinetics 29(9) (1997) 673-682.
[124] M.M. Maricq, J.J. Szente, A kinetic study of the reaction between ethylperoxy radicals and HO2, The Journal of Physical Chemistry 98(8) (1994) 2078-2082.
[125] O. Dobis, S.W. Benson, Reaction of the ethyl radical with oxygen at millitorr pressures at 243-368 K and a study of the Cl+ HO2, ethyl+ HO2, and HO2+ HO2 reactions, Journal of the American Chemical Society 115(19) (1993) 8798-8809.
[126] J. Crowley, F. Simon, J. Burrows, G. Moortgat, M. Jenkin, R. Cox, The HO2 radical UV absorption spectrum measured by molecular modulation, UV/diode-array spectroscopy, Journal of Photochemistry and Photobiology A: Chemistry 60(1) (1991) 1-10.
[127] B. Andersson, R. Cox, M. Jenkin, The effect of methanol on the self reaction of HO2 radicals, International Journal of Chemical Kinetics 20(4) (1988) 283-295.
[128] K. McAdam, B. Veyret, R. Lesclaux, UV absorption spectra of HO2 and CH3O2 radicals and the kinetics of their mutual reactions at 298 K, Chemical physics letters 133(1) (1987) 39-44.
[129] G.A. Takacs, C.J. Howard, Temperature dependence of the reaction hydroperoxo (HO2)+ hydroperoxo at low pressures, The Journal of Physical Chemistry 90(4) (1986) 687-690.
[130] M. Mozurkewich, S.W. Benson, Self - Reaction of HO2 and DO2: Negative temperature dependence and pressure effects, International journal of chemical kinetics 17(8) (1985) 787-807.
[131] S.P. Sander, Low-pressure study of the perhydroxyl (HO2)+ perhydroxyl (HO2) reaction at 298 K, The Journal of Physical Chemistry 88(24) (1984) 6018-6021.
[132] V. Rozenshtein, Y.M. Gershenzon, S. Il'In, O. Kishkovitch, Reactions of HO2 with NO, OH and HO2 studied by EPR/LMR spectroscopy, Chemical physics letters 112(5) (1984) 473-478.
[133] B. Thrush, G. Tyndall, The rate of reaction between HO2 radicals at low pressures, Chemical Physics Letters 92(3) (1982) 232-235.
[134] R. Patrick, M.J. Pilling, The temperature dependence of the HO2+ HO2 reaction, Chemical Physics Letters 91(5) (1982) 343-347.
[135] R.-R. Lii, M.C. Sauer Jr, S. Gordon, Temperature dependence of the gas-phase self-reaction of hydroperoxo in the presence of water, The Journal of Physical Chemistry 85(19) (1981) 2833-2834.
[136] C. Hochanadel, T. Sworski, P. Ogren, Rate constants for the reactions of HO2 with OH and with HO2, The Journal of Physical Chemistry 84(24) (1980) 3274-3277.
[137] A. Ravishankara, P. Wine, J. Nicovich, Pulsed laser photolysis study of the reaction between O (3 P) and HO2, The Journal of Chemical Physics 78(11) (1983) 6629-6639.

[138] L.F. Keyser, Kinetics of the reaction atomic oxygen+ perhydroxyl. fwdarw. hydroxyl+ molecular oxygen from 229 to 372 K, The Journal of Physical Chemistry 86(17) (1982) 3439-3446.
[139] R.-R. Lii, R.A. Gorse Jr, M.C. Sauer Jr, S. Gordon, Rate constant for the reaction of hydroxyl with hydroperoxo radicals, The Journal of Physical Chemistry 84(8) (1980) 819-821.
[140] J. Burrows, D. Cliff, G.W. Harris, B.A. Thrush, J. Wilkinson, Atmospheric reactions of the H02 radical studied by laser magnetic resonance spectroscopy, Proceedings of the Royal Society of London. A. Mathematical and Physical Sciences 368(1735) (1979) 463-481.
[141] W. Hack, A. Preuss, F. Temps, H.G. Wagner, The reaction O+ HO2→ OH+ O2 studied with a LMR‐ESR‐spectrometer, Berichte der Bunsengesellschaft für physikalische Chemie 83(12) (1979) 1275-1279.
[142] E. Assaf, C. Fittschen, Cross Section of OH Radical Overtone Transition near 7028 cm–1 and Measurement of the Rate Constant of the Reaction of OH with HO2 Radicals, The Journal of Physical Chemistry A 120(36) (2016) 7051-7059.
[143] Z. Hong, S.S. Vasu, D.F. Davidson, R.K. Hanson, Experimental study of the rate of OH+ HO2→ H2O+ O2 at high temperatures using the reverse reaction, The Journal of Physical Chemistry A 114(17) (2010) 5520-5525.
[144] N.K. Srinivasan, M.-C. Su, J.W. Sutherland, J.V. Michael, B. Ruscic, Reflected shock tube studies of high-temperature rate constants for OH+ NO2→ HO2+ NO and OH+ HO2→ H2O+ O2, The Journal of Physical Chemistry A 110(21) (2006) 6602-6607.
[145] J.J. Schwab, W.H. Brune, J.G. Anderson, Kinetics and mechanism of the hydroxyl+ hydroperoxo reaction, The Journal of Physical Chemistry 93(3) (1989) 1030-1035.
[146] L.F. Keyser, Kinetics of the reaction hydroxyl+ hydroperoxo. fwdarw. water+ oxygen from 254 to 382 K, The Journal of Physical Chemistry 92(5) (1988) 1193-1200.
[147] P. Dransfeld, H.G. Wagner, Comparative Study of the Reactions of 16OH and 18OH with H16O2, Zeitschrift für Naturforschung A 42(5) (1987) 471-476.
[148] U. Sridharan, L. Qiu, F. Kaufman, Rate constant of the hydroxyl+ perhydroxyl (HO2) reaction from 252 to 420 K, The Journal of Physical Chemistry 88(7) (1984) 1281-1282.
[149] F. Temps, H. Gg. Wagner, Untersuchungen zur Reaktion OH+ HO2→ H2O+ O2 mit Hilfe eines Laser‐Magnetischen Resonanz‐Spektrometers, Berichte der Bunsengesellschaft für physikalische Chemie 86(2) (1982) 119-125.
[150] W. DeMore, Rate constant and possible pressure dependence of the reaction hydroxyl+ hydroperoxo, The Journal of Physical Chemistry 86(1) (1982) 121-126.
[151] M. Braun, A. Hofzumahaus, F. Stuhl, VUV Flash Photolysis Study of the Reaction of HO with HO2 at 1 atm and 298 K, Berichte der Bunsengesellschaft für physikalische Chemie 86(7) (1982) 597-602.
[152] B. Thrush, J. Wilkinson, The rate of reaction of HO2 radicals with HO and with NO, Chemical Physics Letters 81(1) (1981) 1-3.
[153] M.J. Kurylo, O. Klais, A.H. Laufer, Mechanistic investigation of the hydroxyl+ hydroperoxo reaction, The Journal of Physical Chemistry 85(24) (1981) 3674-3678.
[154] R. Cox, J. Burrows, T. Wallington, Rate coefficient for the reaction OH+ HO2= H2O+ O2 at 1 atmosphere pressure and 308 K, Chemical Physics Letters 84(2) (1981) 217-221.
[155] J. Burrows, R. Cox, R. Derwent, Modulated photolysis of the ozone—water vapour system: kinetics of the reaction of OH with HO2, Journal of Photochemistry 16(2) (1981) 147-168.
[156] I. Campbell, C. Gray, Rate constants for O (3P) recombination and association with N (4S), Chemical Physics Letters 18(4) (1973) 607-609.
[157] H. Tchen, Étude cinétique par RPE des atomes d'oxygène 3p dans la post-décharge, Revue de Physique Appliquée 7(3) (1972) 205-212.

[158] I. Campbell, B.A.-N. Thrush, The association of oxygen atoms and their combination with nitrogen atoms, Proceedings of the Royal Society of London. Series A. Mathematical and Physical Sciences 296(1445) (1967) 222-232.
[159] T.C. Marshall, Studies of atomic recombination of nitrogen, hydrogen, and oxygen by paramagnetic resonance, The Physics of Fluids 5(7) (1962) 743-753.
[160] R.R. Reeves, G. Mannella, P. Harteck, Rate of recombination of oxygen atoms, The Journal of Chemical Physics 32(2) (1960) 632-633.
[161] J. Morgan, L. Elias, H. Schiff, Recombination of oxygen atoms in the absence of O2, The Journal of Chemical Physics 33(3) (1960) 930-931.
[162] L. Jerig, K. Thielen, P. Roth, High-temperature dissociation of oxygen diluted in argon or nitrogen, AIAA journal 29(7) (1991) 1136-1139.
[163] W. Watt, A. Myerson, Atom formation rates behind shock waves in oxygen, The Journal of Chemical Physics 51(4) (1969) 1638-1643.
[164] G. Altinay, R.G. Macdonald, Determination of the Rate Constant for the OH (X2Π)+ OH (X2Π)→ H2O+ O (3P) Reaction over the Temperature Range 295 to 701 K, The Journal of Physical Chemistry A 118(1) (2014) 38-54.
[165] M. Sangwan, L.N. Krasnoperov, Disproportionation Channel of Self-Reaction of Hydroxyl Radical, OH+ OH→ H2O+ O, Studied by Time-Resolved Oxygen Atom Trapping, The Journal of Physical Chemistry A 116(48) (2012) 11817-11822.
[166] Y. Bedjanian, G. Le Bras, G. Poulet, Kinetic study of OH+ OH and OD+ OD reactions, The Journal of Physical Chemistry A 103(35) (1999) 7017-7025.
[167] M.S. Wooldridge, R.K. Hanson, C.T. Bowman, A shock tube study of the OH+ OH→ H2O+ O reaction, International journal of chemical kinetics 26(4) (1994) 389-401.
[168] J.W. Sutherland, P.M. Patterson, R.B. Klemm, Rate constants for the reaction, O (3P)+ H2O¶ OH+ OH, over the temperature range 1053 K to 2033 K using two direct techniques, Symposium (International) on Combustion, Elsevier, 1991, pp. 51-57.
[169] G. Wagner, R. Zellner, Temperature Dependence of the Reaction OH+ OH→ H2O+ O, Berichte der Bunsengesellschaft für physikalische Chemie 85(12) (1981) 1122-1128.
[170] G. Farquharson, R.H. Smith, Rate constants for the gaseous reactions OH+ C2H4 and OH+ OH, Australian Journal of Chemistry 33(7) (1980) 1425-1435.
[171] J. Ernst, H.G. Wagner, R. Zellner, Direct Rate Measurements for OH+ OH→ H2O+ O in the Range 1200 – 1800 K, Berichte der Bunsengesellschaft für physikalische Chemie 81(12) (1977) 1270-1275.
[172] W. Rawlins, W. Gardiner Jr, Rate constant of OH+ OH= H2O+ O from 1500 to 2000 K, The Journal of Chemical Physics 60(12) (1974) 4676-4681.
[173] M.A. Clyne, S. Down, Kinetic behaviour of OH X 2 Π and A 2 σ+ using molecular resonance fluorescence spectrometry, Journal of the Chemical Society, Faraday Transactions 2: Molecular and Chemical Physics 70 (1974) 253-266.
[174] W. Gardiner Jr, W. Mallard, M. McFarland, K. Morinaga, J. Owen, W. Rawlins, T. Takeyama, B. Walker, Elementary reaction rates from post-induction-period profiles in shock-initiated combustion, Symposium (International) on Combustion, Elsevier, 1973, pp. 61-75.
[175] M. Mulcahy, R. Smith, Reactions of OH Radicals in the H–NO2 and H–NO2–CO Systems, The Journal of Chemical Physics 54(12) (1971) 5215-5221.
[176] A. Lifshitz, J. Michael, Rate constants for the reaction, O+ H2O→ OH+ OH, over the temperature range, 1500 – 2400 K, by the flash photolysis-shock tube technique: A further consideration of the back reaction,

Symposium (International) on Combustion, Elsevier, 1991, pp. 59-67.
[177] J. Troe, The thermal dissociation/recombination reaction of hydrogen peroxide H2O2 (+ M) double left right arrow 2OH (+ M) III. Analysis and representation of the temperature and pressure dependence over wide ranges, Combustion and Flame 158(4) (2011) 594-601.
[178] S.R. Sellevåg, Y. Georgievskii, J.A. Miller, Kinetics of the gas-phase recombination reaction of hydroxyl radicals to form hydrogen peroxide, The Journal of Physical Chemistry A 113(16) (2009) 4457-4467.
[179] Z. Hong, A. Farooq, E.A. Barbour, D.F. Davidson, R.K. Hanson, Hydrogen peroxide decomposition rate: a shock tube study using tunable laser absorption of H2O near 2.5 μm, The Journal of Physical Chemistry A 113(46) (2009) 12919-12925.
[180] H. Kijewski, J. Troe, Study of the pyrolysis of H2O2 in the presence of H2and CO by use of UV absorption of HO2, International Journal of Chemical Kinetics 3(3) (1971) 223-235.
[181] L. Brouwer, C. Cobos, J. Troe, H.R. Dübal, F. Crim, Specific rate constants k (E, J) and product state distributions in simple bond fission reactions. II. Application to HOOH→ OH+ OH, The Journal of chemical physics 86(11) (1987) 6171-6182.
[182] P.A. Giguère, I. Liu, Kinetics of the thermal decomposition of hydrogen peroxide vapor, Canadian Journal of Chemistry 35(4) (1957) 283-293.
[183] C. McLane, Hydrogen peroxide in the thermal hydrogen oxygen reaction I. Thermal decomposition of hydrogen peroxide, The Journal of Chemical Physics 17(4) (1949) 379-385.
[184] R. Zellner, F. Ewig, R. Paschke, G. Wagner, Pressure and temperature dependence of the gas-phase recombination of hydroxyl radicals, The Journal of Physical Chemistry 92(14) (1988) 4184-4190.
[185] J. Caldwell, R. Back, Combination reactions of hydroxyl radicals in the flash photolysis of water vapour, Transactions of the Faraday Society 61 (1965) 1939-1945.
[186] G. Black, G. Porter, Vacuum ultra-violet flash photolysis of water vapour, Proceedings of the Royal Society of London. Series A. Mathematical and Physical Sciences 266(1325) (1962) 185-197.
[187] D. Fulle, H. Hamann, H. Hippler, J. Troe, High‐pressure range of the addition of HO to HO. III. Saturated laser‐induced fluorescence measurements between 200 and 700 K, The Journal of chemical physics 105(3) (1996) 1001-1006.
[188] R. Forster, M. Frost, D. Fulle, H.F. Hamann, H. Hippler, A. Schlepegrell, J. Troe, High pressure range of the addition of HO to HO, NO, NO2, and CO. I. Saturated laser induced fluorescence measurements at 298 K, The Journal of Chemical Physics 103(8) (1995) 2949-2958.
[189] N.R. Greiner, Hydroxyl radical kinetics by kinetic spectroscopy. III. Reactions with hydrogen peroxide in the range 300-458. degree. K, The Journal of Physical Chemistry 72(2) (1968) 406-410.

Supplementary-2

A Comprehensive Kinetic Modelling Study of Hydrogen Combustion with Data Uncertainty Analysis

Hongxin Wang[a], Nadezda Slavinskaya[b, c], Oskar Haidn[a]

a. Department of Aerospace and Geodesy, Technical University of Munich, 85748 Garching, Germany

b. GRS Association for Plant and Reactor Safety, 85748 Garching, Germany

c. Al-Farabi Kazakh National University, 050040 Almaty, Kazakhstan

Results of the uncertainty analysis

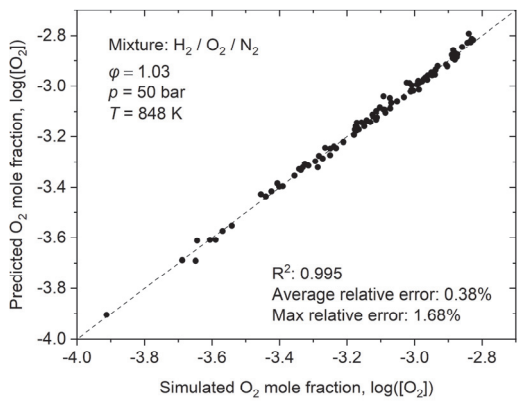

(a)

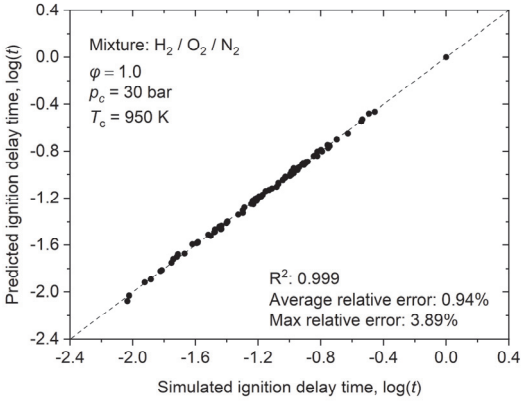

(b)

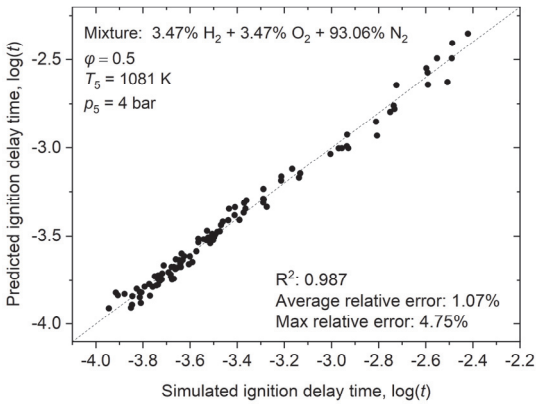

(c)

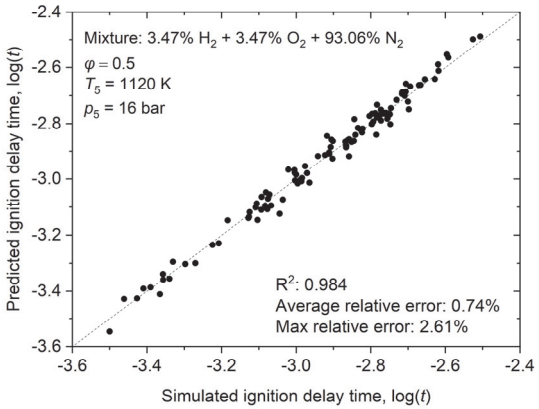

(d)

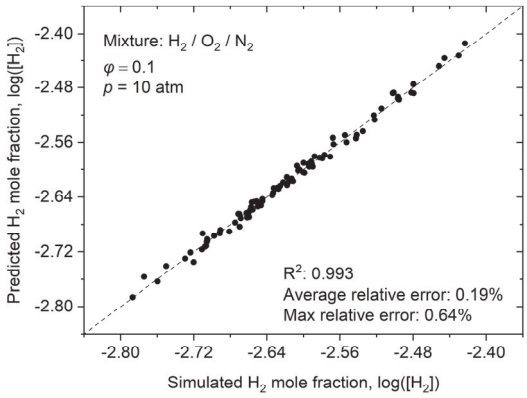

(e)

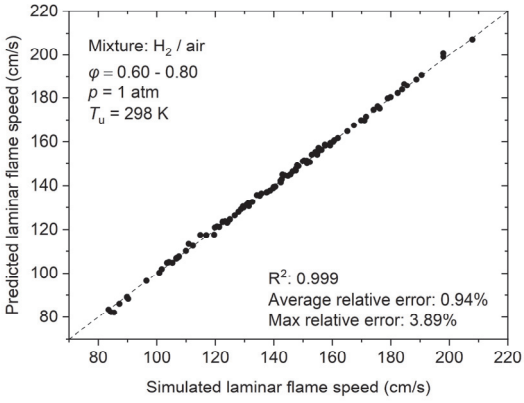

(f)

Figure S2-1. Comparison of the relative uncertainty contributions of different channels to the (a) H_2 mole fractions in the plug flow reactor (PFR) [1]; (b) ignition delay times measured in the rapid compression machine (RCM) [2]; (c) (d) ignition delay times measured in the shock tube; (e) H_2 mole fractions measured in the jet stirred reactor [3]; (f) laminar flame speeds of H_2/air mixture.

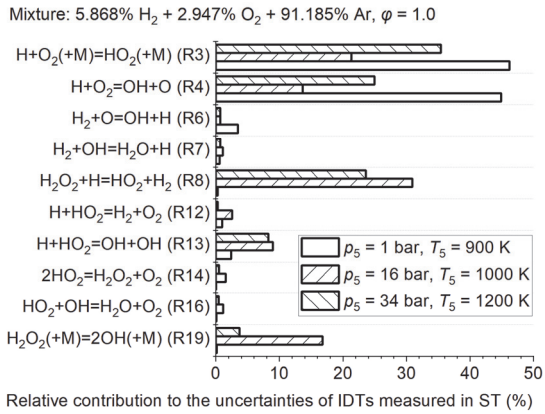

(a)

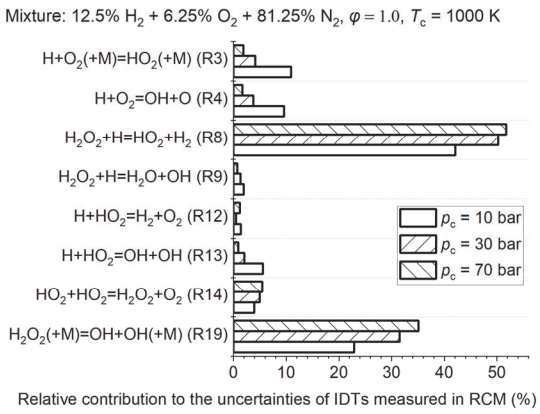

(b)

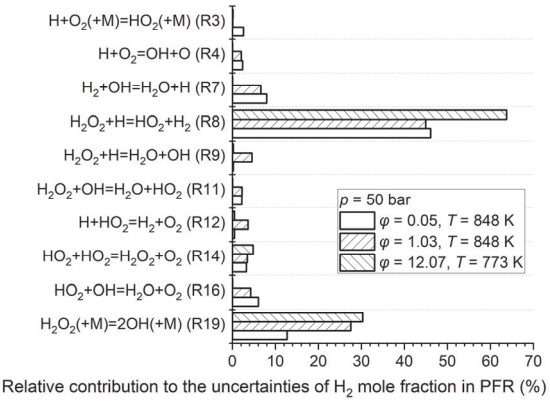

(c)

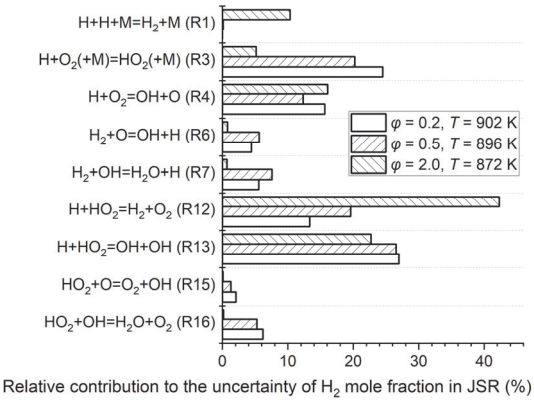

(d)

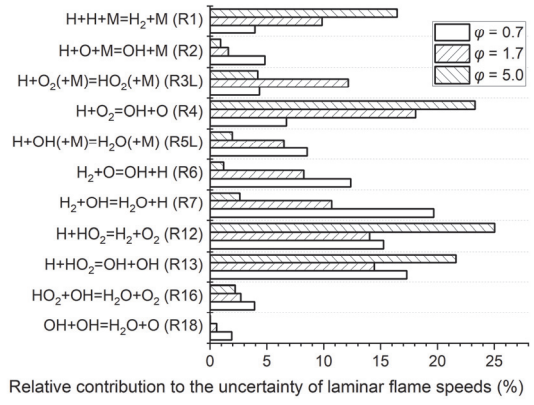

(e)

Figure S2-2. Comparison of the relative uncertainty contributions of different channels to the (a) ignition delay times measured in the shock tube;; (b) ignition delay times measured in the rapid compression machine (RCM); (c) H_2 mole fractions in the plug flow reactor (PFR) [1] (d) H_2 mole fractions measured in the jet stirred reactor [3]; (e) laminar flame speeds of H_2/air mixtures.

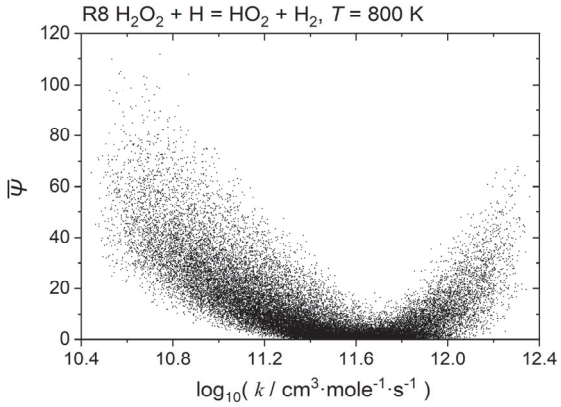

(a) R8 H_2O_2 + H = HO_2 + H_2

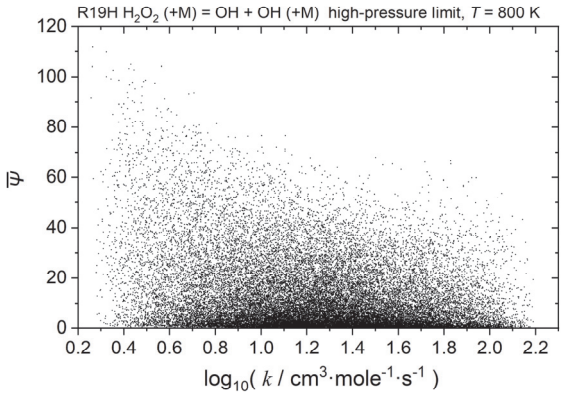

(b) R19 H_2O_2 (+M) = OH + OH (+M)

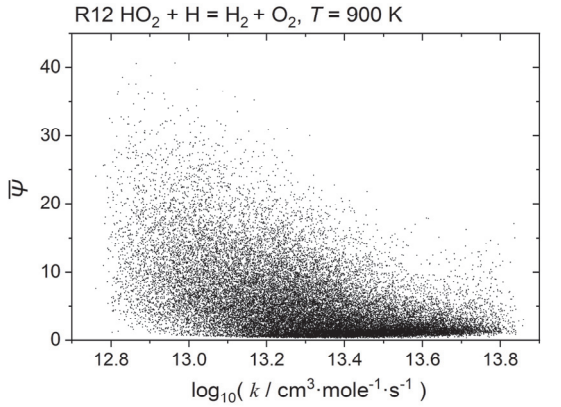

(c) R12 HO_2 + H = H_2 + O_2

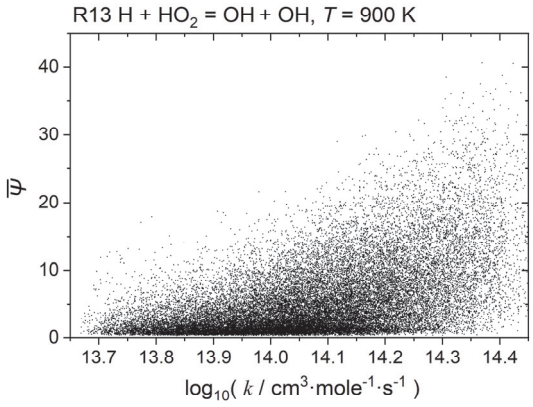

(d) R13 H_2O_2 + H = HO_2 + H_2

Figure S2-3. The distributions of the discrepancy measures on the RRCs of reactions.

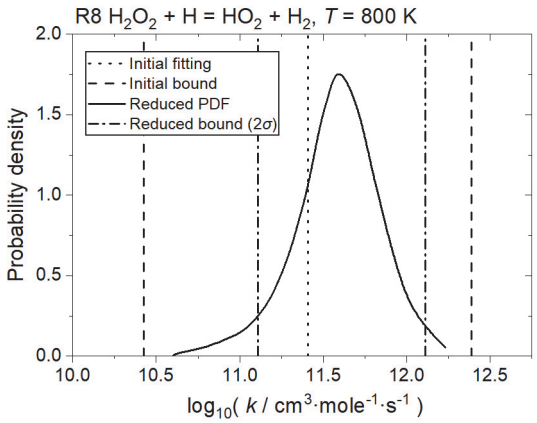

(a) R8 $H_2O_2 + H = HO_2 + H_2$

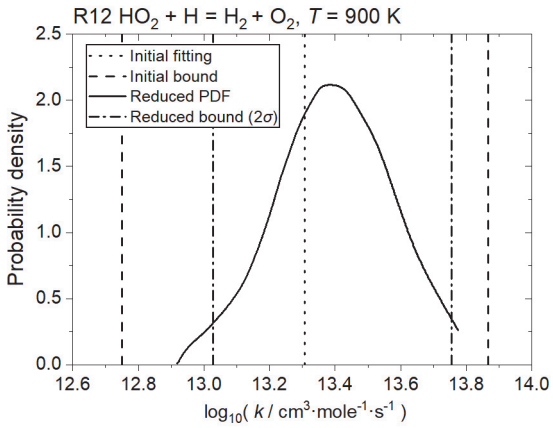

(b) R19 H_2O_2 (+M) = OH + OH (+M)

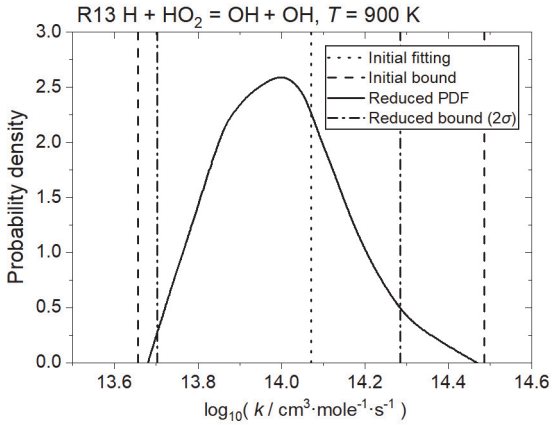

(c) R12 $HO_2 + H = H_2 + O_2$

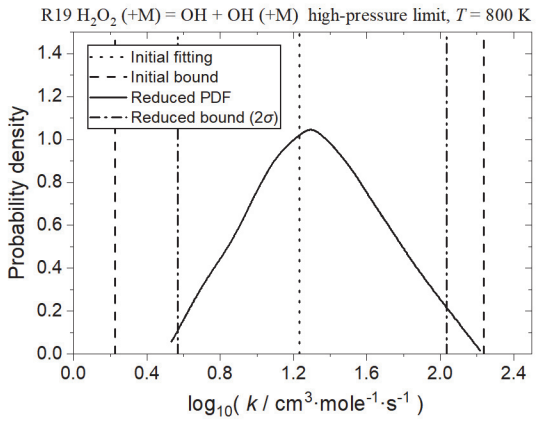

(d) R13 $H_2O_2 + H = HO_2 + H_2$

Figure S2-4. The probability density functions and reduced uncertainties of the studied RRCs calculated based on the average modelling error.

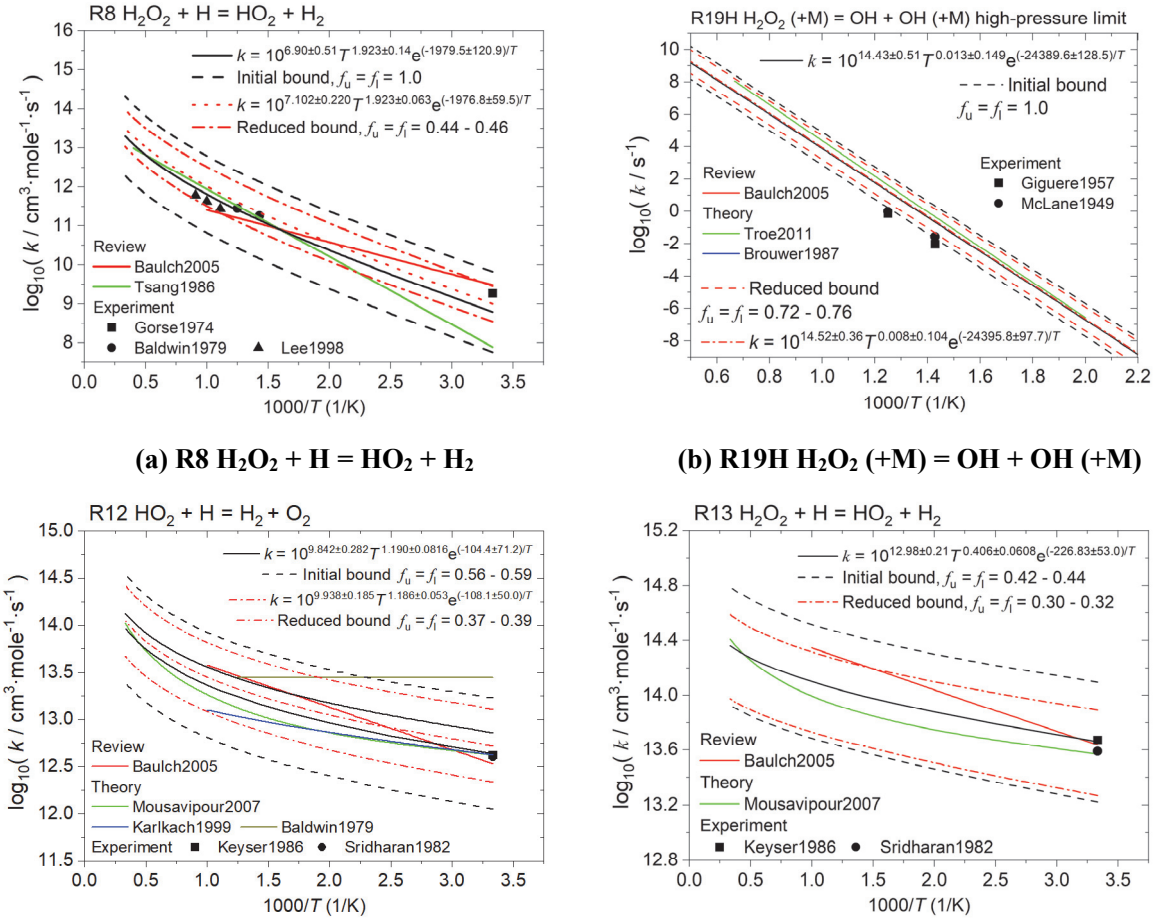

(a) R8 $H_2O_2 + H = HO_2 + H_2$ **(b) R19H H_2O_2 (+M) = OH + OH (+M)**

(c) R12 $HO_2 + H = H_2 + O_2$ **(d) R13 $H_2O_2 + H = HO_2 + H_2$**

Figure S2-5. Comparison of the initial uncertainty bounds (dash lines) and the reduced bounds (dash dot lines) for the RRCs of reactions.

References

[1] H. Hashemi, J.M. Christensen, S. Gersen, P. Glarborg, Hydrogen oxidation at high pressure and intermediate temperatures: Experiments and kinetic modeling, Proceedings of the Combustion Institute 35(1) (2015) 553-560.

[2] A.K. Das, C.-J. Sung, Y. Zhang, G. Mittal, Ignition delay study of moist hydrogen/oxidizer mixtures using a rapid compression machine, International journal of hydrogen energy 37(8) (2012) 6901-6911.

[3] T. Le Cong, P. Dagaut, Oxidation of H2/CO2 mixtures and effect of hydrogen initial concentration on the combustion of CH4 and CH4/CO2 mixtures: Experiments and modeling, Proceedings of the Combustion Institute 32(1) (2009) 427-435.

Supplementary-3

A Comprehensive Kinetic Modelling Study of Hydrogen Combustion with Data Uncertainty Analysis

Hongxin Wang[a], Nadezda Slavinskaya[b, c], Oskar Haidn[a]

a. Department of Aerospace and Geodesy, Technical University of Munich, 85748 Garching, Germany

b. GRS Association for Plant and Reactor Safety, 85748 Garching, Germany

c. Al-Farabi Kazakh National University, 050040 Almaty, Kazakhstan

Compariosn of the measured experimental data and the modelling results.

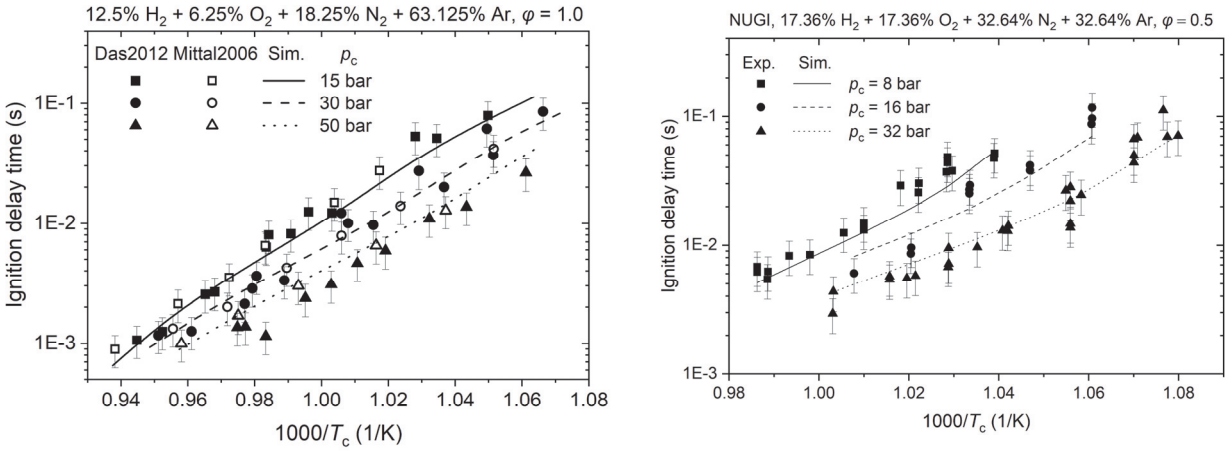

Figure S3-1. Comparison of the simulated and measured ignition delay times in rapid compression machines: (a) Das et al. [1] and Mittal et al. [2]; (b) Keromnes et al. [3] (NUGI).

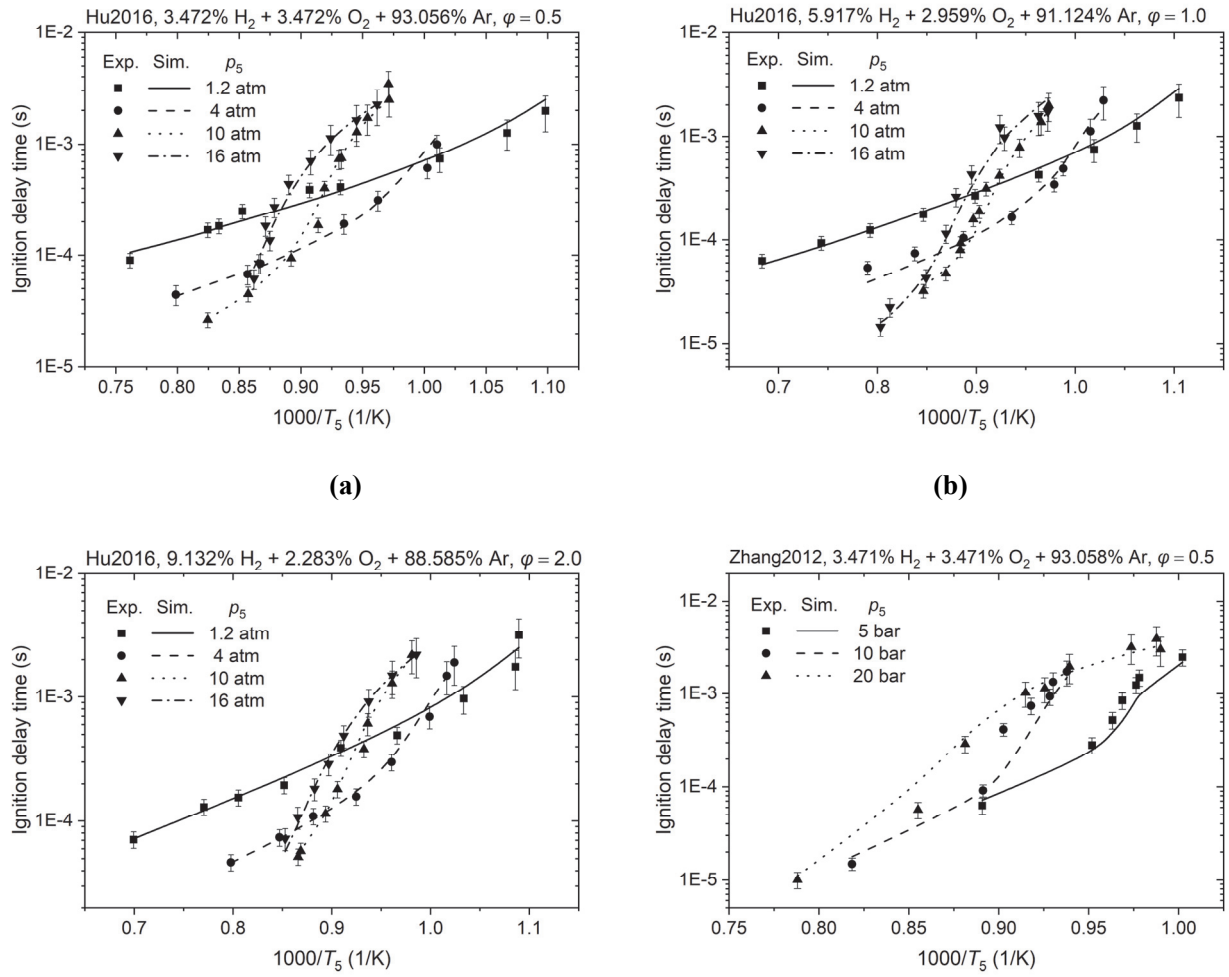

Figure S3-2. Ignition delay times of H_2/O_2/Ar mixtures measured in the shock tube by (a, b, c) Hu et al. [4] and Pan et al. [5] et al.; (d) Zhang et al. [6] (Xi'an Jiaotong University, XJTU).

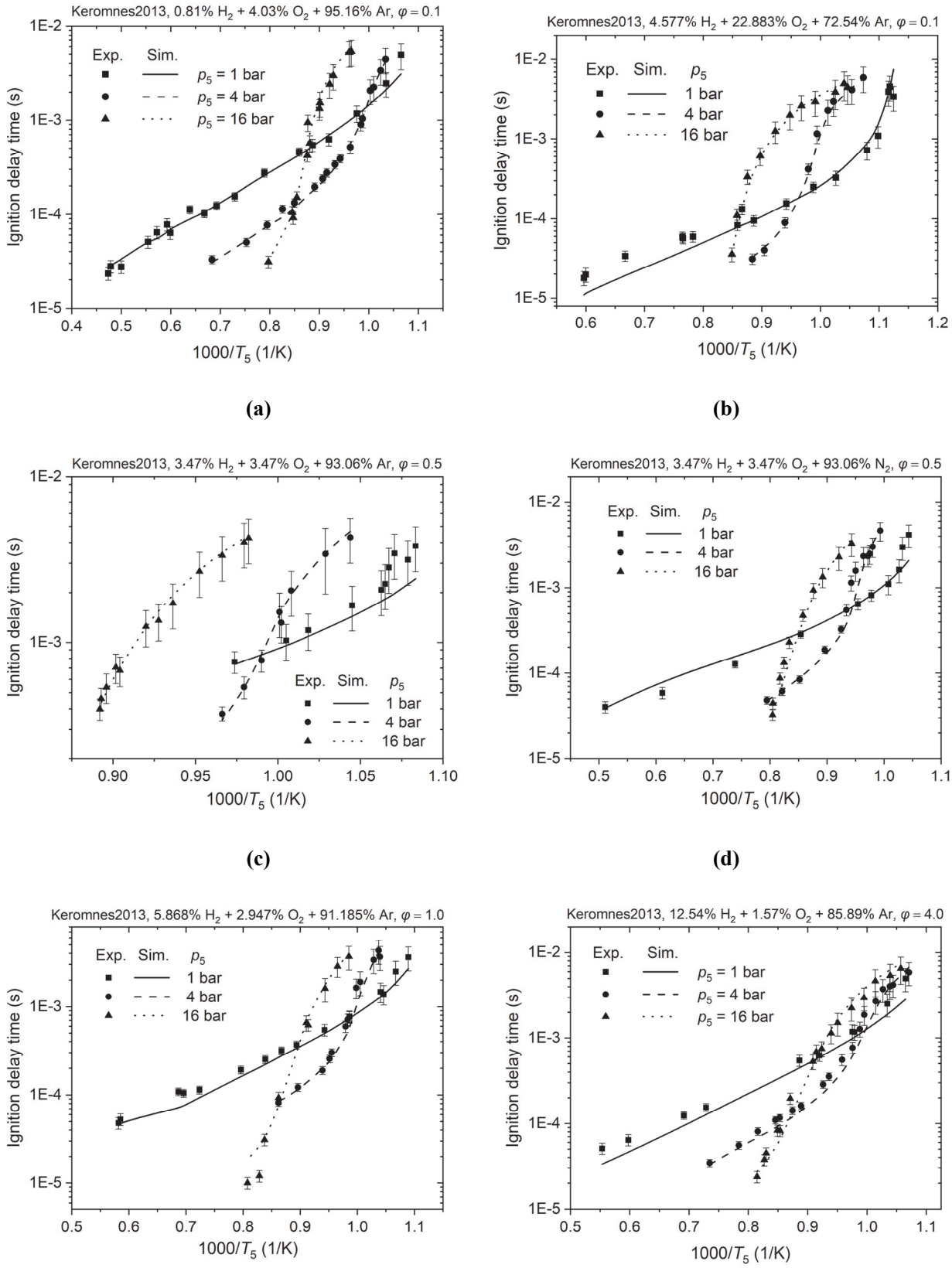

Figure S3-3. Ignition delay times of $H_2/O_2/Ar/N_2$ mixtures measured in the shock tube by Kéromnès et al. [3] and Herzler et al. [7] (German Aerospace Center, DLR).

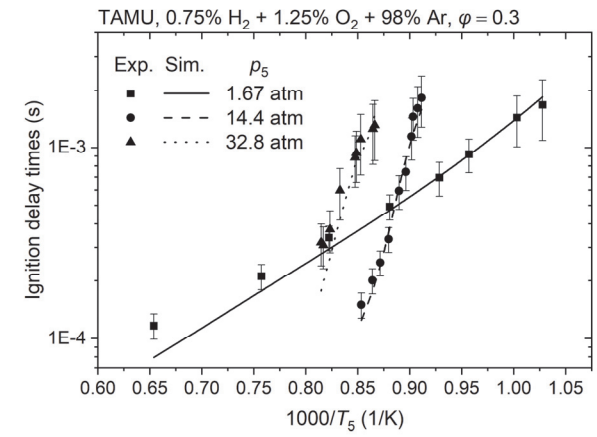

(a)

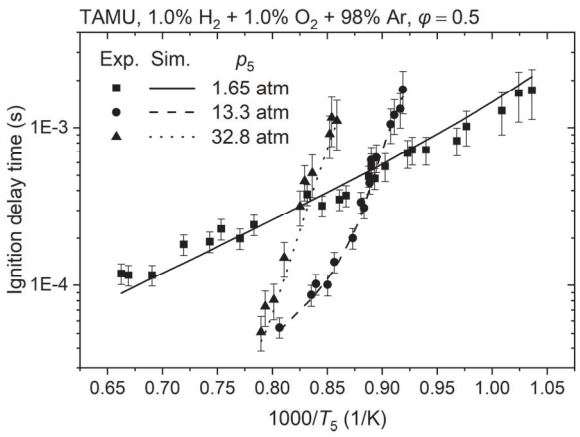

(b)

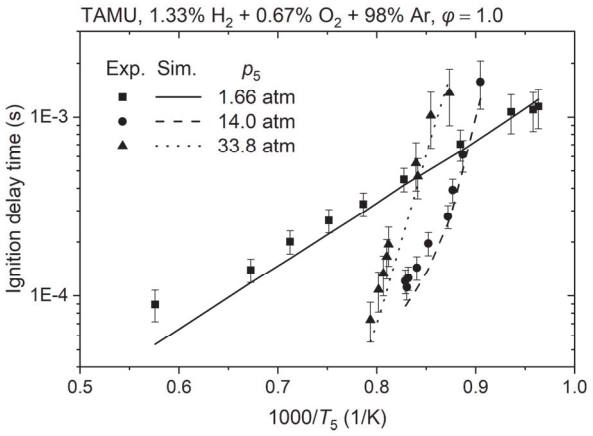

(c)

Figure S3-4. Ignition delay times of H_2/O_2/Ar mixtures measured in the shock tube by Kéromnès et al. [3] (Texas A&M University, TAMU).

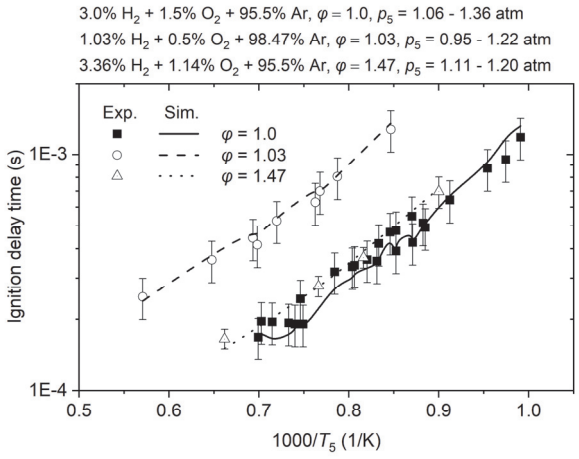

Figure S3-5. Ignition delay times of H_2/O_2/Ar mixtures measured in the shock tube by Petersen et al. [8] (University of Central Florida, UCF).

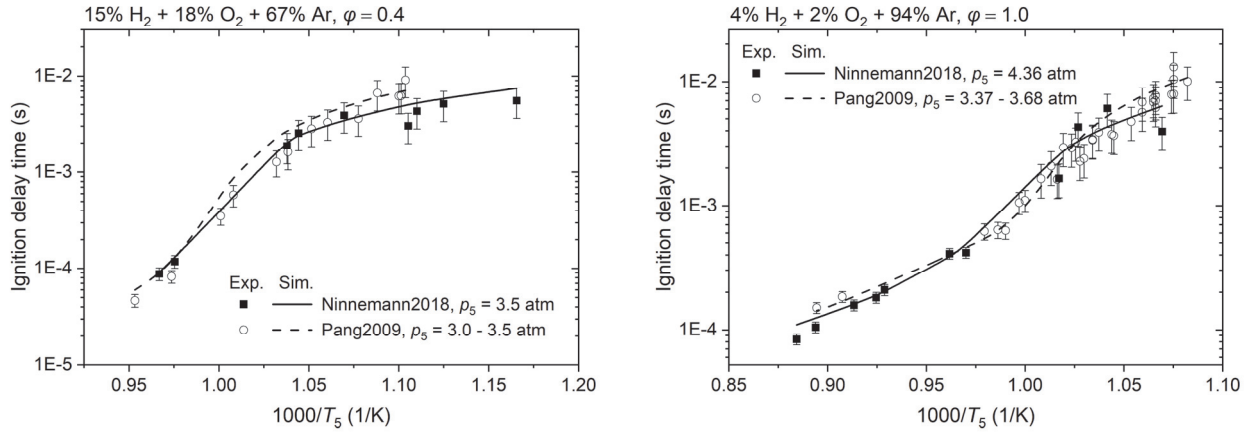

(a) **(b)**

Figure S3-6. Ignition delay times of H_2/O_2/Ar mixtures measured in shock tubes by Ninnemann et al. [9] (University of Central Florida, UCF) and Pang et al. [10] (Stanford University).

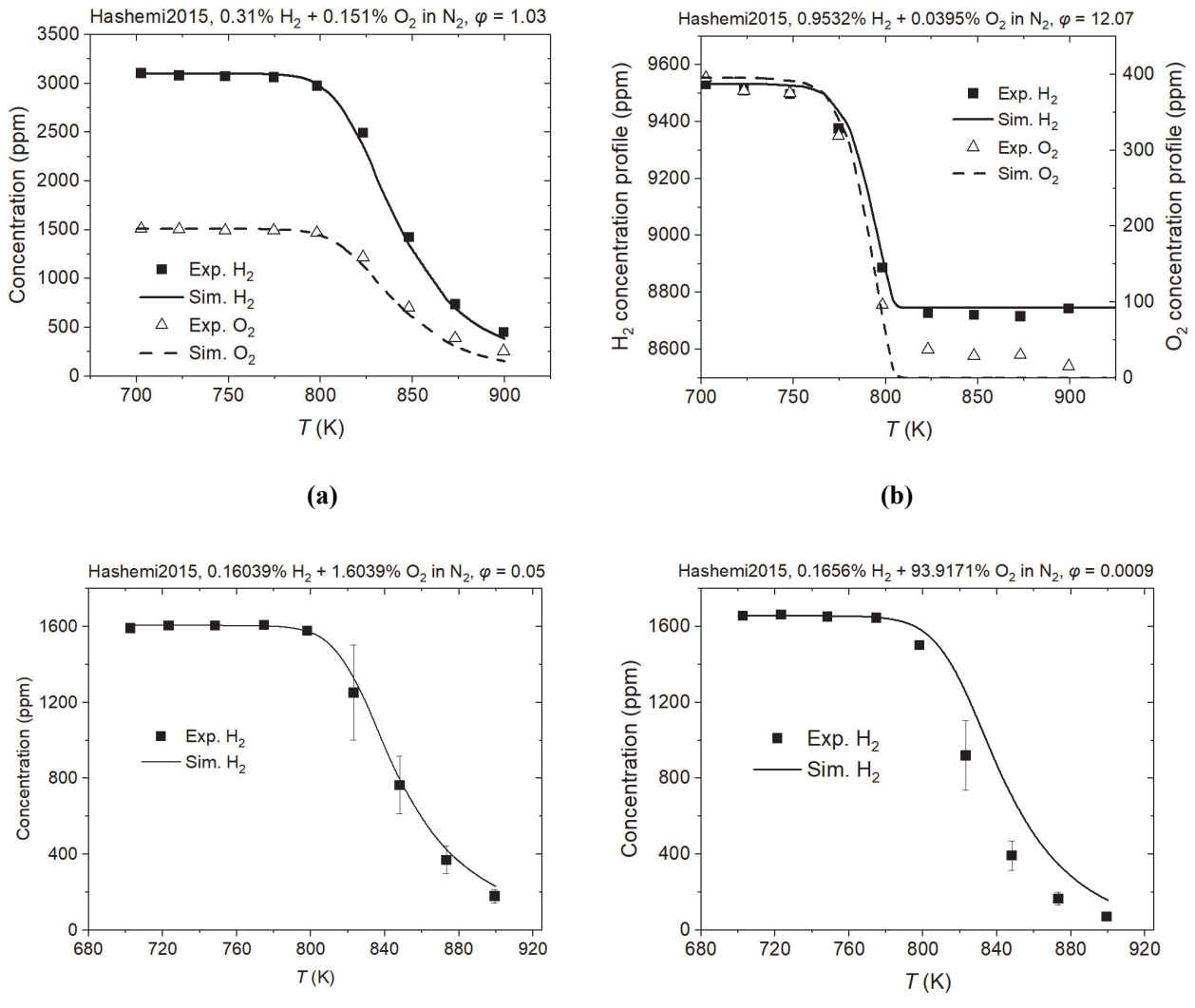

(a) **(b)**

(c) **(d)**

Figure S3-7. Concentration profiles in the plug flow reactor measured by Hashemi et al. [11].

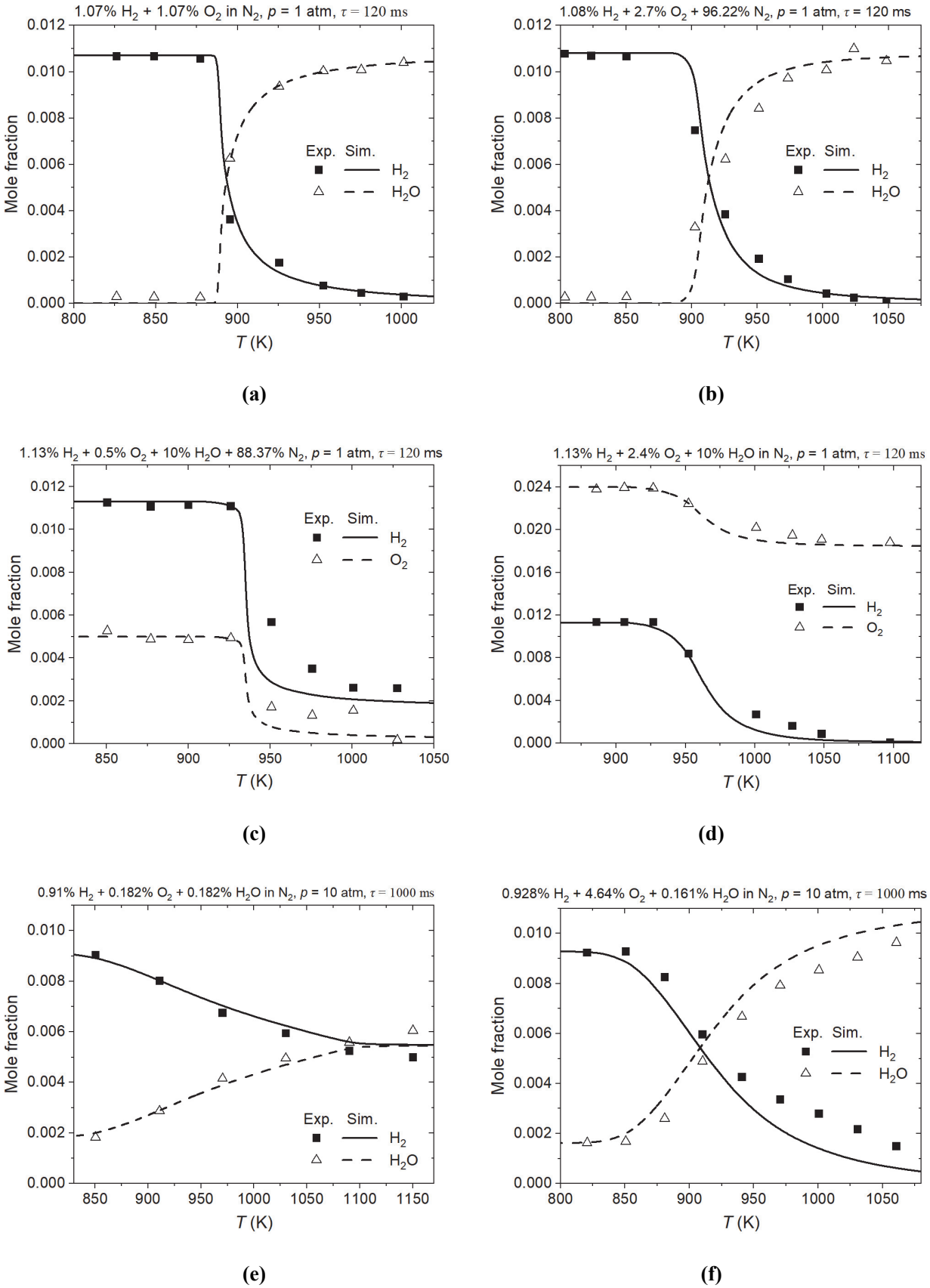

Figure S3-8. Concentration profiles of H_2, O_2, and H_2O in the jet stirred reactor measured by Le Cong and Dagaut [12].

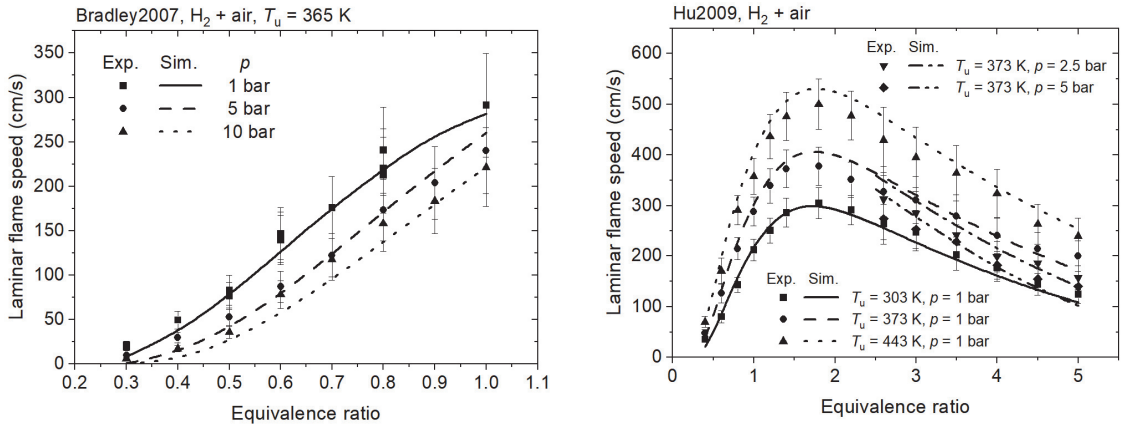

(a) **(b)**

Figure S3-9. Laminar flame speeds of H_2/air mixture at variable pressures and unburned temperatures measured by Bradley et al. [13] and Hu et al. [14].

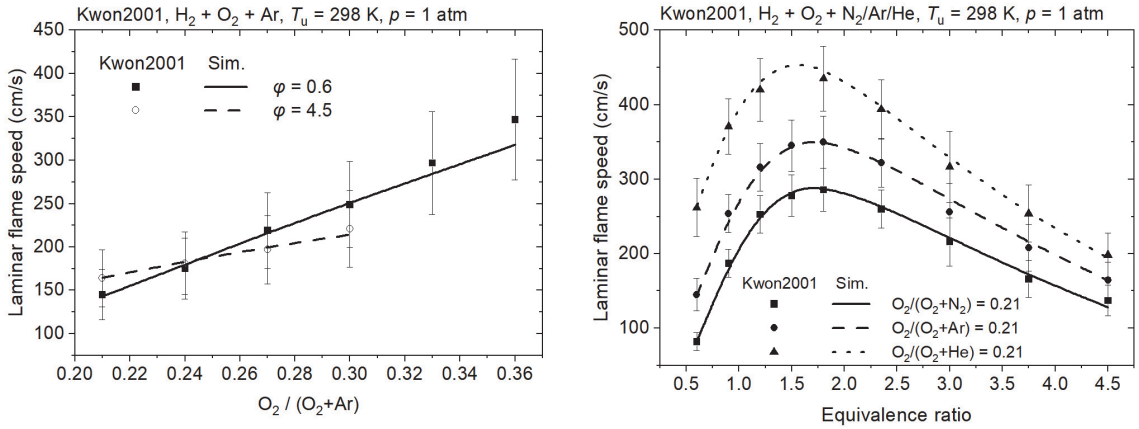

(a) **(b)**

Figure S3-10. Laminar flame speeds of H_2/O_2 and different dilution gases (T_u = 298 K, p = 1 atm) measured by Kwon et al. [15].

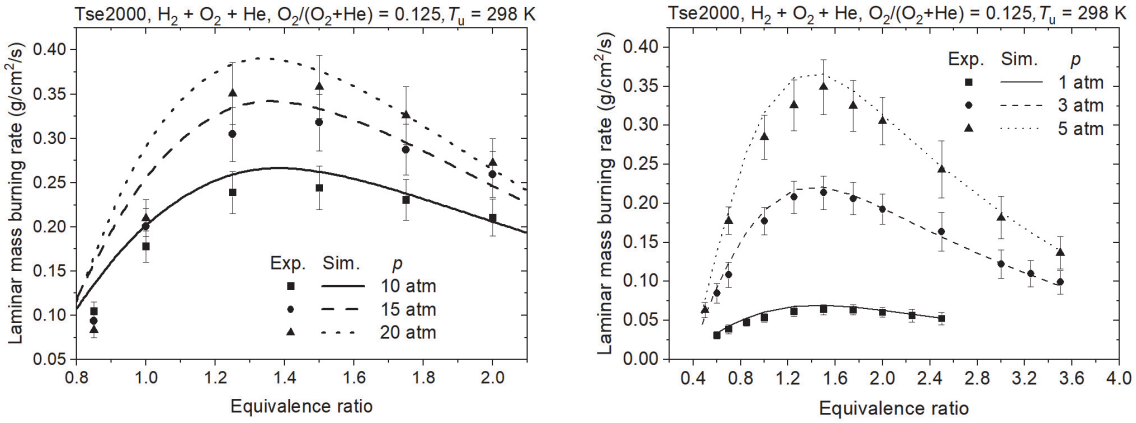

(a) **(b)**

Figure S3-11. Laminar mass burning rates of H_2/O_2/He mixtures at T_u = 298 K and variable pressures measured by Tse et al. [16].

References

[1] A.K. Das, C.-J. Sung, Y. Zhang, G. Mittal, Ignition delay study of moist hydrogen/oxidizer mixtures using a rapid compression machine, International journal of hydrogen energy 37(8) (2012) 6901-6911.

[2] G. Mittal, C.J. Sung, R.A. Yetter, Autoignition of H2/CO at elevated pressures in a rapid compression machine, International Journal of Chemical Kinetics 38(8) (2006) 516-529.

[3] A. Kéromnès, W.K. Metcalfe, K.A. Heufer, N. Donohoe, A.K. Das, C.-J. Sung, J. Herzler, C. Naumann, P. Griebel, O. Mathieu, M.C. Krejci, E.L. Petersen, W.J. Pitz, H.J. Curran, An experimental and detailed chemical kinetic modeling study of hydrogen and syngas mixture oxidation at elevated pressures, Combustion and Flame 160(6) (2013) 995-1011.

[4] E. Hu, L. Pan, Z. Gao, X. Lu, X. Meng, Z. Huang, Shock tube study on ignition delay of hydrogen and evaluation of various kinetic models, international journal of hydrogen energy 41(30) (2016) 13261-13280.

[5] L. Pan, E. Hu, J. Zhang, Z. Zhang, Z. Huang, Experimental and kinetic study on ignition delay times of DME/H2/O2/Ar mixtures, Combustion and flame 161(3) (2014) 735-747.

[6] Y. Zhang, Z. Huang, L. Wei, J. Zhang, C.K. Law, Experimental and modeling study on ignition delays of lean mixtures of methane, hydrogen, oxygen, and argon at elevated pressures, Combustion and Flame 159(3) (2012) 918-931.

[7] J. Herzler, C. Naumann, Shock-tube study of the ignition of methane/ethane/hydrogen mixtures with hydrogen contents from 0% to 100% at different pressures, Proceedings of the combustion institute 32(1) (2009) 213-220.

[8] E.L. Petersen, D.M. Kalitan, M.J. Rickard, Reflected Shock Ignition of SiH4/H2/O2/Ar andSiH4/CH4/O2/Ar Mixtures, Journal of Propulsion and Power 20(4) (2004) 665-674.

[9] E. Ninnemann, B. Koroglu, O. Pryor, S. Barak, L. Nash, Z. Loparo, J. Sosa, K. Ahmed, S. Vasu, New insights into the shock tube ignition of H2/O2 at low to moderate temperatures using high-speed end-wall imaging, Combustion and Flame 187 (2018) 11-21.

[10] G. Pang, D. Davidson, R. Hanson, Experimental study and modeling of shock tube ignition delay times for hydrogen–oxygen–argon mixtures at low temperatures, Proceedings of the combustion institute 32(1) (2009) 181-188.

[11] H. Hashemi, J.M. Christensen, S. Gersen, P. Glarborg, Hydrogen oxidation at high pressure and intermediate temperatures: Experiments and kinetic modeling, Proceedings of the Combustion Institute 35(1) (2015) 553-560.

[12] T. Le Cong, P. Dagaut, Experimental and detailed modeling study of the effect of water vapor on the kinetics of combustion of hydrogen and natural gas, impact on NO x, Energy & Fuels 23(2) (2009) 725-734.

[13] D. Bradley, M. Lawes, K. Liu, S. Verhelst, R. Woolley, Laminar burning velocities of lean hydrogen–air mixtures at pressures up to 1.0 MPa, Combustion and Flame 149(1-2) (2007) 162-172.

[14] E. Hu, Z. Huang, J. He, H. Miao, Experimental and numerical study on laminar burning velocities and flame instabilities of hydrogen–air mixtures at elevated pressures and temperatures, international journal of hydrogen energy 34(20) (2009) 8741-8755.

[15] O. Kwon, G. Faeth, Flame/stretch interactions of premixed hydrogen-fueled flames: measurements and predictions, Combustion and Flame 124(4) (2001) 590-610.

[16] S.D. Tse, D. Zhu, C.K. Law, Morphology and burning rates of expanding spherical flames in H2/O2/inert mixtures up to 60 atmospheres, Proceedings of the Combustion Institute 28(2) (2000) 1793-1800.

Paper III

Fuel 332 (2023) 125945

Contents lists available at ScienceDirect

Fuel

journal homepage: www.elsevier.com/locate/fuel

Full Length Article

A joint hydrogen and syngas chemical kinetic model optimized by particle swarm optimization

Hongxin Wang [a], Chenyi Sun [a], Oskar Haidn [a], Askarova Aliya [c], Chiara Manfletti [a], Nadezda Slavinskaya [b,c,*]

[a] Lehrstuhl für Raumfahrtantriebe, Technical University of Munich, 85748 Garching, Germany
[b] Gesellschaft fur Anlagen-und Reaktorsicherheit GmbH, 85748 Garching, Germany
[c] Al-Farabi Kazakh National University, 050040 Almaty, Kazakhstan

ARTICLE INFO

Keywords:
Syngas
Hydrogen
Chemical kinetic model
Uncertainty
Particle swarm optimization

ABSTRACT

In this work, we propose a novel data-driven framework for detailed kinetic mechanisms optimization applying the heuristic algorithm, namely canonic Particle Swarm Optimization (PSO). The PSO is more effective and robust in coping with uncertainties and incomplete information than deterministic and probabilistic optimization algorithms and is more suitable for machine learning applications. In the proposed framework, to avoid trapping in a local minimum, 1000 local optimums have been obtained and statistically handled to select the final feasible model parameter set with reduced uncertainty intervals and parameter correlations. The developed framework was successfully used for the optimization of the joint H_2 and syngas oxidation chemical kinetic model. The data set collected for the model optimization includes 41 reactions and 16 species, and 3000 experimental data targets supplied with uncertainty boundaries measured in shock tubes, jet stirred reactors, plug flow reactors, and premixed laminar flames under wide ranges of temperature, pressure, equivalence ratio, and H_2/CO ratios. The initially estimated uncertainties of the reaction rate constants for 15 key reactions were significantly constrained. The reaction rate constants for the H_2 oxidation sub-model were re-optimized and their uncertainties were further reduced.

1. Introduction

Syngas (H_2 and CO mixture) has recently attracted lots of attention as the main product of the gasification of coal, the renewable feedstocks (domestic waste, biomass, etc.) [1,2], and the electro-reduction of CO_2 [3], to be further used in different modern power installations [4–6]. To design new effective engines fueled on syngas, tools of computational fluid dynamics need a reliable chemical kinetic model of syngas combustion. Besides playing an important role as a renewable fuel, the oxidation reactions of H_2 and CO are the base for the oxidation model of hydrocarbons.

A big number of syngas kinetic models [7–19] have been designed to reproduce the real reaction process as well as possible. However, due to the lack of possible direct measurement methods of RRCs and high uncertainties in the available experimental data, the obtained models have still a high potential to be improved through the further reduction of uncertainty intervals for the included parameters. Several works [20–22] have been done for the comparison of prediction abilities of different chemical kinetic models for syngas oxidation. >20 detailed or reduced syngas oxidation models were compared. Most modeling results show good agreement with the collected experimental data, but no one of the models can be recognized as a perfect model predicting all the targets accurately [20–22]. Some early models [10,12–14] were developed without sufficient experimental data, and some models [7,15,16,19] were fitted for experimental data of specific temperature and pressure ranges. It motivates our search for further development of the effective framework for the kinetic model uncertainty quantification and minimization and to construct on this base the strongly validated basic H_2/CO oxidation model.

Our first attempt to quantify the uncertainty of the syngas oxidation reaction model was conducted in the work [17] with the methodology of Bound-to-Bound Data Collaboration (B2BDC) [23,24], which prescribes the fixed uncertainty bounds for the involved parameters and non-linear regression approach with solution mapping methodology. Further, in previous work on the H_2 oxidation model [25], the B2BDC was combined with the probabilistic approach, which addresses the uncertainty

* Corresponding author.
E-mail address: Nadezda.Slavinskaya@grs.de (N. Slavinskaya).

https://doi.org/10.1016/j.fuel.2022.125945
Received 5 July 2022; Received in revised form 11 August 2022; Accepted 6 September 2022
Available online 22 September 2022

of parameters and models with probability density functions. In this way, a 19-reaction H_2 oxidation chemical kinetic model was successfully optimized, and the uncertainties of the studied reaction rate constant have been estimated and reduced.

In this work, the optimization strategy has been further developed by an application of the particle swarm optimization (PSO) algorithm instead of the non-linear regression approach and probability density function [25]. The PSO belongs to the heuristic methods which are stochastic and their output possesses some inherent randomness so that the same set of input parameters values and initial conditions can lead to a set of different outputs. After a series of simulations, randomly modifying variables cover as far as possible the space of the solutions to avoid trapping in a local minimum, and randomly obtained outputs, i.e., optimums, can be further statistically handled to obtain the optimal feasible set of parameters and the global optimal solution. The heuristic methods can be effectively used in the application to the inverse problems if the solution to be reached is generally known but the input parameters are not, or are not accurately, as is the case of chemical kinetic models.

The canonic PSO was developed through simplified social model simulation such as bird flocking and fishing schooling by Kennedy and Eberhart [26]. It provides a population-based search procedure in which particles can move through the hyperspace of parameters. While moving in the search space, each particle evaluates the fitness function and adjusts its movement with the new velocity which depends on the history of its own best location (personal best) and the other particles' best location (global best). Gradually particles move close to an optimum of the fitness function like the forage of a flock of birds. In the past two decades, different problem-oriented modifications of the method and various topologies were developed [27–35], which demonstrate the high flexibility of the PSO approach and its high efficiency in the optimization of multidimensional and nonlinear systems with more than one optimum.

Heuristic methods are not actively applied in chemical kinetics. Elliot and co-workers [36–40] applied the genetic algorithm as an alternative to the solution mapping procedure. Tsuchiya and Ross [41] applied a genetic algorithm to determine the RRCs of a chemical kinetic model for the bromate reaction system. Montgomery [42] applied a genetic algorithm to the selection of quasi-steady-state species in reduced chemical kinetic models. Sikalo et al. [43,44] used the genetic algorithm for the reduction of detailed chemical kinetic models and the optimization of the reduced model. Bertolino et al. [45] presented a novel methodology that combines the evolutionary algorithm based on the genetic algorithm with the curve matching index as the objective function. The comparison of PSO and genetic algorithms, performed in the recent work of Rassy et al. [46], revealed the advance of the PSO algorithm for the optimization of detailed chemical kinetic models.

In this study, the principal architecture of the optimization framework using the PSO has been achieved. To elucidate the principal feature of the approach, first, the canonical algorithm [26] with global topology has been realized with the in-house code based on the Python module of Scikit-learn [47] and implemented in the framework. That was applied to the syngas chemical kinetic model optimization and the reduction of model parameters. The model inspection and optimization were based on the following axes: (1) A 16-species and 41-reaction syngas sub-mechanism of the authors' previous works [48,49] and the newest update of the H_2 oxidation sub-model [25]; (2) The literature review and uncertainty analysis of the RRCs involved in the syngas oxidation (Supplementary-1); (3) Experimental data of ignition delay times (IDTs), laminar flame speeds (LFSs), and species concentration profiles with uncertainty quantification and consistency analysis [17,50]; (4) Monte Carlo simulations conducted with Ansys Chemkin Pro [51] and the polynomial regression for construction of the multi-target high-dimensional input–output response function [52,53]; (5) Applying of PSO algorithm optimum searching in the hyperspace of parameters; (6) Statistical analysis of the calculated optimums and correlated parameters; (7) Reduction of the feasible parameter set and the final model optimization.

2. Data set and methodology

2.1. Combustion experimental targets

The published experimental results of the ignition delay times (IDTs) measured in shock tubes (STs) [7,54–63], laminar flame speeds (LFSs) [63–105], and concentration profiles measured in premixed laminar flames (PLFs) [106–108], jet stirred reactors (JSRs) [19,109], and plug flow reactors (PFRs) [110,111] as presented in Table 1 were used as the training set for the model. Around 3000 experimental targets were collected with their uncertainties, u, determined following the data sources, or evaluated based on the earlier published studies [17,50].

2.2. Uncertainty analysis of reaction rate constants

The statistical method of nonlinear regression established in the authors' previous works [25,48,49] has been applied to calculate the uncertainties of the Arrhenius expression parameters $\log_{10}(A)$, n, and E_a:

$$k(T) = 10^{\log_{10}(A)} T^n \exp\left(-\frac{E_a}{T}\right) \quad (1)$$

The lower and upper uncertainty boundaries of the RRC can be calculated:

Table 1
Collected H_2 and syngas oxidation experiments and their test conditions.

Ignition delay time	T_5/K	p_5/bar	**Mixture**
Hu et al. [54–56]	905 – 1463	1.22 – 20.0	$H_2/O_2/Ar$, φ = 0.5 – 2.0
Petersen et al. [57]	1009 – 1752	0.96 – 1.38	$H_2/O_2/Ar$, φ = 1.0 – 1.47
Ninnemann et al. [58]	857 – 1131	3.55, 4.42	$H_2/O_2/Ar$, φ = 0.4, 1.0
Pang et al. [59]	906 – 1118	3.04 – 4.42	$H_2/O_2/Ar$, φ = 0.4, 1.0
Shao et al. [60]	1154 – 1291	39.5 – 253.3	$H_2/O_2/Ar$, φ = 0.25, 1.0
He et al. [61]	913 – 1288	1.013	$H_2/CO/O_2/Ar$, φ = 1.0
Kéromnès et al. [7]	882 – 2234	1.0 – 34.24	$H_2/CO/O_2/Ar$, φ = 0.1 – 4.0
Krejci et al. [63]	982 – 2001	1.4 – 33.2	$H_2/CO/O_2/Ar$, φ = 0.5
Herzler et al. [62]	1019 – 1259	14.1 – 16.9	$H_2/CO/O_2/Ar$, φ = 0.5
Laminar flame speed	T_u/K	p/atm	**Mixture**
H_2 [63–80,86,104]	298 – 443	0.3 – 10.0	$H_2/O_2/N_2$/He/Ar/air φ = 0.23 – 5.08
Syngas [81–105]	298 – 410	0.95 – 20.0	H_2/CO/N_2/He/CO_2/air φ = 0.4 – 5.8
Concentration profile	T/K	p	**Mixture**
JSR: Le Cong et al. [109]	800 – 1150	1, 10 atm	$H_2/O_2/N_2$, φ = 0.2 – 2.33
JSR: Dagaut et al. [19]	800 – 1400	1 atm	CO/H_2/N_2, φ = 0.1 – 2.0
PFR: Hashemi et al. [110]	700 – 900	50 bar	$H_2/O_2/N_2$, φ = 0.0009–12.07
PFR: Glarborg et al. [111]	800 – 1300	1 atm	CO/O_2/H_2O/Ar/N_2 φ = 5.64E-5 – 4.07E-4
PLF: Dixon-Lewis et al. [106]	–	1 atm	$H_2/O_2/N_2$, φ = 2.05
PLF: Vandooren et al. [107]	–	4.75 kPa	$H_2/O_2/Ar$, φ = 1.93
PLF: Knyazkov et al. [108]	–	1 atm	CO/H_2/O_2/Ar, φ = 1.0, 2.0

$$k_{low}(T) = 10^{\log_{10}(A)-s(\log_{10}(A))} T^{n-s(n)} \exp\left(-\frac{E_a + s(E_a)}{T}\right) \quad (2)$$

$$k_{up}(T) = 10^{\log_{10}(A)+s(\log_{10}(A))} T^{n+s(n)} \exp\left(-\frac{E_a - s(E_a)}{T}\right) \quad (3)$$

where $s(\log_{10}(A))$, $s(n)$, and $s(E_a)$ are the standard deviations of $\log_{10}(A)$, n, and E_a determined by the covariation matrix of an applied statistical method of nonlinear regression [48,49,112–114]:

$$s(x_\alpha) = \sqrt{\frac{\Phi}{m-n} D(x_\alpha)} \quad (4)$$

Here, Φ is the final sum of the reduced squares of the deviations.

$$\Phi(\vec{y}, \vec{x}) = \sum_{j\ 1}^{m} \omega_j \left[Y_j^{exp} - \left(f_0(\vec{y}, \vec{x}^*) + \sum_{k\ 1}^{n} \frac{\partial f_j(\vec{y}, \vec{x})}{\partial x_k} \Delta x_k \right) \right]^2 \quad (5)$$

$D(x_\alpha) = \Lambda(x_{\alpha\alpha})$; Λ is the covariance matrix of elements; m is the number of observations; n is the number of unknown model parameters [48,49,112–114].

The uncertainty factor for the RRC is defined as follows:

$$f(T) = \log_{10}\left(\frac{k_{up}(T)}{k_0(T)}\right) = \log_{10}\left(\frac{k_0(T)}{k_{low}(T)}\right) \quad (6)$$

In this study, the finally obtained reduced uncertainty bounds for the RRCs of the H_2 reactions are inherited from our previous work for the H_2 oxidation model [25]. The Arrhenius equation parameters for RRCs of CO and HCO reactions recommended by experimental measurements, theoretical calculations, and the review works of Baulch et al. [115–118] were collected with specific temperature ranges. The detailed information for the collected RRC parameters and the calculated uncertainty intervals, Eq. (2) and (3), for the CO and HCO reactions are presented in Table S1-1 and Fig. S1-1 to S1-21 in Supplementary-1. In this study, the sampling of the RRCs and the optimized RRCs are limited within the determined uncertainty intervals Eq. (2), (3), and (6).

2.3. Monte Carlo simulation and response surface

The mapping of the multidimensional system of the model input–output responses, the response surface [52,53], has been constructed with the second-order polynomial approximation of Monte Carlo simulations as a function of the model parameters, details were described in our previous work [25].

As the magnitudes of the Arrhenius expression parameters show huge differences, the Arrhenius expression parameters are normalized to space [0,1] as follows:

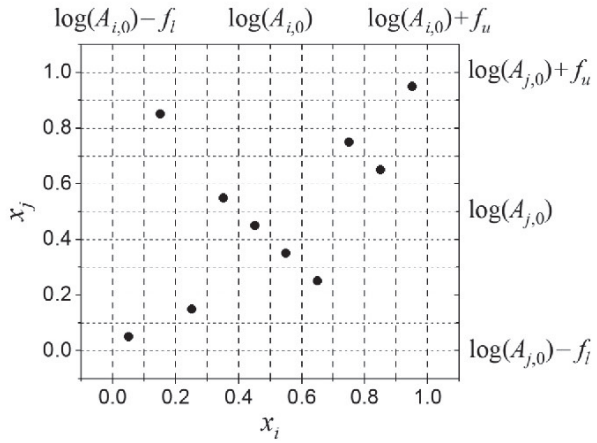

Fig. 1. 10 random numbers sampled with the Latin hypercube method and the determined Arrhenius expression parameters.

$$x_i = \frac{f_{l,i} + \log_{10}(A_i) - \log_{10}(A_{0,i})}{f_{l,i} + f_{u,i}}, \log_{10}(A_i) \in \left[\log_{10}(A_{0,i}) - f_{l,i},\ \log_{10}(A_{0,i}) + f_{u,i}\right] \quad (7)$$

in which $\log_{10}(A_{0,i})$ is the fitted average value and $f_{l,i}$ and $f_{u,i}$ ($f_{l,i} = f_{u,i}$) are the lower and upper bounds for the i^{th} parameter, Eq. (6). In this way, the Arrhenius expression parameters, $\boldsymbol{A}$ (A_1, A_2... A_n), sampled within the determined uncertainty intervals can be mapped to the normalized RRC parameters $\boldsymbol{X}(x_1, x_2 \ldots x_n)$ as follow:

$$\log_{10}(A_i) = \log_{10}(A_{0,i}) - f_{l,i} + x_i(f_{l,i} + f_{u,i}),\ x_i \in [0,\ 1] \quad (8)$$

The Monte Carlo direct simulation of experimental targets has been conducted with Chemkin Pro [51] using the Latin Hypercube sampling method [48] to obtain normalized RRC parameters $\boldsymbol{X}$sampled within space [0, 1] and to randomly determine the Arrhenius expression parameters, as shown by an example of 10 random numbers in Fig. 1. So calculated for each sample $y^{mod}(X)$ has been approximated with the second-order polynomial regression to express the response function, $y^{pre}(X)$, throughout the total of N number of model parameters:

$$y^{mod}(X) \approx y^{pre}(X) = y_0 + \sum_{i\ 1}^{N} \alpha_i x_i + \sum_{i\ 1}^{N} \sum_{j\ 1}^{N} \beta_{ij} x_i x_j \quad (9)$$

in which the first- and second-order polynomial coefficients (α and β) were determined using the least square method realized in an in-house python numerical code [119]. In this study, polynomial regressions with coefficients of determination [120], R^2, higher than 0.98 were obtained for the prediction of IDTs measured in STs and 0.99 for the other experimental data.

2.4. Discrepancy measure

To evaluate the predictive ability of a model depending on $\boldsymbol{X}$, the model discrepancy measure, Ψ, is defined as:

$$\Psi = \frac{1}{M} \sum_{i\ 1}^{M} \frac{1}{N_i} \sum_{j\ 1}^{N_i} \Psi_{ij}^{mod} \quad (10)$$

in which M is the number of the experimental data series and N_i is the point number in the i^{th} data series. The Ψ_{ij}^{mod} for the j^{th} target in the i^{th} data series is defined as follows:

$$\Psi_{ij}^{mod} = \left(\frac{y_{ij}^{mod} - y_{ij}^{exp}}{u\left(y_{ij}^{exp}\right)}\right)^2 \approx \left(\frac{y_{ij}^{pre} - y_{ij}^{exp}}{u\left(y_{ij}^{exp}\right)}\right)^2 \quad (11)$$

where y_{ij}^{exp} is the experimentally measured data, y_{ij}^{mod} is the modeling result, and y_{ij}^{pre} is the results predicted by the response surface, $y^{mod}(X)$, Eq. (9). The experimental uncertainty, $u\left(y_{ij}^{exp}\right)$, is adopted from the reference or evaluated based on the uncertainty analysis of experiments [17,50]. Substituting Eq. (9) and Eq. (11) into Eq. (10), the predictive ability of a model depending on $\boldsymbol{X}$can be evaluated by $\Psi(X)$.

2.5. Uncertainty contribution

To figure out the importance of the different reaction channels of the as-compiled model and to select the active parameters for further model optimization [9,121,122], the relative uncertainty contributions of parameter x_i among the total N number of model parameters has been introduced in our previous work [25] as:

$$C_r(x_i) = \frac{C(x_i)}{\sum_{i\ 1}^{N} C(x_i)} \quad (12)$$

where the uncertainty contribution of parameter x_i is calculated as:

$$C(x_i) = \left[y_{max}^{pre}(x_i) - y_{min}^{pre}(x_i)\right]\Big|_{x_j\ \bar{x}_j,\ j/i} \quad (13)$$

in which $\overline{x}_j$ is the average value of x_j, corresponding to the average value log ($A_{0,i}$) in Eq. (7) and Eq. (8). $y^{pre}_{max}(x_i)$ and $y^{pre}_{min}(x_i)$ are the maximum and minimum y obtained with variable x_i.

The studied uncertainties and the relative uncertainty contributions to the simulated IDTs contributed by different channels are highlighted in Fig. 2. The indexes of the shown reactions are listed in Table 2, which presents the reactions contributing to the model uncertainties of>10 %. The uncertainties contributed by reactions (*R*3), (R4), and (R25) demonstrate obvious different trends if T_5 decreases, Fig. 2a. The channels related to O_2 and HO_2 gain dominance at low-temperature ignition of syngas. The relative uncertainty contributions of the channels to the IDTs are presented in Fig. 2b, in which reactions (*R*3) and (R4) show the highest importance, followed by reactions (R1), (R6), (R8), (R24) and (R25).

16 pre-exponents and 4 third body factors of 15 channels were selected for optimization. The other RRCs parameters in the as-compiled model were kept as constants (A_0). The uncertainty bounds for the third body factors of N_2 and Ar are set as [1.25, 2] and [0.5, 0.8] respectively following the collected recommended RRCs and the review work of Baulch et al. [115–118]. The RRCs optimized in our previous work [25] for H_2 oxidation will be re-optimized and the uncertainty intervals determined in our previous work [25] factors will be further reduced in this study.

3. Uncertainty reduction and model optimization

3.1. Particle swarm optimization (PSO)

In the PSO algorithm, particles with position $\boldsymbol{X}$ present the surrogates of the chemical kinetic model, $\boldsymbol{M(X)}$ based on $\boldsymbol{X}$, Eq. (8); the discrepancy measure $\Psi(X)$, Eq. (10) is defined as the fitness function. The set of particles is initialized as $p = \{p_i, i \in [1 : N_p]\}$, where N_p is the size of the population (all possible surrogates). The particles can move in a 20-dimensional (number of RRC parameters under consideration) search space. The current position of the particle p_i in the different iterations ($t = 0, 1, 2 \ldots t_{max}$) is defined with a vector of its coordinates $X_{pi,t}\left(x^t_{pi,1}, x^t_{pi,2}, \cdots, x^t_{pi,D}\right)$ and a vector of its velocity $V_{pi,t}\left(v^t_{pi,1}, v^t_{pi,2}, \cdots, v^t_{pi,D}\right)$. The position of each particle will be tracked, which is associated with the lowest $\Psi(X)$ achieved up till for the particle with the personal best, X^{per}. The global best, X^{glo}, keeps track of the lowest $\Psi(X)$ obtained so far by all particles within the population. In canonical PSO on the t^{th} iteration, the particle p_i updates its velocity and position of the j^{th}-dimension in the $(t+1)^{th}$ iteration by tracking the personal best position (X^{per}) and global best position (X^{glo}) as follows [26]:

$$v^{t+1}_{pi,j} = w v^t_{pi,j} + c_1 r_{pi,1}\left(x^{per}_{pi,j} - x^t_{pi,j}\right) + c_2 r_{pi,2}\left(x^{glo}_j - x^t_{pi,j}\right) \quad (14)$$

$$x^{t+1}_{pi,j} = x^t_{pi,j} + v^{t+1}_{pi,j} \quad (15)$$

where $x^{per}_{pi,j}$ and x^{glo}_j are the j^{th} components of the personal best location and the global best location respectively; w is the inertia weight determining the "inertial" properties of particles. It reflects the impact of the particle's current velocity on the next iteration. $r_{pi,1}$ and $r_{pi,2}$ are the random numbers that are uniformly distributed between [0, 1] on each iteration. c_1 and c_2 are the acceleration coefficients: c_1 controls the tendency of the particle towards its personal best location, and c_2 adjusts the trend of the particle approaching the global best location.

With Eq. (14) and Eq. (15), the particles can update their velocities in each iteration and converge towards the optimal position, as shown in Fig. 3a. To describe the neighbor relationship and interaction between particles, a global topology, Fig. 3b, is used [123,124].

In the canonic PSO with global topology, it is impossible to guarantee that the found solution is the exact global optimum. But the subsequent statistical analysis of enough large number of local minimums provides adequate and useful information about the confidence region for the model parameters.

The developed framework using the PSO algorithm is shown in the flow chart in Fig. 4. The PSO (in the dashed rectangle) updates the position and velocity of each particle in each iteration step moving towards the personal best and global best. As the computation progresses, particles aggregate or converge around the global best by exploring and exploiting known personal bests in the search space until the max iteration. The finally obtained in the run j global best, X^{glo}_j, defines the best Arrhenius parameter combination found in the individual run and is prescribed to the local optimum j.

In this study, the search space was defined as the 20-D hypercube of the uncertainty intervals [0, 1] for each normalized model parameter $\boldsymbol{X}$ and the 100 particles (surrogate models) randomly initialized within the search space were used. Fig. 5a visualizes the moving of the particles towards the optimal position as the solution of an iteration process in the ternary graph. The algorithm stops searching after the max iteration (we set 50 in this study) is achieved or as the $\Psi(X^{glo})$ stabilizes after 15 iterations, as shown by the history of the predicted Ψ in Fig. 5b. At the end

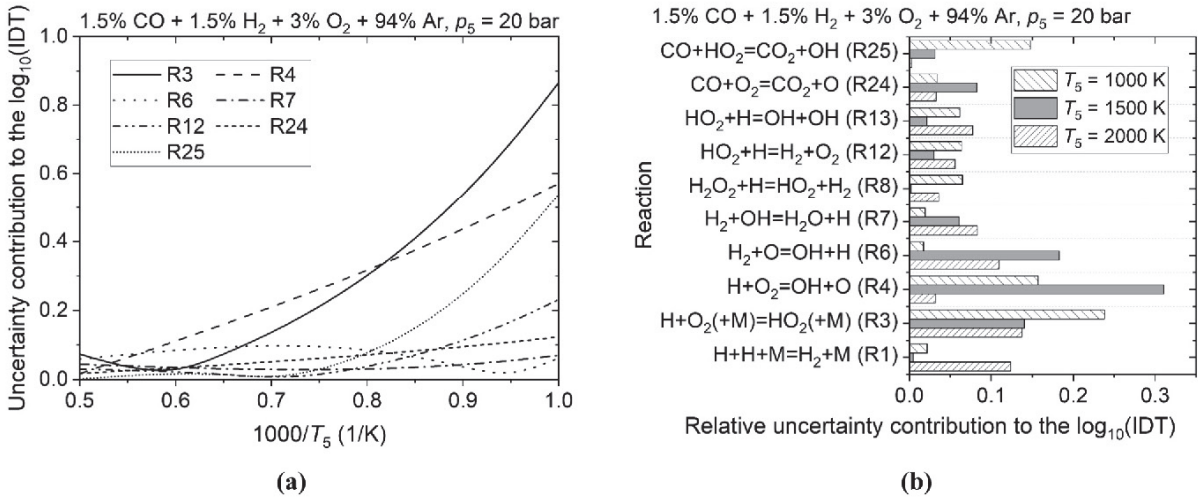

Fig. 2. (a) Uncertainty contributions (C) and (b) relative uncertainty contributions (C_r) of different channels to the modeling ignition delay times of $CO/H_2/O_2$/Ar mixture at 20 bar.

Table 2
Reactions mostly contributed to the modeling uncertainties (X for $C_r > 0.1$, O for $C_r > 0.2$); initial and final uncertainty intervals for their RRCs (Lp for pressure lower than 5 bar, Hp for pressure higher than 5 bar, LT for temperature lower than 1100 K, HT for temperature higher than 1100 K).

No.	Reaction	+M	Initial f_u/f_l	Reduced f_u/f_l	ST				PLF	PFR		JSR	
					Lp		Hp		-	Lp	Hp	Lp	Hp
					LT	HT	LT	LT	-	LT	LT	LT	
R1	$2H + M = H_2 + M$	N_2	0.38	0.26				X	X				
R3L	$H + O_2 + M = HO_2 + M$	Ar	0.17	0.06			O	O	X	O		O	X
R4	$H + O_2 = OH + O$		0.20	0.05	O	O	O	O	O	X		O	X
R5L	$H + OH + M = H_2O + M$	Ar	0.72	0.53					X				
R6	$H_2 + O = OH + H$		0.29	0.18	X	O	X	X	X				
R7	$H_2 + OH = H_2O + H$		0.21	0.12					O		X		X
R8	$H_2O_2 + H = HO_2 + H_2$		0.46	0.23			X	X			O		X
R12	$HO_2 + H = H_2 + O_2$		0.39	0.19					X			O	
R13	$HO_2 + H = OH + OH$		0.32	0.19					X			O	
R16	$HO_2 + OH = H_2O + O_2$		0.27	0.19							X		X
R19H	$H_2O_2 = 2OH$		0.76	0.53							O		X
R19L	$H_2O_2 + M = 2OH + M$	Ar	0.22	0.21							X		X
R23	$CO + OH = CO_2 + H$		0.26	0.06					O	O			
R24	$CO + O_2 = CO_2 + O$		1.6	0.82	X	X		X					
R25	$CO + HO_2 = CO_2 + OH$		1.14	0.65			O						
R28	$HCO + M = H + CO + M$		0.8	0.30					X				

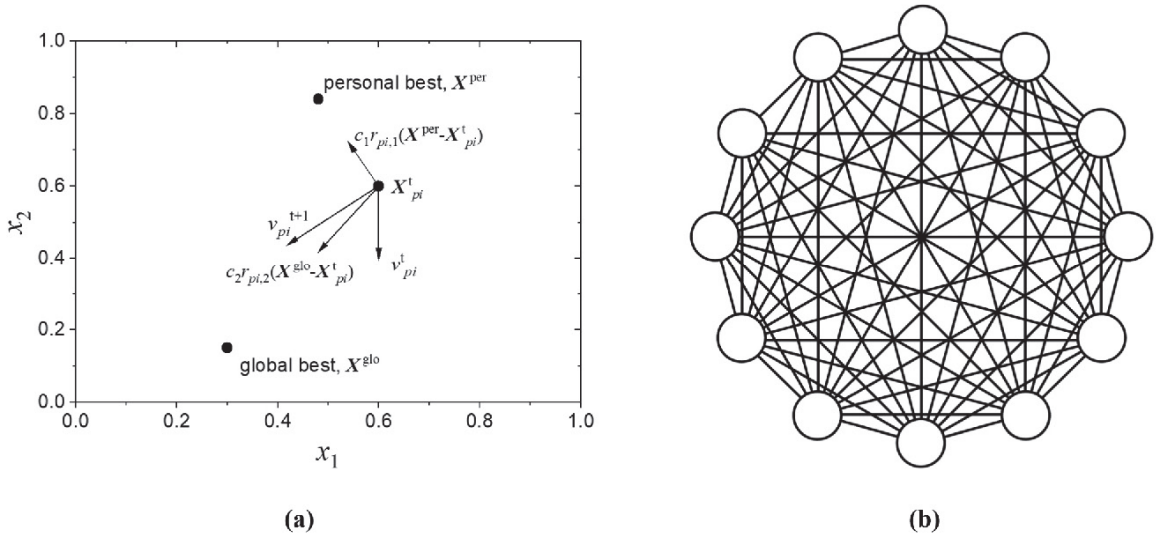

Fig. 3. (a) Update of the particle velocity in the $(t + 1)^{th}$ iteration; (b) global topology of the PSO, circles are particles, in our case surrogates $M(X)$.

of the iterations, the particles decelerate to velocities near 0 and cluster around the global best of the last iteration, X_j^{glo}. The set of parameters is selected and RRCs can be determined by the inverse normalization of the position of the particle.

3.2. Reduction of the RRC uncertainties (confidence region for the model parameters)

The inherent randomness of PSO is realized with the initialization of input parameters for PSO which are randomly defined on each new run, Fig. 3a and Fig. 4: random searching parameters $r_{pi,1}$ and $r_{pi,2}$, the acceleration coefficients c_1 and c_2, which were chosen as $c_1 = c_2 = 1.2$ in this study, and randomly defined Arrhenius preexponents, eq. (8), for active parameters. To minimize the error propagation, the initial feasible parameter set (like we do in B2BDC) [23,24]) was obtained by MC simulations, as explained with an example. Fig. 6 demonstrates the space of solutions, Ψ, for randomly modified rate coefficients of reactions (R3L), (R12), and (R13). The preferable parameters of RRCs of (R3L), (R12), and (R13), which will be adopted for the initialization of PSO, are located within the dark zone where the discrepancy measure has minimal values.

Due to the randomness in the initialization of the particles in each repetition of the PSO run, and the particle velocity update (the random numbers $r_{pi,1}$ and $r_{pi,2}$ in Eq. (14)) in each PSO iteration (the j^{th} iteration), the statistic representative array of the local optimums can be calculated, which are further used for the definition of the confidence region for the model parameters. That is performed through the main step of the framework shown in Fig. 4:

(1) Initialized the parameters and particles for the j^{th} run of PSO;
(2) Calculate $\Psi(X)$ for each particle and update the personal best X^{per} and global best X^{glo} for the i^{th} iteration of PSO;
(3) Update the position (X) and velocity (v) for each particle and return to step (2) until i reaches the max iteration number or the $\Psi(X^{glo})$ stabilizes after 10 iterations;
(4) Record the global best of the final iteration, X_j^{glo}, as the j^{th} local optimum of the searching space, and go to step (1) until $j = 1000$.

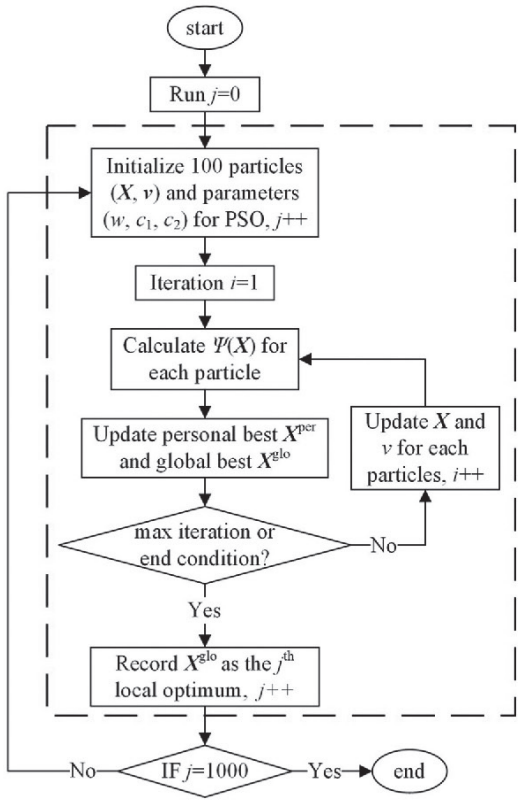

Fig. 4. Flow chart of the optimization framework with the PSO algorithm.

Finally, 1000 local optimums are selected and scattered in an area, where a lower Ψ has a high probability to be obtained, Fig. 7.

3.3. *Correlation of the studied RRCs*

The high-level correlation between RRCs and experimental parameters is organically accounted for in the PSO through the calculation of the particles' positions and velocities in the searching space, which is especially effective for the optimization of the multichannel reactions. Let us take again reactions (R3L), (R12), and (R13):

$$H + O_2 + M = HO_2 + M \quad \text{(R3L)}$$

$$HO_2 + H = H_2 + O_2 \quad \text{(R12)}$$

$$HO_2 + H = OH + OH \quad \text{(R13)}$$

Fig. 8 presents the 95 % confidence ellipsoid obtained for the calculated 1000 local optimums in coordinates of these three reactions. The projections of the particles on the RRC axes are pointed with colored symbols. The projected symbols of the pair reactions (R12)-(R13) show an obvious correlation compared with that of pairs (R3L)-(R12) and (R3L)-(R13). The Pearson correlation coefficients (r) [125] are calculated for the RRCs based on the 1000 local optimums. x_{R12} and x_{R13} demonstrate a significant positive correlation, $r = 0.91$ (Fig. 9a), and

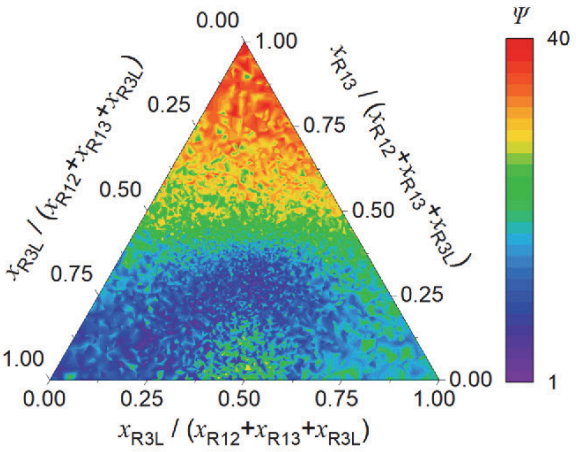

Fig. 6. Distribution of the discrepancy measure (Ψ) in the space of RRCs for reactions (R3L), (R12), and (R13) obtained with MC simulations and the as-compiled model.

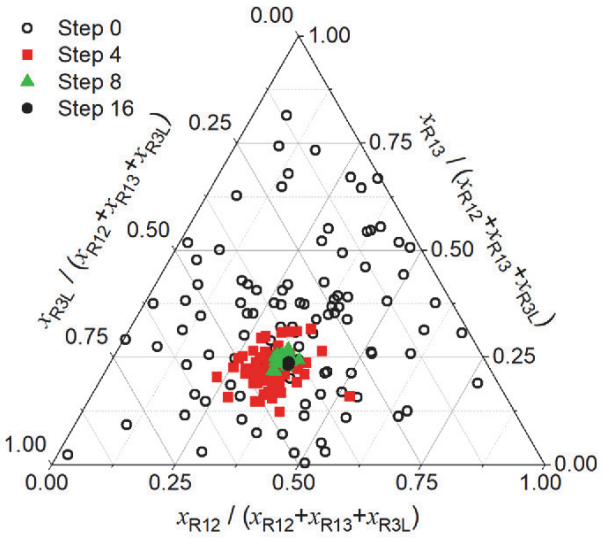

(a)

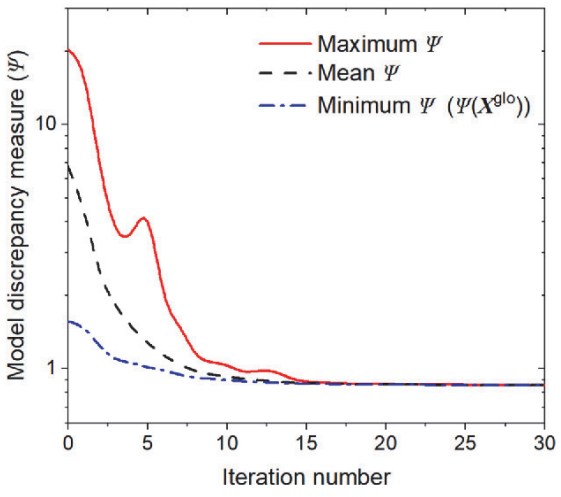

(b)

Fig. 5. (a) The distributions of the particle swarm at different iteration steps; (b) The history of model discrepancy measure (Ψ).

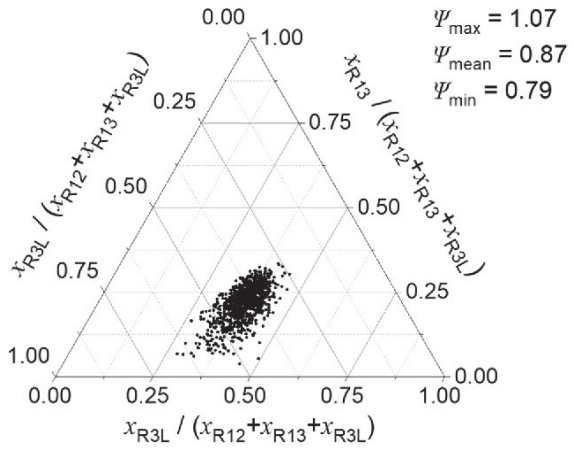

Fig. 7. Distribution of the recorded 1000 local optimums.

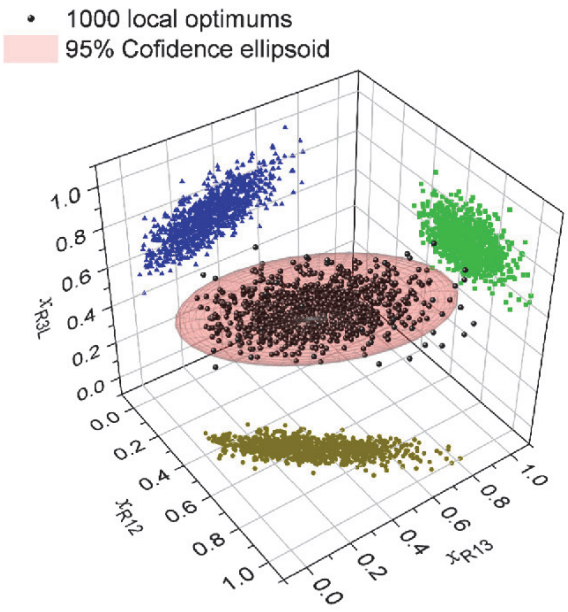

Fig. 8. The 95 % confidence ellipsoid of the 1000 local optimums for x_{R3L}, x_{R12}, and x_{R13}.

define the branching ratio for these two branches of $HO_2 + H$ reaction. The reaction (R3L) is weakly correlated with (R12), $r = 0.25$, points fill the full confidence region so that the RRC uncertainty bounds are approximately not affected by correlation, Fig. 9b.

To reveal the correlations of the studied RRCs and to evaluate the impact of correlation on the final uncertainty bounds, the Pearson correlation coefficients (r) are calculated for each RRC pair based on the 1000 local optimums. These coefficients (r) of the studied channels are presented with color and ellipses in Fig. 10, and the high correlation coefficient pairs ($|r| > 0.5$) are marked with *. Following the pair of (R12)-(R13) (r = 0.91), reactions (R8) and (R19H) show the second-highest $|r|$ (r = -0.83) by sharing reactant of H_2O_2 and the co-influence on the high-pressure and low-temperature oxidation of syngas, Table 2. Two important channels, which define the change in chain reaction of hydrogen autoignition (explosion limits), i.e., $H + O_2 + M = HO_2 + M$ (R3L) and $H + O_2 = OH + O$ (R4) also demonstrate high $|r|$ (r = 0.58).

3.4. Final feasible parameter set

Fig. 11 shows the posterior histograms of x_{R12} and x_{R13} based on the 1000 local optimums, which conform to the assumed normal distributions. To determine the posterior feasible parameter set, the 2-times standard deviation, $2\sigma_i$, which covers 95 % of the distribution, is determined as the reduced bounds for parameter x_i, as shown by the dash lines in Fig. 11. The posterior feasible parameters are sampled within the 2σ bounds:

$$\overline{x}_i - 2\sigma_i < x_i < \overline{x}_i + 2\sigma_i \tag{16}$$

where $\overline{x}_i$ and σ_i are the average value and the standard deviation of x_i based on the 1000 local optimums. The reduced 2σ bounds for the studied parameters are presented in Table 2.

For the high-$|r|$ correlated parameter pairs, the confidence ellipses for the 1000 local optimums are calculated:

$$\begin{bmatrix} x_i - \overline{x}_i \\ x_j - \overline{x}_j \end{bmatrix}^{\mathrm{T}} cov(x_i, x_j)^{-1} \begin{bmatrix} x_i - \overline{x}_i \\ x_j - \overline{x}_j \end{bmatrix} \Big\langle S \tag{17}$$

where S defines the scale of the ellipse (95 % confidence corresponds to $S = 5.991$) and $cov(x_i, x_j)^{-1}$ is the inverse of the covariance matrix of x_i and x_j based on the 1000 local optimums:

$$cov(x_i, x_j)^{-1} = \begin{bmatrix} cov(x_i, x_i) & cov(x_i, x_j) \\ cov(x_j, x_i) & cov(x_j, x_j) \end{bmatrix}^{-1} \tag{18}$$

For the 11 pairs of high-$|r|$ parameters figured out, marked with * in Fig. 10, the intersection of the 2σ bounds and the 95 % confidence ellipse determines the final feasible parameter set. The sampling of x_i and x_j follows the rule of:

$$\begin{cases} \overline{x}_i - 2\sigma_i < x_i < \overline{x}_i + 2\sigma_i \\ \overline{x}_j - 2\sigma_j < x_j < \overline{x}_j + 2\sigma_j \\ \begin{bmatrix} x_i - \overline{x}_i \\ x_j - \overline{x}_j \end{bmatrix}^{\mathrm{T}} cov(x_i, x_j)^{-1} \begin{bmatrix} x_i - \overline{x}_i \\ x_j - \overline{x}_j \end{bmatrix} \Big\langle 5.991 \end{cases} \tag{19}$$

where σ_i and σ_j are the standard deviations based on the respective statistical analysis on parameters x_i and x_i, and the third line defines the 95 % confidence ellipse shown in Fig. 9a.

The performed application of the PSO algorithm reviled its high efficiency. Fig. 12 demonstrates the progress in the obtained results: the reduced uncertainty intervals of the 20 parameters are presented in blue color (Syngas-reduced) in comparison to the results of our previous work [25] for the H_2 oxidation model (red color, H_2-initial) and to the uncertainty bounds for the model as-compiled (black color, H_2-reduced/Syngas-initial), which were normalized to $X \in [0, 1]$, Eq. (7).

It is a good illustration of the problem of model re-optimization arising from dataset (experimental targets and reactions) extension. Compared to the previous work [25] in which only 4 RRCs were reduced for the H_2 oxidation model, the extended dataset, which includes now the experimental data for syngas, revealed the next portion of hydrogen reactions with higher relative uncertainty contributions, namely (R3L), (R4), (R7), (R8), (R12), and (R13), of which uncertainty intervals were reduced by>40 %. Some reactions, like (R1), (R5), (R16), and (R19L), with lower relative uncertainty contributions (only X in Table 2) do not show strong feedback from Ψ and their uncertainty intervals were less reduced (by 5 % to 32 %). The newly added channel for syngas oxidation, $CO + OH = CO_2 + H$ (R23), demonstrates the highest potential for uncertainty reduction (reduced by 77 %).

The application of the PSO algorithm in this study reduced the reliance on human experience and intuition and increased the automation and self-monitoring of the chemical kinetic model optimization works led to the further improvement of reaction rate values. The comparison of the initial and reduced RRC uncertainty bounds for the studied reactions are presented in Fig. S1-1 to S1-21 in Supplementary-1. The 95 % confidence ellipses of the 11 high-$|r|$ reaction pairs are presented in

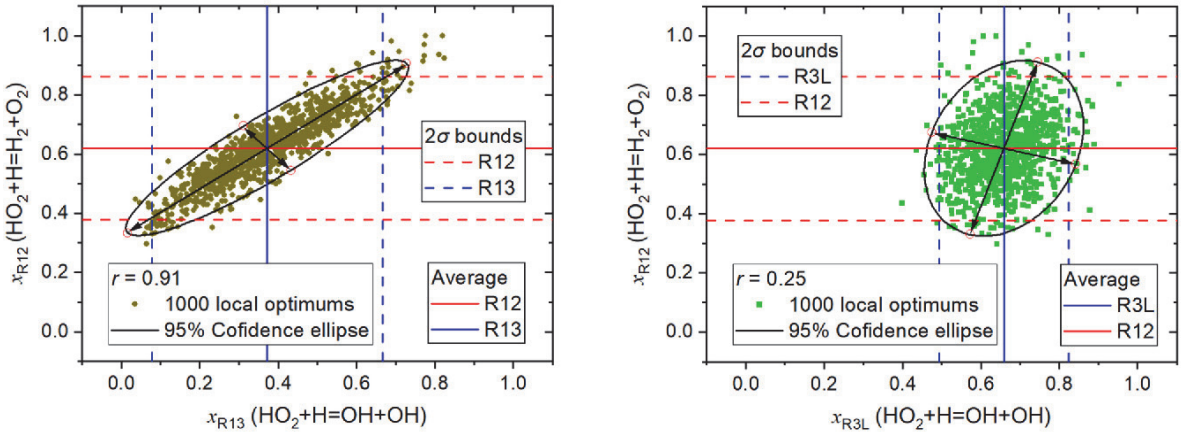

(a) (b)

Fig. 9. Distribution of the 1000 local optimums: (a) reactions (R13)-(R12), r 0.91; (b) reactions (R3L)-(R12), r 0.25.

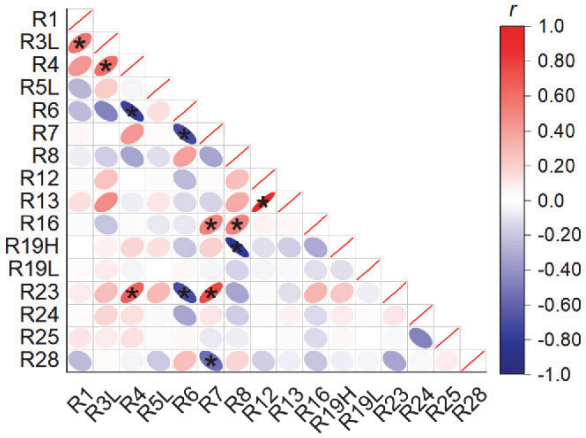

Fig. 10. Pearson correlation coefficients (r) of the studied 16 reaction rate constants and the high-$|r|$ pairs (marked with *, $|r| > 0.5$).

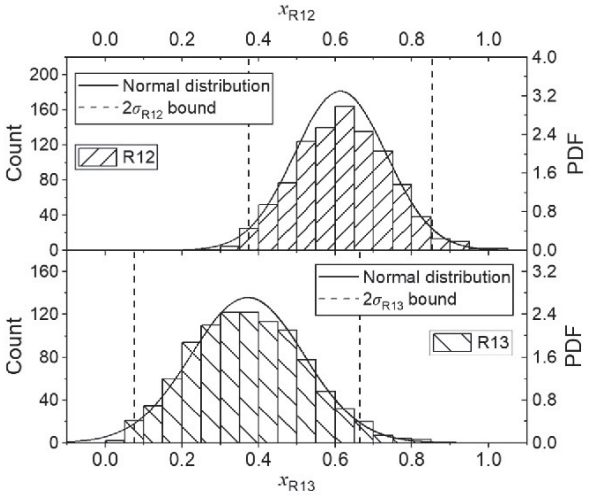

Fig. 11. Posterior distribution of x_{R12} and x_{R13} based on the 1000 local optimums and the assumed normal distributions.

Fig. S1-22 to S1-33 in Supplementary-1.

4. Modeling results and discussion

In this section, the RRCs of the developed joint H_2 and syngas oxidation model will be sampled randomly within the final feasible parameter set (reduced uncertainty intervals and the 95 % confidence ellipses) to show the reduction of the modeling uncertainties. One model with the lowest Ψ among the 1000 local optimums presented in Fig. 7 is designated as the final model and uploaded as Supplementary-3. The modeling results simulated with the models of Varga et al. [18], Kéromnès et al [7] (NUIG syngas), and Konnov [9] were also presented as comparisons. It should be emphasized that all the 1000 local optimums are acceptable models and the final model is one possibility of the feasible parameter sets. The Arrhenius expression parameters of the final model make one possible combination with good prediction ability for the currently collected experimental data. The results of Monte Carlo simulations and modeling results with the final model will be presented. Limited by the length of the paper, the detailed results are presented in Supplementary-2.

4.1. Ignition delay time

The uncertainty contributions of the key reactions are recalculated for their reduced uncertainty intervals. As shown by the comparison of the initial and reduced uncertainty contributions in Fig. 13, most of the uncertainty contributions have been greatly reduced, and declines higher than 50 % were achieved for the reaction ($R3$) and (R4).

Monte Carlo (MC) simulations were conducted with the RRCs sampled within the initial and reduced uncertainty intervals respectively. It can be seen from the comparison of the experimental data and modeling results presented in Fig. 14 that the uncertainty reduction improves the model accuracy and reduces its uncertainties for predicting the IDTs.

The comparison of IDTs simulated with different models is presented in Fig. 15. The model of Kéromnès et al [7] was modified for their measured IDTs [7] and also well predict the IDTs measured by Krejci et al. [63]. The model of Varga et al. [18] was optimized in a comprehensive study and shows good prediction ability for the IDTs of 1.6 atm and 12 atm but predicts earlier ignition at high pressure ($p_5 = 32$ atm).

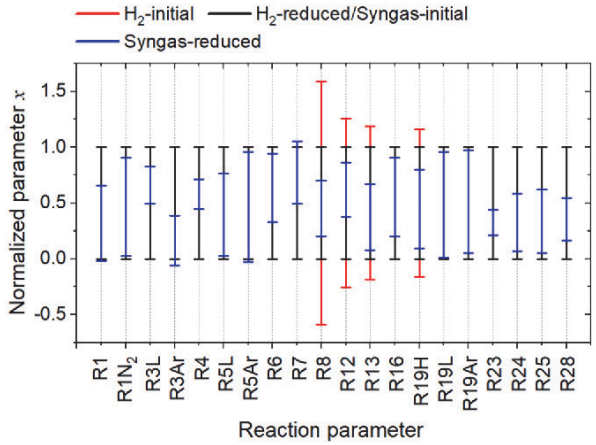

Fig. 12. The initial and reduced uncertainties of the normalized RRC parameters X.

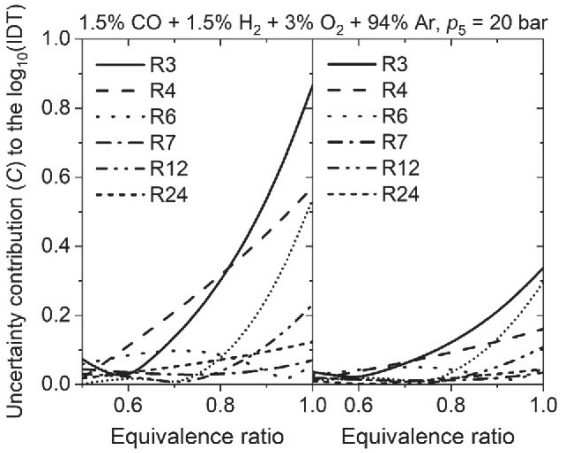

Fig. 13. Initial (left) and reduced (right) uncertainties contributions of the key channels ($C_r > 0.1$) to the simulation of ignition delay times.

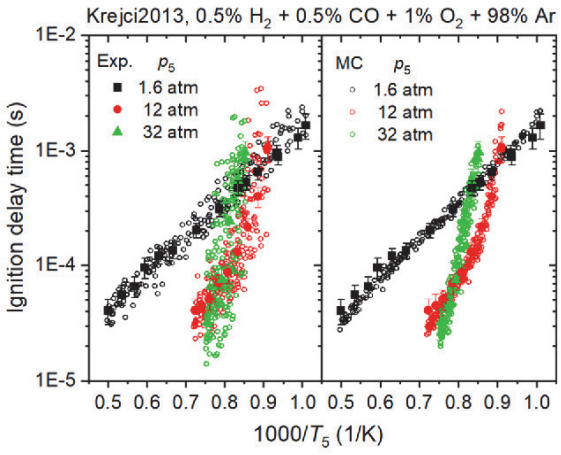

Fig. 14. Measured ignition delay times (Krejci et al. [63], big symbols) and Monte Carlo simulation results (small symbols) with the initial (left) and final (right) parameter sets.

The model of Konnov [9] shows the highest discrepancy measure for the IDTs at high pressures.

The simulations covering wide pressure and temperature ranges have been conducted with the final optimized model for the IDTs of both H_2 [7,54–60,62] and syngas [7,61–63] mixtures. The modeling results show good agreement with the collected experimental data, as presented in Fig. S2-1 to Fig. S2-9 in Supplementary-2.

4.2. Premixed laminar flame

With the initially determined RRC uncertainty intervals, the highest uncertainty (around 25 cm/s) of the modeling LFS at $T_u = 298$ K and $p = 1$ atm is contributed by reaction (R4) $H + O_2 = OH + O$ at fuel-rich conditions, as shown in Fig. 16 (left). By reducing the uncertainty intervals of the studied RRCs, the highest uncertainty contribution is reduced to about 10 cm/s, as shown in Fig. 16 (right).

The RRCs were randomly sampled within the initial and reduced uncertainty intervals, and MC simulations have been conducted for the LFSs at $T_u = 298$ K and $p = 1$ atm, as shown in Fig. 17. Compared to the MC results with initial bounds (red symbols), the distribution of the results with final reduced bounds is concentrated within the uncertainties of experimental data. The 2σ modeling uncertainty bounds [126,127] of the initial and reduced RRC uncertainty intervals are indicated by red and blue dashed lines respectively. The 2σ modeling uncertainties have been reduced by>50 % for conditions with equivalence ratios lower than 2.0, and the modeling uncertainties for fuel reach mixtures have been less reduced due to the high uncertainties of the experimental data.

The final model shows a good prediction ability for the LFSs of mixtures with variable H_2:CO ratios, as shown in Fig. 18. Both models of Varga et al. [18] and Konnov [9] have been optimized for the LFSs and the results show good agreement with the experimental data. Compared with the other three models, the LFSs are overpredicted by the model of Kéromnès et al. [7], as shown in Fig. 19. More modeling results with the final model for LFSs with variable T_u and p are presented in Fig. S2-10 to Fig. S2-25 in Supplementary-2.

4.3. Concentration profile

The idealized 0-D model is applied to the simulation of the JSRs [19,109], and PFRs [110]. The Arrhenius parameters are sampled randomly to get the Monte Carlo simulation results of the concentration profiles in a JSR [19]. As presented in Fig. 20, all the tested model reaches the same equilibrium state at high temperatures, which means

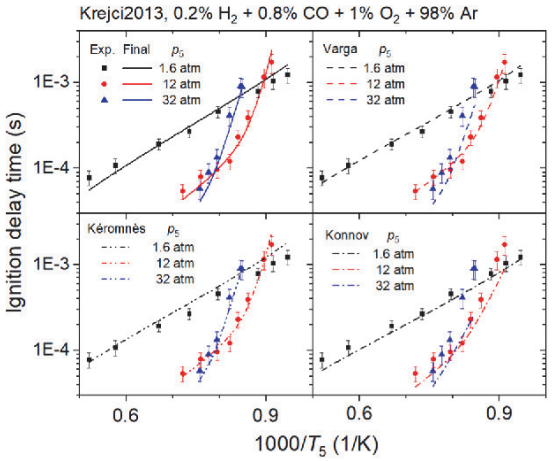

Fig. 15. Measured ignition delay times (Krejci et al. [63], symbols) and simulation results with different models [7,9,18].

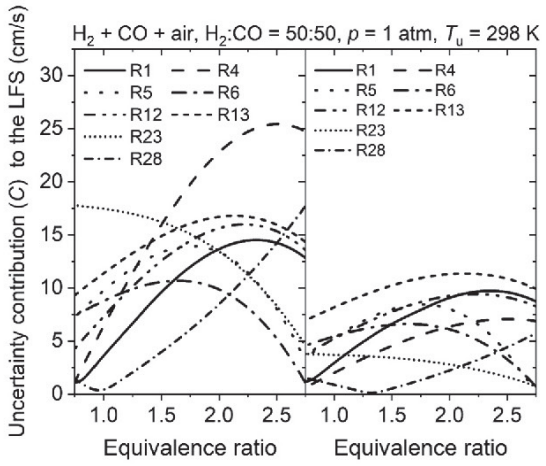

Fig. 16. Initial (left) and reduced (right) uncertainties contributions of the key channels ($C_r > 0.1$) to the laminar flame speed simulation.

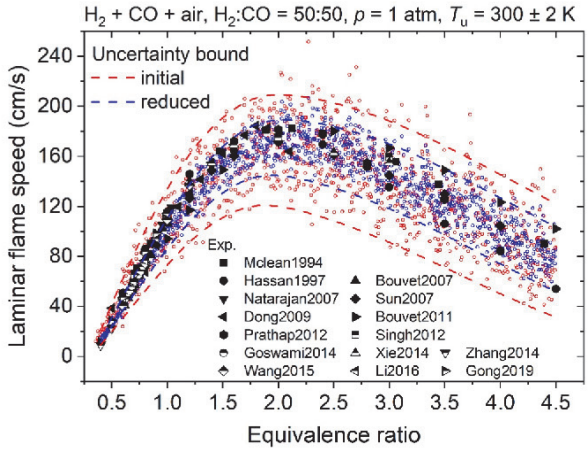

Fig. 17. Laminar flame speeds of Monte Carlo simulations with the initial (red symbols) and reduced (blue symbols) parameter sets. (For interpretation of the references to color in this figure legend, the reader is referred to the web version of this article.)

there is no sense to optimize the model for the targets of mole fractions at high temperatures (>1100 K) or non-reaction temperatures (<850 K). In the unstable temperature range (900–1000 K), the measured concentration profiles rise sharply with the temperature increase and the simulated results also show high gradients to the change of Arrhenius parameters. The high sensitivity of concentration profiles to the temperature, i.e. operating conditions and assumed reactor idealization, and Arrhenius parameters make the optimization difficult with targets on the measured mole fractions so that the input temperatures and residence times are set as optimization targets in this study.

With the reduced final parameter set, the model can predict reactant model fractions in the JSR [19] with much lower modeling uncertainties, as shown in Fig. 20. CO mole fractions measured in the PFR [111] are presented in Fig. 21 with modeling results simulated with different models [7,9,18]. The final model and models of Varga et al. [18] and Kéromnès et al [7] accurately predict the beginning of the CO oxidation (around $T = 1000$ K) and the mole fractions of CO. However, the simulations with the model of Konnov [9] show reactions at lower temperatures (around $T = 950$ K). More results for the simulation of JSR and PFR with the final model are presented in Fig. S2-26 and Fig. S2-27.

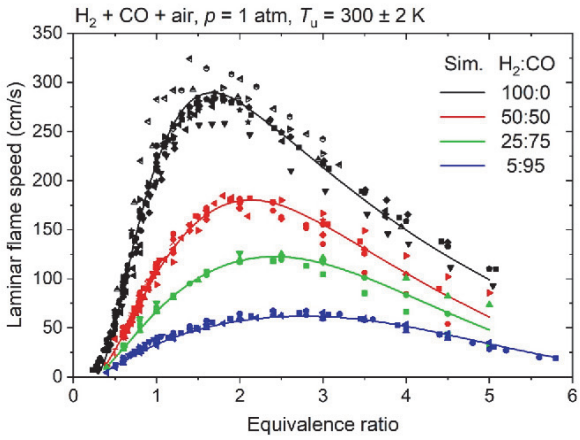

Fig. 18. Comparison of the measured and modeling (final model) laminar flame speeds of H_2/CO/air mixtures at 1 atm (detailed reference information in Supplementary-2).

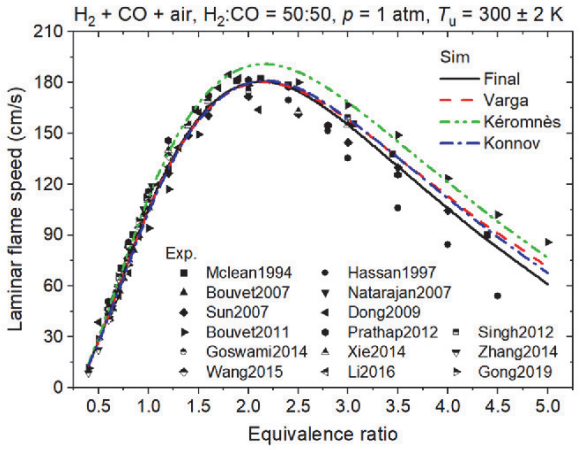

Fig. 19. Laminar flame speeds of H_2/CO/air mixtures measured by experiments [81–94] and simulated with different models [7,9,18].

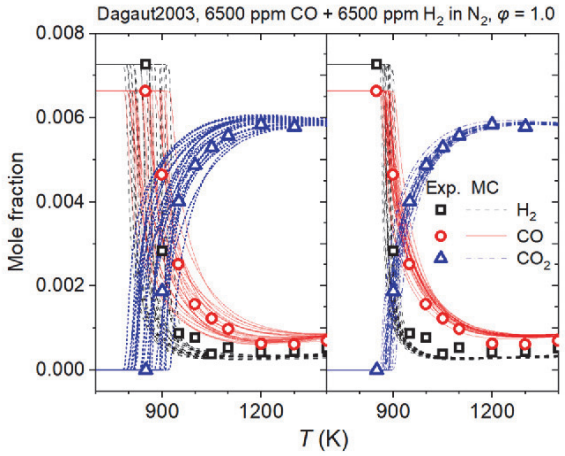

Fig. 20. Mole fractions measured in the jet stirred reactor (Dagaut et al. [19]) and Monte Carlo simulation results with the initial (left) and final (right) parameter sets.

The 1-dimensional premixed laminar flame model in Chemkin Pro [51] was used for the simulation of the concentration profiles in H_2 and syngas premixed laminar flames measured. Limited by the measurement technology for high-temperature flame, the temperature and concentration profiles show high uncertainties [49], so the concentration profiles measured in premixed laminar flames were not specially fitted. A comparison of the modeling results and the experimental data measured by Knyazkov et al. [108] are presented in Fig. 22. More detailed results for the other works are presented in Fig. S2-28 and Fig. S2-29.

5. Conclusion

The novel data-driven framework for detailed kinetic mechanisms optimization applying the heuristic algorithm, namely canonic Particle Swarm Optimization (PSO) was developed and applied to the optimization of the joint H_2 and syngas oxidation chemical kinetic model with 16 species and 41 reactions. The noticeable reduction of uncertainties of 16 Arrhenius pre-exponential factors and 4 third body factors, including further uncertainty minimization for hydrogen reactions being under optimization in the previous work [25] of model development (re-optimization) has been achieved. It is shown that the heuristic method PSO has excellent adaptability, optimization efficiency, and global optimization capability and can be successfully used in the optimization of a chemical kinetic model with not accurately known input parameters and has demonstrated higher effectivity compared with the uncertainty reduction based on probability density functions in our previous work. The inherent randomness of the PSO avoids falling into the local optimal solution and reduces the reliance on human experience and intuition and increases the automation and self-monitoring of the solution.

The data set used in the developed framework includes: the extended reaction model [48,49] including the newest update of the H_2 oxidation sub-model [25] with the reaction rate constants recommended by experimental, theoretical, and review works, based on which the uncertainty intervals of the studied Arrhenius parameters were determined by the statistical analysis; the experimental data with uncertainties provided from shock tubes, jet stirred reactors, plug flow reactors, and premixed laminar flames measured under conditions covered wide ranges of temperature, pressure, equivalence ratio, and H_2/CO ratio. The input–output characteristics of the chemical kinetic system have been revealed by the response function approximated with the second-order polynomial regression.

1000 local optimums were obtained in 1000 runs of PSO performed with randomly defined initial conditions (parameters of algorithm and 100 particles as surrogate reaction models). The best one of them was defined as the final optimized model. The posterior uncertainty intervals of the active parameters have been calculated based on the statistical analysis of these 1000 local minimums. The 11 pairs of strongly correlated reaction rate constants were defined with the Pearson correlation coefficients calculated using all considered 1000 local optimums, based on which the 95 % confidence ellipses and the reduced uncertainty intervals were constructed.

The final model shows good prediction ability for the collected experimental data. It can be used for the computational fluid dynamics simulation of H_2 and syngas oxidation and can be a good basement for the further development of chemical kinetic models for hydrocarbons.

CRediT authorship contribution statement

Hongxin Wang: Methodology, Investigation, Software, Formal analysis, Writing – original draft. **Chenyi Sun:** Software. **Oskar Haidn:** Supervision. **Askarova Aliya:** Investigation. **Chiara Manfletti:** Project administration. **Nadezda Slavinskaya:** Writing – review & editing, Supervision.

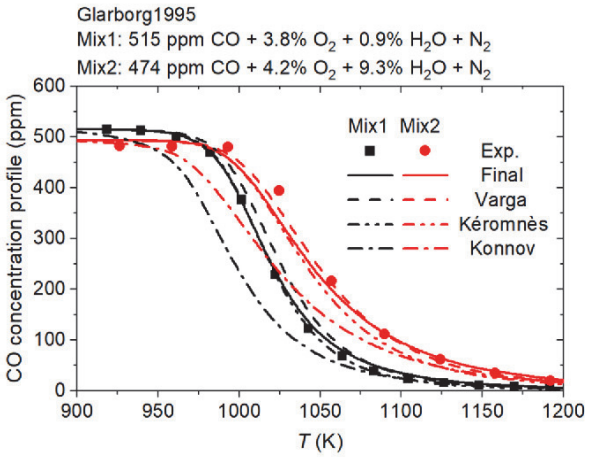

Fig. 21. CO mole fractions measured in the plug flow reactor (Glarborg et al. [111]) and simulated with different models [7,9,18].

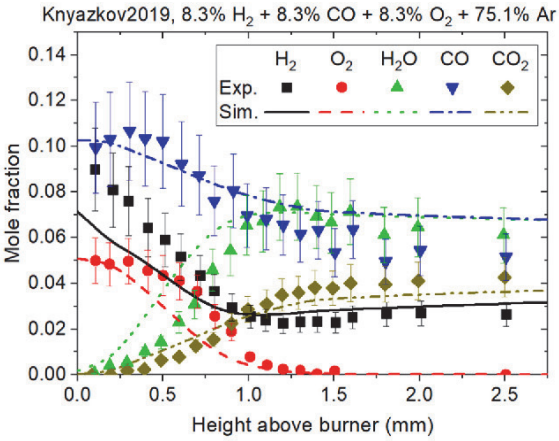

Fig. 22. Measured and simulated concentration profiles in premixed laminar flames [108].

Declaration of Competing Interest

The authors declare that they have no known competing financial interests or personal relationships that could have appeared to influence the work reported in this paper.

Data availability

Data will be made available on request.

Appendix A. Supplementary data

Supplementary data to this article can be found online at https://doi.org/10.1016/j.fuel.2022.125945.

References

[1] Fernández Y, Menéndez J. Influence of feed characteristics on the microwave-assisted pyrolysis used to produce syngas from biomass wastes. J Anal Appl Pyrol 2011;91(2):316–22.
[2] Hlina M, Hrabovsky M, Kavka T, Konrad M. Production of high quality syngas from argon/water plasma gasification of biomass and waste. Waste Manage 2014;34(1):63–6.

[3] Hernández S, Farkhondehfal MA, Sastre F, Makkee M, Saracco G, Russo N. Syngas production from electrochemical reduction of CO 2: current status and prospective implementation. Green Chem 2017;19(10):2326–46.
[4] Pradhan A, Baredar P, Kumar A. Syngas as an alternative fuel used in internal combustion engines: a review. J Pure Appl Sci Technol 2015;5(2):51–66.
[5] Rinaldini CA, Allesina G, Pedrazzi S, Mattarelli E, Savioli T, Morselli N, et al. Experimental investigation on a Common Rail Diesel engine partially fuelled by syngas. Energy Convers Manage 2017;138:526–37.
[6] Kan X, Zhou D, Yang W, Zhai X, Wang C-H. An investigation on utilization of biogas and syngas produced from biomass waste in premixed spark ignition engine. Appl Energy 2018;212:210–22.
[7] Kéromnès A, Metcalfe WK, Heufer KA, Donohoe N, Das AK, Sung C-J, et al. An experimental and detailed chemical kinetic modeling study of hydrogen and syngas mixture oxidation at elevated pressures. Combust Flame 2013;160(6):995–1011.
[8] Konnov AA. Remaining uncertainties in the kinetic mechanism of hydrogen combustion. Combust Flame 2008;152(4):507–28.
[9] Konnov AA. Implementation of the NCN pathway of prompt-NO formation in the detailed reaction mechanism. Combust Flame 2009;156(11):2093–105.
[10] Davis SG, Joshi AV, Wang H, Egolfopoulos F. An optimized kinetic model of H2/CO combustion. Proc Combust Inst 2005;30(1):1283–92.
[11] You X, Packard A, Frenklach M. Process informatics tools for predictive modeling: Hydrogen combustion. Int J Chem Kinet 2012;44(2):101–16.
[12] Smith GP, Golden DM, Frenklach M, Moriarty NW, Eiteneer B, Goldenberg M, et al. GRI 3.0 Mechanism, Gas Research Institute (http://combustion.berkeley.edu/gri-mech/). 1999.
[13] Wang H, You X, Joshi AV, Davis SG, Laskin A, Egolfopoulos F, et al. USC Mech Version II. High-Temperature Combustion Reaction Model of H2/CO/C1-C4 Compounds. http://ignisuscedu/USC_Mech_IIhtm May 2007.
[14] Saxena P, Williams FA. Testing a small detailed chemical-kinetic mechanism for the combustion of hydrogen and carbon monoxide. Combust Flame 2006;145(1–2):316–23.
[15] Mittal G, Sung CJ, Yetter RA. Autoignition of H2/CO at elevated pressures in a rapid compression machine. Int J Chem Kinet 2006;38(8):516–29.
[16] Li X, You X, Wu F, Law CK. Uncertainty analysis of the kinetic model prediction for high-pressure H2/CO combustion. Proc Combust Inst 2015;35(1):617–24.
[17] Slavinskaya N, Abbasi M, Starcke JH, Whitside R, Mirzayeva A, Riedel U, et al. Development of an uncertainty quantification predictive chemical reaction model for syngas combustion. Energy Fuels 2017;31(3):2274–97.
[18] Varga T, Olm C, Nagy T, Zsély IG, Valkó É, Pálvölgyi R, et al. Development of a joint hydrogen and syngas combustion mechanism based on an optimization approach. Int J Chem Kinet 2016;48(8):407–22.
[19] Dagaut P, Lecomte F, Mieritz J, Glarborg P. Experimental and kinetic modeling study of the effect of NO and SO2 on the oxidation of CO-H2 mixtures. Int J Chem Kinet 2003;35(11):564–75.
[20] Alzahrani FM, Sarnusi YS, Vogiatzaki K, Ghoniem AF, Habib MA, Mokheimer E. Evaluation of the accuracy of selected syngas chemical mechanisms. J Energy Res Technol 2015;137(4).
[21] Olm C, Zsély IG, Varga T, Curran HJ, Turányi T. Comparison of the performance of several recent syngas combustion mechanisms. Combust Flame 2015;162(5):1793–812.
[22] Lee HC, Mohamad AA, Jiang L-Y. Comprehensive comparison of chemical kinetics mechanisms for syngas/biogas mixtures. Energy Fuels 2015;29(9):6126–45.
[23] Iavarone S, Oreluk J, Smith ST, Hegde A, Li W, Packard A, et al. Application of Bound-to-Bound Data Collaboration approach for development and uncertainty quantification of a reduced char combustion model. Fuel 2018;232:769–79.
[24] Frenklach M, Packard A, Garcia-Donato G, Paulo R, Sacks J. Comparison of statistical and deterministic frameworks of uncertainty quantification. SIAM/ASA Journal on Uncertainty Quantification 2016;4(1):875–901.
[25] Wang H, Slavinskaya N, Haidn O. A comprehensive kinetic modeling study of hydrogen combustion with uncertainty quantification. Fuel 2022;319:123705.
[26] Kennedy J, Eberhart R. Particle swarm optimization. *Proceedings of ICNN'95-international conference on neural networks*. 4. IEEE; 1995:1942-8.
[27] Shi Y. Particle swarm optimization: developments, applications and resources. *Proceedings of the 2001 congress on evolutionary computation (IEEE Cat. No. 01TH8546)*. 1. IEEE; 2001:81-6.
[28] Kongnam C, Nuchprayoon S. A particle swarm optimization for wind energy control problem. Renewable Energy 2010;35(11):2431–8.
[29] Elsheikh A, Abd EM. Review on applications of particle swarm optimization in solar energy systems. Int J Environ Sci Technol 2019;16(2):1159–70.
[30] Schwaab M, Biscaia Jr EC, Monteiro JL, Pinto JC. Nonlinear parameter estimation through particle swarm optimization. Chem Eng Sci 2008;63(6):1542–52.
[31] Hu X, Eberhart R. Solving constrained nonlinear optimization problems with particle swarm optimization. *Proceedings of the sixth world multiconference on systemics, cybernetics and informatics*. 5. Citeseer; 2002:203-6.
[32] Wang X, Xiao J. PSO-based model predictive control for nonlinear processes. In: International Conference on Natural Computation. Springer; 2005. p. 196–203.
[33] Parsopoulos K, Plagianakos V, Magoulas G, Vrahatis M. Improving the particle swarm optimizer by function "stretching". In: Advances in Convex Analysis and Global Optimization. Springer; 2001. p. 445–57.
[34] Parsopoulos K, Plagianakos V, Magoulas G, Vrahatis M. Stretching technique for obtaining global minimizers through particle swarm optimization. *Proceedings of the particle swarm optimization Workshop*. 29. Indianapolis, USA; 2001:1-8.
[35] Blackwell T, Branke J. Multi-swarm optimization in dynamic environments. In: Workshops on Applications of Evolutionary Computation. Springer; 2004. p. 489–500.
[36] Elliott L, Ingham DB, Kyne AG, Mera NS, Pourkashanian M, Wilson CW. The use of ignition delay time in genetic algorithms optimisation of chemical kinetics reaction mechanisms. Eng Appl Artif Intell 2005;18(7):825–31.
[37] Elliott L, Ingham D, Kyne A, Mera N, Pourkashanian M, Wilson C. Genetic algorithms for optimisation of chemical kinetics reaction mechanisms. Prog Energy Combust Sci 2004;30(3):297–328.
[38] Elliott L, Ingham D, Kyne A, Mera N, Pourkashanian M, Wilson C. Incorporation of physical bounds on rate parameters for reaction mechanism optimization using genetic algorithms. Combust Sci Technol 2003;175(4):619–48.
[39] Elliott L, Ingham D, Kyne A, Mera N, Pourkashanian M, Wilson C. The optimisation of reaction rate parameters for chemical kinetic modelling using genetic algorithms. Turbo Expo: Power for Land, Sea, and Air 2002;36061:563–72.
[40] Harris S, Elliott L, Ingham D, Pourkashanian M, Wilson C. The optimisation of reaction rate parameters for chemical kinetic modelling of combustion using genetic algorithms. Comput Methods Appl Mech Eng 2000;190(8–10):1065–90.
[41] Tsuchiya M, Ross J. Application of genetic algorithm to chemical kinetics: Systematic determination of reaction mechanism and rate coefficients for a complex reaction network. The Journal of Physical Chemistry A 2001;105(16):4052–8.
[42] Montgomery CJ, Yang C, Parkinson AR, Chen J-Y. Selecting the optimum quasi-steady-state species for reduced chemical kinetic mechanisms using a genetic algorithm. Combust Flame 2006;144(1–2):37–52.
[43] Sikalo N, Hasemann O, Schulz C, Kempf A, Wlokas I. A genetic algorithm–based method for the optimization of reduced kinetics mechanisms. Int J Chem Kinet 2015;47(11):695–723.
[44] Sikalo N, Hasemann O, Schulz C, Kempf A, Wlokas I. A genetic algorithm-based method for the automatic reduction of reaction mechanisms. Int J Chem Kinet 2014;46(1):41–59.
[45] Bertolino A, Fürst M, Stagni A, Frassoldati A, Pelucchi M, Cavallotti C, et al. An evolutionary, data-driven approach for mechanism optimization: theory and application to ammonia combustion. Combust Flame 2021;229:111366.
[46] El Rassy E, Delaroque A, Sambou P, Chakravarty HK, Matynia A. On the Potential of the Particle Swarm Algorithm for the Optimization of Detailed Kinetic Mechanisms. Comparison with the Genetic Algorithm. J Phys Chem A 2021;125(23):5180–9.
[47] Pedregosa F, Varoquaux G, Gramfort A, Michel V, Thirion B, Grisel O, et al. Scikit-learn: Machine learning in Python. J Machine Learn Res 2011;12:2825–30.
[48] Slavinskaya N, Mirzayeva A, Whitside R, Starke J, Abbasi M, Auyelkhankyzy M, et al. A modelling study of acetylene oxidation and pyrolysis. Combust Flame 2019;210:25–42.
[49] Wang H, Slavinskaya N, Kanz A, Auyelkhankyzy M, Gao Y, Haidn O. A comprehensive kinetic modeling study of ethylene combustion with data uncertainty analysis. Fuel 2021;299:120833.
[50] Walter G, Wang H, Kanz A, Kolbasseff A, Xu X, Haidn O, et al. Experimental error assessment of laminar flame speed measurements for digital chemical kinetics databases. Fuel 2020;266.
[51] DESIGNS ME. Chemkin-pro. 2011.
[52] Wang H. Uncertainty quantification and minimization. In: Computer Aided Chemical Engineering. Elsevier; 2019. p. 723–62.
[53] Khuri AI, Mukhopadhyay S. Response surface methodology. Wiley Interdiscip Rev Comput Stat 2010;2(2):128–49.
[54] Zhang Y, Huang Z, Wei L, Zhang J, Law CK. Experimental and modeling study on ignition delays of lean mixtures of methane, hydrogen, oxygen, and argon at elevated pressures. Combust Flame 2012;159(3):918–31.
[55] Hu E, Pan L, Gao Z, Lu X, Meng X, Huang Z. Shock tube study on ignition delay of hydrogen and evaluation of various kinetic models. Int J Hydrogen Energy 2016;41(30):13261–80.
[56] Pan L, Hu E, Zhang J, Zhang Z, Huang Z. Experimental and kinetic study on ignition delay times of DME/H2/O2/Ar mixtures. Combust Flame 2014;161(3):735–47.
[57] Petersen EL, Kalitan DM, Rickard MJ. Reflected Shock Ignition of SiH4/H2/O2/Ar andSiH4/CH4/O2/Ar Mixtures. J Propul Power 2004;20(4):665–74.
[58] Ninnemann E, Koroglu B, Pryor O, Barak S, Nash L, Loparo Z, et al. New insights into the shock tube ignition of H2/O2 at low to moderate temperatures using high-speed end-wall imaging. Combust Flame 2018;187:11–21.
[59] Pang G, Davidson D, Hanson R. Experimental study and modeling of shock tube ignition delay times for hydrogen–oxygen–argon mixtures at low temperatures. Proc Combust Inst 2009;32(1):181–8.
[60] Shao J, Choudhary R, Davidson DF, Hanson RK, Barak S, Vasu S. Ignition delay times of methane and hydrogen highly diluted in carbon dioxide at high pressures up to 300 atm. Proc Combust Inst 2019;37(4):4555–62.
[61] He D, Ding Y, Xiong X, Shi S, Du Y, Peng Z, et al. Shock Tube Study of Ignition-Delay Measurements and Kinetic Mechanism Research for Syngas. J Propul Power 2018;34(4):836–43.
[62] Herzler J, Naumann C. Shock tube study of the ignition of lean CO/H2 fuel blends at intermediate temperatures and high pressure. Combust Sci Technol 2008;180(10–11):2015–28.
[63] Krejci MC, Mathieu O, Vissotski AJ, Ravi S, Sikes TG, Petersen EL, et al. Laminar flame speed and ignition delay time data for the kinetic modeling of hydrogen and syngas fuel blends. J Eng Gas Turbines Power 2013;135(2).
[64] Qin X, Kobayashi H, Niioka T. Laminar burning velocity of hydrogen–air premixed flames at elevated pressure. Exp Therm Fluid Sci 2000;21(1–3):58–63.

[65] Pareja J, Burbano HJ, Ogami Y. Measurements of the laminar burning velocity of hydrogen–air premixed flames. Int J Hydrogen Energy 2010;35(4):1812–8.
[66] Liu D, MacFarlane R. Laminar burning velocities of hydrogen-air and hydrogen-air steam flames. Combust Flame 1983;49(1–3):59–71.
[67] Egolfopoulos F, Law CK. An experimental and computational study of the burning rates of ultra-lean to moderately-rich H2/O2/N2 laminar flames with pressure variations. *Symposium (international) on combustion*. 23. Elsevier; 1991:333-40.
[68] Vagelopoulos CM, Egolfopoulos FN, Law CK. Further considerations on the determination of laminar flame speeds with the counterflow twin-flame technique. *Symposium (international) on combustion*. 25. Elsevier; 1994:1341-7.
[69] Huang Z, Zhang Y, Zeng K, Liu B, Wang Q, Jiang D. Measurements of laminar burning velocities for natural gas–hydrogen–air mixtures. Combust Flame 2006;146(1–2):302–11.
[70] Bradley D, Lawes M, Liu K, Verhelst S, Woolley R. Laminar burning velocities of lean hydrogen–air mixtures at pressures up to 1.0 MPa. Combust Flame 2007;149(1–2):162–72.
[71] Günther R, Janisch G. Measurements of burning velocity in a flat flame front. Combust Flame 1972;19(1):49–53.
[72] Dowdy DR, Smith DB, Taylor SC, Williams A. The use of expanding spherical flames to determine burning velocities and stretch effects in hydrogen/air mixtures. *Symposium (International) on Combustion*. 23. Elsevier; 1991:325-32.
[73] Aung K, Hassan M, Faeth G. Effects of pressure and nitrogen dilution on flame/stretch interactions of laminar premixed H2/O2/N2 flames. Combust Flame 1998;112(1–2):1–15.
[74] Tse SD, Zhu D, Law CK. Morphology and burning rates of expanding spherical flames in H2/O2/inert mixtures up to 60 atmospheres. Proc Combust Inst 2000;28(2):1793–800.
[75] Kwon O, Faeth G. Flame/stretch interactions of premixed hydrogen-fueled flames: measurements and predictions. Combust Flame 2001;124(4):590–610.
[76] Lamoureux N, Paillard C-E, Vaslier V. Low hydrocarbon mixtures ignition delay times investigation behind reflected shock waves. Shock Waves 2002;11(4):309–22.
[77] Burke MP, Chen Z, Ju Y, Dryer FL. Effect of cylindrical confinement on the determination of laminar flame speeds using outwardly propagating flames. Combust Flame 2009;156(4):771–9.
[78] Hu E, Huang Z, He J, Miao H. Experimental and numerical study on laminar burning velocities and flame instabilities of hydrogen–air mixtures at elevated pressures and temperatures. Int J Hydrogen Energy 2009;34(20):8741–55.
[79] Varea E, Beeckmann J, Pitsch H, Chen Z, Renou B. Determination of burning velocities from spherically expanding H2/air flames. Proc Combust Inst 2015;35(1):711–9.
[80] Zhang Z, Cheng P, Tan J, Liang J, Li Y, Li G. The uncertainty of laminar burning velocity of premixed H2-air flame induced by the non-uniform initial temperature field inside the constant-volume combustion vessel. Int J Hydrogen Energy 2018;43(45):21049–59.
[81] McLean IC, Smith DB, Taylor SC. The use of carbon monoxide/hydrogen burning velocities to examine the rate of the CO+ OH reaction. *Symposium (international) on combustion*. 25. Elsevier; 1994:749-57.
[82] Hassan M, Aung K, Faeth G. Properties of laminar premixed CO/H/air flames at various pressures. J Propul Power 1997;13(2):239–45.
[83] Bouvet N, Lee S, Gokalp I, Santoro R. Flame speed characteristics of syngas (H2-CO) with straight burners for laminar premixed flames. Third European Combustion Meeting 2007:1–6.
[84] Natarajan J, Lieuwen T, Seitzman J. Laminar flame speeds of H2/CO mixtures: Effect of CO2 dilution, preheat temperature, and pressure. Combust Flame 2007;151(1–2):104–19.
[85] Sun H, Yang S, Jomaas G, Law C. High-pressure laminar flame speeds and kinetic modeling of carbon monoxide/hydrogen combustion. Proc Combust Inst 2007;31(1):439–46.
[86] Dong C, Zhou Q, Zhao Q, Zhang Y, Xu T, Hui S. Experimental study on the laminar flame speed of hydrogen/carbon monoxide/air mixtures. Fuel 2009;88(10):1858–63.
[87] Prathap C, Ray A, Ravi M. Effects of dilution with carbon dioxide on the laminar burning velocity and flame stability of H2–CO mixtures at atmospheric condition. Combust Flame 2012;159(2):482–92.
[88] Singh D, Nishiie T, Tanvir S, Qiao L. An experimental and kinetic study of syngas/air combustion at elevated temperatures and the effect of water addition. Fuel 2012;94:448–56.
[89] Goswami M, Bastiaans R, Konnov A, de Goey L. Laminar burning velocity of lean H2-CO mixtures at elevated pressure using the heat flux method. international journal of hydrogen energy 2014;39(1485):e1498.
[90] Xie Y, Wang J, Xu N, Yu S, Huang Z. Comparative study on the effect of CO2 and H2O dilution on laminar burning characteristics of CO/H2/air mixtures. Int J Hydrogen Energy 2014;39(7):3450–8.
[91] Zhang Y, Shen W, Fan M, Zhang H, Li S. Laminar flame speed studies of lean premixed H2/CO/air flames. Combust Flame 2014;161(10):2492–5.
[92] Wang Z, Weng W, He Y, Li Z, Cen K. Effect of H2/CO ratio and N2/CO2 dilution rate on laminar burning velocity of syngas investigated by direct measurement and simulation. Fuel 2015;141:285–92.
[93] Li H-M, Li G-X, Sun Z-Y, Zhou Z-H, Li Y, Yuan Y. Investigation on dilution effect on laminar burning velocity of syngas premixed flames. Energy 2016;112:146–52.
[94] Gong X, Huo J, Ren Z, Law CK. Extrapolation and DNS-mapping in determining laminar flame speeds of syngas/air mixtures. Combust Flame 2019;200:365–73.
[95] Bouvet N, Chauveau C, Gökalp I, Lee S-Y, Santoro RJ. Characterization of syngas laminar flames using the Bunsen burner configuration. Int J Hydrogen Energy 2011;36(1):992–1005.
[96] Ratna Kishore V, Ravi MR, Ray A. Adiabatic burning velocity and cellular flame characteristics of H2–CO–CO2–air mixtures. Combust Flame 2011;158(11):2149–64.
[97] Burbano HJ, Pareja J, Amell AA. Laminar burning velocities and flame stability analysis of H2/CO/air mixtures with dilution of N2 and CO2. Int J Hydrogen Energy 2011;36(4):3232–42.
[98] Li H-M, Li G-X, Sun Z-Y, Zhou Z-H, Li Y, Yuan Y. Effect of dilution on laminar burning characteristics of H2/CO/CO2/air premixed flames with various hydrogen fractions. Exp Therm Fluid Sci 2016;74:160–8.
[99] Wang S, Wang Z, Elbaz AM, He Y, Chen C, Zhu Y, et al. Effects of CO2 Dilution and CH4 Addition on Laminar Burning Velocities of Syngas at Elevated Pressures: An Experimental and Modeling Study. Energy Fuels 2021;35(22):18733–45.
[100] Prathap C, Ray A, Ravi M. Investigation of nitrogen dilution effects on the laminar burning velocity and flame stability of syngas fuel at atmospheric condition. Combust Flame 2008;155(1–2):145–60.
[101] Das AK, Kumar K, Sung C-J. Laminar flame speeds of moist syngas mixtures. Combust Flame 2011;158(2):345–53.
[102] Zhang X, Huang Z, Zhang Z, Zheng J, Yu W, Jiang D. Measurements of laminar burning velocities and flame stability analysis for dissociated methanol–air–diluent mixtures at elevated temperatures and pressures. Int J Hydrogen Energy 2009;34(11):4862–75.
[103] Han M, Ai Y, Chen Z, Kong W. Laminar flame speeds of H2/CO with CO2 dilution at normal and elevated pressures and temperatures. Fuel 2015;148:32–8.
[104] Grosseuvres R, Comandini A, Bentaib A, Chaumeix N. Combustion properties of H2/N2/O2/steam mixtures. Proc Combust Inst 2019;37(2):1537–46.
[105] Voss S, Hartl S, Hasse C. Determination of laminar burning velocities for lean low calorific H2/N2 and H2/CO/N2 gas mixtures. Int J Hydrogen Energy 2014;39(34):19810–7.
[106] Dixon-Lewis G, Sutton MM, Williams A. Flame structure and flame reaction kinetics-IV. Experimental investigations of a fuel-rich hydrogen+ oxygen+ nitrogen flame at atmospheric pressure. Proceedings of the Royal Society of London A Mathematical and Physical Sciences 1970;317(1529):227-34.
[107] Vandooren J, Bian J. Validation of H2/O2 reaction mechanisms by comparison with the experimental structure of a rich hydrogen-oxygen flame. *Symposium (International) on Combustion*. 23. Elsevier; 1990:341-6.
[108] Knyazkov D, Dmitriev A, Bolshova T, Shmakov A, Korobeinichev O, Markovich D. Experimental and numerical study of the structure of premixed H2/CO/O2/Ar flames at atmospheric pressure. *Journal of Physics: Conference Series*. 1382. IOP Publishing; 2019:012068.
[109] Le Cong T, Dagaut P. Experimental and detailed modeling study of the effect of water vapor on the kinetics of combustion of hydrogen and natural gas, impact on NO x. Energy Fuels 2009;23(2):725–34.
[110] Hashemi H, Christensen JM, Gersen S, Glarborg P. Hydrogen oxidation at high pressure and intermediate temperatures: Experiments and kinetic modeling. Proc Combust Inst 2015;35(1):553–60.
[111] Glarborg P, Kubel D, Kristensen PG, Hansen J, Dam-Johansen K. Interactions of CO, NOx and H2O under post-flame conditions. Combust Sci Technol 1995;110(1):461–85.
[112] Kurbatov V, Silin I. New method for minimizing regular functions with constraints on parameter region. Nucl Instrum Methods Phys Res, Sect A 1994;345(2):346–50.
[113] Sokolov S, Silin I. Preprint JINR D-810. Dubna 1961.
[114] Fokin LR, Slavinskaya N. Thermophysical parameter correlation for low-density gas mixtures: Ar-Xe. Institute for High Temperatures, USSR Academy of Sciences 1987;25(1):40–5.
[115] Baulch DL, Bowman CT, Cobos CJ, Cox RA, Just T, Kerr JA, et al. Evaluated Kinetic Data for Combustion Modeling: Supplement II. J Phys Chem Ref Data 2005;34(3):757–1397.
[116] Baulch D, Cobos C, Cox R, Esser C, Frank P, Just T, et al. Evaluated kinetic data for combustion modelling. J Phys Chem Ref Data 1992;21(3):411–734.
[117] Atkinson R, Baulch D, Cox R, Hampson Jr R, Kerr J, Rossi M, et al. Evaluated kinetic, photochemical and heterogeneous data for atmospheric chemistry: Supplement V. IUPAC Subcommittee on Gas Kinetic Data Evaluation for Atmospheric Chemistry. J Phys Chem Ref Data 1997;26(3):521–1011.
[118] Tsang W, Hampson R. Chemical kinetic data base for combustion chemistry. Part I. Methane and related compounds. J Phys Chem Ref Data 1986;15(3):1087–279.
[119] Shi C. Development of a Program for the Optimization of Chemical Kinetic Mechanism. *Department of Mechanical Engineering*. Master Semester Thesis. Munich: Technical University of Munich; 2021.
[120] Nagelkerke NJ. A note on a general definition of the coefficient of determination. Biometrika 1991;78(3):691–2.
[121] Metcalfe WK, Burke SM, Ahmed SS, Curran HJ. A Hierarchical and Comparative Kinetic Modeling Study of C1–C2 Hydrocarbon and Oxygenated Fuels. Int J Chem Kinet 2013;45(10):638–75.
[122] Hashemi H, Christensen JM, Gersen S, Levinsky H, Klippenstein SJ, Glarborg P. High-pressure oxidation of methane. Combust Flame 2016;172:349–64.
[123] Blackwell T, Kennedy J. Impact of communication topology in particle swarm optimization. IEEE Trans Evol Comput 2018;23(4):689–702.
[124] Figueiredo EM, Ludermir TB. Investigating the use of alternative topologies on performance of the PSO-ELM. Neurocomputing 2014;127:4–12.

[125] Lee Rodgers J, Nicewander WA. Thirteen ways to look at the correlation coefficient. The American Statistician 1988;42(1):59–66.
[126] Sheen DA, You X, Wang H, Løvås T. Spectral uncertainty quantification, propagation and optimization of a detailed kinetic model for ethylene combustion. Proc Combust Inst 2009;32(1):535–42.
[127] Prager J, Najm HN, Sargsyan K, Safta C, Pitz WJ. Uncertainty quantification of reaction mechanisms accounting for correlations introduced by rate rules and fitted Arrhenius parameters. Combust Flame 2013;160(9):1583–93.

Supplementary Material-1

A Joint Hydrogen and Syngas Chemical Kinetic Model Optimized by Particle Swarm Optimization

Hongxin Wang[1], Chenyi Sun[1], Oskar Haidn[1], Askarova Aliya[3], Chiara Manfletti[1], Nadezda Slavinskaya[2, 3]

1. Lehrstuhl für Raumfahrtantriebe, Technical University of Munich, 85748 Garching, Germany

2. Gesellschaft fur Anlagen-und Reaktorsicherheit GmbH, 85748 Garching, Germany

3. Al-Farabi Kazakh National University, 050040 Almaty, Kazakhstan

Recommendations of the reaction rate constants and calculated uncertainty parameters.

Table S1-1. Parameters for Arrhenius equation and uncertainty factors. $k(T)=AT^n exp(-E_a/T)$

Reaction		+M	Reference	ΔT, K	k, cm^3, s, mole, K		
					A	n	E_a, K
R22H	CO+O(+M)=CO_2(+M)		Toby1984 [1]	353-433	6.03E+09	0.00	1630.0
	high-pressure limit		Toby1980 [2]	348-433	1.26E+09	0.00	805.0
			Simonaitis1972 [3]	298-472	1.60E+10	0.00	1460.0
			Kondratev1961 [4]	373-523	9.64E+09	0.00	1060.0
			Avramenko1959 [5]	421-550	1.81E+09	0.50	1510.0
			Wagner1974 [6]	3000-3700	2.08E+10	0.00	0.0
			Clark1969 [7]	2900-4000	1.55E+09	0.00	0.0
			Olschewski1967 [8]	2800-3500	1.12E+10	0.00	0.0
R22L	CO+O(+M)=CO_2(+M)	Ar	Fujii1987 [9]	1700-2500	1.58E+15	0.00	3610.0
	low-pressure limit	He	Fujii1985 [10]	1700-2100	4.37E+15	0.00	2160.0
		CO_2	Toby1984 [11]	353-433	4.32E+20	0.00	5840.0
		He	Sugaw Ara1980 [12]	296	3.63E+12	0.00	0.0
		Ar	Hardy1978 [13]	1300-2200	2.79E+13	0.00	-2280.0
		Ar	Dean1977 [14]	2100-3200	5.79E+13	0.00	0.0
		CO_2	Inn1974 [15]	257-277	8.02E+14	0.00	1780.0
		Ar	Wagner1974 [6]	298-4000	1.01E+19	-1.50	2520.0
		Ar	Inn1973 [16]	296	3.56E+12	0.00	0.0
		CO	Inn1973 [16]	296	1.63E+12	0.00	0.0
		CO_2	Inn1973 [16]	296	1.96E+12	0.00	0.0
		CO	Slanger1972 [17]	250-370	2.36E+15	0.00	2180.0
		CO_2	Slanger1972 [17]	296	2.25E+12	0.00	0.0
		N_2	Slanger1972 [17]	296	8.34E+11	0.00	0.0
		N_2O	Simonaitis1972 [3]	298-472	5.90E+15	0.00	2060.0
		N_2	DeMore1972 [18]	298	2.50E+12	0.00	0.0
		Ar	Baldwin1972 [19]	300-3500	3.00E+14	0.00	1510.0
		CO	Stuhl1971 [20]	300	1.16E+12	0.00	0.0
		He	Stuhl1971 [20]	300	6.17E+11	0.00	0.0
		N_2	Stuhl1971 [20]	300	7.98E+11	0.00	0.0
		Ar	Donovan1971 [21]	300	5.08E+12	0.00	0.0
		He	Slanger1970 [22]	300	2.18E+12	0.00	0.0
		N_2	Slanger1970 [22]	300	5.08E+12	0.00	0.0
		Ar	Slanger1970 [22]	300	2.54E+12	0.00	0.0
		Ar	Lin1969 [23]	1500-3000	2.80E+12	0.00	-12000.0
		O_2	Kondratiev1969 [24]	409-503	6.76E+11	0.00	-1500.0
		O_2	Kondratev1961 [4]	373-523	3.48E+14	0.00	1060.0

Reaction		+M	Reference	ΔT, K	k, cm^3, s, mole, K		
					A	n	E_a, K
R22H^{-1}	CO_2(+M)=CO+O		Wagner1974 [6]	3000-3700	2.07E+10	0.00	0.0
	(+M)		Wagner1974 [6]	3000-3700	8.99E+12	0.00	65300.0
	high-pressure limit		Clark1969 [7]	2900-4000	1.55E+09	0.00	0.0
			Clark1969 [7]	2900-4000	5.13E+07	0.00	37300.0
			Olschewski1967 [8]	2800-3500	2.00E+11	0.00	55900.0
			Olschewski1967 [8]	2800-3500	1.12E+10	0.00	0.0
			Olschewski1966 [25]	2800-3700	2.51E+11	0.00	55400
R22L^{-1}	CO_2(+M)=CO+O	Ar	Eremin1997 [26]	2620-4470	1.09E+14	0.00	48900.0
	(+M)	-	Burmeister1990 [27]	2400-4400	3.65E+14	0.00	52500.0
	low-pressure limit	Ar	Fujii1989 [28]	2300-3400	2.51E+13	0.00	43800.0
		CO_2	Ebrahim1976 [29]	2500-7000	7.47E+12	0.5	52300.0
		Ar	Wagner1974 [6]	3000-4560	5.11E+14	0.00	55600.0
		Ar	Hardy1974 [30]	2700-4300	4.70E+14	0.00	52800.0
		Ar	Olschewski1967 [8]	2800-4400	5.01E+14	0.00	49800.0
		Ar	Olschewski1966 [25]	2800-4400	5.01E+14	0.00	49800.0
		Ar	Fishburne1966 [31]	3000-5000	7.13E+14	0.5	42500.0
		N_2	Fishburne1966 [31]	3000-5000	5.33E+14	0.5	40100.0
		Ar	Michel1965 [32]	2800-4400	5.01E+14	0.00	49800.0
		Ar	Brabbs1963 [33]	2560-2860	3.00E+11	0.5	43300.0
R23	CO+OH=CO_2+H		Wang2017 [34]	1428-1685	1.90E+12	0.00	2760.0
			Li2007 [35]	850-950	2.23E+05	1.89	-583.7
			Wooldridge1996 [36]	1080-2500	2.12E+12	0.00	2629.8
			Bohn1998 [37]	296	1.00E+11	0.00	0.0
			Lissianski1995 [38]	2170-3150	3.30E+06	1.55	-402.0
			Forster1995 [39]	298	5.85E+11	0.00	0.0
			Frost1993 [40]	296	1.08E+11	0.00	0.0
			Smith1985 [41]	298	9.23E+10	0.00	0.0
			Niki1984 [42]	299	1.42E+11	0.00	0.0
			Hofzumahaus1984 [43]	298	1.39E+11	0.00	0.0
			DeMore1984 [44]	298	1.26E+11	0.00	0.0
			Ravishankara1983 [45]	250-350	1.33E+11	0.00	145.0
			Husain1981 [46]	298	8.79E+10	0.00	0.0
			Clyne1979 [47]	293-430	1.32E+11	0.00	88.0
			Biordi1976 [48]	1420-1720	4.60E+11	0.00	0.0
			Vandooren1975 [49]	1000-1800	2.32E+12	0.00	2870.0
			Westenberg1973 [50]	300-915	5.36E+06	1.40	-492.0
			Peeters1973 [51]	1600-1900	1.36E+12	0.00	2770.0
			Gardiner1973 [52]	1200-2500	4.00E+12	0.00	4030.0
			Izod1971 [53]	1400-2200	9.03E+11	0.00	503.2
			Brabbs1971 [54]	1300-1900	4.20E+11	0.00	503.2
			Dean1970 [55]	1700-2600	1.14E+12	0.00	518.3
			Greiner1969 [56]	300-500	1.26E+11	0.00	115.7
			Jost1965 [57]	1380-1720	1.00E+12	0.00	2010.0

Reaction		Reference	ΔT, K	k, cm^3, s, mole, K		
				A	n	E_a, K
R23^{-1}	CO_2+H=CO+OH	Lissianski1995 [38]	2170-3150	2.00E+14	0.00	13500.0
		Wawer1978 [58]	1010-1240	8.99E+13	0.00	12000.0
		Vandooren1975 [49]	650-1800	4.80E+14	0.00	12600.0
		Shub1970 [59]	1200-1400	1.26E+14	0.00	13100.0
		Kochubei1970 [60]	1020-1320	1.01E+14	0.00	12200.0
		Fenimore1958 [61]	1220-1340	3.00E+15	0.00	16800.0
R24	CO+O_2=CO_2+O	Sharipov2011 [62]	800-5000	4.32E+07	1.62	25018.0
		Sharipov2011 [62]	800-5000	7.63E+06	1.67	26950.0
		Thielen1983 [63]	1700-3500	5.06E+13	0.00	31800.0
		Rawlins1974 [64]	1500-2500	1.20E+11	0.00	17612.7
		Gardiner1971 [65]	1400-2500	3.10E+11	0.00	19122.3
		Dean1971 [66]	1750-2590	1.21E+13	0.00	30200.0
		Brabbs1971 [54]	1300-1900	1.60E+13	0.00	20600.0
		Dean1970 [55]	2200-2600	3.49E+12	0.00	25200.0
		Drummond1968 [67]	1190-1850	2.40E+10	0.00	15300.0
		Sulzmann1965 [68]	2400-3000	3.50E+12	0.00	25700.0
		Fenimore1957 [69]	1700-2000	1.20E+12	0.00	12100.0
R24^{-1}	CO_2+O=CO+O_2	Ibragimova1991 [70]	1700-6000	2.71E+14	0.00	33800.0
		Clark1969 [7]	2800-3200	1.55E+13	0.00	16400.0
		Myers1965 [71]	2500-3000	3.85E+09	0.00	20100.0
R25	CO+HO_2=CO_2+OH	Klippenstein2017 [72]	300-2500	8.55E+03	2.52	7830.0
		You2007 [73]	300-2500	1.57E+05	2.18	9030.0
		Vandooren1986 [74]	1200-1600	3.50E+12	0.00	4120.0
		Atri1977 [75]	713-773	5.79E+13	0.00	11500.0
		Vardanyan1975 [76]	878-952	1.02E+14	0.00	11600.0
R26	C+OH=CO+H	Glarborg1986 [77]	300-3000	5.00E+13	0.00	0.0
R27	C+O_2=CO+O	Geppert2000 [78]	15-295	1.70E+14	-0.30	0.0
		Dorthe1991 [79]	298	9.64E+12	0.00	0.0
		Dean1991 [80]	1500-4200	1.20E+14	0.00	2010.0
		Becker1988 [81]	295	2.83E+13	0.00	0.0
		Husain1975 [82]	300	1.57E+13	0.00	0.0
		Husain1971 [83]	300	1.99E+13	0.00	0.0
		Braun1969 [84]	298	1.99E+13	0.00	0.0
		Martinotti1968 [85]	298	1.50E+12	0.00	0.0

Reaction		+M	Reference	ΔT, K	k, cm^3, s, mole, K		
					A	n	E_a, K
R28	HCO+M=H+CO+M	-	Li2007 [35]	850-950	4.750E+11	0.70	7498.0
		Ar	Baulch2005 [86]	500-2500	3.975E+13	0.00	7820.0
		He	Krasnoperov2005 [87]	498-769	4.818E+13	0.00	7938.0
		He	Krasnoperov2004 [88]	298-1229	3.613E+13	0.00	7721.5
		Ar	Friedrichs2002 [89]	835-1230	3.975E+13	0.00	7820.0
		Ar	Fredrichs2002 [89]	600-2500	4.800E+17	0.00	8924.2
		Ar	Hidaka1993 [90]	1200-1890	6.950E+17	-1.00	8554.7
		Ar	Cribb1992 [91]	1900-2700	5.000E+13	0.00	8455.1
		He	Timonen1987 [92]	637-832	2.288E+17	-1.00	8600.0
		He	Wagner1987 [93]	600-1000	1.690E+14	0.00	7950.0
		H_2	Timonen1987 [92]	300-3000	3.487E+17	-1.00	8554.7
		N_2	Timonen1987 [92]	300-3000	1.849E+17	-1.00	8554.7
		Ar	Timonen1987 [92]	300-3000	1.861E+17	-1.00	8554.7
		He	Timonen1987 [92]	300-3000	2.288E+17	-1.00	8605.0
		Ar	Dean1979 [94]	1700-2710	1.506E+14	0.00	7340.0
		Ar	Browne1969 [95]	1000-1700	7.000E+13	0.00	7548.3
R28^{-1}	H+CO+M=HCO+M	Ar	Baulch2005[86]	300-800	7.253E+12	0.200	0.0
		He	Baulch2005[86]	300-800	5.440E+11	0.600	0.0
		He	Wagner1987[93]	333-1000	5.080E+13	0.000	100.0
		CO	Hochanadel1980[96]	298	3.600E+13	0.000	0.0
		CH_4	Hochanadel1980[96]	298	5.800E+13	0.000	0.0
		H_2	Hochanadel1980[96]	298	3.800E+13	0.000	0.0
		N_2	Campbell1978[97]	425	1.440E+14	0.000	0.0
		Ar	Campbell1978[97]	425	9.710E+13	0.000	0.0
		H_2	Wang1973[98]	298-373	1.170E+15	0.000	1006.4
		H_2	Baldwin1972[19]	773	2.300E+14	0.000	0.0
		Ar	Hikida1971[99]	298	2.600E+13	0.000	0.0
		H_2	Hikida1971[99]	298	4.000E+13	0.000	0.0
R29	HCO+H=CO+H_2		Baulch2005 [86]	300-2500	9.033E+13	0.00	0.0
			Friedrichs2002 [89]	295-820	1.100E+14	0.00	0.0
			Ziemer1998 [100]	298	6.810E+13	0.00	0.0
			Hidaka1993 [90]	1200-1890	2.160E+14	0.00	0.0
			Cribb1992 [91]	1900-2700	2.000E+14	0.00	0.0
			Sarkisov1984 [101]	300	1.210E+14	0.00	0.0
			Cherian1981 [102]	250-2000	4.000E+13	0.00	0.0
			Reilly1978 [103]	298	3.310E+14	0.00	0.0
			Jachimowski1977 [104]	1820-2360	1.000E+14	0.00	0.0
			Browne1969 [95]	1000-1700	2.000E+13	0.00	0.0
R30	HCO+O=CO+OH		Baulch2005 [86]	300-2500	3.011E+13	0.00	0.0
R31	HCO+O=CO_2+H		Baulch2005 [86]	300-2500	3.011E+13	0.00	0.0
R32	HCO+OH=CO+H_2O		Baulch2005 [86]	300-2500	1.084E+14	0.00	0.0

Reaction		Reference	ΔT, K	k, cm^3, s, mole, K		
				A	n	E_a, K
-	$HCO+O_2$=products	Matsugi2014 [105]	295	3.31E+12	0.00	0.0
		DeSain2011 [106]	296-673	3.67E+12	0.00	26.0
		Baulch2005 [86]	200-2500	2.71E+10	0.68	-236.0
		Hsu1996 [107]	500-3000	1.21E+10	0.81	-366.0
		Dobe1995 [108]	298	2.60E+12	0.00	0.0
		Temps1984 [109]	296	2.70E+13	0.00	0.0
R33	$HCO+O_2=CO+HO_2$	Ryu2017 [110]	200-1760	1.90E+12	0.18	245.0
		Matsugi2014 [105]	295	3.31E+12	0.00	0.0
		DeSain2011 [106]	296-673	3.67E+12	0.00	26.0
		Colberg2006 [111]	295	3.55E+12	0.00	0.0
		Colberg2006 [111]	739-1108	3.70E+13	0.00	1563.5
		Baulch2005 [86]	200-2500	2.71E+10	0.68	-236.0
		Atkinson2001 [112]	200-400	3.13E+12	0.00	0.0
		Hanoune2001 [113]	294	3.01E+12	0.00	0.0
		Nesbitt1999 [114]	200-398	1.32E+12	0.00	-170.0
		Hsu1996 [107]	500-3000	1.21E+10	0.81	-366.0
		Dobe1994 [115]	298	4.30E+13	0.00	0.0
		Timonen1988 [116]	295-713	7.59E+12	0.00	204.5
		Vandooren1986 [74]	300-1600	2.70E+13	0.00	600
		Temps1984 [109]	296	3.10E+12	0.00	0.0
		Sarkisov1984 [101]	300	2.29E+12	0.00	0.0
		Langford1984 [117]	295	2.80E+12	0.00	0.0
		Cherian1981 [102]	250-2000	3.50E+12	0.00	0.0
		Veyret1981 [118]	298-503	3.31E+13	-0.40	0.0
		Gill1981 [119]	298	2.53E+12	0.00	0.0
		Clark1978 [120]	298	2.41E+12	0.00	0.0
		Shibuya1977 [121]	298	2.41E+12	0.00	0.0
		Washida1974 [122]	298	3.37E+12	0.00	0.0
		Vardanyan1971 [123]	295-713	7.58E+12	0.00	204.5
R34	$HCO+HO_2$=>CO_2+OH+H	Tsang1986 [124]	300-2500	3.00E+13	0.00	0.0
-	HCO+HCO=product	Baulch2005 [86]	230-1000	3.01E+13	0.00	0.0
		Hochanadel1980 [96]	298	1.81E+13	0.00	0.0
		Temps1984 [109]	296	2.70E+13	0.00	0.0
R35	HCO+HCO=>CO+CO+H_2	Hochanadel1980 [96]	298	5.19E+12	0.00	0.0

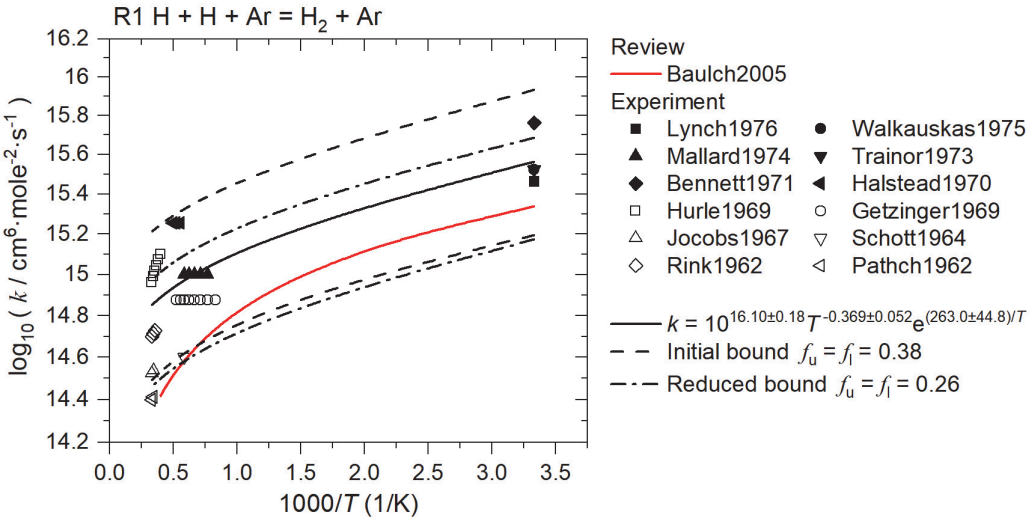

Fig. S1-1. (R1) H + H + Ar = H_2 + Ar [86, 125-135]

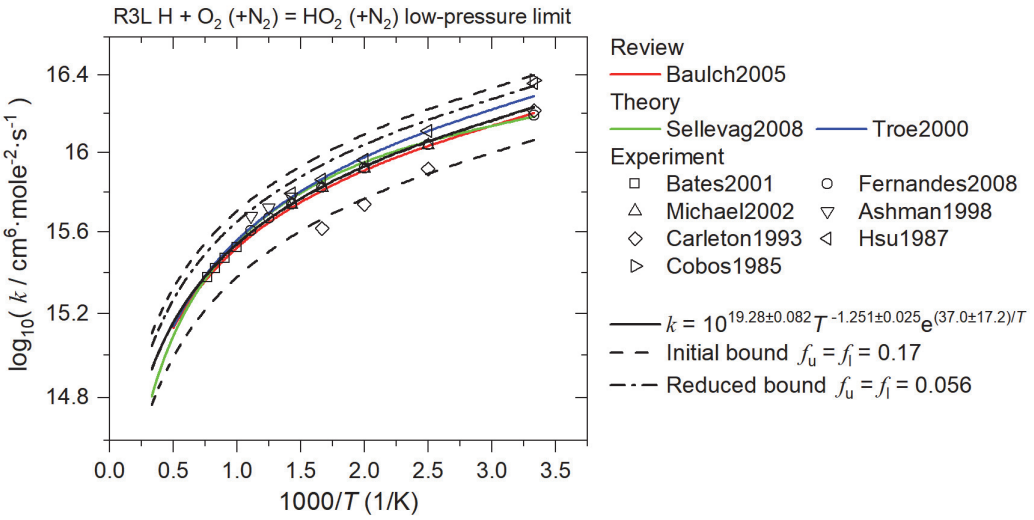

Fig. S1-2. (R3L) H + O_2 (+N_2) = HO_2 (+N_2) low-pressure limit [86, 136-144]

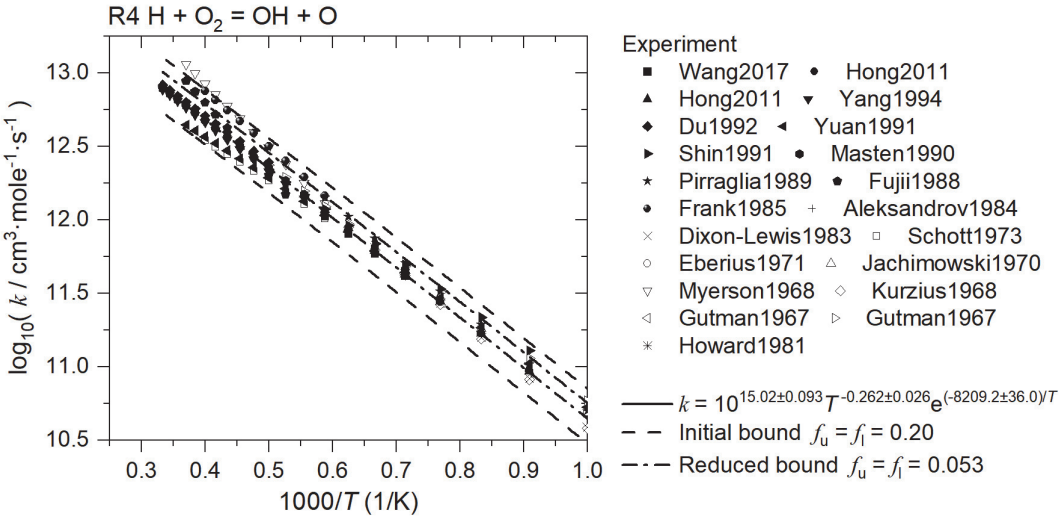

Fig. S1-3. (R4) H + O_2 = OH + O [145-162]

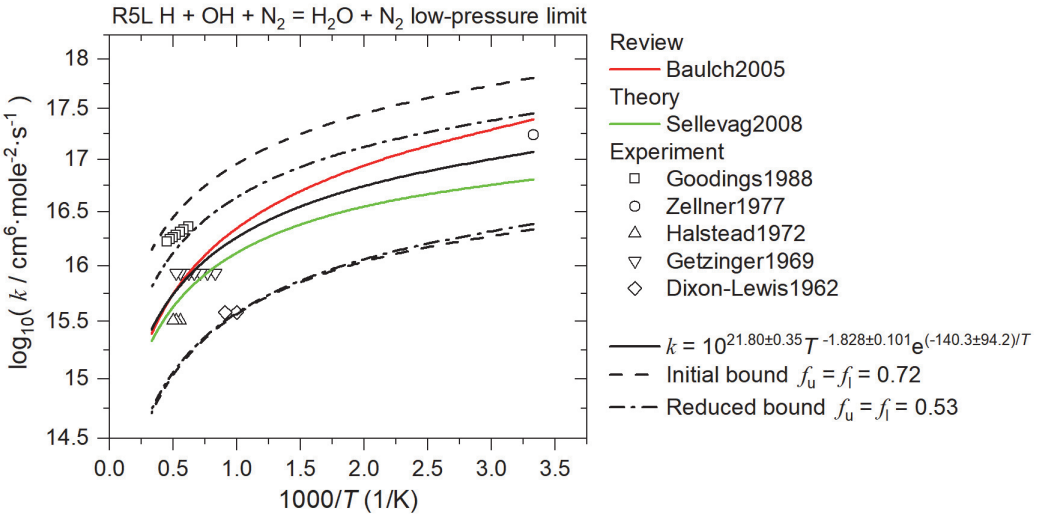

Fig. S1-4. (R5L) H + OH (+N_2) = H_2O (+N_2) low-pressure limit [86, 130, 132, 136, 163-166]

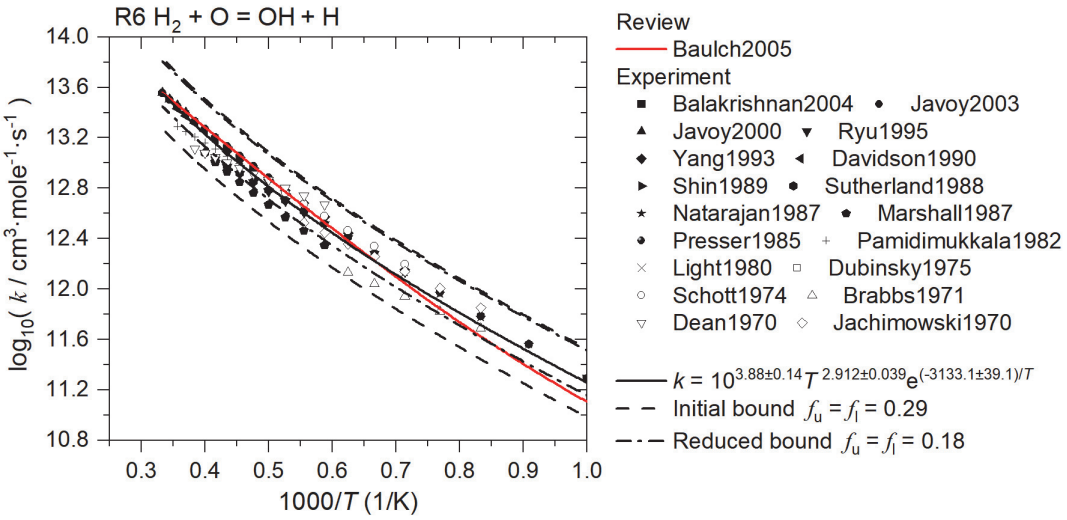

Fig. S1-5. (R6) H_2 + O = OH + H [54, 55, 159, 167-181]

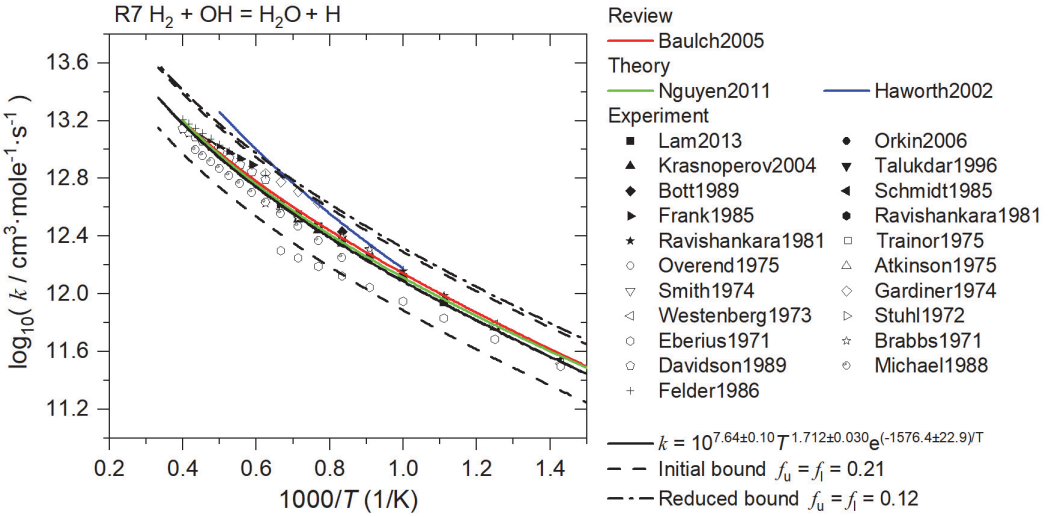

Fig. S1-6. (R7) H_2 + OH = H_2O + H [54, 86, 154, 158, 182-197]

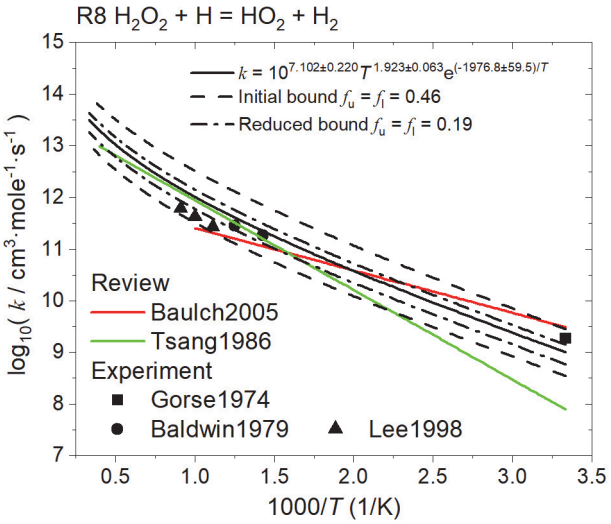

Fig. S1-7. (R8) H_2O_2 + H = HO_2 + H_2 [86, 124, 198-200]

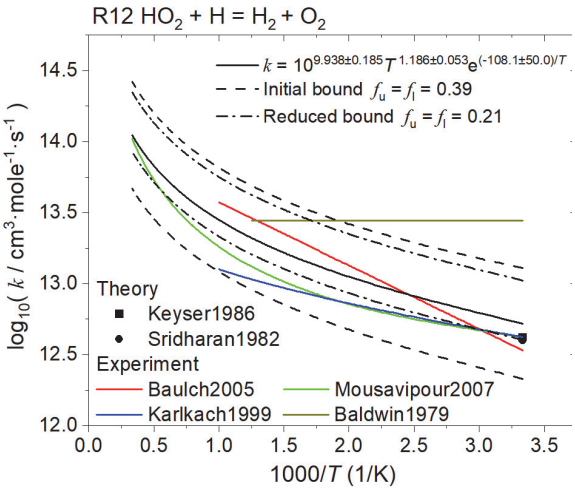

Fig. S1-8. (R12) HO_2 + H = H_2 + O_2 [86, 199, 201-204]

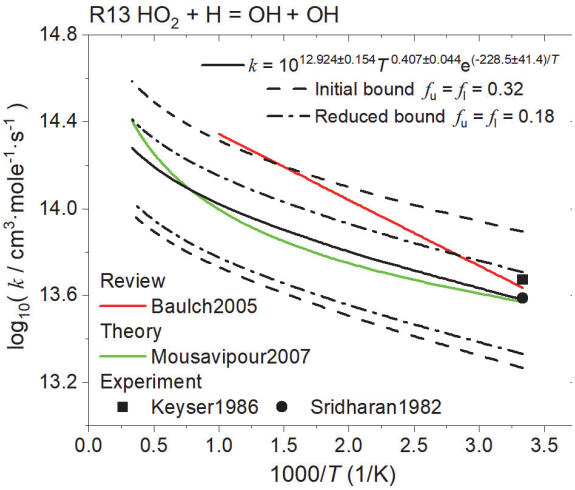

Fig. S1-9. (R13) HO_2 + H = OH + OH [86, 201, 203, 204]

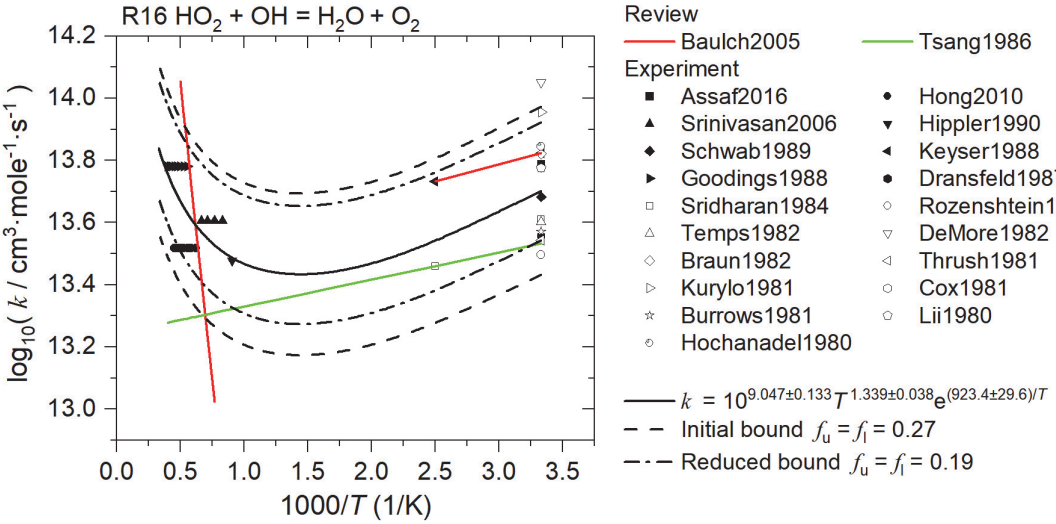

Fig. S1-10. (R16) HO_2 + OH = H_2O + O_2 [86, 124, 163, 205-222]

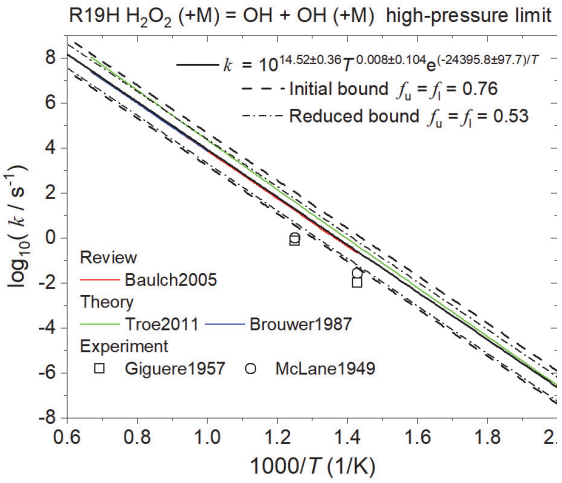

Fig. S1-11. (R19H) H_2O_2 (+M) = OH + OH (+M) high-pressure limit [86, 223-226]

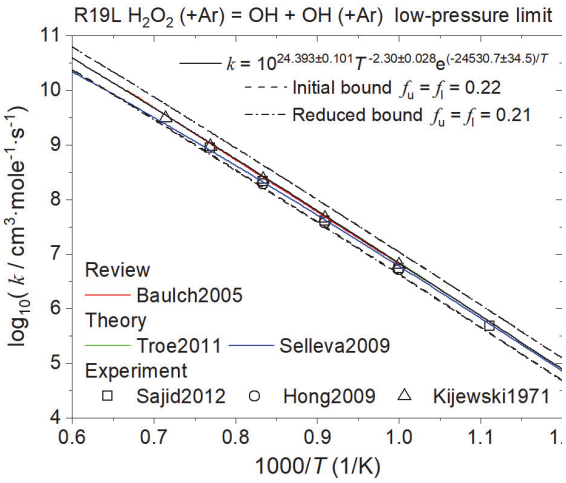

Fig. S1-12. (R19L) H_2O_2 (+Ar) = OH + OH (+Ar) low-pressure limit [86, 223, 227-229]

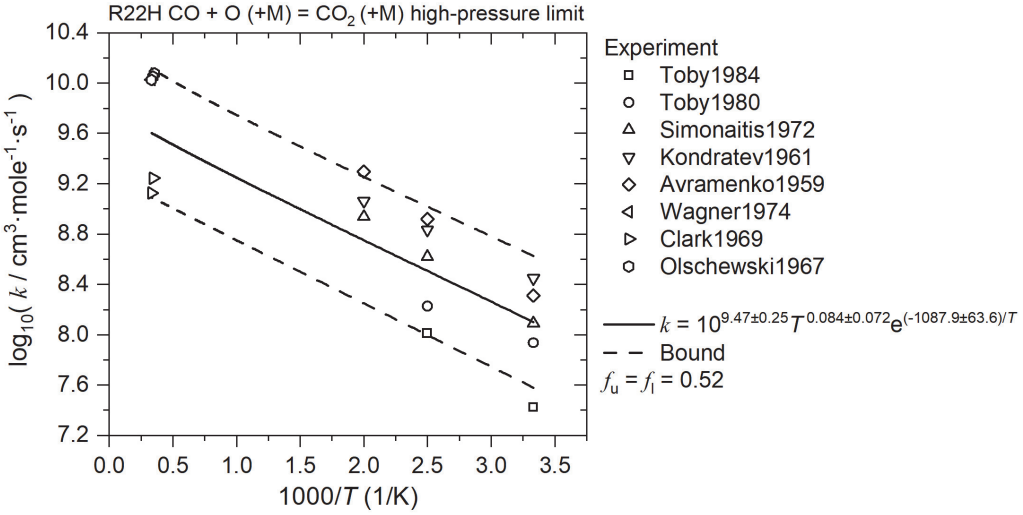

Fig. S1-13. (R22H) CO + O (+M) = CO2 (+M) high-pressure limit [1-8]

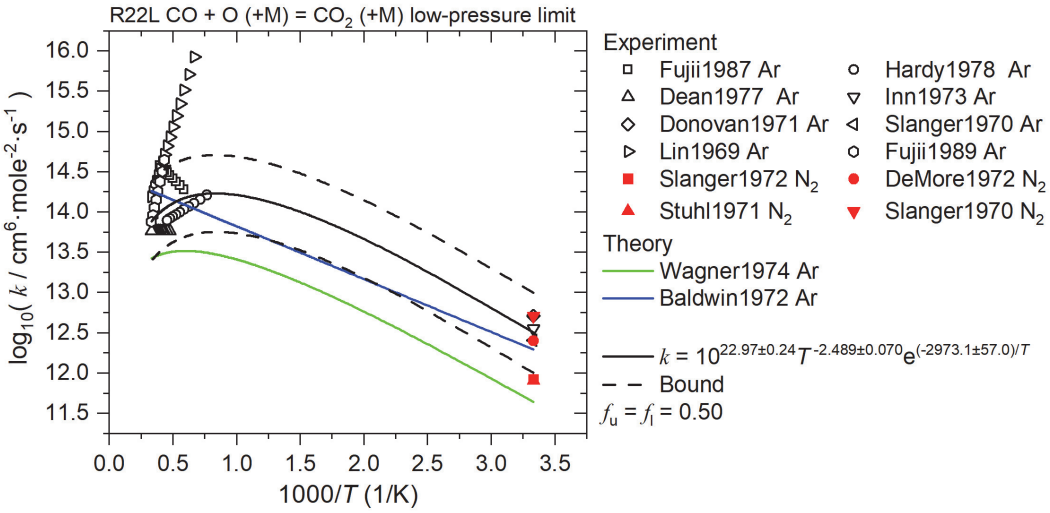

Fig. S1-14. (R22L) CO + O (+M) = CO_2 (+M) low-pressure limit [6, 9, 13, 14, 16, 17, 19, 20, 22, 23]

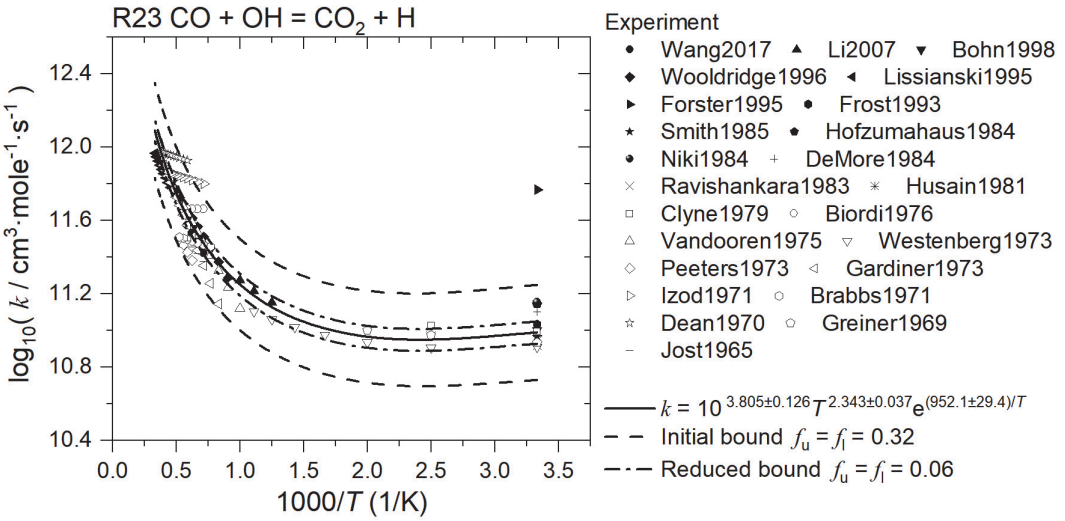

Fig. S1-15. (R23) CO + OH = CO_2 + H [34-57]

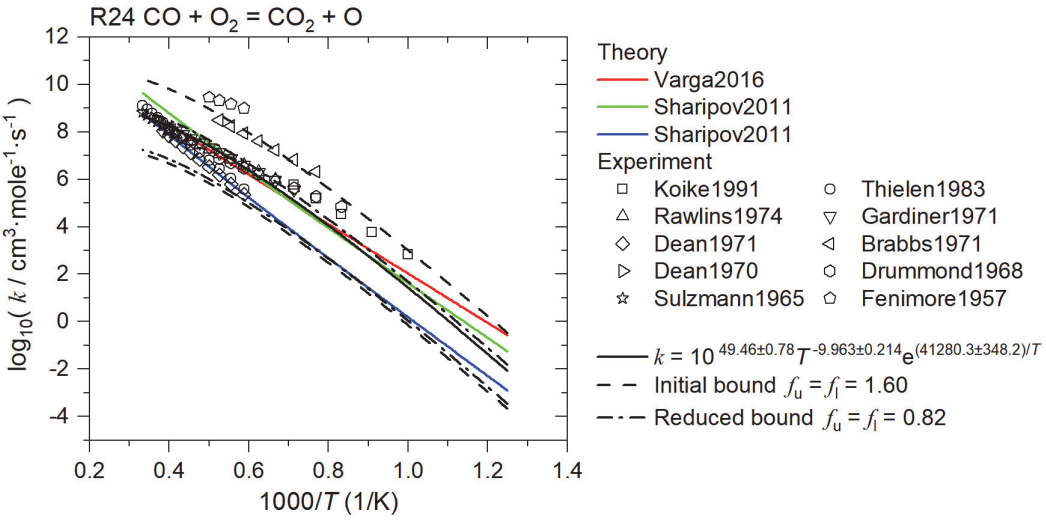

Fig. S1-16. (R24) CO + O_2 = CO_2 + O [54, 55, 62-69]

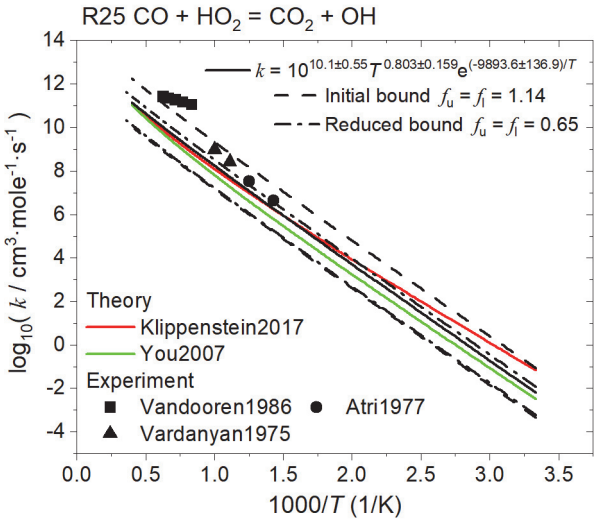

Fig. S1-17. (R25) CO + HO_2 = CO_2 + OH [72-76]

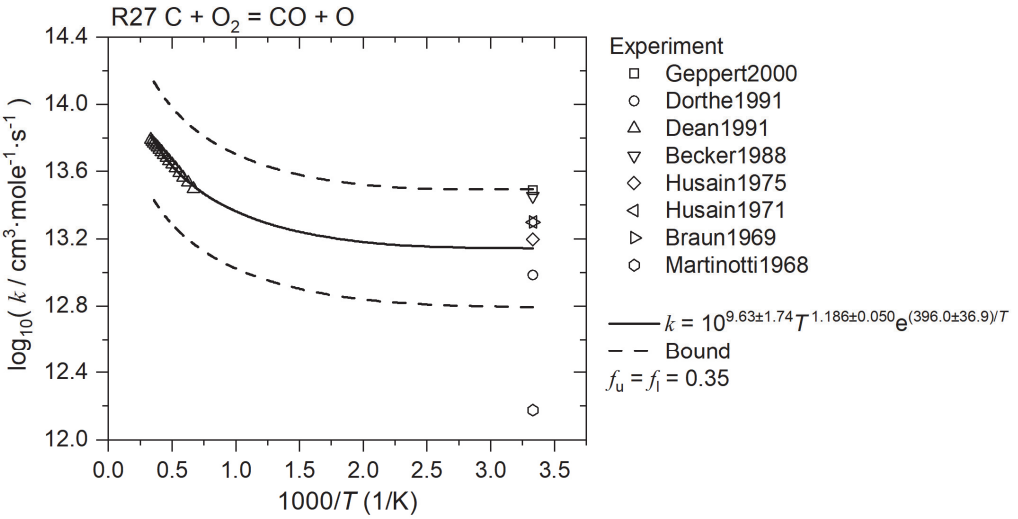

Fig. S1-18. (R27) C + O_2 = CO + O [78-85]

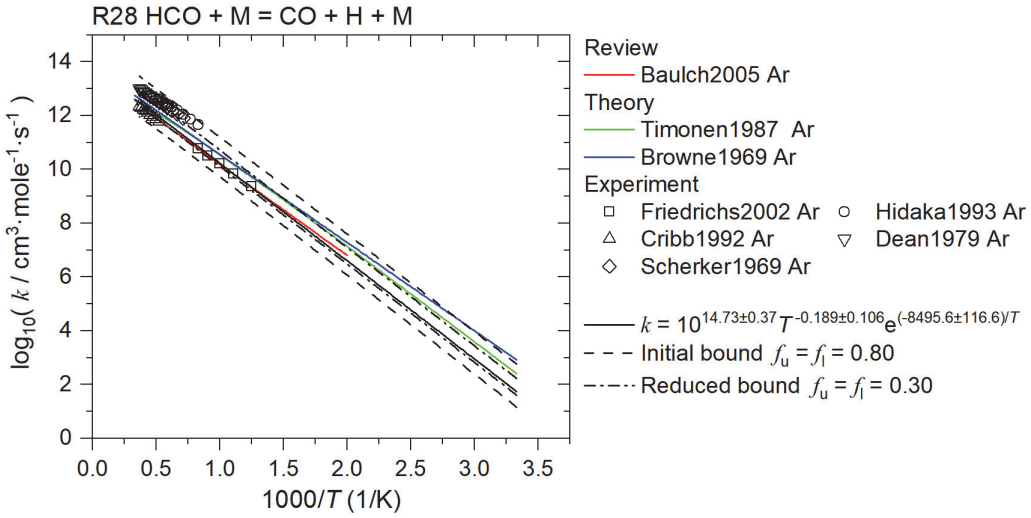

Fig. S1-19. (R28) HCO + M = H + CO + M [86, 89-92, 94, 95]

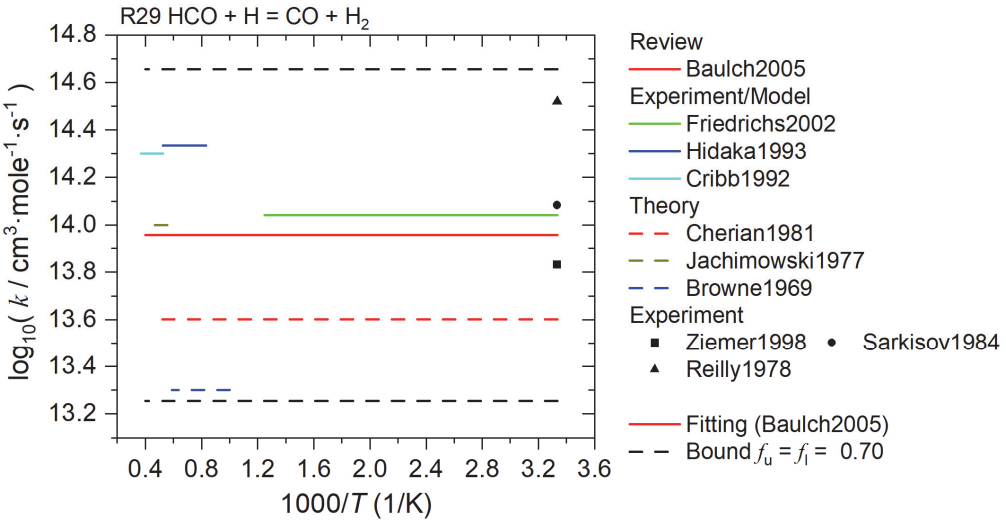

Fig. S1-20. (R29) HCO + H = CO + H_2 [86, 89-91, 95, 100-104]

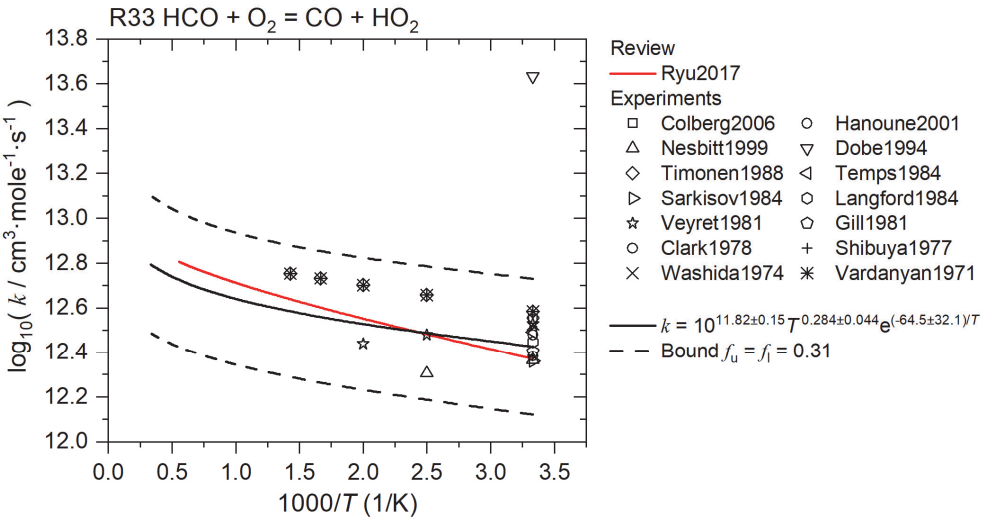

Fig. S1-21. (R33) HCO + O_2 = CO + HO_2 [74, 86, 101, 102, 105-107, 109-123]

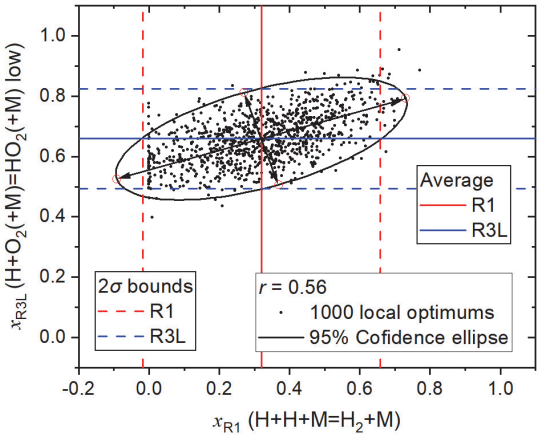

Fig. S1-22. R1-R3L

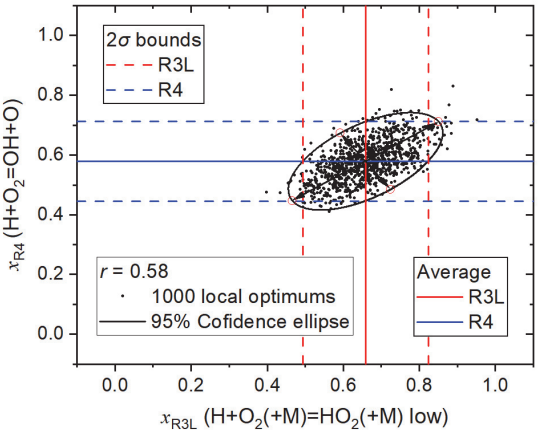

Fig. S1-23. R3L-R4

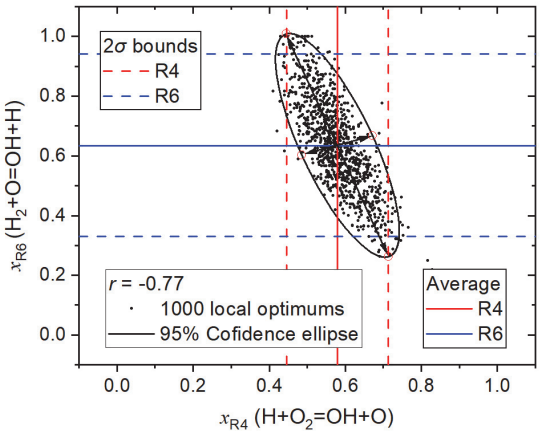

Fig. S1-24. R4-R6

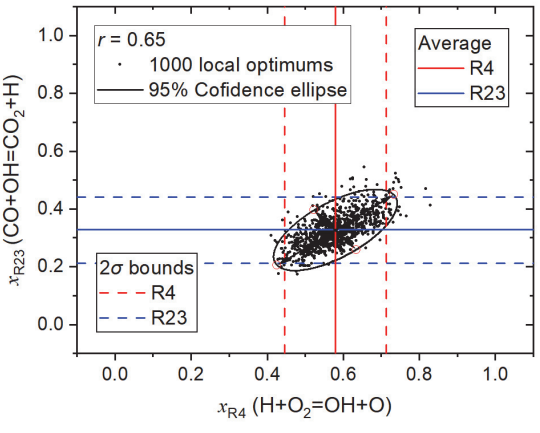

Fig. S1-25. R4-R23

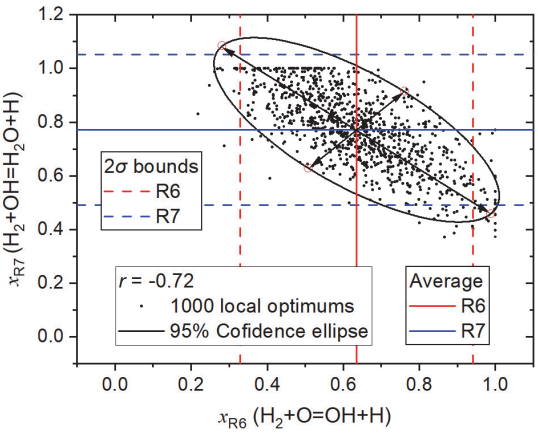

Fig. S1-26. R6-R7

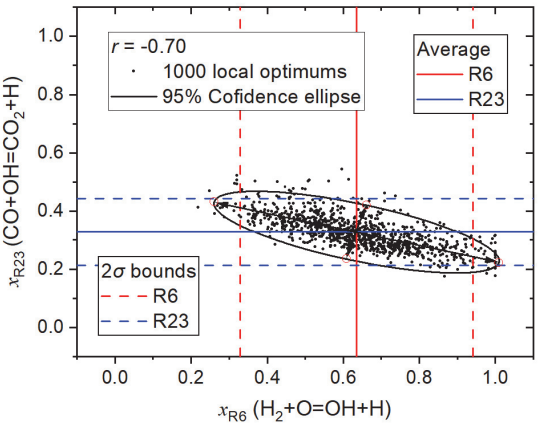

Fig. S1-27. R6-R23

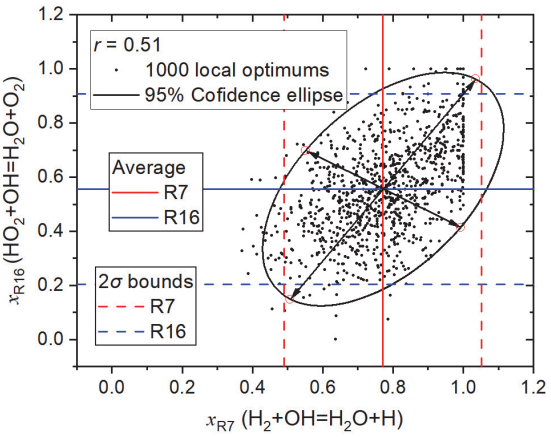

Fig. S1-28. R7-R16

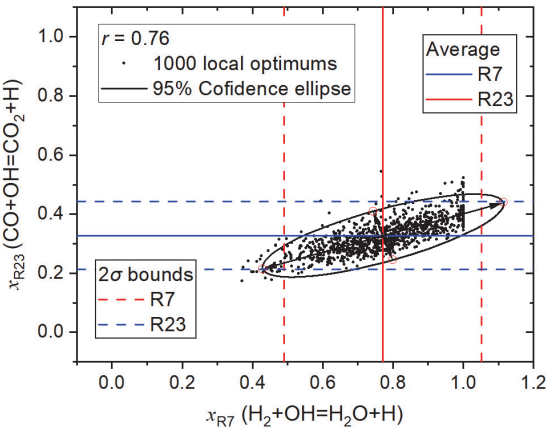

Fig. S1-29. R7-R23

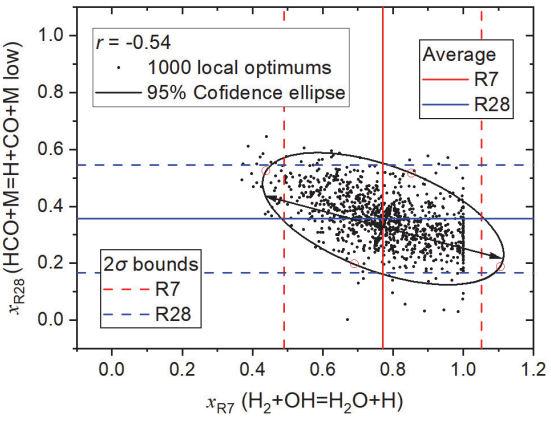

Fig. S1-30. R7-R28

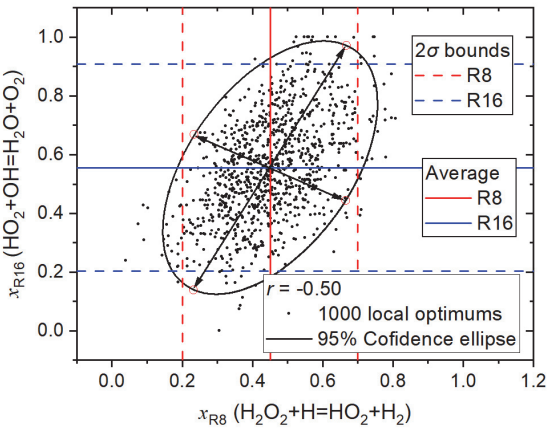

Fig. S1-31. R8-R16

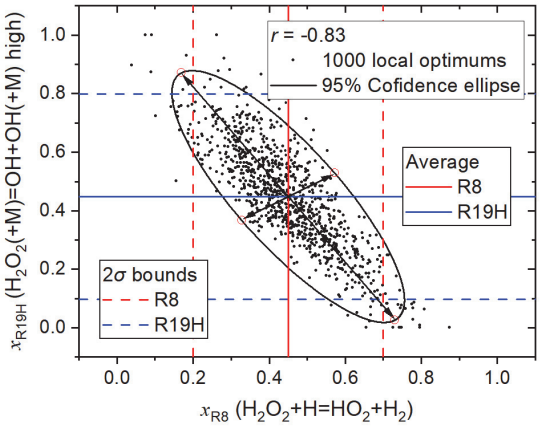

Fig. S1-32. R8-R19H

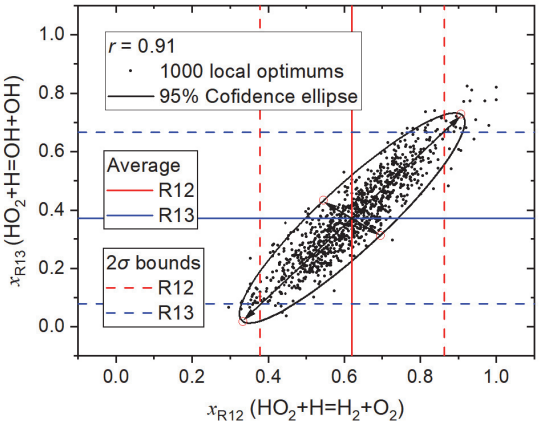

Fig. S1-33. R12-R13

Reference

[1] Toby S, Sheth S, Toby FS. Reaction of carbon monoxide with ozone and oxygen atoms. International Journal of Chemical Kinetics 1984;16(2):149-57.

[2] Toby S, Ullrich E. Reaction of carbon monoxide with ozone: Kinetics and chemiluminescence. International Journal of Chemical Kinetics 1980;12(8):535-46.

[3] Simonaitis R, Heicklen J. Kinetics and Mechanism of the Reaction of O(3P) with Carbon Monoxide. The Journal of Chemical Physics 1972;56(5):2004-11.

[4] Kondrat'ev V, Ptichkin I. Gas-Phase Interaction Between Carbon Monoxide and Ozonized Oxygen. Kinetika i Kataliz 1961;2:449-52.

[5] Avramenko LI, Kolesnikova RV. Kinetics and mechanism of the reaction of oxygen atoms with carbon monoxide. Bulletin of the Academy of Sciences of the USSR, Division of chemical science 1959;8(9):1506-13.

[6] Hardy W, Vasatko H, Wagner H, Zabel F. Neuere Untersuchungen zum thermischen Zerfall von CO2. Teil II. 1974.

[7] Clark TC, Garnett SH, Kistiakowsky GB. Reaction of Carbon Dioxide with Atomic Oxygen and the Dissociation of Carbon Dioxide in Shock Waves. The Journal of Chemical Physics 1969;51(7):2885-91.

[8] Olschewski HA, Troe J, Wagner HG. Studies of unimolecular reactions of triatomic molecules. Symposium (International) on Combustion 1967;11(1):155-61.

[9] Fujii N, Kakuda T, Takeishi N, Miyama H. Kinetics of the high temperature reaction of carbon monoxide with nitrous oxide. The Journal of Physical Chemistry 1987;91(8):2144-8.

[10] Fujii N, Kakuda T, Sugiyama T, Miyama H. Direct determination of the rate constant for the reaction CO + N2O → CO2 + N2. Chemical Physics Letters 1985;122(5):489-92.

[11] TOBY S, SHETH S, TOBY FS. Reaction of Carbon Monoxide with Oxygen Atoms from the Thermal Decomposition of Ozone: Effect of Added Gases. ACS Publications; 1984.

[12] Ko-ichi S, Yo-ichi I, Shin S. Absolute Rate Constants for the Reactions of O(3P) with Several Molecules. Bulletin of the Chemical Society of Japan 1980;53(5):1344-51.

[13] Hardy JE, Gardiner Jr. WC, Burcat A. Recombination of carbon monoxide and oxygen atoms. International Journal of Chemical Kinetics 1978;10(5):503-17.

[14] Dean AM, Steiner DC. A shock tube study of the recombination of carbon monoxide and oxygen atoms. The Journal of Chemical Physics 1977;66(2):598-604.

[15] Inn ECY. Rate of recombination of oxygen atoms and CO at temperatures below ambient. The Journal

of Chemical Physics 1974;61(4):1589-90.

[16] Inn ECY. Rate constant for the reaction CO(1Σ+) + O(3P) + CO2 → 2CO2. The Journal of Chemical Physics 1973;59(10):5431-3.

[17] Slanger TG, Wood BJ, Black G. Kinetics of O(3P) +CO +M Recombination. The Journal of Chemical Physics 1972;57(1):233-8.

[18] DeMore WB. Pressure dependence and mechanism of the reaction of atomic oxygen and carbon monoxide. The Journal of Physical Chemistry 1972;76(24):3527-32.

[19] Baldwin RR, Jackson D, Melvin A, Rossiter BN. The second limit of hydrogen + carbon monoxide + oxygen mixtures. International Journal of Chemical Kinetics 1972;4(3):277-92.

[20] Stuhl F, Niki H. Measurements of Rate Constants for Termolecular Reactions of O(3P) with NO, O2, CO, N2, and CO2 Using a Pulsed Vacuum-uv Photolysis—Chemiluminescent Method. The Journal of Chemical Physics 1971;55(8):3943-53.

[21] Donovan RJ, Husain D, Kirsch LJ. Reactions of oxygen atoms. Part 3.—Reaction of O(23PJ) and O(21D2) with CO and CO2. Transactions of the Faraday Society 1971;67(0):375-81.

[22] Slanger TG, Black G. Reaction Rate Measurements of O(3P) Atoms by Resonance Fluorescence. II O(3P)+CO+M→CO2+M; M=He, Ar, N2. The Journal of Chemical Physics 1970;53(9):3722-5.

[23] Lin MC, Bauer SH. Bimolecular Reaction of N2O with CO and the Recombination of O and CO as Studied in a Single-Pulse Shock Tube. The Journal of Chemical Physics 1969;50(8):3377-91.

[24] Kondratiev VN, Intezarova EI. Interaction between CO and O. International Journal of Chemical Kinetics 1969;1(1):105-11.

[25] Olschewski HA, Troe J, Wagner HG. Untersuchung unimolekularer Reaktionen bei hohen Drucken in Stoßwellen: Zerfall von CS2 und CO2. Berichte der Bunsengesellschaft für physikalische Chemie 1966;70(9-10):1060-4.

[26] Eremin A, Ziborov V, Shumova V, Voiki D, Roth P. Formation of O(1D) atoms in thermal decomposition of CO2. Kinetics and Catalysis 1997;38:1-7.

[27] Burmeister M, Roth P. ARAS measurements on the thermal decomposition of CO2 behind shock waves. AIAA Journal 1990;28(3):402-5.

[28] Fujii N, Sagawai S, Sato T, Nosaka Y, Miyama H. Study of the thermal dissociation of nitrous oxide and carbon dioxide using oxygen(3P) atomic resonance absorption spectroscopy. The Journal of Physical Chemistry 1989;93:5474-8.

[29] Ebrahim NA, Sandeman RJ. Interferometric studies of carbon dioxide dissociation in a free-piston shock tube. The Journal of Chemical Physics 1976;65(9):3446-53.

[30] Hardy W, Vasatko H, Wagner H, Zabel F. Neuere Untersuchungen zum thermischen Zerfall von CO2 1. Teil. Berichte der Bunsengesellschaft für physikalische Chemie 2010;78:76-82.

[31] Fishburne ES, Bilwakesh KR, Edse R. Gaseous Reaction Rates at High Temperature. I. The Dissociation of Carbon Dioxide. The Journal of Chemical Physics 1966;45(1):160-6.

[32] Michel KW, Olschewski HA, Richtering H, Wagner HG. Untersuchung des thermischen Zerfalls von CO2 in Stoßwellen. Zeitschrift für Physikalische Chemie 1965;44(3_4):160-72.

[33] Brabbs TA, Belles FE, Zlatarich SA. Shock-Tube Study of Carbon Dioxide Dissociation Rate. The Journal of Chemical Physics 1963;38(8):1939-44.

[34] Wang S, Davidson DF, Hanson RK. Shock Tube and Laser Absorption Study of CH2O Oxidation via Simultaneous Measurements of OH and CO. The Journal of Physical Chemistry A 2017;121(45):8561-8.

[35] Li J, Zhao Z, Kazakov A, Chaos M, Dryer F, Jr J. A comprehensive kinetic mechanism for CO, CH2O, and CH3OH combustion. International Journal of Chemical Kinetics 2007;39:109-36.

[36] Wooldridge MS, Hanson RK, Bowman CT. A shock tube study of CO + OH → CO2 + H and HNCO + OH → products via simultaneous laser absorption measurements of OH and CO2. International Journal of Chemical Kinetics 1996;28(5):361-72.

[37] Bohn B, Zetzsch C. Formation of HO2 from OH and C2H2 in the presence of O2. Journal of the Chemical Society, Faraday Transactions 1998;94(9):1203-10.

[38] Lissianski V, Yang H, Qin Z, Mueller MR, Shin KS, Gardiner WC. High-temperature measurements of the rate coefficient of the H + CO2 → CO + OH reaction. Chemical Physics Letters 1995;240(1):57-62.

[39] Forster R, Frost M, Fulle D, Hamann HF, Hippler H, Schlepegrell A, et al. High pressure range of the addition of HO to HO, NO, NO2, and CO. I. Saturated laser induced fluorescence measurements at 298 K. The Journal of Chemical Physics 1995;103(8):2949-58.

[40] Frost MJ, Sharkey P, Smith IWM. Reaction between hydroxyl (deuteroxyl) radicals and carbon monoxide at temperatures down to 80 K: experiment and theory. The Journal of Physical Chemistry 1993;97(47):12254-9.

[41] Smith IW, Williams MD. Kinetics of OH (v= 0 and 1) and OD (v= 0 and 1) Studied by Time-Resolved Laser-Induced Fluorescence. Berichte der Bunsengesellschaft für physikalische Chemie 1985;89(3):319-20.

[42] Niki H, Maker P, Savage C, Breitenbach L. Fourier transform infrared spectroscopic study of the kinetics for the hydroxyl radical reaction of 13C16O-carbon monoxide and 12C18O-carbon monoxide. The Journal of Physical Chemistry 1984;88(10):2116-9.

[43] Hofzumahaus A, Stuhl F. Rate constant of the reaction HO+ CO in the presence of N2 and O2. Berichte der Bunsengesellschaft für physikalische Chemie 1984;88(6):557-61.

[44] DeMore W. Rate constant for the OH+ CO reaction: Pressure dependence and the effect of oxygen. International journal of chemical kinetics 1984;16(10):1187-200.

[45] Ravishankara A, Thompson R. Kinetic study of the reaction of OH with CO from 250 to 1040 K. Chemical physics letters 1983;99(5-6):377-81.

[46] Husain D, Plane JM, Slater NK. Kinetic investigation of the reactions of OH (X 2 Π) with the hydrogen halides, HCl, DCl, HBr and DBr by time-resolved resonance fluorescence (A 2∑+–X 2 Π). Journal of the Chemical Society, Faraday Transactions 2: Molecular and Chemical Physics 1981;77(10):1949-62.

[47] Clyne MA, Holt PM. Reaction kinetics involving ground X 2 Π and excited A 2 Σ+ hydroxyl radicals. Part 1.—Quenching kinetics of OH A 2 Σ+ and rate constants for reactions of OH X 2 Π with CH 3 CCl 3 and CO. Journal of the Chemical Society, Faraday Transactions 2: Molecular and Chemical Physics 1979;75:569-81.

[48] Biordi JC, Lazzara CP, Papp JF. Molecular beam mass spectrometry applied to determining the kinetics of reactions in flames II. A critique of rate coefficient determinations. Combustion and Flame 1976;26:57-76.

[49] Vandooren J, Peeters J, Van Tiggelen P. Rate constant of the elementary reaction of carbon monoxide with hydroxyl radical. *Symposium (International) on Combustion.* 15. Elsevier; 1975:745-53.

[50] Westenberg A, DeHaas N. Rates of CO+ OH and H2+ OH over an extended temperature range. The Journal of Chemical Physics 1973;58(10):4061-5.

[51] Peeters J, Mahnen G. Reaction mechanisms and rate constants ofelementary steps in methane-oxygen flames. *Symposium (International) on Combustion.* 14. Elsevier; 1973:133-46.

[52] Gardiner Jr W, Mallard W, McFarland M, Morinaga K, Owen J, Rawlins W, et al. Elementary reaction rates from post-induction-period profiles in shock-initiated combustion. *Symposium (International) on Combustion.* 14. Elsevier; 1973:61-75.

[53] Izod T, Kistiakowsky G, Matsuda S. Oxidation of carbon monoxide mixtures with added ethane or

azomethane studied in incident shock waves. The Journal of Chemical Physics 1971;55(9):4425-32.

[54] Brabbs T, Belles F, Brokaw R. Shock-tube measurements of specific reaction rates in the branched-chain H2-CO-O2 system. *Symposium (International) on Combustion.* 13. Elsevier; 1971:129-36.

[55] Dean A, Kistiakowsky G. Oxidation of carbon monoxide by oxygen in shock waves. The Journal of Chemical Physics 1970;53(2):830-8.

[56] Greiner N. Hydroxyl radical kinetics by kinetic spectroscopy. V. Reactions with H2 and CO in the Range 300–500 K. The Journal of Chemical Physics 1969;51(11):5049-51.

[57] Jost W, Schecker HG, Wagner HG. Messungen der Geschwindigkeit der Einstellung des Wassergas-Gleichgewichtes. Zeitschrift für Physikalische Chemie 1965;45(1_2):47-57.

[58] Wawer A, Zielinski M. A study of carbon-14 transport in the three-component system: 14 CO 2-CO-H 2. Nukleonika 1978;23(9):903-10.

[59] Shub F, Apel'baum L, Temkin M. Kinetics of the homogeneous water gas reaction. Kinet Catal(Engl Transl);(United States) 1970;11(3).

[60] Kochubei V, Moin F. Kinetics of the reaction of CO2 with hydrogen. Kinetika i Kataliz 1969;10:992.

[61] Fenimore C, Jones C. The Reaction of Hydrogen Atoms with Carbon Dioxide at 1200–1350° K. The Journal of Physical Chemistry 1958;62(12):1578-81.

[62] Sharipov A, Starik A. Theoretical study of the reaction of carbon monoxide with oxygen molecules in the ground triplet and singlet delta states. The Journal of Physical Chemistry A 2011;115(10):1795-803.

[63] Thielen K, Roth P. Stoßtwellenuntersuchungen zum Start der Reaktion CO+ O2. Berichte der Bunsengesellschaft für physikalische Chemie 1983;87(10):920-5.

[64] Rawlins W, Gardiner Jr W. Rate constant for carbon monoxide+ molecular oxygen= carbon dioxide+ atomic oxygen from 1500 to 2500. deg. K. Reevaluation of induction times in the shock-initiated combustion of hydrogen-oxygen-carbon monoxide-argon mixtures. The Journal of Physical Chemistry 1974;78(5):497-500.

[65] Gardiner Jr W, McFarland M, Morinaga K, Takeyama T, Walker BF. Initiation rate for shock-heated hydrogen-oxygen-carbon monoxide-argon mixtures as determined by OH induction time measurements. The Journal of Physical Chemistry 1971;75(10):1504-9.

[66] Dean A, Kistiakowsky G. Oxidation of carbon monoxide/methane mixtures in shock waves. The Journal of Chemical Physics 1971;54(4):1718-25.

[67] Drummond L. Shock-initiated exothermic reactions. IV. The oxidation of carbon monoxide. Australian Journal of Chemistry 1968;21(11):2631-40.

[68] Sulzmann K, Myers B, Bartle E. CO Oxidation. I. Induction Period Preceding CO2 Formation in Shock-Heated CO–O2–Ar Mixtures. The Journal of Chemical Physics 1965;42(11):3969-79.

[69] Fenimore C, Jones G. The water-catalyzed oxidation of carbon monoxide by oxygen at high temperature. The Journal of Physical Chemistry 1957;61(5):651-4.

[70] Ibragimova L. Recommended rate constants of CO+ O2-reversible-CO2+ O reactions. KHIMICHESKAYA FIZIKA 1991;10(3):307-10.

[71] Myers B, Sulzmann K, Bartle E. Oxidation of CO. II. Influence of H2 on the Induction Period Preceding Rapid CO2 Formation in Shock-Heated CO–O2–Ar Mixtures. The Journal of Chemical Physics 1965;43(4):1220-8.

[72] Klippenstein SJ. From theoretical reaction dynamics to chemical modeling of combustion. Proceedings of the Combustion Institute 2017;36(1):77-111.

[73] You X, Wang H, Goos E, Sung C-J, Klippenstein SJ. Reaction kinetics of CO+ HO2→ products: ab initio transition state theory study with master equation modeling. The Journal of Physical Chemistry A 2007;111(19):4031-42.

[74] Vandooren J, de Guertechin LO, Van Tiggelen P. Kinetics in a lean formaldehyde flame. Combustion and flame 1986;64(2):127-39.

[75] Atri G, Baldwin R, Jackson D, Walker R. The reaction of OH radicals and HO2 radicals with carbon monoxide. Combustion and Flame 1977;30:1-12.

[76] Vardanyan I, Sachyan G, Nalbandyan A. The rate constant of the reaction HO2+ CO CO2+ OH. International Journal of Chemical Kinetics 1975;7(1):23-31.

[77] Glarborg P, Miller JA, Kee RJ. Kinetic modeling and sensitivity analysis of nitrogen oxide formation in well-stirred reactors. Combustion and flame 1986;65(2):177-202.

[78] Geppert WD, Reignier D, Stoecklin T, Naulin C, Costes M, Chastaing D, et al. Comparison of the cross-sections and thermal rate constants for the reactions of C (3 PJ) atoms with O 2 and NO. Physical Chemistry Chemical Physics 2000;2(13):2873-81.

[79] Dorthe G, Caubet P, Vias T, Barrere B, Marchais J. Fast flow studies of atomic carbon kinetics at room temperature. The Journal of Physical Chemistry 1991;95(13):5109-16.

[80] Dean A, Davidson D, Hanson R. A shock tube study of reactions of C atoms with H2 and O2 using excimer photolysis of C3O2 and C atom atomic resonance absorption spectroscopy. Journal of physical chemistry (1952) 1991;95(1):183-91.

[81] Becker KH, Brockmann KJ, Wiesen P. Spectroscopic identification of C (3 P) atoms in halogenomethane+ H flame systems and measurements of C (3 P) reaction rate constants by two-photon laser-induced fluorescence. Journal of the Chemical Society, Faraday Transactions 2: Molecular and Chemical Physics 1988;84(5):455-61.

[82] Husain D, Young AN. Kinetic investigation of ground state carbon atoms, C (2 3 Pj). Journal of the Chemical Society, Faraday Transactions 2: Molecular and Chemical Physics 1975;71:525-31.

[83] Husain D, Kirsch L. Reactions of atomic carbon C (2 3 PJ) by kinetic absorption spectroscopy in the vacuum ultra-violet. Transactions of the Faraday Society 1971;67:2025-35.

[84] Braun W, Bass A, Davis D, Simmons JD. Flash photolysis of carbon suboxide: absolute rate constants for reactions of C (3P) and C (1D) with H2, N2, CO, NO, O2 and CH4. Proceedings of the Royal Society of London A Mathematical and Physical Sciences 1969;312(1510):417-34.

[85] Martinotti FF, Welch MJ, Wolf AP. The reactivity of thermal carbon atoms in the gas phase. Chemical Communications (London) 1968(3):115-6.

[86] Baulch DL, Bowman CT, Cobos CJ, Cox RA, Just T, Kerr JA, et al. Evaluated Kinetic Data for Combustion Modeling: Supplement II. Journal of Physical and Chemical Reference Data 2005;34(3):757-1397.

[87] Krasnoperov L, Chesnokov E, Stark H, Ravishankara A. Elementary reactions of formyl (HCO) radical studied by laser photolysis—transient absorption spectroscopy. Proceedings of the Combustion Institute 2005;30(1):935-43.

[88] Krasnoperov LN, Chesnokov EN, Stark H, Ravishankara A. Unimolecular dissociation of formyl radical, HCO→ H+ CO, studied over 1− 100 bar pressure range. The Journal of Physical Chemistry A 2004;108(52):11526-36.

[89] Friedrichs G, Herbon JT, Davidson DF, Hanson RK. Quantitative detection of HCO behind shock waves: The thermal decomposition of HCO. Physical Chemistry Chemical Physics 2002;4(23):5778-88.

[90] Hidaka Y, Taniguchi T, Kamesawa T, Masaoka H, Inami K, Kawano H. High temperature pyrolysis of formaldehyde in shock waves. International journal of chemical kinetics 1993;25(4):305-22.

[91] Cribb PH, Dove JE, Yamazaki S. A kinetic study of the pyrolysis of methanol using shock tube and computer simulation techniques. Combustion and flame 1992;88(2):169-85.

[92] Timonen RS, Ratajczak E, Gutman D, Wagner AF. The addition and dissociation reaction atomic

hydrogen+ carbon monoxide. dblharw. oxomethyl. 2. Experimental studies and comparison with theory. Journal of Physical Chemistry 1987;91(20):5325-32.

[93] Wagner AF, Bowman JM. The addition and dissociation reaction atomic hydrogen+ carbon monoxide. dblharw. oxomethyl. 1. Theoretical RRKM studies. Journal of Physical Chemistry 1987;91(20):5314-24.

[94] Dean AM, Craig BL, Johnson RL, Schultz MC, Wang EE. Shock tube studies of formaldehyde pyrolysis. *Symposium (International) on Combustion.* 17. Elsevier; 1979:577-86.

[95] Browne W, Porter R, Verlin J, Clark A. A study of acetylene-oxygen flames. *Symposium (international) on combustion.* 12. Elsevier; 1969:1035-47.

[96] Hochanadel C, Sworski T, Ogren P. Ultraviolet spectrum and reaction kinetics of the formyl radical. The Journal of Physical Chemistry 1980;84(3):231-5.

[97] Campbell IM, Handy BJ. Studies of reactions of atoms in a discharge flow stirred reactor. Part 2.—O+ H 2+ CO system. Journal of the Chemical Society, Faraday Transactions 1: Physical Chemistry in Condensed Phases 1978;74:316-25.

[98] Wang H, Eyre J, Dorfman LM. Activation energy for the gas phase reaction of hydrogen atoms with carbon monoxide. The Journal of Chemical Physics 1973;59(9):5199-200.

[99] Hikida T, Eyre J, Dorfman LM. Pulse radiolysis studies. XX. Kinetics of some addition reactions of gaseous hydrogen atoms by fast lyman-α absorption spectrophotometry. The Journal of Chemical Physics 1971;54(8):3422-8.

[100] Ziemer H, Dobe S, Wagner HG, Olzman M, Viskolcz B, Temps F. Kinetics of the reactions of HCO with H and D atoms. Berichte der Bunsengesellschaft für physikalische Chemie 1998;102(7):897-905.

[101] Sarkisov O, Cheskis S, Nadtochenko V, Sviridenkov E, Vedeneev V. Spectroscopic study of elementary reactions involving HCO, NH2 and HNO. Arch Combust 1984;4:111-20.

[102] Cherian M, Rhodes P, Simpson R, Dixon-Lewis G. Kinetic modelling of the oxidation of carbon monoxide in flames. *Symposium (International) on Combustion.* 18. Elsevier; 1981:385-96.

[103] Reilly J, Clark J, Moore CB, Pimentel GC. HCO production, vibrational relaxation, chemical kinetics, and spectroscopy following laser photolysis of formaldehyde. The Journal of Chemical Physics 1978;69(10):4381-94.

[104] Jachimowski CJ. An experimental and analytical study of acetylene and ethylene oxidation behind shock waves. Combustion and Flame 1977;29:55-66.

[105] Matsugi A, Miyoshi A. Yield of formyl radical from the vinyl+ O2 reaction. International Journal of Chemical Kinetics 2014;46(5):260-74.

[106] DeSain JD, Jusinski LE, Ho AD, Taatjes CA. Temperature dependence and deuterium kinetic isotope effects in the HCO (DCO)+ O2 reaction between 296 and 673 K. Chemical physics letters 2001;347(1-3):79-86.

[107] Hsu CC, Mebel A, Lin M-C. Ab initio molecular orbital study of the HCO+ O2 reaction: Direct versus indirect abstraction channels. The Journal of chemical physics 1996;105(6):2346-52.

[108] Dóbé S, Wagner H, Ziemer H. Rate and stoichiometry of the fast gas titration reaction HCO+ O 2→ CO+ HO 2. Reaction Kinetics and Catalysis Letters 1995;54(2):271-5.

[109] Temps F, Wagner HG. Kinetics of the Reactions of HCO with HCO and O2. Berichte der Bunsengesellschaft für physikalische Chemie 1984;88(4):410-4.

[110] Ryu S-O, Shin KS, Hwang SM. Determination of the Rate Coefficients of the CH4 + O2 → HO2 + CH3 and HCO + O2 → HO2 + CO Reactions at High Temperatures. Bulletin of the Korean Chemical Society 2017;38(2):228-36.

[111] Colberg M, Friedrichs G. Room temperature and shock tube study of the reaction HCO+ O2 using the

photolysis of glyoxal as an efficient HCO source. The Journal of Physical Chemistry A 2006;110(1):160-70.

[112] Atkinson R, Baulch D, Cox R, Crowley J, Hampson Jr R, Kerr J, et al. Summary of evaluated kinetic and photochemical data for atmospheric chemistry. IUPAC Subcommittee on gas kinetic data evaluation for atmospheric chemistry 2001;20.

[113] Hanoune B, Dusanter S, ElMaimouni L, Devolder P, Lemoine B. Rate constant determinations by laser photolysis/diode laser infrared absorption: examples of HCO+ O2→ HO2+ CO and CH2OH+ O2→ HCH (O)+ HO2 reactions at 294 K. Chemical physics letters 2001;343(5-6):527-34.

[114] Nesbitt FL, Gleason JF, Stief LJ. Temperature Dependence of the Rate Constant for the Reaction HCO+ O2→ HO2+ CO at T= 200− 398 K. The Journal of Physical Chemistry A 1999;103(16):3038-43.

[115] Dóbé S, Bérces T, Temps F, Wagner HG, Ziemer H. Formation of methoxy and hydroxymethyl free radicals in selected elementary reactions. *Symposium (International) on Combustion.* 25. Elsevier; 1994:775-81.

[116] Timonen RS, Ratajczak E, Gutman D. Kinetics of the reactions of the formyl radical with oxygen, nitrogen dioxide, chlorine, and bromine. The Journal of Physical Chemistry 1988;92(3):651-5.

[117] Langford AO, Moore CB. Collision complex formation in the reactions of formyl radicals with nitric oxide and oxygen. The Journal of chemical physics 1984;80(9):4211-21.

[118] Veyret B, Lesclaux R. Absolute rate constants for the reactions of the formyl radical HCO with oxygen and nitric oxide from 298 to 503 K. The Journal of Physical Chemistry 1981;85(13):1918-22.

[119] Gill R, Johnson W, Atkinson G. The formation and decay mechanisms of HCO in the photodissociation of gas phase acetaldehyde. Chemical Physics 1981;58(1):29-44.

[120] Clark J, Moore C, Reilly J. HCO radical kinetics: conjunction of laser photolysis and intracavity dye laser spectroscopy. International Journal of Chemical Kinetics 1978;10(5):427-31.

[121] Shibuya K, Ebata T, Obi K, Tanaka I. Rate constant measurements for the reactions of oxomethyl radical with nitric oxide and molecular oxygen in the gas phase. The Journal of Physical Chemistry 1977;81(24):2292-4.

[122] Washida N, Martinez RI, Bayes KD. The oxidation of formyl radicals. Zeitschrift für Naturforschung A 1974;29(2):251-5.

[123] Vardanyan I, Sachyan G, Nalbandyan A. Kinetics and mechanism of formaldehyde oxidation. Combustion and Flame 1971;17(3):315-22.

[124] Tsang W, Hampson RF. Chemical Kinetic Data Base for Combustion Chemistry. Part I. Methane and Related Compounds. Journal of Physical and Chemical Reference Data 1986;15(3):1087-279.

[125] Lynch K, Schwab T, Michael J. Lyman-α absorption photometry at high pressure and atom density kinetic results for H recombination. International Journal of Chemical Kinetics 1976;8(5):651-71.

[126] Walkauskas L, Kaufman F. Gas phase hydrogen atom recombination. *Symposium (International) on Combustion.* 15. Elsevier; 1975:691-9.

[127] Trainor DW, Ham DO, Kaufman F. Gas phase recombination of hydrogen and deuterium atoms. The Journal of Chemical Physics 1973;58(10):4599-609.

[128] Bennett J, Blackmore D. Rates of gas-phase hydrogen-atom recombination at room temperature in the presence of added gases. *Symposium (International) on Combustion.* 13. Elsevier; 1971:51-9.

[129] Mallard W, Owen J. Rate constant for H+ H+ Ar= H2+ Ar from 1300 to 1700 K. International Journal of Chemical Kinetics 1974;6(5):753-61.

[130] Halstead C, Jenkins DR. Rates of H+ H+ M→ H2+ M and H+ OH+ M→ H2O+ M reactions in flames. Combustion and Flame 1970;14(3):321-3.

[131] Hurle I, Jones A, Rosenfeld J. Shock-wave observations of rate constants for atomic hydrogen recombination from 2500 to 7000 K: collisional stabilization by exchange of hydrogen atoms. Proceedings of the Royal Society of London A Mathematical and Physical Sciences 1969;310(1501):253-76.

[132] Getzinger R, Blair L. Recombination in the hydrogen-oxygen reaction: A shock tube study with nitrogen and water vapour as third bodies. Combustion and Flame 1969;13(3):271-84.

[133] Jacobs T, Giedt R, Cohen N. Kinetics of hydrogen halides in shock waves. ii. a new measurement of the hydrogen dissociation rate. The Journal of Chemical Physics 1967;47(1):54-7.

[134] Schott GL, Bird PF. Kinetic Studies of Hydroxyl Radicals in Shock Waves. IV. Recombination Rates in Rich Hydrogen—Oxygen Mixtures. The Journal of Chemical Physics 1964;41(9):2869-76.

[135] Rink JP. Shock tube determination of dissociation rates of hydrogen. The Journal of Chemical Physics 1962;36(1):262-5.

[136] Sellevåg SR, Georgievskii Y, Miller JA. The temperature and pressure dependence of the reactions H+ O2 (+ M)→ HO2 (+ M) and H+ OH (+ M)→ H2O (+ M). The Journal of Physical Chemistry A 2008;112(23):5085-95.

[137] Troe J. Detailed modeling of the temperature and pressure dependence of the reaction H+ O2 (+ M)→ HO2 (+ M). Proceedings of the combustion institute 2000;28(2):1463-9.

[138] Fernandes R, Luther K, Troe J, Ushakov V. Experimental and modelling study of the recombination reaction H+ O 2 (+ M)→ HO 2 (+ M) between 300 and 900 K, 1.5 and 950 bar, and in the bath gases M= He, Ar, and N 2. Physical Chemistry Chemical Physics 2008;10(29):4313-21.

[139] Michael J, Su M-C, Sutherland J, Carroll J, Wagner A. Rate constants for H+ O2+ M→ HO2+ M in seven bath gases. The Journal of Physical Chemistry A 2002;106(21):5297-313.

[140] Bates RW, Golden DM, Hanson RK, Bowman CT. Experimental study and modeling of the reaction H+ O 2+ M→ HO 2+ M (M= Ar, N 2, H2O) at elevated pressures and temperatures between 1050 and 1250 K. Physical Chemistry Chemical Physics 2001;3(12):2337-42.

[141] Ashman PJ, Haynes BS. Rate coefficient of H+ O2+ M→ HO2+ M (M= H2O, N2, Ar, CO2). *Symposium (International) on Combustion.* 27. Elsevier; 1998:185-91.

[142] Carleton KL, Kessler WJ, Marinelli WJ. Hydrogen atom+ oxygen+ M (= N2, H2O, Ar) three-body rate coefficients at 298-750 K. The Journal of Physical Chemistry 1993;97(24):6412-7.

[143] Hsu K-J, Durant J, Kaufman F. Rate constants for H+ O2+ M at 298 K for M= He, N2, and H2O. Journal of physical chemistry (1952) 1987;91(7):1895-9.

[144] Cobos C, Troe J. Theory of thermal unimolecular reactions at high pressures. II. Analysis of experimental results. The Journal of chemical physics 1985;83(3):1010-5.

[145] Wang S, Davidson DF, Hanson RK. Shock Tube and Laser Absorption Study of CH2O Oxidation via Simultaneous Measurements of OH and CO. J Phys Chem A 2017;121(45):8561-8.

[146] Hong Z, Davidson DF, Barbour EA, Hanson RK. A new shock tube study of the H+O2→OH+O reaction rate using tunable diode laser absorption of H2O near 2.5μm. Proceedings of the Combustion Institute 2011;33(1):309-16.

[147] Yang H, Gardiner WC, Shin KS, Fujii N. Shock tube study of the rate coefficient of H + O2 → OH + O. Chemical Physics Letters 1994;231(4-6):449-53.

[148] Du H, Hessler JP. Rate coefficient for the reaction H+O2→OH+O: Results at high temperatures, 2000 to 5300 K. The Journal of Chemical Physics 1992;96(2):1077-92.

[149] Yuan T, Wang C, Yu CL, Frenklach M, Rabinowitz MJ. Determination of the rate coefficient for the reaction hydrogen atom + oxygen .fwdarw. hydrogen + oxygen atom by a shock tube/laser absorption/detailed modeling study. The Journal of Physical Chemistry 1991;95(3):1258-65.

[150] Shin KS, Michael JV. Rate constants for the reactions H+O2→OH+O and D+O2→OD+O over the temperature range 1085–2278 K by the laser photolysis–shock tube technique. The Journal of Chemical Physics 1991;95(1):262-73.

[151] Masten DA, Hanson RK, Bowman CT. Shock tube study of the reaction hydrogen atom + oxygen .fwdarw. hydroxyl + oxygen atom using hydroxyl laser absorption. The Journal of Physical Chemistry 1990;94(18):7119-28.

[152] Pirraglia A, Michael J, Sutherland J, Klemm R. A flash photolysis-shock tube kinetic study of the H atom reaction with O2: H+ O2⇄ OH+ O (962 K≤ T≤ 1705 K) and H+ O2+ Ar⇄ HO2+ Ar (746 K≤ T≤ 987 K). Journal of physical chemistry (1952) 1989;93(1):282-91.

[153] Fujii N, Shin KS. Rate constant for H+ O2→ O+ OH by laser absorption spectroscopy of OH in shock-heated H2-O2-Ar mixtures. Chemical physics letters 1988;151(4-5):461-5.

[154] Frank P, Just T. High temperature reaction rate for H+ O2= OH+ O and OH+ H2= H2O+ H. Berichte der Bunsengesellschaft für physikalische Chemie 1985;89(2):181-7.

[155] Aleksandrov EN, Arutyunov VS, Dubrovina IV, Kozlov SN. Kinetics of hydrogen oxidation near the lower explosion limit. International Journal of Chemical Kinetics 1984;16(7):817-34.

[156] Dixon-Lewis G. Spherically symmetric flame propagation in hydrogen-air mixtures. Combustion science and technology 1983;34(1-6):1-29.

[157] Schott GL. Further studies of exponential branching rates in reflected-shock heated, nonstoichiometric H2COO2 systems. Combustion and Flame 1973;21(3):357-70.

[158] Eberius KH, Hoyermann K, Wagner HG. Experimental and mathematical study of a hydrogen-oxygen flame. Symposium (International) on Combustion 1971;13(1):713-21.

[159] Jachimowski CJ, Houghton WM. Shock-tube study of the induction-period kinetics of the hydrogen-oxygen reaction. Combustion and Flame 1970;15(2):125-32.

[160] Myerson A, Watt W. Atom-Formation Rates behind Shock Waves in Hydrogen and the Effect of Added Oxygen. The Journal of Chemical Physics 1968;49(1):425-33.

[161] Kurzius SC, Boudart M. Kinetics of the branching step in the hydrogen-oxygen reaction. Combustion and Flame 1968;12(5):477-91.

[162] Gutman D, Schott GL. Shock-Tube Study of Chain Branching during the Induction Period of the Hydrogen—Oxygen Reaction. The Journal of Chemical Physics 1967;46(12):4576-84.

[163] Goodings JM, Hayhurst AN. Heat release and radical recombination in premixed fuel-lean flames of H 2+ O 2+ N 2. Rate constants for H+ OH+ M→ H 2 O+ M and HO 2+ OH→ H 2 O+ O 2. Journal of the Chemical Society, Faraday Transactions 2: Molecular and Chemical Physics 1988;84(6):745-62.

[164] Zellner R, Erler K, Field D. Kinetics of the recombination reaction OH+ H+ M→ H2O+ M at low temperatures. *Symposium (International) on Combustion.* 16. Elsevier; 1977:939-48.

[165] Getzinger RW. A shock-wave study of recombination in near-stoichiometric hydrogen-oxygen mixtures. *Symposium (International) on Combustion.* 11. Elsevier; 1967:117-24.

[166] Dixon-Lewis G, Sutton M, Williams A. The kinetics of hydrogen atom recombination. Discussions of the Faraday Society 1962;33:205-12.

[167] Balakrishnan N. Quantum calculations of the O (3 P)+ H 2→ OH+ H reaction. The Journal of chemical physics 2004;121(13):6346-52.

[168] Javoy S, Naudet V, Abid S, Paillard C. Elementary reaction kinetics studies of interest in H2 supersonic combustion chemistry. Experimental thermal and fluid science 2003;27(4):371-7.

[169] Javoy S, Naudet V, Abid S, Paillard C. Rate constant for the reaction of O with H2 at high temperature by resonance absorption measurements of O atoms. International Journal of Chemical Kinetics

2000;32(11):686-95.

[170] Ryu S-O, Hwang SM, Rabinowitz MJ. Rate coefficient of the O+ H2= OH+ H reaction determined via shock tube-laser absorption spectroscopy. Chemical physics letters 1995;242(3):279-84.

[171] Yang H-X, Shin KS, Gardiner W. Rate coefficients for O+ H2→ OH+ H and O+ D2→ OD+ D by kinetic laser absorption spectroscopy in shock waves. Chemical physics letters 1993;207(1):69-74.

[172] Davidson D, Hanson R. A direct comparison of shock tube photolysis and pyrolysis methods in the determination of the rate coefficient for O+ H2→ OH+ H. Combustion and flame 1990;82(3-4):445-7.

[173] Shin KS, Fujii N, Gardiner Jr WC. Rate constant for O+ H2→ OH+ H by laser absorption spectroscopy of OH in shock-heated H2 O2 Ar mixtures. Chemical physics letters 1989;161(3):219-22.

[174] Sutherland J, Michael J, Pirraglia A, Nesbitt F, Klemm R. Rate constant for the reaction of O (3P) with H2 by the flash photolysis—shock tube and flash photolysis—Resonance fluorescence techniques; 504K≤ T≤ 2495K. *Symposium (International) on Combustion.* 21. Elsevier; 1988:929-41.

[175] Natarajan K, Roth P. High temperature rate coefficient for the reaction of O (3P) with H2 obtained by the resonance absorption of O and H atoms. Combustion and flame 1987;70(3):267-79.

[176] Marshall P, Fontijn A. HTP kinetics studies of the reactions of O (2 3 PJ) atoms with H2 and D2 over wide temperature ranges. The Journal of chemical physics 1987;87(12):6988-94.

[177] Presser N, Gordon RJ. The kinetic isotope effect in the reaction of O (3 P) with H2, D2, and HD. The Journal of chemical physics 1985;82(3):1291-7.

[178] Pamidimukkala KM, Skinner GB. Resonance absorption measurements of atom concentrations in reacting gas mixtures. VIII. Rate constants for O+ H2→ OH+ H and O+ D2→ OD+ D from measurements of O atoms in oxidation of H2 and D2 by N2O. The Journal of Chemical Physics 1982;76(1):311-5.

[179] Light GC, Matsumoto JH. Experimental measurement of the rate of the reaction o (3P)+ H2 (v= 0)→ OH (v= 0)+ H at T= 298 K. International Journal of Chemical Kinetics 1980;12(7):451-68.

[180] Dubinsky RN, McKenney DJ. Determination of the Rate Constant of the O+ H2→ OH+ H Reaction using Atomic Oxygen Resonance Fluorescence and the Air Afterglow Techniques. Canadian Journal of Chemistry 1975;53(23):3531-41.

[181] Schott GL, Getzinger RW, Seitz WA. Transient oxygen atom yields in H2 O2 ignition and the rate coefficient for O+ H2→ OH+ H. International Journal of Chemical Kinetics 1974;6(6):921-43.

[182] Lam KY, Davidson DF, Hanson RK. A shock tube study of H2+ OH→ H2O+ H using OH laser absorption. International Journal of Chemical Kinetics 2013;45(6):363-73.

[183] Nguyen TL, Stanton JF, Barker JR. Ab initio reaction rate constants computed using semiclassical transition-state theory: HO + H2 --> H2O + H and isotopologues. J Phys Chem A 2011;115(20):5118-26.

[184] Orkin VL, Kozlov SN, Poskrebyshev GA, Kurylo MJ. Rate Constant for the Reaction of OH with H2 between 200 and 480 K. The Journal of Physical Chemistry A 2006;110(21):6978-85.

[185] Krasnoperov LN, Michael JV. Shock Tube Studies Using a Novel Multipass Absorption Cell: Rate Constant Results For OH + H2and OH + C2H6. The Journal of Physical Chemistry A 2004;108(26):5643-8.

[186] Haworth NL, Bacskay GB, Mackie JC. The Role of Phosphorus Dioxide in the H + OH Recombination Reaction: Ab Initio Quantum Chemical Computation of Thermochemical and Rate Parameters. The Journal of Physical Chemistry A 2002;106(8):1533-41.

[187] Talukdar RK, Gierczak T, Goldfarb L, Rudich Y, Rao BM, Ravishankara A. Kinetics of hydroxyl radical reactions with isotopically labeled hydrogen. The Journal of Physical Chemistry

1996;100(8):3037-43.

[188] Bott J, Cohen N. A shock tube study of the reaction of the hydroxyl radical with H2, CH4, c-C5H10, and i-C4H10. International journal of chemical kinetics 1989;21(7):485-98.

[189] Schmidt V, Zhu G-Y, Becker K, Fink E. Study of OH reactions at high pressures by excimer laser photolysis—dye laser fluorescence. Berichte der Bunsengesellschaft für physikalische Chemie 1985;89(3):321-2.

[190] Ravishankara A, Nicovich J, Thompson R, Tully F. Kinetic study of the reaction of hydroxyl with hydrogen and deuterium from 250 to 1050 K. The Journal of Physical Chemistry 1981;85(17):2498-503.

[191] Trainor DW, von Rosenberg CW. Energy partitioning in the products of elementary reactions involving OH-radicals. Symposium (International) on Combustion 1975;15(1):755-64.

[192] Overend RP, Paraskevopoulos G, Cvetanović RJ. Rates of OH Radical Reactions. I. Reactions with H2, CH4, C2H6, and C3H8 at 295 K. Canadian Journal of Chemistry 1975;53(22):3374-82.

[193] Atkinson R, Hansen DA, Pitts JN. Rate constants for the reaction of the OH radical with H2 and NO (M=Ar and N2). The Journal of Chemical Physics 1975;62(8):3284-8.

[194] Smith IWM, Zellner R. Rate measurements of reactions of OH by resonance absorption. Part 3.—Reactions of OH with H2, D2and hydrogen and deuterium halides. J Chem Soc, Faraday Trans 2 1974;70(0):1045-56.

[195] Gardiner WC, Mallard WG, Owen JH. Rate constant of OH + H2 = H2O + H from 1350 to 1600 K. The Journal of Chemical Physics 1974;60(6):2290-5.

[196] Westenberg AA, deHaas N. Rates of CO + OH and H2 + OH over an extended temperature range. The Journal of Chemical Physics 1973;58(10):4061-5.

[197] Stuhl F, Niki H. Pulsed Vacuum-uv Photochemical Study of Reactions of OH with H2, D2, and CO Using a Resonance-Fluorescent Detection Method. The Journal of Chemical Physics 1972;57(9):3671-7.

[198] Gorse R, Volman D. Photochemistry of the gaseous hydrogen peroxide—carbon monoxide system. II: Rate constants for hydroxyl radical reactions with hydrocarbons and for hydrogen atom reactions with hydrogen peroxide. Journal of Photochemistry 1974;3(1):115-22.

[199] Baldwin RR, Walker RW. Rate constants for hydrogen+ oxygen system, and for H atoms and OH radicals+ alkanes. Journal of the Chemical Society, Faraday Transactions 1: Physical Chemistry in Condensed Phases 1979;75:140-54.

[200] Lee D, Hochgreb S. Hydrogen autoignition at pressures above the second explosion limit (0.6–4.0 MPa). International journal of chemical kinetics 1998;30(6):385-406.

[201] Mousavipour SH, Saheb V. Theoretical study on the kinetic and mechanism of H+ HO2 reaction. Bulletin of the Chemical Society of Japan 2007;80(10):1901-13.

[202] Karkach SP, Osherov VI. Ab initio analysis of the transition states on the lowest triplet H 2 O 2 potential surface. The Journal of chemical physics 1999;110(24):11918-27.

[203] Sridharan U, Qiu L, Kaufman F. Kinetics and product channels of the reactions of perhydroxyl with oxygen and hydrogen atoms at 296 K. The Journal of Physical Chemistry 1982;86(23):4569-74.

[204] Keyser LF. Absolute rate constant and branching fractions for the atomic hydrogen+ hydroperoxyl radical reaction from 245 to 300 K. The Journal of Physical Chemistry 1986;90(13):2994-3003.

[205] Assaf E, Fittschen C. Cross Section of OH Radical Overtone Transition near 7028 cm–1 and Measurement of the Rate Constant of the Reaction of OH with HO2 Radicals. The Journal of Physical Chemistry A 2016;120(36):7051-9.

[206] Hong Z, Vasu SS, Davidson DF, Hanson RK. Experimental study of the rate of OH+ HO2→ H2O+

O2 at high temperatures using the reverse reaction. The Journal of Physical Chemistry A 2010;114(17):5520-5.

[207] Srinivasan NK, Su M-C, Sutherland JW, Michael JV, Ruscic B. Reflected shock tube studies of high-temperature rate constants for OH+ NO2→ HO2+ NO and OH+ HO2→ H2O+ O2. The Journal of Physical Chemistry A 2006;110(21):6602-7.

[208] Hippler H, Troe J, Willner J. Shock wave study of the reaction HO2+ HO2→ H2O2+ O2: Confirmation of a rate constant minimum near 700 K. The Journal of chemical physics 1990;93(3):1755-60.

[209] Schwab JJ, Brune WH, Anderson JG. Kinetics and mechanism of the hydroxyl+ hydroperoxo reaction. The Journal of Physical Chemistry 1989;93(3):1030-5.

[210] Keyser LF. Kinetics of the reaction hydroxyl+ hydroperoxo. fwdarw. water+ oxygen from 254 to 382 K. The Journal of Physical Chemistry 1988;92(5):1193-200.

[211] Dransfeld P, Wagner HG. Comparative Study of the Reactions of 16OH and 18OH with H16O2. Zeitschrift für Naturforschung A 1987;42(5):471-6.

[212] Sridharan U, Qiu L, Kaufman F. Rate constant of the hydroxyl+ perhydroxyl (HO2) reaction from 252 to 420 K. The Journal of Physical Chemistry 1984;88(7):1281-2.

[213] Rozenshtein V, Gershenzon YM, Il'In S, Kishkovitch O. Reactions of HO2 with NO, OH and HO2 studied by EPR/LMR spectroscopy. Chemical physics letters 1984;112(5):473-8.

[214] Temps F, Gg. Wagner H. Untersuchungen zur Reaktion OH+ HO2→ H2O+ O2 mit Hilfe eines Laser-Magnetischen Resonanz-Spektrometers. Berichte der Bunsengesellschaft für physikalische Chemie 1982;86(2):119-25.

[215] DeMore W. Rate constant and possible pressure dependence of the reaction hydroxyl+ hydroperoxo. The Journal of Physical Chemistry 1982;86(1):121-6.

[216] Braun M, Hofzumahaus A, Stuhl F. VUV Flash Photolysis Study of the Reaction of HO with HO2 at 1 atm and 298 K. Berichte der Bunsengesellschaft für physikalische Chemie 1982;86(7):597-602.

[217] Thrush B, Wilkinson J. The rate of reaction of HO2 radicals with HO and with NO. Chemical Physics Letters 1981;81(1):1-3.

[218] Kurylo MJ, Klais O, Laufer AH. Mechanistic investigation of the hydroxyl+ hydroperoxo reaction. The Journal of Physical Chemistry 1981;85(24):3674-8.

[219] Cox R, Burrows J, Wallington T. Rate coefficient for the reaction OH+ HO2= H2O+ O2 at 1 atmosphere pressure and 308 K. Chemical Physics Letters 1981;84(2):217-21.

[220] Burrows J, Cox R, Derwent R. Modulated photolysis of the ozone—water vapour system: kinetics of the reaction of OH with HO2. Journal of Photochemistry 1981;16(2):147-68.

[221] Lii R-R, Gorse Jr RA, Sauer Jr MC, Gordon S. Rate constant for the reaction of hydroxyl with hydroperoxo radicals. The Journal of Physical Chemistry 1980;84(8):819-21.

[222] Hochanadel C, Sworski T, Ogren P. Rate constants for the reactions of HO2 with OH and with HO2. The Journal of Physical Chemistry 1980;84(24):3274-7.

[223] Troe J. The thermal dissociation/recombination reaction of hydrogen peroxide H2O2 (+ M) double left right arrow 2OH (+ M) III. Analysis and representation of the temperature and pressure dependence over wide ranges. Combustion and Flame 2011;158(4):594-601.

[224] Brouwer L, Cobos C, Troe J, Dübal HR, Crim F. Specific rate constants k (E, J) and product state distributions in simple bond fission reactions. II. Application to HOOH→ OH+ OH. The Journal of chemical physics 1987;86(11):6171-82.

[225] Giguère PA, Liu I. Kinetics of the thermal decomposition of hydrogen peroxide vapor. Canadian Journal of Chemistry 1957;35(4):283-93.

[226] McLane C. Hydrogen peroxide in the thermal hydrogen oxygen reaction I. Thermal decomposition of hydrogen peroxide. The Journal of Chemical Physics 1949;17(4):379-85.

[227] Sellevåg SR, Georgievskii Y, Miller JA. Kinetics of the gas-phase recombination reaction of hydroxyl radicals to form hydrogen peroxide. The Journal of Physical Chemistry A 2009;113(16):4457-67.

[228] Hong Z, Farooq A, Barbour EA, Davidson DF, Hanson RK. Hydrogen peroxide decomposition rate: a shock tube study using tunable laser absorption of H2O near 2.5 μm. The Journal of Physical Chemistry A 2009;113(46):12919-25.

[229] Kijewski H, Troe J. Study of the pyrolysis of H2O2 in the presence of H2and CO by use of UV absorption of HO2. International Journal of Chemical Kinetics 1971;3(3):223-35.

Supplementary Material-2

A Joint Hydrogen and Syngas Chemical Kinetic Model Optimized by Particle Swarm Optimization

Hongxin Wang[1], Chenyi Sun[1], Oskar Haidn[1], Askarova Aliya[3], Chiara Manfletti[1], Nadezda Slavinskaya[2, 3]

1. Lehrstuhl für Raumfahrtantriebe, Technical University of Munich, 85748 Garching, Germany

2. Gesellschaft fur Anlagen-und Reaktorsicherheit GmbH, 85748 Garching, Germany

3. Al-Farabi Kazakh National University, 050040 Almaty, Kazakhstan

Results simulated with the final model.

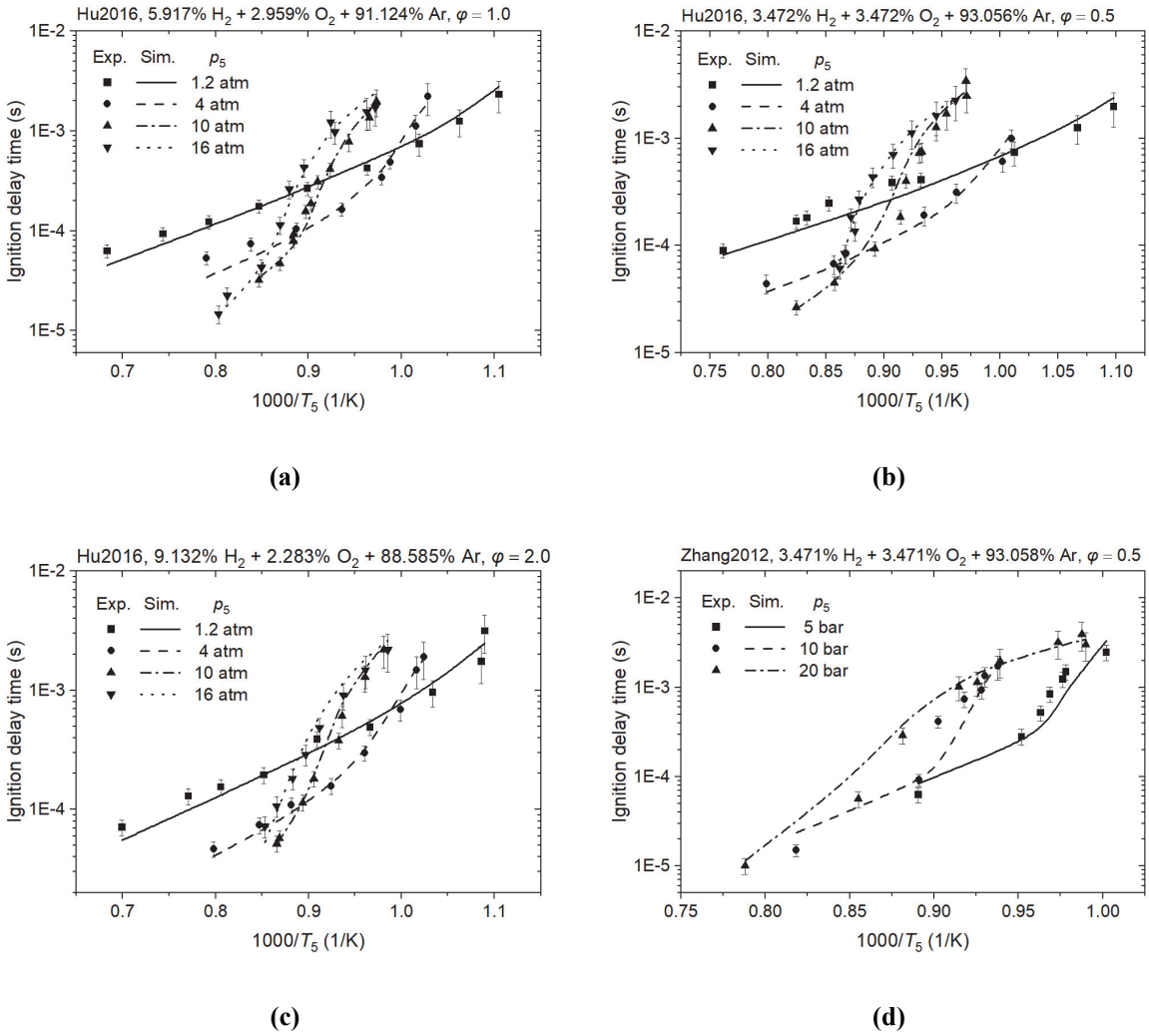

Fig. S2-1. Ignition delay times of $H_2/O_2/Ar$ mixtures measured in the shock tube by Hu et al. [1] and Zhang et al. [2].

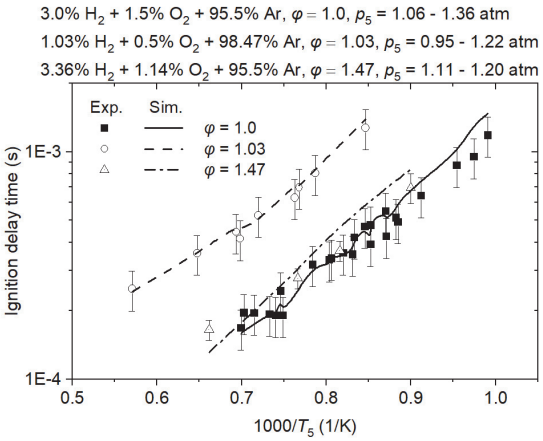

Fig. S2-2. Ignition delay times of $H_2/O_2/Ar$ mixtures measured in the shock tube by Petersen et al. [3].

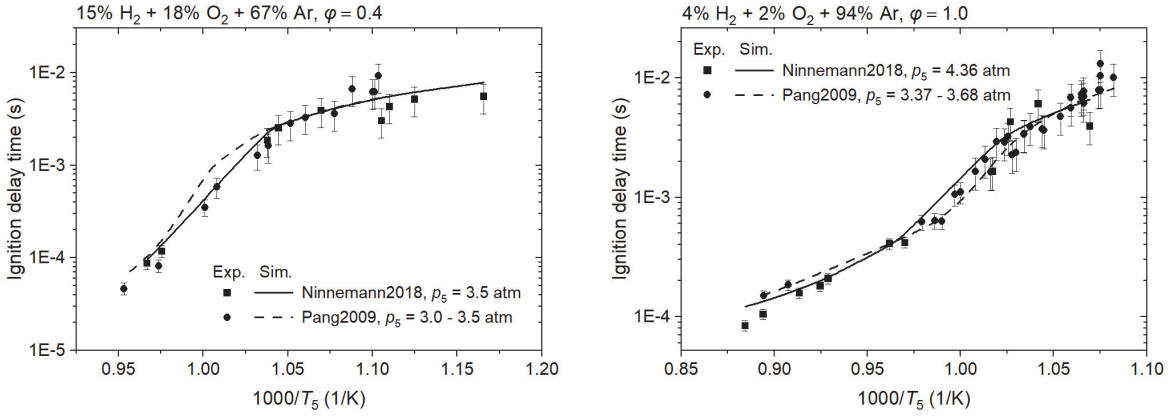

(a) **(b)**

Fig. S2-3. Ignition delay times of $H_2/O_2/Ar$ mixtures measured in the shock tubes by Ninnemann et al. [4] and Pang et al. [5].

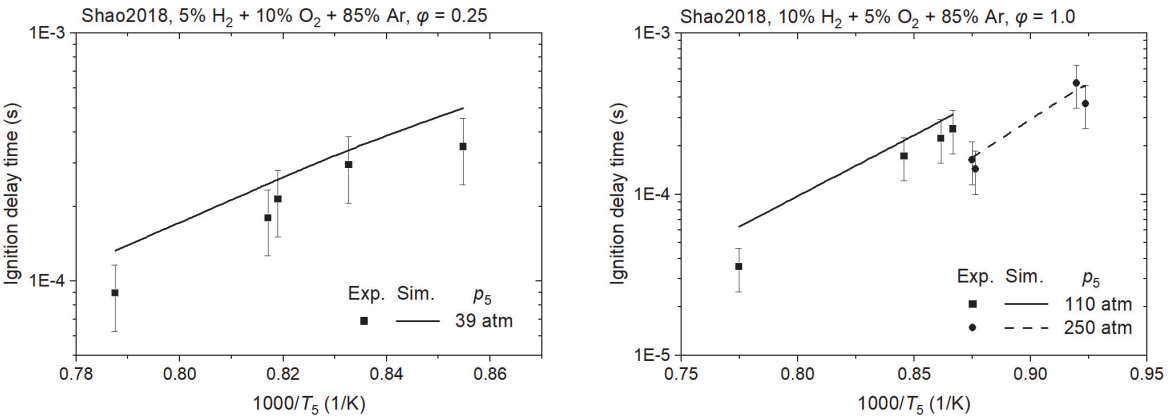

(a) **(b)**

Fig. S2-4. Ignition delay times of H2/O2/Ar mixtures measured in the shock tube by Shao et al. [6].

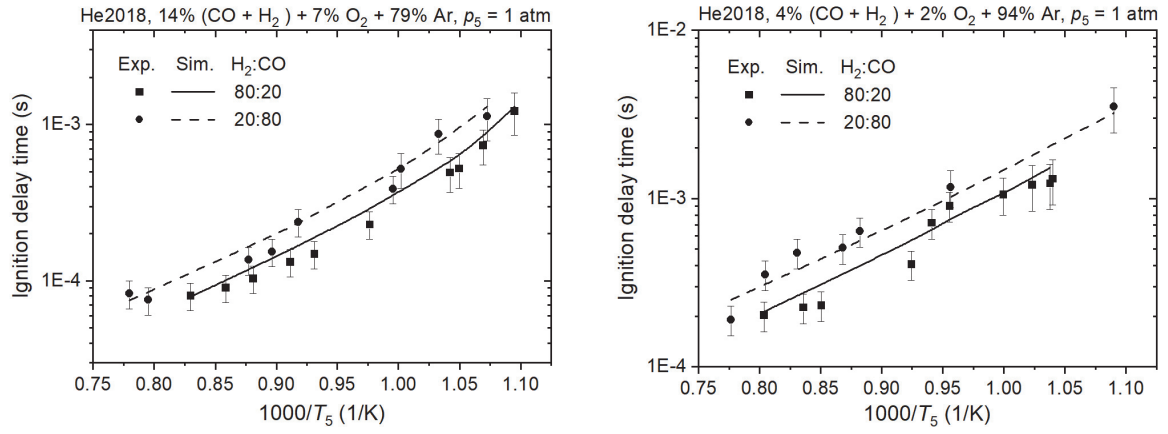

(a) **(b)**

Fig. S2-5. Ignition delay times of $H_2/CO/O_2/Ar$ mixtures measured in the shock tube by He et al. [7].

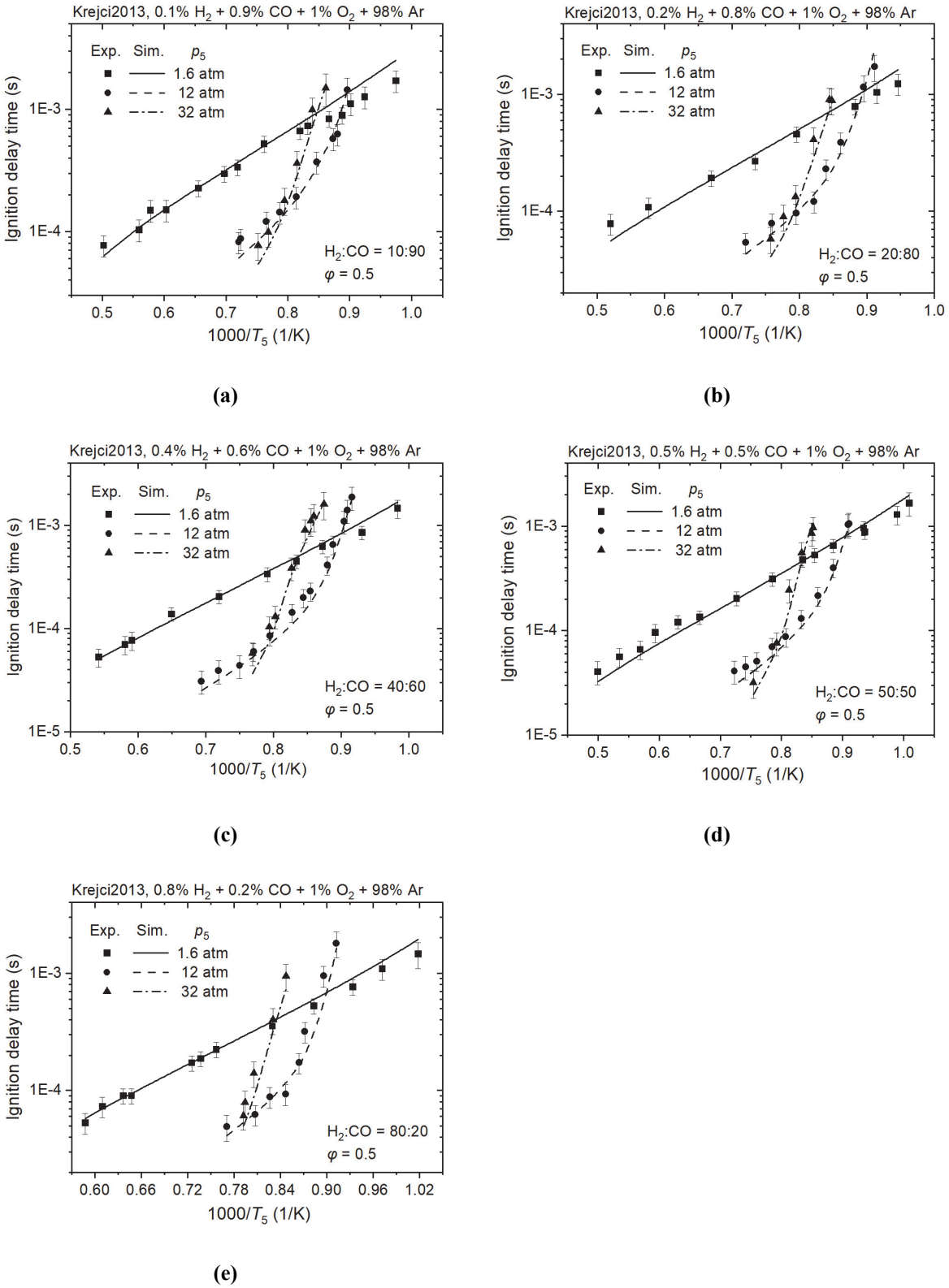

Fig. S2-6. Ignition delay times of $H_2/CO/O_2/Ar$ mixtures measured in the shock tube by Krejci et al. [8].

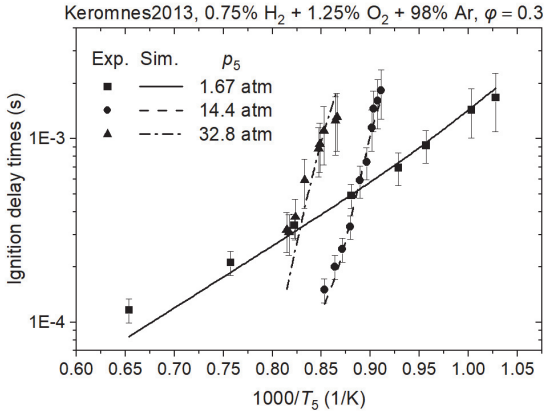

(a)

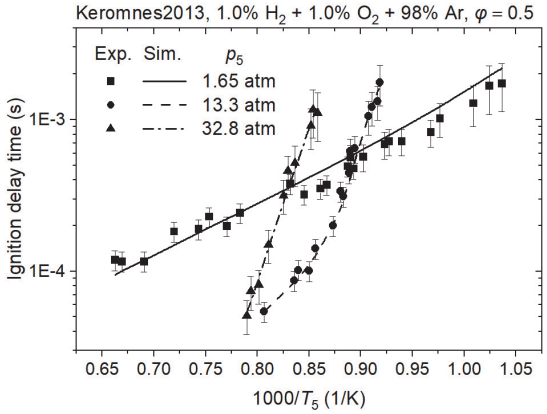

(b)

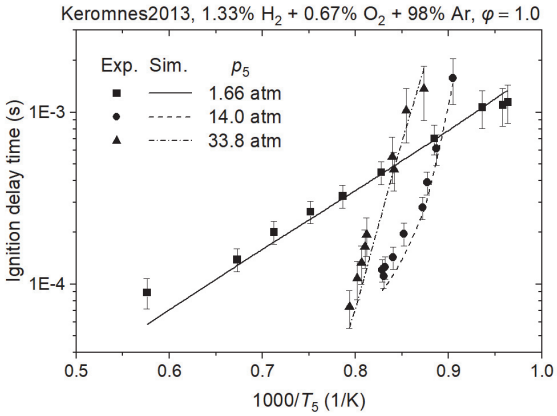

(c)

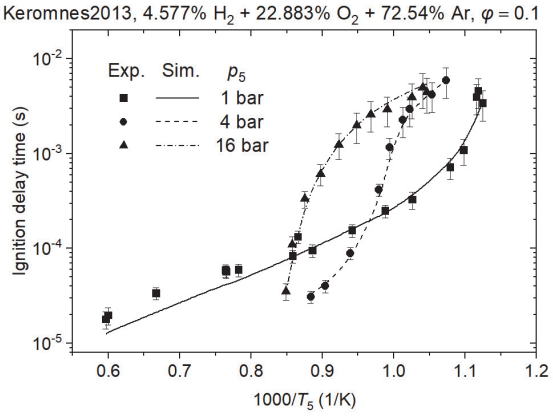

(d)

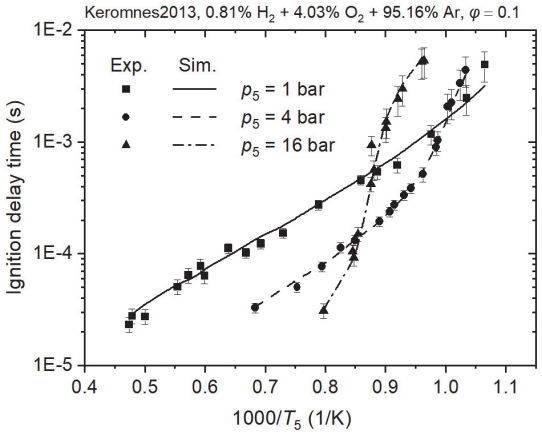

(e)

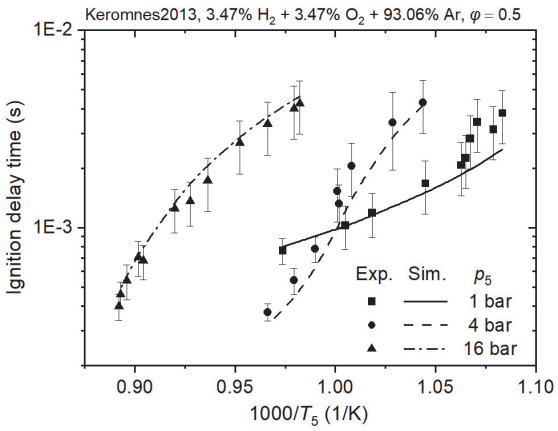

(f)

Fig. S2-7. Ignition delay times of H_2/O_2/Ar mixtures measured in the shock tube by Keromnes et al. [9].

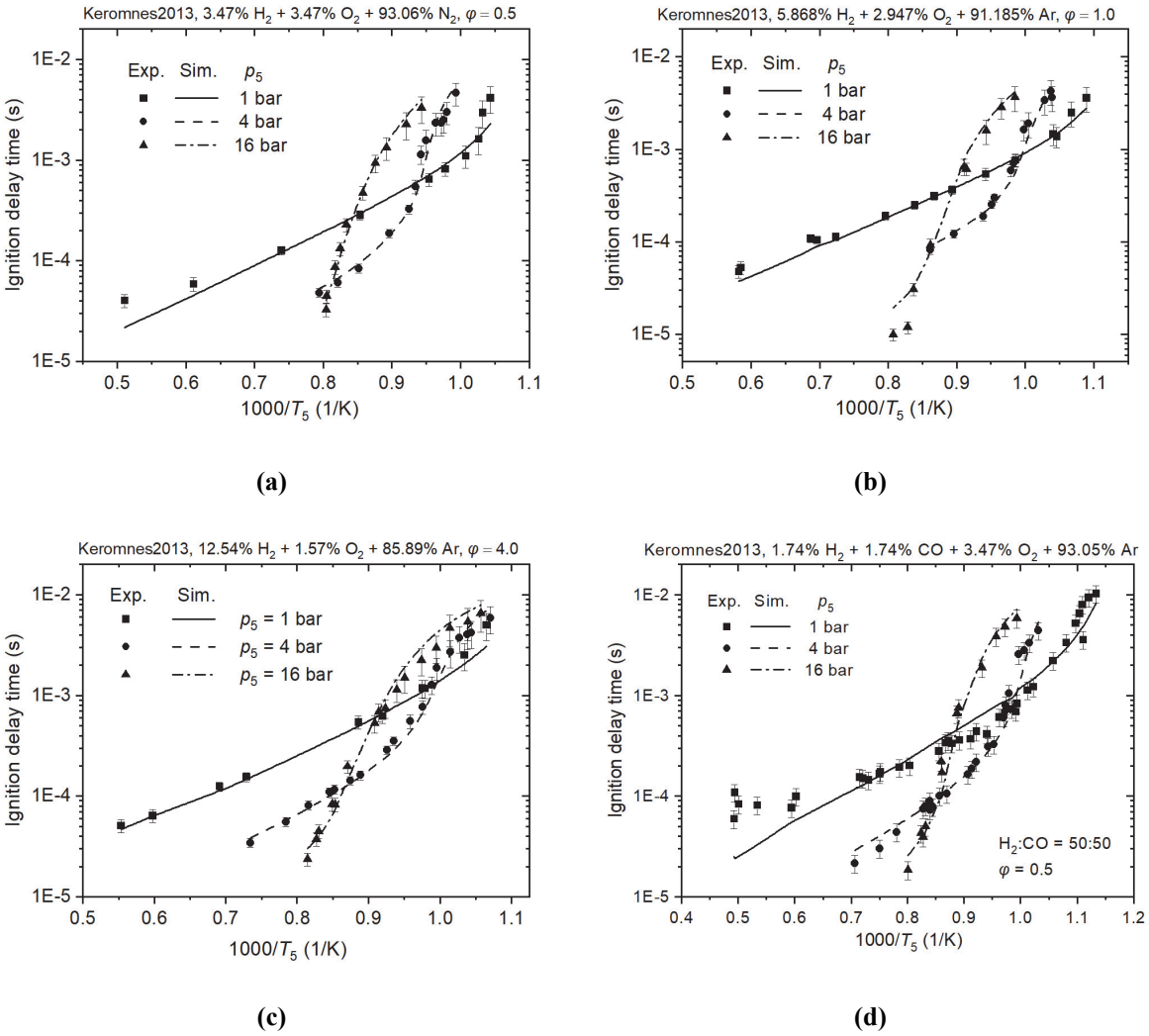

Fig. S2-8. Ignition delay times of H_2/CO/O_2/N_2/Ar mixtures measured in the shock tube by Keromnes et al. [9].

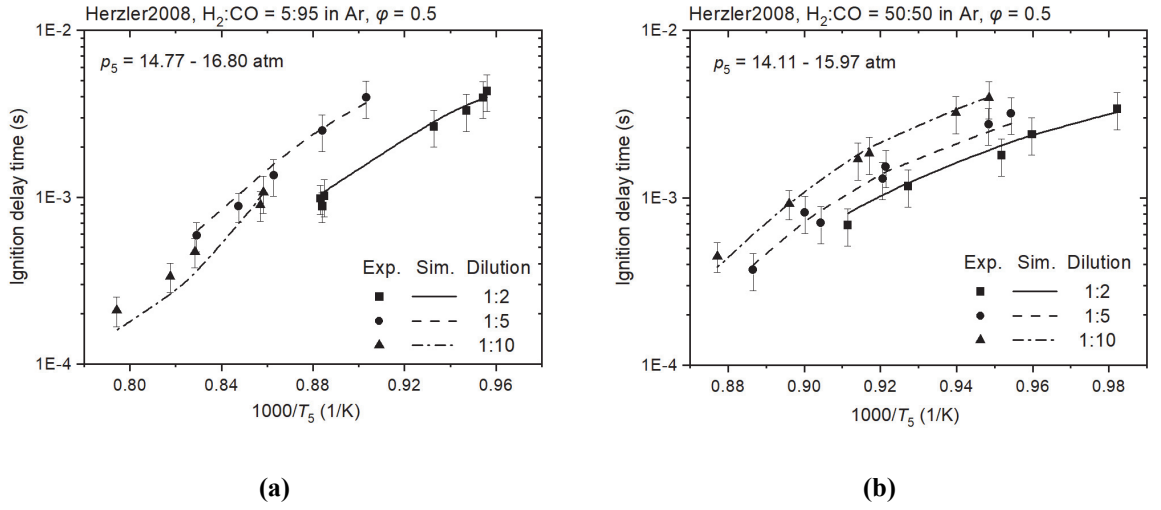

Fig. S2-9. Ignition delay times of H_2/CO/O_2/Ar mixtures measured in the shock tube by Herzler et al. [10].

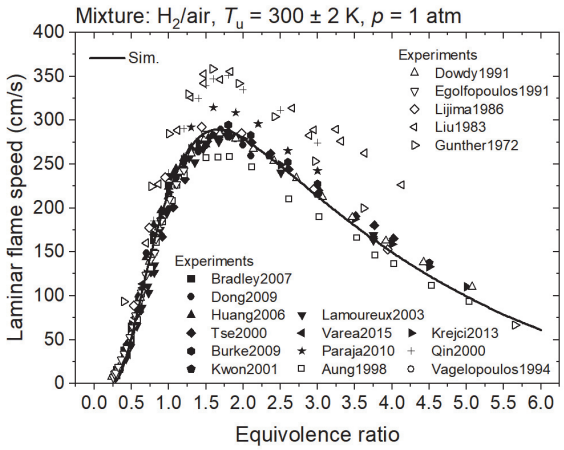

Fig. S2-10. Laminar flame speeds of H_2/air mixtures measured at T_u = 300±2 K and p = 1 atm [8, 11-28].

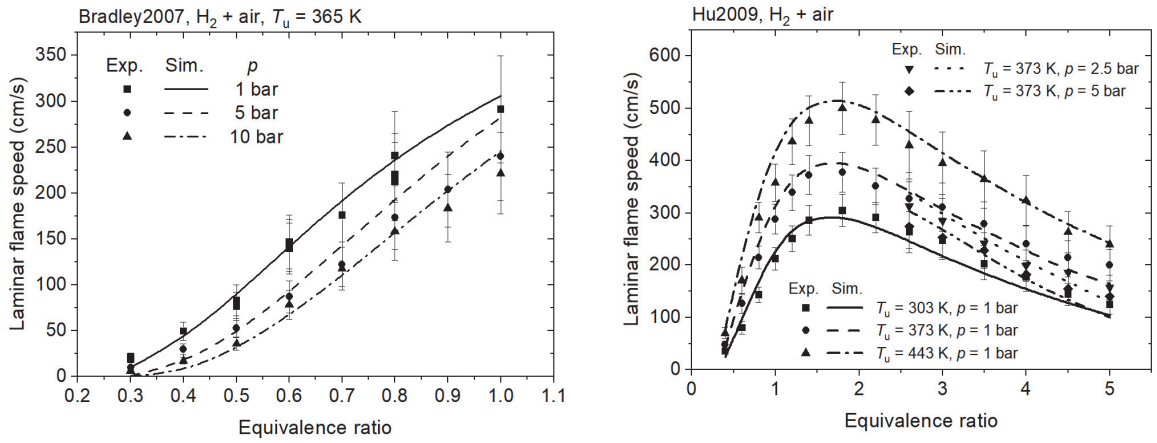

(a) **(b)**

Fig. S2-11. Laminar flame speeds of H2/air mixtures (Tu = 303-443 K, p = 1-10 bar) at variable pressures and unburned temperatures measured by (a) Bradley et al. [18] and (b) Hu et al. [26].

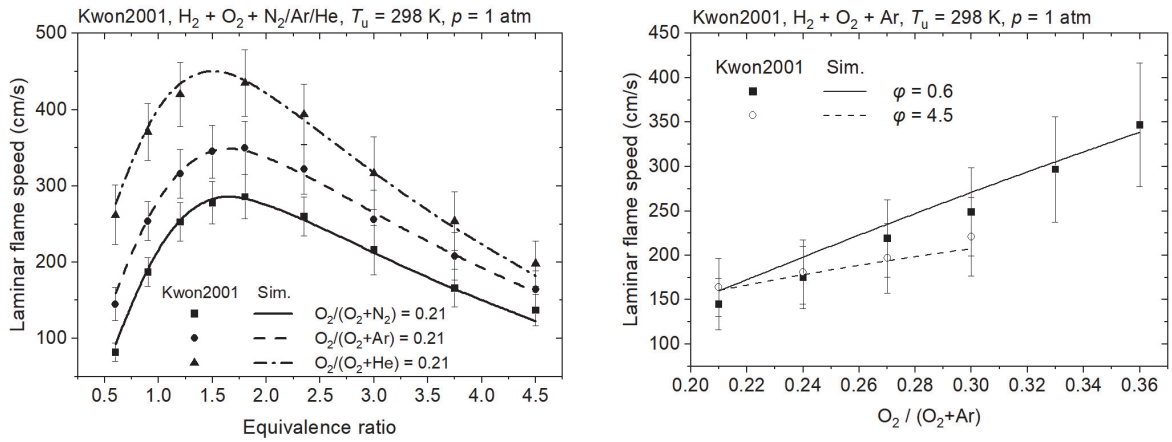

(a) **(b)**

Fig. S2-12. Laminar flame speeds of H_2/O_2/N_2/Ar/He mixtures (T_u = 298 K, p = 1 atm) measured by Kwon et al. [23].

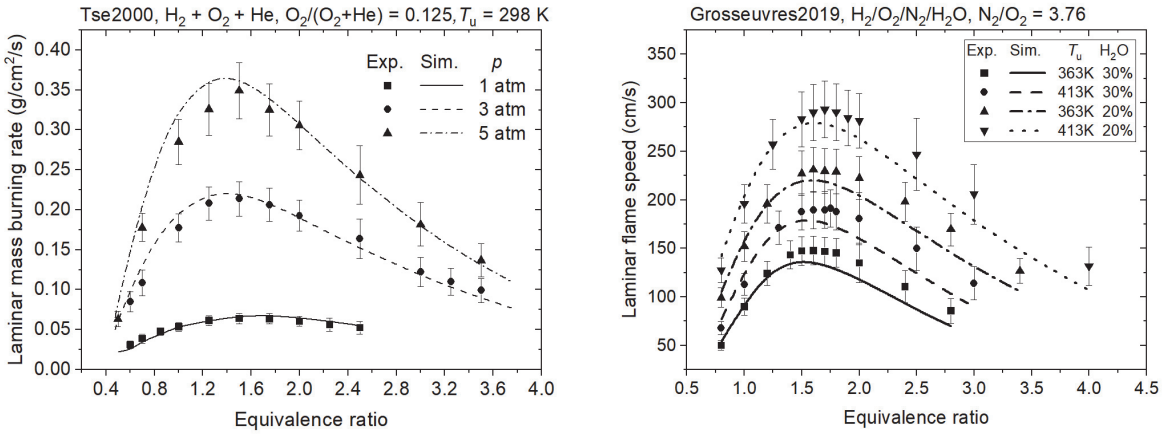

Fig. S2-13. Laminar flame speeds of (a) H_2/O_2/He mixtures (T_u = 298 K, p = 1-5 atm) measured by Tse et al. [22] (b) $H_2/O_2/N_2/H_2O$ mixtures (T_u = 363-413 K, p = 1 atm) measured by Grosseuvres et al. [29].

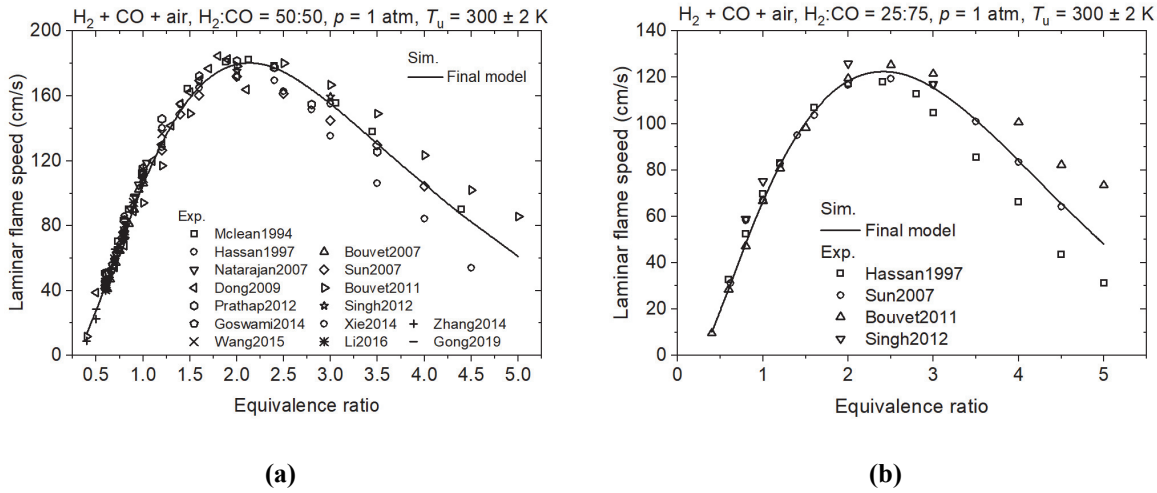

Fig. S2-14. Laminar flame speeds of H_2/CO/air mixtures (T_u = 300±2 K, p = 1 atm): (a) H_2:CO = 50:50 [12, 30-42]; (b) H_2:CO = 25:75 [31, 34, 36, 43]; (c) H_2:CO = 10:90 [12, 31, 39, 43]; (d) H_2:CO = 5:95 [30, 31, 33, 34, 36, 40, 43, 44].

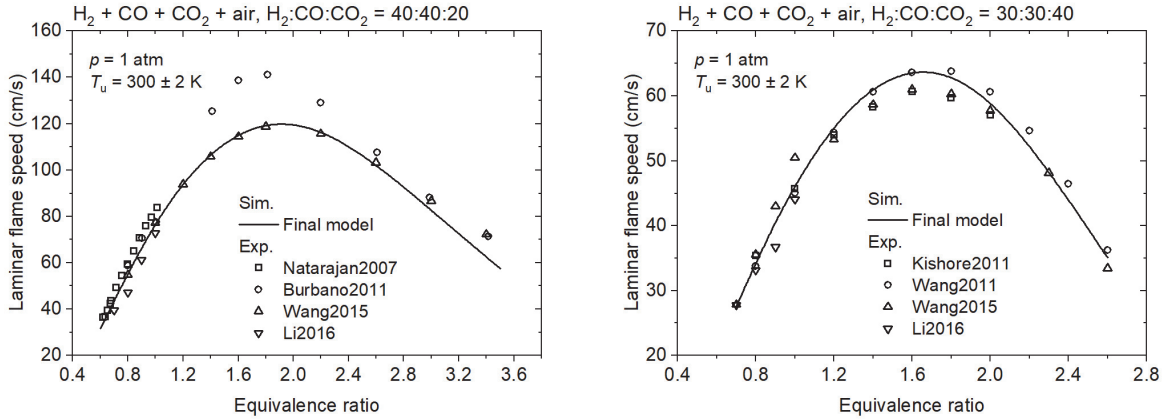

(a) **(b)**

Fig. S2- 15. Laminar flame speeds of H_2/CO/CO_2/air mixtures (T_u = 300±2 K, p = 1 atm) measured by (a) H_2:CO:CO_2 = 40:40:20 [33, 40, 45, 46]; (b) H_2:CO:CO_2 = 30:30:40 [40, 41, 44, 47].

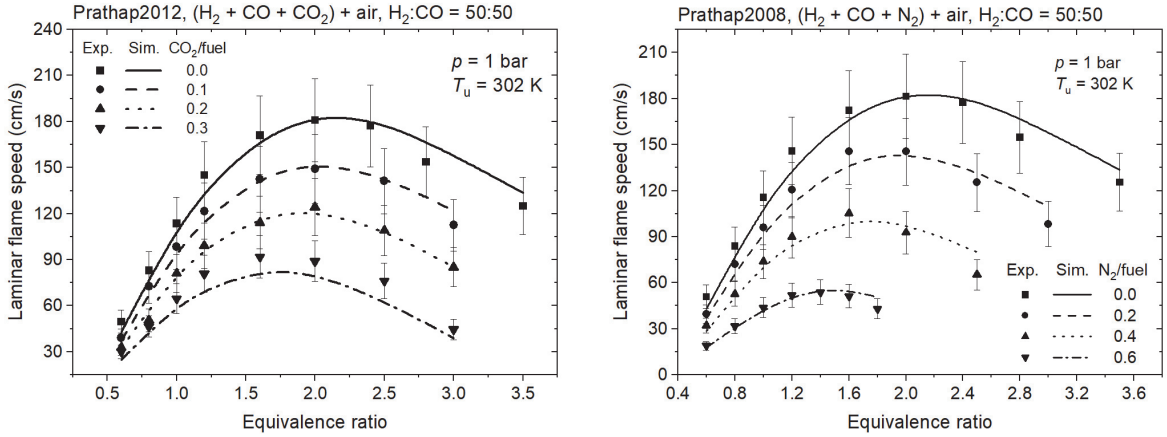

(a) **(b)**

Fig. S2-16. Laminar flame speeds of H_2/CO/N_2/CO_2/air mixtures (T_u = 302 K, p = 1 bar) measured by Prathap et al. [35, 48].

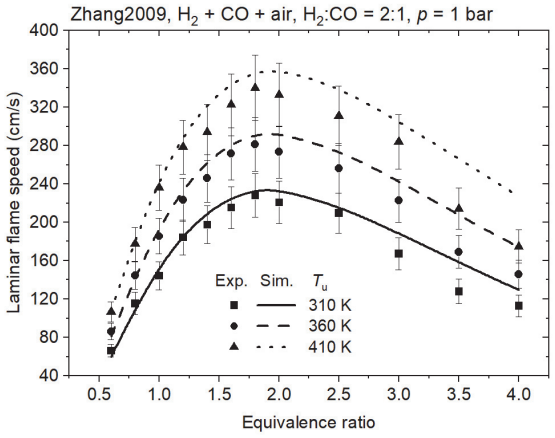

Fig. S2-17. Laminar flame speeds of H_2/CO/air mixtures (T_u = 310-410 K, p = 1 bar) measured by Zhang et al. [49].

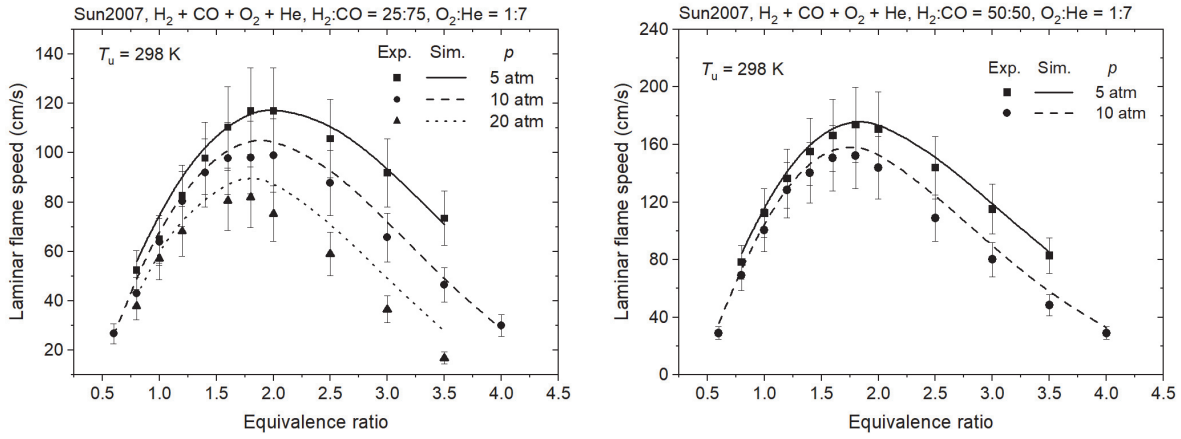

(a) **(b)**

Fig. S2-18. Laminar flame speeds of $H_2/CO/O_2/He$ mixtures (T_u = 298 K, p = 1-20 atm) measured by Sun et al. [34].

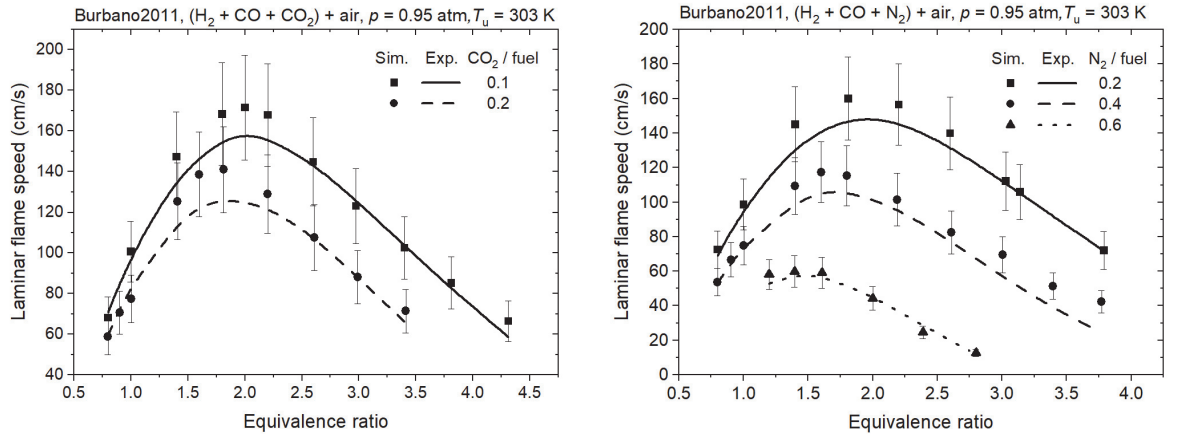

(a) **(b)**

Fig. S2-19 Laminar flame speeds of $H_2/CO/N_2/CO_2$/air mixtures (T_u = 303 K, p = 0.95 atm) measured by Burbano et al. [45].

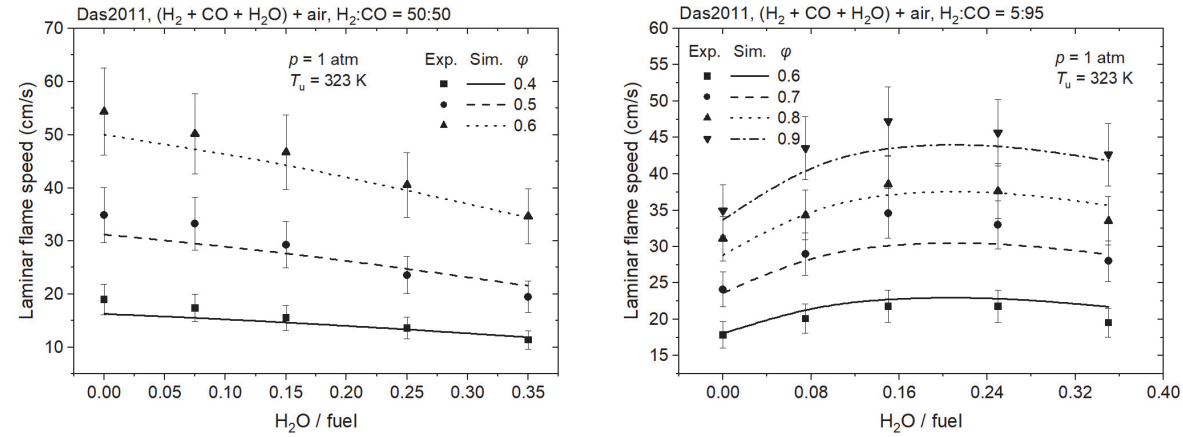

(a) **(b)**

Fig. S2-20 Laminar flame speeds of $H_2/CO/H_2O$/air mixtures (T_u = 323 K, p = 1 atm) measured by Das et al.

[50].

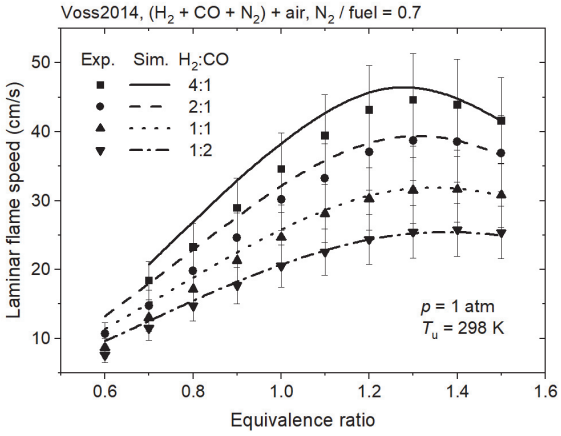

Fig. S2-21 Laminar flame speeds of H_2/CO/N_2/air mixtures (T_u = 298 K, p = 1 atm) measured by Voss et al. [51].

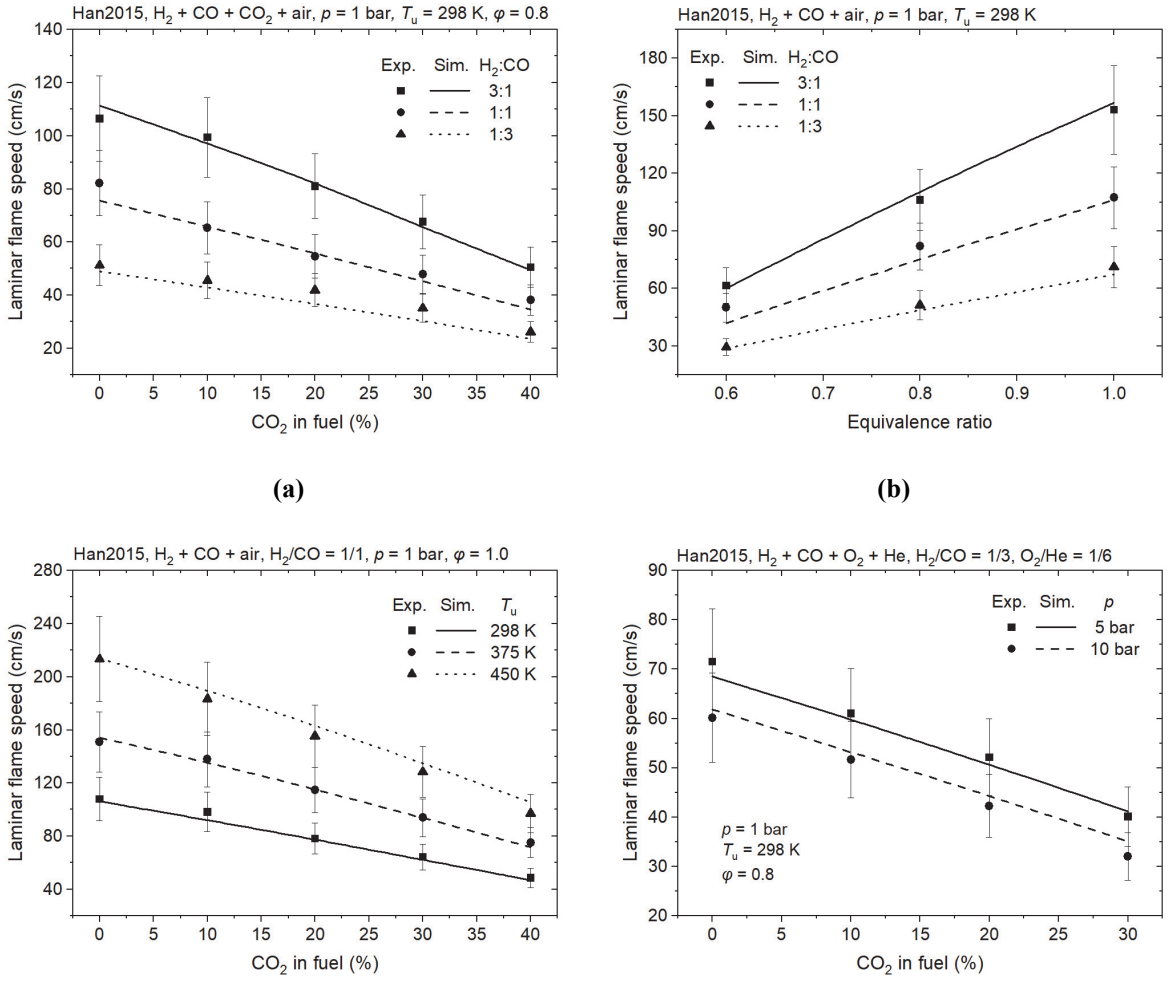

Fig. S2-22 Laminar flame speeds of H_2/CO/CO_2/O_2/He/air mixtures (T_u = 298-450 K, p = 1-10 bar) measured by Han et al. [52].

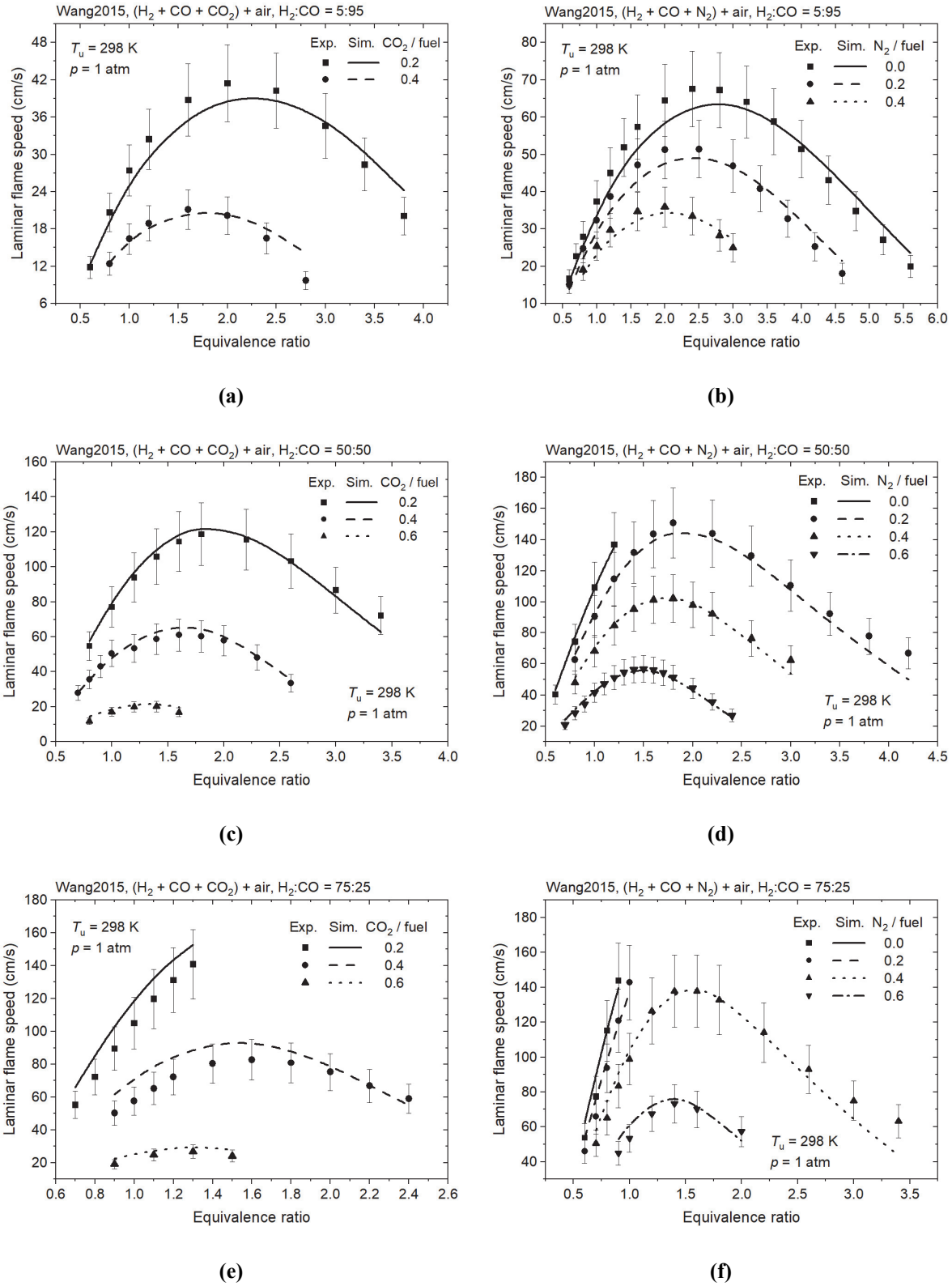

Fig. S2-23 Laminar flame speeds of H_2/CO/N_2/CO_2/air mixtures (T_u = 298 K, p = 1 atm) measured by Wang et al. [40].

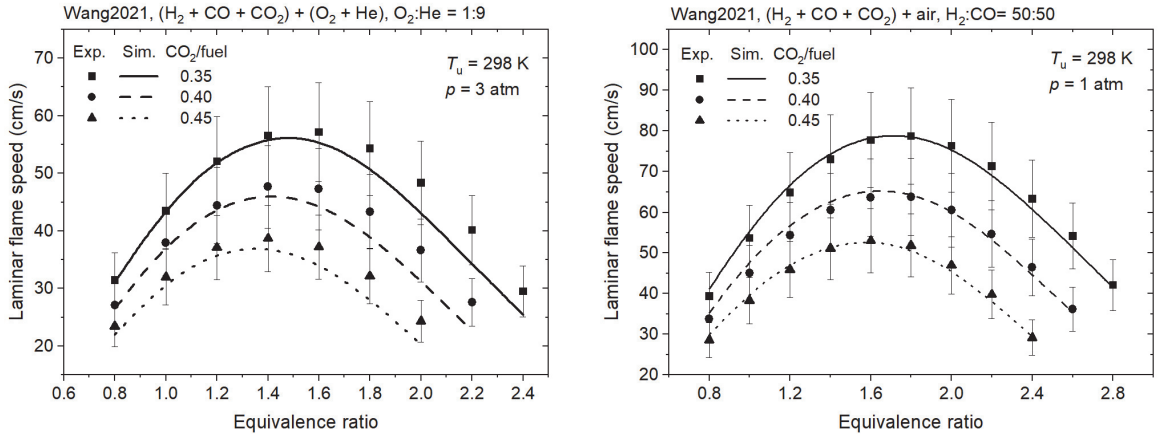

(a) **(b)**

Fig. S2-24 Laminar flame speeds of H2/CO/CO2/O2/He/air mixtures (Tu = 298 K, p = 1-3 atm) measured by Wang et al. [47].

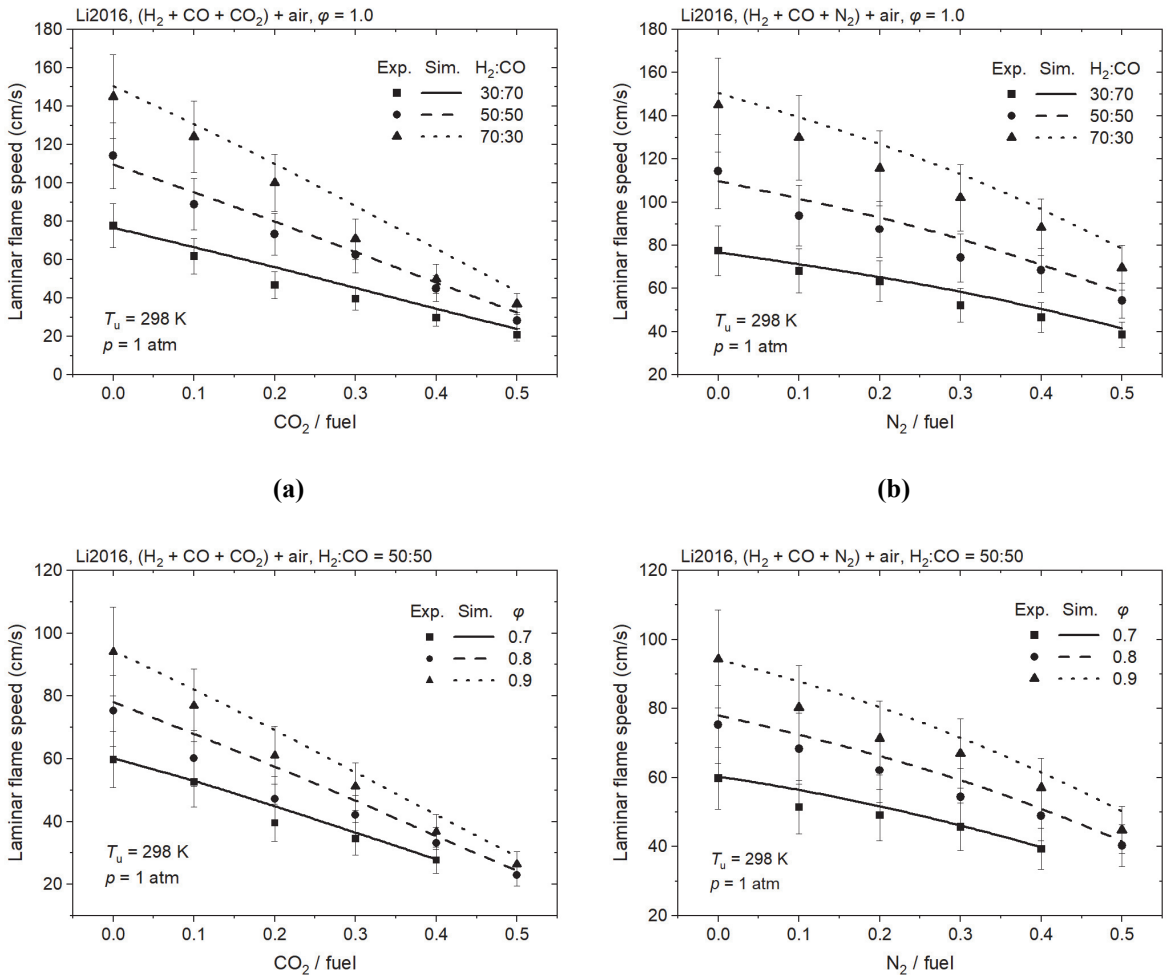

(a) **(b)**

(c) **(d)**

Fig. S2-25 Laminar flame speeds of H_2/CO/N_2/CO_2/air mixtures (T_u = 298 K, p = 1 atm) measured by Li et al. [41].

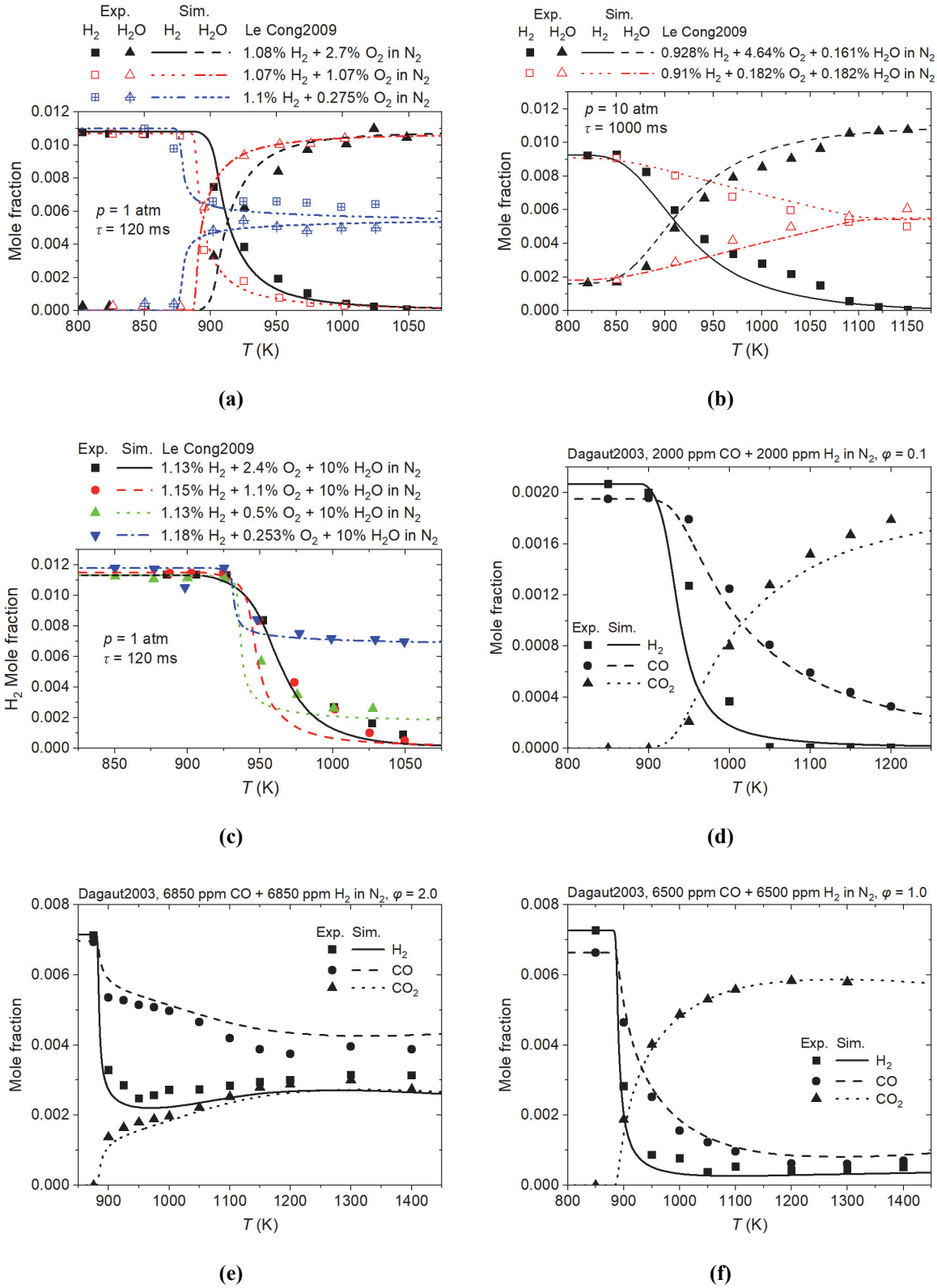

Fig. S2-26. Concentration profiles of H_2, H_2O, CO, and CO_2 measured in the jet stirred reactor by Le Cong and Dagaut et al [53, 54].

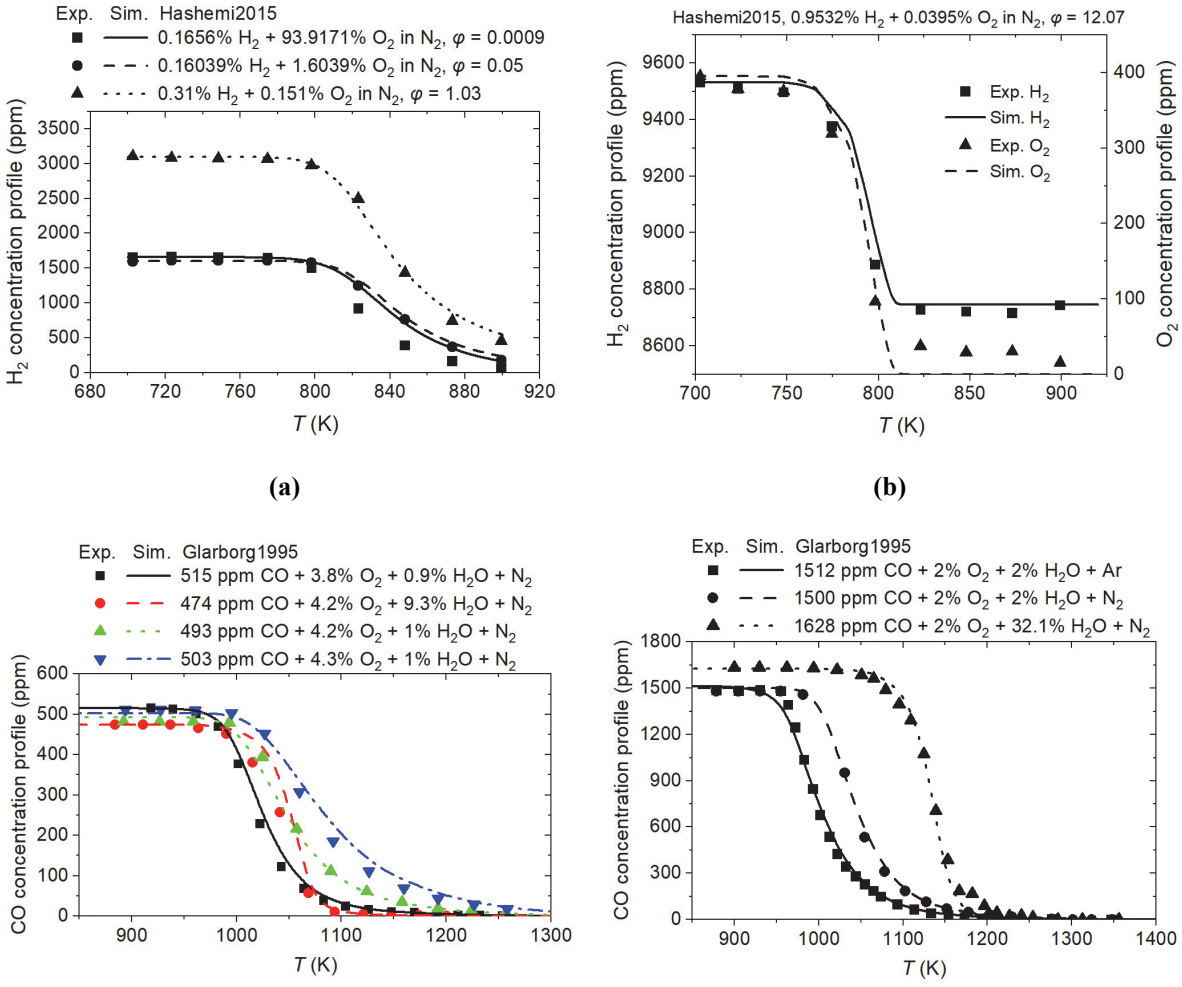

Fig. S2-27. Concentration profiles of H_2, O_2, and CO measured in the plug flow reactors by Hashemi and Glarborg et al. [55, 56].

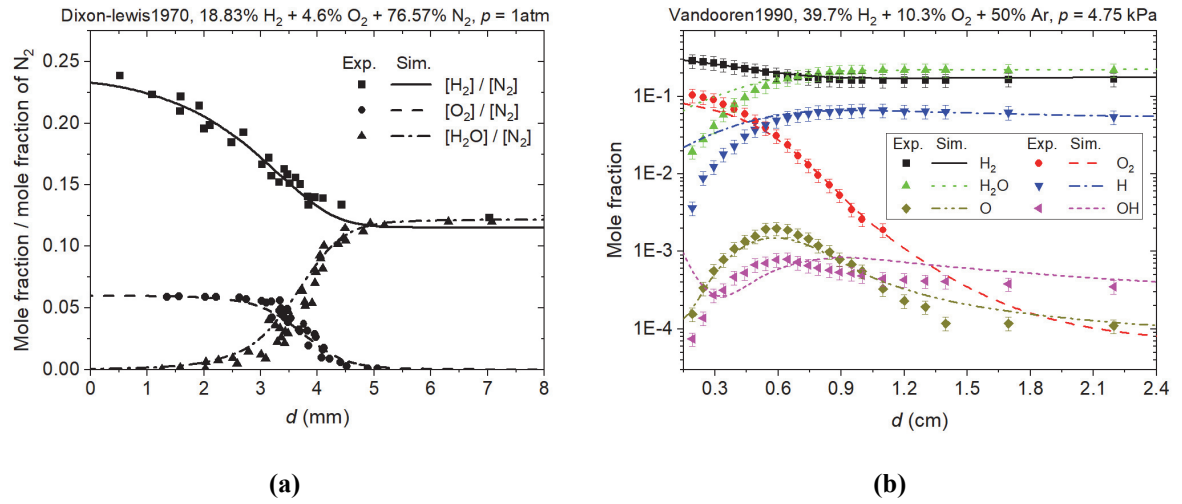

Fig. S2-28. Concentration profiles measured in the premixed laminar flame by Dixon-Lewis et al. [57] and Vandooren et al. [58].

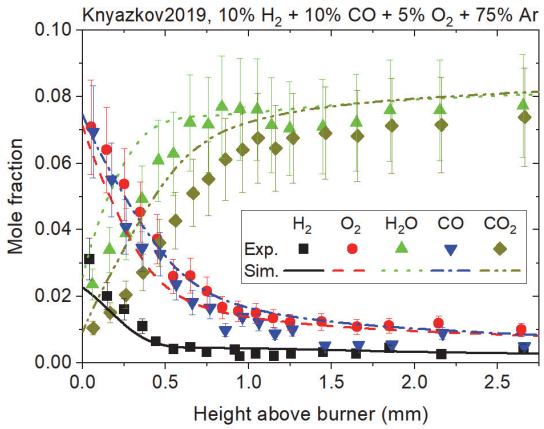

(a)

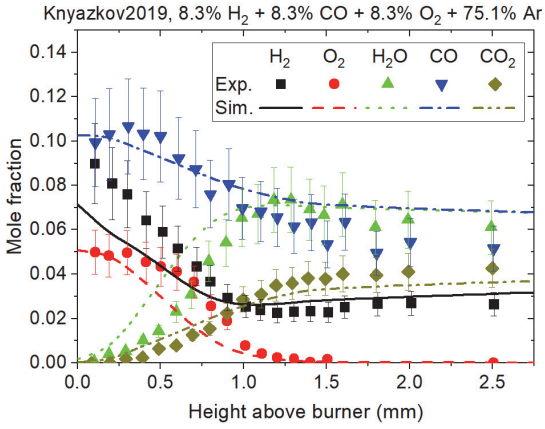

(b)

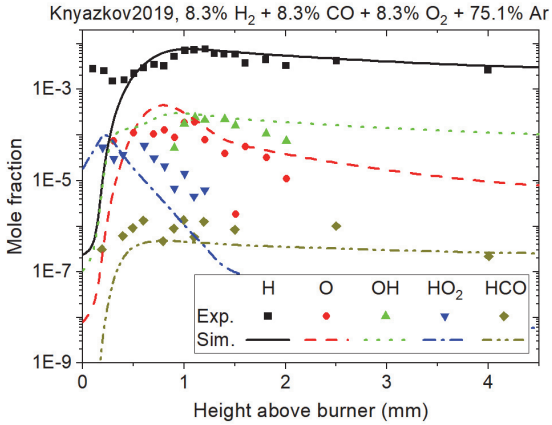

(c)

Fig. S2-29. Concentration profiles measured in the premixed laminar flame by Knyazkov et al [59].

Reference

[1] Hu E, Pan L, Gao Z, Lu X, Meng X, Huang Z. Shock tube study on ignition delay of hydrogen and evaluation of various kinetic models. International Journal of Hydrogen Energy 2016;41(30):13261-80.

[2] Zhang J, Hu E, Pan L, Zhang Z, Huang Z. Shock-Tube Measurements of Ignition Delay Times for the Ethane/Dimethyl Ether Blends. Energy & Fuels 2013;27(10):6247-54.

[3] Petersen EL, Kalitan DM, Rickard MJ. Reflected Shock Ignition of SiH4/H2/O2/Ar andSiH4/CH4/O2/Ar Mixtures. Journal of Propulsion and Power 2004;20(4):665-74.

[4] Ninnemann E, Koroglu B, Pryor O, Barak S, Nash L, Loparo Z, et al. New insights into the shock tube ignition of H2/O2 at low to moderate temperatures using high-speed end-wall imaging. Combustion and Flame 2018;187:11-21.

[5] Pang G, Davidson D, Hanson R. Experimental study and modeling of shock tube ignition delay times for hydrogen–oxygen–argon mixtures at low temperatures. Proceedings of the Combustion Institute 2009;32(1):181-8.

[6] Shao J, Choudhary R, Davidson DF, Hanson RK, Barak S, Vasu S. Ignition delay times of methane and hydrogen highly diluted in carbon dioxide at high pressures up to 300 atm. Proceedings of the Combustion Institute 2019;37(4):4555-62.

[7] He D, Ding Y, Xiong X, Shi S, Du Y, Peng Z, et al. Shock Tube Study of Ignition-Delay Measurements and Kinetic Mechanism Research for Syngas. Journal of Propulsion and Power 2018;34(4):836-43.

[8] Krejci MC, Mathieu O, Vissotski AJ, Ravi S, Sikes TG, Petersen EL, et al. Laminar flame speed and ignition delay time data for the kinetic modeling of hydrogen and syngas fuel blends. Journal of Engineering for Gas Turbines and Power 2013;135(2).

[9] Kéromnès A, Metcalfe WK, Heufer KA, Donohoe N, Das AK, Sung C-J, et al. An experimental and detailed chemical kinetic modeling study of hydrogen and syngas mixture oxidation at elevated pressures. Combustion and Flame 2013;160(6):995-1011.

[10] Herzler J, Naumann C. Shock tube study of the ignition of lean CO/H2 fuel blends at intermediate temperatures and high pressure. Combustion Science and Technology 2008;180(10-11):2015-28.

[11] Qin X, Kobayashi H, Niioka T. Laminar burning velocity of hydrogen–air premixed flames at elevated pressure. Experimental Thermal and Fluid Science 2000;21(1-3):58-63.

[12] Dong C, Zhou Q, Zhao Q, Zhang Y, Xu T, Hui S. Experimental study on the laminar flame speed of hydrogen/carbon monoxide/air mixtures. Fuel 2009;88(10):1858-63.

[13] Pareja J, Burbano HJ, Ogami Y. Measurements of the laminar burning velocity of hydrogen–air premixed flames. International Journal of Hydrogen Energy 2010;35(4):1812-8.

[14] Liu D, MacFarlane R. Laminar burning velocities of hydrogen-air and hydrogen-air steam flames. Combustion and Flame 1983;49(1-3):59-71.

[15] Egolfopoulos F, Law CK. An experimental and computational study of the burning rates of ultra-lean to moderately-rich H2/O2/N2 laminar flames with pressure variations. *Symposium (international) on combustion.* 23. Elsevier; 1991:333-40.

[16] Vagelopoulos CM, Egolfopoulos FN, Law CK. Further considerations on the determination of laminar flame speeds with the counterflow twin-flame technique. *Symposium (international) on combustion.* 25. Elsevier; 1994:1341-7.

[17] Huang Z, Zhang Y, Zeng K, Liu B, Wang Q, Jiang D. Measurements of laminar burning velocities for natural gas–hydrogen–air mixtures. Combustion and Flame 2006;146(1-2):302-11.

[18] Bradley D, Lawes M, Liu K, Verhelst S, Woolley R. Laminar burning velocities of lean hydrogen–air mixtures at pressures up to 1.0 MPa. Combustion and Flame 2007;149(1-2):162-72.

[19] Günther R, Janisch G. Measurements of burning velocity in a flat flame front. Combustion and Flame 1972;19(1):49-53.

[20] Dowdy DR, Smith DB, Taylor SC, Williams A. The use of expanding spherical flames to determine burning velocities and stretch effects in hydrogen/air mixtures. *Symposium (International) on Combustion.* 23. Elsevier; 1991:325-32.

[21] Aung K, Hassan M, Faeth G. Effects of pressure and nitrogen dilution on flame/stretch interactions of laminar premixed H2/O2/N2 flames. Combustion and flame 1998;112(1-2):1-15.

[22] Tse SD, Zhu D, Law CK. Morphology and burning rates of expanding spherical flames in H2/O2/inert mixtures up to 60 atmospheres. Proceedings of the Combustion Institute 2000;28(2):1793-800.

[23] Kwon O, Faeth G. Flame/stretch interactions of premixed hydrogen-fueled flames: measurements and predictions. Combustion and Flame 2001;124(4):590-610.

[24] Lamoureux N, Paillard C-E, Vaslier V. Low hydrocarbon mixtures ignition delay times investigation behind reflected shock waves. Shock waves 2002;11(4):309-22.

[25] Burke MP, Chen Z, Ju Y, Dryer FL. Effect of cylindrical confinement on the determination of laminar flame speeds using outwardly propagating flames. Combustion and Flame 2009;156(4):771-9.

[26] Hu E, Huang Z, He J, Miao H. Experimental and numerical study on laminar burning velocities and

flame instabilities of hydrogen–air mixtures at elevated pressures and temperatures. international journal of hydrogen energy 2009;34(20):8741-55.

[27] Varea E, Beeckmann J, Pitsch H, Chen Z, Renou B. Determination of burning velocities from spherically expanding H2/air flames. Proceedings of the Combustion Institute 2015;35(1):711-9.

[28] Zhang Z, Cheng P, Tan J, Liang J, Li Y, Li G. The uncertainty of laminar burning velocity of premixed H2-air flame induced by the non-uniform initial temperature field inside the constant-volume combustion vessel. International Journal of Hydrogen Energy 2018;43(45):21049-59.

[29] Grosseuvres R, Comandini A, Bentaib A, Chaumeix N. Combustion properties of H2/N2/O2/steam mixtures. Proceedings of the Combustion Institute 2019;37(2):1537-46.

[30] McLean IC, Smith DB, Taylor SC. The use of carbon monoxide/hydrogen burning velocities to examine the rate of the CO+ OH reaction. *Symposium (international) on combustion.* 25. Elsevier; 1994:749-57.

[31] Hassan M, Aung K, Faeth G. Properties of laminar premixed CO/H/air flames at various pressures. Journal of Propulsion and Power 1997;13(2):239-45.

[32] Bouvet N, Lee S, Gokalp I, Santoro R. Flame speed characteristics of syngas (H2-CO) with straight burners for laminar premixed flames. *Third European Combustion Meeting.* 2007:1-6.

[33] Natarajan J, Lieuwen T, Seitzman J. Laminar flame speeds of H2/CO mixtures: Effect of CO2 dilution, preheat temperature, and pressure. Combustion and flame 2007;151(1-2):104-19.

[34] Sun H, Yang S, Jomaas G, Law C. High-pressure laminar flame speeds and kinetic modeling of carbon monoxide/hydrogen combustion. Proceedings of the Combustion Institute 2007;31(1):439-46.

[35] Prathap C, Ray A, Ravi M. Effects of dilution with carbon dioxide on the laminar burning velocity and flame stability of H2–CO mixtures at atmospheric condition. Combustion and Flame 2012;159(2):482-92.

[36] Singh D, Nishiie T, Tanvir S, Qiao L. An experimental and kinetic study of syngas/air combustion at elevated temperatures and the effect of water addition. Fuel 2012;94:448-56.

[37] Goswami M, Bastiaans R, Konnov A, de Goey L. Laminar burning velocity of lean H2-CO mixtures at elevated pressure using the heat flux method. international journal of hydrogen energy 2014;39(1485):e1498.

[38] Xie Y, Wang J, Xu N, Yu S, Huang Z. Comparative study on the effect of CO2 and H2O dilution on laminar burning characteristics of CO/H2/air mixtures. international journal of hydrogen energy 2014;39(7):3450-8.

[39] Zhang Y, Shen W, Fan M, Zhang H, Li S. Laminar flame speed studies of lean premixed H2/CO/air flames. Combustion and Flame 2014;161(10):2492-5.

[40] Wang Z, Weng W, He Y, Li Z, Cen K. Effect of H2/CO ratio and N2/CO2 dilution rate on laminar burning velocity of syngas investigated by direct measurement and simulation. Fuel 2015;141:285-92.

[41] Li H-M, Li G-X, Sun Z-Y, Zhou Z-H, Li Y, Yuan Y. Investigation on dilution effect on laminar burning velocity of syngas premixed flames. Energy 2016;112:146-52.

[42] Gong X, Huo J, Ren Z, Law CK. Extrapolation and DNS-mapping in determining laminar flame speeds of syngas/air mixtures. Combustion and Flame 2019;200:365-73.

[43] Bouvet N, Chauveau C, Gökalp I, Lee S-Y, Santoro RJ. Characterization of syngas laminar flames using the Bunsen burner configuration. International Journal of Hydrogen Energy 2011;36(1):992-1005.

[44] Ratna Kishore V, Ravi MR, Ray A. Adiabatic burning velocity and cellular flame characteristics of H2–CO–CO2–air mixtures. Combustion and Flame 2011;158(11):2149-64.

[45] Burbano HJ, Pareja J, Amell AA. Laminar burning velocities and flame stability analysis of H2/CO/air mixtures with dilution of N2 and CO2. International Journal of Hydrogen Energy 2011;36(4):3232-42.

[46] Li H-M, Li G-X, Sun Z-Y, Zhou Z-H, Li Y, Yuan Y. Effect of dilution on laminar burning characteristics of H2/CO/CO2/air premixed flames with various hydrogen fractions. Experimental Thermal and Fluid Science 2016;74:160-8.

[47] Wang S, Wang Z, Elbaz AM, He Y, Chen C, Zhu Y, et al. Effects of CO2 Dilution and CH4 Addition on Laminar Burning Velocities of Syngas at Elevated Pressures: An Experimental and Modeling Study. Energy & Fuels 2021;35(22):18733-45.

[48] Prathap C, Ray A, Ravi M. Investigation of nitrogen dilution effects on the laminar burning velocity and flame stability of syngas fuel at atmospheric condition. Combustion and Flame 2008;155(1-2):145-60.

[49] Zhang X, Huang Z, Zhang Z, Zheng J, Yu W, Jiang D. Measurements of laminar burning velocities and flame stability analysis for dissociated methanol–air–diluent mixtures at elevated temperatures and pressures. International Journal of Hydrogen Energy 2009;34(11):4862-75.

[50] Das AK, Kumar K, Sung C-J. Laminar flame speeds of moist syngas mixtures. Combustion and Flame 2011;158(2):345-53.

[51] Voss S, Hartl S, Hasse C. Determination of laminar burning velocities for lean low calorific H 2 /N 2 and H 2 /CO/N 2 gas mixtures. International Journal of Hydrogen Energy 2014;39(34):19810-7.

[52] Han M, Ai Y, Chen Z, Kong W. Laminar flame speeds of H2/CO with CO2 dilution at normal and elevated pressures and temperatures. Fuel 2015;148:32-8.

[53] Le Cong T, Dagaut P. Experimental and detailed modeling study of the effect of water vapor on the kinetics of combustion of hydrogen and natural gas, impact on NO x. Energy & Fuels 2009;23(2):725-34.

[54] Dagaut P, Lecomte F, Mieritz J, Glarborg P. Experimental and kinetic modeling study of the effect of NO and SO2 on the oxidation of CO-H2 mixtures. International journal of chemical kinetics 2003;35(11):564-75.

[55] Glarborg P, Kubel D, Kristensen PG, Hansen J, Dam-Johansen K. Interactions of CO, NOx and H2O under post-flame conditions. Combustion Science and Technology 1995;110(1):461-85.

[56] Hashemi H, Christensen JM, Gersen S, Glarborg P. Hydrogen oxidation at high pressure and intermediate temperatures: Experiments and kinetic modeling. Proceedings of the Combustion Institute 2015;35(1):553-60.

[57] Dixon-Lewis G, Sutton MM, Williams A. Flame structure and flame reaction kinetics-IV. Experimental investigations of a fuel-rich hydrogen+ oxygen+ nitrogen flame at atmospheric pressure. Proceedings of the Royal Society of London A Mathematical and Physical Sciences 1970;317(1529):227-34.

[58] Vandooren J, Bian J. Validation of H2/O2 reaction mechanisms by comparison with the experimental structure of a rich hydrogen-oxygen flame. *Symposium (International) on Combustion.* 23. Elsevier; 1990:341-6.

[59] Knyazkov D, Dmitriev A, Bolshova T, Shmakov A, Korobeinichev O, Markovich D. Experimental and numerical study of the structure of premixed H2/CO/O2/Ar flames at atmospheric pressure. *Journal of Physics: Conference Series.* 1382. IOP Publishing; 2019:012068.